The Evolution of Speed: an empirical and comparative analysis of drag-reducing scales in early fishes

Thomas Merrick Fletcher

Submitted in accordance with the requirements for the degree of Doctor of Philosophy

The University of Leeds, School of Earth and Environment

September 2015

The candidate confirms that the work submitted is his/her own, except where work which has formed part of jointly authored publications has been included. The contribution of the candidate and the other authors to this work has been explicitly indicated below. The candidate confirms that appropriate credit has been given within the thesis where reference has been made to the work of others.

(Overleaf) Juxtaposition of modern mako shark swimming alongside extinct jawless thelodonts (~415 million years old), and 'acanthodians' (~385 million years old). Published with kind permission of artist James McKay.

" The animal glides, dreamlike through its watery world, and in to our subconscious. It's one of the last great predators to roam free on the planet, a creature of fearful symmetry. "

Sir David Frederick Attenborough, 1995

Acknowledgements

I am indebted to my supervisors, Professors Jeffrey Peakall, Paul Wignall, and John Altringham for their advice, encouragement, and forbearance while conducting this research. It is testament to their scientific curiosity and trust that this project was allowed to mutate, in ways none of us could have imagined. It was great fun and a genuine honour to work with such different but oddly harmonious personalities, all of whom are true natural philosophers. I'm particularly proud to be John's final PhD student, bringing him back to his fishy roots. I wish him a very happy and lengthy retirement.

I would like to thank Doctors Gareth Keevil and Rob Thomas, and Russell Dixon of the Sorby Environmental Fluid Dynamics Laboratory, without whose technical aid much of this work would not have been possible. Technical support was also provided by Dr Richard Walshaw using the scanning electron microscope, Dr Samuel Allshorn of the Cohen Laboratory, Hannah Elms, Ruth Anderson Beck. Additionally, I would like to thank everyone who I have discussed this work with for their honest advice and useful feedback, especially my examiners Tracy Aze and Matt Friedman. I would like to thank Dr Henning Blom for scale material from his collection, Dr Martin Rücklin for sharing µCT scan data, James Dale of the Blue Planet Aquarium for cadaverous *Polypterus* material, and Victoria Bendall for access to shark specimens at the Centre for Environment, Fisheries & Aquaculture Science. I thank Sue Lindsay and Carole Burrow for contributing scale images, and Sue Turner for help acquiring literature. For access to museum collections I thank Martha Richter and Lorna Steele (British Museum of Natural History, London), Mathew Riley (Sedgwick Museum, Cambridge), Mathew Lowe (University of Cambridge Zoological Museum, Cambridge), Katie Hewitt (Lapworth Museum of Geology, Birmingham), and a special thanks to Dr Stig Walsh of the National Museums of Scotland. The project was funded by Natural Environment Research Council doctoral training grant NE/J50001X/1, and case partner Speedo Ltd.

I thank James McKay for the stunning cover art overleaf, a juxtaposition created with genuine warmth, passion, and masterful imagination. I of course thank my family, Dan, Nikki, the Nudds, Fletchers and Robinsons, and particularly my unflinchingly devoted grandparents, Viv and Graham, Tom and Peggy. I know how lucky I am to have you all. To my wonderful friends and adopted family, I owe special thanks. As my long-time carers, enablers and therapists, their terrible influence and drunken nonsense has improved my life immeasurably.

Finally, I thank my parents Neil and Pam most of all, for their nearly three decades of limitless patience and support. For the life I love so much, I am truly proud to dedicate this work to them.

Abstract

From their earliest origins fishes have developed a suite of adaptations for locomotion in water. Even without data from behaviour, soft tissue, and extant relatives, it is possible to infer a wealth of palaeobiological and palaeoecological information. As in extant species, aspects of gross morphology such as streamlining, fin position and tail type are optimised even in the earliest fishes, indicating similar life strategies have been present throughout their evolutionary history. Drag-reducing riblets ornamenting the scales of fast-moving sharks have been subject to particularly intense research, but this has not been extended to extinct forms. The crowns of shark scales are exposed directly to the aquatic environment offering a unique opportunity to elucdate scale function in some of their long-extinct Palaeozoic relatives.

This thesis is the first comprehensive study of scale function in fossil fishes, and demonstrates that sophisticated adaptations for drag-reduction existed at a remarkably early stage in fish evolution. It is shown that riblet spacing reflects swimming speed in modern sharks, and that drag-reduction morphology evolved in the denticles of the earliest vertebrates, including the oldest examples known (~460 million years ago). Comparative analysis between modern sharks and fossil taxa reveals distinct and diverse regionalisation of scale features across the body, as well as ontogenetic changes. In addition to riblet spacing, the variation of other scale features is investgated quantitatively in modern sharks, revealing the importance of riblet angle in overall drag reduction. Furthermore, experimental skin friction measurements of fossil fish scales demonstrate the potential drag reduction of a diverse range of morphologies, even without riblets.

Table of Contents

List of Tables

Chapter 3

Chapter 5

Chapter 6

Chapter 7

List of Figures

Chapter 2

Figure 2.8. Vertical cross sections of turbulent flow (velocity = 3 m s^{-1}) of streamwise vortices over a) a flat plate, and; b) riblets. Mean velocity profiles for flow in cross-flow directions shown enlarged for riblets. Adapted from Bechert et al., 1997; and Lee & Lee, 2001.

Figure 2.9. Mechanism of drag-reduction by bristling scales. Placoid scales in; a) resting position in attached boundary layer; and b) erect position in detached recirculating flow.

Figure 2.10. Proposed mechanism of drag-reduction by streamwise injection. a) Diagram of vortices formed across a scaled plate with patterns of fluid suction and ejection (white arrows); b) lateral section view, and; c) transverse section view. Mean flow direction indicated by black arrow. Based on Bechert et al., 1986.

Figure 2.11. Examples of hypothesised swimming morphotypes of extinct and extant fishes. a) *Saurichthys* (Triassic); b) *Aspidorhynchus* sp. (Middle Jurassic – Late Cretaceous); c) *Belone belone* (extant needlefish); d) *Dorypterus* sp. (Permian); e) *Proscinetes* sp. (Jurassic); f) *Stromateus fiatola* (extant pomfret); g) *Trachinotus falcatus* (extant permit); h) *Bobasatrania* sp. (Triassic); i) *Cheirodus* sp. (Carboniferous); j) *Chaetodon* sp. (extant butterflyfish); k) *Tarrasius* sp. (Carboniferous); l) *Clinoporus biporosus* (extant ladder klipfish); m) *Rebellatrix divaricerca* (Early Triassic); n) *Hypsocormus* sp. (mid-late Jurassic); o) *Scomber scombrus* (extant Atlantic mackerel); p) *Parasemionotus* sp. (Early Triassic); q) *Mesolepis* sp. (Carboniferous); r) *Oncorhynchus mykiss* (extant rainbow trout); s) *Carpiodes cyprinus* (extant quillback); t) *Perleidus* sp. (Early – Middle Triassic); u) *Paracentrophorus* sp. (Early Triassic); v) *Serranus hepatus* (extant brown comber). After Helfman et al., 2009; Wendruff & Wilson, 2011; Belles-Isles, 1992; Webb, 1984; Kogan et al., 2011; Barbieri & Martin, 1996; and Braun & Reif, 1982.

Figure 2.12. Recent phylogenetic hypothesis; a) of all 'fishes' and their relatives; b) and timescale of the evolution of Palaeozoic 'fishes' and their relatives, including pituriaspids. c) Reconstruction of the early Cambrian myllokunmingiid *Haikouichthys ercaicunensis*. Extinct taxa are symbolised with a dagger (†), question marks indicate uncertain phylogenetic placement, and inverted commas denote possibly paraphyletic taxa. Details of analyses and taxonomic groupings are detailed in the original source references; a) modified from Friedman & Sallan, 2012; b) redrawn from Janvier, 2015, and; c) from Zhang & Hou, 2004. Scale bar is 5mm

Figure 2.13. Reconstructions of representative Palaeozoic 'Agnathans'; a) the conodont animal, from Aldridge et al., 1993; b) the Silurian anaspid *Cowielepis*, from Blom, 2008; c) the Early Devonian galeaspid *Macrothyraspis*, based on Wang et al. 2005 and; d) the Early

Devonian heterostracan *Errivaspis*, from Mark-Kurik & Botella, 2009; e) the Early Devonian furcacaudiform thelodont *Cometicercas*, from Wilson & Caldwell, 1998; f) the Ordovician arandaspid *Sacambamaspis*, modified from Gagnier, 1993 [in Benton, & Harper, 2013] and Pradel et al., 2007 and; g) the osteostracan *Diademaspis*, from Keating et al., 2012. Not to scale.

Figure 2.14. Reconstructions of representative Palaeozoic gnathostome fish groups. The placoderms a) *Oxyosteus*, from Moy-Thomas & Miles, 1971, and; b) *Rolfosteus* (creative commons image); the 'acanthodians' c) Nerepisacanthus, from Burrow, 2011, and; d) *Acanthodes*, from Zidek, 1976. The chondricthyans e) *Akmonistion*, from Coates & Sequeira, 2001, and; f) *Cladoselache* (creative commons image); and the osteichthyans g) *Guiyu*, from Zhu et al., 2009, and; h) *Eusthenopteron*, from Schultze, 1984. Not to scale.

Figure 2.15. Reconstruction of the Carboniferous chondrichthyan *Iniopteryx rushlaui* from Zangerl and Case, 1973, showing large hook-like denticles on leading edge of fin.

Figure 2.16. a) Diversity of caudal fins in some Palaeozoic fish groups, and; b) occurrence of dorsal fins (green), paired fins (red), and anal fins (blue) in some Palaeozoic fish groups. From a) Pradel et al., 2007, and; b) Sansom et al., 2010; 2013.

Figure 2.17. Variation in the integument of some living fishes. Clockwise from top left: Simplified cross-sections of the leptoid scales of a) *Phoxinus phoxinus* (common minnow), and; b) *Scomber scombrus* (mackerel); c) the ganoid scales of *Polypterus senegalus* (Cuvier's bichir); and d) the placoid scales of *Isurus oxyrinchus* (shortfin mako shark). Modified from Whitear, 1986 and Motta et al., 2012.

Figure 2.18. Dermal denticles of the angelshark *Squatina squatina* from the mid-body flank region of the a) mucus-coated dorsal and b) ventral surface. Adult female, total length 1240mm, sampled at Centre for Environment Fisheries and Aquaculture Science (CEFAS), United Kingdom.

Figure 2.19. Dermal denticles from a) the flank ('FB2', Figure. 3.3); and b) the tail ('T1', Figure 3.3) of the small-spotted catshark Scyliorhinus canicula. Adult male specimen from Pembrokeshire, United Kingdom, 535mm total length.

Figure 2.20. a) Simplified phylogeny of Palaeozoic vertebrates showing incidences of monoodontode (blue) and polyodontode scales, with cross sections of the osteichthyan *Cheirolepis*; the 'acanthodian' *Nostolepis*; the chondrichthyan *Cladoselache*, and the placoderm *Ohiolepis*; b) 'non-growing' forms of putative chondrichthyan, and; c) 'growing'

forms of putative chondrichthyan scale. From a) Qu et al., 2013 and; b-c) Hanke & Wilson, 2010.

Chapter 3

Figure 3.1. Schemes and terms applied for differentiating body regions in thelodonts, including the mouth/rostral area (brown), postpectoral or trunk (red), and the tail region or precaudal (blue). a) *Loganellia scotica* after Märss & Ritchie, 1997 further defining lateral (orange), and pinnal scales (green); b) *Phlebolepis elegans* after Märss, 1986; and c) *Furcacauda fredholmae* after Wilson & Caldwell, 1998.

Figure 3.2. Standardised scale regions for taxa referenced in text. a) an 'acanthodian'; b, an early osteichthyan; c) a modern shark; d) a modern teleost; and e) a thelodont agnathan. Based on Reif, 1985; Märss, 1986; Märss & Ritchie, 1998; and Wilson, 1998.

Figure 3.3. A) Standardised sampling locations for shark specimens (*Lamna nasus* shown) and; b) sampling locations and a higher density sampling grid specific to *Centrophorus granulosus*. Locations are; H1, tip of rostrum; H2, middle of head; H3, back of head at start of gills; MG, exposed outer skin from the central gill; P1, proximal dorsal surface of pectoral fin; P2, middle dorsal surface of pectoral; P3, distal dorsal surface of pectoral; FF1, top of flank anterior along vertical transect running upwards from the back of the pectoral fin; FF2, midline of flank anterior along same transect; FF3, bottom of flank anterior along same transect; D1, distal-most point of dorsal fin; D2, middle of dorsal fin; D3, centre proximal-most point of dorsal fin; FB1, top of flank posterior along vertical transect running upwards from the back of the anal fin; FB2, midline of flank posterior along same transect; FB3, bottom of flank posterior along same transect; Cl, centre of pelvic clasper; T1, proximal centre of tail/caudal fin; T2, middle of tail along axial midline; T3, distal-most of axial midline where the caudal fin forks inwards. Images not to scale. For ease of reference, a simplified version of this figure is presented in section 6.1.

Figure 3.4. Example of evenly distributed riblet measurements of a flank scale of *Carcharhinus brachyurus* (copper shark). Image modified for illustrative purposes courtesy of Sue Lindsay, Microscopy and Microanalysis Unit, Australian Museum, Sydney.

Figure 3.5. Technique for measuring riblet angle. This scale crown shows one central riblet (orange) surrounded by two at diverging angles in the downstream direction. Riblet angle was calculated as the downstream angle of the left riblet(s) relative to the central riblet ('Angle 1)

minus the downstream angle of the right ('Angle 2'). Negative values indicate diverging in the down-stream direction, and positive values are converging in the downstream direction. In this example from the mid-gills of *Lamna nasus* ('MG', Figure 3.3), the angle is -18˚ (diverging).

Figure 3.6. An articulated specimen of *Lanarkia horrida* (NHMUK PV42009), highlighted in purple. Detail of the dorsal and flank region with anterior/head region towards the right of the image, scale bar is 2mm.

Figure 3.7. The tessellation of thelodont flank scales in articulated material. a) *Thelodus mackintoshi* (NHMUK PV52445) and; b) *Loganellia scotica* (NHMUK PV 11282). Scale bar 1mm.

Figure 3.8. The tessellation of 'acanthodian' flank scales in articulated material. a) *Acanthodes sulcatus* (NHMUK PV57555); b) *Cheiracanthus latus* (NHMUK PV50105); c) *Ptomacanthus anglicus* (NHMUK PV19998); d) *Diplacanthus longispinus* (NHMUK PV1369). Scale bar 1mm.

Figure 3.9. High resolution synchrotron radiation X-ray tomographic microscopy (SRXTM) scan of a *Loganellia scotica* (Thelodonti) flank scale, MNHN GBP384 (Muséum national d'Histoire naturelle, Paris), from the Silurian of Scotland. Scan data provided by Martin Rücklin, Naturalis Biodiversity Center, Leiden. Figured in Rücklin et al., 2011. Surface mesh lines hidden for clarity, images not to scale.

Figure 3.10. X-ray microtomograph images of a *Lophosteus* sp. (Osteichthyes) flank scale from the Silurian of Estonia (Ohesaare Cliff). Uncatalogued specimens provided by Henning Blöm, Uppsala University. Images not to scale.

Figure 3.11. X-ray microtomograph images of a *Phlebolepis elegans* (Thelodonti) flank scale from the Silurian of Estonia (Silma Cliff, Saaremaa). Uncatalogued specimens provided by Henning Blöm, Uppsala University. Images not to scale.

Figure 3.12. X-ray microtomograph images of a *Poracanthodes* sp. (Acanthodii) flank scale from the Silurian of Estonia (Ohesaare Cliff). Uncatalogued specimens provided by Henning Blöm, Uppsala University. Images not to scale.

Figure 3.13. X-ray microtomograph images of a *Nostolepis striata* (Acanthodii) flank scale from the Silurian of Estonia (Ohesaare Cliff). Uncatalogued specimens provided by Henning Blöm, Uppsala University. Images not to scale.

Figure 3.14. Completed *Loganellia* scale (MNHN GBP384) block showing tessellated scale surface (top), and individual scale volumes embedded and merged with blank rectangular prisms, placed beside each other before further merging operations (bottom).

Figure 3.15. Top view of two completed and joined Loganellia scale plate blocks (top), and detail of the interdigitating scale units (bottom).

Figure 3.16. Design template for the individual plate blocks, on which a scaled surface was applied. a) top view of block; b) back view; c) oblique view showing concave truncated pyramids and holes for steel rod supports; d) side view, asterisk shows the only dimensional variable of the blocks, herein referred to as block thickness, and; e) oblique view showing corresponding convex truncated pyramids used to guide assembly of plate.

Figure 3.17. Design of individual block of *Loganellia scotica* test plate. a) top view of block showing scaled surface and downstream direction (black arrow); b-c) oblique views of whole block; d) side view; e-f) surface detail showing scale tessellation and downstream direction (black arrow). Scale height above flat upper surface is 0.6mm, block thickness is 10.4mm, see text.

Figure 3.18. Design of individual block of *Lophosteus* sp. test plate. a) top view of block showing scaled surface and downstream direction (black arrow); b-c) oblique views of whole block; d) side view; e-f) surface detail showing scale tessellation and downstream direction (black arrow). Scale height above flat upper surface is 0.27mm, block thickness is 10.0mm, see text.

Figure 3.19. Design of individual block of *Phlebolepis elegans* test plate. a) top view of block showing scaled surface and downstream direction (black arrow); b-c) oblique views of whole block; d) side view; e-f) surface detail showing scale tessellation and downstream direction (black arrow). Scale height above flat upper surface is 0.35mm, block thickness is 12.4mm, see text.

Figure 3.20. Design of individual block of *Poracanthodes* sp. test plate. a) top view of block showing scaled surface and downstream direction (black arrow); b-c) oblique views of whole block; d) side view; e-f) surface detail showing scale tessellation and downstream direction (black arrow). Scale height above flat upper surface is 0.55mm, block thickness is 10.56mm, see text.

Figure 3.21. Design of individual block of *Nostolepis striata* test plate. a) top view of block showing scaled surface and downstream direction (black arrow); b-c) oblique views of whole block; d) side view; e-f) surface detail showing scale tessellation and downstream direction (black arrow). Scale height above flat upper surface is 0.97mm, block thickness is 10.47mm, see text.

Figure 5.1. Scanning electron micrographs of flank scales of a) the porbeagle shark *Lamna nasus* and; b) the 'acanthodian' *Nostolepis* sp. cf. *N. gaujensis*. Scale bar on each image is 200 µm. 'acanthodian' image reprinted from Burrow et al., 2009 with permission from Carole Burrow.

Figure 5.2. Schematic vertical cross sections of turbulent-flow of streamwise vortices over a) a flat plate, and; b) riblets. Mean velocity profiles for flow in streamwise (green) and cross-flow (orange) directions shown for riblets. Adapted for illustrative purposes from Bechert et al., 1997, and Lee & Lee, 2001.

Figure 5.3. Boxplot showing riblet spacing measurements for 'acanthodians', thelodonts and modern sharks (n = number of species) possessing distinct parallel grooves and riblets on the scale crown surface. Boxes represent 25-75 percent quartiles with median values at vertical division line. Statistically significant differences (Table 5.1) are indicated by left adjoining lines, those in red indicate p values that show no significant difference after false discovery rate (FDR) correction. Determination of shark speed categories was based on ecological and experimental speed data, detailed in the methods section.

Chapter 6

Figure 6.1. Standardised sampling locations (orange squares) used throughout this study, and midline transect (yellow line) from anterior-most to posterior-most sampling locations. Scheme detailed in section 3.1. Example shown is *Lamna nasus*, not to scale.

Figure 6.2. Shark squamation along the midline ('H1-3, FF2, FB2, T1-3', Figure 6.1.) showing scale variation from anterior to posterior. Note: It is clear from material figured in the literature (Reif, 1985a), that the scales of *Squalus acanthias* have similarly smooth rostral scales, in contrast to the sample presented here (bottom left).

Figure 6.3. Heat map of a) mean scale width (µm) and; b) scale crown aspect ratio (length/width). Distribution interpolated across entire body from standardised sample locations (Figure 6.1.).

Figure 6.4. Examples of *Lamna nasus* dermal denticles with low aspect ratio (width/length) in the head region and high aspect ratio scale bases on the flank. Heat map of scale base aspect ratio distribution from 19 sample locations (excluding claspers) of a 183cm male, and three flank semi-landmarks, interpolated across entire body, and weighted according to standard error.

Figure 6.5. a) Transect of shark midline, showing mean riblet spacing (µm) at different sampling locations. b) 'Heat map' of mean riblet spacing (µm) distribution from 19 sample locations and semi-landmarks, interpolated across entire body, and weighted according to standard error.

Figure 6.6. a) Transect of *Lamna nasus* midline, showing mean riblet angle (degrees) of all specimens at different sampling locations. b) Heat map of mean riblet angle (degrees) distribution from 19 sample locations, and flank semi-landmarks, interpolated across entire body, and weighted according to standard error. Left, scanning electron microscope images of example riblet angles, from top to bottom; riblets converging ('H1' head scale from 183cm male), parallel ('D3' dorsal fin scale from 215cm female) and diverging ('H3' head scale from 127cm female).

Figure 6.7. Heat maps of mean riblet spacing (top), mean riblet angle (middle), and mean scale width (bottom) distribution for all immature (left) and mature (right) specimens of *Lamna nasus*. Images generated using sampling points detailed in Chapter 3.1.3.

Chapter 7

Figure 7.1. Raw velocity measurements (m/s) showing corrected bases of velocity profiles (vertical bars) at horizontal positions 200-400mm, for smooth control plate (dark blue), *Loganellia scotica* (red), *Lophosteus* sp. (green), *Phlebolepis elegans* (purple), *Poracanthodes* sp. (cyan), and *Nostolepis striata* (orange). Data below the inferred wall level was excluded from all analyses that follow. See section 3.2 for Methods and Materials.

Figure 7.2. Mean velocity profiles (corrected base locations) of test plates at 200-400mm from leading edge. Including the smooth control plate (dark blue), and the scaled plates *Loganellia scotica* (red), *Lophosteus* sp. (green), *Phlebolepis elegans* (purple), *Poracanthodes* sp. (cyan), and *Nostolepis striata* (orange). See Appendix II, Figures S2.8-2.13 for individual plots.

Figure 7.3. Semilog plot of mean velocity profiles (corrected) of all test plates at 200-400mm from leading edge. Including smooth control plate (dark blue), and the scaled plates *Loganellia scotica* (red), *Lophosteus* sp. (green), *Phlebolepis elegans* (purple), *Poracanthodes* sp. (cyan), and *Nostolepis striata* (orange). See Appendix II, Figures S2.8-2.13 for individual plots.

Figure 7.4. Bar chart showing percentage of raw negative velocity (U = < 0 m/s) measurements recorded at a near-wall corrected position of 0.5mm vertical (z) position for all plates at all horizontal positions (x = 200-400mm).

Figure 7.5. Boundary layer height (99% maximum velocity) across the test plates. Including the smooth control plate (dark blue dashed), and the scaled plates *Loganellia scotica* (red), *Lophosteus* sp. (green), *Phlebolepis elegans* (purple), *Poracanthodes* sp. (cyan), and *Nostolepis striata* (orange). See Appendix II for full data and individual plots.

Figure 7.6. Skin friction coefficient at horizontal positions x = 200-400mm for the smooth control plate (dark blue), *Loganellia scotica* (red), *Lophosteus* sp. (green), *Phlebolepis elegans* (purple), *Poracanthodes* sp. (cyan), and *Nostolepis striata* (orange).

Chapter 8

Figure 8.1. Scratch marks on the scales of a 680mm (total length) male *Chilloscyllium plagiosum* a) from the rostrum and; b) detail of the posterior tip of a scale from the trunk region ('FF3', section 3.1.). Scales are orientated anterior upwards.

Figure 8.2. Distribution of scale features in *Lamna nasus*, compiled for ease of reference from figures 6.4-6.6, in Chapter 6. Top: transect of shark midline, showing mean riblet spacing (µm) of all specimens of *Lamna nasus* at different sampling locations. Middle: heat map of scale base aspect ratio distribution of a 183cm male *Lamna nasus* from 19 sample locations (excluding claspers), and three flank semi-landmarks, interpolated across entire body, and weighted according to standard error. Bottom: transect of shark midline, showing mean riblet angle (degrees) of all specimens of *Lamna nasus* at different sampling locations

Figure 8.3. Scanning electron micrograph of the Silurian osteichthyan fish *Lophosteus* sp., from Ohesaare Cliff, Estonia. Material courtesy of Henning Blom.

Figure 8.4. Scanning electron micrographs of the 'acanthodian' *Milesacanthus* sp. (a,b) and the modern porbeagle shark *Lamna nasus* (c,d) scales. A) *Milesacanthus* sp. aff. *M. antarctica* flank scale in ventral view showing detail of base, modified from Hairapetian, 2006. B) Dorso-lateral view of scale from unknown body position of *Milesacanthus antarctica* NMV P228907, modified from Burrow et al. 2009. C-d) Flank scales (FF2) of a 183cm male *Lamna nasus* in c) ventral view and; d) lateral view.

1. Introduction

1.1. Hydrodynamics of Fossil Fishes

Swimming has evolved at some point in every class of vertebrate, demonstrating the advantages to locomotion in water. Movement from land in to water or simply upwards beyond its floor, means a species can exploit previously unavailable food sources and habitat, move and escape in three-dimensional space. There is no prospect of limitless variety in nature; the form and behaviour of an organism is strictly governed by the physical world, and the organisms around it. Those species which swim freely in water are no exception, and there are remarkable convergences in nature and in our own technology which reflect this. Fishes - a diverse and disparate group of non-tetrapod vertebrates - provide some of the best examples of convergent evolution in the animal kingdom. Shark scales (and those of rays to a lesser extent) are a good example of this, and are the only surviving group of fishes to still possess dermal denticles: a scale type which erupts through the soft skin tissue. This contact between hard tissue and environment offers a unique opportunity to explicate the function of extinct ‘‘acanthodian’’ and thelodont scales. Herein, the hydrodynamics of long extinct fishes are investigated, both experimentally and comparatively, in light of the drag-reduction strategies of modern sharks.

1.2. Research Motivation and Relevance

Since Aristotle (notably ‘De Motu Animalium’) swimming has fascinated biomechanicians, but it is only since the turn of the 20th century that rigorous experimental approaches to research have been applied. A flourish of publications in the mid 1970s (e.g. Webb, 1975; Wu et al., 1975; Aleyev, 1977) enlivened the modern field, and the pure research they synthesised remain important references. Since this point much fish hydrodynamics research has been driven by commercial or industrial applications, biomimetics, and increasingly the sub-discipline of biorobotics (e.g. Dean & Bhushan, 2010). Many of the fundamental questions raised in these earlier texts remain unanswered or little-explored, especially those of purely biological interest. Sharks are a prime example of this trend, heralded as the inspiration for a suite of drag-reducing and antifouling applications, but in reality only a minority of these studies concern shark ecology.

When living animals cannot be observed, anatomy is the next best source of information, with gross morphology, stomach contents, and even the braincase reflecting ecology and behaviour. Much of this information is lost as the animal decays and so cannot be applied to

the majority of fossil taxa. Scales however are a resistant hard tissue, known to be ecologically significant, and reduce drag in many pelagic sharks (Reif, 1985). Their small size and relative physical resilience means scales have high preservation potential in the fossil record, and so a central question emerged. Can research inspired by shark scales be used retrospectively to study their biology, and that of their ancestors?

The continued interest in shark-inspired technology has resulted in a much deeper understanding of some fundamental mechanisms of shark scale drag-reduction. The motivation for this work has been to further explore how applied research can secondarily benefit our understanding of modern sharks, and of fossil fishes (specific aims and objectives are detailed next). The approach was two-fold, and alongside more traditional functional analyses (e.g. comparative anatomy, geometric morphometrics), engineering methods were also used (facilitated by the Sorby Environmental Fluid Dynamics Laboratory, University of Leeds). The continually improving resolution and decreasing cost of rapid prototyping, made this empirical approach possible, and skin friction of fossil fishes could be measured for the first time. This approach, and the lack of any similar research, makes this project timely and relevant to a number of disciplines, including biology, ecology, engineering, fluid mechanics, geology, and palaeontology.

1.3. Aims and Objectives

A comparative approach using modern sharks was adopted from the outset, serving two main roles; to identify potential morphofunctional correlates which could be explored in fossil taxa (Chapters 4, 5, and 6), and to guide assumptions in the experimental study (Chapter 7). The largest assumption was that the fossil material used in modelling the species' skin was representative of the entire squamation. Scale morphology is known to change dramatically across the bodies of most shark species (Reif, 1985a), and even between individuals of the same species. It was therefore crucial to investigate the magnitude of this variability, and justify the comparison between modern sharks and Palaeozoic taxa. This thesis is a synthesis of three studies, the primary and overarching aims of which were to:

1) Investigate the convergence and functional significance of dermal denticle morphology in modern sharks and fossil taxa.

Objectives:

- Assemble a dataset of images of scales of known body location.

- Investigate functional correlates, and classify scale morphotypes.
- Measure scale variables related to hydrodynamic function in modern sharks and between individuals of a single species.
- Map and analyse patterns of distribution of scale features if found.
- Test hypothesised relationship between riblet spacing and speed in modern sharks (Reif, 1985), and extend to fossil relatives.

2) Empirically test the efficacy of a range of dermal denticles in reducing skin friction drag.

Objectives:

- Based on morphofunctional correlates in modern sharks, identify suitable fossil species and material for replicating a diversity of fish skins.
- Scan material using micro computed tomography, and use modelling software to tessellate scales on a test plate based on articulated modern and fossil skin.
- Rapid prototype replica fish skin, and assemble rig for flume study. Laser Doppler anemometry used to measure fluid velocity across test plates, and smooth control plate.
- Skin friction to be approximated and relative drag-reductions interpreted.

3) Provide a context-driven analysis of the evolution of drag-reducing adaptations in fishes.

Objectives:

- Use experimental data to supplement functional interpretations made with comparative approaches.
- Classify fossil denticles described in literature (of known body location) using morphotype scheme, to track occurrence through time and functional trends.

1.4. Associated publications and declaration of author contributions

In all cases, the doctoral candidate was the primary and corresponding author of material written for publication. This material was often subject to additional edits and review by the co-authors. This, and extensive discussion throughout the drafting process has undoubtedly

improved the quality of the manuscripts and by extension this dissertation. General acknowledgments can be found on page IV, and specific credits (including personal communications) are given in text. However, to address the obfuscation of authorship credit, all concomitant papers (at varying stages of publication) to this thesis are detailed below, including candidate and co-author contributions.

(1) Fletcher T. M., Altringham J. D., Peakall J., Wignall P. B., Dorrell R. M. (2014) Hydrodynamics of fossil fishes. Proceedings of the Royal Society B: Biological Sciences 281, 20140703.

Related chapters 2, 8. TMF researched and wrote the manuscript, major editorial changes were contributed by JDA, JP, and PBW, and minor changes by RMD.

(2) Fletcher T. M., Altringham J. D., Peakall J., Wignall P. B. (SUBMITTED) Denticle Déjà Vu: remarkable scale convergence in modern sharks and Palaeozoic fishes.
Related sections 2.4, 2.6, 3.1, and 4. TMF performed all research, and wrote the manuscript. JDA, JP, and PBW contributed minor editorial changes.

(3) Fletcher T. M., Altringham J. D., Peakall J., Wignall P. B., McFarlane L. A., Bell M. A. (SUBMITTED) The Evolution of Speed: function and significance of drag-reducing riblets in the fossil record of fishes.
Related chapters 3.1, 4.4, and 6.2.3. TMF performed the research, and wrote the manuscript with major contributions from JDA, JP, and PBW. MAB, LAF, and JDA contributed to statistical analysis, MAB produced figure 5.4 and ran the PDR analysis following reviewer comments.

(4) Fletcher T. M., Altringham J. D., Peakall J., Wignall P. B., Bendall, V. A., Brown W. J. (IN PREP) Dermal denticle in modern sharks: functional factors affecting scale morphology.
Related chapters 2.2-2.4, 3.1, 6. TMF performed the research and wrote the manuscript. JDA, JP, and PBW contributed minor editorial changes. VAB provided material and facilities, and WJB assisted with figure production.

(5) Fletcher T. M., Altringham J. D., Peakall J., Wignall P. B., Dorrell R. M., Keevil, G. M. (IN PREP) Skin friction drag-reduction by fossil fish scales: A novel application for laser Doppler anemometry.

Related chapters 2, 3.2, and 7. TMF, JDA, GMK, JP, and PBW designed the project and made major intellectual contributions. TMF performed the research with the technical assistance of GMK, and RMD contributed to statistical analysis.

1.5. Thesis organisation

The primary goal of this project was to experimentally determine the relative drag-reduction of different Palaeozoic fish scale morphologies. To complement empirical data and comprehensively assess hydrodynamic adaptations, alternative functions and influences on morphology had to be considered. The aforementioned publications were self-contained works exploring one or many of these concepts, and as such there was inevitable overlap in introductory and discussed content. To limit repetition and provide a more coherent narrative, the succeeding Chapter 2 is a thorough and complete synthesis of the literature reviewed for all aspects of the study. This includes the hydrodynamics of modern and fossil fishes, and work to date on scale function.

Chapter 3 details methodologies for all studies, but as comparative analyses were a crucial foundation and supplemental to experimental work, they precede lab-based content where possible. This convention is continued for the results, beginning with Chapter 4 'Comparative analysis and functional interpretations of scale morphology', Chapter 5 'Drag-reducing riblets in modern sharks and fossil fishes', and Chapter 6 ' Modern shark scale variability analysis'. Experimental results are presented in Chapter 7 'Experimental analysis of drag-reduction by fossil fish scales', before interpretations and implications of all results are discussed in Chapter 8. Chapter 9 concludes with an address of the primary aims established in Chapter 1, discussing the contributions to knowledge this thesis presents. It also serves as retrospective; assessing the limitations of this investigation and of those which guided its course. Finally, a brief but optimistic prospective is presented to encourage future work in this fascinating and truly interdisciplinary subject.

2. Background

In this chapter the fundamental fluid principles which often govern morphology will be described before types of drag and drag-reduction are defined. The hydrodynamics of modern fishes will be reviewed, including whole-body adaptations and passive mechanisms of drag-reduction, with an emphasis on scale morphology. Active flow control, including behavioural aspects of drag-reduction will then be discussed before ecological correlates are identified. This discursive prologue to modern fish hydrodynamics will supplement the synthesis of research to date on fossil fishes that follows, including a geological context to observed trends and patterns. Finally, the alternative functions of fish scales are presented, and their usefulness for biomechanical analyses is discussed.

2.1. Fundamental Fluid Principles

a) Fluid properties

The motion in swimming organisms depends on the forces the animal imparts on a fluid, and that fluid's properties. In water (an almost incompressible fluid) an important factor affecting drag and lift in fishes is the Reynolds number (Reynolds, 1883; Azuma, 1992). The Reynolds number (Re) is an expression of the ratio of inertial and viscous forces (below), and is influenced by the animal's size and speed (section 2.3.1).

$$Reynolds\ number\ = \frac{velocity\ (m/s) x\ linear\ travelled\ distance(m)}{kinematic\ viscocity\ (m^2/s)}$$

Equation 2.1. Equation for calculating dimensionless Reynolds number (Reynolds, 1883), where kinematic viscosity is equal to dynamic viscosity kg/(m/s) divided by fluid density (kg/m^3).

At low Re, and predominantly viscous effects, the greatest influence on drag will be surface friction, due to moving through a relatively viscous medium with little momentum from the propulsive forces the animal generates (Aleyev, 1977; Azuma, 1992). It is the point at which

the Re is great enough for inertial forces to take priority in the design of the organism that they are broadly classified as nektonic, rather than planktonic (Aleyev, 1977).

When viscous forces (those holding fluid particles together) dominate, fluid flow is laminar and particles move in parallel ordered lines. As fluid velocity increases, inertial forces dominate and the flow becomes turbulent, characterised by irregular movements, but still with average motion in the mean direction of flow.

b) Boundary layer development and separation

As a fluid of uniform flow (Figure 1a) passes over a wall, molecules in contact with the surface decelerate due to shear stress from friction. The flow velocity above this decelerating fluid then becomes retarded, as particles move over slower-moving particles below. Counteracting this, the fastest moving fluid in the main flow-stream above drags the underlying fluid along and a velocity profile is formed (Figure 1b.). The region between the wall to the point at which the fluid velocity is at 99% of the maximum 'free stream' velocity is called the boundary layer.

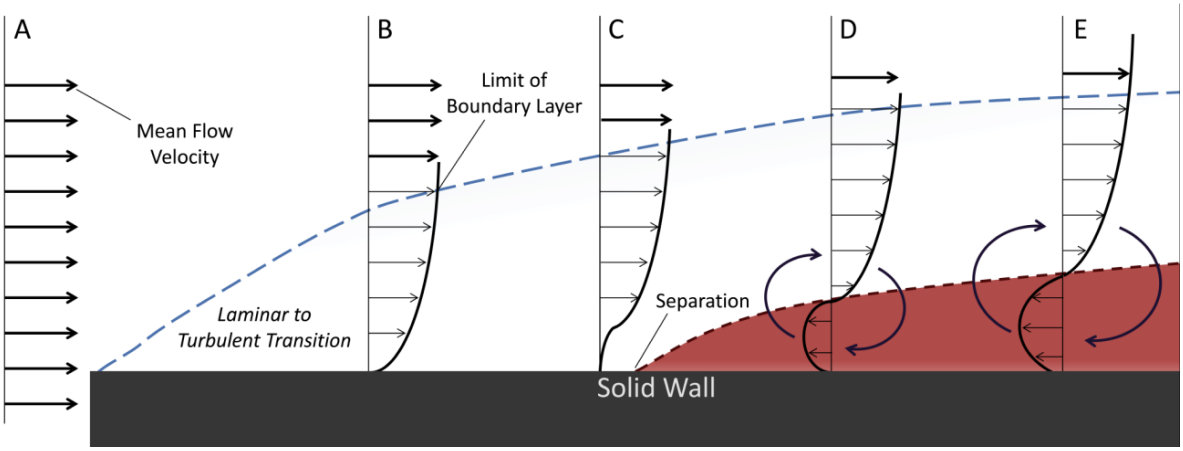

Figure 2.1. Stages of boundary layer development (A-E) on a flat plate, subject to an adverse pressure gradient. Arrows show flow direction, with length indicating velocity and mean flow velocity emboldened, boundary layer in blue, and zone of vortex formation or 'wake' in red.

In an adverse pressure gradient, such as behind the widest point of a fish's body, the rising static pressure (pressure energy per unit volume) of the fluid implies a reduction of dynamic pressure (kinetic energy per unit volume) and thus a decrease in flow velocity (Batchelor, 1977; Figure 2.1c). Reduction of flow velocity induces flow to separate and reverse, forming

counter rotating vortices near the wall (Figure 2.1d, e). This is referred to as boundary layer separation, which increases the effective size of the object to be propelled through the fluid and thus also the amount of drag suffered (Fish, 1998).

2.2. Drag

2.2.1. Types of drag

Drag refers to fluid forces opposing the movement of an object, impeding velocity (Azuma, 1992). For our purposes drag can be divided into two types; pressure (or form) drag, and friction drag. Pressure drag describes the energy used to move fluid out of the way of the front of the body and push it behind it again (form drag). Another important component of pressure drag in submerged bodies is that produced by lifting surfaces such as fins. This is referred to as induced drag and is produced as higher pressure fluid below a hydrofoil (lifting surface) flows around the trailing edge towards the lower pressure upper surface. This produces vortices, meaning some fluid rotates against mean flow, increasing drag (Aleyev, 1977; Fish, 1998).

Skin friction drag concerns the finer interactions of fluid flowing over a plane, and is defined as any reduction in fluid velocity caused by shear stresses and forces acting on the 'wetted' skin surface (Azuma, 1992; Fish, 1998). As illustrated in Figure 2.2, minimal pressure drag could be achieved in laminar conditions with a long and pointed pencil-like body, where skin friction is the predominant drag component. However, there must be a trade-off with physiological limitations, and the minimal body volume requirement of the fish. Streamlining achieves this, and (dependant on individual requirements) nektonic species are most often elliptical and teardrop-shaped (Figure 2.2d). Consequently for the majority of pelagic fishes skin friction is an important component of drag, and the biological strategies for reducing it are the primary focus of this thesis.

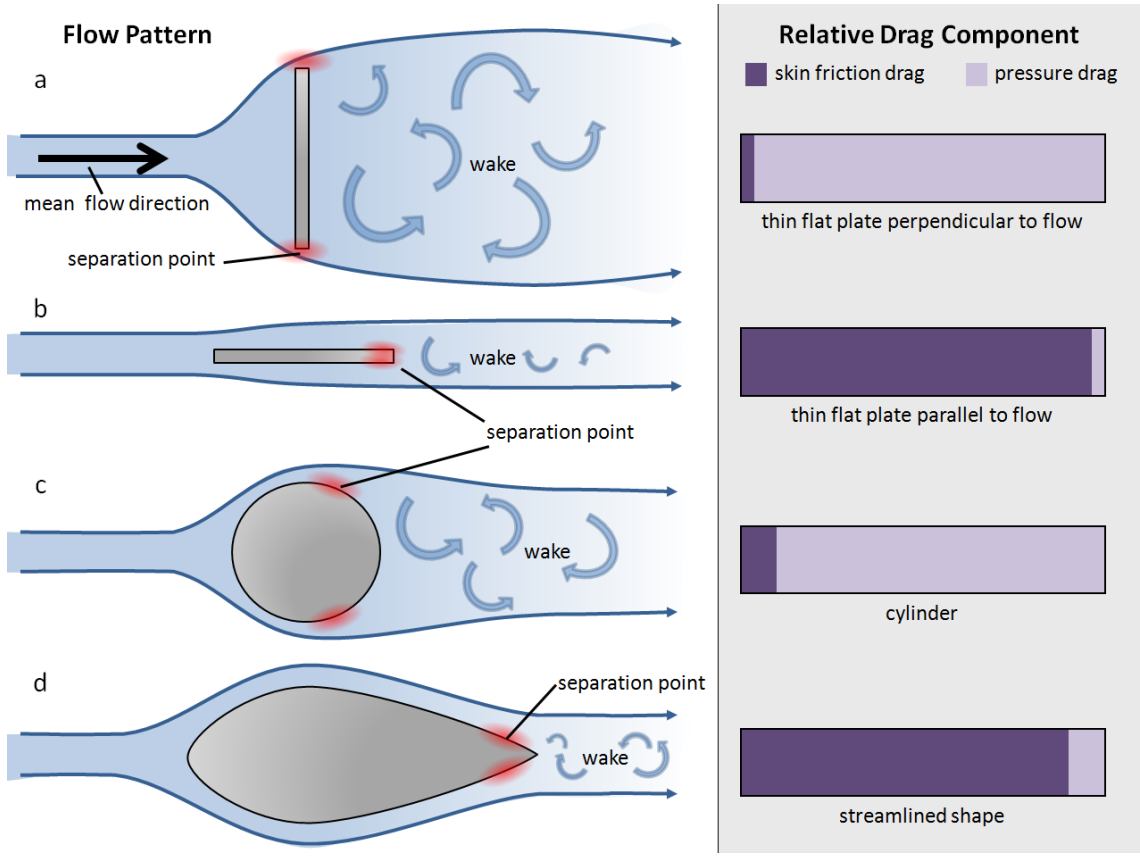

Figure 2.2. Flow patterns (blue arrows) and relative drag components of submerged objects; a) thin flat plate perpendicular to flow direction (black arrow); b) thin flat plate parallel to flow; c) cylinder; and d. streamlined shape. Based on Talay, 1975.

2.2.2. Drag reduction

Drag reduction is crucial to efficient locomotion through a fluid, especially in the relatively viscous and dense medium of liquid water. Beyond more general adaptations to life in water (e.g. streamlining), a surprisingly large number of 'imaginative solutions' (Fish, 1998) have also evolved to reduce drag which will be discussed next (section 2.3). Drag-reduction can help fish achieve faster burst and cruising speeds to escape, hunt and travel longer distances. However for the majority of fish the greatest benefit is the lower energetic expense of everyday swimming, including holding a stationary position against currents. The way in which a fish reduces drag varies according to physiology, behaviour and morphology of the species. The external morphology is remarkably plastic in response to hydrodynamic constraints (e.g. Fischer-Rousseau, 2010), which is especially fortunate in those instances where behavioural and physiological data are not available (e.g. very rare or extinct taxa). The mechanisms of drag reduction will now be discussed.

2.3. Hydrodynamics of Modern Fishes

2.3.1. Gross morphology

a) Body size

As discussed, fishes face differing fluid conditions depending on Reynolds number (Equation 2.1), determined by fluid properties and the fish's body length and speed (Figure 2.3). For example a tuna of length 3 metres, travelling at its highest observed speed of 22.2 m/s (McGowan, 1999) has a Reynolds number 5.11 x 10^7. In larger organisms like this, inertial forces are a more important influence on drag, and adaptations are primarily aimed at preserving attached laminar flow or controlling turbulent boundary layers at higher speeds through relatively inviscid fluids (Videler, 1993). Depending on body shape and skin properties, the point of transition can vary between 9.0 x 10^4 to 3.0 x 10^6, and possibly even higher in some cases (Aleyev, 1977). The flow type is intractably linked to Reynolds number, so fish must not only adjust their adult morphology and behaviour to reduce drag, but also adjust to continually changing fluid mechanics throughout ontogeny.

Adult fishes range in size from millimetres (e.g. *Paedocypris)* (Kottelat et al., 2005) to many metres (e.g. *Rhincodon*, and the extinct *Leedsichthys*) (Liston et al., 2013). Small fish larvae face very low Re (Figure 2.3) and in some species up to 98% of their swimming can be in the viscous or intermediate flow regime (Müller et al., 2000). While essentially planktonic (unable to fight currents), they can generate thrust to move through their relatively viscous fluid to avoid sinking (Videler, 1993). There is debate as to whether changes during ontogeny reflect optimal functionality for differing Re values (Weihs, 1980), or are just an energetically expensive stage of growth before achieving a streamlined adult form (Müller & Videler, 1996; McHenry & Lauder, 2006). While adult fish are the principal focus of this thesis, the increasing Reynolds number with size and speed, and the associated change in flow regime are an important consideration. Flows around objects of the same shape with the same Reynolds number are said to be dynamically similar, which – crucially - allows for scaling in modelling experiments (Webb, 2006).

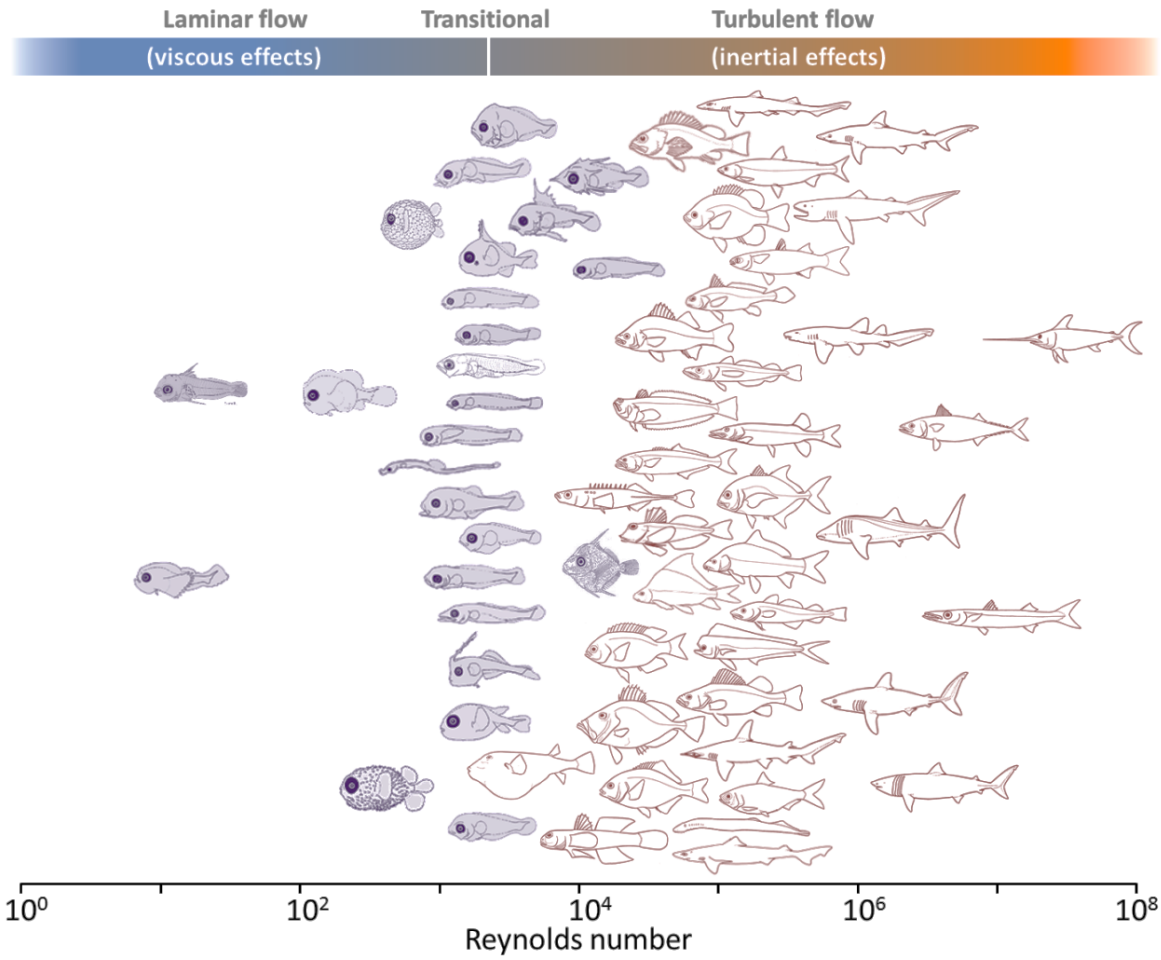

Figure 2.3. Mean Reynolds number of some larval and adult fish taxa in water at 10°C showing relative influence of viscous and inertial forces. Dynamic viscosity (N s/m^2 x 10^{-3}) of seawater from McGowan, 1999; approximate transition value from Nachtigall, 2001. Fish speed and length data from (alphabetically) Block et al., 1992; Carey, 1982; Carey & Clark, 1995; Carey et al., 1990; Carlson et al., 1999; Domenici, 2010 (and references therein); Froese & Pauly, 2014; Gazzola, 2014 (and references therein); Goldman & Anderson, 1999; Graham et al., 1990; Gunn et al., 1999; Jones, 1973; Huish & Benedict, 1977; Johnson et al. 2009; Klimley et al., 2002; Lowe et al., 1998; McKibben & Nelson, 1986; Medved, 1983; Nakamura et al., 2010; Nelson et al., 1997; Priede, 1984; Sambilay Jr., 1990; Semmens et al., 2013; Sims, 2000; Sundstrom et al., 2001; Tricas, 1981. Fish images from Leis & Carson-Ewart, 2000; Nelson, 2006; and Froese & Pauly, 2014.

b) Distribution of mass and buoyancy

Buoyancy is the weight of water the animal displaces, and when deducted from the animal's weight gives an apparent weight. In pelagic fishes this apparent weight is near zero with

neutral buoyancy, and the distribution of volume determines the centre of buoyancy (Blake, 1983; Videler; 1993). If the centre of mass is not in the same position along the body as the centre of buoyancy, the animal must correct for the resulting rotation. To do this the fish may have a gas bladder, a large, low density liver (as in sharks), or use its fins (section 2.3.3) or other lifting surfaces (section 2.3.2) to equalise horizontal and vertical forces (Videler, 1993). Negative buoyancy improves stability, and while more energy is required to swim and overcome gravity, there is clearly a benefit to those benthic fishes facing strong currents (Webb, 2006). Many Palaeozoic fishes are presumed to have been negatively buoyant because of their heavy armour (Moy-Thomas & Miles, 1971). A trend for this armour to be lost may be related to the migration of many fishes in to the pelagic realm during the Devonian (Lauder & Liem, 1983; Klug et al., 2010).

c) Streamlining and body profile

Streamlining is a fundamental way to decrease form drag as it optimises pressure gradients which develop across the body. Many fishes are dorso-ventrally or laterally compressed (e.g. flatfishes, lookdowns respectively), or long and torpedo-like (e.g. barracuda) to minimise their impact against the fluid as they move. Body shape should act to maintain a favourable pressure gradient and – ideally - laminar flow, with the widest part of the body in the centre (Blake, 1963). In some of the fastest-moving fishes, protrusions from the body surface can be tucked into fairings that maintain the streamlined shape, where even the eyes do not protrude (Helfman et al., 2009).

While lift is usually actively achieved with specialised surfaces such as the pectoral and caudal fins (section 2.3.3), the gross morphology sometimes plays a role. The bodies of animals such as sturgeon, many sharks and sea turtles resemble a typical wing profile (Figure 4). In these cases, the body as whole can act as a lifting surface, counteracting negative buoyancy by creating low pressure on the upper surface, and deflecting fluid downwards (Aleyev, 1977). This is often coupled antagonistically with an asymmetrical tail which can stabilise the pitch of forward movement (section 2.3.3.).

A diverse suite of adaptations for drag-reduction have evolved in fishes, and can be categorised broadly as either passive (reliant on morphology), or active mechanisms (reliant on behavioural actions), discussed next.

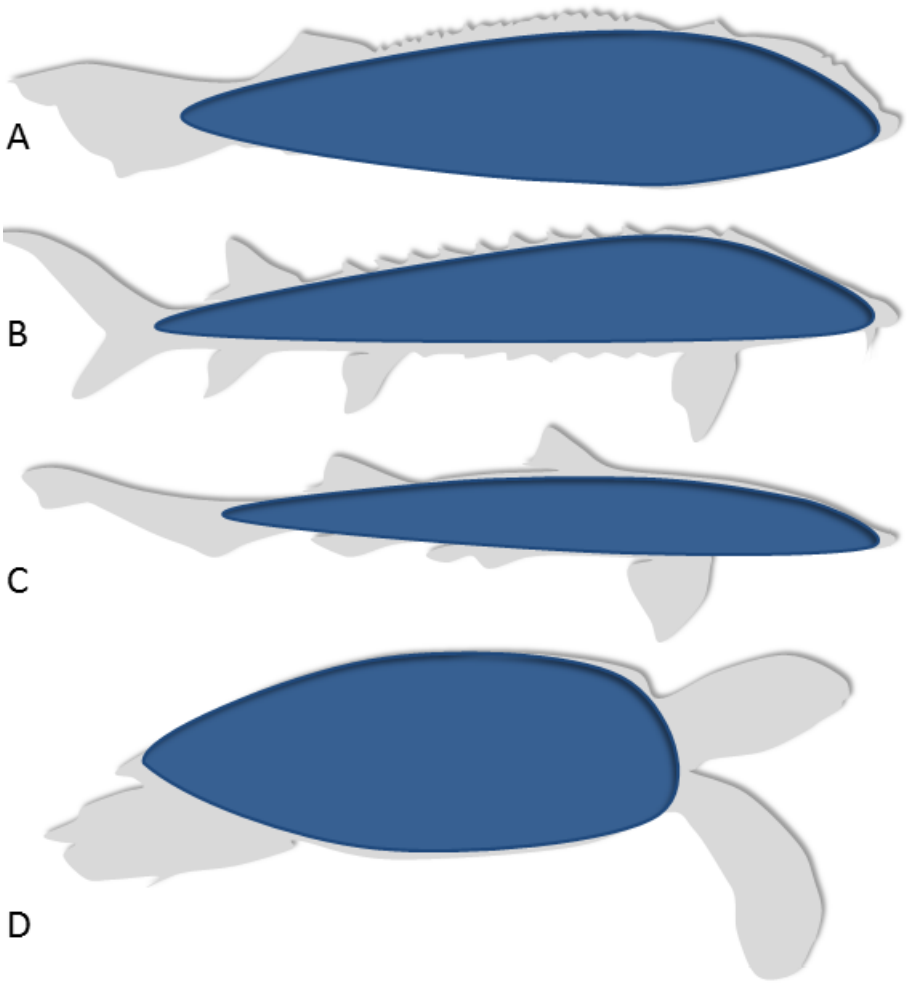

Figure 2.4. Sagittal sections of aquatic animals with wing profile body shapes. a) the Palaeozoic jawless fish Cephalaspis b) the modern sturgeon *Acipenser* ; c) the modern hound shark *Triakis* ; d) modern green sea turtle *Chelonia mydas*. Modified from Aleyev, 1977.

2.3.2. Passive mechanisms of drag reduction

a) Collagen

In the skin of sharks and other fishes there are highly ordered collagen fibre bundles spiralling about the axis of the animal in both directions, forming a tight mesh. Collagen itself is relatively inelastic, but as part of a lattice can stretch in the direction which bisects the angle of intersection. In sharks this angle can be anything from 40-90 degrees in different regions of the body and acts to maintain a tight external surface during flexure (Motta, 1977; Meyer & Seegers, 2012). This prevents folding of the skin (Motta, 1977; Wainwright, 1978; Long et al., 1996; Lindgren, 2011), which would increase form drag, and reduces the energy required to restore body shape after a thrust swing, in essence acting as an external tendon. In the caudal

fin of the white shark (*Carcharadon carcharias*), this mesh accounts for 50% of the dorsal lobe stiffness, despite making up only 6% of its thickness (Lingham-Soliar, 2005). In terrestrial animals the collagen fibres are normally much less strictly organised, and folding is allowed to occur (Kardong, 2008). In air, folding has a much smaller effect on drag, and can infer benefits such as greater freedom of movement, and a greater surface area for thermoregulatory purposes (e.g. Lillywhite & Stein, 1987). Skin folds appear during very fast movement in dolphins, and other aquatic mammals, and for a time was thought to be a passive control on turbulent flow although a convincing mechanism was never provided (Aleyev, 1977; Fish, 2006).

b) Mucus and polymer additives

The epithelium produces mucus from specialised goblet cells at or near the surface of the skin with functions including hormone-release, protection against pathogens (mainly due to its rapid turnover), an osmotic barrier, and drag-reduction (Shephard, 1994). The thick layer of stiff mucus found on exposed skin of modern bramble sharks also serves as general mechanical protection, and is found convergently in bottom-dwelling rays and skates (Reif, 1985).

From a hydrodynamic perspective, a general smoothing effect has been suggested, with the mucus effectively filling irregularities in the scale surface (Aleyev, 1977), but there appears to be a more complex mechanism involved. Long-chain polymers found in fish mucus, even in small quantities can reduce drag significantly (Toms, 1949; Berman, 1978; Yang, 2009). Experiments show that mucus dissolved in water can increase the Reynolds number at which transition between laminar and turbulent flow occurs, firstly maintaining laminar flow and then acting to prevent full separation. Mucus is perhaps the most important feature of the integument because it can make the greatest contribution to drag reduction (Hoyt, 1975). For example, it has been shown using turbulent flow rheometry (a method for measuring the flow of matter under applied force) that the Pacific Barracuda can reduce drag by 66% through dissolution of mucus (Rosen & Cornford, 1971). The in situ drag-reducing effect has also been shown experimentally by comparing real and wax models of trout (Daniel, 1981). Teleost fishes very often have smooth, round, cycloid scales on their head, but ctenoid scales with spine-like projections posterior of the widest point of the body. These comb-like structures bordering the posterior margin of the scale could be maximising the surface area for mucus dissemination, helping to reduce turbulent drag (Bushnell & Moore, 1991). While we can speculate that extinct fishes reduced drag with mucus, the fossil record rarely preserves integumentary structure. More fundamentally, it is difficult to account for mucus properties, its rate of

production, thickness, or the fish's behaviour. Dermal denticles have no epithelium overlying the crowns, but lie embedded in the skin with their outer surface in direct contact with water flow. As such, mucus production is restricted to small areas below the crowns, between the scale bases. Modern sharks possess mucus glands, but the production rate, properties and function of the mucus is very poorly understood for most species. The most explicit mention of hydrodynamic function of shark mucus is in the context of olfaction, in which the authors assumed a negligible influence on fluid flow (Rygg et al., 2013).

c) Heat exchange

Aquatic mammals and some fishes (e.g. tuna) are warm-blooded and it has been suggested that by heating the surrounding fluid, these animals can reduce its viscosity (Fish, 1998). In tuna, friction drag could hypothetically be reduced by 14%, but this could only be achieved with unrealistically prolonged contact with the water (Webb, 1975; Fish and Hui, 1991), rather than the estimated 0.1 seconds (Walters, 1962). For this reason it is unlikely that heat exchange is a major contributor to drag reduction; it is mentioned here as one of several soft tissue adaptations that cannot be accounted for in fossil taxa.

d) Laminarisation

Laminarisation is the promotion of well-ordered laminar flow, and in terms of drag-reduction is the ideal way to minimise pressure drag. However, this is only the case where the boundary layer is attached (Figure 2.5), and in adverse pressure gradients (pressure drops downstream), detachment is more likely to occur (Webb, 1975), resulting in high pressure drag, and the highest relative total drag (Figure 2.5). In a favourable pressure gradient, skin friction is the largest contributor to total drag, but streamlined bodies rarely preserve laminar flow beyond the widest point of the body. The Reynolds number, a measure of the relative influence of inertial and viscous forces means very small planktonic organisms (and some juvenile nektonic organisms), or slow-moving animals encounter only laminar conditions. This work will be addressing drag-reduction by fishes which are fast and large enough to chiefly encounter (and have adapted to) inertial fluid forces and turbulent flow. Reversion of an attached flow from the turbulent to laminar regime occurs naturally if a favourable pressure gradient (low to high downstream) is encountered. However, early workers postulated that riblets (the linear streamwise valleys ornamenting the surface of shark scales), and the teeth-like structures of ctenoid scales (ctenii) act to physically 'comb' fluid, and re-laminarise turbulent flow via

physical baffling. The mechanism of riblet drag-reduction is now better understood (and discussed later), and their action is more complex than simple vortex diffusion (see 3.2.2). Although very little has been written about the function of ctenii, laminarisation is unlikely as the structures do not extend beyond the laminar sublayer (section 2.1) and therefore do not interact with the turbulent flow (Bushnell & Moore, 1991).

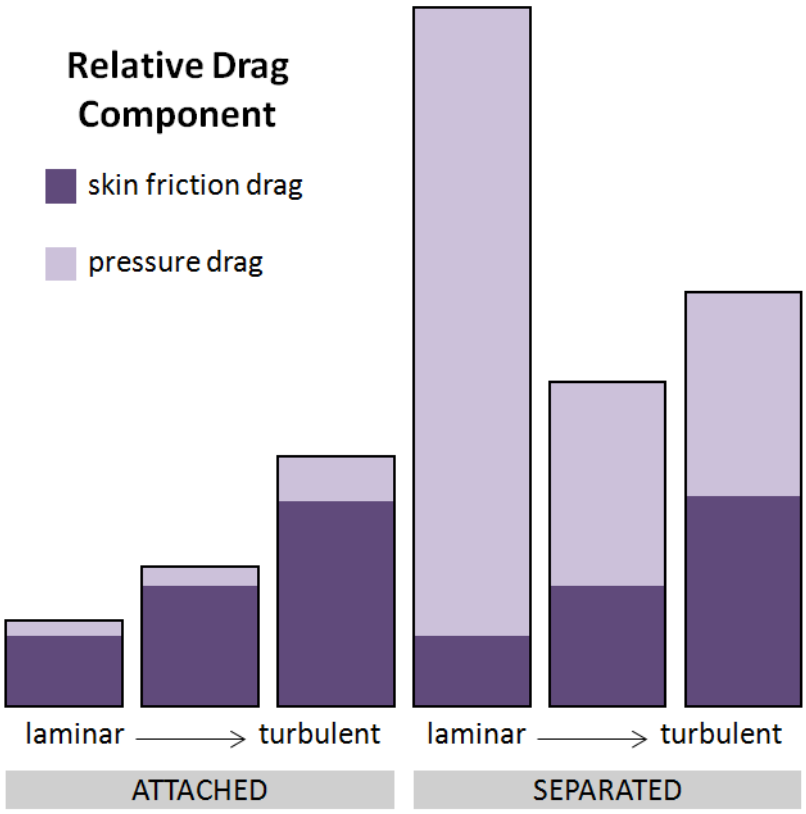

Figure 2.5. Relative total drag, and drag composition for different boundary-layer flow conditions over a streamlined object. Redrawn from Webb, 1975.

e) Turbulisors

The typical streamlined fish shape consists of two regions; the contractor and the diffuser. The contractor extends from the anterior tip of the body to the point of maximum cross-sectional area, and the diffuser from this point to the rear. Typically, when water passes over the contractor region of a fish (from the anterior leading edge to the widest point of the body) laminar flow is maintained as dynamic pressure is high, pushing the fluid against the surface, minimising drag (Fish, 1998). However, in the diffuser region (the narrowing area towards the tail), dynamic pressure decreases and flow rotation and reversal (boundary layer separation or

'stall') is prone to occur (Aleyev 1977; Batchelor 1977). Turbulisors (which can include surface roughness, fins and gill efflux) help trigger the transition from laminar to turbulent flow by seeding vortices and disrupting the smooth and ordered movement of fluid molecules. This means streamwise but 'messier' flow transfers some fluid momentum back towards the surface, meaning the boundary layer remains attached for longer.

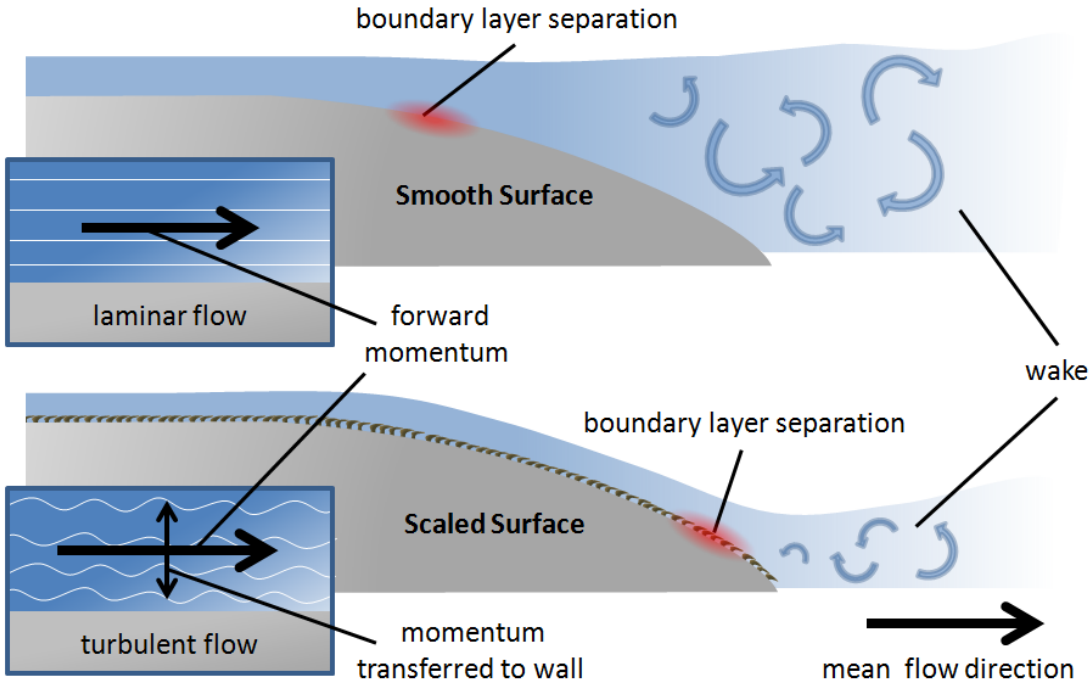

Figure 2.6. Boundary layer development and separation across a fish-like form, showing the hypothesised effect of a turbulisor on flow regime and wake formation.

To delay boundary layer separation (and in some cases maximise the area of lift) many species use turbulisors at the widest point of their body to induce turbulent flow. In fishes where the contractor is coated with larger and smoother scales, there tend to be rougher scales in the diffuser region. In sharks too, the scales are often relatively smoother on the head (Reif, 1985). Moreover the distribution of pressure across the surface in motion appears to be positively influenced by the presence of scales, affecting thrust as well as overall drag reduction although the mechanism is unknown (Oeffner and Lauder, 2012).

Ctenii are the small comb-like projections found on the posterior edge of ctenoid scales in teleosts and a limited number of other groups (e.g. Polyodontidae) (Grande et al., 2002). There is strong evidence that their role is hydrodynamic, as they occur only after the widest point on the body where turbulent transition is likely (Figure 2.7). Ctenoid scales have been interpreted as 'combing' the turbulent flow to a more stable regime (Aleyev, 1977). Ctenii would actually

increase turbulence if they were large enough, but are considered subroughness within the laminar sublayer, having little effect on friction drag. It is more likely that their presence increases the surface area from which mucus can dissolve into the fluid stream (Bushnell & Moore, 1991; section 2.3.2.).

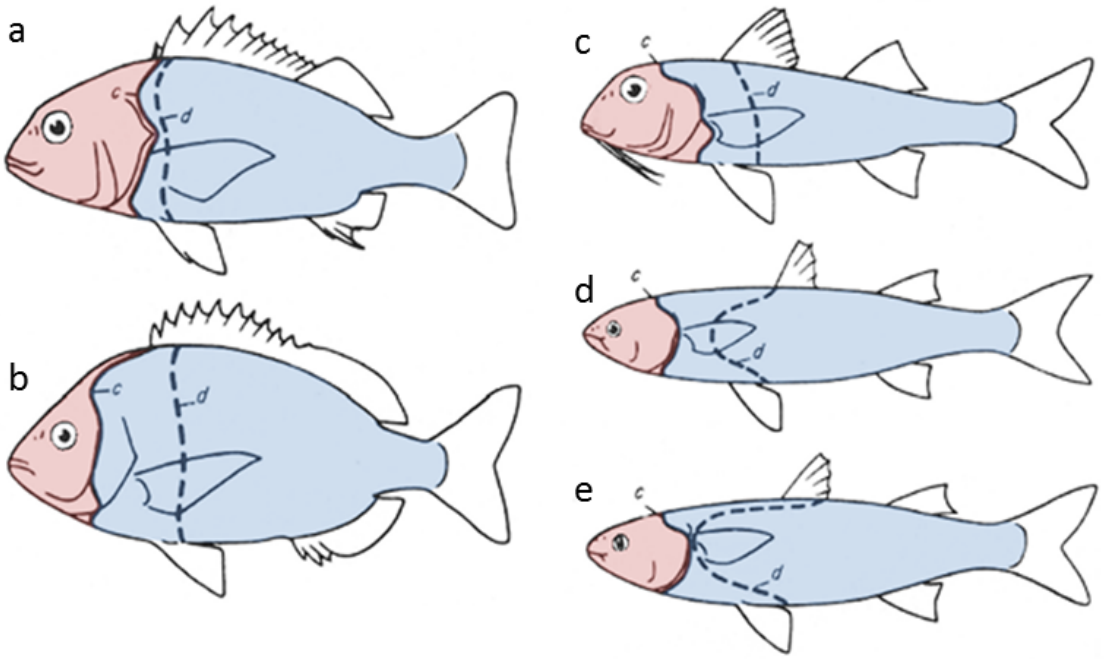

Figure 2.7. Regions of the fish skin surface covered by cycloid (red) and ctenoid (blue) scales and the general boundary between these zones (solid line, c), and the border between contractor and diffuser zones (dashed line, d). A) *Pomadasis guoraca* (Indian grunter); b) *Diplodus annularis* (annular seabream); c) *Mullus barbatus pomticus* (Black Sea red mullet); d) *Liza auratus* (golden grey mullet); e) *Mugil cepahlus* (flathead mullet). Modified from Aleyev, 1977 (after Burdak, 1968).

The hydrodynamic function of ctenoid scales is supported further when assessing the ontogenetic development of this scale type. Young and small *Mugil saliens* (modern leaping mullet fish) develop cycloid scales over the entire body, but after the animal is large enough to experience larger Reynolds numbers (Figure 2.3, section 2.3.1) and – crucially - transition these are replaced by ctenoid scales (Videler, 1993; Figure 2.7). Ctenoid scales mostly grow behind the gills, with some cteniod scales also growing to control highly turbulent flow exiting the gills (Videler, 1993). They begin to form on the flanks, where transverse folds are more likely to form during swimming (Aleyev 1977; Sire, 2004). Skin flexure is an important function (Ganguly

& Mookerjee, 1947) as skin folds have the potential to increase drag considerably; it is a convergence of all nektonic organisms to maintain a tight, collagen-rich skin (Aleyev, 1977; Lindgren et al., 2007; 2011; Lingham-Soliar & Plodowski, 2007; Smith & Buchy, 2008).

Lastly, the tubercles on the rostrum (sword) of fishes such as *Istiophorus* (sailfish) may act as a turbulisor, with the surface of the sword propagating a turbulent boundary layer which is already thick by the time it reaches the main portion of the head (Aleyev, 1977; Videler, 1995).

f) Compliant surfaces

A compliant surface refers to an elastically responsive wall surface texture that can respond to external fluctuations in pressure. A compliant coat can reduce the intensity of downstream perturbations by up to 19%, lowering total drag by up to 7% (Choi et al., 1997). In order to work, the surface roughness must remain small enough so as not to extend up above the viscous sublayer (see section 2.1). The material properties must also be such that the coat responds at the right frequency to the turbulent fluctuations. Faster moving fluid subjecting a wall to higher frequency (and potentially higher energy) perturbations requires stiffer material properties to minimise the deformation-driven roughness which would otherwise increase drag (Choi et al., 1997). It is also possible to delay the transition from laminar to turbulent flow by fine-tuning compliant coatings to changing Reynolds number (principally velocity) across the wall (Carpenter et al., 2000). The rib-like structures on some scale surfaces are hypothesised to support and improve adherence to this layer of soft tissue (Burdak, 1972), but there have been no experimental attempts to demonstrate the hydrodynamic advantage in fishes. As a soft-tissue surface structure, the material properties of compliant surfaces cannot be accounted for in fossil material, however evidence for this passive mechanism of drag-reduction is considered next.

A related phenomenon investigated by many biomechanicians was skin compliance and folding, known to occur during swimming, particularly in dolphins. The calculated drag of a dolphin based on solid models, observed speeds and estimations of muscle output (Gray, 1936) appeared to show that dolphins were swimming faster than they ought to be, and 'Gray's Paradox' emerged. The most debated potential solution to this problem is that low friction drag could be achieved by maintaining laminar flow across the body (Kramer, 1960; 1961). Mechanisms for this include skin folding whereby vortices are shifted downstream (Sokolov et al., 1969; Aleyev, 1977; Nagamine et al., 2004), changing fluid properties in the boundary layer through elevated body temperature (Lang & Daybell, 1963; Fish & Hui, 1991,),

skin sloughing and eye secretions (Sokolov et al., 1969; Uskova et al., 1983 [in Russian, referenced in Fish & Lauder, 2006]), and even microvibrations (Ridgway & Carder, 1993). Recent studies have begun to reinvigorate ideas that dolphin skin acts as a compliant damping complex (e.g. Pavlov, 2006), but the historical need to explain Gray's paradox has complicated the field enormously.

Gray's paradox is now known to be flawed, with unrealistic estimations of muscle power (Fish & Lauder, 2006; Askew & Marsh, 1997), and the observed dolphins may have enhanced their swimming using the ship's wake (Lang, 1966; Williams et al., 1992; Weihs, 2004; Fish & Lauder, 2006; Noren, 2008). It is now known that dolphins can swim in short rapid bursts while maintaining fully attached turbulent flow (the preferred scenario over boundary layer separation, Figure 2.5). This is supported by experiments which added extra turbulisors to a gliding dolphin model, which did not affect drag (Lang & Daybell, 1963).

g) Riblets

To limit the drag produced by attached turbulent flow, which is much lower than any separated flow (Fish, 1998) many fast-moving sharks have placoid scales with pronounced parallel riblets. These streamwise ridges limit lateral transfer of momentum (Figure 2.8), training the vortices in the direction of flow (Garcia-Mayoral & Jiménez, 2011; Oeffner & Lauder, 2012). The vortices that form are also held away from the wall by the riblet tips, reducing drag by up to 10% (Bechert et al., 1997). Experimental analyses of riblet optimisation have shown that more narrowly-spaced riblets reduce drag more efficiently at higher speeds (Dean & Bhushan, 2010). This is reflected in sharks, with riblet spacing from 40-80μm in the fastest species, and wider in slower sharks (Reif 1985a, Chapter 5).

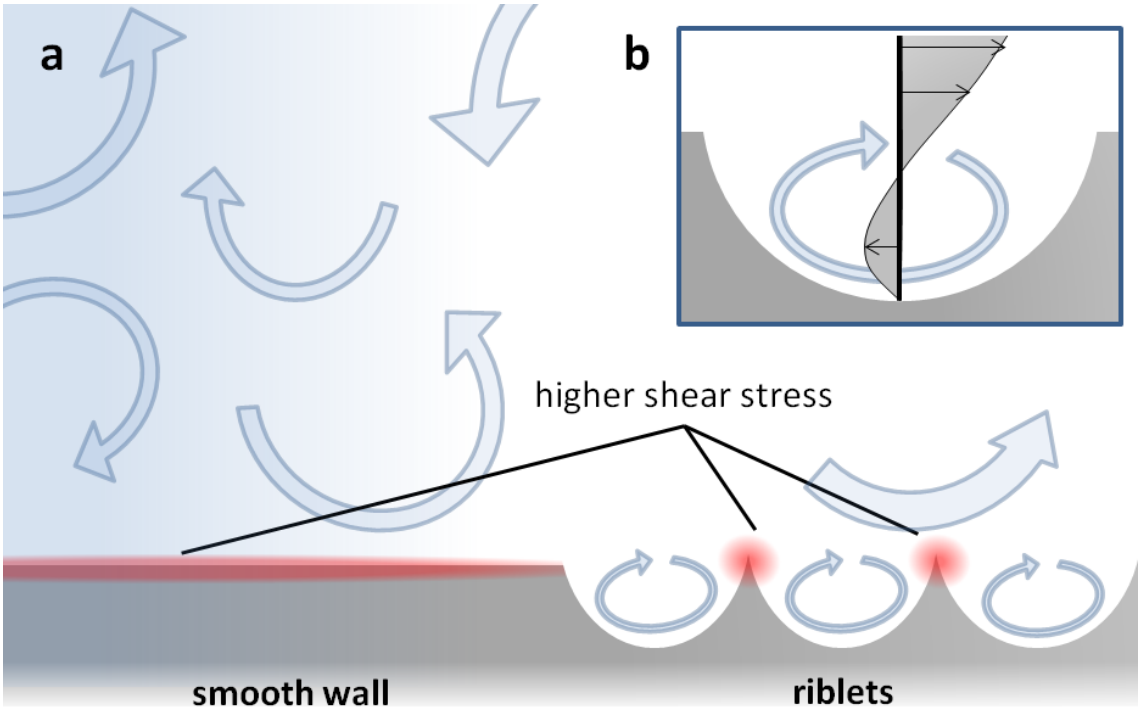

Figure 2.8. Vertical cross sections of turbulent-flow (velocity = 3 m s^{-1}) of streamwise vortices over a) a flat plate, and; b) riblets. Mean velocity profiles for flow in cross-flow directions shown enlarged for riblets. Adapted from Bechert et al., 1997; and Lee & Lee, 2001.

h) Converging and diverging riblets

Early experimental evidence suggested that drag-reduction is reduced if parallel riblets are misaligned from the streamwise direction by >15°, with no benefit >30° (Walsh & Lindemann, 1984). However, the riblets of denticles have long been thought to also redirect flow across the body surface (Reif, 1978). Of particular interest has been redirection at a small scale, towards openings such as the nostrils and pit organs, and away from the eyes and lateral line pore openings (Reif, 1978, 1982, 1985; Cigala-Fulgosi & Gandolfi, 1983; Raschi & Tabit, 1993; McKenzie et al., 2014). Recent studies on the physics of converging and diverging riblets suggest a more complicated process than simple redirection. Diverging riblets decrease turbulent disturbances and velocity fluctuations, which would help reduce 'noise' at the ear-like lateral line organs downstream. Equally, the requirement for turbulence in olfaction is met by converging riblets, which act to increase these fluctuations and hence mixing (Koeltzsch et al., 2002; Nugroho et al., 2013). Convergent riblets around pit organs are more difficult to explain, and as a result their function is not fully understood (Peach & Marshall, 2000), but similar fluid movement is predicted. Larger-scale hydrodynamic studies on riblet angle have concentrated on the direction of the whole scale, assuming the riblets were parallel to flow,

but this is not always the case. The v-shaped central keel of some shark pectoral fin scales has been interpreted as a vortex generator; turbulisors whose function is to maintain boundary layer attachment (Bechert et al., 1985). Despite this early work, very little additional research has been conducted, and the present study is the first to map riblet angle distribution across the entire body of a shark.

i) Bristling

In some of the fastest sharks the bases of the scales have a high aspect ratio (wide and short in the streamwise direction) to facilitate pivoting away from the body (Pershin et al., 1976 [in Bushnell & Moore, 1991; Bechert et al., 1986). When flow begins to rotate or reverse, the scales are erected (by up to 50° in mako sharks) and prevent backflow, and even contribute to thrust (Motta et al., 2012). The erect crowns also cause small, embedded vortices to form between the scales, and streamwise flow is able to skip over the gaps (Lang et al., 2008). This 'bristling' action is most pronounced on the flank region where separation is most likely, but this has been studied in a small number of taxa.

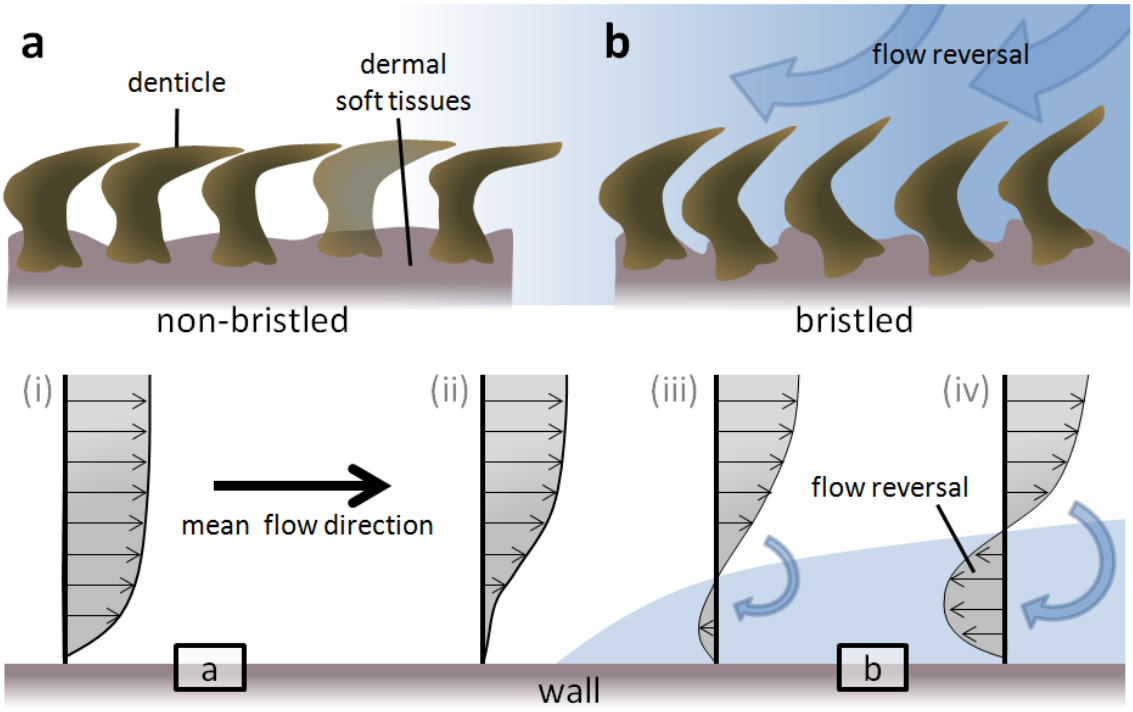

Figure 2.9. Mechanism of drag-reduction by bristling scales. Placoid scales in; a) resting position in attached boundary layer; and b) erect position in detached recirculating flow.

j) Passive streamwise injection and dynamic dampening

In the ribbonfish *Desmodema*, the negative pressure gradient experienced across most of the body's posterior could be reduced with subdermal canals (Walters, 1963), known to achieve laminar flow by redistributing fluid between high and low pressure regions (Fish, 1999). It has been suggested that streaks of low and high pressure which form across the surface could also be controlled by exchanging fluid with the reservoir beneath scale crowns (Bechert et al., 1986; Figure 2.10). The riblets of shark scales form gutters where the crown of one scale overlies the riblets of another. If a region of low pressure formed above these gutters, fluid would be injected passively to counteract it. In experimental studies porous surfaces increase drag (although see Nagamatsu et al., 1984), where injection is perpendicular to the surface (Kong & Schetz, 1983; Wilkinson, 1983). However, the orientation of shark scale gutters would cause injection to occur in the streamwise direction, an arrangement which has yet to be tested. Denticles of the fastest pelagic sharks often have very thin neck regions, which may accommodate a larger reservoir of fluid for this purpose.

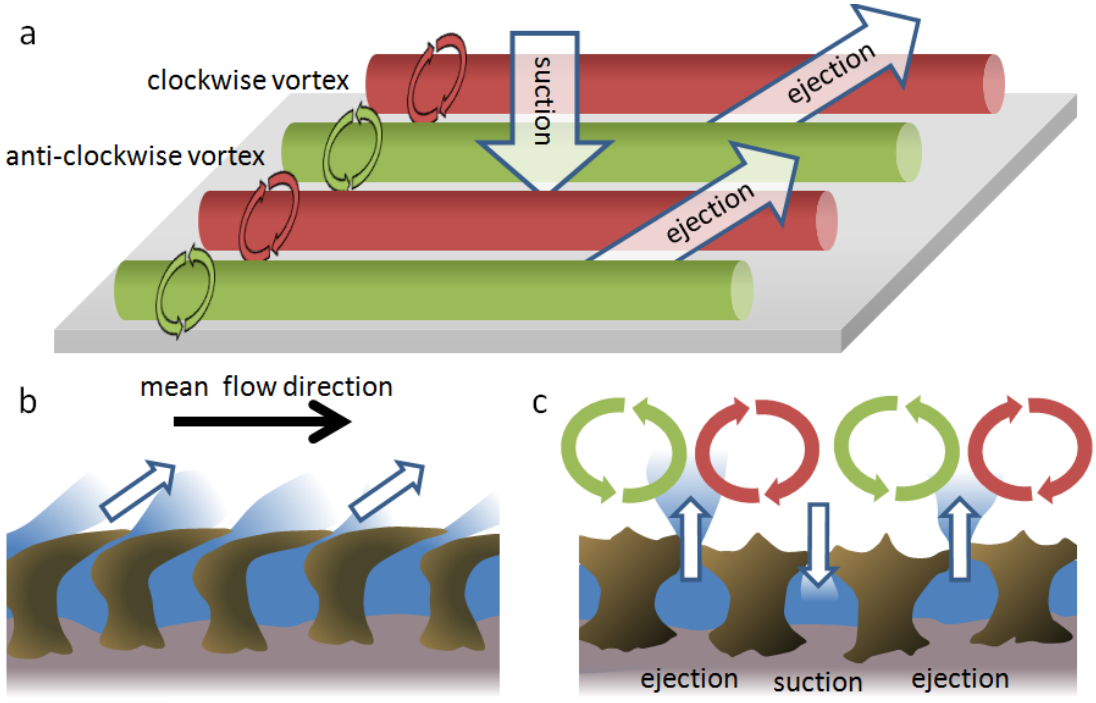

Figure 2.10. Proposed mechanism of drag-reduction by streamwise injection. A) Diagram of vortices formed across a scaled plate with patterns of fluid suction and ejection (white arrows); b) lateral section view, and; c) transverse section view. Mean flow direction indicated by black arrow. Based on Bechert et al., 1986.

k) Passive vortex manipulation

The slow-moving boxfishes (Ostraciidae) are encased in a carapace of sutured dermal bone, known to function in defence (Walker, 2000). Despite the rigidity of their box-like body, these fish are capable of high manoeuvrability and can achieve high drag reduction (Bartol et al., 2003; 2005; 2008; Van Wassenbergh et al., 2015). This is a passive process whereby the animal's uniquely shaped body propagates vortices across the surface. These vortices form as needed to stabilise the fish's body, but also accelerate fluid they entrain helping to improve velocity and reduce drag (Bartol et al., 2002).

Another example of passive vortex manipulation can be found in the humpback whale flipper (and possibly the extinct *Protospyraena*), which is lined at its anterior leading edge with large rounded tubercles (Fish & Battle, 1995). These tubercles delay boundary layer separation by generating vortices in the troughs and reducing the adverse pressure gradient downstream (Miklosovic et al., 2004). By keeping the boundary layer attached for longer more lift can be achieved (Bushnell & Moore, 1991), even at the high angles of attack the flippers face during the whale's complex feeding behaviour. For example at 10˚ angle of attack the tubercles increased the lift to drag ratio by 17.6% (Watts & Fish, 2001). In modern sharks, tubercles which form the scalloped hydrofoil of hammerhead sharks may be acting in much the same way (Bushnell & Moore, 1991). Hammerheads are known to turn at tighter angles more frequently than other genera, with little roll and at higher speeds (Nakaya, 1995; Kajiura et al., 2003), however the hydrodynamic roles of tubercles in this group have yet to be studied in detail.

Passive vortex manipulation is rare in both modern and extinct taxa, but actively controlling flow is a very common method of stabilisation control and thrust production, discussed next.

2.3.3. Active control of flow

Active flow control involves physical exertion by the animal, to either reduce drag, produce thrust, or both. Behavioural and physiological adaptations will be discussed first, followed by those typically associated with thrust production. Fishes use a well-tuned combination of these passive and active adaptations to suit their lifestyle and while behaviour and soft tissue can rarely be preserved in the fossil record, it is important to review and discuss all adaptations for drag-reduction.

a) Cooperative drag-reduction/ drafting

Moving in formation is a well-known phenomenon associated with drag-reduction in numerous species, including dolphins (e.g. Weihs, 2004; section 2.3.2), whales (Richardson et al., 1985; Fish et al., 2013), fishes (Weihs, 1973; Partridge et al., 1983) lobsters (Bill & Herrnkind, 1976), and even ducklings (Fish, 1994; 1995). Known as drafting, this behaviour is thought to reduce drag by using the vortices produced by a leading animal's locomotion. The velocity of fluid encountered by those directly behind or diagonally behind the leader (depending on the vortex pattern) can be significantly lower and therefore reduces the energy required to swim through it (Fish, 1999). Though this could be classified as a passive method of drag reduction, it does require constant repositioning of the follower to optimise the effect, which in fishes could help reduce energetic exertion by 4-6 times (Weihs, 1974; Fish, 1999).

b) Breaching

Breaching, also known as 'porpoising' (Bushnell & Moore, 1991) is the action of leaping out of the water to minimise drag. Air is a much thinner fluid and presents much less resistance than the relatively viscous medium of water. For air-breathers this is particularly advantageous, as the costly hydrodynamic requirement to breathe can be offset by the locomotary energy saved in air (Hui, 1987; 1989; Fish, 1993). Many animals swim with a ballistic trajectory to maximise airborne distance (Fish, 1999), but some such as flying fishes have enlarged pectorals as lifting surfaces which can extend this distance substantially (Au & Weihs, 1980; Hui, 1987; Azuma, 1992; Fish, 1990).

Those animals moving at or just under the water surface experience much greater drag because of wave formation (Webb et al., 1991; Videler, 1993). However, trapping air under fur or feathers is one adaptation which may help offset this energetic expense, and has been suggested as an additional benefit of breaching (Azuma, 1992).

c) Mass transfer and boundary layer acceleration

Scombrid fishes swim with their mouths open to ram ventilate their gills, and this can keep flow laminar for 13-100% longer over the body (Aleyev, 1977). However, many fishes may also maintain an attached boundary layer by 'blowing' fluid from their gills (positioned at or near

the widest point of the body [Figure 2.7]) downstream (Walters, 1962; Webb, 1975), By introducing extra momentum in the downstream direction along the wall, the boundary layer becomes thinner and less likely to detach, counteracting retarding flow and reducing drag (Bushnell & Moore, 1991; Lighthill, 1969; Fish, 1999).

d) Caudal fin morphology

As the primary producer of thrust, the tail is a hugely important aspect of fish locomotion, and has been discussed in the context of counteracting negative buoyancy (e.g. Grove & Newell, 1936; Harris, 1936; Affleck, 1950; Alexander, 1965; Hopson, 1974; Belles-Isles, 1987; section 2.3.1.). Given the movement of the tail during swimming, decoupling active and passive flow control is difficult to justify, and studies using static models are of limited value (Bunker & Machin, 1991). Recent studies of the hydrodynamics of the epicercal tail of modern sharks e.g. (Ferry & Lauder, 1996; Liao & Lauder, 2000; Wilga & Lauder, 2002) are of more use, as they constrain the possible behaviours with a given morphology. An asymmetrical (heterocercal) tail allows forward propulsion, but the greater relative flexibility of the upper lobe (hypocercal) or lower lobe (epicercal), generates forces (downward or upward respectively) in the vertical plane. Many early fishes likely had hypocercal tails (e.g. myllokunmigiids, hagfishes, lampreys, euconodonts, anaspids, galeaspids and most thelodonts [section 2.5]), or epicercal tails (e.g. pituriaspids, 'acanthodians', placoderms, chondrichthyans, osteichthyans, [Pradel et al., 2007]).

In stabilising pitch, a lobed and asymmetrical caudal fin usually corresponds to a transversely asymmetrical body shape, with a more rounded surface on the side of the longer lobe. This is possibly because the wake created by the rounded surface is higher above the skin surface and the caudal fin must extend out of the vortex zone (Aleyev, 1977). Much like a hydrofoil, the curved surface (for example on the upper side of a sturgeon) can reduce flow velocity relative to the flatter side, creating a pressure differential and directing flow capable of producing lift (section 2.3.1).

The tail can also indicate the likely swimming speed of the fish, because boundary layer separation at higher speeds occurs in the middle portion of the tail. In most cases, slow-swimming fishes have rounded unlobed tails, which give the fish a larger surface area for membrane stability, but perform weakly at high cruising speeds when vortices form across the surface. The solution for faster (and sustained) movement is to discard this central portion, and indeed some of the fastest fishes (e.g. Scombridae, Xiphiidae, Istiophoridae) have very

concave caudal fins with narrow lobes that avoid the vortex zone (Lauder, 2000). The peduncle (immediately anterior to the caudal fin) tends to be narrow (and sometimes keeled) in these fishes, as propulsion is generated primarily from undulations of the caudal fin. Deeply concave tails are not suited to rapid acceleration and sharp direction changes, so there exists a functional spectrum (Aleyev, 1977; Webb, 1977). While there are studies that have sought to quantify this ecomorphological correlation in modern fishes e.g. (Azuma, 1992; Motta et al., 1995; Pulcini et al., 2008), fossil taxa have not received the same treatment (but see Friedman, 2010).

e) Dorsal fin morphology

The principal functions of the dorsal fin (and possibly the dorsal finlets) are to prevent roll and to enlarge the surface area giving stability during quick turns (Blake, 1983). The dorsal fin is positioned posteriorly in fishes with a pike-like (sagittiform) morphology that are capable of short bursts of rapid acceleration, with relatively little manoeuvring as they dart forwards (Videler, 1993). Fishes that require manoeuvrability during rapid and sustained swimming have their dorsal fins further forwards where they may be actively erected at critical moments and then repositioned flush to the body surface (section 2.4.1). Alternatively, the dorsal fin acts for defence in extant species with spines (e.g. many catfishes, *Squalas acanthias*, *Heterodontus portusjacksoni*); which was presumably the function in extinct spinose species such as 'acanthodians' and hybodont sharks.

f) Paired fins

In fishes with an epicercal tail, like most sharks, the pectoral fins act to counteract the pitch of posteriorly-produced lifting forces and are consequently fairly immobile (Videler, 1993). Acting in much the same way, the pectoral fins of primitive Triassic teleosts are abdominal and orientated horizontally to stabilize trajectory and to a lesser degree brake. In later teleosts the pectorals are more dorsal and hinge vertically, playing a more active role in propulsion e.g. *Diodon*. Pectoral fins can act as hydrofoils and produce lift, e.g. *Acipenser* (sturgeon) and *Prionace* (blue shark), but their overall importance has been questioned [Wilga & Lauder, 2004]), whereas in faster swimming fishes they are more pointed (Wainwright et al., 2002), acting as stabilisers. The Triassic *Potanichthys* and Thoracopterus are exceptional cases, resembling modern (and unrelated) flying fishes, its enlarged pectoral fins were probably used to glide above the water surface (Tintoria & Sassi, 1992; Xu et al., 2012). Pelvic fins are thought

to be the least important for stabilisation, which may underlie their secondary loss in several lineages including sticklebacks, true eels and seahorses (e.g. Brown et al., 2011).

2.4. Ecomorphology

2.4.1. Patterns in gross morphology

Throughout the evolution of fishes there have been repeated convergences on strikingly similar body types (e.g. Belles-Isles, 1992; Friedman, 2010; Kocher et al., 1993; and Figure 2.11]). Mako sharks and tuna, are both fast pelagic predators and have convergent external morphology, but their internal mechanical design is strikingly similar as well, despite 400 million years of phylogenetic separation (Donley et al., 2004). Many factors influence morphology but all relate to movement and hydrodynamics, and schemes which classify swimming morphotypes (e.g. Webb, 1984) are powerful tools for reconstructing the palaeobiology of extinct species, regardless of phylogenetic association.

a) Rapid acceleration

Elongate arrow-like fishes (Figure 2.11 a-c) like pike, barracuda and others, have a dorsal and anal fin positioned posteriorly, to assist the tail in bursts of rapid acceleration, but they are relatively inefficient at steady swimming (Webb, 1988). The Triassic fish *Saurichthys* is superficially similar to modern needlefish (*Belone belone*), which has served as an analogue for a computational fluid dynamical study, highlighting the effectiveness of this dart-like morphology (Kogan et al., 2011).

b) High manoeuvrability

Lateral compression and deepening of the body (Figure 2.11 d-j) are often associated with high flexibility (difficult to infer in fossil taxa) in fishes such as the Pomacanthidae (angelfishes) and Chaetodontidae (butterflyfishes) acanthomorphs (Figure 2.11j). This allows greater manoeuvrability, with a reduced ‘turning circle’ (Videler, 1993), as the sides of the fish offer a large surface area for braking and rapid changes in direction. Examples in the fossil record include pycnodonts (Poyata-Ariza, 2005), the acanthomorphs *Aipichthys* and *Pycnosteroides*, the osteichthyans *Ebenaqua* and *Cleithrolepis*, and the thelodont *Furcacauda*.

c) Active demersal

Fish inhabiting complex demersal environments (Figure 2.11 k-l) tend to have elongate bodies, tapering backwards e.g. moray eel (*Muraena helena*), and lungfishes. Such is the focus on low-speed manoeuvrability that the pectoral fins may become the primary thrust generators, and become more robust to negotiate spatially challenging habitats. Conversely, species that propel themselves with anguilliform (eel-like) swimming may show a reduction or even complete loss of the pectoral fins (Belles-Isles, 1992).

d) Sustained swimming

There is always a trade-off between manoeuvrability, energetic efficiency and speed (see 'Generalists' Figure 2.11p-v), and cruisers prioritise sustained high-speed swimming. These fishes (e.g. tunas and their relatives) have a higher aspect ratio and a more hydrodynamically optimal torpedo-like body, but also larger heads to prevent recoil energy being lost as they beat their lunate caudal fins (Belles-Isles, 1992).

e) Dorsoventral compression and the ground effect

Boundary layers form against all walls interacting with a flow, including riverbeds and seafloors, and there is a thin layer of lower velocity water at the interface (the laminar sublayer). By exploiting this layer, dorsoventrally compressed benthic fishes expend less energy maintaining their position at rest. Flatfishes in particular can withstand significant water velocities before being dislodged (Arnold & Weihs, 1977; Videler, 1993), and secondary migration of the eyes to accommodate this strategy can be tracked in their evolution (Friedman, 2008).

Similar flattening is seen in the Early Devonian placoderm *Gemuendina stuertzi*, the agnathan *Drepanaspis*, and the thelodont *Turinia pagei*, which has been compared with the extant angel sharks (*Squatina* sp.) in form and lifestyle (Turner, 1992). In addition to being flattened, some extant fishes are small enough to move in the boundary layer of fast-flowing rivers (e.g. *Etheostoma tetrazonum*), where their morphology can be surprisingly independent of hydrodynamic influences (Carlson & Lauder, 2011).

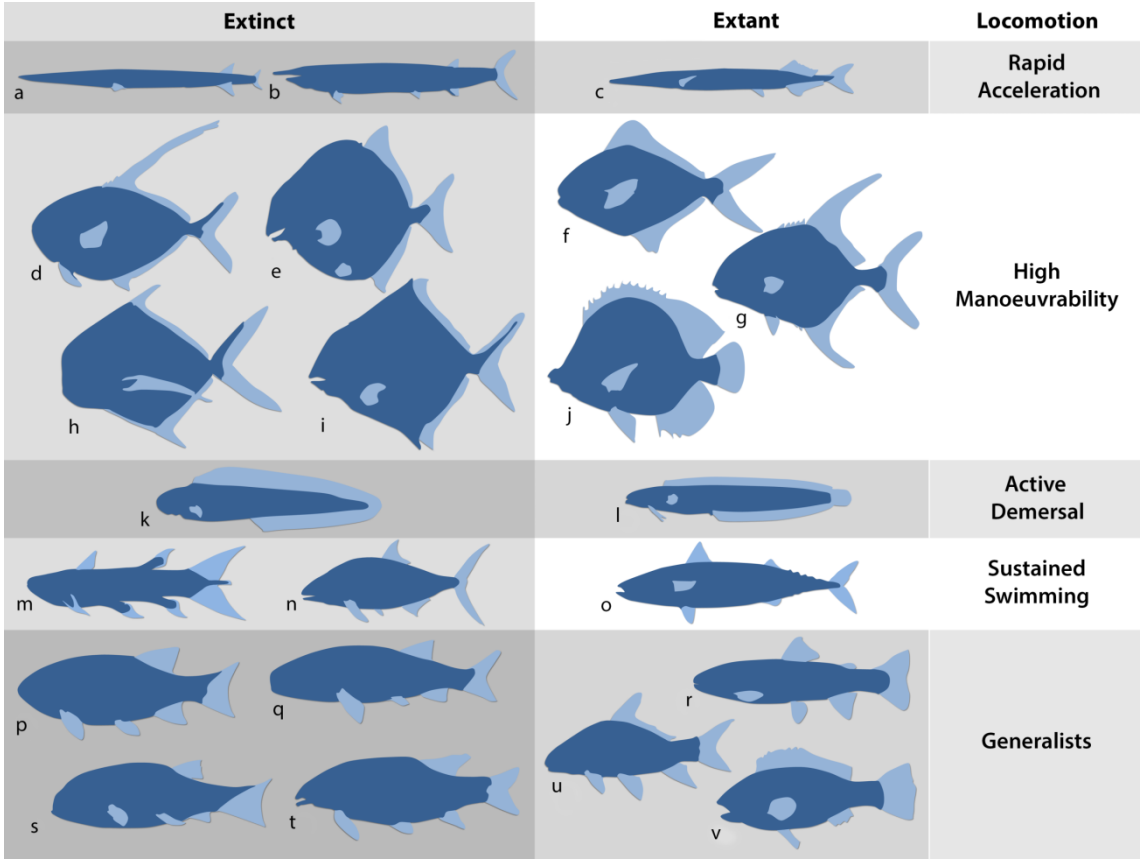

Figure 2.11. Examples of hypothesised swimming morphotypes of extinct and extant fishes. a) *Saurichthys* (Triassic); b) *Aspidorhynchus* (mid-Jurassic – Late Cretaceous); c) *Belone belone* (extant garfish); d) *Dorypterus* (Permian); e) *Proscinetes* (Jurassic); f) *Stromateus fiatola* (extant pomfret); g) *Trachinotus falcatus* (extant permit); h) *Bobasatrania* (Triassic); i) *Cheirodus* (Carboniferous); j) *Chaetodon* (extant butterflyfish); k) *Tarrasius* (Carboniferous); l) Clinoporus biporosus (extant ladder klipfish); m) Rebellatrix divaricerca (Early Triassic); n) *Hypsocormus* (mid-late Jurassic); o) *Scomber scombrus* (extant Atlantic mackerel); p) *Parasemionotus* (Early Triassic); q) *Mesolepis* (Carboniferous); r) *Oncorhynchus mykiss* (extant rainbow trout); s) *Carpiodes cyprinus* (extant quillback); t) *Perleidus* (Early – Middle Triassic); u) *Paracentrophorus* (Early Triassic); v) *Serranus hepatus* (extant brown comber). After Helfman et al., 2009; Wendruff & Wilson, 2011; Belles-Isles, 1992; Webb, 1984; Kogan et al., 2011; Barbieri & Martin, 1996; and Braun & Reif, 1982.

2.5. Hydrodynamics in the Fossil Record of Vertebrates

This section synthesises existing knowledge of drag-reduction in Palaeozoic fishes (and other relevant taxa), before briefly discussing long-term hydrodynamic trends in their early evolution. Fish scales are discussed separately in section 2.6.

2.5.1. Agnathans

a) The first 'fishes'

Locomotion is an advantage to almost every aspect of a pelagic species' survival, whether it be finding a mate or habitat, feeding, or avoiding being predated. In a competitive ecosystem it pays to be able to exploit opportunities in the water column, and this is no less true for fossil organisms than in modern communities. Tracking the early evolution of swimming proper is difficult to constrain in fishes, partially because of the subjective classification of what makes a 'fish' (Figure 2.12a-b). The larval stages of tunicates (sea squirts) for example are equipped with muscular tails, resembling some of the early Cambrian fishes of China, and with a fossil record that is possibly much older, perhaps even Ediacaran (Vickers-Rich, 2007). Some of the earliest 'fishes' including *Myllokunmingia* and *Haikouichthys* (Shu et al., 1999; 2003) of the early Cambrian of China, have dorsal fins and muscular tails (Zhang & Hou, 2004). Regardless of affinity *Haikouichthys* (Figure 2.12c) and its less commonly-preserved relatives have a clear head and tail region, and as such are presumed to have been capable swimmers. The extant lancelet is known to use cilia to swim after hatching, with muscle flexure and undulatory swimming gradually taking over and becoming more complex as the animal gets larger and faster (Stokes, 1997). This ontogenetic progression to full swimming is shared by other vertebrates (e.g. Kimmel, 1993) and may offer a parallel to the earliest stages of the evolution of undulatory swimming.

Early chordates lack control surfaces such as pectoral fins, so it is presumed that the tail was the primary thrust generator (Clark, 1964; Shadwick & Lauder, 2006; Pradel et al., 2007). Those modern fishes (and aquatic tetrapods) with reduced pectoral fins have much lower locomotor control and rely on high flexibility to direct force, as would likely the earliest fishes (Graham et al., 1987; Deliagina, 1997; Shadwick & Lauder, 2006). The term 'fish' is usually defined as vertebrates with a mineralised skeleton (cartilage or bone), thought important for defence, and locomotary innovation through improved muscle attachment (Long, 2011). Bony

fragments have been found as early as the late Cambrian (Young et al., 1996), including possibly the oldest agnathan (jawless fishes) *Anatolepis* (Smith & Sansom, 1995), although some argue that these are arthropod remains (Smith & Coates, 2001).

b) Euconodonts

Well-preserved euconodonts or 'conodont animals' (differentiating the organism from the tooth-like oral elements) have revealed bodies which were superficially eel-like with elongate muscular tails (Figure 2.13a), and that the 'elements' used for biostratigraphy are in fact teeth (Briggs & Clarkson, 1983). The microstructure of these elements resembles dentine/enamel-like tissue, which is unique to true vertebrates, and an important taxanomic character (e.g. Murdock et al., 2014). However, there has been a great deal of debate over their exact phylogenetic placement (Figure 2.13; Briggs, 1992; Blieck et al., 2010; Turner; 2010), and it has even been suggested that conodonts are stem-gnathostomes (Donoghue, 2000). Their hydrodynamics are seldom discussed, but some workers have suggested the muscle fibres of *Promissum* (a late Ordovician conodont from South Africa) are too small for rapid bursts of swimming (Gabbott et al., 1995).

c) Anaspida

The anaspids were fairly small and primitive fishes, found in Silurian and Devonian of the once Euramerican continent (Long, 2011). An interesting development in anaspids including *Pharyngolepis* and *Cowielepis* (Figure 2.13b) was their fin-like lateral projections which had an internal skeleton and musculature. This was a distinct advantage for manoeuvrability as a suprabenthic organism coping with turbulence higher in the water column (Coates, 2003). Species from late Devonian Canadian deposits had a long row of gill arches (up to 30 pairs in *Euphanerops*), and have been central to discussions of an anaspid relationship to lampreys (Figure 2.12, and; Janvier et al., 2006).

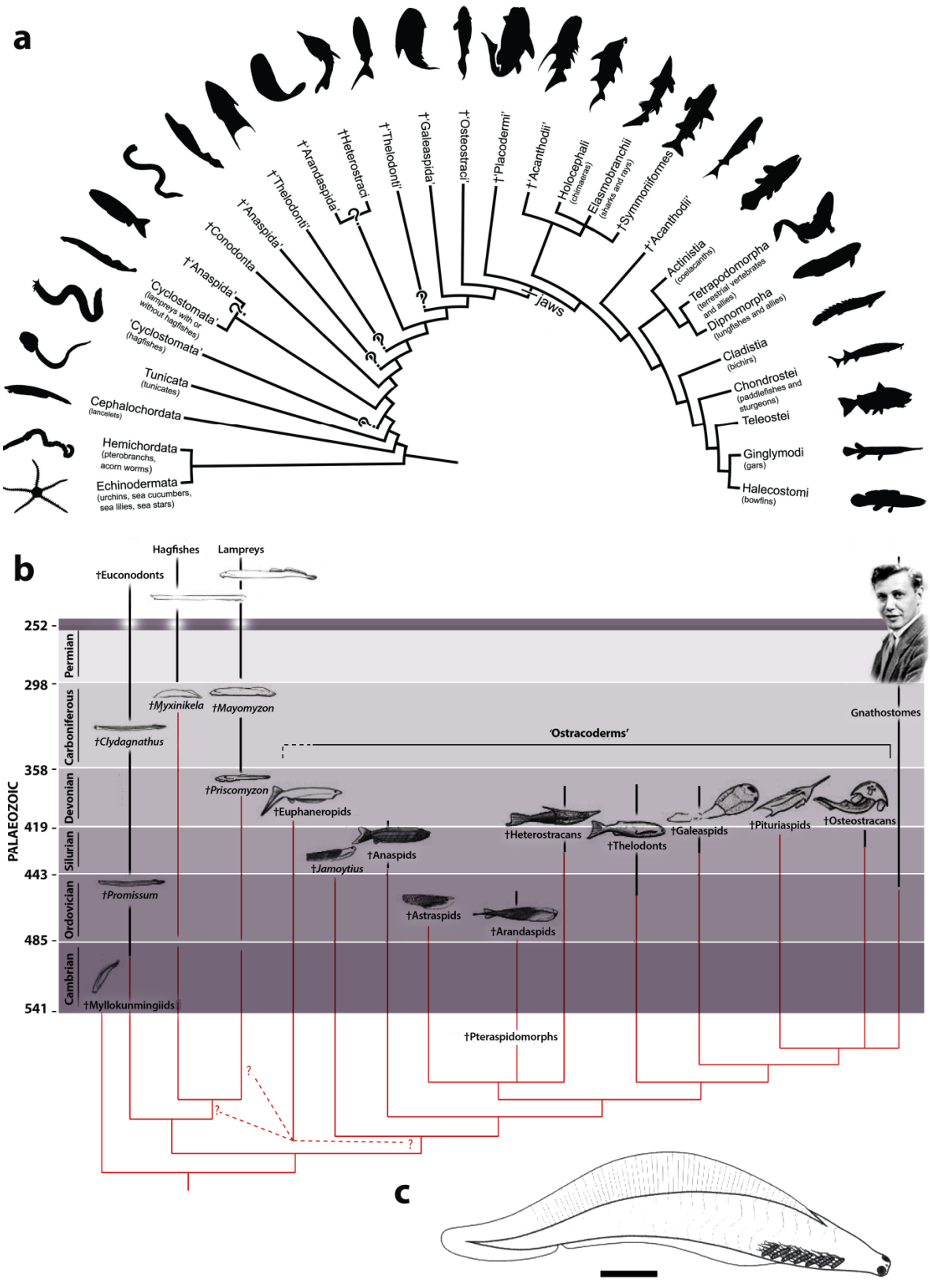

Figure 2.12. Recent phylogenetic hypothesis; a) of all 'fishes' and their relatives; b) and timescale of the evolution of Palaeozoic 'fishes' and their relatives, including pituriaspids. c) Reconstruction of the early Cambrian myllokunmingiid *Haikouichthys ercaicunensis*. Extinct taxa are symbolised with a dagger (†), question marks indicate uncertain phylogenetic placement, and inverted commas denote possibly paraphyletic taxa. (continued overleaf)

(continued) Details of analyses and taxonomic groupings are detailed in the original source references; a) modified from Friedman & Sallan, 2012; b) redrawn from Janvier, 2015, and; c) from Zhang & Hou, 2004. Scale bar is 5mm.

d) Pteraspidomorphi

Members of this group have been found in both marine and freshwater deposits from the late Ordovician (Sansom et al., 2001) until the late Devonian. The earliest pteraspidomorphs were small fishes with symmetrical (homocercal) tails and full body armour (e.g. *Astraspis*) which probably fed by filter feeding. Arandaspids such as *Sacambamaspis* (Figure 13f.) and later forms such as the heterostracans ('different shelled'), had hypocercal tails (enlarged lower lobe) and armour chiefly around the head (Pradel et al., 2007). This was sutured and grew incrementally producing growth rings (Keating et al., 2015), providing defence. Freedom to move the tail more, however crudely, would have allowed the animal to plough bottom sediments, using the pharyngeal pouches to filter edible material, probably small prey animals and detritus (Halstead, 1973; Purnell, 2002).

Slow-moving fishes with negative buoyancy often have asymmetric, epicercal caudal fins, used in part to create vertical lifting forces. This may have been the case for the heavily armoured, early Devonian pteraspid *Errivaspis waynensis* (Figure 2.13d.) although attempts to reconstruct its hydrodynamics have focussed on the underside of the bony head shield as a simple lifting surface (Kermack, 1943), raised in pitch by the downward force of the tail. On this premise, workers have suggested that *Errivaspis* were both benthic, moving in short powered bursts (Aleyev, 1977), and facultative pelagic planktivores (Belles-Isles, 1987).

As discussed, fishes can reduce drag passively by controlling vortices which form across the body (section 2.3.2). Recent wind tunnel experiments have shown that the cephalic shield of *Errivaspis waynensis* acts very much like a delta wing (Botella & Fariña, 2008), creating vortices roughly parallel to the leading edge. In essence, fluid flows over these vortices and is also pulled in, accelerating as the vortex widens posteriorly and creates lower pressure. This would have provided an important source of lift during swimming and produced stabilising vortices to aid yaw control, just as in modern boxfishes (Bartol et al., 2002; 2003; 2005; 2008). Later forms did develop stabilising lateral projections on the head (cornua) in parallel to a reduction in armour, suggesting selection for mobility and manoeuvrability (Hildebrand and Goslow, 2001; Benton, 2005).

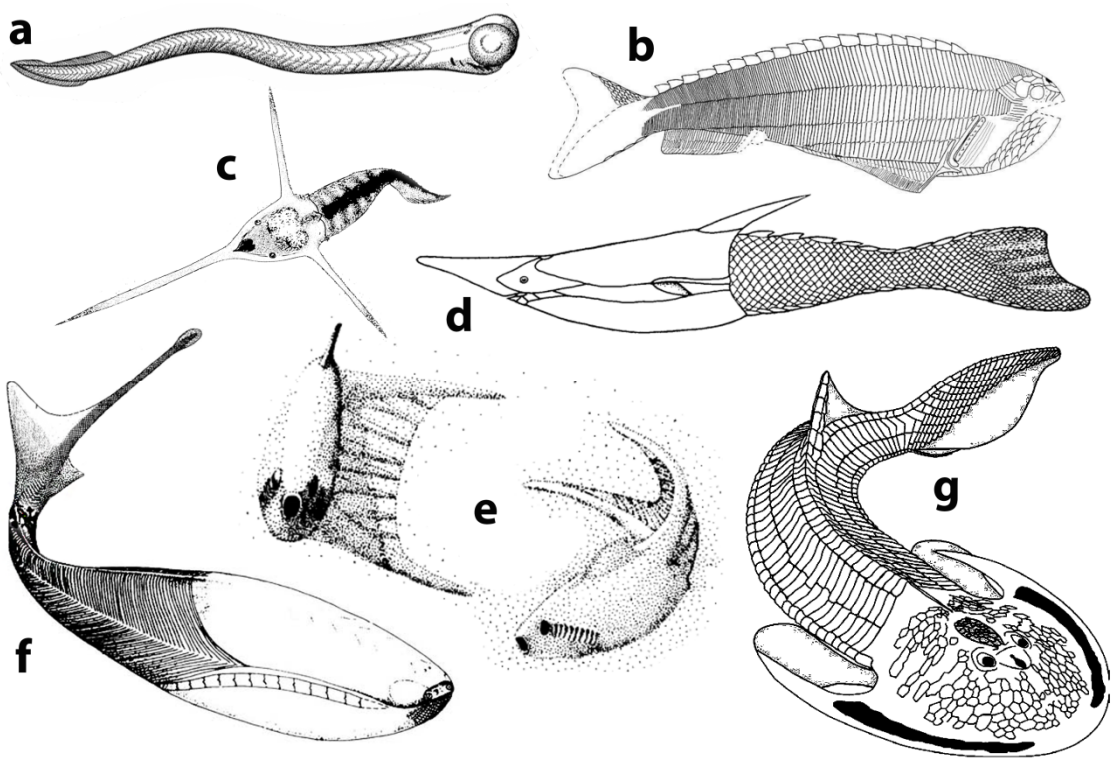

Figure 2.13. Reconstructions of representative agnathan Palaeozoic fish taxa; a) the conodont animal, from Aldridge et al., 1993; b) the Silurian anaspid *Cowielepis*, from Blom, 2008; c) the Devonian galeaspid *Macrothyraspis*, based on Wang et al. 2005 and; d) the early Devonian heterostracan *Errivaspis*, from Mark-Kurik & Botella, 2009; e) the Devonian furcacaudiform thelodont *Cometicercas*, from Wilson & Caldwell, 1998; f) the Ordovician arandaspid *Sacambamaspis*, modified from Gagnier, 1993 [in Benton, & Harper, 2013] and Pradel et al., 2007 and; g) the osteostracan *Diademaspis*, from Keating et al., 2012. Not to scale.

e) Thelodonti

Despite their biostratigraphic use, thelodonts have not received much palaeobiological attention from researchers (although see Turner, 1992) partly because only a small proportion of species are described from articulated remains (Wilson and Märss, 2009). Thelodonts have lozenge-shaped scales made of dentine which would have surrounded a pulp cavity, much like a tooth (Märss, et al., 2007). These scales were varied in shape across the body, but tended to be larger and more elongate towards the tail (Long, 2011). Researchers have previously noted the resemblance of thelodont scales to those of modern sharks (e.g. Märss et al., 2007; Chernova & Vorob'eva, 2012) but this has never been explored in any systematic detail.

Many species were flattened, dorsally compressed benthic animals (Turner, 1982, Long, 2011). However, some of the earliest examples of well-developed symmetrical tails are found in the

furcacaudiform thelodonts (literally 'fork-tailed'). *Furcacauda* (Figure 2.13e) was a deep-bodied species which was laterally compressed, probably pelagic and highly manoeuvrable like the modern butterflyfish (Figure 2.11j).

f) Galeaspida

Galeaspids (Silurian-Devonian) are an unusual fish group with a diverse range of head shield morphologies (Zhu & Gai, 2007), considered forerunners to the jawed gnathostomes (Gai et al., 2011). They are characterised by a lack of paired fins, and a large opening at the front of the head shield which was a modified 'nostril' used for water intake. A detailed study of the galeaspid *Shuyu zhejiangensis* has shown that this nostril intake leads to a nasopharyngeal complex, which in hagfish leads to the pharynx (so they could smell the water as it flowed through). The nasopharyngeal complex in lampreys, *Shuyu* (and supposedly other osteostracans) and jawed vertebrates is a dead-end pouch, referred to as a nasohypophyseal organ (Gai et al., 2011). It is a complex feature, but is worth mentioning here as it is an important step which accommodated the development of jaws. The Devonian galeaspid *Rhegmaspis* and others have an elongate rostrum and streamlined head shield, interpreted as reducing drag and improving manoeuvrability (Zhi-Kun et al., 2015). It is unknown how much feeding specialisations influenced morphology in this and similar taxa but compared to dorsally flattened galeaspids, species such as *Rhegmaspsis*, *Macrothyraspis* (Figure 2.13c), and others with elongate rostra certainly appear to be much more active swimmers (Janvier, 1996).

g) Pituriaspida

Very little is known about pituriaspids, found in Devonian sediment of just one locality in Western Queensland, Australia (Young, 1991). *Pituriaspis doylei* (one of only two known pituriaspid species) had a long rostral elongation, but unlike similarly endowed galeaspids also has pectoral fins. This may represent a step towards stabilisation, helping improve the yaw, roll and pitch control of movement, and fins are also an additional source of lift and thrust.

h) Osteostraci

The osteostracans are a clade of stem gnathostomes (Figure 2.12), and a sister group to jawed fish proper (Forey and Janvier, 1993; Sansom, 2009). They share girdle-supported paired fins

and an epicercal tail with the gnathostomes, but their braincases have primitive lamprey-like features (Long, 2011). This relationship has also been confirmed in a recent analysis of the group, which also detailed the unique case of secondary loss of paired fins in the trematapids (Sansom, 2009). The best known of these is *Cephalaspis,* a genus in the Cephalaspidomorphi (the only class within the Osteostracomorphi) which contains over 100 species (e.g. *Diademaspis*, Figure 2.13g). The fossilised sutureless head shields of some species are always of similar size, which is a feature of adult animals that have undergone a larval stage and metamorphosis (Moy-Thomas & Miles, 1971). As with many other Palaeozoic fishes, the tail was heterocercal and thought to both counteract negative buoyancy (Helfman et al., 2009) and likely correct pitch for ploughing sediment.

2.5.2. Non-tetrapod gnathostomes

a) Placoderms

The Devonian period saw a huge diversity of gnathostomes (jawed fishes), after their 'long-fuse' evolution throughout the Silurian (Friedman & Sallan, 2012), the most basal members of which are the placoderms. Placoderms ('plate-skinned'), a large class of Silurian-Devonian fishes are now thought to be paraphyletic stem gnathostomes (Brazeau, 2009; Zhu et al., 2013; Zhu et al., 2013; Brazeau & Friedman, 2014). They may have replaced the pteraspids and osteostracans in morphospace, and were the dominant and most diverse Devonian fishes, achieving global distribution in both marine and freshwater (Young, 2010). They had depressed, sometimes flattened bodies and bony plates which covered the front of the body (Denison, 1978). In the arthrodire placoderms, these bony carapaces (covering the head and shoulder regions) were mobile (Long, 2011). The complex of plates around the mouth (which self-sharpened to form a blade like beak), in partnership with the huge bite forces that could be generated no doubt contributed to their success (Anderson & Westneat, 2003).

While many placoderms are fairly conservative in their morphology (interpreted as benthic and slow-moving), some species had large and pointed snouts. Rostral elongation for drag-reduction and pelagic life is most convincing in placoderms such as *Oxyosteus* (Figure 2.14a), *Rolfosteus* (Figure 2.14b), and *Carolowilhelmina*, as they superficially resemble billfishes (Dennis & Miles, 1979; Mark-Kurik & Carls, 2002). In these three genera large pectoral fins may have been used in a similar way to those of modern billfishes; for high-speed manoeuvres in partnership with a large rudder-like dorsal fin. However, it is not clear if the small tubercles which ornament the bony plates of placoderms extended on to the snout. This surface

roughness is known to aid transition of the boundary layer in sailfish (Aleyev, 1977; Sagong et al., 2013, and; section 2.3.2), but no hydrodynamic modelling has been performed to test this.

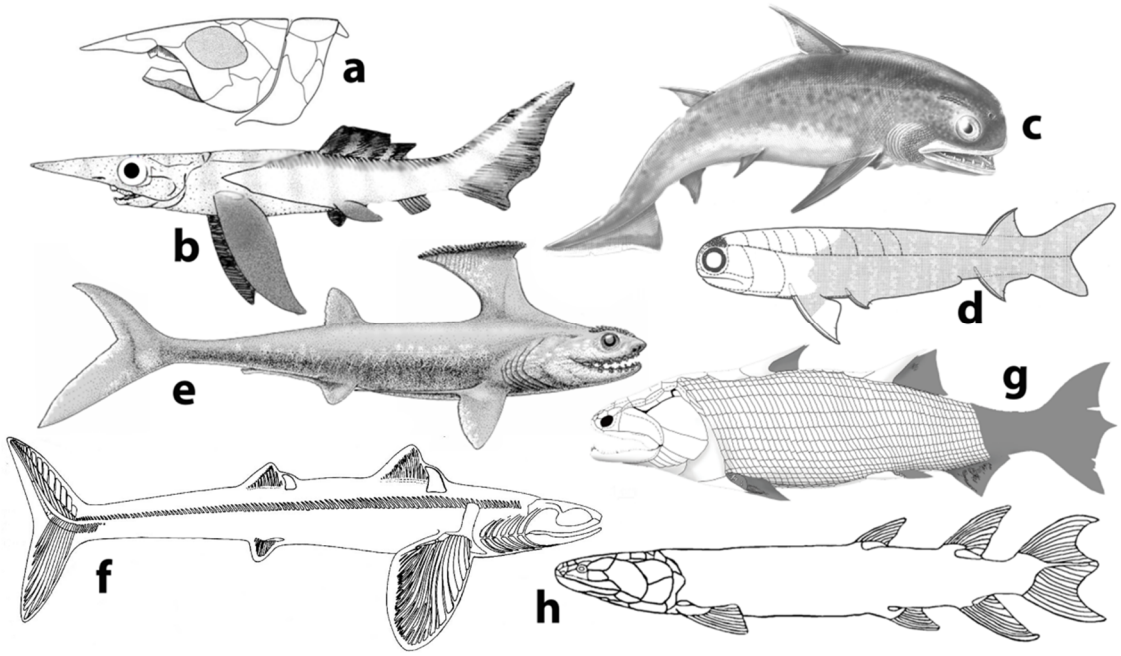

Figure 2.14. Reconstructions of representative Palaeozoic gnathostome fish groups. The placoderms a) *Oxyosteus*, from Moy-Thomas & Miles, 1971, and; b) *Rolfosteus* (creative commons image); the 'acanthodians' c) *Nerepisacanthus*, from Burrow, 2011, and; d) *Acanthodes*, from Zidek, 1976. The chondricthyans e) *Akmonistion*, from Coates & Sequeira, 2001, and; f) *Cladoselache* (Benton, 2005); and the osteichthyans g) *Guiyu*, from Zhu et al., 2009, and; h) *Eusthenopteron*, from Schultze, 1984. Not to scale.

b) 'Acanthodians'

'Acanthodians' ('spiny sharks') are a paraphyletic grouping of jawed fishes, which in recent analyses have either been split between the Chondricthyes (sharks and relatives) and Osteichthyes (bony fishes), or placed as stem chondricthyans (e.g. Davis et al, 2012; Zhu et al., 2013; Brazeau & Friedman., 2014; Giles et al., 2015), with support generally for the latter. 'Acanthodians' are typically small (mostly ~20cm), with an elongate spindle-like body and heterocercal tail (Figure 2.14c-d), commonly discussed as evidence for an active pelagic lifestyle (Denison, 1979). This is supported in part by the identification of an Early Devonian 'acanthodian' swimming trace, produced by a non-anguilliform (eel-like) swimming style (Wisshak et al., 2004), although the fish would have to be in direct contact with the substrate

to produce the trace. Perhaps because of the widespread acceptance that 'acanthodians' were active predators, scale hydrodynamics are very rarely discussed (but see Reif, 1982; Hanke, 2012, and section 2.6).

c) Chondrichthyes

Despite their remarkable diversity, especially in the Carboniferous (e.g. Lund, 1990; Benton; 2005), the hydrodynamics of Palaeozoic sharks (Figure 2.14e, f) have only been discussed in a very general sense, often with focus on the heterocercal tail (section 2.3.3). A notable exception is the large 'brush' dorsal fin of the early Carboniferous shark *Akmonistion* (Figure 2.14e), which for a long time was thought to be a significant hydrodynamic disadvantage, creating drag that would prohibit fast swimming (e.g. Coates & Sequeira, 2001). However, after modelling this drag was found to be much smaller than expected (Criswell et al., 2013), highlighting the importance of testing assumed functions experimentally.

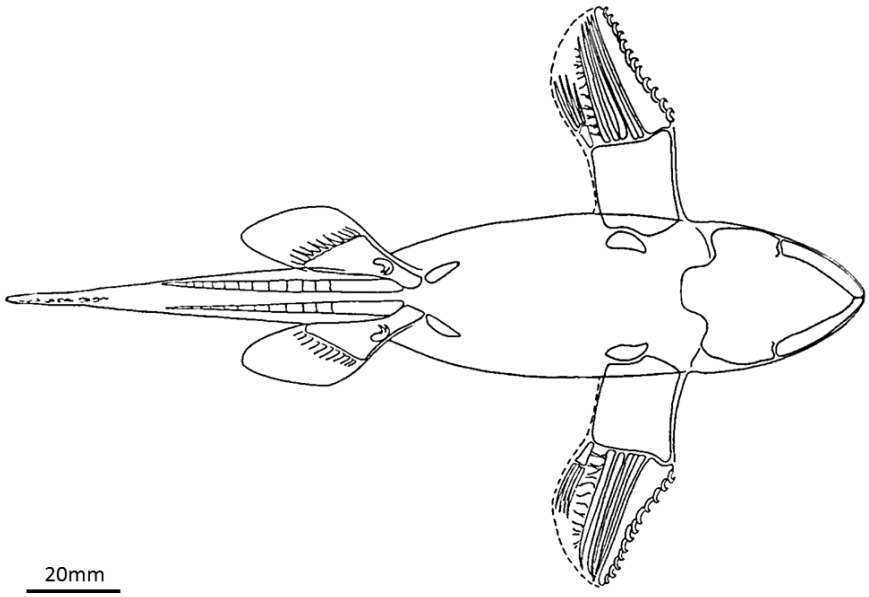

Figure 2.15. Reconstruction of the Carboniferous chondrichthyan *Iniopteryx rushlaui* from Zangerl and Case, 1973, showing large hook-like denticles on leading edge of fin.

The Devonian-Carboniferous iniopterygians, all have enlarged pectoral fins, mounted high on the flank, just as in extant hatchetfishes and flying fishes. Although untested, it has been argued that because these fishes are adapted to breach from the water to avoid predators and reduce drag (section 2.3.3), iniopterygians may have done the same (Lund, 1990). In another

iniopterygian, *Iniopteryx rushlaui*, (Fish & Lauder, 2006), large hook-like dermal denticles on the leading edge of the pectoral fins are thought to function like the tubercles of humpback whale flippers (section 2.3.2). However, as this has never been tested experimentally there is little to contradict the original interpretation that these scales are defensive, or even sexual (Zangerl & Case, 1973). Scale functions, particularly of modern sharks are the subject of this thesis, and existing literature is reviewed in section 2.6.

d) Osteichthyans

Osteicthyans include the actinopterygians (ray-finned fishes) and sarcopterygians (lobe-finned fishes), and constitute ~98% of all vertebrate species (Nelson, 2006). The early evolution of this group is poorly understood, represented by scales and jaw fragments of the late Silurian fishes *Andreolepis* and *Lophosteus* (Botella et al., 2007).

An interesting development in many early osteichthyans is the symmetrical fork-like tail, possibly including the earliest articulated member *Guiyu*, Figure 2.14g (although the tail is not preserved in this taxon). A forked tail (sometimes referred to as double-truncate) is a trade-off between manoeuvrability and drag-reduction with a large enough surface area for rapid thrust production but not enough to promote deleterious vortices that would affect pressure drag (section 2.3.3). The Late Devonian sarcopterygian *Eustenopteron* (Figure 2.14h) is superficially very similar to that of a pike, and therefore considered an ambush predator. The posteriorly positioned dorsal and anal fins act like a dart, guiding the fish in one direction rapidly to capture prey such as 'acanthodians' (Arsenault, 1982; Cote et al., 2002). This is in contrast with the early Triassic fork-tailed coelacanth *Rebellatrix divaricarca*, where these fins are further forwards to allow manoeuvrability at high speeds; unique in a group that is generally slow-moving (Wendruff & Wilson, 2011).

Unlike other fish groups, the huge diversity of modern osteichthyans means there are usually plenty of analogues to help elucidate the ecology and hydrodynamics of their extinct ancestors. Unfortunately this cannot be said of the earliest osteicthyan and actinopterygian scales, which are thick rhomboidal units, often with a surface ornament. The closest living analogues are 'ganoid fishes' such as gars and bichirs, which do not have this ornament, and therefore functional comparison is limited (section 2.6).

2.5.3. Aquatic tetrapods

Although the focus of this thesis is Palaeozoic fishes and their modern analogues, secondarily aquatic vertebrates are subject to the same physical constraints. They therefore offer insight into hydrodynamic adaptations which may have evolved convergently, and independently of phylogenetic relatedness. The most famous case of convergent evolution in aquatic tetrapods is the tail fin, which is often secondarily heterocercal (e.g. mosasaurs, early ichthyosaurs) (Massare, 1994). However, a well-preserved *Stenopterygius* (Jurassic ichthyosaur) was found to have collagen fibres supporting the dorsal fin and, significantly, a dorsal lobe of the tail (Lingham-Soliar, 1999; Lingham-Soliar & Plodowski, 2007). This supports the long-standing view that ichthyosaurs were fast thunniform swimmers, but also highlights the problems of interpreting incomplete fossil remains (Massare, 1994).

Experimental modelling has been performed for a wide range of aquatic tetrapods, including Palaeozoic amphibians (e.g. Cruickshank & Skews, 1980), however the majority of studies on extinct taxa concern Mesozoic reptiles e.g. ichthyosaurs, plesiosaurs, mosasaurs (e.g. Massare, 1988). Of these, none have investigated skin texture, despite reports of scale ornamentation in some taxa and their potential role in drag-reduction. For example the late Cretaceous mosasaur *Plotosaurus* (Lindgren et al., 2010) has non-imbricated and fairly rounded scales on the head, but further back towards the flank they are rhomboidal and overlap, as in many modern sharks (Reif, 1985), 'acanthodians' and thelodonts (section 3.1.2). It has also been suggested that *Plotosaurus* used riblets to reduce drag (section 2.3.2; Lindgren, 2009), however there are several important problems with this interpretation. The most important issue is that of riblet spacing, which in modern pelagic sharks is generally between 50-150 micrometres. The slowest moving tend to have wider riblet spacing, until drag-reduction is no longer an important influence on morphology and the scales become spinier or blocky (section 4.1.1; Reif, 1985). The inter-keel distance in *Plotosaurus* is 766µm, and in *Ectenosaurus clidastoides* (a mosasaur) was 1062µm. Similar diamond-shaped shark scales with a dominant central keel belong to the modern *Cirrhigaleus asper* (roughskin spiny dogfish), which has an interkeel distance of ~430µm (note: this passage was written before the publication of Palmer & Young; 2015, who have adopted this view).

Interestingly, there is geochemical evidence that large marine reptiles such as ichthyosaurs, plesiosaurs and mosasaurs could maintain high body temperatures, even in cold climates (Bernard et al., 2010). As discussed it has been suggested that elevated body temperature can change the viscous properties of the relatively cool surrounding fluid (section 2.3.2). This

method of drag reduction is unlikely due to the short amount of time that the water would be in contact with the body (Fish, 1998).

2.5.4. Palaeozoic trends in hydrodynamic evolution

Assessing the evolutionary significance of the hydrodynamic innovations discussed so far is difficult because it requires disentangling the many factors which contribute to the success or failure of a species. While this is also a problem for modern ecologists, palaeontologists are in a unique position to track morphological trends over tens to hundreds of millions of years.

This work focuses on how morphology relates to hydrodynamic function of scales (section 2.6); however it is useful to summarise and discuss overarching evolutionary trends associated with drag-reduction and locomotion in Palaeozoic fishes. *Haikouichthys* and its relatives lived during the Cambrian radiation, and are heralded as the first 'fish', likely moved freely in the water column (Long, 2011). Articulated body fossils are rare in the Ordovician but mineralised microremains such as scales are abundant (Sansom et al., 1996; Young, 1997; Sansom et al., 2001; 2012), demonstrating the foothold fishes already had at this early stage. Conodonts emerge at the end-Cambrian, likely swimming in much the same simple eel-like fashion. Like the myllokunmingiids, cononodonts were scaleless, and may have employed a mucus coat to reduce drag, in addition to defensive and osmotic functions (Shephard, 1994). The lack of articulated material makes palaeoecology, taxonomy, and diversity difficult to investigate for this interval, including – unfortunately - the effects of the end-Ordovician mass extinction (Friedman & Sallan, 2012). From the limited information available it is likely that the earliest jawed vertebrates arose in the early Silurian, but were relatively rare compared to agnathan taxa, which dominated marine faunas (Boucot & Janis, 1983) in to the Early Devonian (Janvier, 1996; Friedman & Sallan, 2012). Many agnathans were heavily armoured around the head, but the trunk region was always more flexible, often covered in small plates or scales, which afford greater flexibility and freer movement of the caudal fin.

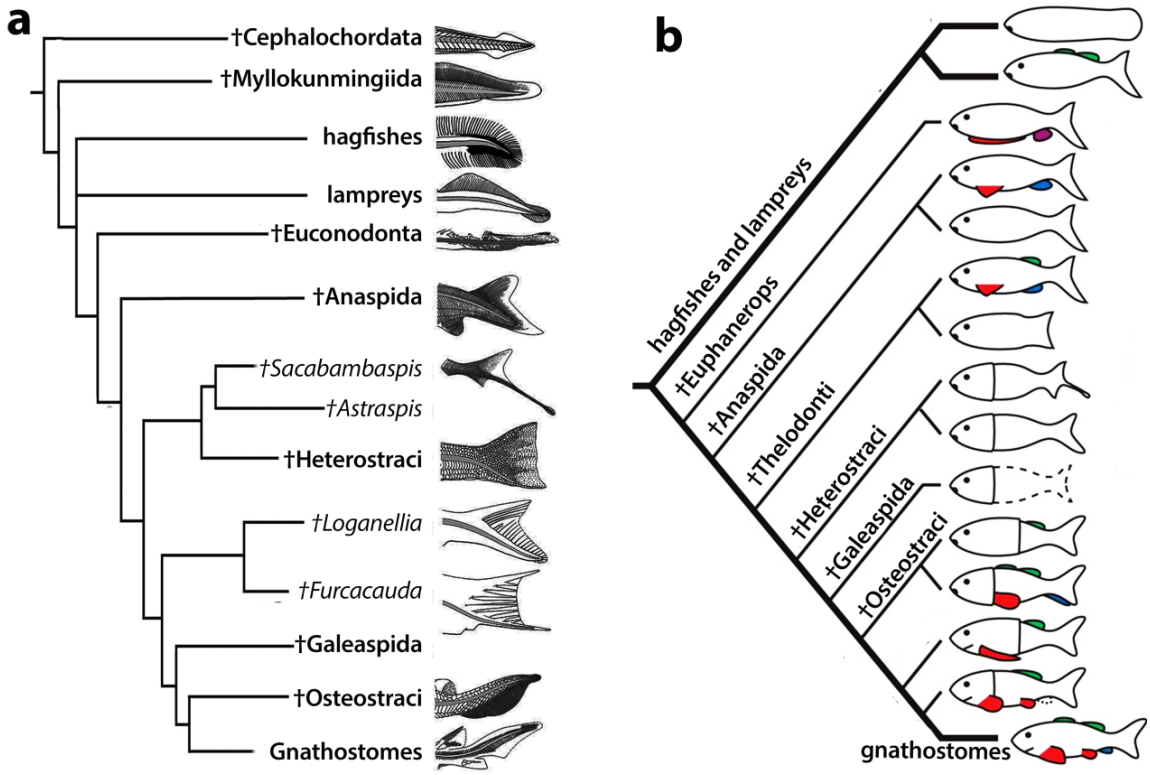

Figure 2.16. A) Diversity of caudal fins in some Palaeozoic fish groups, and; b) occurrence of dorsal fins (green), paired fins (red), and anal fins (blue) in some Palaeozoic fish groups. From a) Pradel et al., 2007, and; b) Sansom et al., 2010; 2013.

The caudal fins of early agnathans are normally heterocercal (section 2.3.3; Figure 2.16a), with a larger upper lobe (Pradel et al., 2007). Symmetrical tail shapes evolved in groups such as furcacaudid thelodonts (Figure 2.16a) during the Devonian, but the hydrodynamic and ecological significance is still unclear. Heterocercal tails, as well as producing forward thrust, are thought to counteract negative buoyancy (or positive in some cases, e.g. flying fishes) and correct the animal's pitch (section 2.3.3)(Aleyev, 1977). A major issue is that without observing the living fish or knowing its internal anatomy, factors such as buoyancy cannot be accounted for, and the heterocercal tail may either be for a benthic lifestyle with pelagic excursions or slow, efficient cruising (like many deepwater sharks). In addition it has also been suggested that the external morphology of caudal fins does not reflect the hydrodynamic action, which is affected by lobe stiffness, behaviour, and flow conditions (Lauder, 2000). This limitation aside, it is interesting to note the general trend from very simply symmetrical lobe-like tails, to the heterocercal condition in early Palaeozoic agnathans, and then to complex symmetrical designs in a huge number of ray-finned fishes and other more recent groups (Webb, 2006).

Throughout the Palaeozoic there is a trend for swimming to become more complex, and there is a general loss of the eel-like (anguilliform) style of swimming as fins evolve (Sansom et al., 2010; 2013). This involved reduced body undulation and stiffening of the trunk, with the majority of thrust produced by the far posterior of the body (Webb, 1982; Webb, 2006). This is concomitant with the gradual addition of stabilising fins (Figure 2.16b), which themselves become more mobile, with greater degrees of freedom (Moy-Thomas & Miles, 1971), especially in the actinopterygians (e.g. Lauder & Drucker, 2004). There is also a trend for reduced skeletal mass in Palaeozoic fishes, with the evolution of thinner scales (section 2.6) and reduced armour in many groups. Increased mass is beneficial for stability in benthic, current-swept habitats (Webb, 2006), so this trend may be related to an increased reliance on paired fins for flow control (Carr, 1995).

2.6. Fish Scales

The integument is a composite organ of three layers, the epidermis, the dermis and a basement membrane between them. This simple arrangement evolved into many familiar structures including hair, sweat and mammary glands, feathers, teeth and scales (Pough et al., 2007). Scales are diverse in form, development, and function, and by the broadest definition are small units of hard mineralised tissue, which may be discrete or overlapping plates.

a) Scale types

In fishes, there are four broadly defined scale types (leptoid, cosmoid, ganoid, and placoid), most of which are essentially a hardened integument fold (specifically the dermis), often with ossified dermal bone as its key constituent (Ehrlich, 2015). Leptoid scales (Figure 2.17a, b) grow concentrically and overlap, exposing only the posterior portion which can have either a smooth (cycloid) or toothed (ctenoid) trailing edge (section 2.3.2). Cosmoid scales are composed of two layers of bone with a cap of dentine-like cosmine above it, and grow as lamellar bone is added at the base. Ganoid scales (e.g. *Polypterus*, Figure 2.17c) are similar to cosmoid scales but have extra layers of hard enamel-like ganoin overlying the cosmine. Placoid scales or 'dermal denticles' (Figure 2.17d) are tooth-like in cross section, with bone at the base, dentine above it, and a cap of enamel (Helfman et al., 2009). These scales are embedded in the dermis, which is unique to the cartilaginous fishes; chondrichthyes. In elasmobranchs (sharks, skates, and rays) particularly, scale morphology has long been recognised as biomechanically

significant, reflecting the relative importance to a species of functions such as defence, and drag-reduction (Reif 1985a), discussed next.

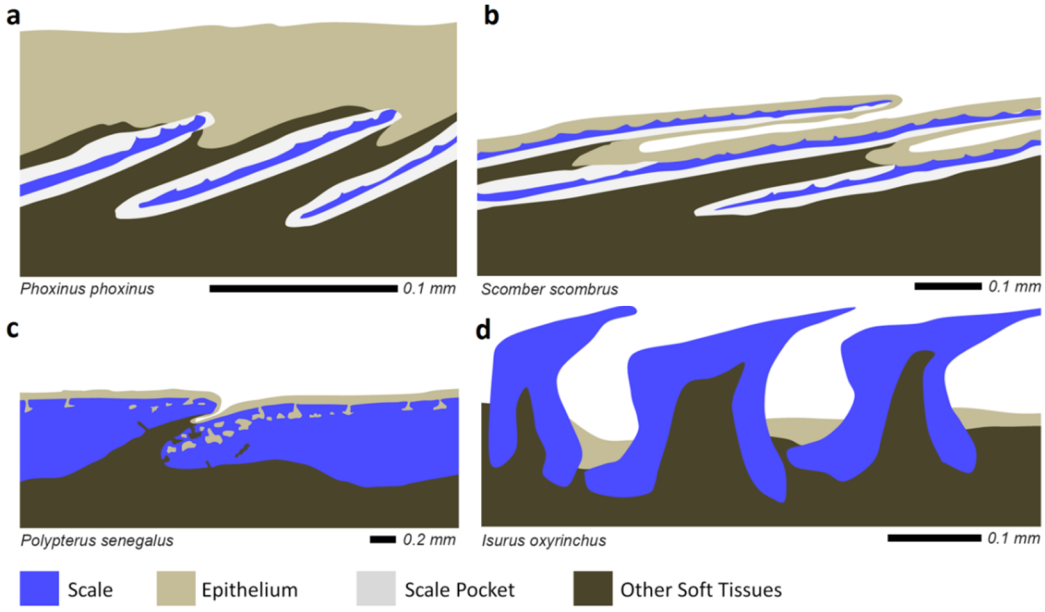

Figure 2.17. Variation in the integument of some living fishes. Clockwise from top left: Simplified cross-sections of the leptoid scales of a) *Phoxinus phoxinus* (common minnow), and; b) *Scomber scombrus* (mackerel); c) the ganoid scales of *Polypterus senegalus* (Cuvier's bichir); and d) the placoid scales of *Isurus oxyrinchus* (shortfin mako shark). Modified from Whitear, 1986 and Motta et al., 2012.

b) Physiological functions

Fishes are known to use scales as a calcium and phosphorus reservoir, which can be exploited when supply is limited or during breeding (Whitear, 1986; Metz et al., 2014). Scales are also thought to act as a physical barrier to osmosis (Whitear, 1986), preventing the unwanted loss or gain of water and mineral ions, but this function in sharks is undocumented.

c) Abrasion defence

As a hard tissue barrier, any form of scale will serve a protective role against abrasion and minor mechanical stresses (Reif, 1985). However, the morphology of shark scales is of particular interest as they are in direct contact with the surrounding environment. This is apparent in many rays, and benthic shark species, where the animals' ventral surface (in direct

contact with the substrate) is often covered in a dense mat of rounded and blocky scales. In angel sharks (*Squatina* sp.) there is a particular distinction from the dorsal side, which in contrast is sparsely covered with small mushroom-like denticles (Figure 2.18). In the benthic longtail carpet sharks (Hemiscylliidae), scales are again smooth and robust, very often with scratch marks in the stream wise direction betraying their intimate contact with hard substrates (Reif, 1985). It is likely that any ornament relief (such as drag-reducing riblets) proud of the scale surface would be susceptible to excessive wear, without conveying a functional benefit to more sluggish benthic animals.

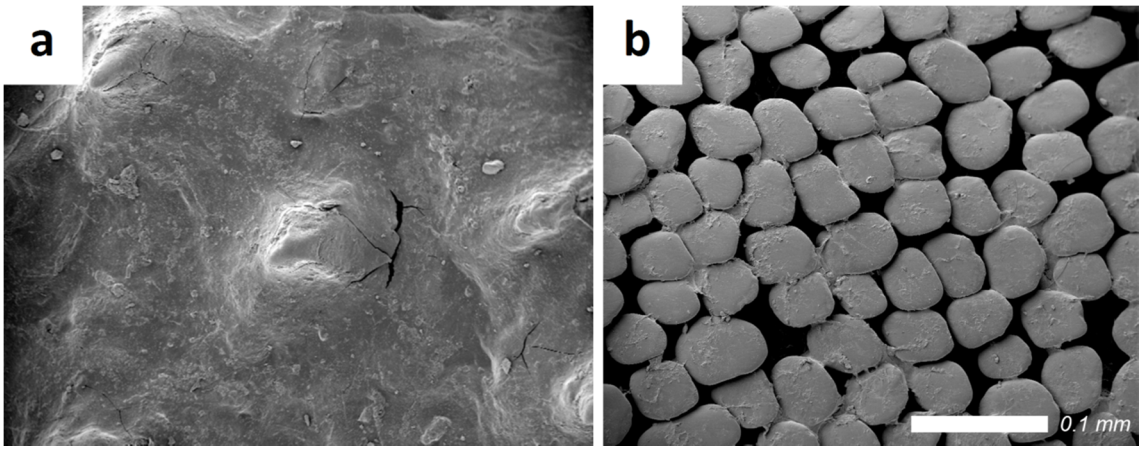

Figure 2.18. Dermal denticles of the angelshark *Squatina squatina* from the mid-body flank region of the a) mucus-coated dorsal and b) ventral surface. Adult female, total length 1240mm, sampled at Centre for Environment Fisheries and Aquaculture Science (CEFAS), United Kingdom.

d) Predator defence

As a primary defence many fishes throughout the Phanerozoic evolved body spines, commonly on the dorsal fin, and in some cases envenomated (Smith & Wheeler, 2006). Scales modified to be spiny or spine-like are much less common in teleosts than chondricthyans (but see Carnevale & Santini, 2006), but the reason for this is unknown.

Smaller scale units, regardless of morphology allow for much greater flexibility than large stiff plates, while still providing physical protection (Browning et al., 2013). In many extinct jawless fishes (section 2.5.1) and modern armoured catfish, rigid bony tissue surrounds the head, but the flank and tail have smaller scute-like elements where the greater flexure is required for swimming. In teleosts the overlapping scales help maximise robustness and flexibility without

too much additional weight (Vernrey & Barthelat, 2014), prompting biomimetic research looking to improve armour (Zhu et al., 2012; 2013). The overlap between scale units is clearly an important part of the mechanical role of skin, but individual scales can be very robust as well. Bichirs, arapaima, gars, and others have scales which can individually withstand large external forces (Bruet et al., 2008; Yang et al., 2013; Zimmermann et al., 2013). In the case of modern bichirs (*Polypterus* sp.), there are thick peg and socket joints connecting the scales, which are made up of layers of a dense mineralised tissue called ganoin, making the integument as a whole particularly tough (Kerr, 1952; Smith et al., 2006; Song et al., 2011).

e) Parasites and antifouling

Parasites are a ubiquitous problem for most aquatic animals and have a long fossil record (e.g. Cressey, 1989), although there are frequently difficulties associating them with specific hosts. Evidence for external parasitism of fishes can be found as early as the Middle Devonian (~385 mya), in taxa such as heterostracans, antiarch placoderms, and sarcopterygians (Lukševics et al., 2009). Just as barnacles compromise the streamlining of ships, there is a well-documented deleterious influence of ectoparasites and other epibionts on drag in fishes (e.g. Wagner et al., 2003; Östlund-Nilsson et al., 2005; Binning et al., 2013) and a range of other marine taxa (e.g. Wahl, 1996; Bates & Loydell, 2003; Donovan et al., 2003). Many parasites of pelagic sharks have highly specialised adaptations to hold their bodies close to the surface (e.g. Benz, 1992), but it has been suggested that smoother, flatter scales are relatively easier for the parasite to attach to (Raschi & Tebit, 1992). There is also a relatively low incidence of ectoparasitic attachment in sharks with spiney and spine-like scale types (Reif, 1985). Spined and spine-like scales occur in the birdbeak dogfish (*Deania calcea*) which has a dense covering of almost vertical trident-like denticles, presenting a very unappealing attachment surface for epibionts (Reif, 1985a). This is thought to be the principle function of such scales, especially in schooling sharks (Reif 1985a), and similarly shaped scales have been reported in a range of fossil taxa (e.g. Martill et al., 2013; section 4.2).

f) Other non-hydrodynamic functions

Little has been written about unusual scale functions in non-chondrichthyan taxa, however a role in mating and spawning has been suggested for the modern roughbelly darters (*Percina* sp.), which have ctenoid scales with long backward-pointing spines (Page, 1976).

In bioluminescent sharks protection can be afforded from blocky and shallow scales for abrasion resistance (e.g. *Etmopterus virens*), or elongate spiny scales that resist parasite attachment (e.g. *Etmopterus spinax*). Despite this variation (even between closely related species), all reflect a trade-off between a protective function, and the requirement to expose the photophore-rich epidermis between the scale bases (Reif, 1985b). However, this condition is rare; restricted to just two squalid subfamilies; the kitefin (Dataltiinae) and lantern sharks (Etmopteridae).

Alternative functions of the spiney, or spine-like scale type for sharks includes aiding juveniles split the eggcase during hatching (Grover, 1974), and even feeding as discovered recently. The small-spotted catshark (*Scyliorhinus canicula*) has scales which protrude more towards the tail region (Figure 2.19), originally suggested to be a hydrodynamic adaptation (Bone, 1975). Recently however, these sharks have been observed bracing large food items with their tails, anchoring it in place to bite more effectively. This behaviour is particularly common in juveniles, whose scales protrude from the tail surface an order of magnitude more than the adults', and which can tackle larger, otherwise unavailable prey (Southall & Sims, 2003). While it is probable that this behaviour occurs in other species, it should be noted that only a small proportion of the denticles are involved in this feeding action, and for the majority parasite resistance is still their likeliest primary function.

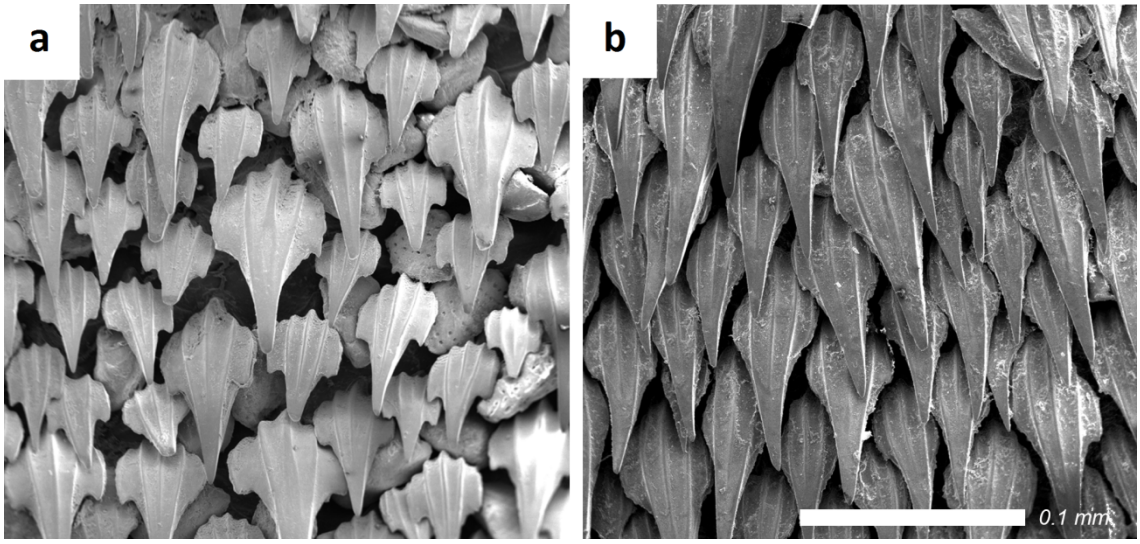

Figure 2.19. Dermal denticles from a) the flank ('FB2', Figure. 3.3); and b) the tail ('T1', Figure 3.3) of the small-spotted catshark *Scyliorhinus canicula*. Adult male specimen from Pembrokeshire, United Kingdom, 535mm total length.

g) Scale histology of Palaeozoic fishes

Scale histology is an important field in modern ichthyology and palaeontology, allowing the study of tissue development and the early evolution of skeletal mineralisation (e.g. Donoghue, 2002; Donoghue et al., 2006; Sire, 2009). The focus of this thesis is the external morphology of scales, and physical interactions with the immediate environment. Yet, as discussed the majority of fishes have scales which sit in a pocket of soft tissue (Figure 2.17), the properties of which cannot be accounted for if only hard parts are preserved during fossilisation. Soft tissue features can have a significant effect on drag (section 2.3.2), so it is important to understand this potential source of error. The primitive fish condition is a dermal (skin) skeleton composed of discrete mineralised (dentine) units known as odontodes (Qu et al., 2013; Figure 2.20). In most modern fishes this dermal skeleton has been lost (except for 'teeth' proper, fin spines, and rarely throat denticles), except in modern chondrichthyans (sharks, rays and ratfishes) which have a well-developed dermal skeleton of placoid scales. These scales are single odontodes (monoodontode) which do not grow continually, but are rather replaced with larger developing scales (Hanke & Wilson, 2010). Thelodonts are the only other group to have monoodontode scales, unlike other primitive Palaeozoic taxa in which the scales formed from multiple odontodes (polyodontode) attached to a bony base (Sansom et al., 2001). Polyodontode scales grow larger without being shed, suggesting there may have been a soft tissue covering, and not fully exposed to the water (Qu et al., 2013). Groups reported to have taxa with polyodontode scales include early chondrichthyans, osteostracans, heterostracans, 'placoderms', osteichthyans, and early 'acanthodians' (e.g. Denison, 1979; Karatajūtė-Talimaa, 1995; Sire et al., 2009; Qu et al., 2015).

While it is reasonable to assume thelodont scales were exposed directly to fluid flow, other groups are more difficult to interpret. For example the 'acanthodians' are known to be paraphyletic, with some members classed as osteichthyans (bony fishes), and others as stem chondrichthyans (Brazeau, 2009; Zhu et al., 2013). Relatively extensive histology of 'acanthodian' scales has shown most grow by the concentric addition of surrounding layers, meaning soft tissue would have surrounded and covered the crown. However, a select few 'acanthodians' (e.g. *Nostolepis robusta*) grow by adding to the sides and base (Denison, 1979; Karatajūtė-Talimaa, 1998). Additionally, it has been suggested that 'acanthodians' (and some ray-finned fishes) are capable of post-eruptive repair and growth. The scale would erupt, periodically sink in to the dermis and then re-erupt (Reif, 1982; Sire et al., 1987; Donoghue, 1998; Donoghue & Purnell, 1999), exposed directly to the immediate environment. The only reconstructions of epidermal tissue in the integument of Palaeozoic fishes (Reif, 1982), shows the odontodes at least partially exposed (the extent of which is unknown), a view supported by

current workers (personal communication Zerina Johanson). This and other potential limitations, justification for the inclusion of taxa, and experimental design are discussed next.

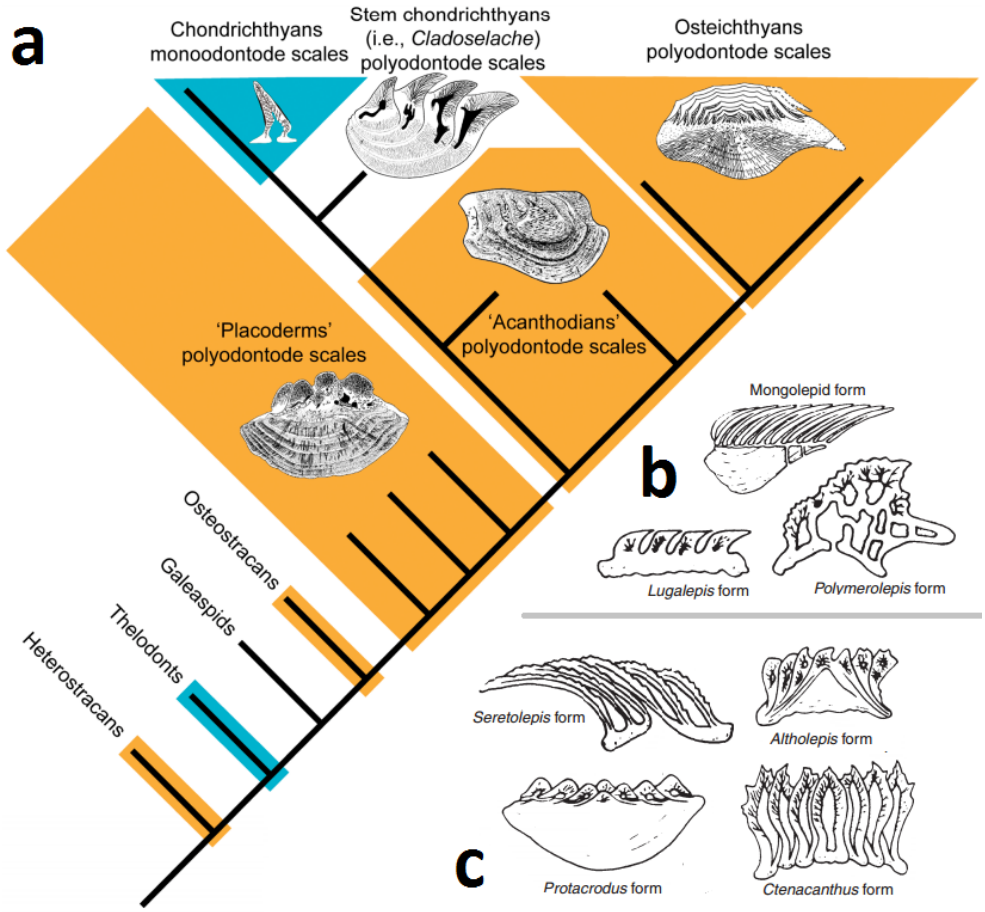

Figure 2.20. a) Simplified phylogeny of Palaeozoic vertebrates showing incidences of monoodontode (blue) and polyodontode scales, with cross sections of the osteichthyan *Cheirolepis*; the acanthodian *Nostolepis*; the chondrichthyan *Cladoselache*, and the placoderm *Ohiolepis*; b) 'non-growing' forms of putative chondrichthyan, and; c) 'growing' forms of putative chondrichthyan scale. From a) Qu et al., 2013 and; b-c) Hanke & Wilson, 2010.

2.7. Limitations of Research to Date

A primary aim of this project was to empirically measure the drag-reduction of fossil fish skin for the first time. That this has not been attempted previously reflects the theoretical and practical limitations, and the complex interactions of abiotic and biotic factors affecting drag.

a) Material and modelling

Vertebrate microremains or 'ichthyoliths' are often the only available early Palaeozoic vertebrate fossils (Janvier, 2015). As gross morphology is often the focus of biomechanical studies, this has undoubtedly limited attempts to model the hydrodynamics of these early fishes.

From a practical perspective, any accurate modelling (physical or otherwise) requires a good replica of the structure being studied. Ideally this would be real material e.g. fresh shark skin (Lang et al., 2014), but this is not possible with extinct organisms as fossil material is often highly altered, valuable and fragile (although see Alexander, 1984; Albert et al., 2009). Alternatives can include a moulded cast (e.g. Han et al., 2008), manual rendering (e.g. Aleyev, 1977; Rickards et al., 1998), or rapid prototyping (e.g. Bartol et al., 2002; Wen et al., 2014). Rapid prototyping has been in development for decades, but only recently has it become widespread and cost effective enough for practical use. Any artificial model will have flaws, whether due to human error or the manufacturing process, and all systems of measurement have limited resolution. A common solution is for structures to be scaled up to minimise these sources of error (e.g. Lang et al., 2011), while accounting for the change in Reynolds number. In some cases the model's verisimilitude can be compromised to minimise the influence of variables beyond the research focus (e.g. Melchin & Doucet, 1996). In all but the most complex systems, simplifying or isolating one aspect of a structure is an effective way of studying its mechanics. An advantage of rapid prototyping is that the geometry of a three-dimensional object can be modified to test a range of morphologies, with much greater precision and speed than traditional rendering. Additionally, this improves replication, and allows concomitant testing using computational fluid mechanics.

b) Soft tissue

Regardless of growth or internal structure, most fish scales are covered in epithelial tissue of varying thickness (Figure 2.19a-c.) which can help reduce drag in various ways (section 2.3.2). Therefore fossilised surfaces may not reflect the texture or properties of the skin as it would have been in life, a significant problem for modelling. Palaeontological fluid mechanical studies have all but ignored soft tissue, concentrating instead on gross morphology of animals with hard exoskeletons e.g. trilobites (Miller, 1975; Fortey, 1985), eurypterids (Plotnick & Baumiller, 1988), crinoids (Baumiller & Plotnick, 1989; Plotnick & Bauer, 2014), cephalopods

(Chamberlain & Westermann, 1976), brachiopods (Alexander, 1984), and others. In this respect, those studies modelling active flow control (such as fins or tails) of soft-skinned animals are potentially the most flawed, because of the variable flexibility of structures (section 2.3.3), the precise shape of which must be subjectively approximated (e.g. DeBlois, 2013).

c) Interdisciplinary applications

Despite their popular appeal and the huge interest in biomimetic drag-reduction technologies, the study of riblet optimisation has never been quantitatively applied to shark ecology. Seminal work by Reif (1985) reported a correlation between ecology and scale morphology but at the time the mechanism of riblet action was not fully understood. Furthermore, the scheme for interpreting scale function (Reif, 1982b) has yet to be extended to include extinct fishes. Those papers describing thelodont and 'acanthodian' scales occasionally mention modern sharks for analogy (e.g. Märss, 2007), but are never more than cursory comparisons. Herein, the function of scale morphotypes will be discussed and interpreted for both modern sharks, and the extinct thelodonts and 'acanthodians', supported by experimental analysis.

3. Methods and Materials

This thesis presents data for both comparative analyses and an experimental approach to investigating fish scale function. Methods and materials for the comparative approach are described first in sections 3.1, excluding elements that strongly informed the design of the concomitant flume experiments, which are detailed in section 3.2.

3.1. Functional morphology and comparative anatomy study

3.1.1. Body regions

It has long been recognised that denticles are highly variable between species, including extinct, non-chondrichthyan taxa such as thelodonts. Dermal denticle morphology is known to be equally, and sometimes more, variable between the body regions of a single species, now demonstrated in a large number of taxa (particularly Reif, 1985a). The morphological variety of scales across the body is now routinely accounted for and reliably recorded in articulated modern material, but this is still an issue for palaeontologists, especially those attempting to classify isolated scales. Regionalisation can also be problematic when attempting to interpret a general function for the scale set as a whole and ultimately the species.

In fossil taxa such as thelodonts which are rarely preserved as articulated specimens, regional morphologies are usually presented as scale sets to justify erecting novel taxa (e.g. Turner, 1999). Several methods of dividing the body have been proposed for thelodonts (Figure 3.1), but all recognise three distinct regions; the rostrum, pre-pectoral and post-pectoral or flank. The body regions of thelodonts, 'acanthodians' and sharks were standardised for comparison (Figure 3.2). The rostral or pre-orbital zone extends from the snout to the back of the eye, after which the pre-pectoral region extends to where the back of the pectoral fin attaches to the body. The flank extends from the pectoral fin attachment to the peduncle (or its equivalent) of the tail, not including fins.

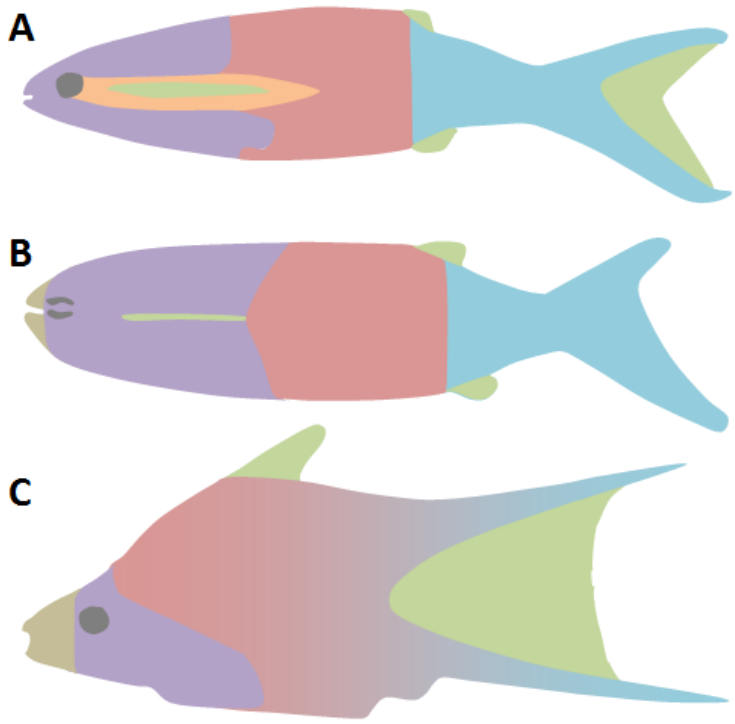

Figure 3.1. Schemes and terms applied for differentiating body regions in thelodonts, including the mouth/rostral area (brown), pre-orbital (purple), postpectoral or trunk (red), and the tail region or precaudal (blue). A) *Loganellia scotica* after Märss & Ritchie, 1997 further defining lateral (orange), and pinnal scales (green); b) *Phlebolepis elegans* after Märss, 1986; and c) *Furcacauda fredholmae* after Wilson & Caldwell, 1998.

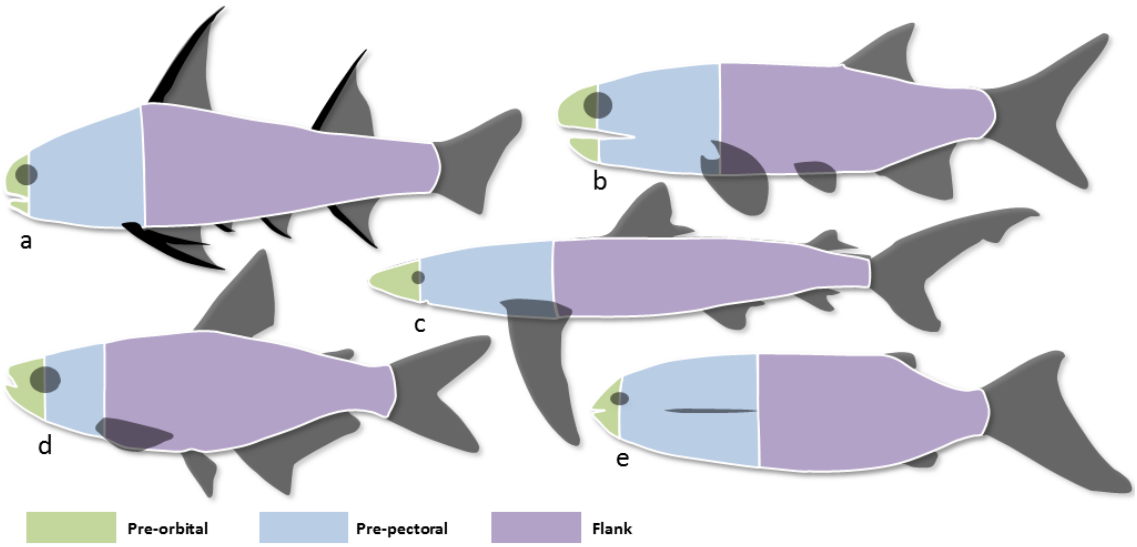

Figure 3.2. Standardised scale regions for taxa referenced in text. A) an 'acanthodian'; b, an early osteichthyan; c) a modern shark; d) a modern teleost; and e) a thelodont agnathan. Based on Reif, 1985; Märss, 1986; Märss & Ritchie, 1998; and Wilson, 1998.

3.1.2. Specimens and sampling

a) Specimens and taxa selection

Modern shark taxa were selected on the basis of their availability, and to represent the diversity of gross morphology, scale types and ecologies (Table 3.1). Fresh cadaverous material of *Lamna nasus*, *Squalus acanthias* and *Squatina squatina* was sourced from the Centre for Environment Fisheries and Aquaculture Science (CEFAS) and *Scyliorhinus canicula* was found beached in Pembrokeshire, UK. Taxidermied specimens of *Chiloscyllium plagiosum*, *Chiloscyllium punctatum* and *Centrophorus granulosus* were sourced from a commercial supplier based in the Philippines.

A wide range of fossil fish material from a number of institutions was examined for comparative analysis and to inform the plate design of the experimental study (section 3.2). Particular focus remained on Palaeozoic taxa, especially those with dermal denticles, of which notable specimens are detailed in Appendix II, Table S2.1. While this was very useful, the majority of quantitative scale data for Palaeozoic taxa were taken from the literature, particularly figured scales in macroscopic photographs and scanning electron micrographs. These were measured in the same way as the modern material. For details of fossil taxa selected for the experimental analysis see section 3.2.

c) Sampling and microscopy

For modern taxa total body length was measured (tip of snout to end of tail) of frozen and dried cadaverous specimens (Table 3.1), before 10mm^2 skin samples were taken at 19 standardised sampling locations (20, including male-specific claspers), shown in Figure 3.3. To produce dorsal-view scanning electron micrographs (Appendix I, Figures S1.6-1.10, S1.23-1.27) skin pieces were manually cleaned of excessive underlying soft tissue, sterilised with ethanol and dried between filter paper under a light weight. These dry, flat squares of skin were mounted on to 12mm diameter aluminium stubs with graphite adhesive, and gold coated before imaging.

Table 3.1. Details of the shark specimens sampled for this study

Species	Order	Ecology	Length (mm)	Sex	Utility to Present Study
Centrophorus granulosus (Bloch & Schneider, 1801)	Squaliformes	Pelagic	480	M	Crown dimensions
Chiloscyllium plagiosum (Anon [Bennett], 1830)	Orectolobiformes	Demersal	680	M	Comparative anatomy
Chiloscyllium punctatum (Müller & Henle, 1838)	Orectolobiformes	Demersal	730	F	Comparative anatomy
Lamna nasus (Bonnaterre, 1788)	Lamniformes	Pelagic	1270	F	Scale width, riblet spacing, angle, and number
			1860	F	As above
			2150	F	As above
			1460	M	As above
			1830	M	As above, and scale base geometry
Scyliorhinus canicula (Linnaeus, 1758)	Carcharhiniformes	Demersal	535	M	Comparative anatomy
Squalus acanthias (Linnaeus, 1758)	Squaliformes	Pelagic	1020	F	Comparative anatomy
Squatina squatina (Linnaeus, 1758)	Squatiniformes	Demersal	1240	F	Comparative anatomy

Sex determined by presence or absence of genital claspers. Length (mm), measured as maximum distance from tip of rostrum to tip of tail. Cadaverous material acquired from both commercial sources, and the Centre for Environment Fisheries and Aquaculture Science (CEFAS), UK.

Previous work on the skin of mako sharks (e.g. Lang et al., 2008) has revealed a bristling action of shark scales, and a long and thin base in a direction perpendicular to the streamline is thought to accommodate a pivoting action. To explore the distribution of bristling scales, the aspect ratio of the scale base was investigated in the porbeagle shark *Lamna nasus*. The 183cm male porbeagle was the largest male, and was selected for the scale base investigation as it also enabled sampling of the genital claspers, an area of presumably low bristling. Measuring the aspect ratio of the denticle bases required isolating the scales from the soft tissue. To examine 3D structure in more detail, sample material remaining from the SEM mounts was soaked in 35% H_20_2 for 24-48 hours to remove soft tissue. Isolated scales were carefully washed, dried, mounted on stubs with adhesive strips, and then gold-coated for SEM imaging. A selection of *Chiloscyllium punctatum* and *C. plagiosum* scales was treated in the same way for qualitative analysis.

3.1.3. Comparative analyses

a) Qualitative analysis

Simple observations including sketches and photographs were recorded of examined material, with particular reference to scale morphology and functional interpretation. Comparisons of the dorsal surface of the scale crown were prioritised, especially in the early stages of the project. This was to assess the occurrence and adaptations for drag reduction at the exposed surfaces, riblets, turbulising structures and ultrasculpture (microscopic ornament). As each specimen was examined, these features were drawn and/or described, and interpretations of function compiled in a dataset alongside stratigraphic and body region data. Scales of different species were only compared with other scales from the same region of the body, as it was know that scale morphology could be highly variable (e.g. Reif, 1985a). This broad and traditional approach was an important basis for the entire project, and helped substantiate original and published hypotheses of scale function. A scheme for the functional classification of fossil fish scales was constructed, and from this the functions of flank scales of over 200 taxa were proposed (sections 4.2 and 4.3). Scale type occurrence throughout geological time was then compared to the incidence of scale types in modern sharks, providing additional insight into the palaeoecology of the extinct species.

b) Modern shark scale variation

Measurements were made of 15-20 scales per sample using ImageJ (U. S. National Institutes of Health, Bethesda, Maryland, USA, http://imagej.nih.gov/ij/, 1997-2014). Where scale features

were not clear or measurable (e.g. proximal pectoral fin 'P1', Figure 3.3), or organs such as the claspers were missing, data were omitted. This method allowed for scales with converging or diverging riblets to be included in the riblet spacing analysis, although as discussed later, heavily converging or diverging scale types were not included in the interspecies (multi-taxon) riblet spacing study. Mean riblet spacings were calculated from 15 measurements, taken evenly across the crown surface of each denticle (Figure 3.4). As a result the porbeagle dataset consisted of approximately 20,400 individual riblet spacing measurements, in addition to the concurrently recorded exposed scale width, length, riblet number, and riblet angle, described next.

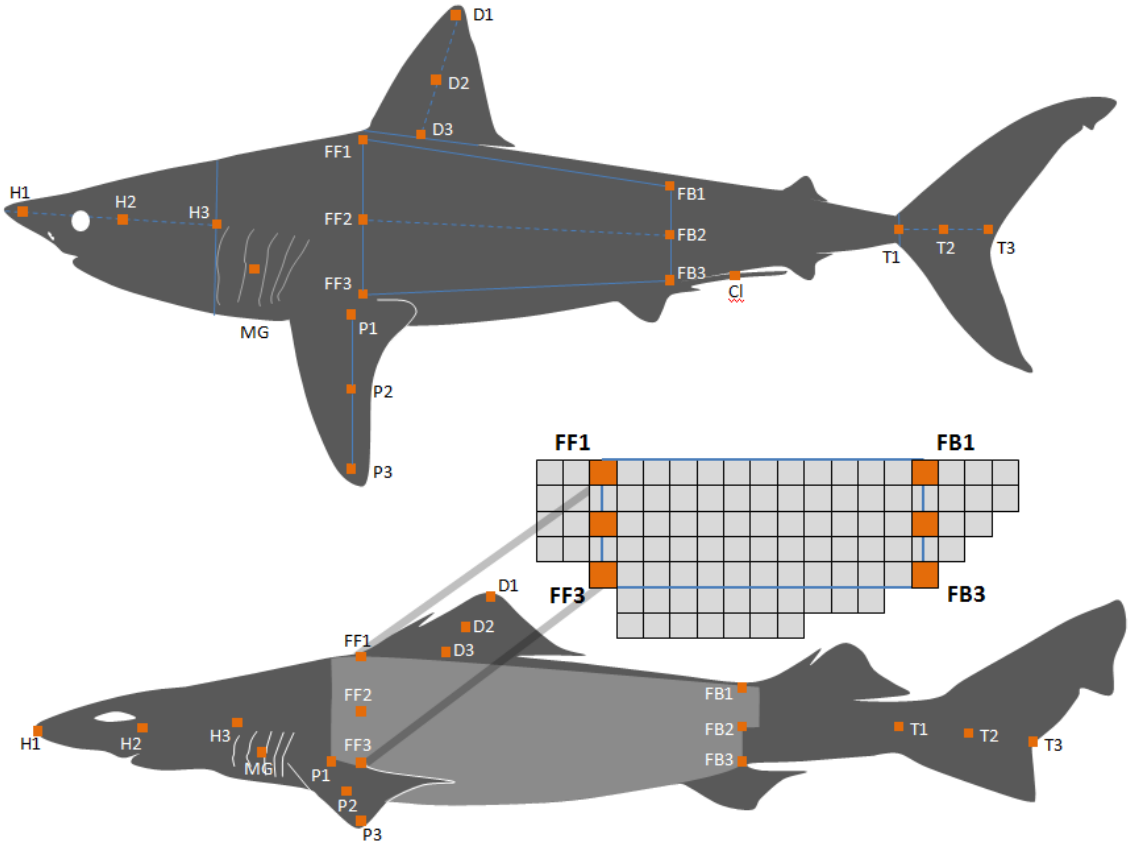

Figure 3.3. A) Standardised sampling locations for shark specimens (*Lamna nasus* shown) and; b) sampling locations and a higher density sampling grid specific to *Centrophorus granulosus*. Locations are; H1, tip of rostrum; H2, middle of head; H3, back of head at start of gills; MG, exposed outer skin from the central gill; P1, proximal dorsal surface of pectoral fin; P2, middle dorsal surface of pectoral; P3, distal dorsal surface of pectoral; FF1, top of flank anterior along vertical transect running upwards from the back of the pectoral fin; FF2, midline of flank anterior along same transect; FF3, bottom of flank anterior along same transect; D1, distal-most point of dorsal fin; D2, middle of dorsal fin; D3, centre proximal-most point of dorsal fin; FB1, top of flank posterior along vertical transect running upwards from the back of the anal fin; FB2, midline of flank posterior along same transect; FB3, bottom of flank posterior along

same transect; Cl, centre of pelvic clasper; T1, proximal centre of tail/caudal fin; T2, middle of tail along axial midline; T3, distal-most of axial midline where the caudal fin forks inwards. Images not to scale. For ease of reference, a simplified version of this figure is presented in section 6.1. Semilandmarks for heat mapping were equidistant between FF1 –FB1, FF2-FB2, FF3-FB3.

Scale width was measured as the maximum exposed distance from one side of the visible scale crown to the other, perpendicular to the stream direction. Exposed crown length was measured as distance of the visible crown in the stream-wise direction (Figure 3.4). Riblet angle (convergence or divergence of riblets in the streamwise direction) was calculated by measuring the downstream angle of riblets on the left of the scale crown (Figure 3.5, 'Angle 1'), and subtracting the angle of those on the right (Figure 3.5, 'Angle 2'). In most cases these were riblets either side of the largest central rib (as in Figure 3.5). Positive values using this method signified riblets were converging, and negative values were diverging in the stream-wise direction.

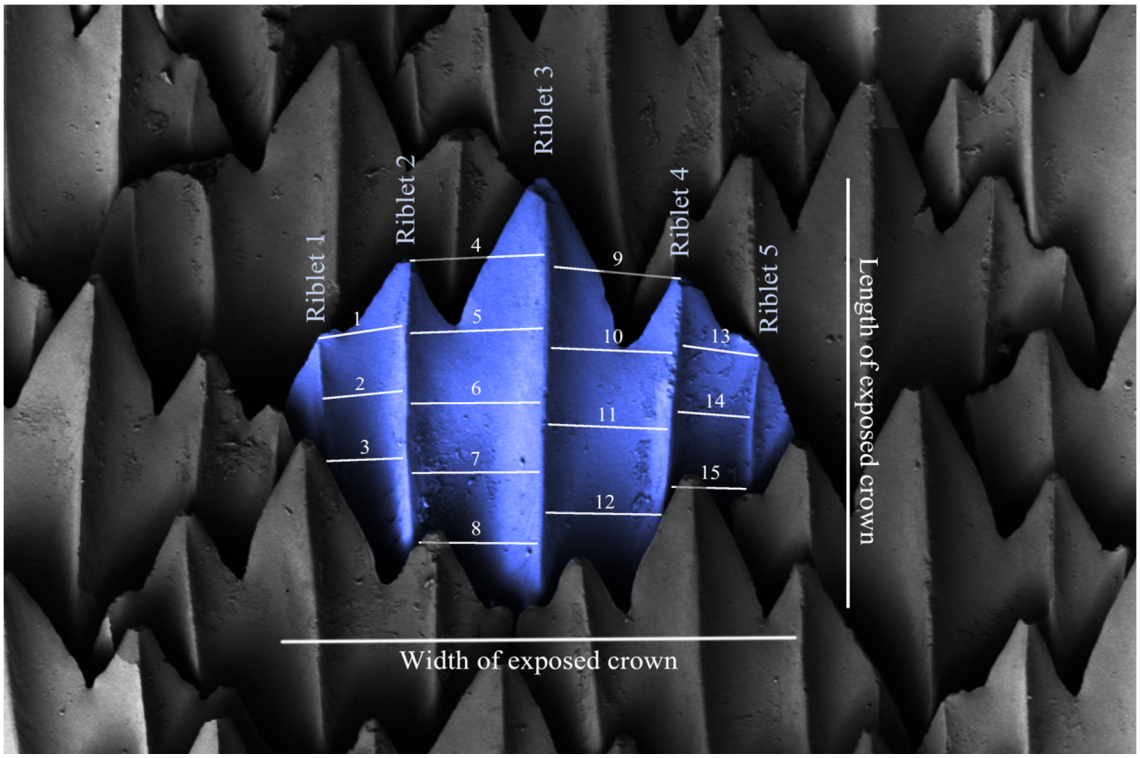

Figure 3.4. Example of evenly distributed riblet measurements of a flank scale of *Carcharhinus brachyurus* (copper shark). Image modified for illustrative purposes courtesy of Sue Lindsay, Microscopy and Microanalysis Unit, Australian Museum, Sydney.

The width (perpendicular to streamwise direction) and length of the bases of *Lamna nasus* denticles were also measured in ImageJ, and the aspect ratio calculated as width divided by length. Body region "heat maps" were then produced using Matlab (The MathWorks, Inc.). Means of a given variable e.g. riblet spacing, riblet number, scale width, riblet angle etc. were applied to the sampling locations defined in Figure 3.3. These landmarks of known value were then used for interpolation across a 2D lateral aspect image of the species, with the relative influence of each landmark defined by its standard error. The influence of the dorsal and pectoral fins, although connected to the flank, had a disproportionate influence on the proximal flank values of the heat maps. To reduce this effect, additional, intermediate landmarks were calculated between flank landmarks. Colour schemes were assigned to width and length (black to white), aspect ratio (dark blue to white), riblet angle (dark blue to red), and riblet spacing measurements (dark red to white) to visually differentiate these data types. Data were checked for normality using Shapiro-Wilk tests, before Student's t-tests for significant difference were used for directly comparing two groups, and Tukey's range test used for whole body comparisons to minimise error. Tests including descriptive statistics were performed using Excel (Microsoft) and PAST (Hammer et al., 2001) software packages. Significance was accepted when $p < 0.05$.

c) Riblet spacing analysis

To determine the relative size of different body regions, lateral aspect images of representative members of extant fish families were traced using ImageJ. These were sourced from one text (Nelson, 2006) to ensure consistency of artistic representation of the taxa. From this the two dimensional area of the body regions could be calculated; namely the preorbital, prepectoral, and postpectoral (Figure 3.2). In total 123 lateral view images were analysed, representative of 119 families of extant fishes. To monitor the accuracy of this process, the full area of the fish was traced and the area calculated, against which the sum of the three areas could be compared and the discrepancy calculated. The process was repeated until a difference of below 1% was achieved. Rays, skates and other dorso-ventrally flattened demersal fishes were not included, as in these groups extensions of the pectoral fin often precluded their being processed in this way.

The results of this investigation (Appendix I, S1.5) showed that mean largest area was the flank (74% area), followed by the post-orbital (20%) and pre-orbital (6%). This and an analysis of 50 modern shark species (Appendix I, Table S1.30) using an alternative body region standardisation, yielded similar results (S1.28-2.29). This informed the decision to use the flank

(as discussed, a hydrodynamically significant region) as representative of the fish's squamation. However, it was first necessary to gain a better understanding of the variation of scale morphology within these body regions to justify comparisons between species. This was achieved by comparing the riblet spacing of different body regions in *Lamna nasus*, which confirmed that the flank (sampling locations 'FF1-3' and 'FB1-3', Figure 3.3) is an area of low variation compared to other smaller regions. Data are presented in full in results Chapter 7. Flank scales are also more commonly reported than other scale types, making them good candidates for a systematic approach to functional interpretation.

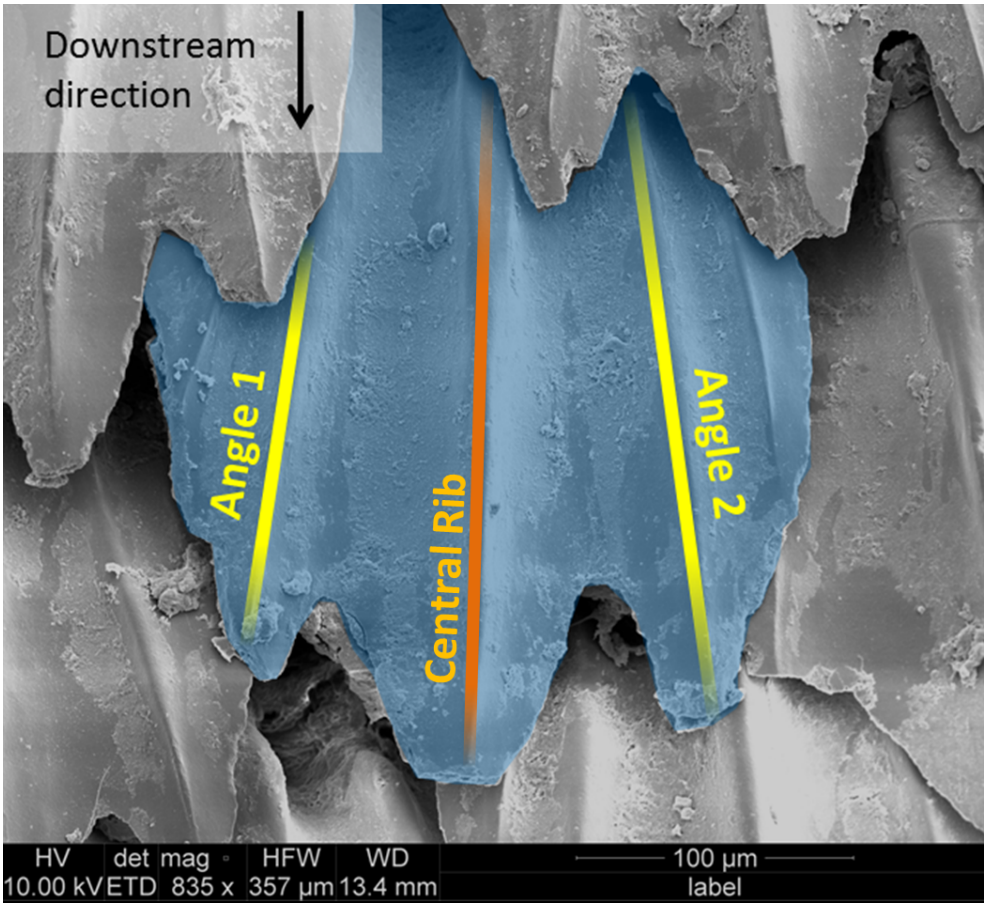

Figure 3.5. Technique for measuring riblet angle. This scale crown shows one central riblet (orange) surrounded by two at diverging angles in the downstream direction. Riblet angle was calculated as the downstream angle of the left riblet(s) relative to the central riblet ('Angle 1) minus the downstream angle of the right ('Angle 2'). Negative values indicate diverging in the down-stream direction, and positive values are converging in the downstream direction. In this example from the mid-gills of *Lamna nasus* ('MG', Figure 3.3), the angle is -18˚ (diverging).

Scanning electron micrographs of the flank region of 50 modern sharks, were analysed, from both newly imaged and existing figured material. In all cases images detailed the crowns of the denticles that are often still embedded in the skin and articulated. Fossil material was rarely articulated, but isolated scales were only included if they were from the flank region, sometime referred to as the 'trunk'. There were 11 extinct fishes with riblets that met this requirement, of which six were 'acanthodians' and five were thelodonts. Riblet spacing measurements were taken using ImageJ software, as the linear distance between riblet peaks. Where possible 15 measurements were taken, evenly distributed across the scale surface regardless of the number of riblets (e.g. Figure 3.4), with several measurements along the length of the riblet-formed grooves. This method helped correct for sub-parallel riblets, and those scales whose riblets were larger towards the centre, ensuring a reliable mean measurement for the entire crown. In modern sharks a maximum of 15 scales were measured per sample, although several flank sample locations from the same shark were also included for some taxa to calculate overall mean riblet spacing for the flank. Number of scales analysed, total measurements, and sample references for each taxa are detailed in Appendix I.

For consistency, extant shark speed categories were based principally on Reif's (1985a) classification. Those not included in his scheme were assigned a group based on ecological similarity to a species of known category. For example the uncategorised great hammerhead shark *Sphyrna mokarran* has a very similar ecology to the thresher shark *Alopias vulpinus*, a 'fast' species in Reif's scheme. Available ecological data include relative speed of known prey items, migratory records, satellite tracking, and in a small number of cases direct speed measurements (Appendix I, Table S1.32).

The relationship between riblet spacing (the only morphological scale trait used) and swimming speed in sharks was investigated initially with standard descriptive statistics and a Student's T-test of difference between the groups. However, feedback from an anonymous reviewer prompted efforts to account for possible phylogenetic signals. Co-author Dr Mark Bell performed phylogenetic least squares regression (PGLS) using the pgls function in the 'caper' package for R (Orme et al., 2013). The 229-species shark phylogeny of Vélez-Zuazo and Agnarsson (Velez-Zuazo & Agnarsson, 2011) was used since it is the most complete and includes 41 of the species we studied (Appendix I). The response variable 'speed' was a three-state ordinal variable ('Fast', 'Moderate', and 'Slow/Scavenger/Ambush'). The inclusion of discrete variables in PGLS analysis has been shown to give results comparable to multinomial variables (Jetz & Freckleton, 2015).

3.2. Experimental Skin Friction of Fossil Fishes

To investigate the effect of scale shape on skin friction drag, flat plates of reconstructed and rapid prototyped fossil fish squamations were produced. These were submerged in a flume tank, and velocity across the plates was measured using laser Doppler anemometry.

3.2.1. Preliminary scale tessellation study

In order to reconstruct the skin of fossil fishes accurately and help standardise the way repeating scale units tessellate for experimental comparison, a large number of articulated specimens were examined. This included the modern shark samples of section 3.1, and a range of Palaeozoic taxa, detailed in Appendix II. In addition to the shark-like condition, the inclusion of the early oseichthyan *Lophosteus* required the examination of the modern 'ganoid fish' squamation seen in bichirs (*Polypterus* sp.). These are amongst the few surviving members of the 'Chondrostei', a subclass of ray-finned fishes thought to have originated in the late Silurian (the first being *Andreolepis hedei*). Examination of a 460mm (total length) cadaverous specimen of *Polypterus ornatipinnis* (ornate bichir; acquired from the Blue Planet Aquarium, Cheshire) confirmed published accounts of a thick mucus coating of the epithelium which overlies the scales. A similar condition was found in a cadaverous juvenile 116mm long *Polypterus senegalus* (Cuvier's bichir; acquired as waste from a tropical fish retailer).

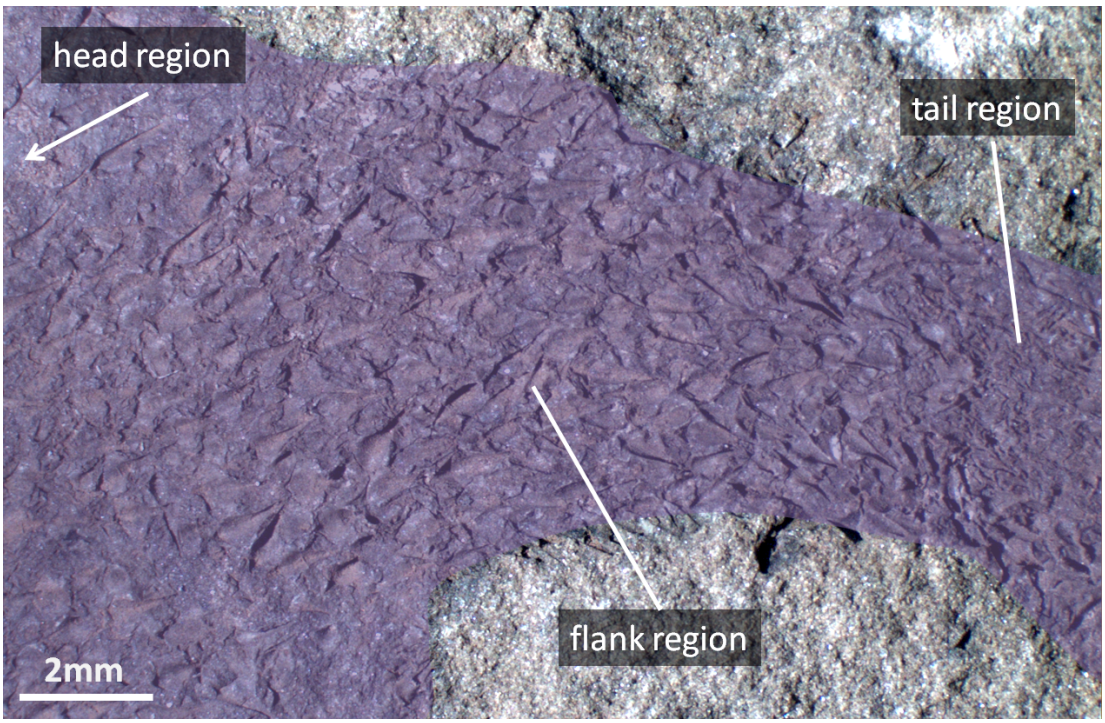

Figure 3.6. An articulated specimen of *Lanarkia horrida* (NHMUK PV42009), highlighted in purple. Detail of the dorsal and flank region with anterior/head region towards the right of the image, scale bar is 2mm.

The flank region was quickly identified as an area of relatively low scale variation in all taxa, modern and extinct. Within the flank region, which was always the largest externally exposed area of the body (see section 3.1) there were subtle changes in morphology towards the fins, head, and tail regions. However, as demonstrated in *Lamna nasus* (section 3.1) this variation was much lower than in other body regions. Scales of all 'acanthodian' and thelodonts examined formed ordered diagonal rows, with the scale bases either flush to one another or tightly packed. *Lanarkia horrida* (Figure 3.6) was the only exception, with most scales randomly arranged. However, on exceptional specimens of this species the largest spine-like scales are arranged in long rows across the body with smaller scales between them. All other examined thelodont and 'acanthodian' taxa had scales which, in well-preserved articulated remains, tessellated uniformly in diagonal rows (Figures 3.7 and 3.8).

It was also confirmed that directional features of scales from the flank region (such a ridges, spines or tubercles) invariably align with the direction of flow from head to tail. In addition, microscope examination of modern shark skin showed that the neck region of the scale (narrow region between the relatively wider crown and base) is a useful indicator of how deeply it is embedded within the soft tissue.

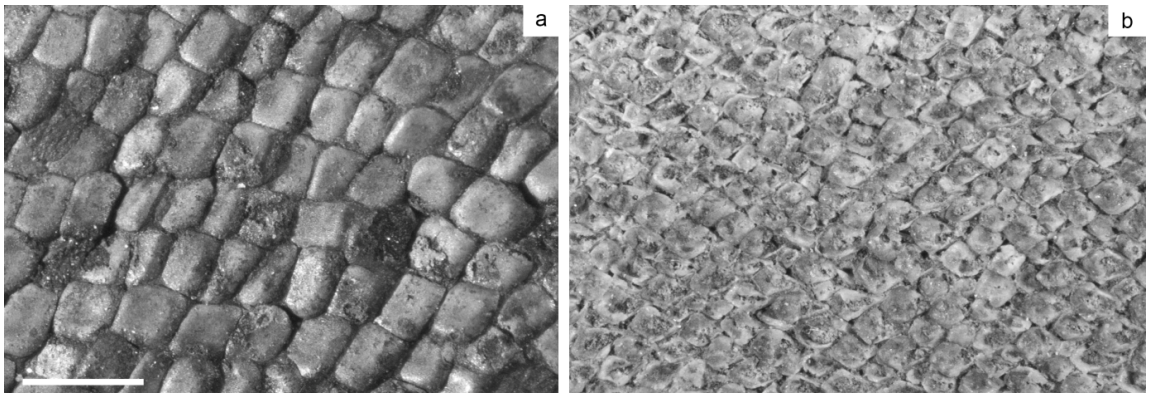

Figure 3.7. The tessellation of thelodont flank scales in articulated material. A) *Thelodus mackintoshi* (NHMUK PV52445) and; b) *Loganellia scotica* (NHMUK PV11282). Scale bar 1mm.

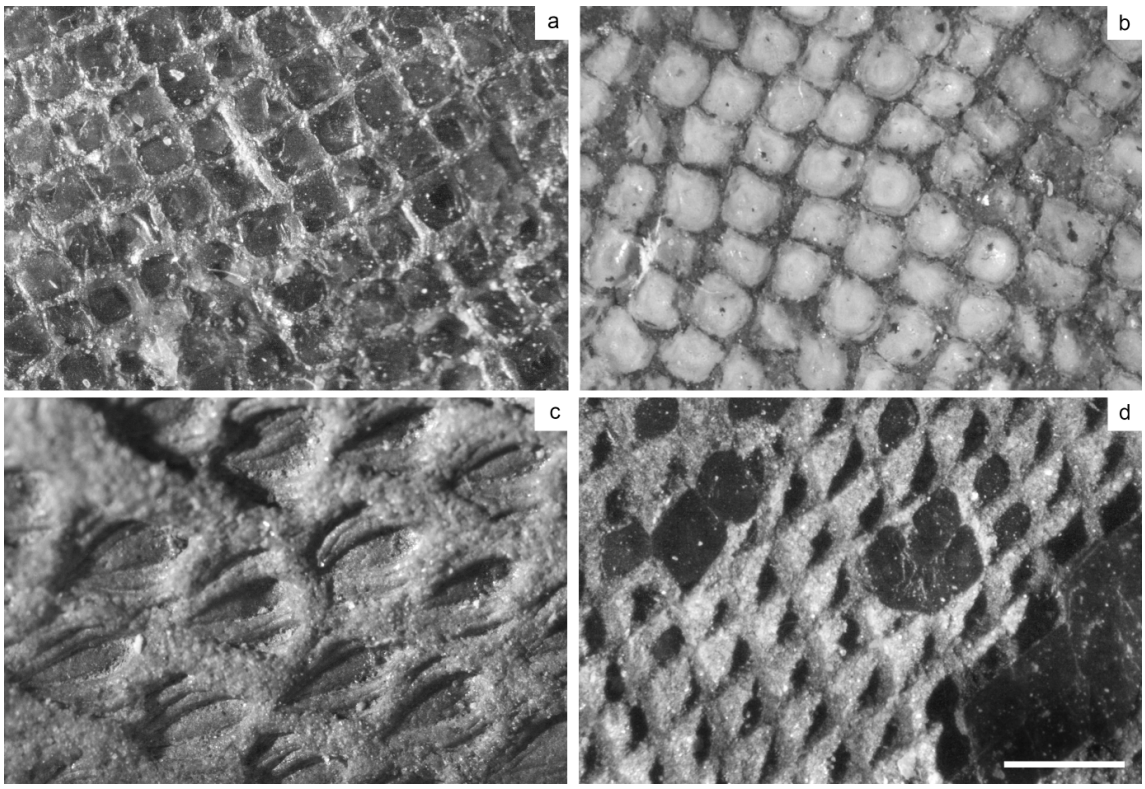

Figure 3.8. The tessellation of 'acanthodian' flank scales in articulated material. A) *Acanthodes sulcatus* (NHMUK P57555); b) *Cheiracanthus latus* (NHMUK PV50105); c) *Ptomacanthus anglicus* (BNHM P19998); d) *Diplacanthus longispinus* (NHMUK PV1369). Scale bar 1mm.

Table 3.2. Fossil material selected for flume experiments.

Species	Higher Taxon	Age	Locality	Material Source	Scan Data
Loganelia scotica	Thelodonti	Silurian	Scotland	Martin Rücklin (MNHN GBP384)	Synchrotron (data donated)
Lophosteus sp.	Osteichthyes	Silurian	Ohesaare Cliff, Estonia	Henning Blom (uncatalogued)	On-site µCT
Nostolepis striata	Acanthodii	Silurian	Ohesaare Cliff, Estonia	Henning Blom (uncatalogued)	On-site µCT
Phlebolepis elegans	Thelodonti	Silurian	Silma Cliff, Saaremaa, Estonia	Henning Blom (uncatalogued)	On-site µCT
Poracanthodes sp.	Acanthodii	Silurian	Ohesaare Cliff, Estonia	Henning Blom (uncatalogued)	On-site µCT

3.2.2. Fossil Taxa Selection and Material

Flank scales were selected to represent the more commonly encountered morphologies in Palaeozoic fishes (Table 3.2), and reflect their diversity of function. Monetary constraints prohibited the testing of more than five rapid-prototyped scale plates, so priority was given to those taxa with hydrodynamical features of interest, discussed next.

a) *Loganellia scotica*

This thelodont (Figure 3.9) has lozenge-shaped flank scales, which are smooth and rounded at the front, tapering to a point at the posterior. This specimen was selected to represent blockier scales, which do not have a pronounced crown or neck region. In articulated material, these scales have low relief, and tessellate tightly to form a rough but relatively simple surface.

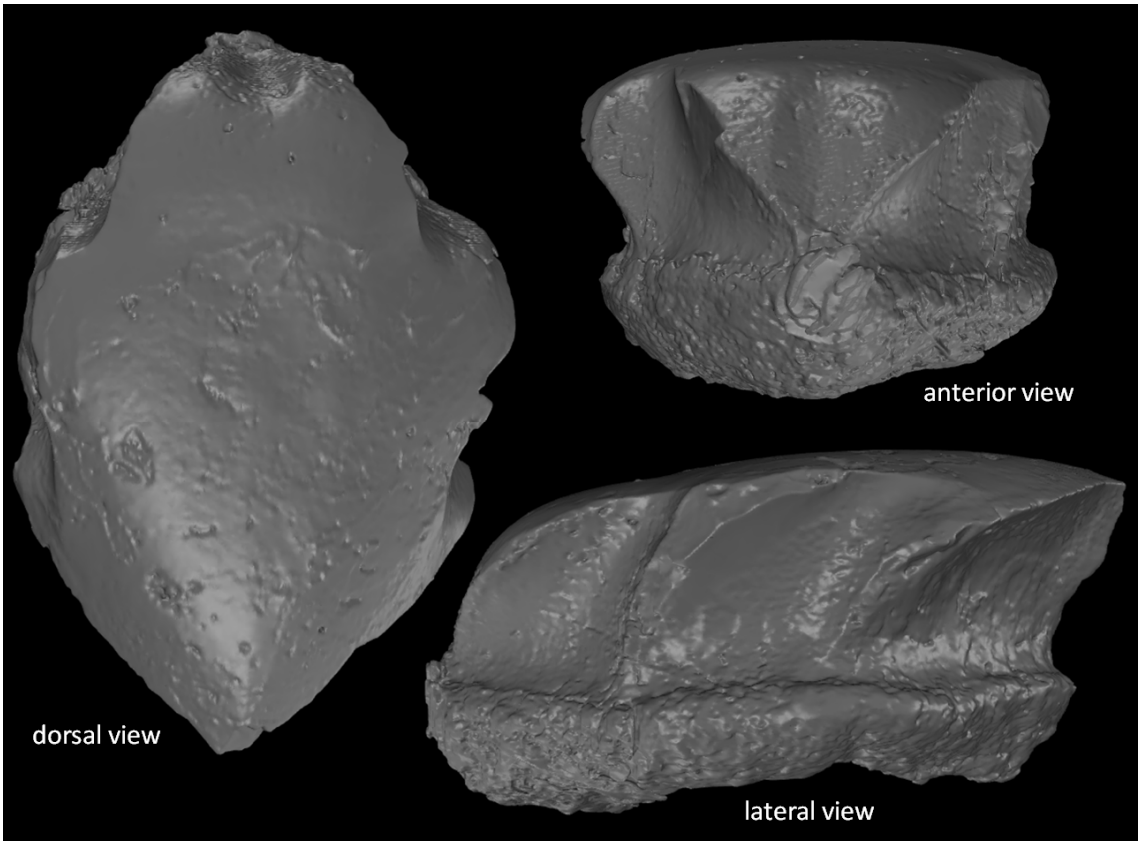

Figure 3.9. High resolution synchrotron radiation X-ray tomographic microscopy (SRXTM) scan of a *Loganellia scotica* (Thelodonti) flank scale, GBP384 (Muséum national d'Histoire naturelle, Paris), from the Silurian of Scotland. Scan data provided by Martin Rücklin, Naturalis Biodiversity Center, Leiden. Figured in Rücklin et al., 2011. Surface mesh lines hidden for clarity, images not to scale, fish scale length is 105µm.

b) *Lophosteus* sp.

Lophosteus is an osteichthyan with thick, robust scales ornamented with large tubercular projections pointing backwards in a streamwise direction (Figure 3.10). This fish is neither an 'acanthodian' nor a thelodont, however the specimen was chosen as it represents blockier but directional scale morphotypes. The scales of this taxon were likely covered in soft tissue (see section 2.7) and mucus as in the modern *Polypterus*. This element of the study aimed to investigate drag-reduction of scale crown shapes rather than specific values for individual taxa, so the inclusion of *Lophosteus* was an interesting way to expand the variety of morphotypes under investigation.

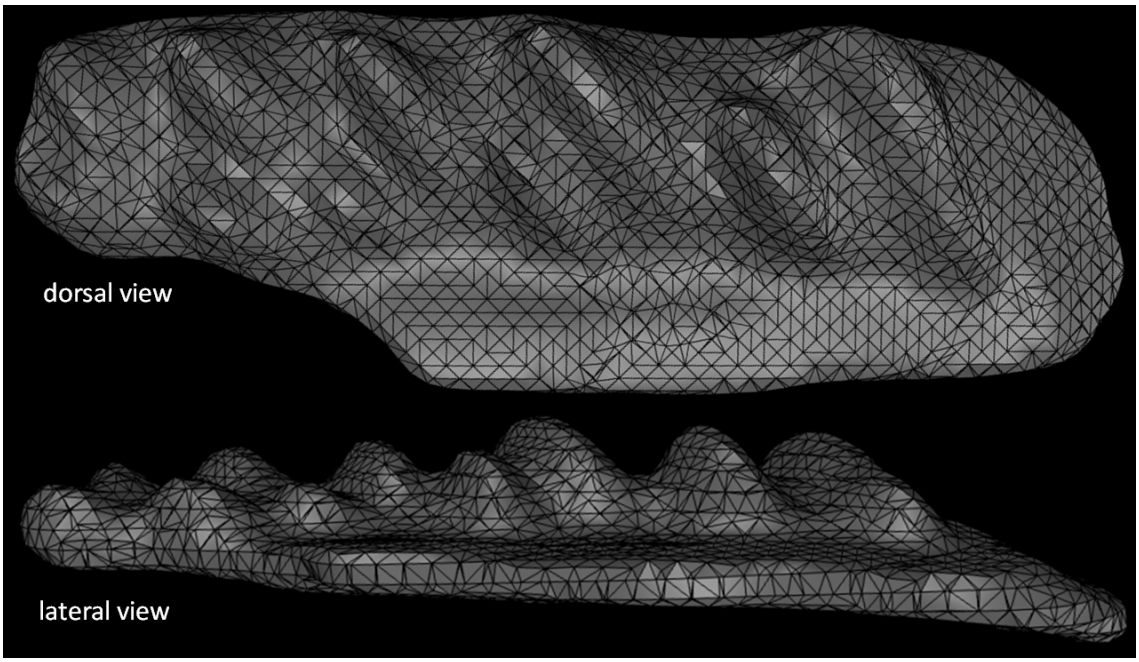

Figure 3.10. X-ray microtomograph images of a *Lophosteus* sp. (Osteichthyes) flank scale from the Silurian of Estonia (Ohesaare Cliff). Specimens provided by Henning Blöm, Uppsala University. Images not to scale, fish scale length is 2.8mm.

c) *Phlebolepis elegans*

Phlebolepis is a common and relatively well-studied thelodont, which has elliptical and fairly flat scales. On the trunk these scales have variable riblets running in a generally streamwise direction, often with a dominant central keel (Figure 3.11). In articulated specimens the scales pack tightly with no overlap. This specimen was selected to represent scales with riblets, although it lacks the distinct neck region of many pelagic shark scales. It should be noted that

while this particular specimen exemplifies the ribletted surface ornament, it is an inconsistent character in this species and as such was not included in the spacing analysis of section 3.1.3c. The focus of the experimental analysis remained on testing the hydrodynamics of different scale morphotypes, rather than any specific taxa.

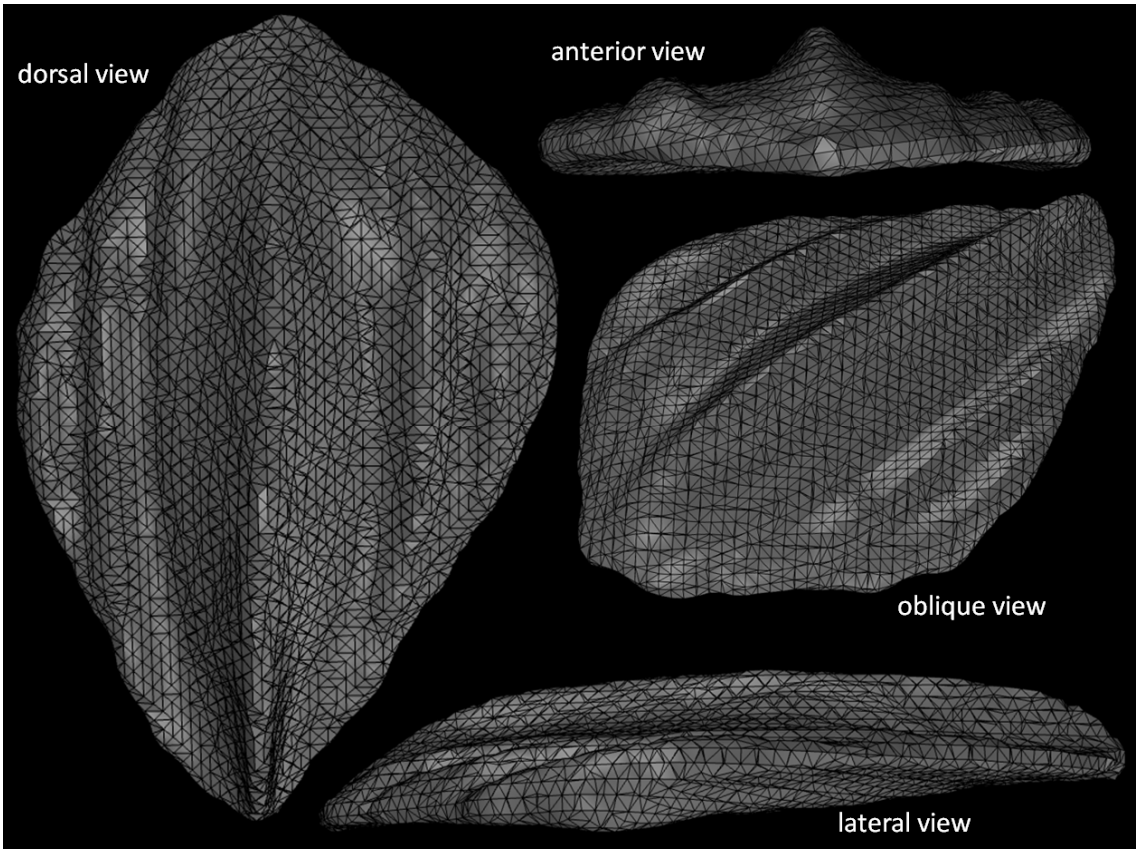

Figure 3.11. X-ray microtomograph images of a *Phlebolepis elegans* (Thelodonti) flank scale from the Silurian of Estonia (Silma Cliff, Saaremaa). Specimens provided by Henning Blöm, Uppsala University. Images not to scale, fish scale is 1.3mm.

d) *Poracanthodes* sp.

This 'acanthodian' has a kite-shaped scale crown with a flat and smooth upper surface, ornamented with small pores (Figure 3.12). Articulated material figured in the literature (Valiukevičius, 1992) shows tight packing of the crowns which occasionally overlap a little at the posterior margins. The specimen was selected to represent the typical 'shark-like' scale shape, with its distinct neck region and large overhanging crown, without the riblets.

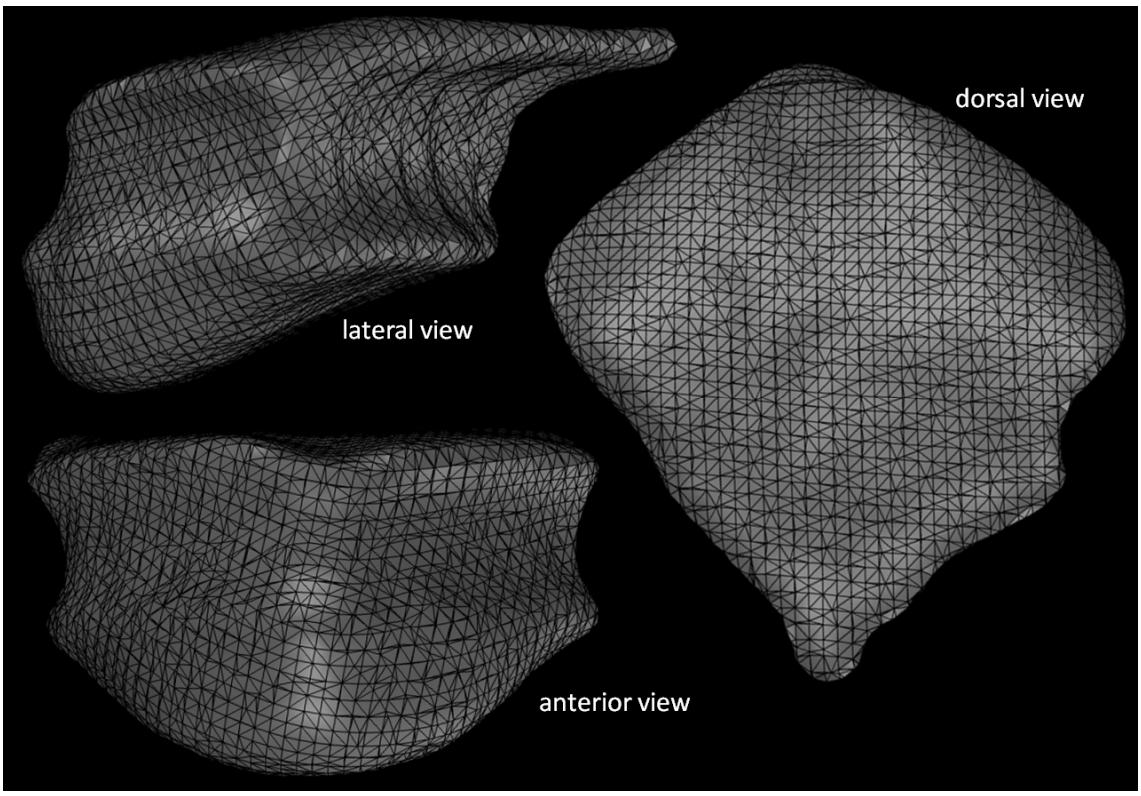

Figure 3.12. X-ray microtomograph images of a *Poracanthodes* sp. (Acanthodii) flank scale from the Silurian of Estonia (Ohesaare Cliff). Specimens provided by Henning Blöm, Uppsala University. Images not to scale, fish scale length is 1.5mm.

e) *Nostolepis striata*

This 'acanthodian' has blocky scales, with a pointed posterior to the crown (Figure 3.13). The crown often has riblets at the anterior which may or may not extend and converge towards the posterior tip. The pointed tip itself is angled steeply, projecting upwards above the scale base. The specimen was chosen to represent the spine-like scales of many groups, which theoretically do not reduce drag as their primary function.

3.2.3. Virtual Skin Reconstruction and Standardisation

a) Scaling

Scale volumes (Figures 3.9-3.13) were first imported in to Meshlab software (http://meshlab.sourceforge.net/), where they were resampled to reduce file size, and a

Poisson surface reconstruction was performed to simplify the mesh without losing crown detail. Limited computing power and resolution of three dimensional printing resulted in a trade-off between scale size and rendering quality. After many design iterations, it was eventually decided that a minimum standard scale size of 2mm was possible without loss of the details we intended to study (e.g. riblets, tubercles). Resizing was performed in the CAD (computer-aided design) program Rhinoceros 3D (Robert McNeel & Associates), before the scale unit was positioned on a blank square block so that the neck of the scale was parallel to its surface (Figure 3.14).

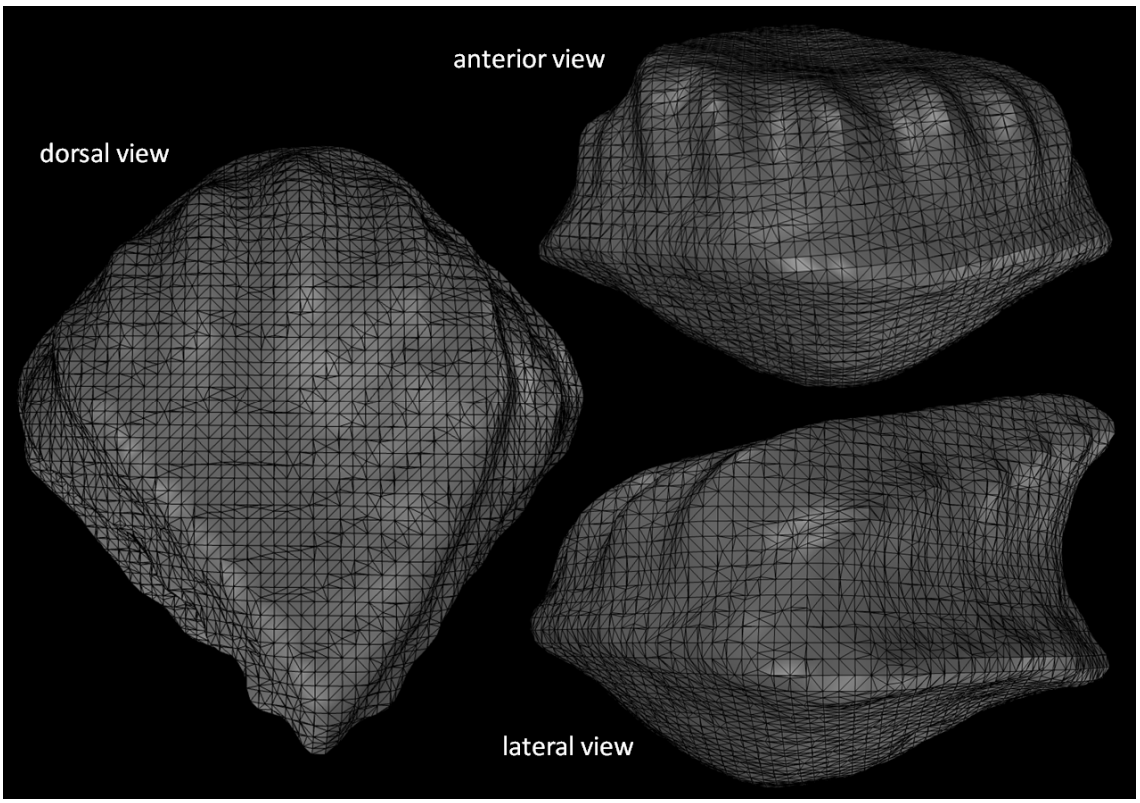

Figure 3.13. X-ray microtomograph images of a *Nostolepis striata* (Acanthodii) flank scale from the Silurian of Estonia (Ohesaare Cliff). Specimens provided by Henning Blöm, Uppsala University. Images not to scale, fish scale length is 679µm.

b) Positioning

In modern shark skin, denticles lie in the soft tissue on a level with the thinner scale neck (between the base and crown), and the distinct neck region of many fossil fish scales suggest a similar arrangement. *Phlebolepis* and *Lophosteus* do not have a distinct neck region, however

the crowns of these scales can be easily differentiated from the bases, and were positioned so that when tessellated only the crown surfaces were exposed.

c) Tessellation and merging

Once correctly positioned, further scale units were added to recreate the diagonal rows observed in both modern sharks and fossil material. This was a slow and precise process of fine-tuning the optimal packing of scales units, taking care to avoid large spaces or unnatural tessellation patterns (i.e. not observed in the examined reference material). As scales were added to the array, Boolean mesh merges were performed in Rhino 3D, which helped produce small patches of scales which could themselves be duplicated and merged. After each merging process, it was necessary to recheck the health of the mesh to ensure errors were not duplicated. Although laborious, this step was vital to successfully render the stereolithic surface geometry files which would eventually be printed.

When these scale arrays were merged with the blank plate block (described next), the tessellation pattern was modified to produce a more realistic and uniform surface across the entire plate. This involved positioning some scale units in such a way that they interdigitated with those of the blocks on either side (Figure 3.15).

3.2.4. Scale Plate Design

Scale plates of 500mm were required to provide adequate wall length for the boundary layer to develop, and while a longer plate would have been better to allow this, the cost of production was prohibitive. There were major technical difficulties in producing a 500 x 100mm single plate, particularly the large computing power required to tessellate thousands of repeating scale units. It was therefore necessary to design individual scale blocks, which could be connected tightly in series and secured to the flume rig. These blocks were designed to accommodate the scales on a stiff and flat surface, supported by two steel rods which ran through the length of the assembled plate, pulling the individual blocks together when bolted at either end. Two convex truncated pyramids on one side of the block, with corresponding concave holes on the other were included to prevent flexure of the plate and guide the surface scales towards a flat plane when tightened (Figure 3.16). The width of the blocks (i.e. the width of the plate) was always 100mm and the height 20mm, however the thickness of each block was dictated by the tessellation of the scales (asterisk of Figure 3.16d). Therefore the number

of individual blocks required to complete a 500mm plate varied slightly depending on scale type, and was an unavoidable concession (see Figures 3.17-3.21).

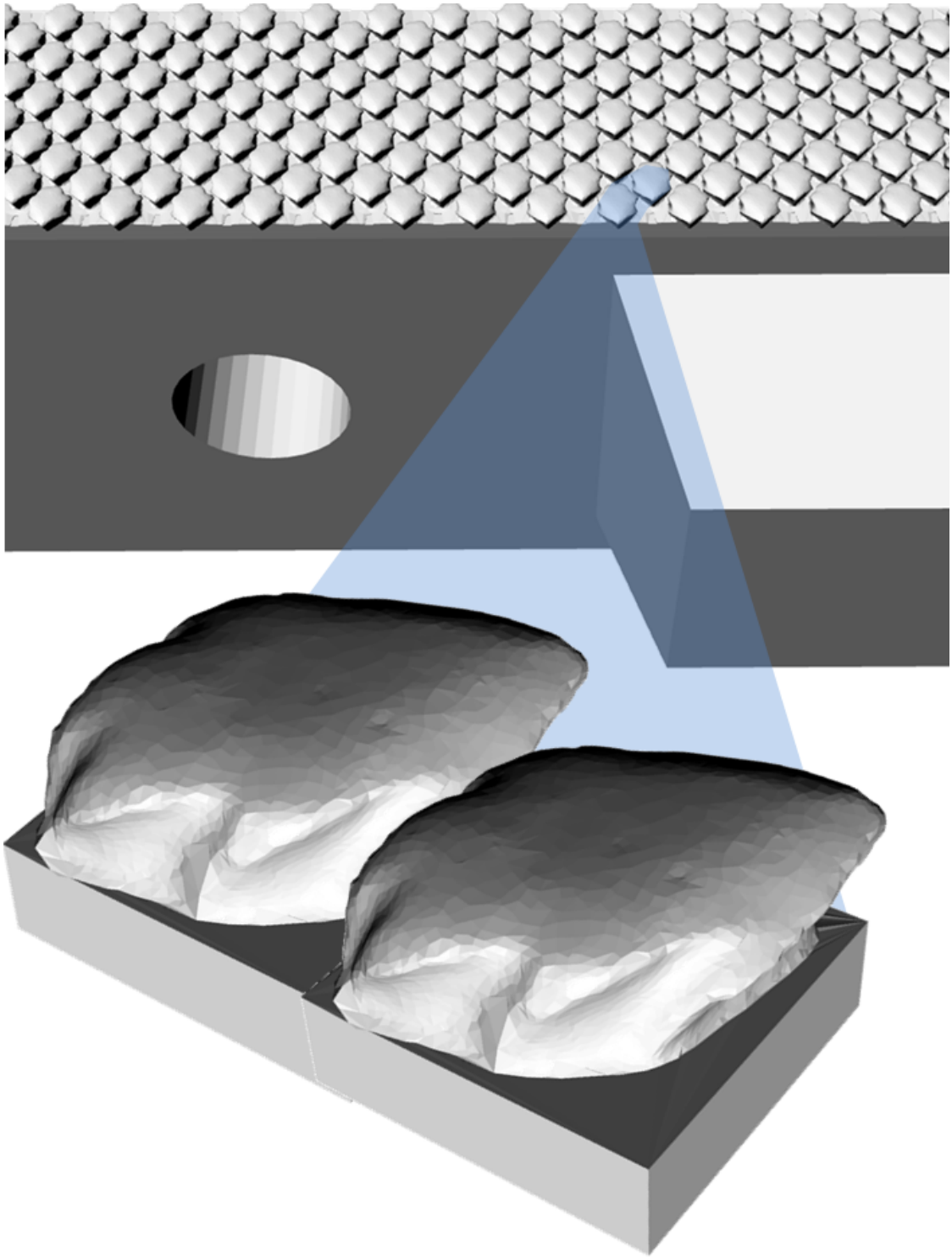

Figure 3.14. Completed *Loganellia* scale block showing tessellated scale surface (top), and individual scale volumes embedded and merged with blank rectangular prisms, placed beside each other before further merging operations (bottom).

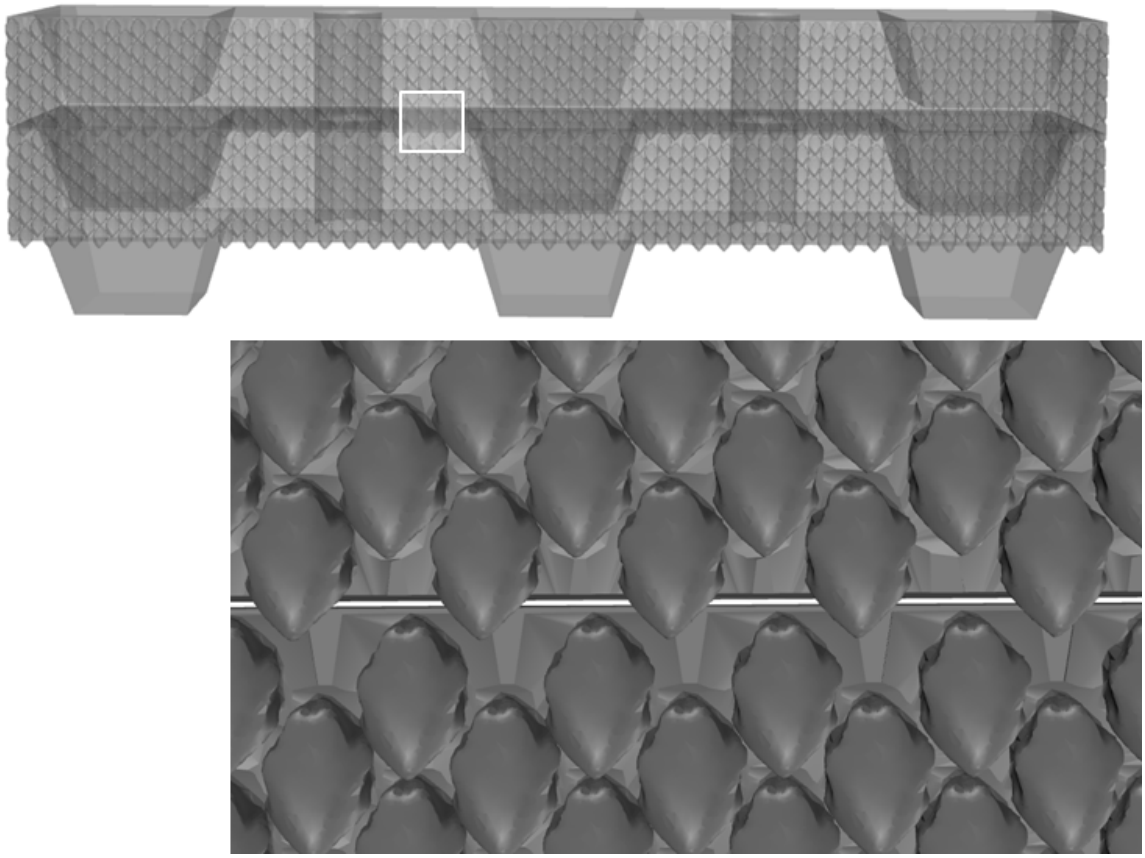

Figure 3.15. Top view of two completed and joined *Loganellia* scale plate blocks (top), and detail of the interdigitating scale units (bottom). All plate blocks are 100mm in length.

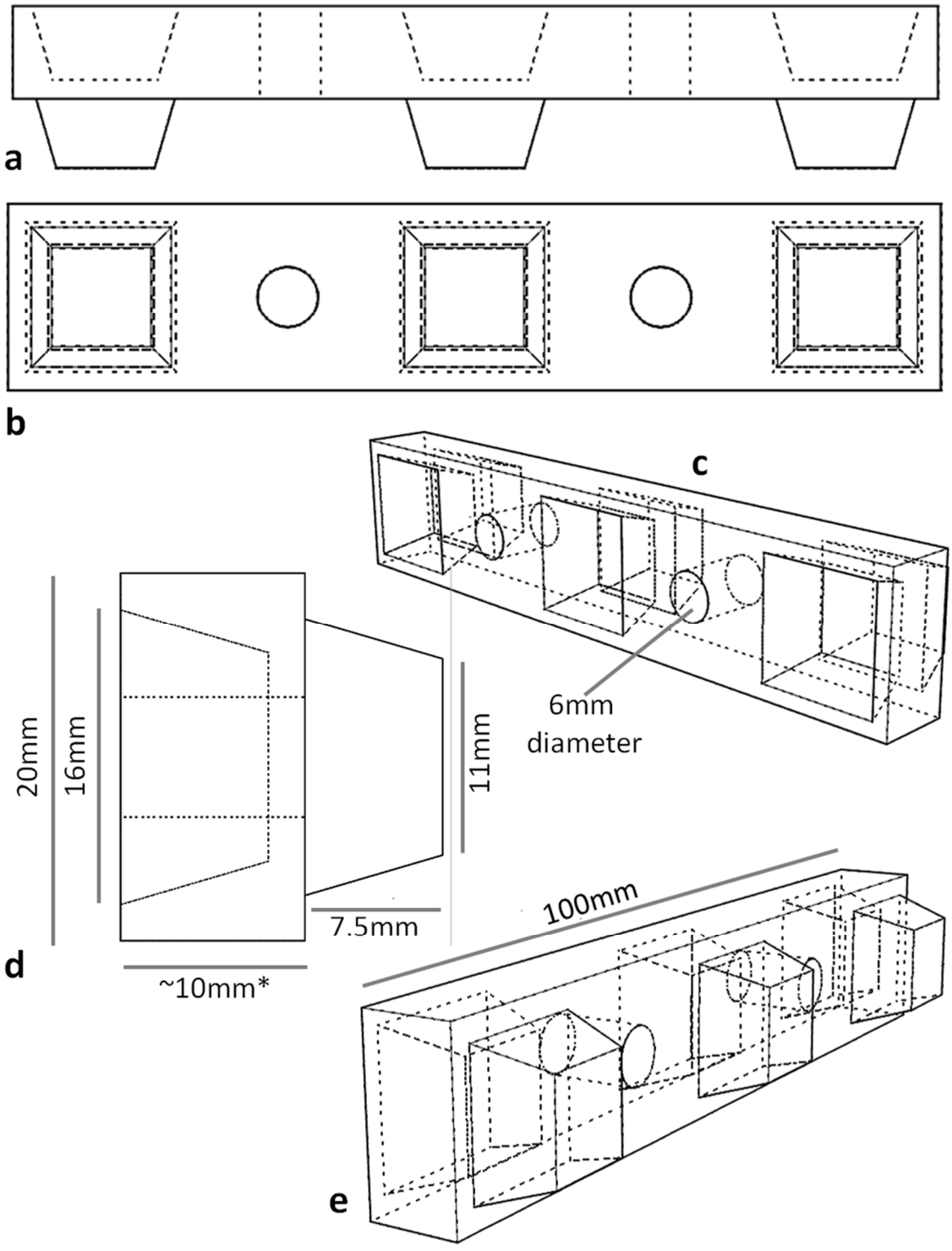

Figure 3.16. Design template for the individual plate blocks, on which a scaled surface was applied. a) top view of block; b) back view; c) oblique view showing concave truncated pyramids and holes for steel rod supports; d) side view, asterisk shows the only dimensional variable of the blocks, herein referred to as block thickness, and; e) oblique view showing corresponding convex truncated pyramids used to guide assembly of plate.

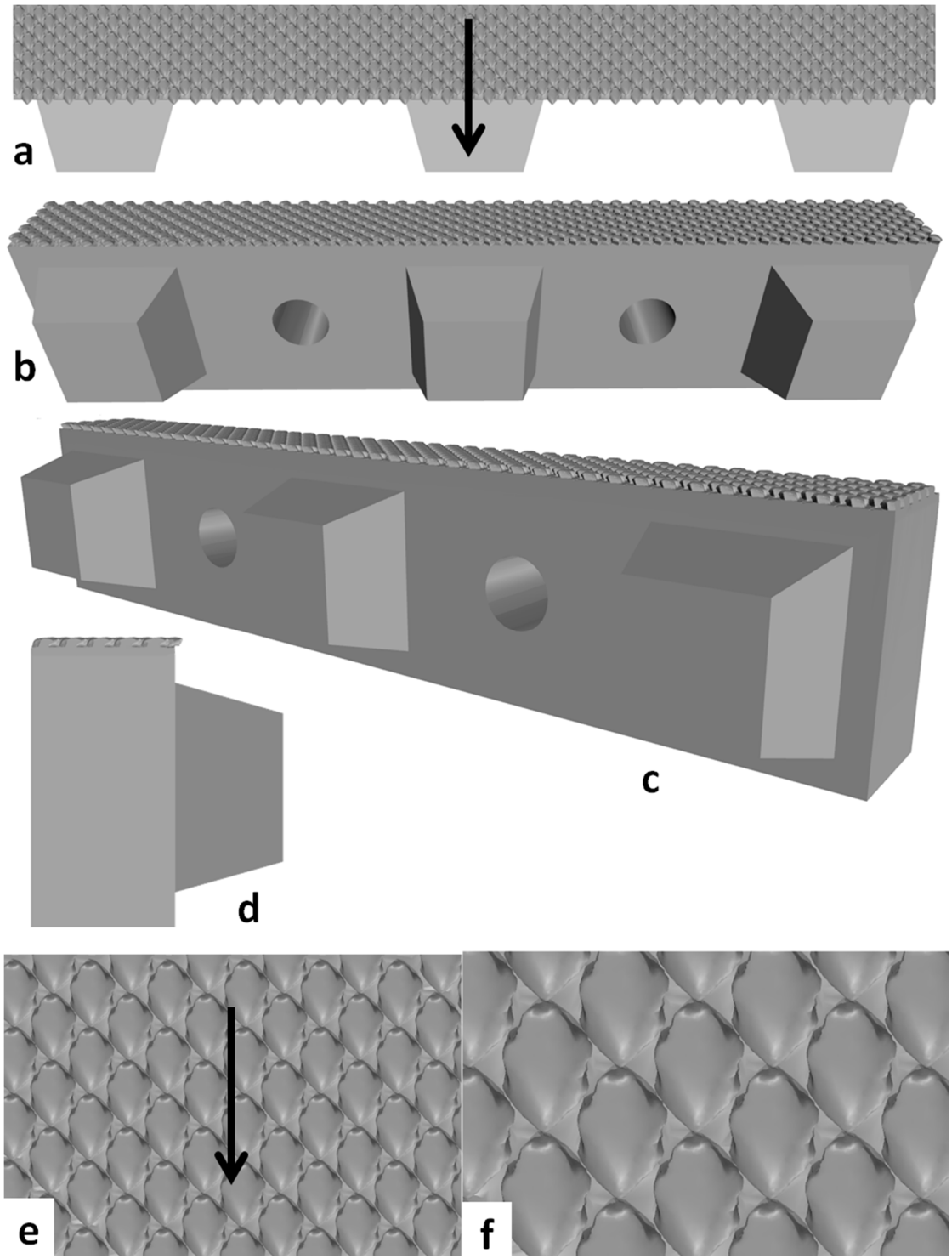

Figure 3.17. Design of individual block of *Loganellia scotica* test plate. a) top view of block showing scaled surface and downstream direction (black arrow); b-c) oblique views of whole block; d) side view; e-f) surface detail showing scale tessellation and downstream direction (black arrow). Scale length standardised to 2mm, height above flat upper surface is 0.6mm, block thickness is 10.4mm, see text.

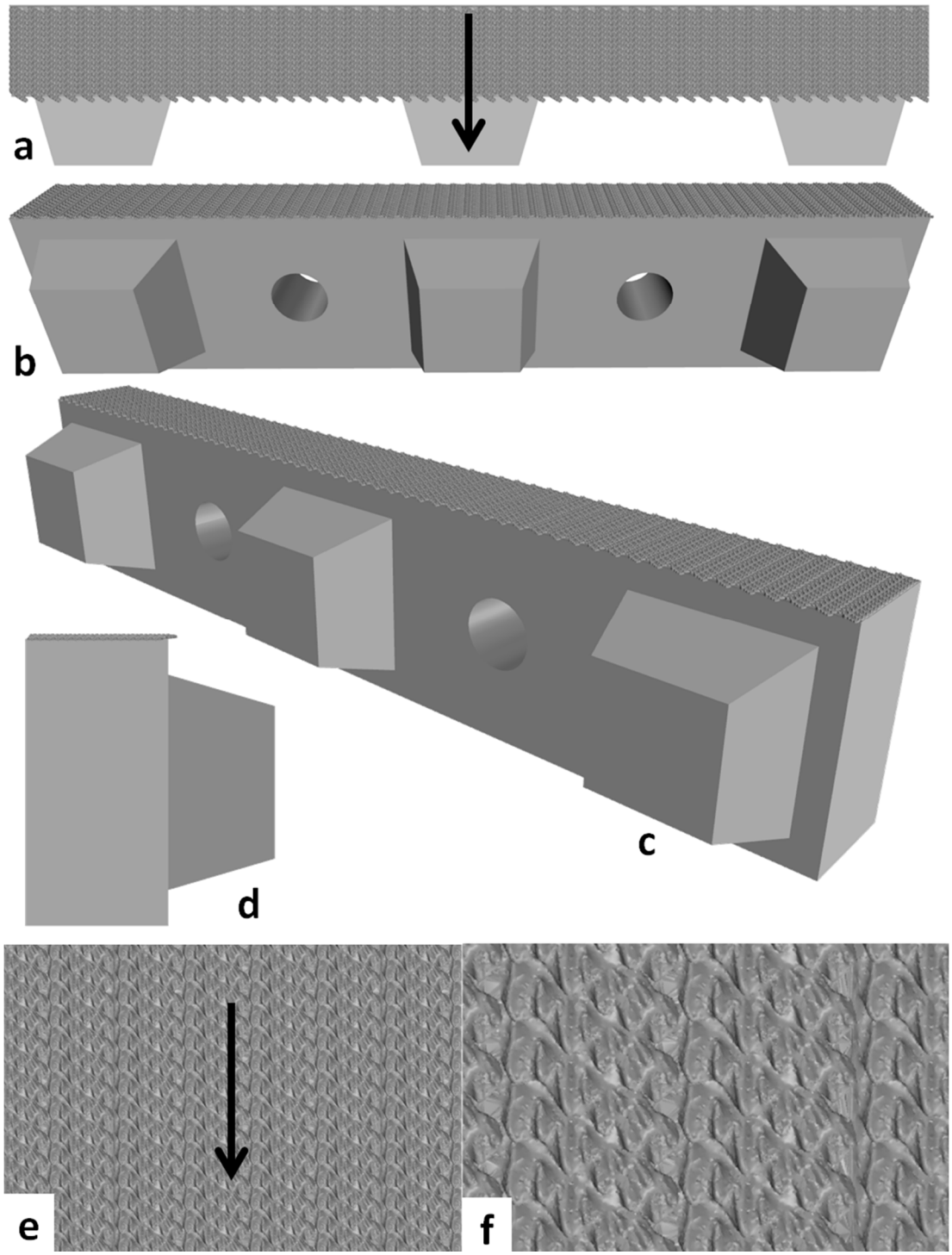

Figure 3.18. Design of individual block of *Lophosteus* sp. test plate. a) top view of block showing scaled surface and downstream direction (black arrow); b-c) oblique views of whole block; d) side view; e-f) surface detail showing scale tessellation and downstream direction (black arrow). Scale length standardised to 2mm, height above flat upper surface is 0.27mm, block thickness is 10.0mm, see text.

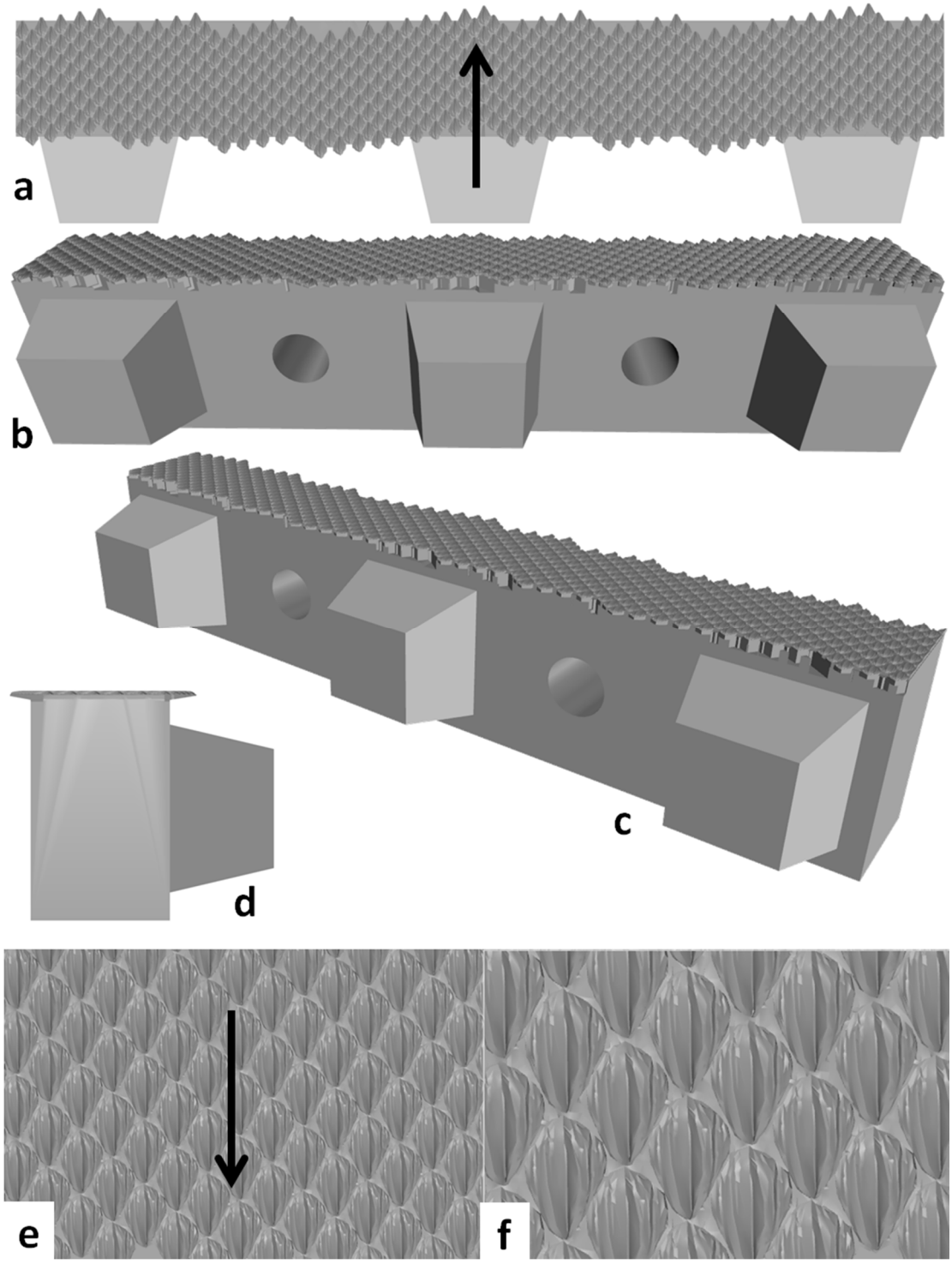

Figure 3.19. Design of individual block of *Phlebolepis elegans* test plate. a) top view of block showing scaled surface and downstream direction (black arrow); b-c) oblique views of whole block; d) side view; e-f) surface detail showing scale tessellation and downstream direction (black arrow). Scale length standardised to 2mm, height above flat upper surface is 0.35mm, block thickness is 12.4mm, see text.

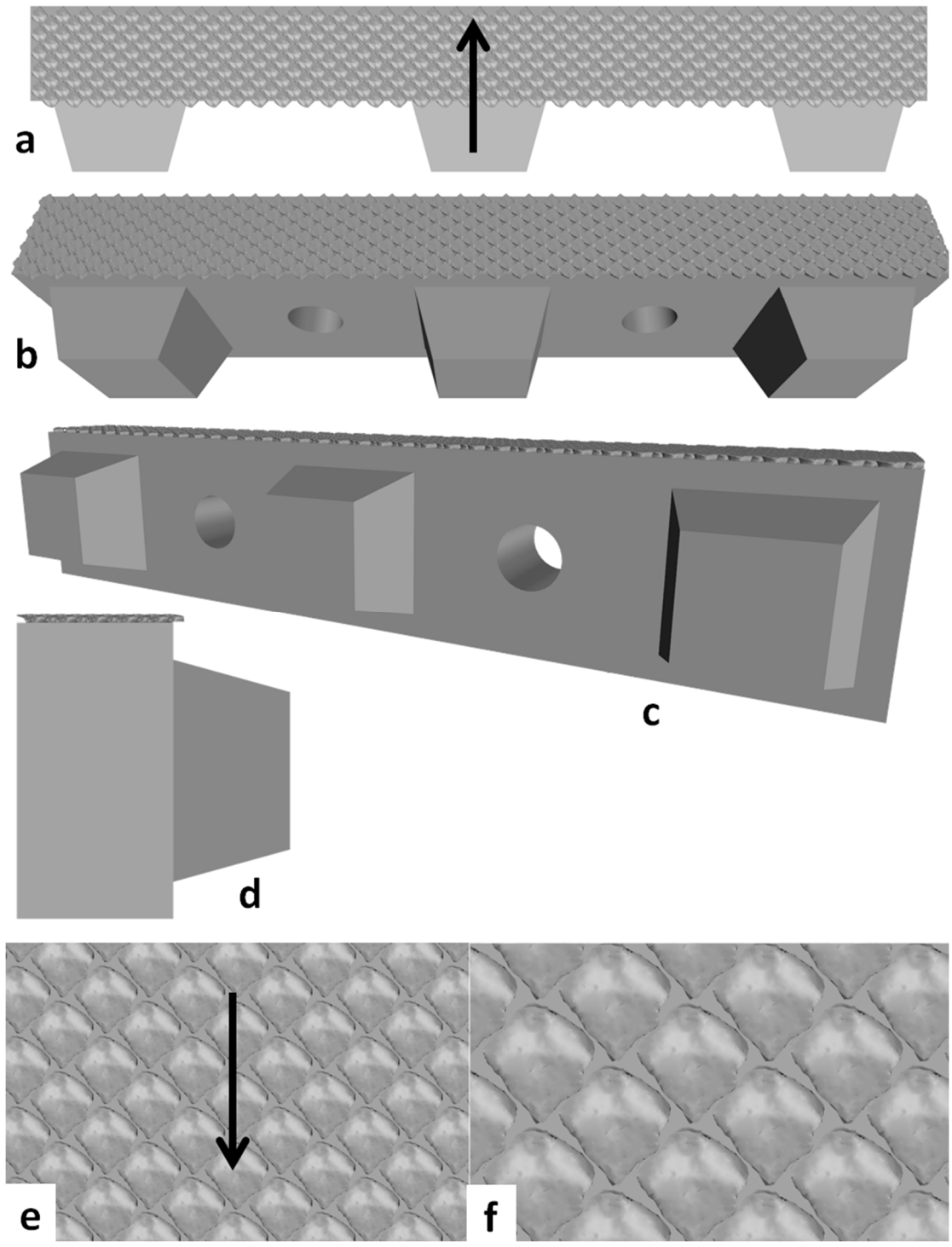

Figure 3.20. Design of individual block of *Poracanthodes* sp. test plate. a) top view of block showing scaled surface and downstream direction (black arrow); b-c) oblique views of whole block; d) side view; e-f) surface detail showing scale tessellation and downstream direction (black arrow). Scale length standardised to 2mm, height above flat upper surface is 0.55mm, block thickness is 10.56mm, see text.

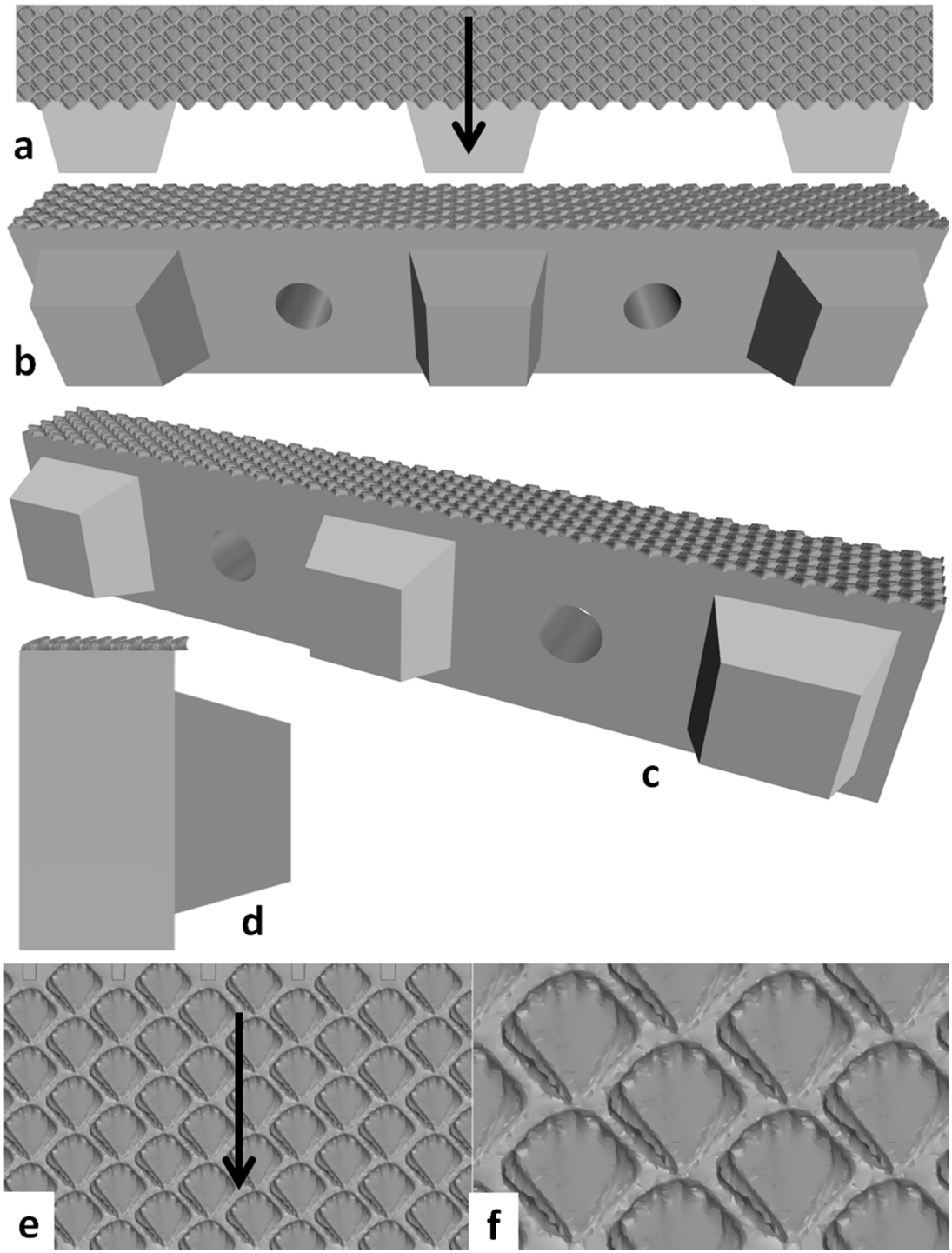

Figure 3.21. Design of individual block of *Nostolepis striata* test plate. A) top view of block showing scaled surface and downstream direction (black arrow); b-c) oblique views of whole block; d) side view; e-f) surface detail showing scale tessellation and downstream direction (black arrow). Scale length standardised to 2mm, height above flat upper surface is 0.97mm, block thickness is 10.47mm, see text.

3.2.5. Rig Assembly and Flume Setup

a) Flume tank flow

An 8.5 m recirculating hydraulic flume tank, with 30cm cross-sectional width and 30cm depth was used to conduct the experimental skin friction analysis. The flume is equipped with a stack of laminarising tubes upstream (the vane) of the measurement zone, designed to minimise small perturbations, which can propagate to alter the flow structure downstream. To determine if there was an intrinsic structure to normal flume flow, velocity was measured in the centre of the flume using laser Doppler anemometry (discussed next, section 3.2.6) for 10 minutes. Over this period mean velocity was 0.32m/s, ranging from 0.2-0.44 m/s (n = 59490), with a standard error of 0.0001 m/s.

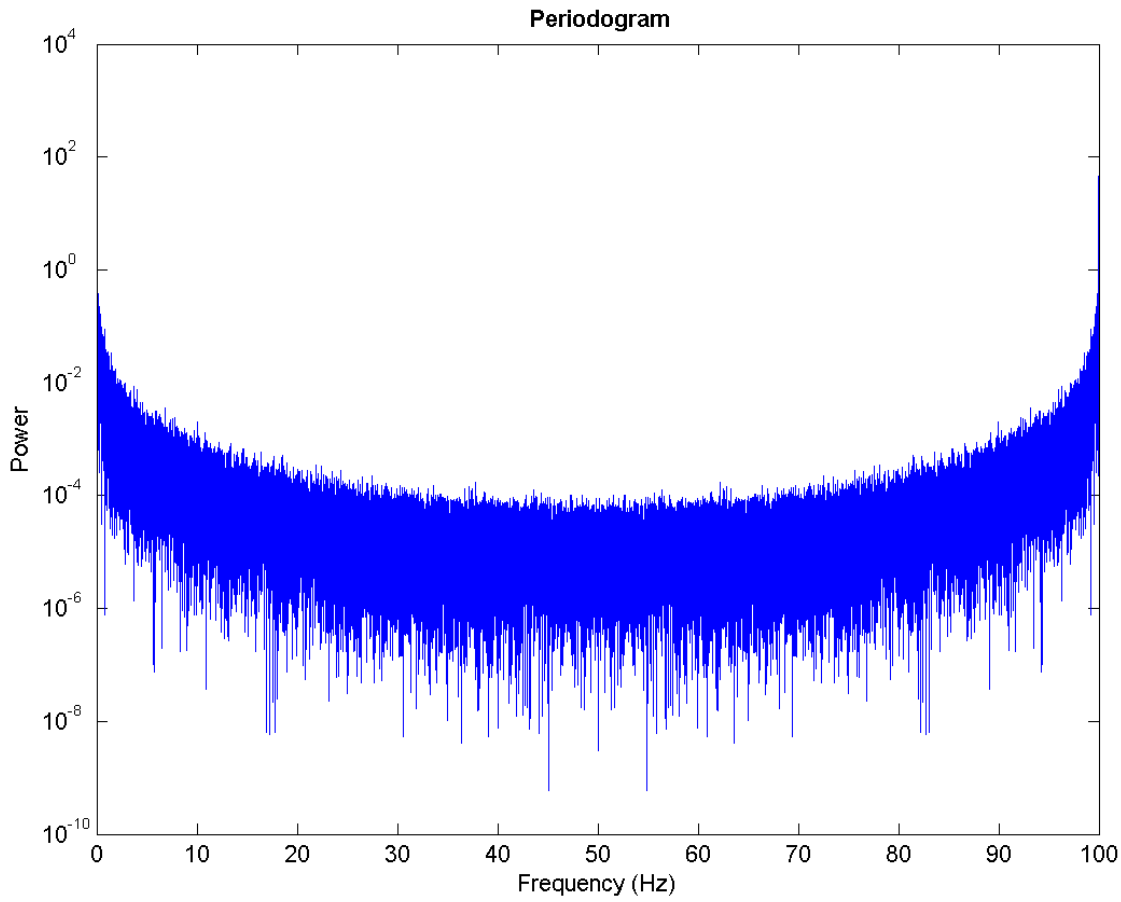

Figure 3.22. Periodogram of velocity measurements recorded at the mid-centre of the flume tank using laser Doppler anemometry, over 10 minutes at mean flume speed 0.32 m/s.

A periodogram was produced (using code contributed by Dr Gareth Keevil), using this data (Figure 3.22), which showed there were fluctuations in velocity. A way of compensating for this, would be to increase the measurement time at each spatial position. However, measuring velocity at each of the 410 spatial positions (described next) for 10 minutes would require over 68 hours to complete each plate. Standard error of velocity measurements during the 10 minute run (n = 59530) was 0.0001 m/s. When 20 time intervals of 30 second were randomly selected (https://www.random.org/) from the same dataset, the mean standard error was 0.0005 m/s (mean n = 2848). On this basis, a 30 second linger time was chosen, reducing the experimental run time to ~6 hours.

b) Rig assembly

An adjustable aluminium frame was constructed above the flume, which held a single aluminium supporting beam vertically in to the centre of the flume, approximately 4m downstream of the vane (Figure 3.23a). A gimble was attached to the end of this beam, which in turn was bolted to the back of the plate allowing small adjustments to be made to the angle of the plate. It was important to achieve as horizontal and flat a surface as possible for the laser Doppler anemometry to return spatially accurate velocity measurements, and to minimise any pressure gradients, so a high sensitivity spirit level was used while adjusting the plate. The plate assembly was held scale-face downwards ~16cm from the base of the flume tank (Figure 3.23b), to reduce the influence of surface waves, which are a potential source of error, especially in shallower flume tanks.

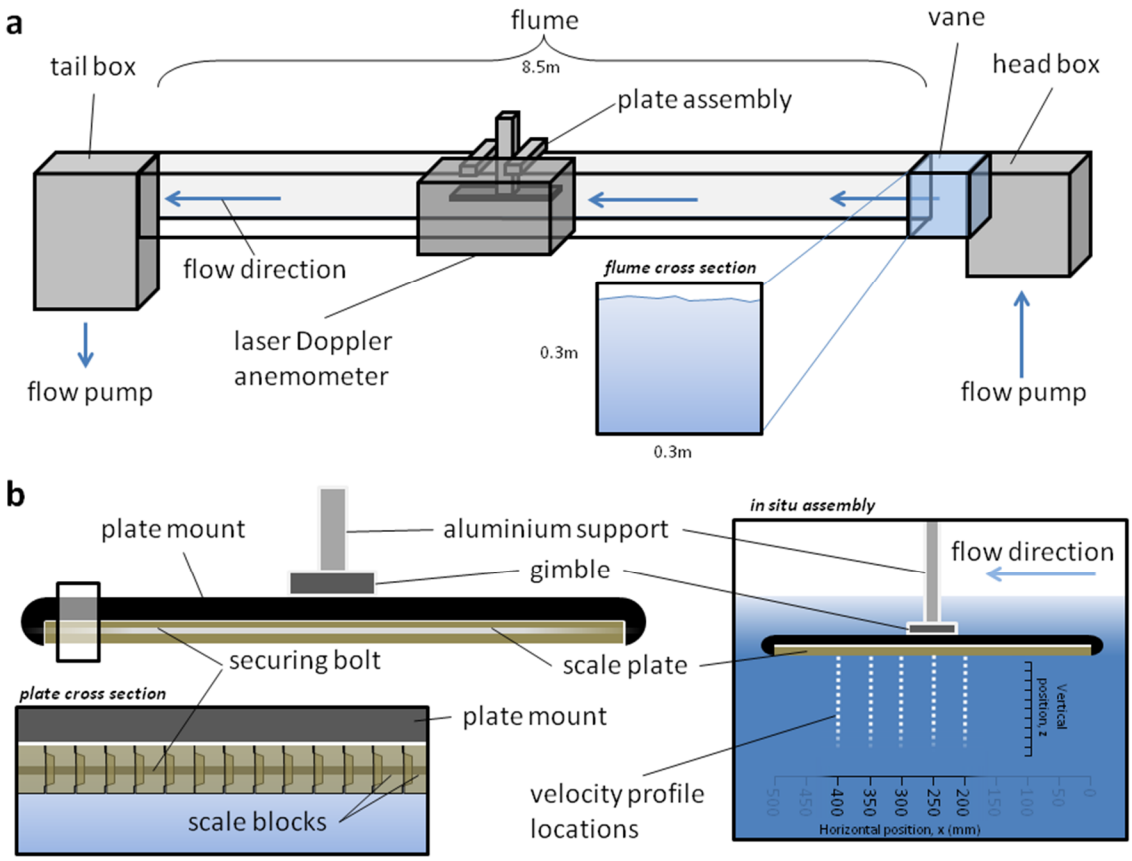

Figure 3.23. Flume tank setup; a) general schematic of flume system, and; b) detail of plate assembly and rig within flume tank. During operation, the flume was blacked out to minimise exposure to laser light. Not to scale.

c) Flume operation

Once secured, the flume was filled with water and any bubbles adhering to the scaled surface were removed by hand. While operating, the flume was blacked-out to minimise exposure to laser light during experimental runs, and before the flume was activated a protective hood was bolted over the supporting rig. The flume pump was then activated to run at ~50 cm/s (maximum speeds over each plate ranged from 0.49 - 0.533 m/s) which is in the range of cruising speeds for many extant fishes of a similar size to the fossil taxa (~5-25cm) (e.g. Bainbridge, 1957; Fishbase). This speed was used for all scale plates as the experiment sought a relative comparison of scale hydrodynamics, and not precise species-specific data.

3.2.6. Laser Doppler Anemometry

a) Experimental setup

Laser Doppler anemometry (LDA) uses the Doppler effect of laser light hitting a seeding particle to measure flow velocity, and is alternatively referred to as laser Doppler velocimetry (Durst et al., 1991). An interferometer splits a laser light (argon-ion) in to two coherent beams; the reference and measurement beams. Particles in the fluid flow alter the frequency of light intensity depending on their velocity, and the shift relative to the reference beam can be used to calculate this velocity. The benefits of this method include the high temporal and spatial resolution, with around 100 2D point measurements per second, a traverse accuracy of ±0.1 mm, and laser Doppler anemometer accuracy of 0.3mm (Yeh & Hall, 2008). No calibration of the equipment is required, and as a non-intrusive and remote method, the measurement process has no effect on flow.

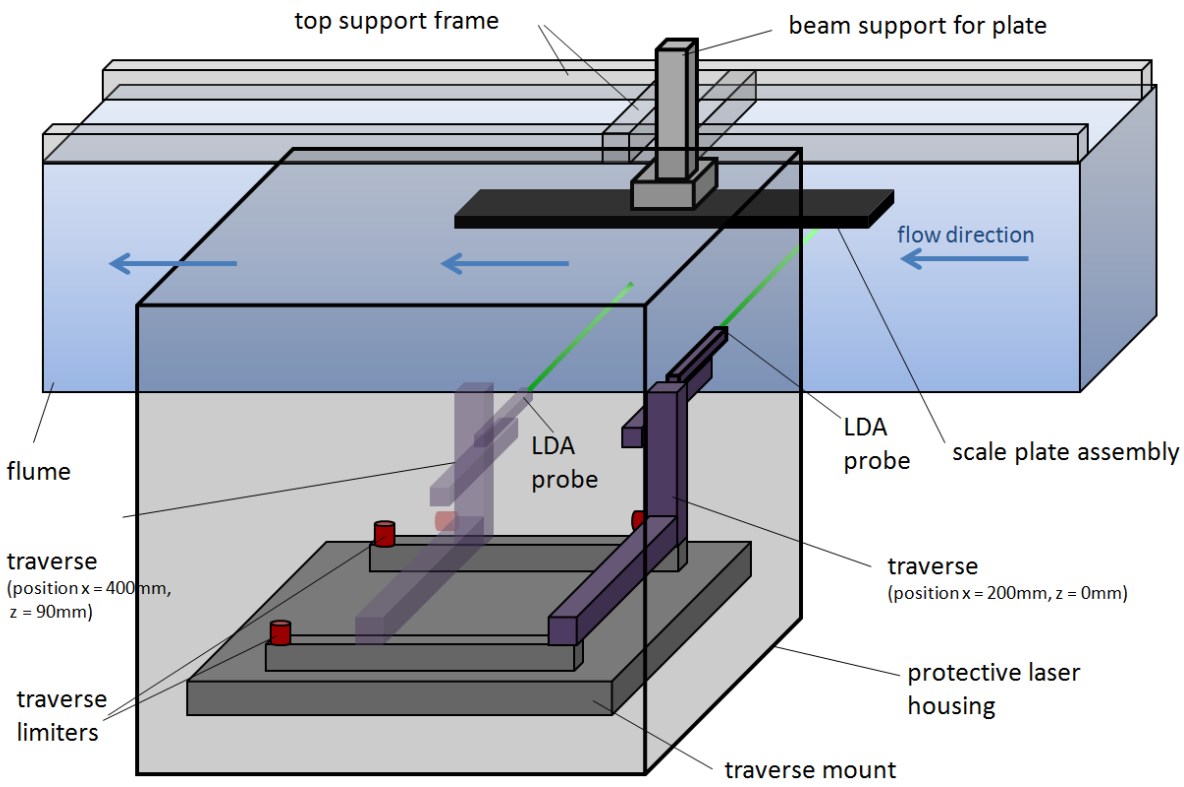

Figure 3.24. Diagram of laser Doppler anemometer and flume setup. Not to scale.

For this study, a Dantec fibre-optic LDA system was used, in conjunction with a motorised traverse to allow navigation to specific measurement locations both along the length of the

plate, and downwards away from the plate surface in to the freestream. During the experiment, seeding was added to the flow which the LDA detects to measure velocity, the seeding used was 10 µm diameter hollow borosilicate glass spheres (which have no effect on flow), coated with silver to increase reflectivity.

b) Measurement locations

A grid of measurement locations was created to record velocity profiles at five horizontal distances (x axis) along the plate. Each profile consisted of 82 positions (e.g. Appendix II, section A2.2) from the point closest to the wall (z = 0 mm) in to the freestream (z = 100 mm), with a higher density of measurements in the region closest to the wall (Figure 3.25).

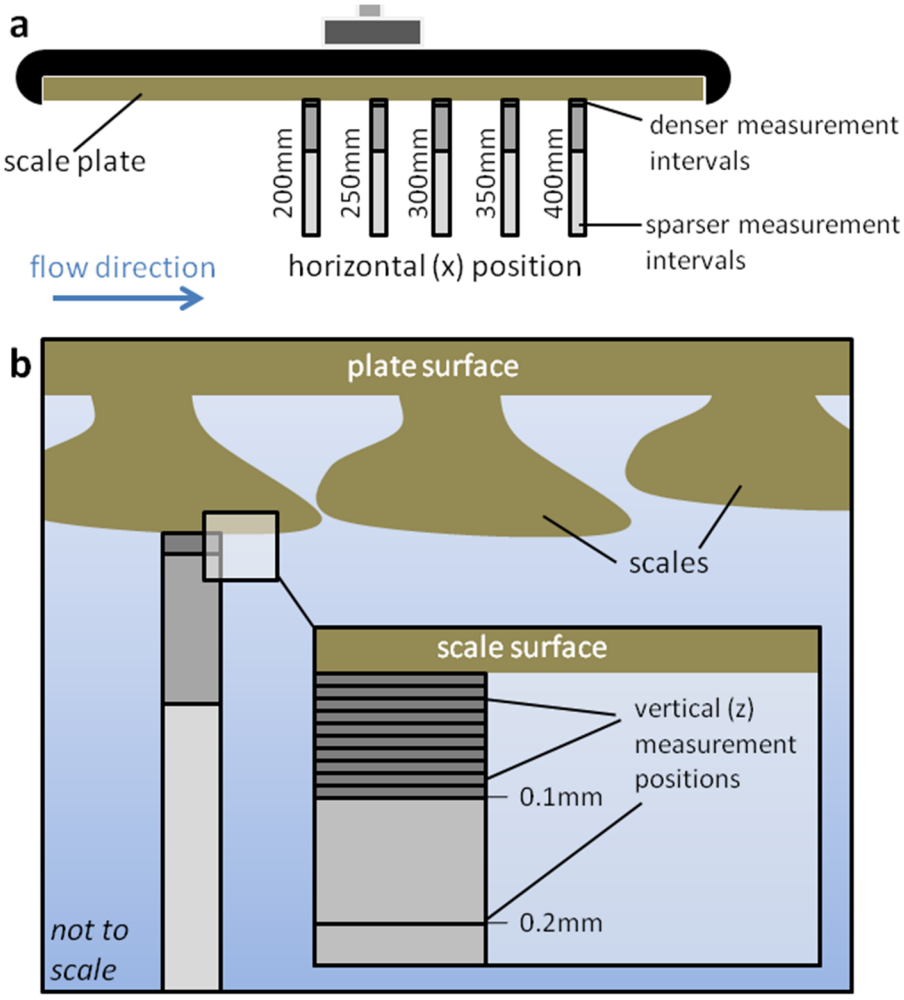

Figure 3.25. Diagram showing the density of measurements at positions across the plate (x = 200-400mm), and positions away from the wall surface (z = 0-90mm).

The plate was fixed in a flat orientation, however even a small tilt could alter the position of z = 0mm across the 500 mm surface. This along with variable scale morphology produced erroneous results when the probe was measuring the velocity of the plate rather than the fluid travelling over its surface. The higher density of velocity measurements close to the wall helped minimise the loss of data resolution in this region, even after post-hoc corrections were made to the position of z = 0mm. The extent of data loss at the base of each profile is detailed in section 7.1, and Appendix II.

3.2.7. Data Processing

a) Mean velocity

The LDA system records a large number of velocity measurements at set positions relative to the test plate for a linger time of up to 30 seconds (see section 3.2.6). Measurement rate is dependent on the fluid velocity and LDA sensitivity, however by altering seeding density a maintained rate of 100 measurements per second was achieved. As the LDA system generated text files of measurements for every z, x position, it was necessary to preprocess this large volume of raw data and calculate the mean velocity for each position using Matlab (The Mathworks, Inc., USA).

b) Profile base corrections

Once means had been calculated for every position, it was necessary to retrospectively estimate the position of the first measurement closest to the wall. The true base of each profile was obscured during flume testing to protect workers from laser light. As a result the variable scale geometry and sub-millimetre tilting across the 500mm plate limited the accuracy of manually estimating vertical measurement positions relative to the test plate. To do this, mean velocity measurements were plotted as a vertical profile and the intersection with zero velocity was identified. To refine and standardise this process, the differences between consecutive measurements were calculated from the highest vertical position to the base. The true base was defined as the wall-most measurement at which velocity had reached 0.005m/s or more from the previous (higher in the profile) measurement (an example is presented in Figure 3.26). Following this procedure, the vertical (z) axis was also corrected, allowing for the non-uniform spacing in measurement positions.

a

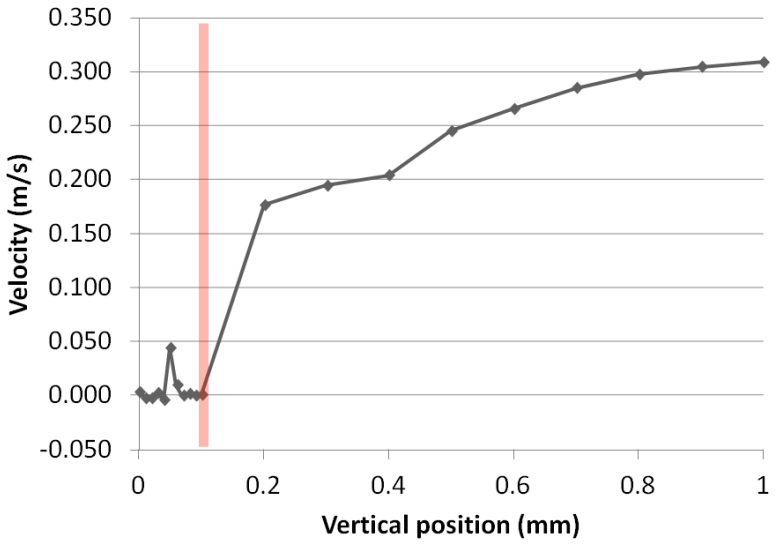

b

Vertical position (mm)	Velocity (m/s)	Difference (m/s)
0	0.003	-0.005
0.01	-0.002	0.000
0.02	-0.002	0.005
0.03	0.003	-0.006
0.04	-0.004	0.048
0.05	0.045	-0.035
0.06	0.010	-0.010
0.07	0.000	0.002
0.08	0.002	-0.002
0.09	0.000	0.001
0.1	***0.001***	***0.175***
0.2	0.177	0.018
0.3	0.194	0.010
0.4	0.204	0.041
0.5	0.245	0.021
0.6	0.266	0.019
0.7	0.285	0.012
0.8	0.297	0.007
0.9	0.304	0.005
1	0.309	

Figure 3.26. Example of data correction, identifying the true base of a velocity profile from a plot of raw data a), and differences between consecutive measurements; b). Corrected base position (red lines) defined as wall-most measurement at which velocity has reached less than 0.005m/s (bold italics) and had ideally decreased from the vertically higher measurement by 0.005m/s or more (green text). Red text denotes velocity differences 0.005 m/s or smaller than vertically higher value, or negative values (reversed flow).

All statistical tests and the calculations that follow use only data from these corrected plots. All mean measurements, including values not included in the analyses are reported in Appendix II. Raw unprocessed measurements of velocity were retained, as they provided interesting near-wall information which mean values for velocity may not show as clearly.

c) Boundary layer thickness

Using Matlab the boundary layer thickness was calculated, by first plotting each velocity profile with a fitted second degree polynomial curve, and extracting the vertical (z) position at which 99% of the freestream velocity was reached. Freestream velocity was defined as mean velocity at the vertical position furthest from the wall, which because of the base correction process described previously meant the mean average of this vertical distance was 89.499 (n = 30), ranging from 81.35 – 89.97. Boundary layer thicknesses were then plotted for qualitative comparison, and basic descriptive statistics performed using PAST.

d) Drag calculations

Within the boundary layer, fluid flow decreases towards the wall, as shear stresses increase until a 'no-slip' condition is reached and fluid is stationary next to the wall. In the region above this velocity gradually increases proportionally with decreasing shear stresses, until free stream velocity is reached. Theoretical predictions of flow in the viscous sublayer and log law region can be used to approximate the near-wall velocity gradient and skin friction.

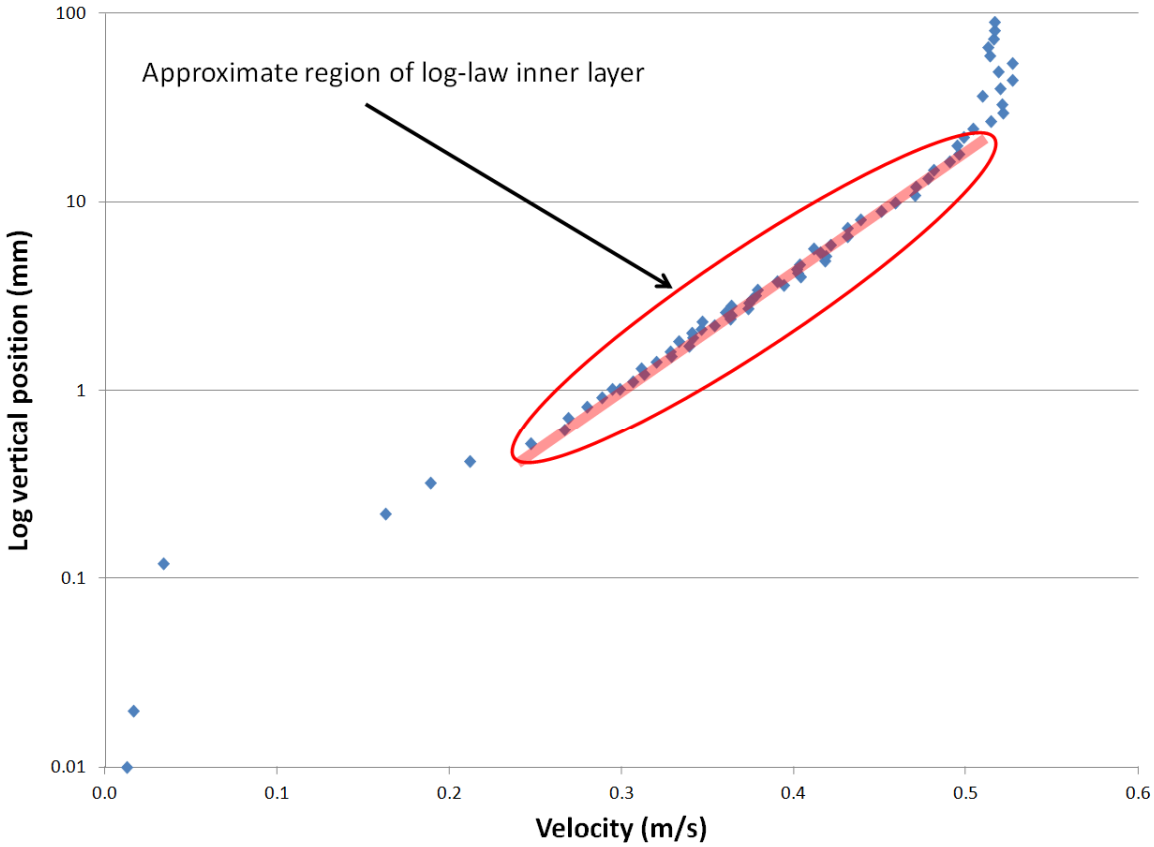

Figure 3.27. Example semilog plot of velocity profile, showing approximate position of log-law inner region and a line of best fit. The gradient of this best fit line approximates the frictional velocity, which itself is used to calculate dimensionless wall units (y+). The inner log-law region, defined as y+ = >30 - <100 was used to fine tune this line of best fit by iterative exclusion of data outside this region.

First, log distance from the wall (y) was plotted against velocity (u) for all corrected experimental data of a given profile (e.g. 250mm from the leading edge of the *Lophosteus* plate) and a line of best fit was applied (Figure 3.27). The gradient of this line is equal to the frictional velocity divided by Von Karmen's dimensionless constant (0.41), applied to turbulent

conditions where a no-slip condition is reached. Using the frictional velocity (U*) value, the distance from the wall was converted to dimensionless distance y+, according to Equation 3.1.

$$y^{+} = \frac{\text{Distance from the Wall X Frictional Velocity}}{\text{Fluid Viscosity}}$$

$$y^{+} = \frac{y\, u*}{v}$$

Equation 3.1. Equations for the calculation of dimensionless wall unit y^{+} (Schlichting & Gersten, 1999).

Using this dimensionless distance referred to as wall units (Equation 3.1), the log law region could be defined further, as y+ = >30 - <100. Once data which fell outside this region was excluded, another iteration of the same process of line fitting and calculating U* (frictional velocity) was performed (Equation 3.2). This was repeated until U* values converged to 4 decimal places. Instances where this process resulted in a feedback loop were examined and the mean U* approximation calculated.

$$frictional\ velocity = \sqrt{\frac{shear\ stress\ at\ wall}{fluid\ density}}$$

$$u* = \sqrt{\frac{\tau}{\rho}}$$

Equation 3.2. Equation used to calculate frictional velocity (U*) during approximation process described in text (Schlichting & Gersten, 1999).

Freestream velocity was calculated as the mean velocity of all measurements taken beyond the boundary layer, and using the frictional velocity values, skin friction could be calculated (Equation 3.3).

$$\text{Skin friction coefficient} = \frac{\text{Frictional Velocity}^2}{\frac{1}{8}\ \text{x Freestream Velocity}^2}$$

$$Cf = \frac{U^{*2}}{\frac{1}{8}\ \text{x } U_{\infty}{}^2}$$

Equation 3.3. Equation used for the calculation of skin friction coefficient (Schlichting & Gersten, 1999).

Descriptive and basic statistical tests were then performed using PAST software. Results of this experimental data are presented in Chapter 7, and are discussed in Chapter 8.

4. Comparative Functional Analysis of Scale Morphology

Scale form is a reflection of physical and ecological constraints, so by studying a wide range of modern sharks in addition to the morphometric approaches presented in Chapters 5 and 6, the scale functions of extinct taxa can be inferred. Using specimens and data from the literature, museum collections and fresh modern shark material, scale morphotypes are first identified. To control for regional variation in morphology only the flank, a relatively large (section 3.1) and homogeneous (Chapter 6) region, was used for this analysis, unless otherwise stated. Specialised scale types are identified first as extreme end-members of a hypothesised functional gradient, before intermediate forms are identified and their possible functions discussed.

4.1. Comparative Analysis

4.1.1. Specialised scale morphotypes

a) Blocky, flat scales

Examination of a large number of extant sharks revealed blocky non-overlapping flank scales are found in slow-moving, deep water sharks (section 4.2.1), and the scale type is relatively uncommon (e.g. *Etmopterus bigelowi*, Figure 4.1). Extinct taxa with this scale type on the flank include the Siluro-Devonian (~423-411mya) 'acanthodian' *Gomphonchus hoppei* (Figure 4.1), and the Devonian (~419-383mya) thelodont *Turinia australiensis* among others (Appendix I). The relatively large scale bases suggest there was exposed skin between the crowns. This is a feature found in some modern gulper sharks, where this exposed skin is coated in thick mucus, the function of which is likely protection (Reif, 1985b). As there are no obvious features of hydrodynamic benefit, or specialism for parasite defence, it is assumed herein that the function of these scales is general abrasion protection and mechanical defence.

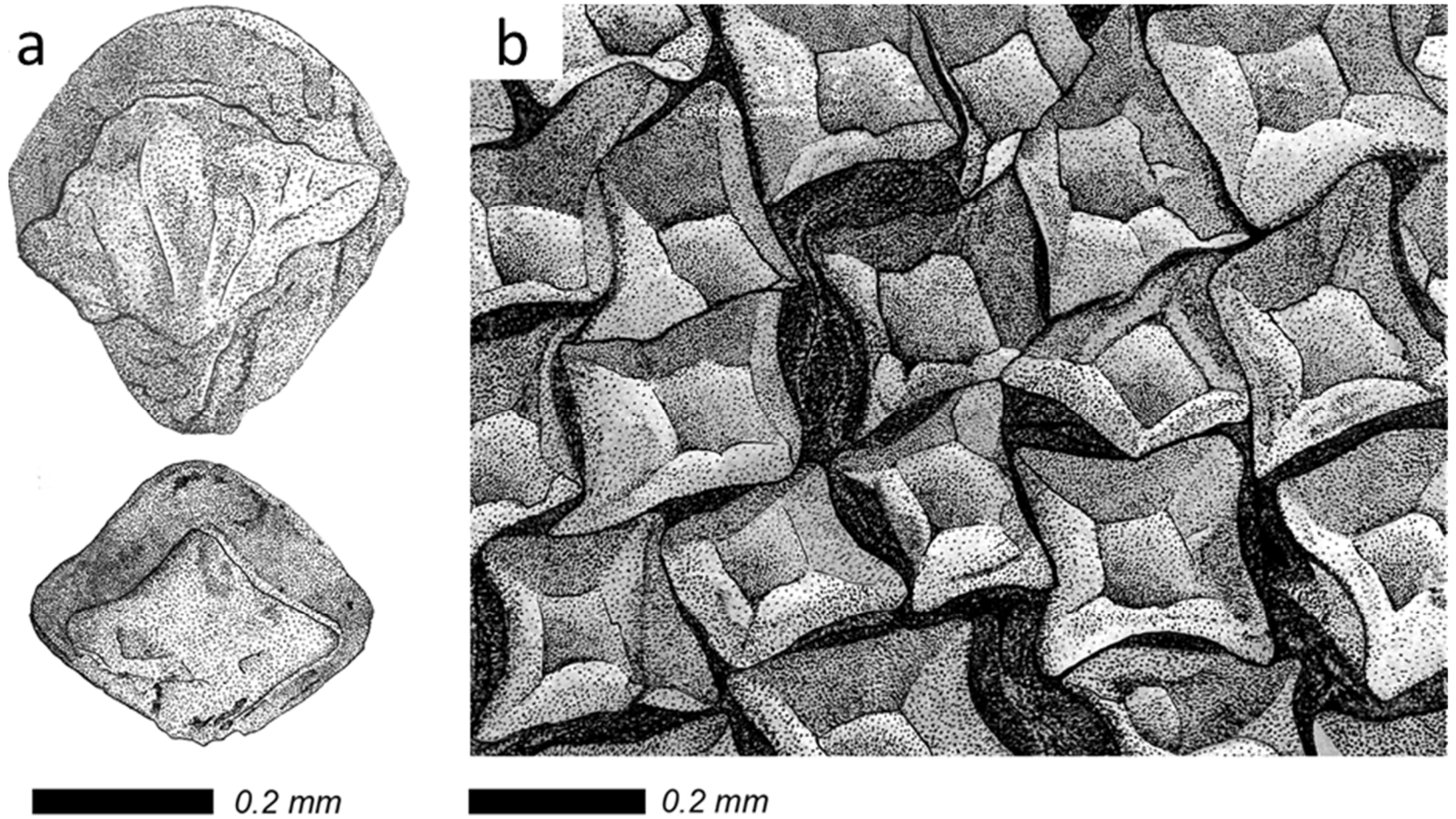

Figure 4.1. Representative examples of blocky flank scales; a) the 'acanthodian' *Gomphonchus hoppei* (drawn from material figured in Valiukevičius, 2005); and b) the modern lantern shark *Etmopterus bigelowi* (drawn from material figured in Castro, 2011).

b) Spiny, and spine-like scales

Spine-like scales are typically elongate and diamond-shaped, coming to a sharper point at the posterior, supported by ridges at the base and up to the tip. These are found in a variety of slow-moving pelagic sharks, including the basking shark *Cetorhinus maximus* (Figure 4.2), the Cuban dogfish *Squalus cubensis*, and many catsharks (*Scyliorhinus* sp.) and lantern sharks (*Etmopterus* sp.) among others (Appendix I).

Spine-like scales and scales with multiple spines are common in Palaeozoic taxa, and constitute the majority of thelodont morphotypes in particular. In modern sharks, spiny scales (differing from singular 'spine-like' scales) have numerous points emanating from the crown, commonly as three elevated ridges, of which the central spine is usually the longest. Extant examples include the marbled catshark, *Galeus area*, and the brier shark, *Deania calcea* (Figure 4.2), which has extraordinary trident-like scales. Palaeozoic taxa with spiny scales include the the thelodont *Paralogania martinssoni* (Figure 4.2) and the 'acanthodian' *Acanthospina irregulare* (Figure 4.2) with spines pointing backwards, raised at 50-60 degrees from the base of the scale in some cases.

c) Uniform parallel riblets

Scales with parallel riblets have a fairly regular pattern of three or more distinct antero-posterior aligned peaks and troughs, which are either spaced evenly or may become slightly closer together away from the medial axis of the crown (Figure 4.3). This scale type is specialised for drag-reduction, and is found in many pelagic sharks including the shortfin mako *Isurus oxyrhinchus* (Motta et al., 2012), considered the fastest shark species (http://www.flmnh.ufl.edu/). Riblets are a key focus of this project, and are further investigated in Chapters 5, 6 and 7.

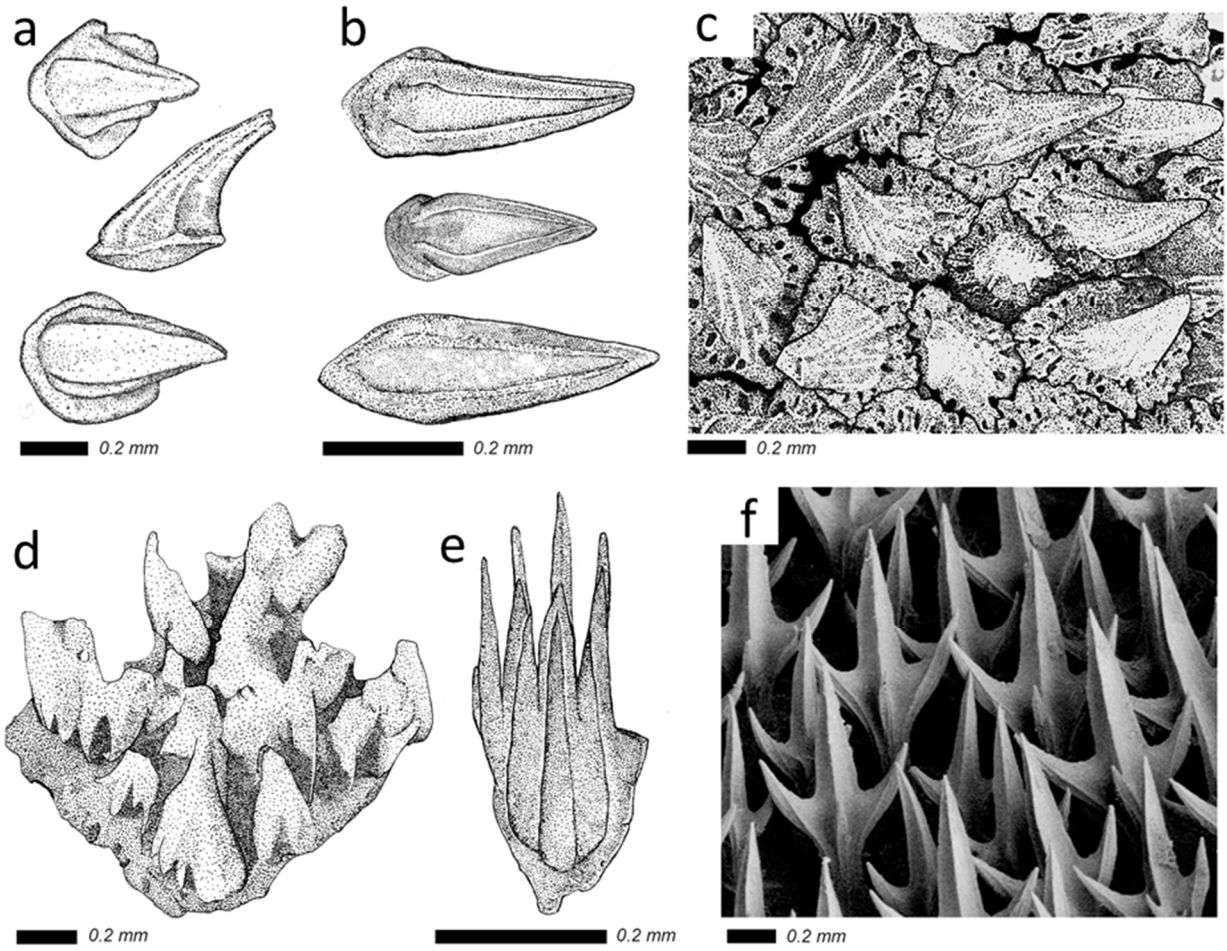

Figure 4.2. Representative examples of spine-like (a-c) and spiny scales (d-f). A) the 'acanthodian' *Nostolepis fragilis* (drawn from material figured in Valiukevičius, 2003); b) the thelodont *Loganellia exilis* (drawn from material figured in Märss et al., 2006); c) the modern basking shark *Cetorhinus maximus* (drawn from material figured in Castro, 2011); d) the 'acanthodian' *Acanthospina irregulare* (drawn from material figured in Valiukevičius, 2003); e) the thelodont *Paralogania martinssoni* (drawn from material figured in Märss, 2003); and f) the brier shark *Deania calcea* (courtesy of Sue Lindsay, Australian Museum).

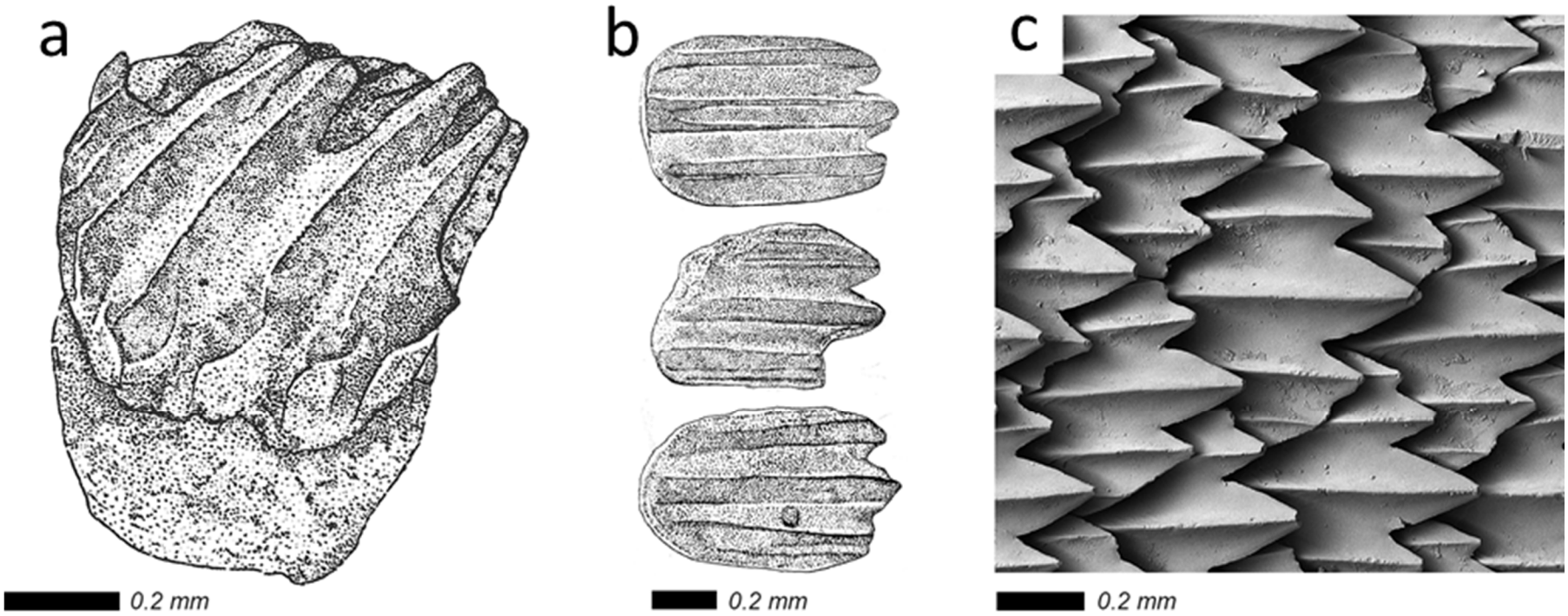

Figure 4.3. Representative examples of flank scales with uniform parallel riblets; a) the 'acanthodian' *Nostolepis gaujensis* (drawn from material figured in Burrow et al., 2009); b) the thelodont *Canonia grossi* (drawn from material figured in Karatajūtē-Talimaa, 2002); and c) the modern requiem shark *Carcharhinus brachyurus* (courtesy of Sue Lindsay, Australian Museum).

4.1.2. Intermediate scale forms

a) Smooth teardrop scales

Smooth teardrop or kite-like scales are found in the modern angel sharks *Squatina* sp. (Figure 4.4), which are bottom dwelling ambush predators. Several 'acanthodians' and thelodonts (Figure 4.4) share this scale shape, but it is relatively rare. In isolation, the pointed trailing edge could potentially seed deleterious vortices, but an array of tessellated scales together could act as a turbulisor, cultivating small-scale turbulence to transfer moment back towards the wall and keep the boundary layer attached for longer across the skin surface. However, as in blocky and flat scales, with a smooth surface wearing more evenly, resisting abrasion from the substrate is likely also important.

b) Converging ridges

Here the ridges on the crown converge towards a point at the posterior edge of the scale, with the grooves becoming more shallow and narrow towards this edge (Figure 4.5). This arrangement of converging ridges is known to increase turbulent disturbances at the surface (Koeltzsch, 2002). However, encouraging transition to a turbulent boundary layer in this way is a possible mechanism of reducing overall drag; it being the less deleterious alternative to full boundary layer separation.

Some gulper sharks including *Centrophorus granulosus* have converging ridges on the crowns of rhomboidal scales (Figure 4.5) which, because of their large base are separated and do not overlap. The exposed skin in between the crowns is coated in stiff mucus, as in bramble sharks (Silas & Selveraj, 1972), suggesting a protective function. Additionally, the hard tooth-like scales will afford some abrasion resistance, and the ornament of the scale crowns would also help reduce biofouling if the ridge spaces were smaller than the epibiont attempting to attach to the surface (Bixler & Bhushan, 2012). For these reasons, and based on the occurrence of this scale type in generally slow-moving and demersal sharks (section 4.2), their primary functions are likely both abrasion defence and parasite resistance.

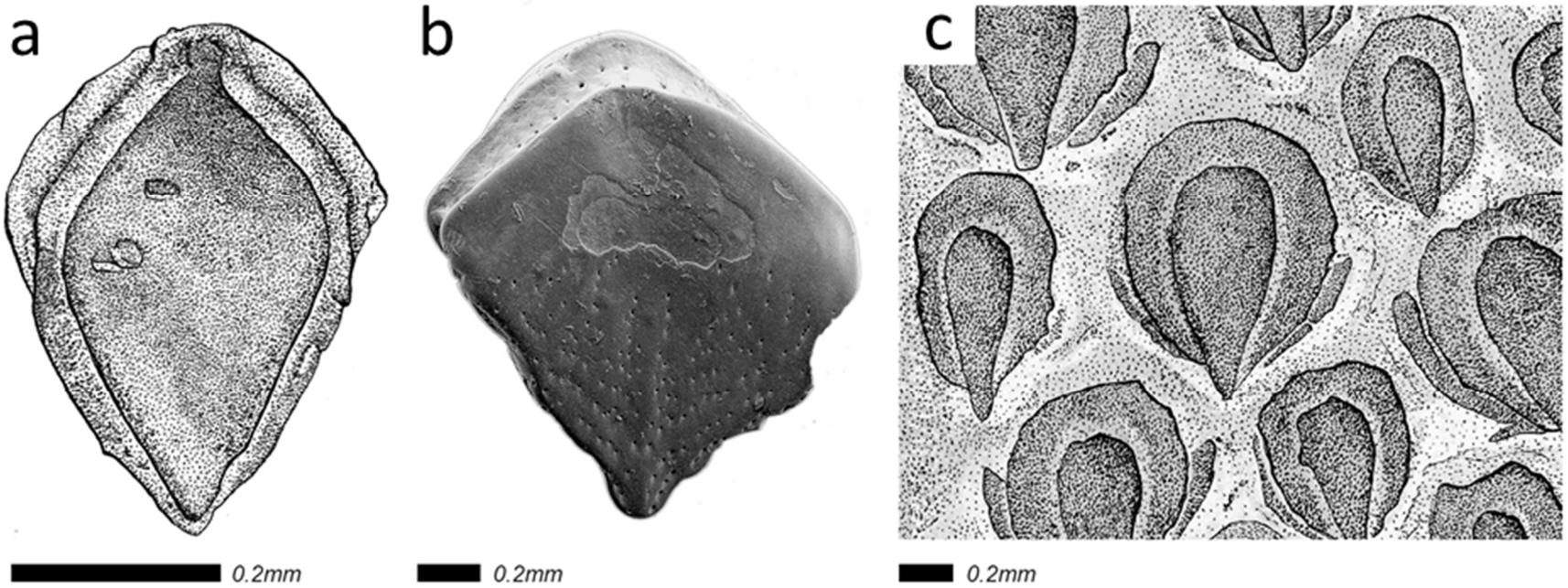

Figure 4.4. Representative examples of smooth teardrop flank scales; a) the thelodont *Loganellia grossi* (drawn from material figured in Märss et al., 2006); b) the 'acanthodian' *Poracanthodes* sp. (section 3.1) and; c) the modern angel shark *Squatina californica* (drawn from material figured in Castro, 2011).

c) Riblets on the leading edge

In some cases the parallel riblets are restricted to the anterior portion of the crown, for example in bamboo sharks (Hemiscyllidae), and some 'acanthodians' (Figure 4.6). The function of this morphology is not immediately apparent, but three hypotheses are presented. In the epaulette shark *Chiloscyllium punctatum* (Figure 4.6), there is a distinct overlap of the crowns, and this helps achieve a dense scale covering for mechanical defence against abrasion, like the smooth teardrop-like scales described above. It is also possible that riblets at the leading edge reduce the surface area of the overlying scale in contact with it. This would reduce inter-scale friction, and therefore the energy cost of flexure during swimming. Although small, it is reasonable to suggest the cumulative benefit of reducing scale-scale contact between thousands of scales could be a significant energetic benefit.

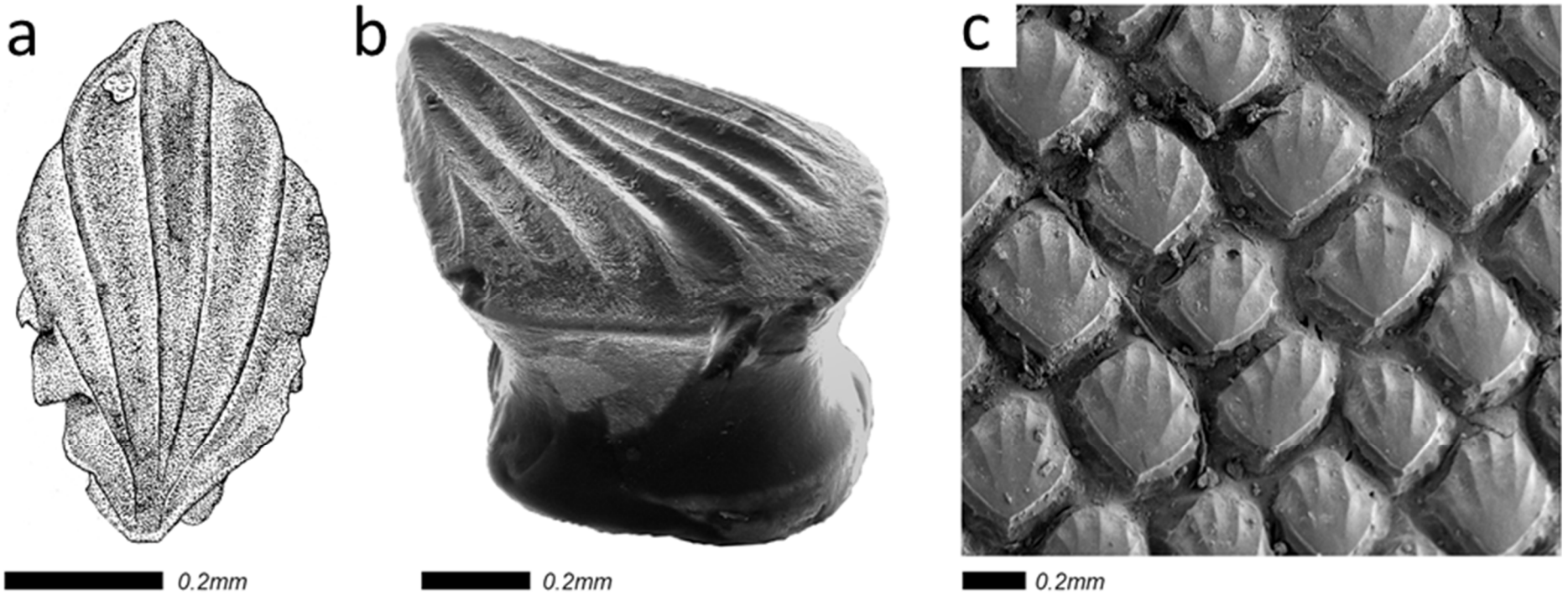

Figure 4.5. Representative examples of flank scales with converging ridges; a) the thelodonts *Overia adraini* (drawn from material figured in Märss et al., 2006); and b) *Thelodus laevis* (micrograph produced using material provided by Henning Blom); c) the modern gulper shark *Centrophorus granulosus* (section 3.1).

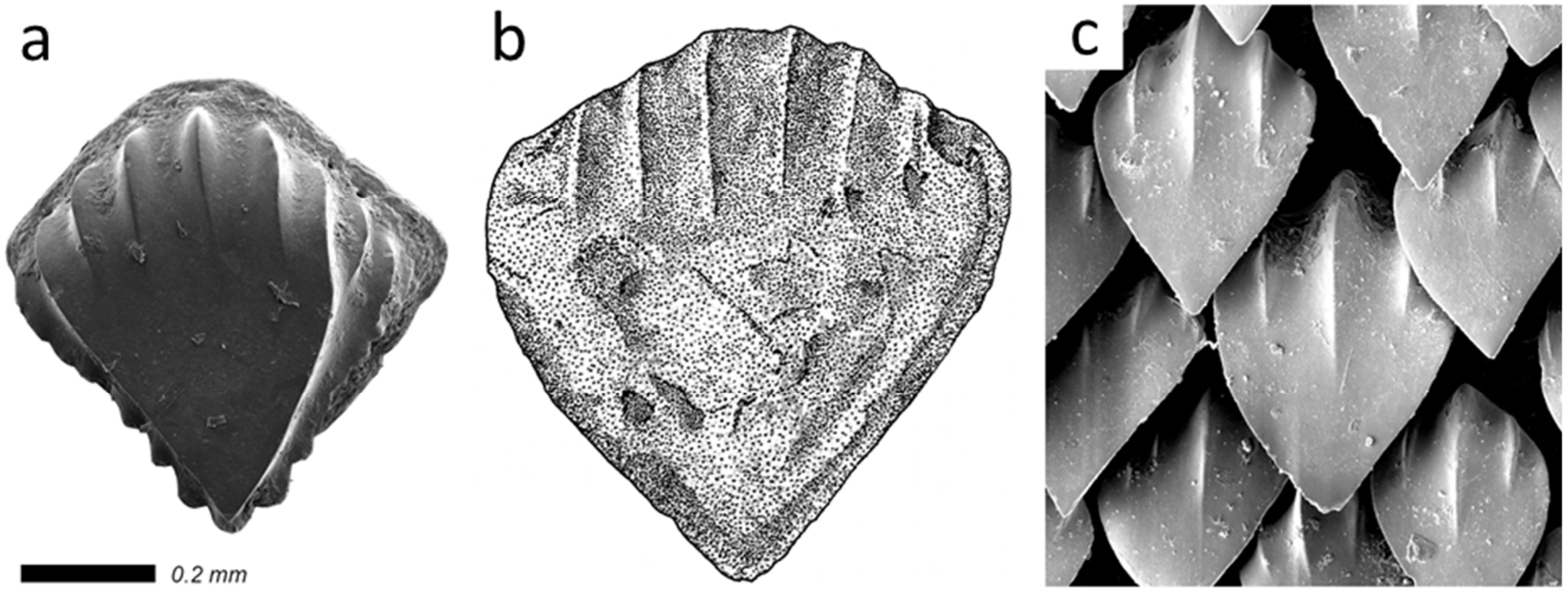

Figure 4.6. Representative examples of flank scales with leading edge riblets; a) the 'acanthodian' *Nostolepis gracilis* (section 3.2); b) the 'acanthodian' *Cheiracanthoides planus* (drawn from material figured in Vaiukevičius, 2005); and c) the modern bamboo shark *Chiloscyllium punctatum* (section 3.1).

Chiloscyllium scales have parallel streamwise riblets that rarely extend into the posterior half of the crown. Scratches were observed across the surface of the crown which did not extend into the anterior region, and in articulated material they can be seen supporting the overlapping scale at the peaks of the ridges which often appear worn (Figure 4.7). The scales of *Scyliorhinus canicula* sometimes possess small polygonal structures (known as ectodermal pits) at the front of the crowns, especially on the head and anterior of the flank. They are well-ordered, low relief structures normally ~12-16µm diameter and hexagonal (Figure 4.7). The function of these pits is discussed further in Chapter 6.

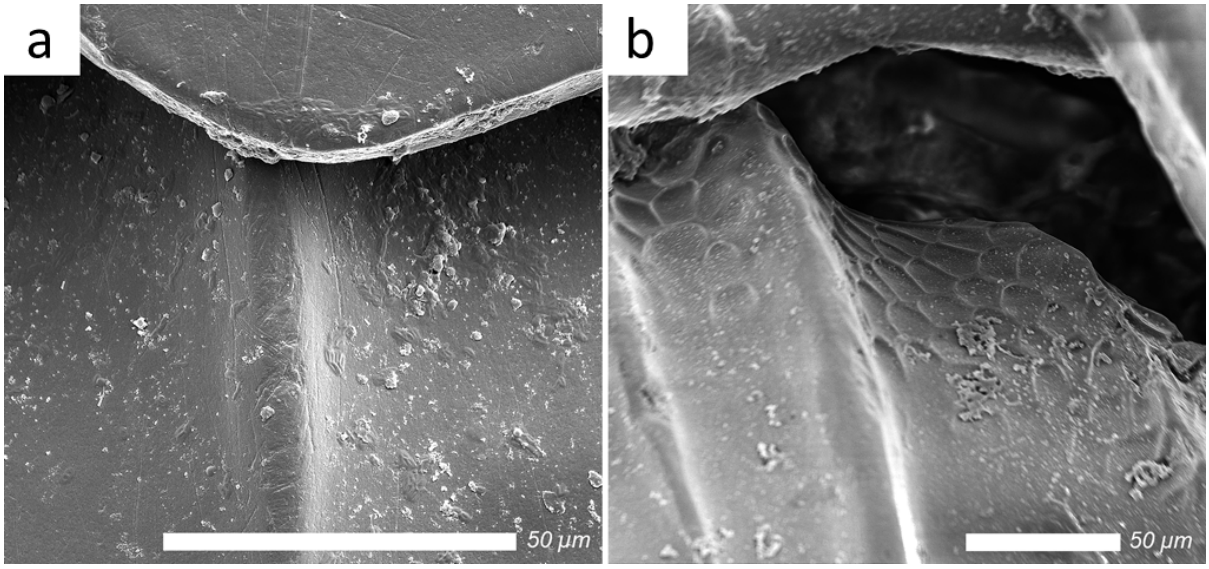

Figure 4.7. Points of interest on shark denticles. A) overlapping head scales ('H3') of *Chiloscyllium plagiosum* (section 3.1) showing riblet wear, and scratch marks. b) Overlapping flank scales ('FB1') of *Scyliorhinus canicula* (section 3.1) showing polygonal ultrasculpture. Scale bars are 50µm.

Reducing inter-scale friction goes some way to explaining the unexposed riblets of bamboo sharks, however it is important to note that 'acanthodian' scales with this ornament do not overlap, and the value of a partial ornament remains unclear. As discussed, riblets that extend the entire length of the crown help modern sharks reduce skin friction during swimming. Realistically, species such as *Nostolepis gracilis* (Figure 4.6.) may still have achieved drag-reduction with partial riblets, but even if this were the case there are many more 'acanthodians' with converging, non-parallel riblets along the anterior edge of the crown. Like those modern sharks with converging ridges over the entire scale, one could speculate that it is an antifouling adaptation, preventing the attachment of parasites.

d) Keel-dominated parallel riblets

Keel-dominated forms have one central antero-posterior riblet extending the full length of the scale. Parallel secondary riblets run alongside, and their length often determines the overall shape of the scale crown. The riblets are sometimes held on isolated 'wings', which can give the scale a cuspate appearance (Figure 4.8). Where the central keel dominates the ornament, a ribletting effect is often still achieved through tessellation with other scales (Figure 4.8). Riblet spacing was hypothesised to correlate with swimming speed in modern sharks, with slower speeds associated with wider spacing (Reif, 1985a), which is confirmed in Chapter 5. As space for riblets and grooves is restricted by the diameter of the crown surface, it is likely that these keels serve to extend the groove width across several scales, and by doing so are optimised for drag-reduction at slower swimming speeds.

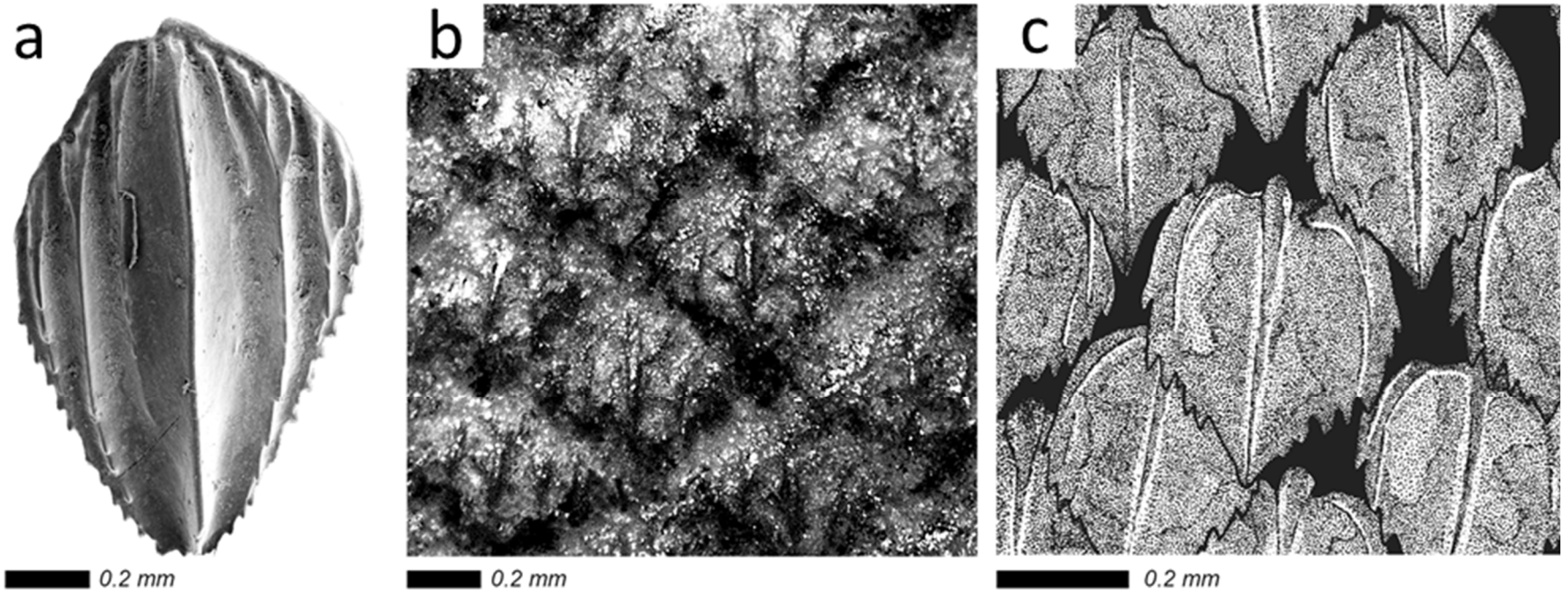

Figure 4.8. Representative examples of keel-dominated flank scales; a. the thelodont *Phlebolepis elegans*; b. the 'acanthodian' *Vernicomacanthus waynensis* (Natural History Museum, London); and the modern gulper shark *Centrophorus squamosus* (drawn from material figured in Castro, 2011).

4.2. Scale Morphotype Occurrence

4.2.1. Modern sharks

The occurrence of different scale types in modern sharks of known ecology is an important basis for interpreting their function. Dermal denticles from the flank of 125 modern shark species were examined from both published and fresh material, and categorised based on ecology (source FishBase; Froese & Pauly, 2014). The scales were then assigned to one of the seven morphotype categories described so far (Appendix I).

The incidence of the defined scale types in different ecological ranks was striking (Figure 4.9), with a clear association between parallel riblets and pelagic ecology. None of the sharks classified as 'fast' or 'moderate speed' (n= 42) had smooth or blocky scales on the flank, nor did they have converging ridges ornamenting their surface. Parallel riblets also occur in demersal and slow pelagic sharks, but are much less prevalent (~23%, n= 81) than blockier or spiny morphotypes. Other patterns are difficult to distinguish, however spiny and spine-like scales do occur more frequently in sharks living on or near the sea floor, where the necessity for physical defence may be elevated.

Based on the literature and results presented so far, a semi-quantitative basis for the interpretation of fossil scales can be constructed (Figure 4.10). It includes several intermediate forms, and accounts for the majority of scale morphologies encountered in modern sharks, and the 'acanthodian' and thelodont fossil record.

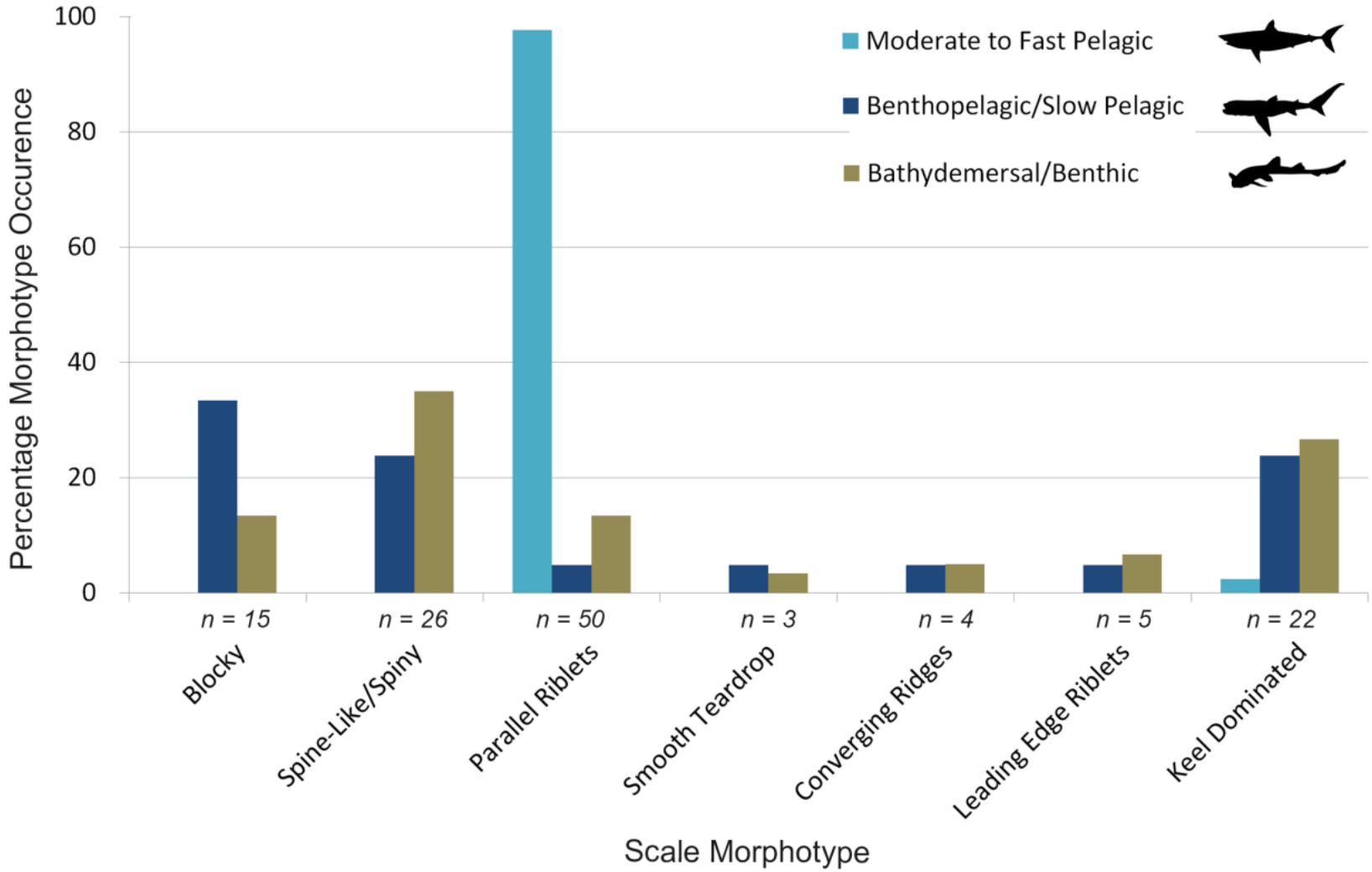

Figure 4.9. Percentage occurrence of scale morphotypes in modern sharks of different ecologies (n =125).

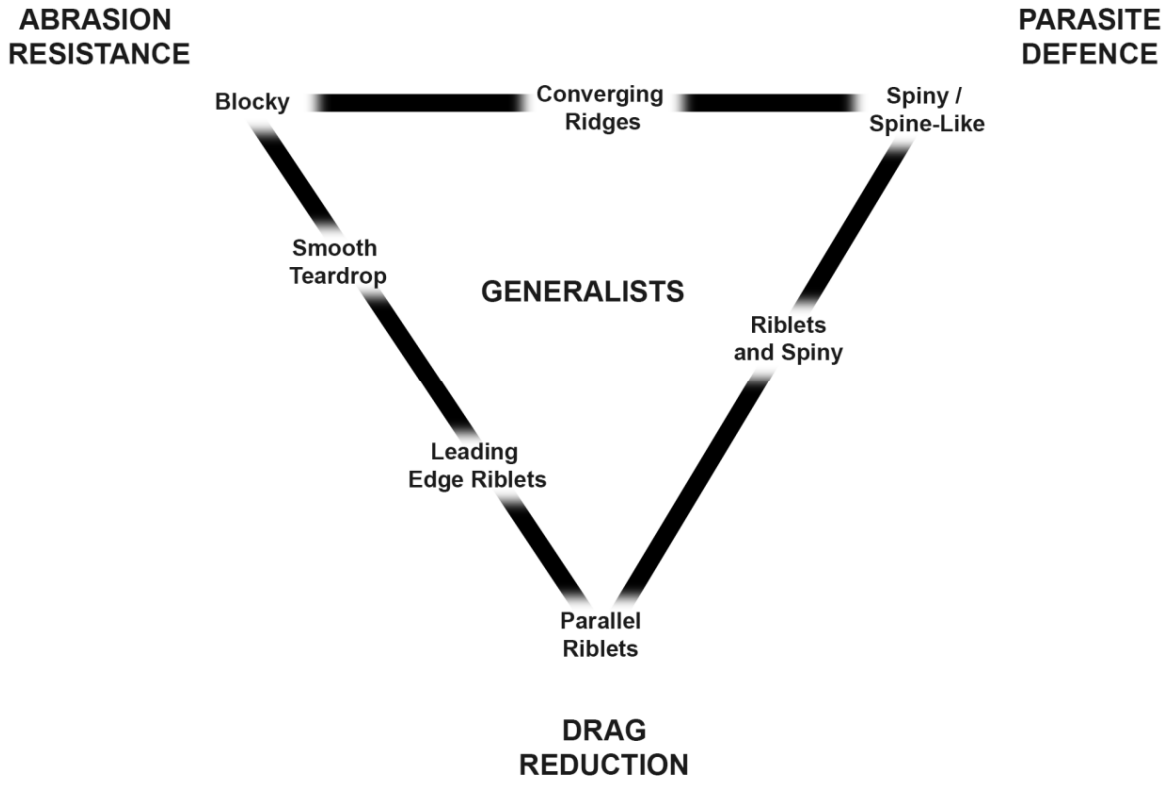

Figure 4.10. Hypothesised functions of flank dermal denticles.

4.2.2. Stratigraphic occurrence

Using the framework described above the global incidence of scale type (and hence function) can be tracked throughout the mid-Palaeozoic, when thelodont, 'acanthodian', and early chondrichthyans dominated the oceans (Figure 4.11). All of these groups were included in the survey of 208 taxa with published scale data. Of these, 182 recorded the body region as the flank (or equivalent terminology), and of these 167 could be classified as a particular scale type. Scale functions were then applied using Figure 4.10, with scores of 1 for specialised single function scales, and intermediate morphotypes were scored 0.5 for each function.

What this reveals is the presence of complex ecologies from at least the Llandovery (~440 million years ago), which includes active pelagic taxa. There appears to be a continuous increase in those species prioritising drag-reduction throughout the Silurian, and into the early Devonian. This is in accord with previously observed patterns of faunal diversity throughout the end Silurian and early Devonian, showing a large-scale shift from benthic to nektonic lifestyles in a suite of disparate taxa (Klug et al., 2010).

4.3. Scale Regionalisation in Modern and Fossil Taxa

Scale morphology of modern sharks can vary enormously (Chapter 6), and a suite of scale types can be found at different body regions of the same species. Examination of articulated remains (detailed in Appendix I) and figured material of thelodonts, 'acanthodian's and early-chondrichthyans proper revealed similar variation in fossil taxa. Commonly, head scales were rounder in shape, with lower relief of crown ornamentation such as spines (if present). Of the 98 taxa with both head and flank scales recorded, only 6 had spines on the head region, and all were thelodonts. Among these were *Lanarkia horrida* and *Drepanolepis maerssae* both of which have much shorter spines on the head, than those of the flank region. Converging riblets were common on the head (n = 21), as were smooth but star-shaped scales (n = 27), although there was little consistency in the associated flank scale morphology. The clearest trend in the majority of taxa was the streamwise elongation of flank scales relative to those on the head, which was also observed in modern shark taxa. Scale regionalisation in modern sharks is the subject of Chapter 6, and is discussed in Chapter 8.

4.4. Summary

In this chapter, the flank scales of thelodonts, 'acanthodians' and early chondricthyans are compared with modern shark analogues. Comparative analysis suggests that blocky and smooth scales of the flank are adapted for abrasion resistance and general mechanical defense, whereas spiny or spine-like scales function to resist parasite attachment. Those flank scales with uniform parallel riblets or those with keels aligned in the streamwise direction are here interpreted as reducing skin friction drag, as in modern sharks. The occurrence of parallel riblets in modern sharks of differing ecologies is presented which supports this view. Intermediate forms are herein described and a flowchart of flank scale function is presented. Using this framework, the stratigraphic occurrence of scale functions is analysed revealing an increase in drag-reducing scale types throughout the Silurian relative to abrasion resistance and parasite defence. Lastly, the head and flank scales of fossil taxa are compared (based on examined and figured material), and an overarching trend for rounder and lower relief head scales is identified.

In Chapter 5 the significance of riblet spacing for drag reduction is investigated in more detail, and in Chapter 7, the skin friction of a number of commonly encountered scale morphotypes is tested experimentally for the first time.

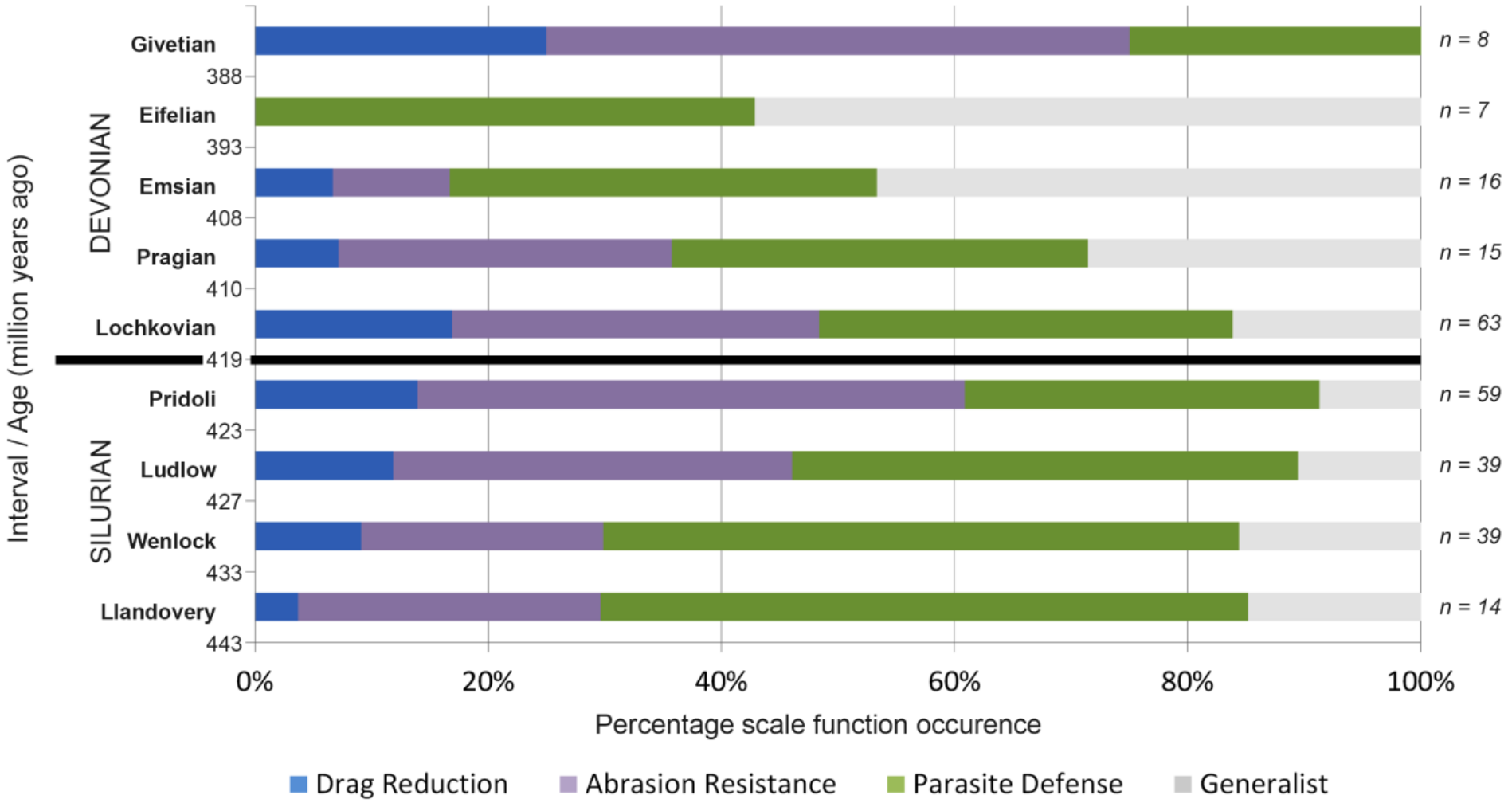

Figure 4.11. Functional composition of mid – Palaeozoic taxa with dermal denticles based on flank scale morphology. See Appendix 1 for full data and references.

5. Drag-reducing Riblets in Modern Sharks and Fossil Fishes

In this chapter, biomimetic investigations of riblet spacing are used retrospectively to investigate the hydrodynamics of the animals which inspired the technology. Ecological data of modern sharks is used to determine if riblet spacing is related to speed, and further extended to fossil taxa for the first time. A summary of the background to this investigation is presented first for ease of reference.

5.1. Riblet optimisation

As demonstrated in Chapter 4, there are striking convergences in the dermal denticle morphology of modern sharks with fossil taxa, with scales adapted to a greater or lesser degree for four distinct functions; parasite defence, abrasion resistance, drag reduction, and luminescence (Reif, 1985a). The first three can be identified from scale morphology because the crowns of dermal denticles are exposed directly to the environment (Whitear et al., 1986), allowing their function to be assessed independently of overlying tissue and mucus.

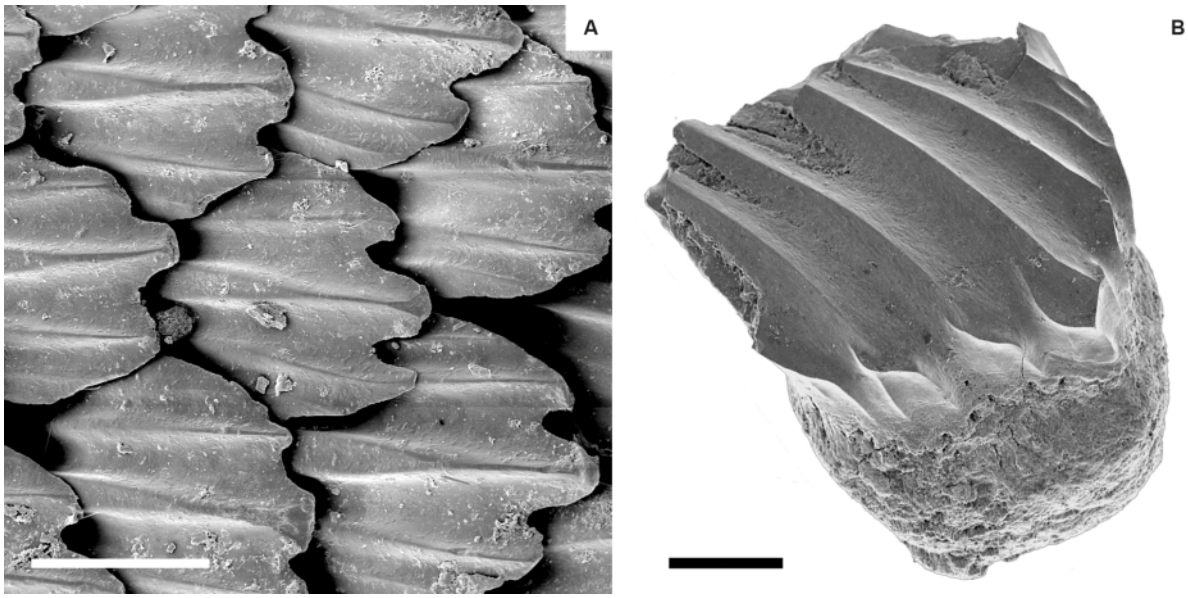

Figure 5.1. Scanning electron micrographs of flank scales of a) the porbeagle shark *Lamna nasus* and; b) the 'acanthodian' *Nostolepis* sp. cf. *N. gaujensis*. Scale bar on each image is 200 µm. 'acanthodian' image reprinted from (Burrow et al., 2009) with permission from Carole Burrow.

The parallel riblets ornamenting the surface of some fish scales (Figure 5.1) have been identified as a key drag-reducing feature, and those of fast pelagic sharks have been the inspiration for numerous biomimetic applications, including swimsuits, and drag-reduction on planes and ships (Bixler & Bhushan, 2012). Riblets act to control vortices which form across the scale surface in a turbulent flow regime, by reducing their lateral drift, and pinning the vortices in place. This reduces the lateral transfer of momentum, meaning drag – any impedance/loss of velocity – is reduced as well. Riblets also lift these vortices up and out of the valleys in between the riblet peaks, minimising the surface area rotating fluid is in contact with. This means less force is required to overcome the friction imparted by that surface, and drag is reduced (Bechert & Hoppe, 1985; Bechert et., 2000; García-Mayoral & Jiménez, 2011; Dean & Bhushan, 2012; Oeffner & Lauder, 2012; Figure 5.2). Scales of modern sharks become larger as they are shed and replaced throughout the animal's life, but riblet spacing on the flank remains fairly constant (Raschi & Tabit, 1992), suggesting a tight optimal range related to lifestyle (although see section 6.3).

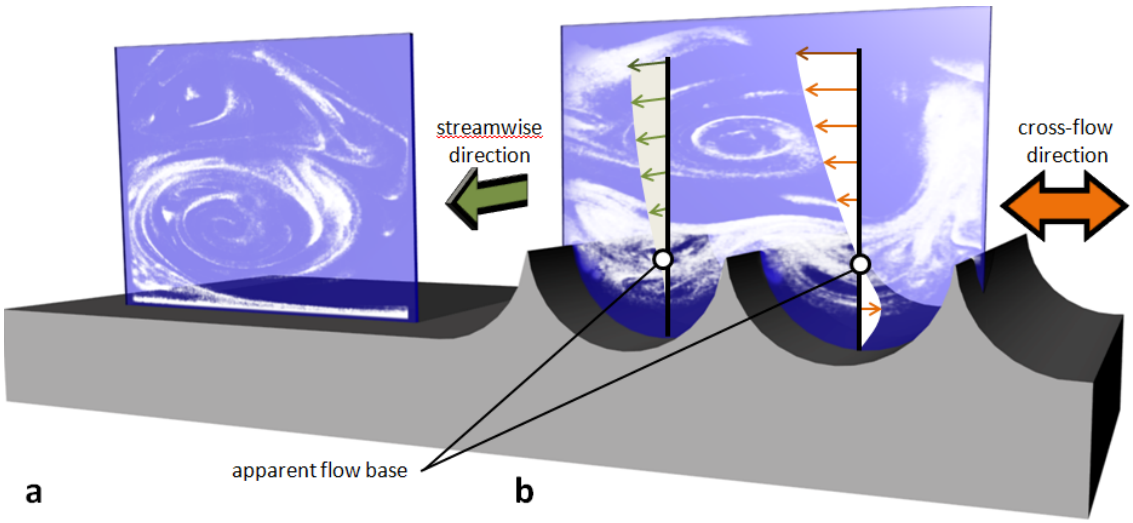

Figure 5.2. Schematic vertical cross sections of turbulent-flow of streamwise vortices over a) a flat plate, and; b) riblets. Mean velocity profiles for flow in streamwise (green) and cross-flow (orange) directions shown for riblets. Adapted for illustrative purposes from Bechert et al., 1997, and Lee & Lee, 2001.

Since some of the earliest work recognising the potential drag-reducing properties of riblets, experimental studies have sought to optimise their geometry (e.g. Walsh & Lindemann, 1984). To function effectively, riblets must be spaced more narrowly than the vortices that form across the scale, keeping them above and out of the valleys between the peaks (Figure 5.2b). It was found that smaller riblet spacing was directly related to greater drag-reduction in faster flows, with 2-3 riblet peaks needed to support a vortex (Bechert et al., 2000). However, this understanding of riblet optimisation has never been applied retrospectively to study the sharks that inspired the design.

In Chapter 4, it was demonstrated that denticles of modern sharks are comparable to those found in many long extinct groups including the stem chondrichthyan 'acanthodians' (Davis et al., 2012; Zhu et al., 2013) and the jawless thelodonts from the Palaeozoic (~383-425 million years ago) (Märss et al., 2007), some of which have riblets on their crowns (e.g. Figure 5.1b). Fossil fish hydrodynamics are seldom investigated (Fletcher et al., 2014), not least because three dimensional structures are rarely preserved. While only some fossil taxa in this study are known from articulated remains (Miles, 1973; Turner, 1982; Young & Burrow, 2004), their scales can provide key hydrodynamic information. The riblets of 50 modern shark species were compared to test the hypothesis that narrower spacing will be found in relatively faster extant shark species. The riblet spacings of fossil taxa were then measured for comparison.

5.2. Riblet Spacing Analysis

Scanning electron micrographs of the flank region of 50 modern sharks, 6 'acanthodians' and 5 thelodonts were analysed, from both newly imaged and existing figured material. Riblet spacing was measured as detailed in section 3.1.3c, and was the only scale trait measured for this analysis. The relationship between riblet spacing and swimming speed in sharks was investigated by Dr Mark Bell using phylogenetic least squares regression (PGLS). For full methodology see section 3.1.3c.

Taken as a whole, riblet spacing data did not depart significantly from a normal distribution, but since there were few data in some groups and some distributions were not normal, tests for differences in riblet spacing between groups were performed using Mann-Whitney tests, correcting for multiple testing with the False Discovery Rate method (FDR) Benjamini & Hochberg, 1995), using the p.adjust function in R. The PGLS test showed that there was a strong negative correlation between riblet spacing and swimming speed, after taking phylogeny into account ($r^2 = 0.244$, F 8.272, $p < 0.001$). Figure 5.3 shows distributions of riblet

spacing in the three shark and two fossil species groups, and Figure 5.4 shows relative riblet spacings of modern shark species on a recent phylogeny (Vélez-Zuazo & Agnarsson, 2011). Table 5.1 shows the results of Mann-Whitney post hoc comparisons.

The analysis of riblets in modern sharks revealed a significant trend towards decreased riblet spacing with increased swimming speed. Mean riblet spacing for 'fast' sharks was 63µm, 'moderate' was 91µm (44% wider than 'fast'), and 'slow' was 111µm (75% wider than 'fast'). The extinct thelodonts and 'acanthodians' had the narrowest mean riblets at 50µm and 62µm respectively, with spacing comparable with the fastest modern sharks.

Table 5.1 shows riblet spacing is significantly smaller in the 'Fast' sharks than in both 'Moderate' and 'Slow/Scavenger/Ambush' modern species. There was no significant difference between 'Fast' modern sharks and the 'acanthodians', or thelodonts. Both the 'Moderate' and 'Slow/Scavenger/Ambush' species have significantly wider riblet spacing than the two fossil categories, with the exception that the 'Moderate' and 'acanthodians' are not significant following a p value correction using FDR.

Table 5.1. Comparisons of riblet spacing between ecological categories. Significant results (<0.05) are highlighted in bold. Values in brackets represent p values following Mann-Whitney tests and False Discovery Rate correction. Courtesy of Dr Mark Bell.

		Moderate	**Slow**	**Thelodonts**	**'Acanthodian'**
Fast	W	101	6	71	79
	p	**0.001 (0.011)**	**<0.001 (<0.001)**	0.169 (0.507)	0.268 (0.536)
Moderate	W	-	39	104	113
	p	-	**0.001** (0.17)	**0.003 (0.021)**	**0.016** (0.081)
Slow	W	-	-	35	39
	p	-	-	**0.003 (0.02)**	**0.008 (0.049)**
Thelodonts	W	-	-	-	11
	p	-	-	-	0.537 (0.537)

Empirical studies of biomimetic models show that decreasing riblet spacing has a greater drag-reducing effect at higher speeds (Dean & Bhushan, 2010), and this negative relationship between riblet spacing and speed in modern species of shark can now be demonstrated. This may be related to a decrease in vortex wavelength with increasing velocity, when more closely-packed riblets are needed to hold the vortices above the riblet valleys. The small riblet tips reduce the contact between the vortex and the fish by lifting them out of the riblet valley, reducing wall shear stress and skin friction (Bechert et. al. 1997; Lee & Lee, 2001). Extinct taxa with narrowly spaced riblets appear to have been similarly adapted for speed and efficiency. Furthermore, there is evidence that some of the earliest known fishes were similarly well adapted for drag-reduction. The Middle Ordovician (~460 million years ago) fishes *Tantalepis gatehousi* (Sansom et al., 2012) and *Areyonga oervigi* (Young, 1997) (possible chondricthyans) were not included in the main analysis as the scales found were of unknown position on the body. However their mean riblet spacing was 69µm and 77µm respectively, placing them within the fast-moderate speed modern sharks.

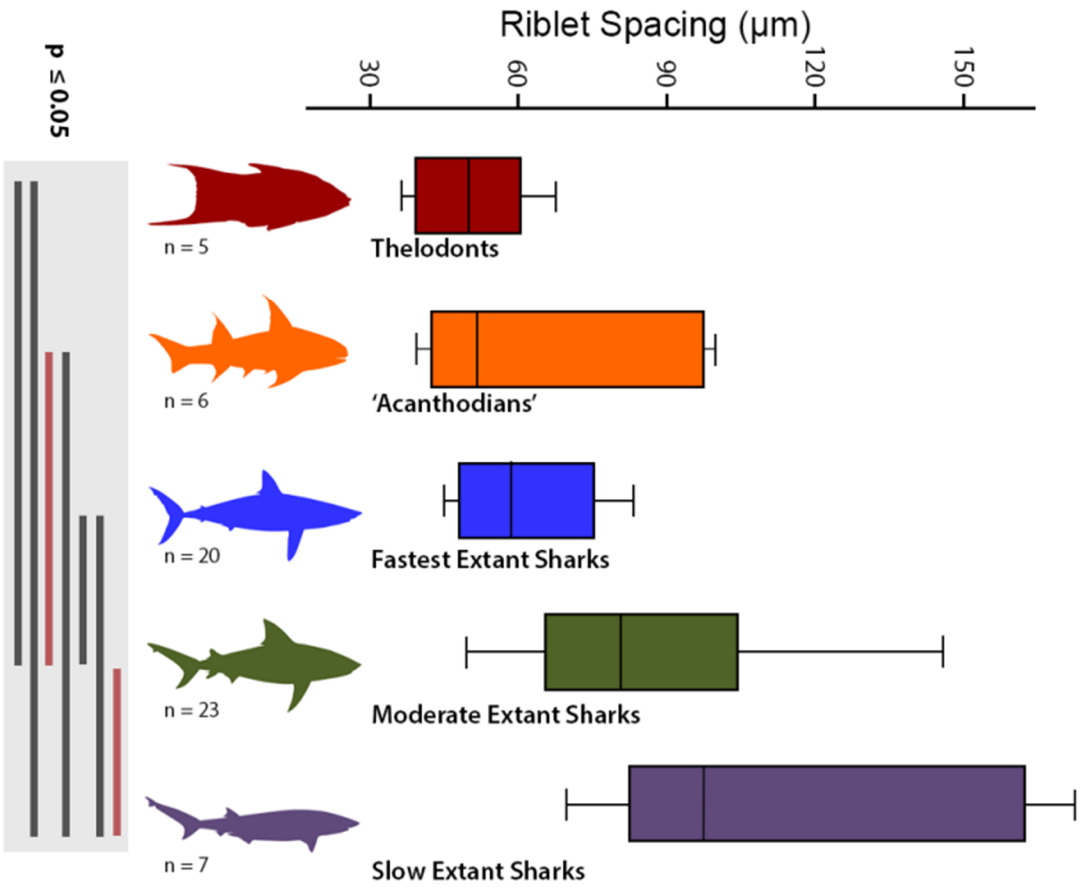

Figure 5.3. Boxplot showing riblet spacing measurements for acanthodians, thelodonts and modern sharks (n = number of species) possessing distinct parallel grooves and riblets on the

scale crown surface. Boxes represent 25-75 percent quartiles with median values at vertical division line. Statistically significant differences (Mann-Whitney) (Table 5.1) are indicated by left adjoining lines, those in red indicate p values that show no significant difference after FDR correction. Determination of shark speed categories was based on ecological and experimental speed data, detailed in the methods section.

The smallest riblet spacing of the 'acanthodians' studied was the Lower to upper Middle Devonian (~407-383 mya) genus *Milesacanthus* (Burrow, et al., 2006; 2009), at 40µm. *Milesacanthus* scales resemble those of the shortfin mako shark (*Isurus oxyrhinchus*), which can be highly flexible, especially in the flank region where adverse pressure gradients are likely to develop at high speeds or during manoeuvres (Lang et al., 2008). The erection of these scales, known as 'bristling', acts to prevent boundary layer separation by retarding any reversing flow (Motta et al., 2012). In this and *Lamna nasus* (Chapter 6) the scales have a hinge-like base, wider than it is long and smaller than the crown above. *Milesacanthus* also had scales with a relatively small base, and a base length to width ratio very similar to the mako shark, suggesting a similar bristling action.

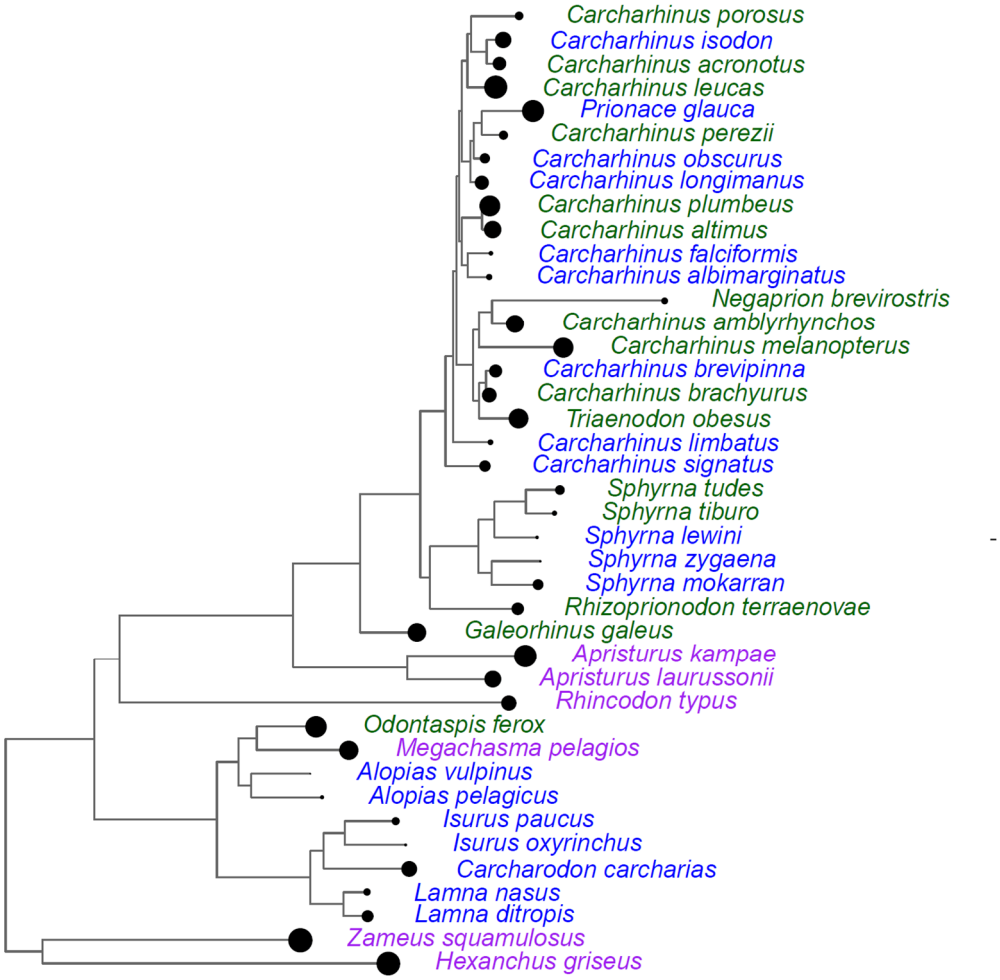

Figure 5.4. Plot showing the phylogeny of species included in this study which also feature in the Vélez-Zuazo and Agnarsson, 2011 dataset. Species are coloured by speed categories 'slow' (purple), 'moderate' (green), and 'fast' (blue) as in Figure 4 of the main text. Mean spacing values illustrated by circles at each tip, where larger circles equal larger riblet spacing. This figure was produced and the PDR analysis performed by co-author Dr Mark Bell.

The occurrence of innovative drag-reducing morphology in fossil taxa as advanced as that seen in the fastest modern sharks is significant. This optimal scale riblet spacing is found in the earliest groups of scaled fishes, suggesting that there was a significant selective advantage to being built for speed. An expansion into the pelagic realm during the Devonian from a predominantly benthic fauna, a progression referred to as the 'nektonic revolution' (Klug et al., 2010), is certainly consistent with selection for hydrodynamic efficiency; there is nowhere for prey to hide in open water and speed can give both predator and prey a selective advantage.

5.3. Summary

In this chapter phylogenetic generalised least-squares regression is used to demonstrate a strong relationship between riblet spacing and swimming speed in modern shark species. The smallest spacing of riblets is associated with the fastest extant sharks, and the largest spacing occurs in the slowest pelagic species. The appearance of riblets in fossil species suggest that such a drag-reduction morphology evolved in the earliest vertebrates, including some of the oldest examples known (~460 million years ago). Applying this observation to the fossil record it appears some Palaeozoic taxa match the apparent optimum riblet spacing for drag-reduction found in faster pelagic sharks. This implies adaptation for fast, efficient swimming. The results demonstrate that riblet spacing is fine-tuned to the species' ecology, and that novel and sophisticated drag-reduction adaptations existed at the dawn of fish evolution.

In the next chapter, the variation in scale features (ncluding riblet spacing) between and within species are investigated, principally in the modern porbeagle shark *Lamna nasus*.

6. Modern shark scale variability analysis

In Chapter 4, the flank scales of fossil and modern shark scales were compared to inform interpretations of their function. The flank is the largest region of the fish body (section 3.1), and this chapter demonstrates the relative homogeneity of scales in this region as well. It is on this basis that the flank region is considered representative of general scale function, for comparison between taxa. It is noted in section 4.3 however that scale morphology can differ between body regions, in both modern shark taxa and their extinct Palaeozoic relatives. Quantitative analysis of scale regionalisation is rare for modern sharks (Cigala Fulgosi & Gandolfi, 1983; Crooks, 2013), and to date only Reif's 1985 work has addressed hydrodynamically relevant scale features. A thorough investigation of modern shark material is presented in this chapter, which forms a crucial basis for understanding the regionalisation of scales in fossil taxa.

6.1. Morphological regionalisation

a) General observations

Qualitative examination of sampled modern shark material (section 3.1) revealed several patterns of scale regionalisation. Scales from the rostral region of the head ('H1', Figure 6.1) tend to be smoother, with noticeably lower relief of crown structures such as riblets (if present). In addition to the smoothness of the individual scale crowns, and the rostral skin surface in general, the directionality i.e. a 'streamlined' geometry of the scale crown is also much smaller. Scales in this region also tend to tessellate on all sides of the crown, rather than overlapping each other. The porbeagle shark *Lamna nasus* showed little change from head to tail, however in contrast to regions more posterior, scales at the tip of the rostrum did not overlap, and were very tightly packed. Both examined *Chiloscyllium* species also had blocky and rhombic head scales with little overlap, but after this point scales become more elongate with greater overlap.

This pattern of overlap is not repeated in *Scyliorhinus canicula* (Figure 6.2.), which has flat, kite-shaped scales on the tip of the head, which overlapped but still formed a relatively smooth surface. After this point, scale shape quickly graded to spine-like teardrops, the size of which varied greatly across the rest of the head and flank. Of the material examined for this study, only *Centrophorus granulosus* had rough surface structures on the scale crown with radial ridges converging to a central point. This rostral scale type is very similar to many 'acanthodian' head scales, and just as in *C. granulosus* flank scales are more elongate and

streamlined in shape. Like many 'acanthodian' and thelodont taxa, scale overlap was not observed at any sampled point on the body. At the tail, scale shape is generally similar to that of the flank; however tail scales tended to be relatively smaller, with tighter packing than body regions upstream.

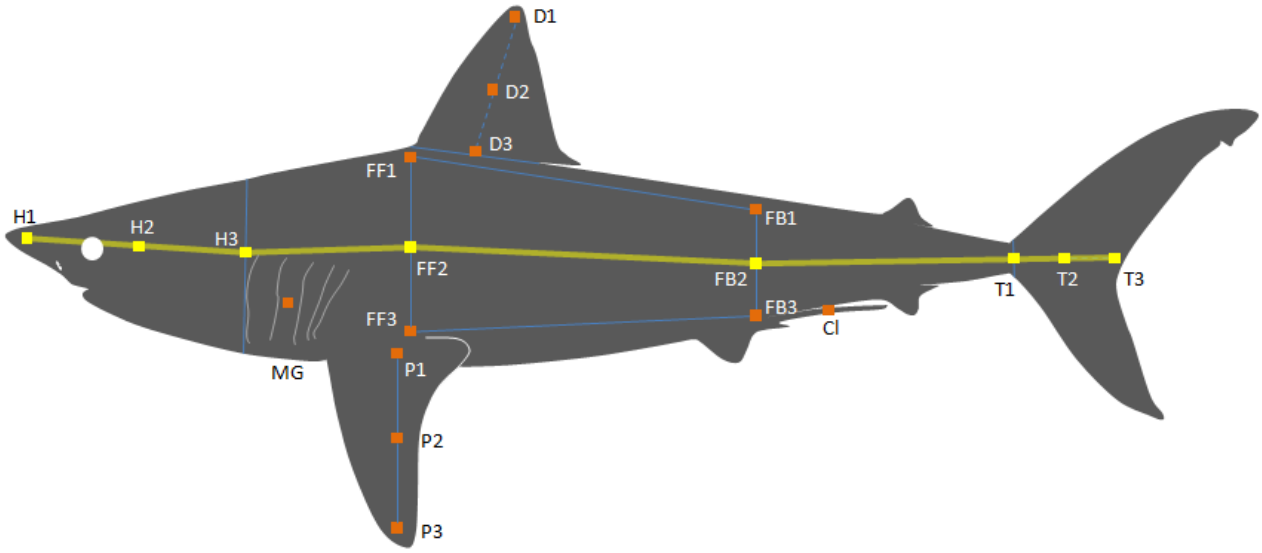

Figure 6.1. Standardised sampling locations (orange squares) used throughout this study, and midline transect (yellow line) from anterior-most to posterior-most sampling locations. Scheme detailed in section 3.1. Example shown is *Lamna nasus*, not to scale.

6.2. Crown and base dimensions

To investigate the size and basic geometry of scale crowns across the body of modern sharks, the width and length of scales at different sampling locations were measured. Two species were chosen, based on availability of material, and to represent contrasting modern shark ecologies. The scales of the slow-moving, deepwater gulper shark *Centrophorus granulosus* do not overlap, and the entire scale crown geometry can be measured in situ. On this basis the flank of *C. granulosus* was chosen for a higher density of sampling. This was to test that the flank region was sufficiently homogeneous enough to justify basing ecological interpretations on scales sampled from any generically described 'flank scale' in the literature. The larger, faster-moving porbeagle *Lamna nasus* and many other pelagic shark species have scales which overlap, which presented a problem for measuring large numbers of scales in a limited time period. The exposed/visible scale lengths and widths were also measured to approximate the degree of scale overlap and crown size respectively. The base aspect ratio was also calculated

for isolated and manually mounted scales, to test the hypothesis that wider thinner scale bases occur in areas prone to bristling (Lang et al. 2008).

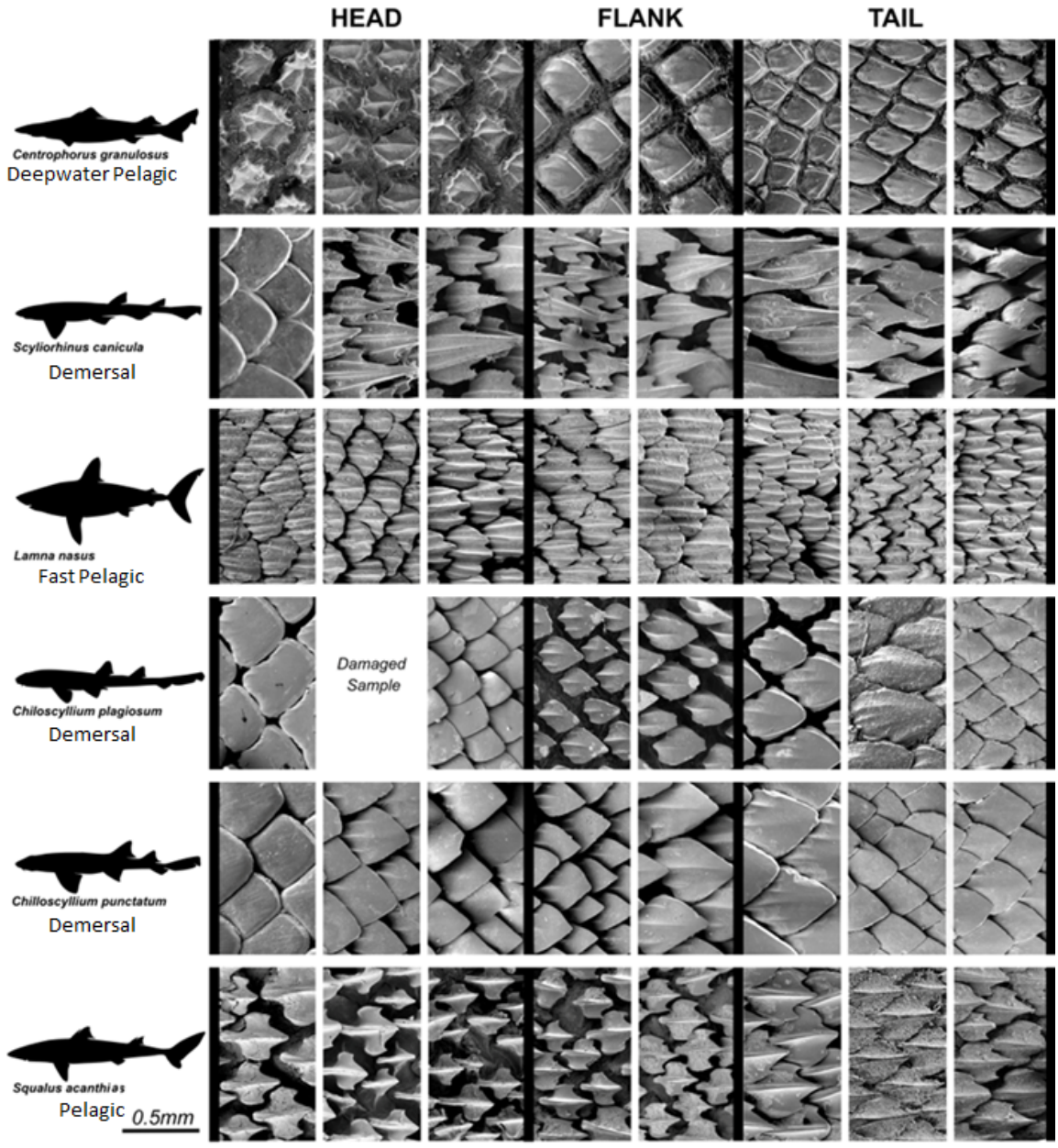

Figure 6.2. Shark squamation along the midline ('H1-3, FF2, FB2, T1-3', Figure 6.1.) showing scale variation from anterior to posterior. Note: It is clear from material figured in the literature (Reif, 1985a), that the scales of *Squalus acanthias* have similarly smooth rostral scales, in contrast to the sample presented here (bottom left). Ecological data based on Ebert et al., 2013.

6.2.1. Crown size and geometry of *Centrophorus granulosus*

Significant differences in both crown width and aspect ratio were found between most sampling positions (Table 6.1). The pectoral fin ('P3', Figure 6.1., Figure 6.3) had the smallest scales with mean width of 94±3.0µm (SE), and mean length of 153±4.4µm, and the largest scales were 333±5.0µm (SE) wide at the dorsal-most anterior of the flank, and 387±10.4µm at the base of the dorsal fin ('FF1' and 'D3' respectively).

Compared to the 6-point sampling scheme ('FF1-3' and 'FB1-3', Figure 6.3), width and length means were lower (0.9%, and 4.9% respectively) than the higher-resolution treatment, which sampled 59 positions within the same bounds (Appendix I). However, a t-test revealed no significant difference between the values obtained by these sampling methods for either length ($p = 0.84$, f 2.5) or width ($p = 0.23$, f 1.5). Mean scale aspect ratio (length/width) ranged from 0.90 at the anterior-most centre of the flank ('FF2') to 1.78 at the middle of the tail ('T2'). Scales were significantly longer and narrower in the tail and dorsal and pectoral fins compared with the flank (Table 6.1) supporting earlier qualitative observations (section 6.1).

6.2.2. Crown size and geometry of *Lamna nasus*

As discussed, the overlap of scales in this species can obscure the crown and prevent accurate measurement, but the exposed width can still provide an approximate indication of scale size. Significant differences in scale width were found between most body regions (Table 6.2), and across the midline of the shark there is a general decrease in scale width from anterior to posterior with tail scales being ~14% smaller than those on the flank and head. Additionally the pectoral and dorsal fin mean scale widths were 10-12% smaller than the flank and head (see Appendix I for individual specimen plots). A similar pattern was found for exposed scale length, with the largest values at the tip of the rostrum ('H1') and the proximal region of the pectoral fin (Table 6.3). Mean aspect ratio (width/length) of exposed scale crown rises gradually across the midline, with an increase of 6% (longer thinner scales) from the head to front flank region. The tail scales have even longer exposed length relative to width, with an exposed aspect ratio 11.9% greater than at the head. This supports earlier observations that scales tend to be longer and narrower towards the tail, a pattern also observed in actinopterygians (pers. comm. Matt Friedman).

Maturity occurs in male *Lamna nasus* at ~8 years between 165-195cm, and ~13 years in females at 195-245cm (Francis & Duffy, 2005; Ebert et al. 2013; Natanson et al., 2002). Widths and lengths measured for the *Lamna nasus* sharks showed significantly wider and longer

crowns in mature animals (Figure 6.5, Tables 6.2, 6.3), likely because denticles are shed during growth and replaced by larger scales. Scale widths and lengths were also significantly greater in female animals, perhaps reflecting the larger average size of female specimens of this species used in this analysis.

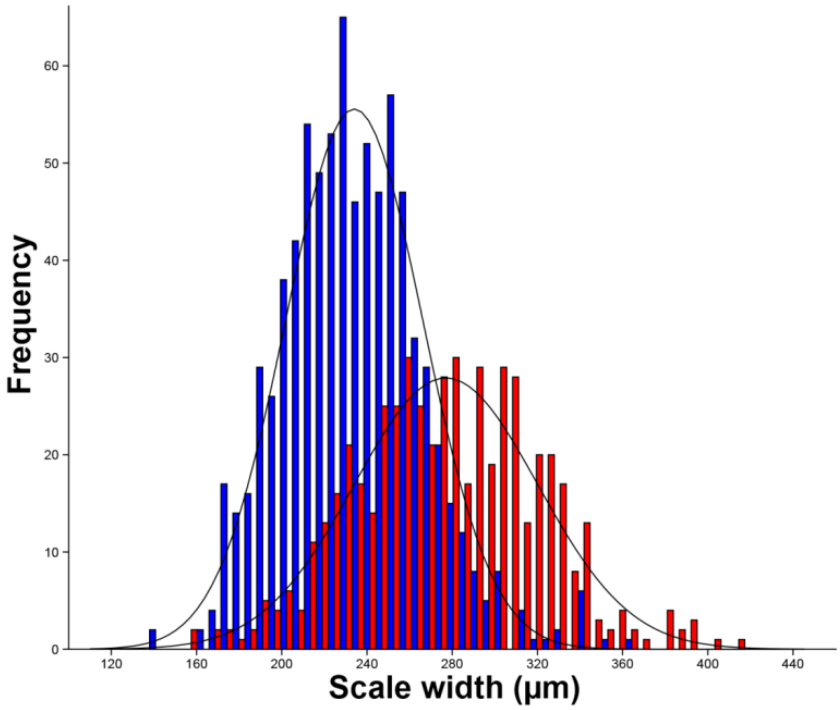

Figure 6.5. Histogram showing mean scale width of immature (blue) and mature (red) *Lamna nasus*. Males over 165 cm and females over 195 cm defined as mature (according to Ebert et al., 2013).

6.2.3. Scale base geometry of *Lamna nasus*

Across the midline of the shark there is an increase in scale base aspect ratio of ~47% (i.e. becoming wider, relative to length) from head to flank ('H1'-'FB2', Figure 6.4). Scale base aspect ratio differs significantly between most body regions, tending to be lower in the fins and snout (Table 6.4.). These are areas where scale stability and embedded strength in the dermis may be more important than the pivoting bristling action encouraged downstream, especially across the flank. Another possibility is that there are changes in scale packing in different regions, which require the scale bases be smaller in areas of higher scale density. Alternatively base morphology may be influenced by the differing orientation of collagen fibres across the body, which are vital for maintaining the elasticity of shark skin.

Table 6.1. Descriptive statistics and tests for difference of crown width (µm) and crown aspect ratio in *Centrophorus granulosus* (48cm, male).

CROWN WIDTH (µm)							p-value*						
Sample	N	Mean	SE	25%	Median	75%	H	Mg	P	D	FF	FB	Cl
All Scales	298	214.2	4.60	153.3	198.10	289.2							
Head (H)	45	214.3	4.71	195.0	217.5	22.1							
Mid Gills (Mg)	15	160.4	2.83	150.5	157.2	169.2	**<0.001**						
Pectoral Fin (P)	45	131.3	5.94	88.2	142.1	164.0	**<0.001**	0.312					
Dorsal Fin (D)	45	187.2	14.91	112.5	128.5	318.3	0.413	0.428	**<0.001**				
Flank Front (FF)	45	288.5	6.38	257.9	285.9	329.2	**<0.001**	**<0.001**	**<0.001**	**<0.001**			
Flank Back (FB)	45	315.8	3.42	300.4	315.3	334.7	**<0.001**	**<0.001**	**<0.001**	**<0.001**	0.403		
Claspers (Cl)	13	169.6	4.16	157.5	167.7	182.3	**0.012**	0.997	0.059	0.871	**<0.001**	**<0.001**	
Tail (T)	45	179.2	4.02	155.8	176.5	200.0	0.116	0.829	**0.005**	0.999	**<0.001**	**<0.001**	0.995
CROWN ASPECT RATIO (L/W)							p-value†						
Sample	N	Mean	SE	25%	Median	75%	H	Mg	P	D	FF	FB	Cl
All Scales	285	1.29	0.02	1.03	1.21	1.50							
Head (H)	45	1.16	0.03	1.01	1.15	1.32							
Mid Gills (Mg)	15	0.98	0.04	0.87	0.97	1.08	0.119						
Pectoral Fin (P)	45	1.56	0.06	1.28	1.54	1.72	**<0.001**	**<0.001**					
Dorsal Fin (D)	45	1.43	0.03	1.24	1.40	1.62	**<0.001**	**<0.001**	0.596				
Flank Front (FF)	45	1.02	0.02	0.95	1.00	1.11	0.305	1.000	**<0.001**	**<0.001**			
Flank Back (FB)	45	1.05	0.02	0.98	1.07	1.11	0.847	**<0.001**	**<0.001**	**<0.001**	0.990		
Claspers (Cl)	13	1.44	0.04	1.32	1.44	1.56	**<0.001**	**<0.001**	0.660	1.000	**<0.001**	**<0.001**	
Tail (T)	45	1.57	0.06	1.21	1.60	1.85	**<0.001**	**<0.001**	1.000	0.489	**<0.001**	**<0.001**	0.553

*Crown Width - ANOVA [F(7, 290) = 70.41, p = <0.001], p-values from Tukey's post hoc test, emboldened results significantly different (95% confidence interval).† Crown Aspect Ratio - ANOVA [F(7, 314) = 37.68, p = <0.001], p-values from Tukey's post hoc test, emboldened results significantly different (95% confidence interval).

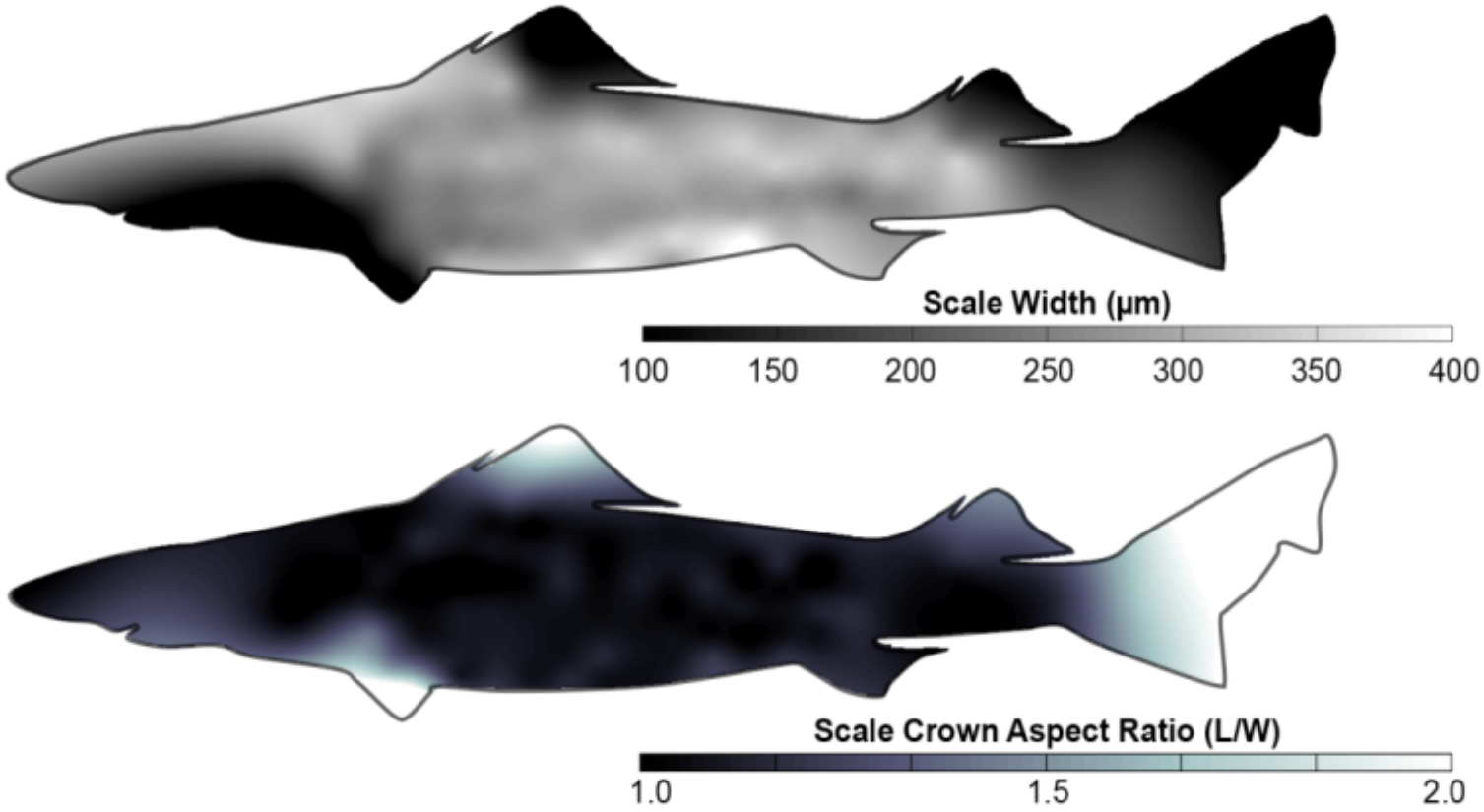

Figure 6.3. Heat map of a) mean scale width (µm) and; b) scale crown aspect ratio (length/width). Distribution interpolated across entire body from standardised sample locations (Figure 6.1.).

Table 6.2. Summary statistics and test for difference of *Lamna nasus* scale width measurements (all micrometres, µm).

Sample		N	Mean	SE	25%	Median	75%	p-value*	F
All Scales		1421	250.70	1.12	221.00	246.44	276.02		
Sex	Male	570	241.85	1.69	213.43	234.68	265.04	**<0.001**	1.11
	Female	851	256.63	1.46	227.13	252.52	282.58		
Maturity	Immature	851	233.47	1.10	211.97	231.64	253.66	**<0.001**	1.78
	Mature	570	276.44	1.79	247.52	276.49	305.92		

Sample	N	Mean	SE	25%	Median	75%	p-value† H	Mg	P	D	FF	FB
Head (H)	225	263.86	2.48	235.27	257.79	290.07						
Mid Gills (Mg)	75	259.30	3.89	236.64	252.42	272.21	0.931					
Pectoral Fin (P)	225	240.39	2.56	213.21	231.93	266.61	**<0.001**	**<0.001**				
Dorsal Fin (D)	225	234.41	2.54	208.04	228.88	256.01	**<0.001**	**<0.001**	0.785			
Flank Front (FF)	225	261.00	2.78	229.88	254.93	282.36	0.993	1.000	**<0.001**	**<0.001**		
Flank Back (FB)	221	273.76	2.95	242.65	266.42	301.82	0.213	**0.010**	**<0.001**	**<0.001**	**0.037**	
Tail (T)	225	228.34	2.43	202.40	223.46	256.44	**<0.001**	**<0.001**	0.061	0.775	**<0.001**	**<0.001**

SE = Standard error

Maturity = Males over 165cm and females over 195cm defined as mature, according to Ebert et al. 2013.

* p-value from Student's T-test. Emboldened values significantly different (95% confidence interval).

† ANOVA [F(6, 1414) = 41.68, p = <0.001], p-values from Tukey's post hoc test, emboldened results significantly different (95% confidence interval).

Table 6.3. Summary statistics and test for difference of *Lamna nasus* exposed scale length measurements (µm).

Sample		N	Mean	SE	25%	Median	75%	p-value*	F
All Scales		1421	250.70	1.12	221.00	246.44	276.02		
Sex	Male	570	208.43	1.89	175.34	203.97	235.13	**<0.001**	1.15
	Female	851	244.89	1.66	211.89	240.50	275.05		
Maturity	Immature	851	216.23	1.42	186.99	215.20	243.45	**<0.001**	1.75
	Mature	570	251.21	2.30	214.61	251.12	290.78		

							p-value†					
Sample	N	Mean	SE	25%	Median	75%	H	Mg	P	D	FF	FB
Head (H)	225	249.01	2.97	217.16	244.72	280.28						
Mid Gills (Mg)	75	261.63	5.84	229.28	262.15	284.71	0.143					
Pectoral Fin (P)	225	244.29	3.13	206.56	240.74	273.50	0.964	**0.009**				
Dorsal Fin (D)	225	222.32	2.79	190.22	220.17	251.72	**<0.001**	**<0.001**	**<0.001**			
Flank Front (FF)	225	232.36	3.17	202.22	232.97	259.03	**0.014**	**<0.001**	0.196	0.398		

SE = Standard error

Maturity = Males over 165cm and females over 195cm defined as mature, according to Ebert et al. 2013.

* p-value from Student's T-test. Emboldened values significantly different (95% confidence interval).

† ANOVA [F(6, 1414) = 41.68, p = <0.001], p-values from Tukey's post hoc test, emboldened results significantly different (95% confidence interval).

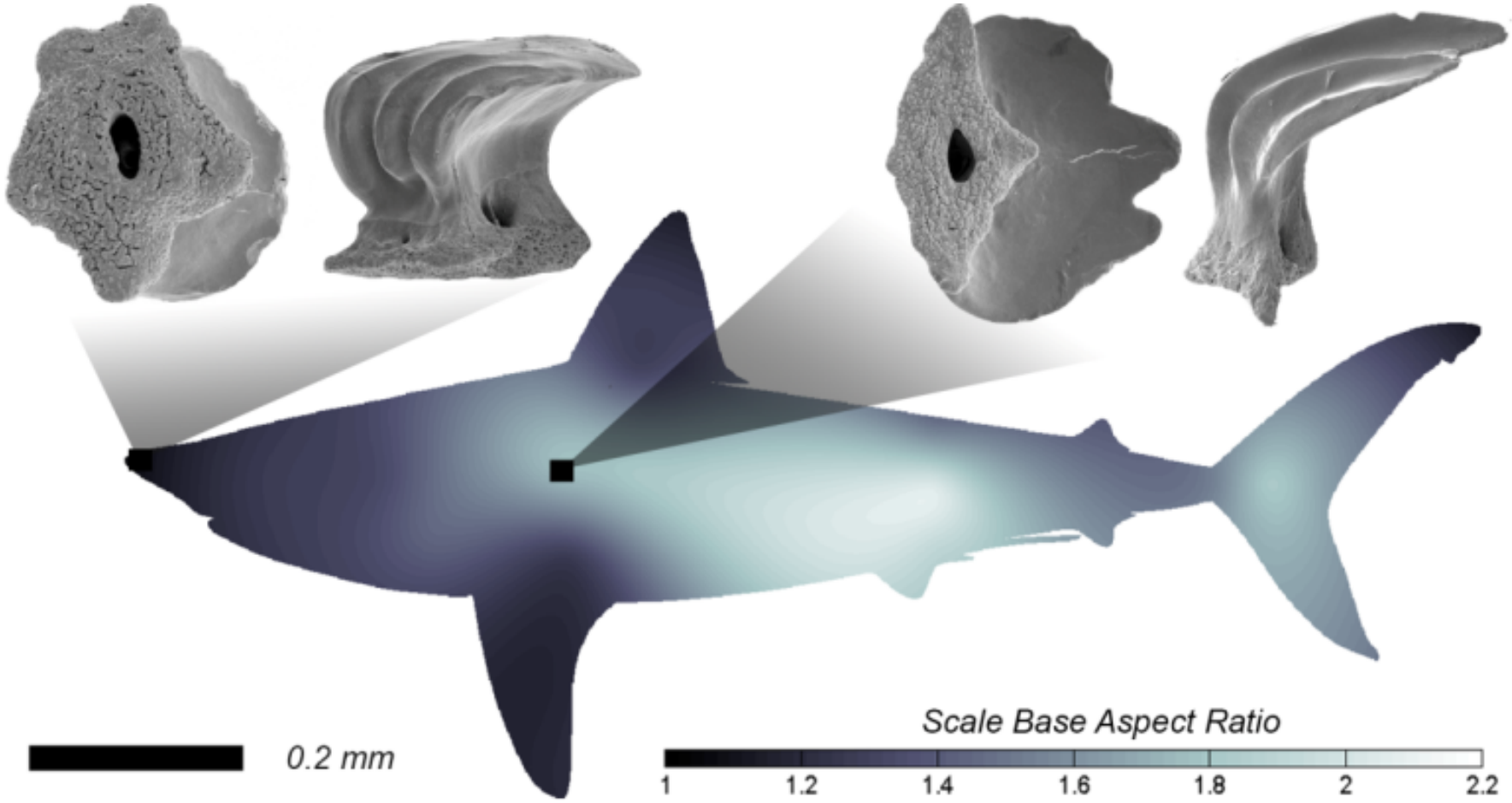

Figure 6.4. Examples of *Lamna nasus* dermal denticles with low aspect ratio (width/length) in the head region and high aspect ratio scale bases on the flank. Heat map of scale base aspect ratio distribution from 19 sample locations (excluding claspers) of a 183cm male, and three flank semi-landmarks , interpolated across entire body, and weighted according to standard error.

Table 6.4. Summary statistics and tests for difference of *Lamna nasus* scale base aspect ratio (width/length), male specimen 183cm. Statistical differences highlighted in bold italic.

							p-value†						
Sample	N	Mean	SE	25%	Median	75%	H	Mg	P	D	FF	FB	Cl
All Scales	487	1.49	0.02	1.16	1.40	1.72							
Head (H)	62	1.25	0.04	1.05	1.23	1.37							
Mid Gills (Mg)	25	1.52	0.08	1.15	1.44	1.8	**0.007**						
Pectoral Fin (P)	75	1.23	0.03	1.06	1.21	1.35	1.000	**0.002**					
Dorsal Fin (D)	75	1.30	0.03	1.14	1.27	1.42	0.997	0.067	0.978				
Flank Front (FF)	75	1.59	0.05	1.33	1.54	1.76	**<0.001**	0.980	**<0.001**	**0.003**			
Flank Back (FB)	75	1.90	0.06	1.53	1.81	2.20	**<0.001**	**<0.001**	**<0.001**	**<0.001**	**0.002**		
Claspers (Cl)	25	1.09	0.05	0.86	1.12	1.25	0.462	**<0.001**	0.647	0.111	**<0.001**	**<0.001**	
Tail (T)	75	1.76	0.05	1.51	1.73	2.00	**<0.001**	**0.036**	**<0.001**	**<0.001**	0.359	0.623	**<0.001**

† ANOVA [F(7, 479) = 34.69, p = <0.001], p-values from Tukey's post hoc test, emboldened results significantly different (95% confidence interval).

Table 6.5. Summary statistics of *Lamna nasus* scale riblet spacing measurements, all in micrometres (µm).

Sample		N	Mean (µm)	SE	25%	Median	75%	p-value*	F
	All Scales	1346	54.89	0.29	46.61	54.71	62.16		
Gender	Male	540	55.7	0.39	48.88	55.09	62.00	**0.021**	1.56
	Female	806	54.3	0.40	45.05	54.08	62.39		
Maturity	Immature	806	52.87	0.36	45.23	52.15	59.28	**<0.001**	1.12
	Mature	540	57.90	0.46	49.66	57.77	66.20		

							p-value†					
Sample	N	Mean	SE	25%	Median	75%	H	Mg	P	D	FF	FB
Head (H)	225	59.84	0.50	55.18	59.45	64.58						
Mid Gills (Mg)	75	59.04	0.78	54.94	57.76	63.91	0.972					
Pectoral Fin (P)	150	48.63	0.49	44.43	47.74	52.63	**<0.001**	**<0.001**				
Dorsal Fin (D)	225	43.69	0.38	39.5	43.58	47.38	**<0.001**	**<0.001**	**<0.001**			
Flank Front (FF)	225	58.32	0.52	53.51	57.58	63.24	0.601	0.983	**<0.001**	**<0.001**		
Flank Back (FB)	221	64.22	0.63	58.37	64.46	70.31	**<0.001**	**<0.001**	**<0.001**	**<0.001**	**<0.001**	
Tail (T)	225	51.33	0.70	44.43	49.38	56.25	**<0.001**	**<0.001**	**0.035**	**<0.001**	**<0.001**	**<0.001**

SE = Standard error

Maturity = Males over 165cm and females over 195cm defined as mature, according to Ebert et al. 2013.

* p-value from Student's T-test. Emboldened values significantly different (95% confidence interval).

† ANOVA [F(6, 1339) = 170.4, p = <0.001], p-values from Tukey's post hoc test, emboldened results significantly different (95% confidence interval).

6.3. *Lamna nasus* Riblet Spacing and Number

Optimisation studies suggest that smaller riblet spacing is more effective at reducing drag at higher speeds (Dean & Bhushan, 2010). It may therefore be expected that some regions of a shark's body are more often exposed to faster moving fluid than others, perhaps reflected by differences in riblet spacing. As with riblet angle, it was also hypothesised that individuals within a species of the same waters would have differing riblet spacing distributions depending on growth stage or sex-dependent ecologies. To test these hypotheses, the number of riblets and their spacing was measured in several *Lamna nasus* specimens of both genders and differing stages of maturity (Table 3.1).

Mean riblet number for all scales of all specimens (n = 1346) was 3.88±0.0, median 4, ranging from 2-6. Riblet number was not correlated strongly with width (Pearson r = 0.38), and only loosely positively correlated with riblet spacing (Pearson r = 0.53).

A mean riblet spacing of 54.9±0.3µm in *Lamna nasus* (n = 1346) places them among the fastest modern pelagic sharks, whose riblet spacing generally ranges from ~45-80µm (Reif, 1985; Chapter 5). Riblet spacing differed significantly between the majority of body regions (Table 6.5.). Across the midline of the shark (Figure 6.6.) there was a gentle increase in riblet spacing of ~11% from the head to the back of the flank. As the freestream velocity remains constant, the downstream increase in riblet spacing may reflect a thickening boundary layer, and the downstream decrease in velocity of fluid in direct contact with the shark (investigated further in Chapter 7). Other leading edge surfaces have similarly narrow-spaced riblets compared to the rest of the body (mean flank, gill and tail), ~16% and 25% smaller on the pectoral and dorsal fins respectively. Downstream along the midline from the flank to tail, riblet spacing decreases sharply by ~23% (see Appendix I for individual specimen plots). The tail is where thrust is generated, and narrower riblet spacing is likely reflected by the greater lateral component of body movement, and the resulting increase in fluid velocity in this region.

The difference in mean riblet spacing between the sexes is tiny (Table 6.5, Appendix I), and just 1.4µm greater in females. Total length is not strongly correlated to mean riblet spacing (Pearson r = 0.541), however average female specimen length was 11.5cm greater than males, and may account for the small discrepancy.

Mature *Lamna nasus* had on average 8.7% wider riblet spacing than immature specimens. If the theoretical assumption that smaller riblet spacing is more efficient at higher speeds is correct, this suggests the larger sharks are swimming more slowly in real terms (see section 8.2.1). A more likely explanation is that a thicker boundary layer is developing over the longer

adults, and as such near wall velocity is reduced over the flank region. As demonstrated next (section 6.4), the angles at which riblets lie on the scale crown also vary between body regions, and throughout ontogeny. Based on similarities in the distributions of these features (Figures 6.6, 6.7) it is unlikely that riblet angle and spacing are performing entirely separate hydrodynamic processes, and a combination of these factors may contribute to optimisation for drag-reduction, although the relationship remains unclear (see section 6.4).

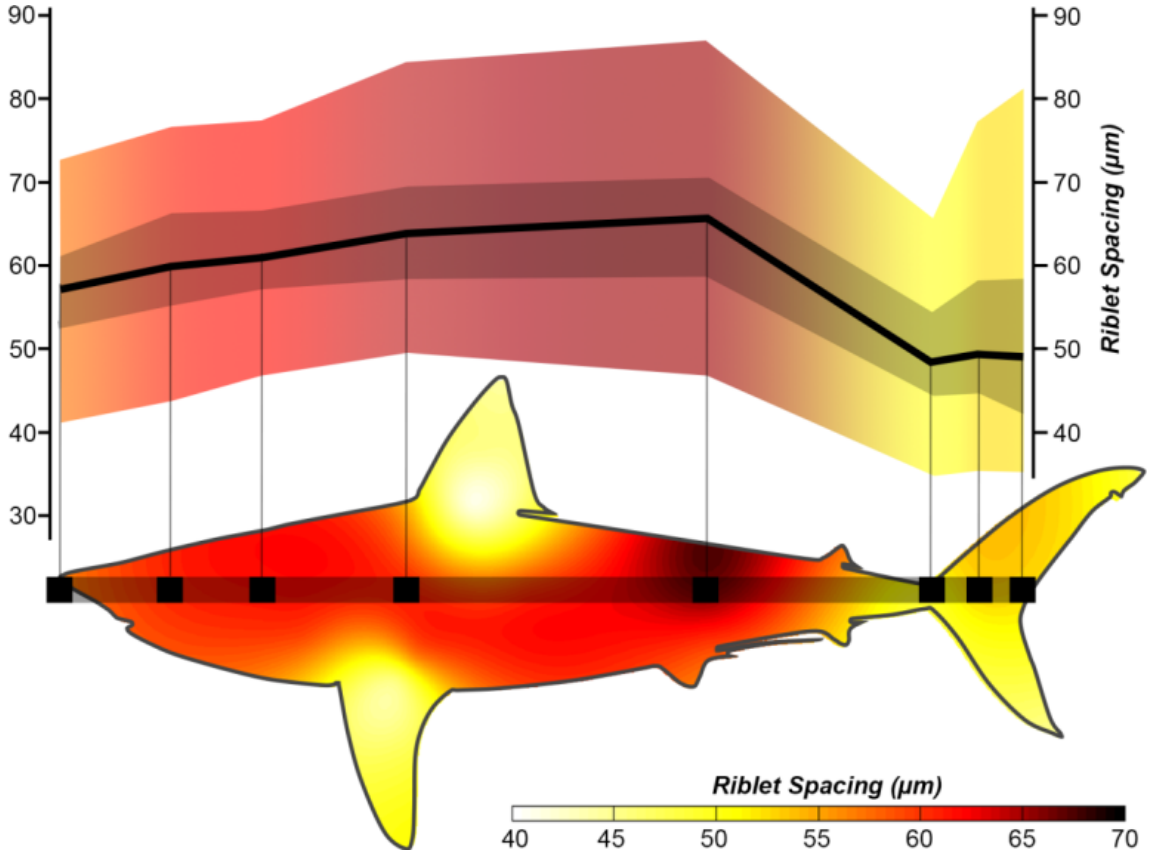

Figure 6.6. a) Transect of shark midline, showing mean riblet spacing (µm) at different sampling locations. b) 'Heat map' of mean riblet spacing (µm) distribution from 19 sample locations and semi-landmarks (Appendix I), interpolated across entire body, and weighted according to standard error.

Table 6.6. Summary statistics of *Lamna nasus* downstream scale riblet convergence (> 0°) and divergence (< 0°) angles.

Sample		N	Mean (°)	SE	25%	Median	75%	p-value†	F
All Scales		1800	-3.74	0.22	-9.89	-3.92	1.31		
Sex	Male	720	-3.71	0.38	-10.84	-3.20	2.00	0.897	1.4
	Female	1080	-3.76	0.26	-9.35	-4.34	0.76		
Maturity*	Immature	1080	-6.65	0.27	-13.02	-6.96	-1.50	**<0.001**	1.3
	Mature	720	0.62	0.29	-4.60	-0.21	4.21		

Sample	N	Mean	SE	25%	Median	75%	p-value† H	Mg	P	D	FF	FB
Head (H)	300	-3.48	0.64	-11.17	-4.08	3.15						
Mid Gills (Mg)	100	-8.67	0.74	-14.17	-8.45	-3.42	**<0.001**					
Pectoral Fin (P)	220	5.50	0.62	-1.17	3.83	10.16	**<0.001**	**<0.001**				
Dorsal Fin (D)	300	-1.34	0.31	-4.39	-1.36	1.36	**0.009**	**<0.001**	**<0.001**			
Flank Front (FF)	300	-5.14	0.52	-11.15	-6.05	-0.19	0.335	**<0.001**	**<0.001**	**<0.001**		
Flank Back (FB)	280	-7.91	0.42	-2.37	-7.64	-2.37	**<0.001**	0.959	**<0.001**	**<0.001**	**0.007**	
Tail (T)	300	-6.26	0.38	-1.43	-6.41	-1.43	**0.006**	**0.033**	**<0.001**	**<0.001**	0.775	0.347

SE = Standard error

Maturity = Males over 165cm and females over 195cm defined as mature, according to Ebert et al. 2013.

* p-value from Student's T-test. Emboldened values significantly different (95% confidence interval).

† ANOVA [F(6, 1793) = 74.95, p = <0.001], p-values from Tukey's post hoc test, emboldened results significantly different (95% confidence interval).

6.4. Converging and Diverging Riblets of *Lamna nasus*

Riblets are known to be an important source of drag-reduction in sharks, but the effect of riblet angle on shark scales has not been investigated. After studying a large number of *Lamna nasus* SEM images it was observed that the downstream angle at which riblets lie across the crown changes at different body locations. These changes in riblet angle relative to the central keel produce both diverging and converging riblet patterns, without any association to sensory structures (e.g. pores). Here riblet angles are measured across the body of individual species, in order to examine spatial variations in riblet convergence/divergence and any changes in riblet angle. This analysis is repeated for juvenile and adult specimens and for male and female species in order to investigate changes with maturity and sex.

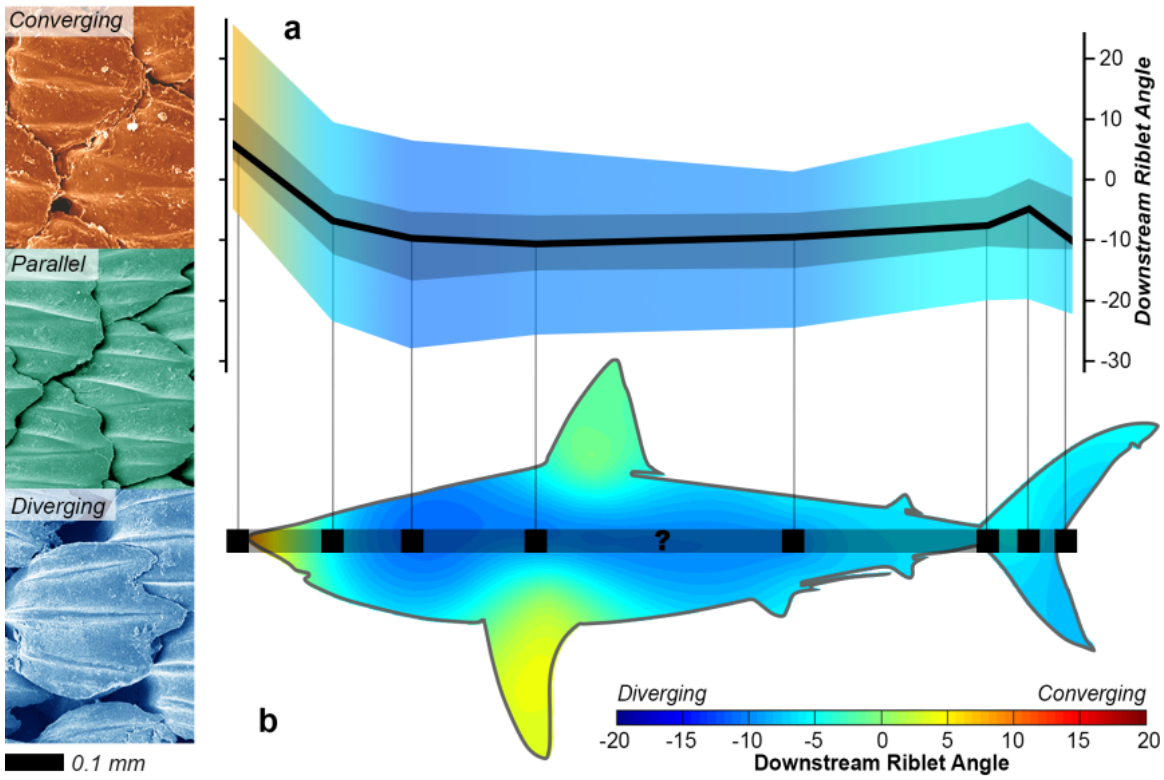

Figure 6.7. A) Transect of *Lamna nasus* midline, showing mean riblet angle (degrees) of all specimens at different sampling locations. B) Heat map of mean riblet angle (degrees) distribution from 19 sample locations, and flank semi-landmarks (Appendix I), interpolated across entire body, and weighted according to standard error. Left, scanning electron microscope images of example riblet angles, from top to bottom; riblets converging ('H1' head scale from 183cm male), parallel ('D3' dorsal fin scale from 215cm female) and diverging ('H3' head scale from 127cm female).

Across the midline, mean riblet angles are convergent on the snout but decrease (by up to 18°) to be divergent across the flank, before becoming convergent again at the tail (Figure. 6.7). The majority of body regions differed significantly in riblet angle (Table 6.6), with the most convergent riblets on the pectoral and snout ('P1' and 'H1', Figure 6.1), and the most divergent at the back of the head and flank ('H3', 'FF2' and 'FB2').

It is apparent that the method of drag reduction changes as the animal grows. With only a tiny change in variance (61.8µm immature, and 60.6µm mature), mature shark scale riblets at every sampled position are slightly more convergent than in immature specimens. Riblet angle for mature sharks ranged from 3.3° more convergent than juveniles at the base of the dorsal fin ('D3') to 14.5° more convergent at the ventral-most region of the flank posterior ('FB3'). Mean riblet angles of all immature specimens diverge by 6.7˚ and are significantly different ($p = <0.001$) to the mature riblet angles which converge slightly by mean 0.6˚ (Table 6.6., Figure 6.7).

As riblet angle and spacing were measured separately, correlation between individual scales could not be tested, but mean riblet angle and spacing of the same regions of the same individuals ($n = 89$) showed little correlation (Pearson $r = -0.19$). Tested separately, the correlation between riblet spacing and angle is stronger, for both immature (Pearson $r = -0.39$), and mature sharks (Pearson $r = -0.41$). This data and the pattern of both riblet spacing and angle observed (Figures 6.6, 6.7) suggests they are interrelated, and the two factors must be discussed together to fully understand scale regionalisation for optimised drag reduction.

6.5. Unifying Scale Features for Optimal Drag-reduction

In *Lamna nasus* there is a trend from head to flank for the riblet spacing to increase, and angle to become more divergent, and from flank to tail riblet spacing decreases and angle become near parallel (Figures 6.6, 6.7). Without a thorough basis in experimental data, it is difficult to disentangle the hydrodynamic effects of riblet spacing and angle. Idealised converging riblets in pipe flow are capable of seeding vortices and encouraging turbulent perturbations, while diverging riblets are thought to have the opposite effect, reducing turbulent fluctuations in pressure (Nugroho et al., 2013, section 2.3.2). If the convergent riblets of shark scales create turbulence in a similar way, it may aid the prolonged attachment of the boundary layer downstream by transferring momentum towards the skin surface (section 2.3.2). The relatively narrow riblet spacing on these leading edge surfaces may reflect the higher velocity fluid of a thinner boundary layer, at an earlier stage of development. Downstream, riblets may be

optimised for slower moving fluid as the turbulent boundary layer thickens, coupled with gently diverging riblets optimised to reduce the turbulent fluctuations which contribute to drag.

Observed differences between the occurrences of these features in *Lamna nasus* specimens of different maturity, offers some clues (Figure 6.8). As a shark grows, the distance from leading to trailing edges increases and so larger animals may be more prone to premature boundary layer separation creating a larger wake. This increases pressure drag enormously (Figure 2.5), so maximising the boundary layer attachment is especially important for larger animals. If increased convergence of the riblets make them more effective turbulisors, this may explain their presence on more mature individuals. There is clearly potential for much more extensive research in this area.

6.6. Summary

In this chapter the variation in modern shark scales was investigated. In section 6.1, the regionalisation of scale morphology was quantitatively assessed in a diverse range of sharks. A general trend was identified in most taxa of rounder, non-overlapping scales on the rostrum, which are often more elongate and overlapping on the flank. In section 6.2.1 this pattern of elongation was confirmed quantitatively in *Centrophorus granulosus*, a deepwater slow-moving shark chosen as the scales do not overlap in any region. This allowed the in situ measurement of scale crown dimensions, which were least variable in scales of the flank region. In section 6.2.2 the same analysis was applied to the fast pelagic porbeagle shark *Lamna nasus*. and although scales overlapped more extensively, observations of decreased scale size in the tail region relative to the flank (section 6.1) were confirmed. In section 6.2, the scale base geometry of *Lamna nasus* was measured in a mature male specimen, in different body regions. Base geometry is thought to reflect bristling action in sharks (e.g. Lang et al., 2008), and data herein is the first time scale base geometry has been quantitatively assessed across the entire body of a shark. Bases capable of greater pivoting were found on the flank, confirming findings in *Isurus oxyrhinchus* (Lang et al., 2011), but further to this non-pivoting scales were also recorded in areas such as the head and claspers for the first time.

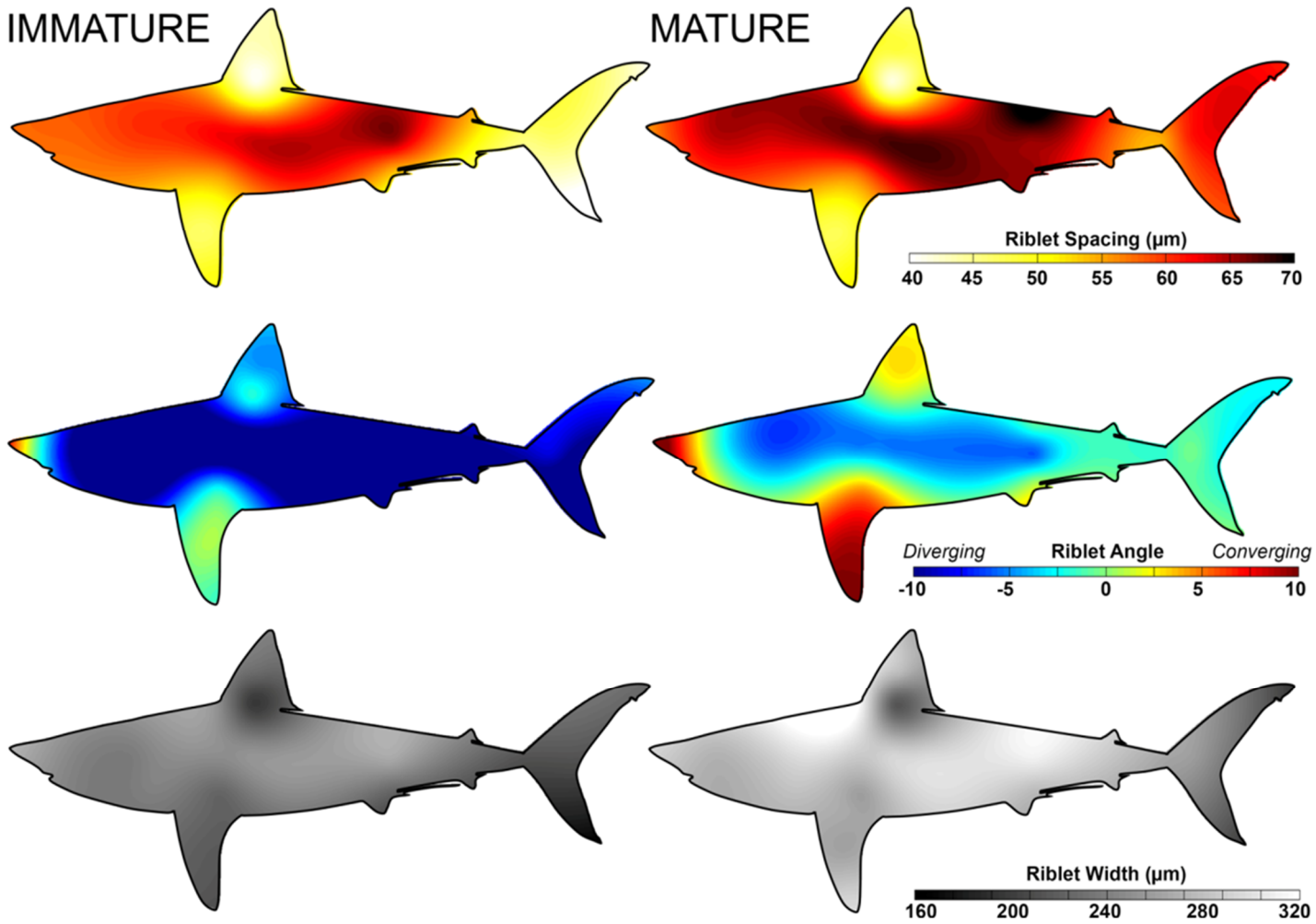

Figure 6.8. Heat maps of mean riblet spacing (top), mean riblet angle (middle), and mean scale width (bottom) distribution for all immature (left) and mature (right) *Lamna nasus* specimens. Images generated using sampling points detailed in Chapter 3.1.3.

In section 6.3 and 6.4 data for the distribution of riblet number, spacing and angles are presented for five specimens of *Lamna nasus* of varying age and gender. Riblet number was not correlated strongly with width and only loosely positively correlated with riblet spacing. Riblet spacing differed significantly between the majority of body regions and across the midlines of the shark (Figures 6.6, 6.7). There was a gentle increase in riblet spacing from the head to the back of the flank, before decreasing towards the tail. Riblet angles are convergent on the snout but decrease (by up to 18°) to be gently divergent across the flank, before becoming convergent again at the tail. Little difference was found between genders but mature specimens had significantly wider riblet spacing and more convergent riblet angle. In section 6.5, riblet spacing and angle are discussed together in the context of overall scale optimisation for drag-reduction.

In the next chapter, boundary layer development will be discussed further, and experimental data will be presented which tests the effect of scale morphology on skin friction.

7. Experimental Analysis of Drag-reduction by Fossil Fish Scales

In the previous chapter, a comparative approach for interpreting scale function was taken which explored patterns of scale occurrence between body regions, different taxa, and even individuals of the same species. While this is a solid basis for identifying functionally relevant adaptations, it is only with experimental testing that biomechanical hypotheses can be convincingly validated. Form drag is influenced by a host of environmental factors, as well as the fish's body shape, musculature, and behaviour. As this - principally soft-tissue - information is rarely preserved in the fossil record, there are many assumptions involved in modelling and measuring this kind of drag. Instead of form drag, the focus of this chapter is skin friction, which is the drag caused by friction of fluid moving over the surface of an object. The hard scales of modern sharks are exposed directly to fluid flow, so by reconstructing the skin of fossil fishes with similarly exposed scale crowns, skin friction can be calculated for a range of extinct taxa. These are not intended as accurate species-specific values, rather as an indicator of the different drag-reducing potential of generic scale shapes. By taking this approach, the results can be applied to a far wider range of taxa, with a solid experimental basis to supplement the comparative approach to interpreting scale function.

Fossil scale specimens representing five flank scale morphotypes were selected and µCT scanned to obtain three-dimensional surface geometry. Computer-aided design (CAD) software was used to first scale all fish scales to 2mm (in their longest direction), and reconstruct the pattern of squamation. These were rapid-prototyped as flat plates for testing in a flume tank, and laser Doppler anemometry was used to measure velocity profiles along the length of the plates. Boundary layer development and skin friction drag calculations were performed to compare reconstructed fish skin with a smooth control. For full methodology, see section 3.2.

7.1. Data Acquisition and Processing

Flume runs lasted an average 229 minutes per plate, with LDA data recorded for a maximum of 30 seconds at 82 vertical positions per profile, and five profiles per plate (see Section 3.2.6). A total of 16,100,813 velocity measurements were recorded for this analysis, with a mean data acquisition of 232 measurements per second.

Normal boundary layer development results in lower fluid velocity at the wall, and so fewer seed particles can be detected within a limited linger time. This was observed by eye for all velocity profiles, however there were regions of noise in validation values, frequency of data acquisition, and the velocity measurements. Perhaps as a result, there was no statistical correlation between vertical position and percentage data validation (Pearson r = -0.01, p = 0.58, n = 2441), or vertical position and data count (Pearson r = 0.05, p = 0.01, n = 2460). Relative standard deviation of validation (coefficient of variance) values range from 0.6 - 36.6%, with little change towards the wall (Figure A2.8.). However, at or close to the wall mean relative standard deviation (RSD) for data frequency is relatively higher, particularly between 0-0.4mm (mean = 133.6%, range = 119.5-172.8%), whereas further away from the wall (≥0.05mm) values are more consistent (mean RSD = 38.2%, range = 17.1-84.0%). This is important, as it may reflect the differing height and geometry of scale types, which limits the accuracy of navigation in the vertical (z) plane (see Section 3.2). The vertical location of the wall (and true zero) must be inferred retrospectively, by identifying decreases in fluid speed towards zero velocity at the wall. The method of correction is described in Section 3.2.7, and raw data including the corrected position of the wall are detailed in Appendix 2. Erroneous measurements of the solid wall were excluded from all drag calculations and statistical treatments that follow.

As Figure 7.1 shows, there is a downward tilt of ~0.9mm across the measurement region 200-400mm from the leading edge (~0.2°). The influence of scale geometry is difficult to disentangle from this tilt in most cases but *Nostolepis* (Figure 7.1 in orange) at point x = 300mm shows a marked increase in wall height relative to the general downward trend across the entire plate. This suggests that an area closer to the scale tip was the base of the true profile rather than a depression between the scales.

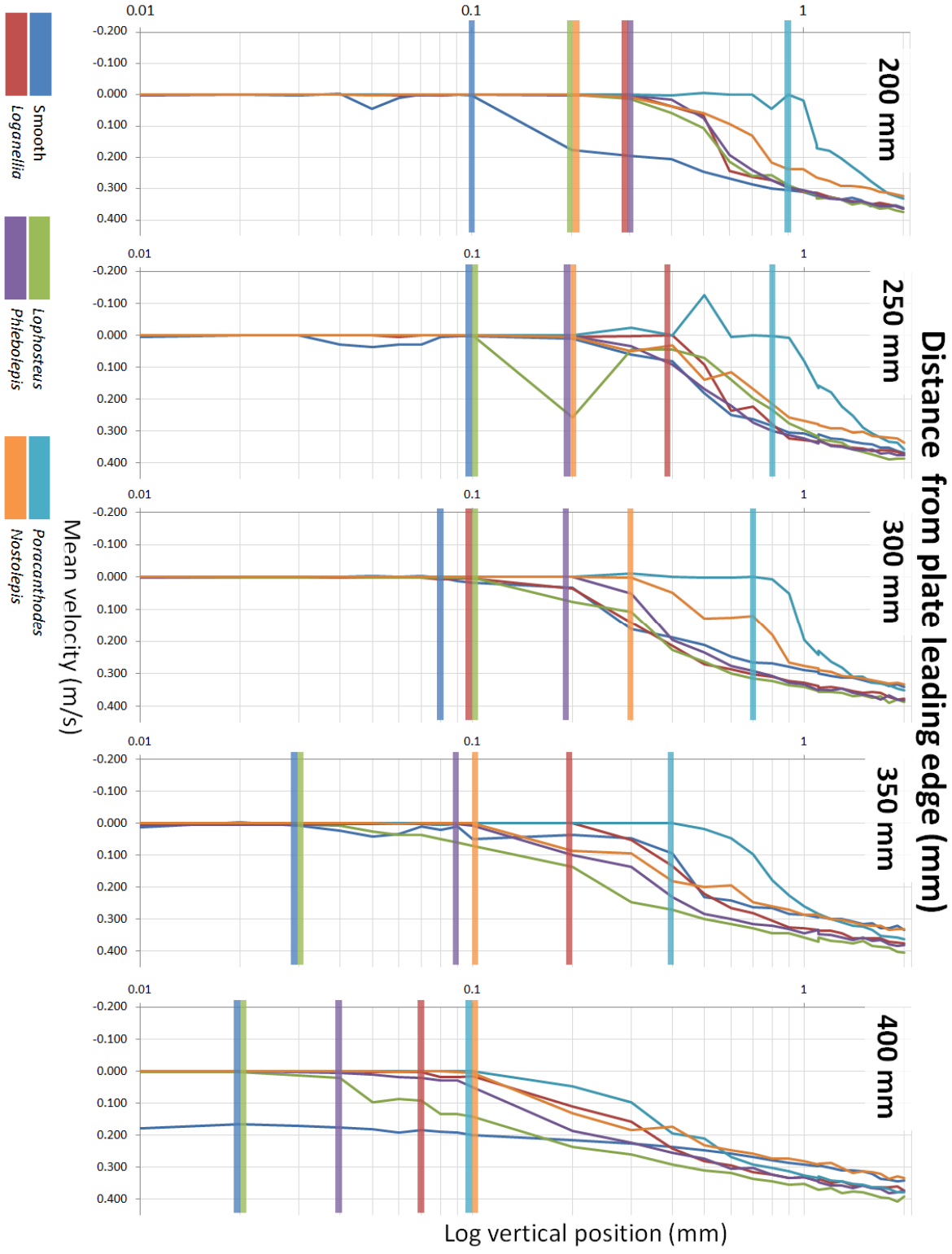

Figure 7.1. Raw velocity measurements (m/s) showing corrected bases of velocity profiles (vertical bars) at horizontal positions 200-400mm, for smooth control plate (dark blue), *Loganellia scotica* (red), *Lophosteus* sp. (green), *Phlebolepis elegans* (purple), *Poracanthodes* sp. (cyan), and *Nostolepis striata* (orange). Data below the inferred wall level was excluded from all analyses that follow. See section 3.2 for Methods and Materials.

7.2. Mean Velocity Profiles

Data for all test plates, and at all positions (Figures 7.2) show normal velocity profiles, with the slowest fluid moving closest to the plate surface (wall), gradually increasing at greater distances away in to the freestream. The shape of the velocity profiles is rather angular with a slower-moving band of fluid close to the wall, a small region of increasing velocity, and then a steep ascent to the freestream. This is associated more with turbulent boundary layers, where there is larger-scale mixing of fluid layers. Freestream velocity is reached at approximately 50cm/s, where the wall no longer has an effect on fluid velocity. From semilog plots (Figure 7.3) three regions can be differentiated by eye, the viscous sublayer at the base, a relatively straight log-law region, and the outer layer, where freestream velocity is reached. Near-wall velocity at the 200mm and 400mm positions is greatest on the smooth plate but remains relatively lower than scaled plates between these points. In the log-law region, it is more difficult to disentangle relative velocity, however it is clear that the smooth control and *Nostolepis* have lower velocities than the other plates. The highest log-law region velocities were observed in the *Loganellia*, *Lophosteus*, and *Phlebolepis* plates, although these are difficult to differentiate by eye. In a downstream direction from 200-400mm, velocity gradients in the log-law region separate in to two increasingly distinct groups of plates. The *Nostolepis* and smooth plate velocity gradients become lower than the other plates downstream. *Loganellia*, *Lophosteus*, *Phlebolepis* and to a lesser degree *Poracanthodes* have slightly steeper gradients in the log-law region and velocity is relatively higher and contrasts strongly with the slower group of plates (Figure 7.3). The behaviour of plates in these groups suggests similar flow patterns, however qualitative assessment alone is not enough to justify this hypothesis.

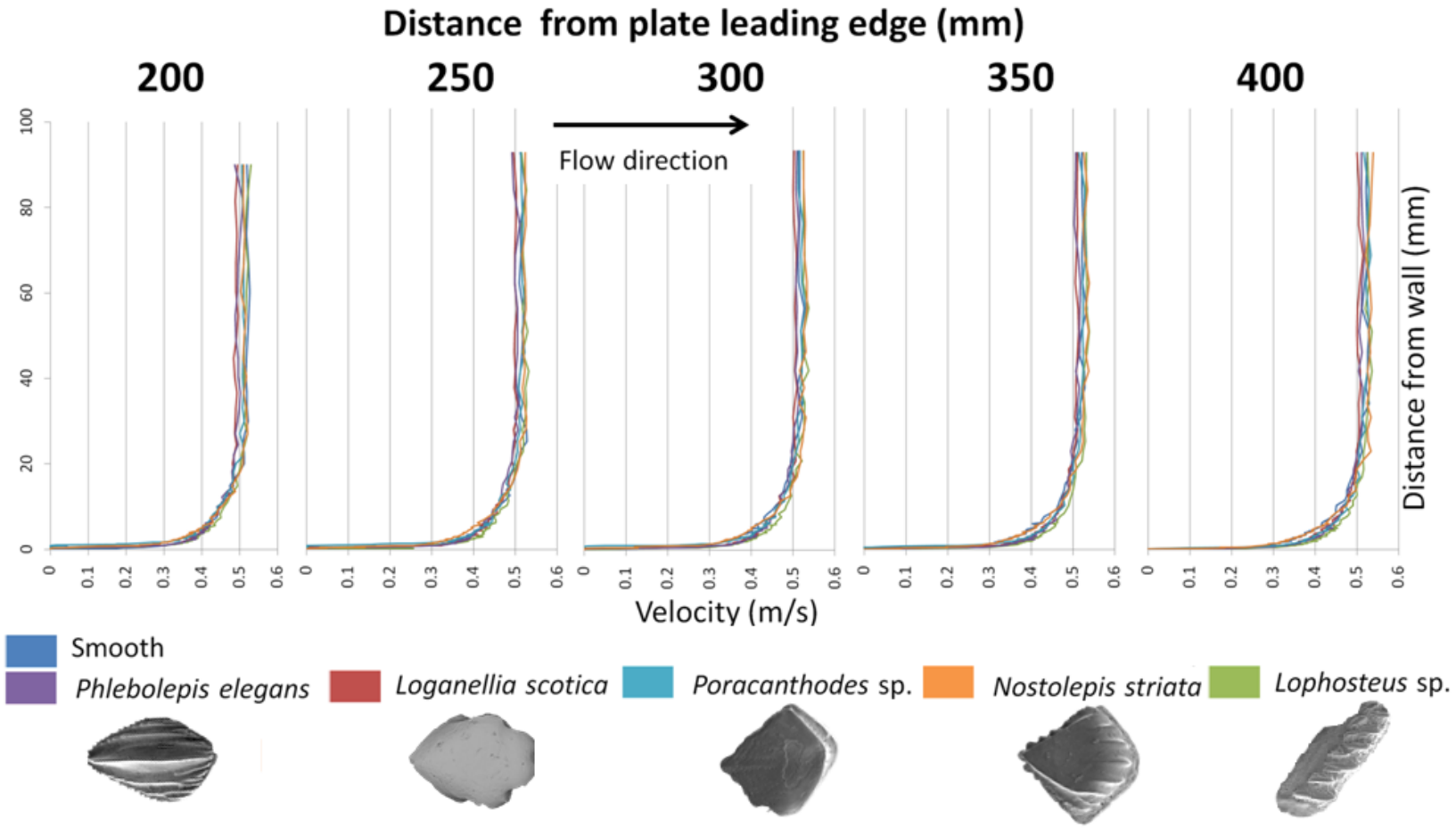

Figure 7.2. Mean velocity profiles (corrected base locations) of test plates at 200-400mm from leading edge. Including the smooth control plate (dark blue), and the scaled plates *Loganellia scotica* (red), *Lophosteus* sp. (green), *Phlebolepis elegans* (purple), *Poracanthodes* sp. (cyan), and *Nostolepis striata* (orange). See Appendix II for full data and individual plots.

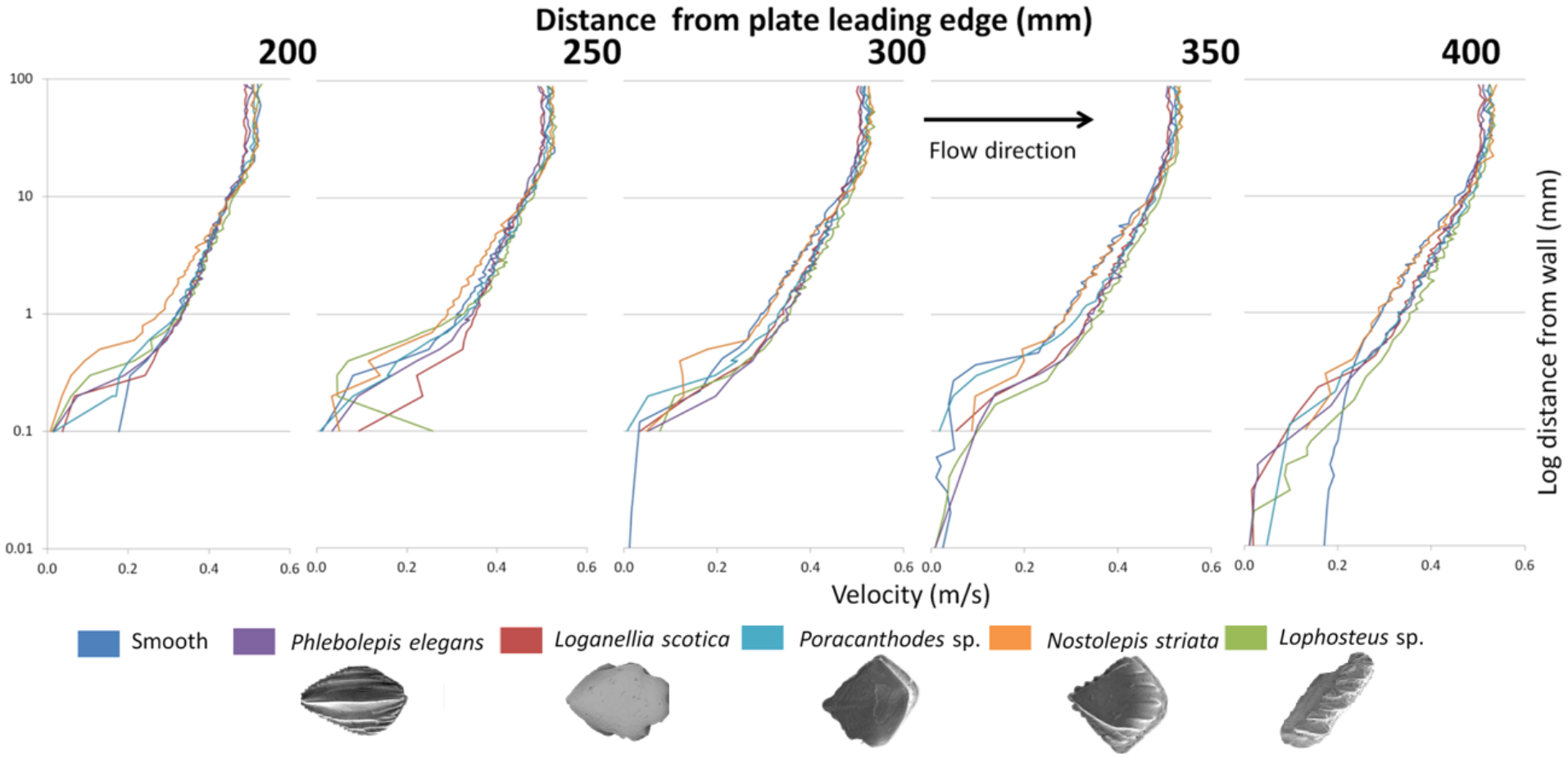

Figure 7.3. Semilog plot of mean velocity profiles (corrected) of all test plates at 200-400mm from leading edge. Including the smooth control plate (dark blue), and the scaled plates *Loganellia scotica* (red), *Lophosteus* sp. (green), *Phlebolepis elegans* (purple), *Poracanthodes* sp. (cyan), and *Nostolepis striata* (orange). See Appendix II for full data and individual plots.

7.3. Boundary Layer Development

The boundary layer is the fluid influenced by shear stress at the wall, and is the vertical point of a profile at which fluid travels at 99% of the maximum freestream velocity. The mean velocity values discussed earlier suggest the boundary layers of all plates remained attached during the experiment, without recirculating flow near the wall. However, examination of all raw data recorded at 0.5mm from the wall suggests a more complicated picture (Figure 7.4), with a small percentage of measurements below 0 m/s velocity, indicating minor flow stagnation or reversal within the 30 second measurement time. Instances of negative velocity account for between 0-3% (n = 69 782) of measurements in all plates, except *Nostolepis* which is noticeably larger. At the leading edge (x = 200mm) of the *Nostolepis* test plate, 18.23% of measurements were negative (n = 4016), and remains above 10% across the plate until it falls to 0.03% (n = 3842) at the furthest downstream position (x = 400mm). It should be noted that negative values are relatively small, suggesting normal fully attached transitional or fully turbulent boundary layer behaviour, rather than full separation. Negative velocity measurements obtained for the *Nostolepis* of 0.5mm vertical position at x = 200mm had a mean average velocity of -0.003 m/s, ranging from -0.0 - 0.3 m/s (n = 732). This is an important observation as it highlights the importance of large sample sizes provided by laser Doppler anemometry, and supports the use of mean velocities in this analysis.

Boundary layer development was different across all plates (Figure 7.5), however there was a general upwards trend in most cases. *Nostolepis* shows the most consistent boundary layer growth across the plate, and coupled with earlier observations of fluctuating near-wall velocity suggesting laminar to turbulent transition has already occurred further upstream than the measurement regions x = 200-400mm. In the transition region, boundary layer thickness is known to fluctuate as larger-scale fluid interactions begin to occur. This could explain the highly variable boundary layer thicknesses of other plates such as *Loganellia* and *Phlebolepis*. Both *Lophosteus* and *Phlebolepis* have very similar boundary layer shapes with a steep decrease towards x = 250mm and a gentle rise towards 350mm, and dropping again at 400mm. The smooth control plate has an almost identical shape, except the boundary layer thickness was much lower at the first measurement position. One interpretation is that the higher roughness of the scaled plates caused transition to a turbulent condition upstream of the measurement region. However it may also have been caused by upstream detachment, and proceeding reattachment of the boundary layer at x = 250mm. This is unclear, as the near-wall (z = 0.5mm) raw measurements for both the *Lophosteus* and *Phlebolepis* plates show very few negative velocity measurements which we would expect to find in both if periodic

detachment was occurring. Differences in boundary layer development, and the possible implications are discussed in Chapter 6.

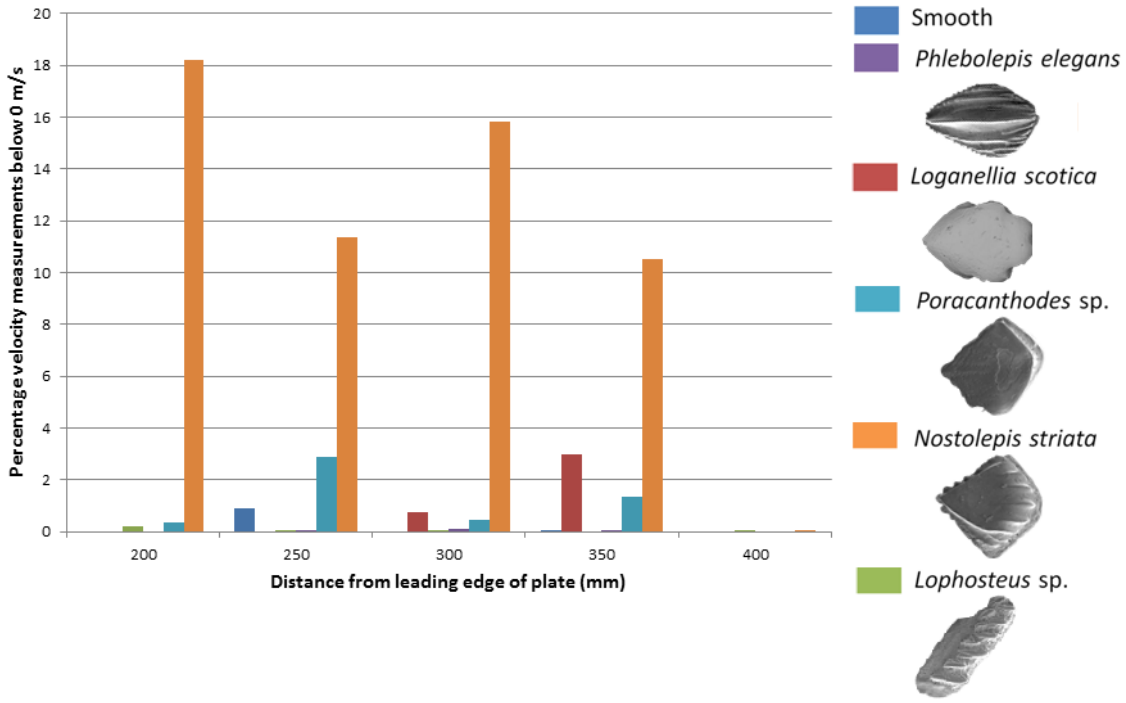

Figure 7.4. Bar chart showing percentage of raw negative velocity (U = < 0 m/s) measurements recorded at a near-wall corrected position of 0.5mm vertical (z) position for all plates at all horizontal positions (x = 200-400mm).

7.4. Skin Friction Coefficients

Frictional shear velocities were calculated for all profiles of all plates using Matlab (see section 3.2.7, and Appendix II for code script). Skin friction was then calculated (Figure 7.6), using these frictional velocity calculations, and the freestream velocity (section 3.2.7.). The distribution of skin friction measurements across the plates is rather variable, but there is a gentle upwards trend towards the end of the plate in most cases. This is typified by *Phlebolepis*, which after the first 200mm position rises gently to approximately the same skin friction as the smooth control at 400mm, the last downstream measurement position. This supports observations of the boundary layer, which suggest a turbulent boundary layer of fluctuating thickness. A clear exception to this trend is the *Nostolepis* plate, which at 200mm has the largest skin friction coefficient of all plates and all profiles.

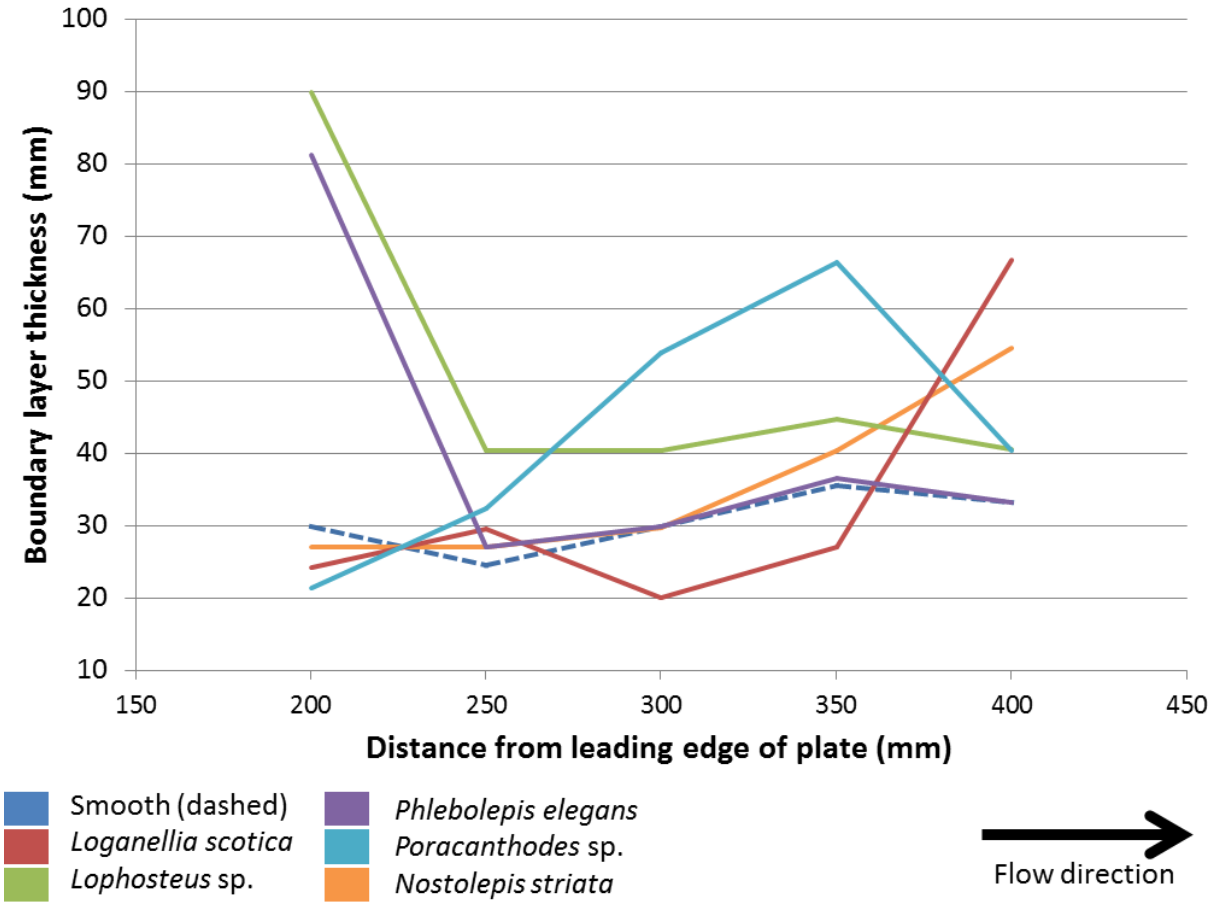

Figure 7.5. Boundary layer height (99% maximum velocity) across the test plates. Including the smooth control plate (dark blue dashed), and the scaled plates *Loganellia scotica* (red), *Lophosteus* sp. (green), *Phlebolepis elegans* (purple), *Poracanthodes* sp. (cyan), and *Nostolepis striata* (orange). See Appendix II for full data and individual plots.

Nostolepis had the largest skin friction for most horizontal positions, and at 0.025, the largest mean value over the entire plate as well. This was ~27.7% higher than the smooth control plate average, which is in effect the relative skin friction drag (Table 7.1.). This perhaps reflects the relative height of the crown spines, which at 0.97mm make *Nostolepis* the tallest (height away from the wall) scales in this study. This alone is not a satisfactory explanation for increased drag however, as the height of the crowns of the *Poracanthodes* scales and *Loganellia* are 0.55 and 0.6mm high respectively, and both reduce skin friction drag relative to the smooth (0mm high) plate. *Loganellia* is particularly interesting in this case as it reduces skin friction drag across the plate by ~33.5% relative to the smooth control (Table 7.1.). This is on a par with the scales of *Lophosteus*, which was 35.4% lower than the smooth control, and has the lowest scale height at 0.27mm. That the skin friction relative to the smooth plate was so similar for scales of such contrasting height, suggests that relative smoothness is only part

of a more complicated mechanism of drag reduction. *Lophosteus* was in fact the plate which reduced skin friction the greatest, and at the 250mm position is ~52.6% lower than the equivalent position on the smooth plate.

Table 7.1. Percentage reduction in skin friction drag, relative to the smooth control plate.

Plate	Horizontal Position (mm)				
	200	250	300	350	400
Smooth*	-	-	-	-	-
Loganellia	28.175	45.760	32.344	39.533	21.598
Lophosteus	26.665	52.541	25.195	39.625	32.809
Phlebolepis	21.402	39.017	44.789	35.614	4.856
Poracanthodes	3.315	5.555	11.949	-4.116	13.611
Nostolepis	-83.737	-52.922	6.195	11.632	-19.535

*control plate

Skin friction values across the smooth and *Poracanthodes* plate are very similar, rising towards the 350mm position before falling towards 400mm. *Poracanthodes* was chosen to represent scales with little surface ornament but a generic shark-scale morphology, so again it is interesting to note that skin friction at most positions in this scaled plate is lower than the smooth control (Figure 7.6.). *Lophosteus* and *Loganellia* plates are also very similar in skin friction distribution across the plate, with a steep rise between 250-300mm and falling again towards the end of the plate. Faster moving flow would decrease boundary layer thickness, and increase the average mean velocity at measurement positions in the log-law region of a profile, and in doing so increase the calculated skin friction coefficient. This peak of skin friction occurs more closely to the leading edge in *Loganellia* and *Lophosteus*, and approximately 50mm downstream for *Poracanthodes* and the smooth control. These plates have a sigmoidal distribution of skin friction values, and although much more subtle the *Phlebolepis* plate appears to follow the same pattern.

Calculated as a whole, all but the *Nostolepis* plate reduced skin friction drag relative to the smooth plate (Table 7.1). This is a clear indication that the presence of scales can dramatically reduce skin friction (6-35 %) relative to a flat surface, even though the scales have significant inherent topography (0.3-1 mm). *Nostolepis* has an erect backward pointing spine-like

posterior to the scale crown, and was originally chosen to represent defensive, anti-parasitic scale types. Therefore, it is perhaps not surprising that this scale type had a deleterious effect on skin friction, although the mechanism remains unclear.

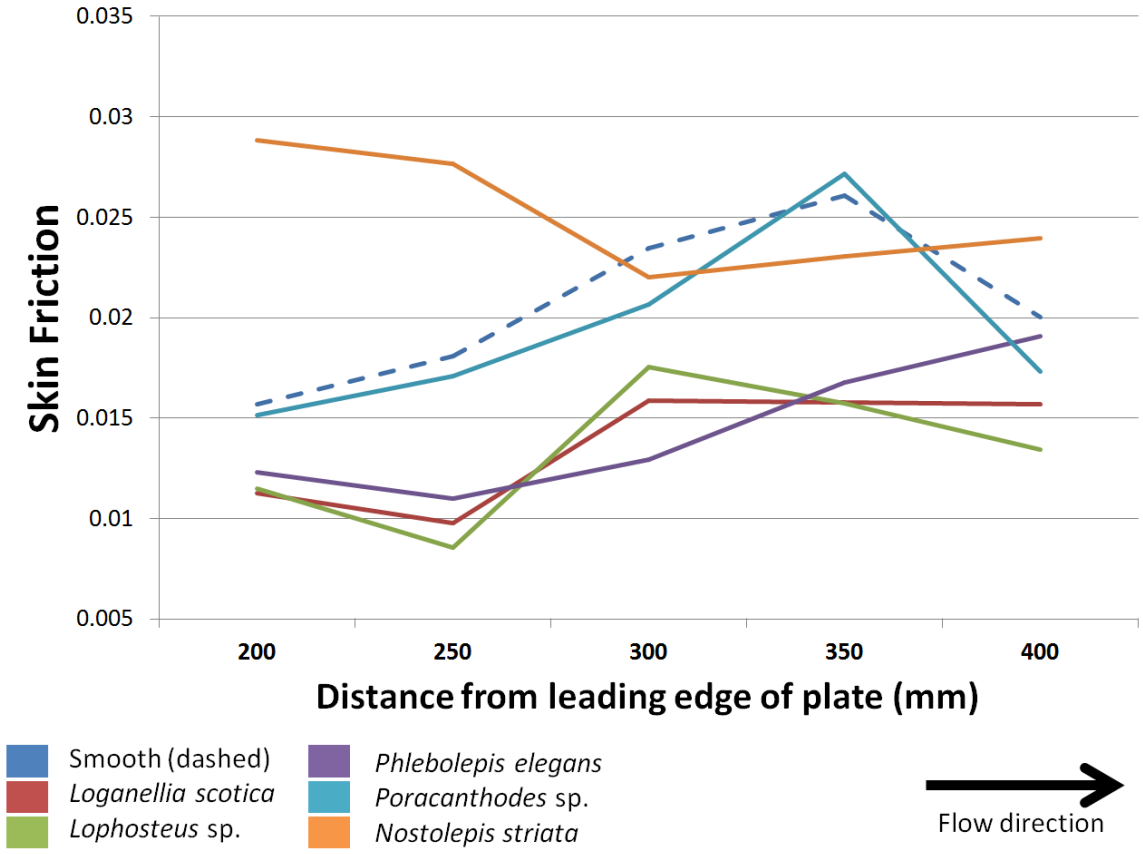

Figure 7.6. Skin friction coefficient at horizontal positions x = 200-400mm for the smooth control plate (dark blue), *Loganellia scotica* (red), *Lophosteus* sp. (green), *Phlebolepis elegans* (purple), *Poracanthodes* sp. (cyan), and *Nostolepis striata* (orange).

7.5. Summary

In this chapter, the skin friction of five commonly encountered scale morphotypes was measured using laser Doppler anemometry. Compared with the smooth control, all but one scale type (*Nostolepis*) reduced skin friction drag (by 6-35%), including scales without riblets. A discussion of these results in combination with the preceding comparative analyses is presented next, in Chapter 8.

8. Functional Morphology of Modern and Extinct Fish Scales: a synthesis and future research directions

This chapter is a discussion of the results presented so far, of the comparative and experimental approaches used to investigate the functional morphology. Section 8.1 focusses on alternative functions of shark-like scales, before adaptations for drag-reduction in modern sharks and fossil taxa are discussed in section 8.2. Implications for the early evolution of speed are presented in 8.3, and suggestions for future research are proposed. Finally, original contributions to knowledge and significant findings are summarised in section 8.4 to conclude this thesis.

8.1. Functions of Modern Shark Denticles

Denticles of modern sharks are comparable to those found in many long extinct groups including the stem chondrichthyan 'acanthodians' and the jawless thelodonts from the Palaeozoic (~383-425 million years ago). Modern sharks therefore provide an excellent analogue for these taxa, and can yield a host of ecological information not available from the fossil record. The parallel riblets ornamenting the surface of most pelagic shark scales have been identified as a key drag-reducing feature, and those of fast pelagic sharks have been the inspiration for numerous biomimetic applications, including swimsuits, and drag-reduction on planes and ships. Almost all active pelagic sharks have uniform or keeled riblets on the crown surface, and of the species studied this was the most common scale type in modern taxa. Drag reduction is discussed in section 8.2, but there are other important functions of shark scales which must also be considered.

In section 4.2 a framework for the interpretation of scale function has been developed, which builds on work by Reif on modern sharks (Reif, 1985), extending it in to the fossil record for the first time. In contrast to Reif's scheme, only three major functions are proposed, abrasion resistance, parasite/antifouling defence and drag-reduction; bioluminescence as used by Reif (1985a) is not utilised. Scales adapted to accommodate photophores in modern sharks also have features associated with protection; either by mechanical resistance with blocky and shallow scales (e.g. *Etmopterus virens*), or as a parasite defence with elongate spines (e.g. *Etmopterus spinax*). This reflects a trade-off between this protection function, and exposing the photophore-rich epidermis between the scale bases (Reif, 1985b). As a soft-tissue feature, bioluminescence cannot be directly detected in the fossil record, and is itself rare in modern

taxa; restricted to just two squalid subfamilies; the kitefin (Dataltiinae) and lantern sharks (Etmopteridae). For these reasons bioluminescence is not considered a major function of scales.

(a) Abrasion resistance

Blocky low-relief scales which lack a crown ornament are most likely adapted for abrasion resistance. Intuitively, any features (such as spines) proud of the scale surface would be susceptible to greater wear on contact with a solid substrate. These scales lack specialised adaptations known to reduce drag in other taxa (e.g. riblets), and while there is evidence presented here that generic surface roughness can help reduce drag, it is clearly not a strong influence on scale form. This is apparent in many rays, and benthic shark species, where blocky scale types occur predominantly on the underside of the body (author's observations). There is further regionalisation of scale type in benthic species, with scales of the rostrum generally much smoother and rounder than on the flank (section 6.1). The hydrodynamic advantages of this arrangement are discussed later (section 8.2), but in benthic species the arrangement of scales at the rostrum may additionally relate to foraging activity. The tip of the rostrum would be the area most susceptible to wear when searching for food. Wear patterns observed on scales at the tip of the rostrum (snout) of the epaulette sharks *Chilloscyllium plagiosum* and *Chilloscyllium punctatum* are not always in the streamline direction (anterior to posterior). In fact many of the superficial scratches observed on the scale crown surfaces are perpendicular to the stream, (e.g. Figure 8.1a). Observations by the author of the foraging activities of living epaulette sharks (commonly found in the pet trade and public aquaria) support the hypothesis that these scratches occur during feeding activities as the head moves from side to side. Epaulette sharks – uniquely – can negotiate spatially complex areas by 'walking' with their pectoral fins, and have even been observed on land travelling between rock pools, reflected by similarly random scratch directions on the trunk scales (Figure 8.1b).

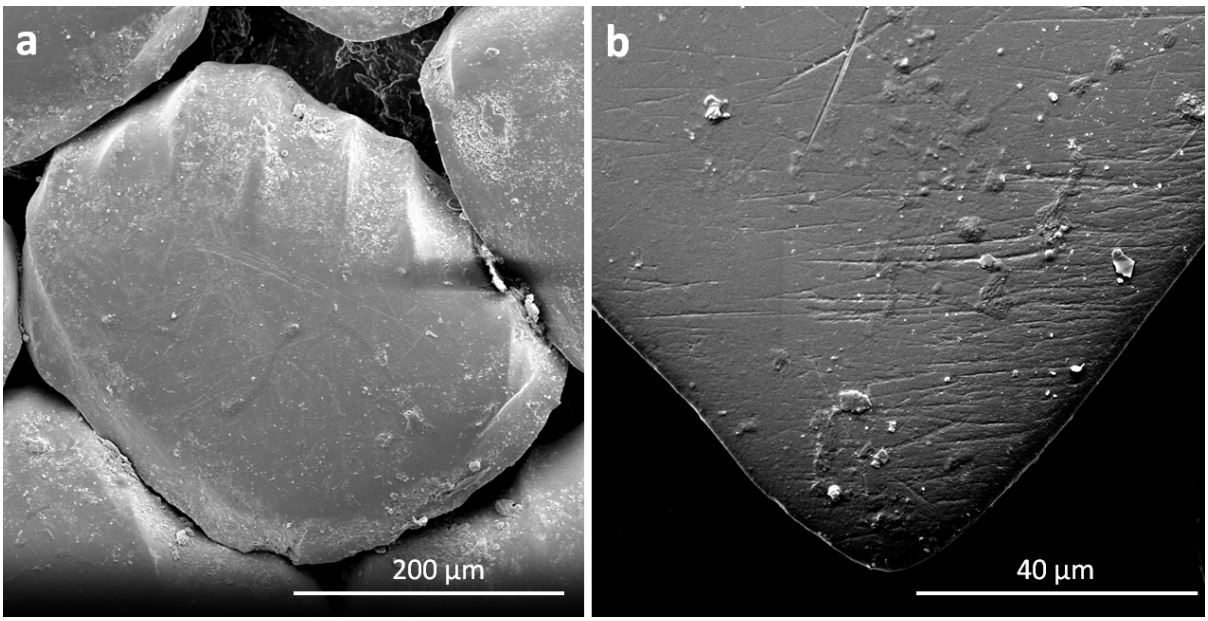

Figure 8.1. Scratch marks on the scales of a 680mm (total length) male *Chilloscyllium plagiosum* a) from the rostrum and; b) detail of the posterior tip of a scale from the trunk region ('FF3', section 3.1.). Scales are orientated anterior upwards.

(b) Parasite / antifouling defence

In accord with previous work (Reif, 1985a) spined-and spine-like scales are here interpreted as a defence against parasites. There is little published experimental evidence, however work on sailfish concluded that similarly pointed v-shaped scales did not reduce skin friction (Sagong et al., 2008), nor did they help delay boundary layer separation (Sagong et al., 2013). There is also ecological support for this as a primary function. Firstly, there is a lack of documented ectoparasite infection in shark species with this scale type. While absence of parasites is not evidence in itself, there are many more accounts of infestation of pelagic species with other scale types (e.g. Cheung & Ruggieri, 1983; Russo, 2013). In addition, the hypothesis that erect spines contribute to drag is supported by the experimental analysis (Chapter 7), discussed later. This suggests a functional trade-off between defensive and drag-reducing features for pelagic species, and between drag-reduction and abrasion resistance for benthic species.

An important consideration is the anti-fouling function of riblets, recognised in biomimetic studies as a solution for self-cleaning (Bixler & Bhushan, 2013). Riblets increase the exposed surface area of the scale crown, and it follows that this should not only encourage growth and encrustation, but also make it more difficult to dislodge these organisms. However, while total surface area is increased, the accessible surface for attachment of larger organisms is reduced to the peaks of the riblets, much like a cattle grid. The smaller riblet spacing would physically

prevent the attachment of even the smallest epibionts (encrusting organisms). The effect of very small epibionts on drag would be small initially, increasing surface roughness (and therefore skin friction) and reducing the efficacy of the riblets by altering their geometry. However, fouling is an additive process and these 'pioneer' fouling organisms could form the substrate for progressively larger species (Bixler et al., 2014). Eventually these masses could begin to compromise streamlining, negatively affecting the way fluid moves across the body surface and increasing form drag. Additionally, riblets which help maintain higher fluid velocity across the body surface (Chapter 7) may as a result reduce the time an encrusting organism has to attach, and increase the force of fluid entraining and washing them away relative to a completely smooth surface. Others have reported lower encrustation on scaled shark skin when compared to naked animals such as whales (Bixler et al., 2014), which are apparently more prone to biofouling.

Sharks optimise their riblet spacing for drag-reduction at different speeds (Chapter 5), but there is an additional anti-fouling benefit at higher speeds as well. If the potential for fouling was greater in the photic zone, this extra function would be particularly advantageous for the faster pelagic species inhabiting it. Notably, slower-moving deep water sharks often do not have riblets at all, instead possessing blocky or spiny denticles thought to function as abrasion resistance and parasite defence respectively (Reif, 1985).

On examining uncleaned shark scales under the scanning electron microscope, very little fouling was detected on either the fast-swimming lamnid shark *Lamna nasus* or the demersal and relatively slow-moving *Scyliorhinus canicula*. The latter does not have riblets proper, rather converging ridges, which support spines at the posterior of the crown. In this case it may be the spines that prevent biofouling, reducing the size of crevices which could serve as potential holdfasts. Unlike the 'flushing' hypothesis described above, this is the basis for improving biomimetic sharkskin surfaces for antifouling, whereby riblet spacing is optimised to deter different species of epibiont, rather than for reducing drag (e.g. Carman et al, 2006; Schumacher et al., 2007). Living sharks enjoy the benefit of shedding their scales as they grow, which presumably helps clean the skin as well. The rate of replacement has never been measured empirically, so the contribution of this process to maintaining a clean skin is unknown. Regardless of the mechanism it is clear that riblets do help reduce fouling, which in turn would help reduce skin friction, firstly by keeping the riblets clean, and also by minimising the extra surface roughness which may begin to increase both skin friction and pressure drag.

(c) Passive gripping

An intriguing hypothesis that has emerged from this project is that the epaulette sharks could be using their scales as grips for more efficient benthic locomotion. Their scales are blocky and smooth, but with robust pointed tips on the crown. These often show signs of wear, especially on the ventral surface. When 'walking' the animal bends its body to place one pectoral fin in a bracing position before pulling forward the other pectoral fin as the body bends in the other direction, assisted by the pelvic fins. As the scale crowns tilt slightly upwards they may act like a crampon. With the shovel tip of the crown embedded in the substrate, it could provide a great deal of grip. In addition, the pointed tip could be removed from the sediment with relative ease. If a small amount of bristling is possible (i.e. the scale crown angle is changeable), this would also baffle sediment behind the scale crown (which is also slightly concave), meaning more force could be applied, increasing purchase with the sediment. Evidence for this function is limited so far, with this being the first discussion of passive gripping in a shark species. As discussed, wear is greater on the ventral scales of the *Chiloscyllium* species examined, suggesting disproportionate exposure to the hard substrate.

8.2. Drag Reduction of Shark-like Scales

8.2.1. Riblets

Riblets act to control vortices that form across the scale surface in a turbulent flow regime, by reducing their lateral drift, and pinning the vortices in place (e.g. Garcia-Mayoral & Jiménez, 2011; Oeffner & Lauder, 2012). This reduces the lateral transfer of momentum, meaning drag – any impedance/loss of velocity – is reduced as well. Riblets also lift these vortices up and out of the valleys in between the riblet peaks, minimising the surface area rotating fluid is in contact with. This means less force is required to overcome the friction imparted by that surface, and drag is reduced.

In Chapter 5, the ecological significance of riblet spacing was investigated quantitatively for the first time. Empirical studies of biomimetic models show that decreasing riblet spacing has a greater drag-reducing effect at higher speeds (Dean & Bhushan, 2010). This may be related to a decrease in vortex wavelength with increasing velocity, when more closely-packed riblets are needed to hold the vortices above the riblet valleys. While the mechanism remains unclear, this negative relationship between riblet spacing and speed in modern species of shark has herein been convincingly demonstrated. The analysis of riblets in modern sharks revealed a significant trend towards decreased riblet spacing with increased swimming speed. Mean

riblet spacing for ‘fast’ sharks was 63µm, ‘moderate’ was 91µm (44% wider than ‘fast’), and ‘slow’ was 111µm (75% wider than ‘fast’). This is the first quantitative confirmation of the hypothesis that riblet spacing is related to speed (Reif, 1985a). It is also the first time biomimetic optimisation has been retroactively applied to the animals which originally inspired the technology.

Extinct taxa with narrowly spaced riblets appear to have been similarly adapted for speed and efficiency. Of all the categories, the extinct thelodonts and ‘acanthodians’ had the narrowest mean riblet spacing at 50µm and 62µm respectively, akin to the ‘fast’ and ‘moderate’ modern sharks. Of the ‘acanthodians’ studied, *Milesacanthus* (of the Lower to upper middle Devonian, ~407-383 million years ago) had the narrowest mean riblet spacing at 40µm (Burrow, et al., 2006; 2009). However, the thelodont genus *Canonia* had a mean riblet spacing of 37µm, which is the narrowest of all taxa studied. ‘Acanthodians’ and thelodonts are quite small animals (of those examined by the author, typically 10-30cm), and it is therefore important to recognise the implications of this discovery. Smaller riblet spacing is more efficient at reducing drag at higher speeds, but the cruising speeds of large active modern sharks is surprisingly slow. For example the shortfin mako shark *Isurus oxyrhinchus* has a riblet spacing of 46µm, and is widely considered the fastest shark (e.g. Stevens, 2008). However it has a sustained cruising speed of just 0.5-0.9 m/s (Block et al. 1992; Klimley et al., 2002), which is a much more plausible speed for a smaller fish. Indeed the average cruising speeds of modern taxa in the 10-30cm length range is just over 1 m/s (http:/www.fishbase.org).

Furthermore, there is evidence that some of the earliest known fishes were similarly well adapted for drag-reduction. The middle Ordovician (~460 million years ago) fishes *Tantalepis gatehousi* and *Areyonga oervigi* (possible chondricthyans) were not included in the main analysis as the scales found were of unknown position on the body. However their mean riblet spacing was 69µm and 77µm respectively, placing them firmly within the fast-moderate speed modern sharks. As riblets tend to occur more prominently on the flank (Chapters 4 and 6), there is a strong likelihood that these scales are at least broadly representative of overall squamation. There is therefore strong evidence that novel drag-reducing adaptations evolved in, or before the middle Ordovician.

A major finding of Chapter 6 is that the nature of drag-reduction by riblets cannot always be described by spacing alone. In areas where riblets are broadly parallel (such as the flank), direct comparisons can be made (such as Chapter 5), however in other areas of the body, riblets with converging or diverging riblet patterns paint a more complicated picture. The dataset of riblet angle measurements assembled for *Lamna nasus* in Chapter 6, is the first of its kind in any shark species, and like riblet spacing shows clear regional variation (Figure 8.2).

Experimental evidence suggests that drag-reduction diminishes if parallel riblets are misaligned from the freestream direction by >15°, with no benefit >30° (Walsh & Lindemann 1984). Non-parallel riblets at diverging angles have been shown to decrease turbulent disturbances and velocity fluctuations, with the opposite effect for converging riblets (Koeltzsch et al., 2002; Nugroho et al., 2013). Additionally, the v-shaped central keel of some shark pectoral fin scales has been interpreted as a vortex generator; turbulisors whose function is to maintain boundary layer attachment (Bechert et al. 1985; section 2.3.2). The data reported in Chapter 6 supports this view, by demonstrating the occurrence of convergent scales on these and other leading edges, such as the rostrum and dorsal fin. Due to the sampling scheme used, information about the pattern of riblet angle from the tip of a leading edge downstream is only available for the head region. Despite this, the pattern is very clear with strongly converging scales at the tip, becoming more divergent downstream within a very short distance, restricted to the anterior of the head region. If the putative work discussed is correct and converging riblets create turbulence, it suggests that turbulent flow is being encouraged almost immediately at the tip of the snout, before scales with parallel to divergent riblets 'rein in' that turbulence downstream.

In most teleost fishes this transition is triggered at the point of maximum body girth with the relatively rougher ctenoid scales and gill efflux affecting the diffuser region, where separation is prone (section 2.3.2.). If as the evidence suggests the transition occurs before the point of maximum body girth for *Lamna nasus*, a more appropriate comparison may be the sailfish *Istiophorus*. It has been suggested that the tubercles of the rostrum tip of sailfish may act as a turbulisor (Aleyev, 1977; Videler, 1995). Experimental data supports this hypothesis, but it is important to note that at cruising speeds overall drag was largely unaffected, although skin friction was lower immediately behind the rostrum (Sagong et al., 2013). It may be that sailfish turbulisors act solely to counter the increased drag created by the larger wetted surface of the elongate rostral feeding appendage at cruising speeds, and is less important at higher (and untested) speeds.

Chapter 6 also presents evidence that both riblet angle and spacing change throughout ontogeny. Riblets of immature *Lamna nasus* diverge while those in mature individuals slightly converge, and are ~7µm more widely spaced than immature specimens. As these are new observations and have not been tested experimentally, it is difficult to disentangle the hydrodynamic effects of riblet spacing and angle.

If the theoretical assumption that smaller riblet spacing is more efficient at higher speeds is correct, it suggests the larger sharks have lower absolute swimming. Alternative explanations for this result are that the juveniles have faster burst speeds than the larger animals. While it may be intuitive to assume larger animals are moving at faster speeds, there is little evidence to support this and as discussed, the normal swimming speeds of adult sharks can be surprisingly slow. Younger and smaller sharks are more vulnerable to predation, leading many species to utilise shallow water as nurseries during their earliest years before moving further offshore (Castro, 1993). The benefits of relatively faster speed are clear for younger sharks, but do not fully explain the wider spacing in adult specimens of *Lamna nasus*.

A relatively larger mean boundary layer thickness over the adult animals would go some way to explaining this result, with slower moving fluid in contact with the shark. As a shark grows, the distance from leading to trailing edges increases and so larger animals may be more prone to premature boundary layer separation creating a larger wake. This increases pressure drag enormously (Figure 2.5), so maximising the boundary layer attachment is especially important for larger animals. If increased convergence of the riblets make them more effective turbulisors (section 8.2.2), this may explain their presence on more mature individuals. The relatively narrow riblet spacing on the leading edge surfaces (e.g. rostrum) may reflect the higher velocity fluid of a thinner boundary layer, at an earlier stage of development. Downstream, riblets may be wider due to reduction in fluid velocity, caused by a combination of skin friction, and pressure-related thickening of the turbulent boundary layer. The gently diverging riblets of the flank may be optimised to dampen turbulent fluctuations which contribute to drag. Further investigation of ontogenetic changes in this species' ecology is required to explore this hypothesis, and there is clearly potential for much more extensive research in this area.

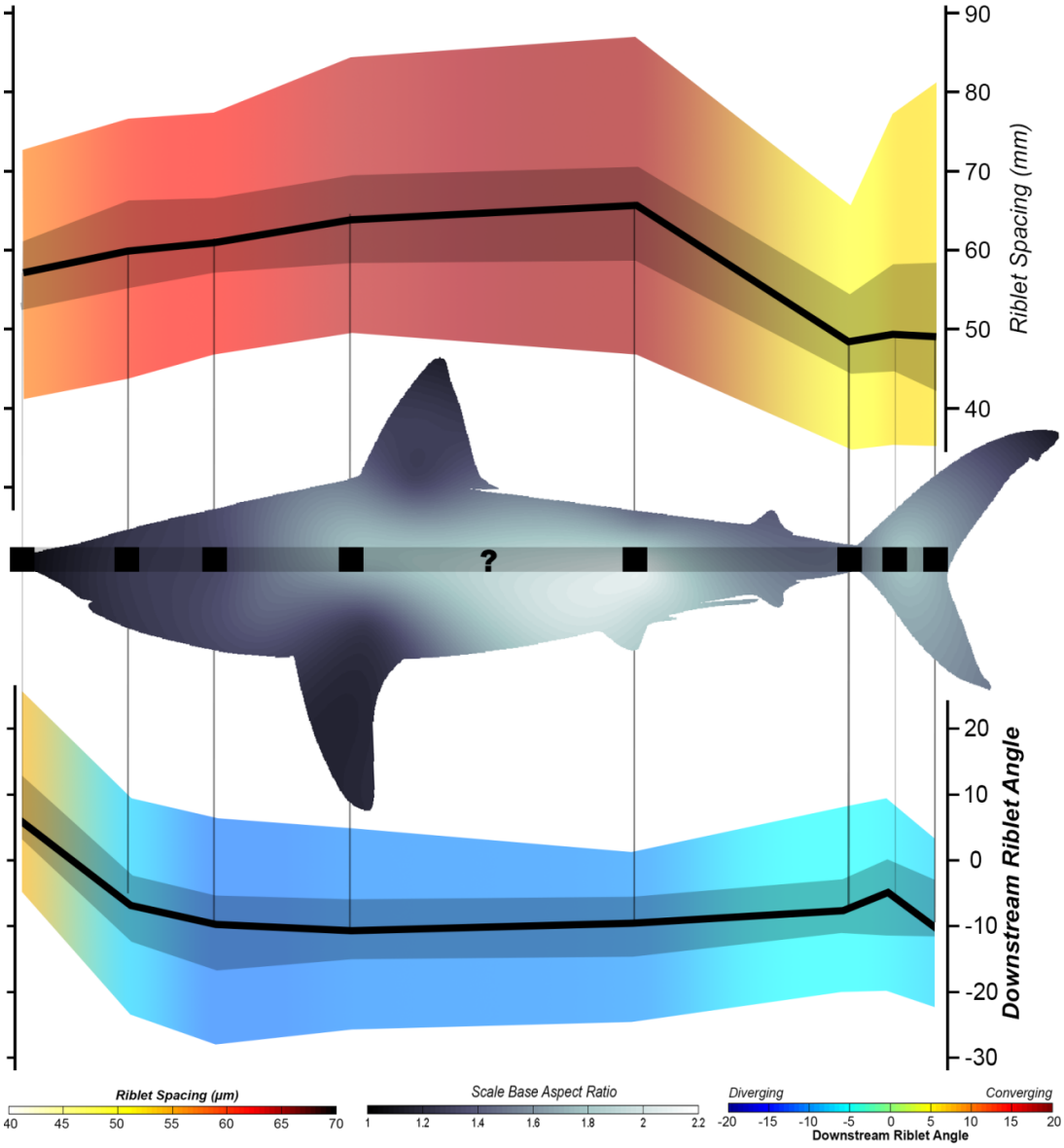

Figure 8.2. Distribution of scale features in *Lamna nasus*, compiled for ease of reference from figures 6.4-6.6, in Chapter 6. Top) Transect of shark midline, showing mean riblet spacing (µm) of all specimens of *Lamna nasus* at different sampling locations. Middle) Heat map of scale base aspect ratio distribution of a 183cm male *Lamna nasus* from 19 sample locations (excluding claspers), and three flank semi-landmarks (Appendix 1), interpolated across entire body, and weighted according to standard error. Bottom) Transect of shark midline, showing mean riblet angle (degrees) of all specimens of *Lamna nasus* at different sampling locations.

In Chapter 7 representative scale morphotypes of Palaeozoic fishes were subjected to flume analysis, and is the first study to measure skin friction drag of any extinct vertebrate. The jawless thelodont fish *Phlebolepis* was chosen to represent taxa with riblets, and the results confirm previous reports (discussed in section 2.3.2.) that riblets do reduce skin friction drag.

This result is particularly interesting because in order to control for scale size and overcome the practical limitations of 3D printing, all specimens were scaled to 2mm length. This is an issue which will inevitably be addressed in future as the quality and economy of 3D printing improves, but as a consequence of scaling in this study the riblet spacing was ~58% wider (between 151-336µm) than the original specimen (96-213µm). The freestream velocity was fairly slow during these experiments (~0.5m/s), and consequently may have controlled for this. Skin friction was reduced by 5-45% across the plate relative to the smooth control, out-performing the pointed *Nostolepis* scale, and the typically shark-like scale shape of *Poracanthodes*, both of which do not have riblets. It is difficult to ascribe this drag reduction to riblet action alone however. Calculated as a whole, all but the *Nostolepis* plate reduced skin friction drag relative to the smooth plate. The greatest drag reduction was recorded for *Lophosteus* (~35%), a scale ornamented with stream-wise orientated tubercles (Figures 3.10; 3.18; 8.3). This demonstrates that scales do not necessarily increase skin friction even if they increase surface roughness.

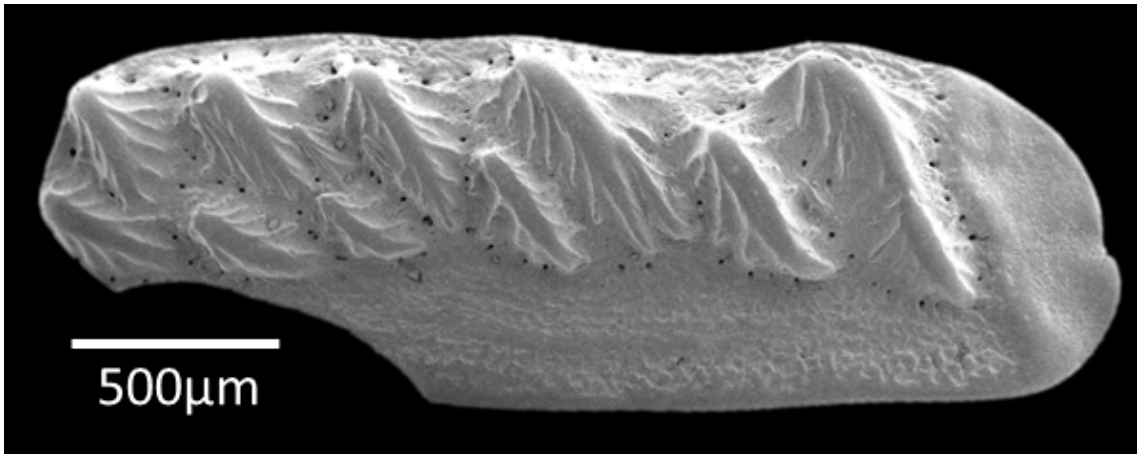

Figure 8.3. Scanning electron micrograph of the Silurian osteichthyan fish *Lophosteus* sp., from Ohesaare Cliff, Estonia. Material courtesy of Henning Blom.

The riblet action described so far operates in part by reducing the lateral transfer of momentum by controlling the drift of vortices which form across the skin surface. When tessellated, the *Lophosteus* scale tubercles align to form broken streamwise ridges, which may be acting in a similar way to the riblets of *Phlebolepis*. In support of this, the boundary layer thicknesses at successive points along the *Phlebolepis* and *Lophosteus* plates were very similar. Riblets also act to reduce the surface area in contact with the base of the boundary layer, reducing the interaction of moving fluid and the solid wall. This may explain the relatively low

skin friction drag reduction of *Poracanthodes*, in which the crowns tessellate tightly to produce a large and flat surface. Perhaps as a consequence the skin friction distribution across the *Poracanthodes* and smooth plates was also very similar. Boundary layer thickness grew much more rapidly in *Poracanthodes* than other plates, which likely reflects subtler differences in scale geometry.

Skin friction drag in *Loganellia* was ~33.5% lower than that of a smooth plate, despite lacking riblets or any streamwise ornamentation. These stubby scales are rounded at the anterior and softly pointed at the posterior, with curved upward and backward directed channels at the sides (Figure 3.9). It is possible that these channels are directing flow upwards away from the wall, and reducing skin friction by passive streamwise injection, as discussed in section 2.3.2. Alternatively, like the riblets, any form of lifting the flow base to interact with structures of lower surface area than the wall proper, would reduce skin friction drag (Dean & Bhushan, 2010). Further experimental work is required to test these hypotheses, and visualise flow movement between and above the scales. Simple techniques such as dye-flow analysis with high speed cameras would provide an adequate basis for a more in-depth investigation, using high resolution particle image velocimetry. Alternatively LDA could be applied, although this would require very high spatial accuracy of the position of the measurement volume relative to the scale structures.

8.2.2. Turbulisors

Turbulisors trigger the transition from laminar to turbulent flow by disrupting the smooth and ordered movement of fluid molecules. This means streamwise but 'messier' flow transfers some fluid momentum back towards the surface, meaning the boundary layer remains attached for longer. The turbulisor role of fish squamation is a little discussed aspect of their overall hydrodynamics, but there is compelling evidence of its importance in drag-reduction. The most convincing biological evidence of turbulisors in fishes is the distribution of ctenoid and cycloid scales across the bodies of teleosts (Figure 2.7; section 2.3.2). Smooth cycloid scales cover the head and often the gills, but after this point towards the posterior, rough ctenoid scales dominate. A similar distribution of scale types can be found in many modern sharks (Figure 6.2.), thelodonts and 'acanthodians', as detailed in Chapter 4. Commonly, the scales of leading edge surfaces are smoother, but also stubbier (smaller neck region below the crown), tessellating more closely together, and with shorter spines (if present at all). Flank scales are almost always more elongate, and the crown extends more proudly from the scale base, often with a streamlined ornament.

In Chapter 7, evidence was presented which demonstrates that scales can reduce skin friction even in the absence of riblets. A possible explanation is that vortices that are kept elevated by scales interact with a smaller surface area relative to a smooth wall, reducing skin friction. Scale morphology may therefore reflect a crucial trade-off between the production of turbulence to benefit the scales downstream, and controlling the turbulence they encounter from scales upstream. The prolonged attachment of a turbulent boundary layer in such a wide array of modern pelagic shark species highlights the predominant influence of whole-body hydrodynamics on scale morphology.

8.2.3. Bristling

Minimal skin friction is achieved by preserving an attached fully laminar flow regime (Figure 2.5), but the effects of pressure drag must also be considered. A perfectly smooth surface offers the most favourable conditions for laminar flow, but as discussed is more prone to boundary layer separation (reversal of near-wall flow), especially in unfavourable pressure gradients. Flow separation is essentially stall, and pressure drag increases enormously across the body surface if it occurs prematurely (Fish, 1998, Figure 2.5-2.6). In some of the fastest pelagic sharks the passive bristling of scales is hypothesised to reduce drag and contribute to thrust, and it has been suggested that the aspect ratio of the scale base reflects the degree of pivoting the scale is capable of (Pershin et al., 1976 [in Bushnell & Moore, 1991]; Bechert et al., 1986; Motta et al. 2012).

The first systematic treatment of scale base morphology for any shark is presented in Chapter 7. The results show scales with the widest and shortest bases in the streamwise direction are found in the flank region of *Lamna nasus*. In addition, those scales with the squarer base type were found on leading edge regions such as the fins and rostrum. Scale overlap can only be roughly estimated using exposed scale length as this assumes identical crown size across the body. However, qualitative examination of articulated skin strongly suggests a requirement for bristling scales to have both larger and overlapping crowns. This a significant finding, as it highlights the limitations of modelling immobile scales for experimental analyses, and the requirement to further understand soft-tissue systems of drag-reduction. The immobile bases of scales found on leading edge surfaces may reflect a decreased likelihood of flow separation in these regions, and as such bristling may not be required, perhaps even increasing drag. There is little evidence for bristling in the fossil record so far, however the Middle Devonian acanthodian *Milesacanthus* (Figure 8.2) also had scales with a relatively small base, and a base length to width ratio very similar to those of the *Lamna nasus* flank scales (section 6.1.2),

suggesting a similar action. *Milesacanthus* has riblets on the crowns, which have a spacing (~39-42µm) comparable to the fastest sharks (Chapter 5), but is only 20-22cm in length (based on reconstruction of Young & Burrow, 2004). This suggests that even small fishes can benefit from scale bristling, although the degree to which body size affects the mechanism of drag-reduction is currently unclear.

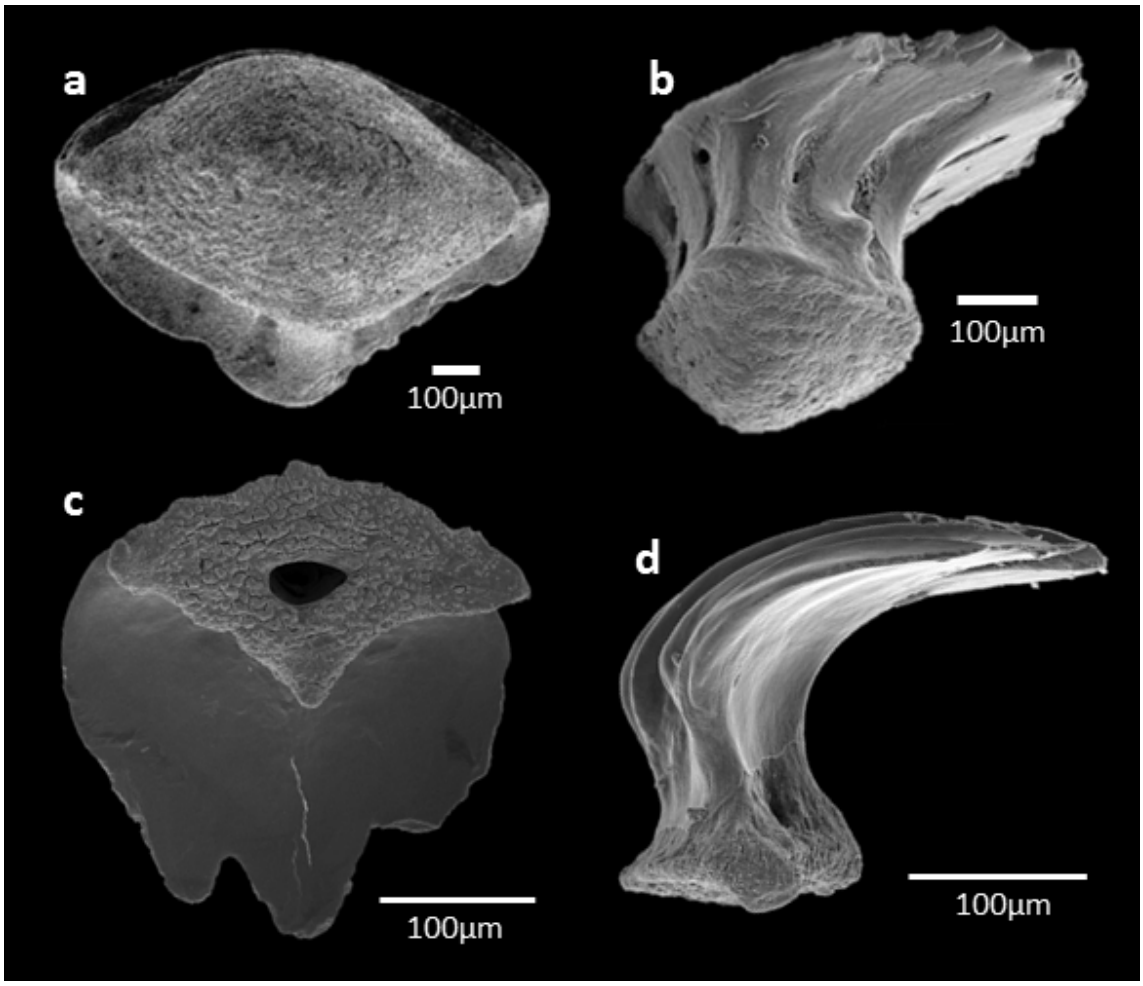

Figure 8.4. Scanning electron micrographs of the 'acanthodian' *Milesacanthus* sp. (a,b) and the modern porbeagle shark *Lamna nasus* (c,d) scales. A) *Milesacanthus* sp. aff. *M. antarctica* flank scale in ventral view showing detail of base, modified from Hairapetian, 2006. B) Dorso-lateral view of scale from unknown body position of *Milesacanthus antarctica* NMV P228907, modified from Burrow et al. 2009. C-d) Flank scales (FF2) of a 183cm male *Lamna nasus* in c) ventral view and; d) lateral view.

8.3. The Evolution of Speed

There are remarkable similarities between the scales of modern sharks and their extinct relatives. In section 4.2 flank scale function of 167 extinct species was interpreted based on comparative and experimental data, and their stratigraphic occurrence is presented in Figure 4.11. This shows that complex ecologies were established from at least the Llandovery (~440 million years ago), which includes active pelagic taxa. There appears to be a continuous increase in those species prioritising drag-reduction throughout the Silurian, and into the early Devonian. After this point drag-reducing scales become less common compared to morphotypes associated with abrasion resistance and parasite defence. This is coincident with the burgeoning success of actinopterygian fishes in particular, and may relate to a shift from hard scale based drag reduction, to soft-tissue mechanisms (e.g. compliant surfaces, mucus).

However, table 8.1 shows the results of chi squared comparison at each interval, revealing only one significant shift in functional composition between the Emsian-Eifelian (~393 million years ago. This step shows an increase in parasite defence and unknown/generalist morphologies, and temporary loss of the drag-reduction and abrasion resistance functions. It is not clear if this signal reflects genuine change in ecology or a sampling bias of different beds. This thesis has explored the use of scales as a potential source of previously unrecoverable ecological data, so tracking functional trends in more detail should be a priority for future work.

The chi squred analysis suggests that the functional makeup of Palaeozoic fish communites was largely independent of changing palaeogeography, palaeoclimate, large-scale evolutionary trends, and any other factors contributing to palaeoecology.

Table 8.1. Chi squared results comparing the functional composition of scales found between time intervals from the Llanvirn (Ordovician) to Fammenian (late Devonian). Categories of scale function included drag reduction, abrasion resistance, parasite defense and unknown/generalist (for those scales with multiple functions). Those omitted results could not be calculated due to small 'expected' sample numbers.

Chi (p)	Llanvirn-Caradoc	Caradoc-Ashgill	Ashgill-Llandovery	Llandovery-Wenlock	Wenlock-Ludlow	Ludlow-Pridoli	Pridoli-Lochkovian	Lochkovian-Pragian	Pragian-Emsian	Emsian-Eifelian	Eifelian-Givetian	Givetian-Frasnian	Frasnian-Fammenian
All data	-	-	0.21	0.92	0.52	0.55	0.31	0.63	0.58	0.72	**0.05**	-	-
Excl unknown	0.39	-	0.59	0.92	0.61	0.56	0.56	0.90	0.81	0.75	0.27	0.88	0.84

As discussed, the distribution of scale types across the body plays an important role in drag reduction, particularly the prevention of boundary layer separation. The first unambiguous occurrence of this scale regionalisation in the fossil record is in the thelodont *Sandivia melnikovi* of the Upper Ordovician (~458-443 mya) of Russia (Karatajūtė-Talimaa, 1997). The scales of modern sharks, 'acanthodians' and thelodonts were directly exposed to fluid flow (section 2.6) however the soft tissue context of these structures is unknown and so the skin friction cannot be tested in the same way. It should be noted that many heavily armoured fishes show a similar pattern, with a smooth head region of large bony plates, and smaller scales along the flank. This is possibly because of the requirement for increased skin flexure in this region, with smaller or overlapping scales perhaps helping to maintain an uninterrupted, regular surface for both drag reduction and defence.

Nevertheless, some of the earliest fish scales have narrowly spaced riblets, suggesting that drag-reduction and fast speeds evolved as early as the Middle Ordovician, ~460 million years ago.

8.4. Conclusions

This thesis has focussed on the hydrodynamics of fish scales, with an emphasis on modern sharks and Palaeozoic taxa. A combination of research methods has been employed, including comparative anatomy, morphometrics, and the novel application of laser Doppler anemometry for experimental analysis.

8.4.1. Original contributions to knowledge

The present work has demonstrated a number of novel findings on the function and evolution of scales in fishes, including:

(1) There is a remarkable convergence in scale morphology between 'acanthodians', thelodonts and modern sharks, and clear potential for further hydrodynamic and palaeoecological investigations.

(2) In modern sharks, scale morphology can vary dramatically between body regions. Scales on the head tend to be rounder, tessellating tightly with little or no overlap to maintain smooth laminar flow in a favourable pressure gradient towards the widest point of the body. After this point, where boundary layer separation is prone to occur scales are often rougher and overlap more, possibly to induce turbulence and delay separation in this region.

(3) Almost all active pelagic sharks have uniform riblets on the crown surface, and of the species studied this was the most common scale type in modern taxa. The occurrence of ribletted scales in extinct species was much lower, but drag-reducing scales rose in prominence in concurrence with the 'nekton revolution' throughout the end-Silurian and early Devonian.

(4) Riblet spacing reflects speed in modern sharks and optimal riblet spacing for the fastest sharks is narrower, in accord with existing biomimetic research. Thelodonts and 'acanthodians' have similar narrowly spaced riblets, placing many within the range of the fastest extant shark species. Evidence is also presented suggesting the oldest fish scales (~460 million year ago) were not only capable of reducing drag, but were optimised for similarly high speeds.

(5) Variation in scale features between body regions in *Lamna nasus* reveal regional fine-tuning of riblet spacing and riblet angle. Evidence is presented which suggests the two riblet properties are related, and are of hydrodynamic signifincance.

(6) Experimental data suggests the pointed scale type (associated with parasite resistance) increased skin friction significantly. However, a variety of other fossil fish scales are capable of reducing skin friction, even those without riblets.

8.4.2. Future Work

(a) Modern shark ecology

With limited fossil data, modern biomechanical analogues are an important source of information. Throughout this study, a common and persistent issue was the lack of data for modern sharks, with just a handful of references offering quantitative scale and swimming speed data. When compiled, reported swimming speeds of shark species were variable, and could not be used as a basis for quantitative analysis. There is also a conspicuous bias towards the larger more aggressive species, which represent a narrow slice of true shark diversity. With more information available the ecological basis for speed categorisation was judged more reliable, however the rare and smaller species of shark were often still neglected.

It is clear from the data presented herein that denticle morphology can change quite markedly between body regions. A clear aim for the future is to map scale features in much wider range of taxa, and further investigate the ecological and hydrodynamic basis for the ontogenetic and sex-specific differences we have observed in *Lamna nasus*. An important aspect of this is the accurate reporting of scale sampling locations, so that direct comparisons can be made.

Lastly, there are basic questions about scale biology which remain unanswered, for example the replacement rate of denticles, or possible physiological functions such as calcium storage.

Denticle replacement may play a role in self-cleaning, and the reduction of biofouling on the skin which may otherwise increase drag. The riblets too may be acting to prevent epibiont attachment, but the efficacy has only been demonstrated in biomimetic studies, and the mechanism in living sharks remains unclear.

(b) Modern shark hydrodynamics

It is apparent from these results that riblet spacing is directly related to speed, which supports previous experimental work. However, riblet angle has not received the same intensive research focus, or attempts at optimisation for industrial and commercial applications. It is very important that the fundamental hydrodynamic actions of divergent and convergent riblets are fully understood, and further studying their role and occurrence in modern sharks is a first step to this end. Similarly, the hypothesis that streamwise injection of fluid from an under-crown reservoir could reduce drag in modern sharks remains completely unexplored.

The hydrodynamic function of mucus in sharks has never been investigated, which is surprising as in other taxa mucus is known to reduce drag. There is also good evidence that the ctenii (comb-like projections of many teleost scales) of some fish scales (discussed in Chapter 2) are involved in the efficient dissemination of mucus in areas prone to boundary layer separation. Since the original research decades ago, focus has shifted away from soft-tissue mechanics of living animals, to the development of synthetic compliant surfaces and polymers. The relative difficulty of modelling soft tissue systems is undoubtedly a factor contributing to their historical neglect, but must be addressed if we are to understand the true complexity of drag-reduction in modern and extinct taxa.

(c) Prospectus

There has been a huge surge in interest in fossil biomechanics, fuelled by increases in computing power and the application of engineering techniques for novel biological analyses (e.g. Fletcher et al., 2010). Fishes in their myriad forms have been largely neglected, despite constituting a significant proportion of vertebrate diversity. This work is a step towards understanding the physical constraints which have influenced their evolution for over half a billion years. Furthering this work will help improve our technology, in the new field of palaeobiomimetics. Moreover, it will help shed light on the complex mechanics of our deepest ancestors, and the modern marine life we are obliged to understand and protect.

"So long, and thanks for all the fish"

Douglas Noel Adams, 1978

REFERENCES

1. Aburomia R., Khaner O., & Sidow A. (2003) Functional evolution in the ancestral lineage of vertebrates or when genomic complexity was wagging its morphological tail. In *Genome Evolution*. Springer Netherlands, 45-52.
2. Affleck R. J. (1950) Some points on the function, development and evolution of the tail in fishes. *Proceedings of the Zoological Society of London* **120**, 349-368.
3. Albert J. S., Johnson D. M., & Knouft J. H. (2009) Fossils provide better estimates of ancestral body size than do extant taxa in fishes. *Acta Zoologica* **90**, 357-384.
4. Aldridge R. J., Briggs D. E., Smith M. P., Clarkson E. N. K., & Clark N. D. L. (1993) The anatomy of conodonts. *Philosophical Transactions of the Royal Society B: Biological Sciences* **340**, 405-421.
5. Alexander R. M. (1965) The lift produced by the heterocercal tails of selachii. *Journal of Experimental Biology* **43**, 131-138.
6. Alexander R. M. (1966) Lift produced by the heterocercal tail of Acipenser. *Nature* **210**, 1049-1050.
7. Alexander R. R. (1984) Comparative hydrodynamic stability of brachiopod shells on current-scoured arenaceous substrates. *Lethaia* **17**, 17–32.
8. Aleyev Y. G. (1977) *Nekton*. The Hague, Netherlands: Dr W. Junk B.V. Publishers.
9. Anderson A. M. (1976) Fish trails from the early Permian of South Africa. *Palaeontology* **19**, 397-409.
10. Anderson A. (1970) An analysis of supposed fish trails from interglacial sediments in the Dwyka Series, near Vryheid, Natal. *Proceedings of the Second Gondwana Symposium* **1970**, 637-645.
11. Anderson E. J., MacGillivray P. S., & DeMont M. E. (1997) Scallop shells exhibit optimization of riblet dimensions for drag reduction. *The Biological Bulletin* **192**, 341-344.
12. Anderson E. J., Mcgillis W. R., & Grosenbaugh M. A. (2001) The boundary layer of swimming fish. *Journal of Experimental Biology* **204**, 81-102.
13. Anderson E. J. (2005) Advances in the visualization and analysis of boundary layer flow in swimming fish (Doctoral dissertation, Massachusetts Institute of Technology and Woods Hole Oceanographic Institution).
14. Anderson P. S. L., Friedman M., Brazeau M. D., & Rayfield E. J. (2011) Initial radiation of jaws demonstrated stability despite faunal and environmental change. *Nature* **476**, 206–209.
15. Andreev P. S., Coates M. I., Shelton R. M., Cooper P. R., Smith M. P. & Sansom I. J. (2015) Upper Ordovician chondrichthyan-like scales from North America. *Palaeontology* **58**, 691-704.

16. Antonucci F., Costa C., Aguzzi J., & Cataudella S. (2009) Ecomorphology of morpho-functional relationships in the family of sparidae: A quantitative statistic approach. *Journal of Morphology* **270**, 843-855.
17. Arnold G. P. & Weihs D. (1977) The hydrodynamics of rheotaxis in the Plaice (*Pleuronectes platessa* L.). *The Journal of Experimental Biology* **75**, 147-169.
18. Arsenault M. (1982) *Eusthenopteron foordi*, a predator on *Homalacanthus concinnus* from the Escuminac Formation, Miguasha, Quebec. *Canadian Journal of Earth Sciences* **19**, 2214-2217.
19. Askew G.N. & Marsh R.L. (1997) The effects of length trajectory on the mechanical power output of mouse skeletal muscles. *Journal of Experimental Biology* **200**, 3119–31
20. Au D. & Weihs D. (1980) At high speeds dolphins save energy by leaping. *Nature* **284**, 548-550.
21. Azuma A. (1992) *The Biokinetics of Flying and Swimming.* Tokyo: Springer-Verlag.
22. Bambach R. K. (2006) Phanerozoic biodiversity mass extinctions. *Annual Review of Earth and Planetary Science* **34**, 127-155.
23. Bandyopadhyay P. (1986) Mean flow in turbulent boundary layers disturbed to alter skin friction. *Journal of Fluids Engineering* **108**, 127-140.
24. Barbieri L. & Martin M. (1996) Swimming patterns of Malagasyan Triassic Fishes and environment. *Geological Society of Denmark, On Line Series* **1**, 1.
25. Barret R. D., Rogers S. M., & Schluter D. (2008) Natural selection on a major armor gene in threespine stickleback. *Science* **322**, 255-257.
26. Bartol I. K., Gharib M., Webb P. W., Weihs D. & Gordon, M. S. (2005) Body-induced vortical flows: a common mechanism for self-corrective trimming control in boxfishes. *Journal of Experimental Biology* **208**, 327-344.
27. Bartol I. K., Gordon M. S., Gharib M., Hove J., Webb P.W. & Weihs D. (2002) Flow patterns around the carapace of rigid-bodied, multipropulsor boxfishes (Teleostei: Ostraciidae). *Integrative and Comparative Biology* **42**, 971- 980.
28. Bartol I.K., Gordon M.S., Webb P.W., Weihs D. & Gharib M. (2008) Evidence of self-correcting spiral flows in swimming boxfishes. *Bioinspiration & Biomimetics* **3**, 014001.
29. Bartol I. K., Weihs D., Webb P. W., Hove J. R. & Gordon M. S. (2003) Hydrodynamic stability of swimming in ostraciid fishes: roles of the carapace in the smooth trunk-fish *Lactophrys triqueter* (Teleostei: Ostraciidae*). Journal of Experimental Biology* **206**, 725-744.
30. Batchelor G. K. (1977) *An Introduction to Fluid Dynamics.* New York: Cambridge University Press.
31. Bates D. E. B. & Loydell D. K. (2000) Parasitism on graptoloid graptolites. *Palaeontology* **43**, 1143–1151.

32. Baum J. K. & Worm B. (2009) Cascading top-down effects of changing oceanic predator abundances. *Journal of Animal Ecology* **78**, 699-714.
33. Baumiller T. K. & Plotnick R. E. (1989) Rotational stability in stalked crinoids and the function of wing plates in *Pterotocrinus depressus. Lethaia* **22**, 317-326.
34. Bechert D. W., Bruse M., Hage W., VanderHoeven J. G. T. & Hoppe G. (1997) Experiments on drag-reducing surfaces and their optimization with an adjustable geometry. *Journal of Fluid Mechanics* **338**, 59-87.
35. Bechert D. W., Hoppe G. & Reif W.-E. (1985) On the drag reduction of the shark skin. *American Institute Of Aeronautics And Astronautics Shear Flow Control Conf., Boulder, CO, 12–14 March* **85**, 1-18.
36. Bechert D. W., & Bartenwerfer M. (1989) The viscous flow on surfaces with longitudinal ribs. *Journal of Fluid Mechanic* **206**, 105-129.
37. Bechert D. W., Bruse M. & Hage W. (2000) Experiments with three-dimensional riblets as an idealized model of shark skin. *Experiments in Fluids* **28**, 403-412.
38. Becher D. W., Brus M., Hage W., & Meye R. (2000) Fluid mechanics of biological surfaces and their technological application. *Naturwissenschaften* **87**, 157-171.
39. Belles-Isles M. (1987) La nage et l'hydrodynamique de deux Agnathes du Paléozoïque: *Alaspis macrotuberculata* et *Pteraspis rostrata*. *Neues Jahrbuch für Geologie und Paläontologie – Ahbhandlungen* **175**, 347-376.
40. Belles-Isles M. (1992) The modes of swimming of sarcopterygians. In *Fossil fishes as living animals.* (ed. E. Mark-Kwik). pp. 117-130. Academia, 1. Tallinn: Academy of Sciences of Estonia.
41. Benjamini Y. & Hochberg Y. (1995) Controlling the False Discovery Rate: a powerful and practical approach to multiple testing. *Journal of the Royal Statistical Society Series B (Methodological) 57*, 289-300.
42. Benton M. J. & Harper D. A. (2013) Introduction to paleobiology and the fossil record. John Wiley & Sons, London.
43. Bergstrom D. J., Akinlade, O. G. & Tachie M. F. (2005) Skin friction correlation for smooth and rough wall turbulent boundary layers. *Journal of Fluids Engineering* **127**, 1146-1153.
44. Berman N. S. (1978) Drag reduction by polymers. *Annual Review of Fluid Mechanics* **10**, 47-64.
45. Bernadsky G., Sar N. & Rosenberg E. (1993) Drag reduction of fish skin mucus: Relationship to mode of swimming and size. *Journal of Fish Biology* **42**, 797-800.
46. Bernard A., Lécuyer C., Vincent P., Amiot R., Bardet N., Buffetaut E. & Prieur A. (2010) Regulation of body temperature by some Mesozoic marine reptiles. *Science* **328**, 1379-1382.

47. Beznosov P. (2009) A redescription of the Early Carboniferous acanthodian *Acanthodes lopatini* Rohon, 1889. *Acta Zoologica* **90**, 183-193.
48. Bill R. G. & Herrnkind W. F. (1976) Drag reduction by formation movement in spiny lobsters. *Science* **193**, 1146-1148.
49. Binning S.A., Roche D.G. & Layton C. (2013) Ectoparasites increase swimming costs in a coral reef fish. *Biology Letters* **9**, 20120927.
50. Bixler G. D., & Bhushan B. (2012) Biofouling: lessons from nature. *Philosophical Transactions of the Royal Society A: Mathematical, Physical and Engineering Sciences* **370**, 2381-2417.
51. Bixler G. D. & Bhushan B. (2012) Fluid drag reduction with shark-skin riblet inspired microstructured surfaces. *Advanced Functional Materials* **23**, 4507-4528.
52. Bixle G. D., & Bhushan B. (2013) Shark skin inspired low-drag microstructured surfaces in closed channel flow. *Journal of Colloid and Interface Science* **393**, 384-396.
53. Blackwelder R. F. (1989) Some ideas on the control of near-wall eddies, *AIAA Paper No. 89-1009*.
54. Blake R. W. (1983) *Fish Locomotion*. Cambridge, UK: Press Syndicate of the University of Cambridge.
55. Blake R. W. (2004) Fish functional design and swimming performance. *Journal of Fish Biology* **65**, 1193-1222.
56. Blake R. W., Chan K. H. S. & Kwok E. W. Y. (2005) Finlets and the steady swimming performance of *Thunnus albacares*. *Journal of Fish Biology* **67**, 1434-1445.
57. Blieck A., Turner S., Burrow C. J., Schultze H. P., Rexroad C. B., Bultynck P., & Nowlan G. S. (2010) Fossils, histology, and phylogeny: why conodonts are not vertebrates. *Episodes-Newsmagazine of the International Union of Geological Sciences* **33**, 234.
58. Blob R. W., Bridges W. C., Ptacek M. B., Maie T., Cediel R. A., Bertolas M. M. & Schoenfuss H. L. (2008) Morphological selection in an extreme flow environment: body shape and waterfall-climbing success in the Hawaiian stream fish *Sicyopterus stimpsoni*. *Integrative and Comparative Biology* **48**, 734-749.
59. Block B. A., Booth D., & Care F. G. (1992) Direct measurement of swimming speeds and depth of blue marlin. *Journal of Experimental Biology* **166**, 267-284.
60. Blom, H. (1999) Vertebrate remains from Upper Silurian–Lower Devonian beds of Hall Land, North Greenland. *Geology of Greenland Survey Bulletin* **182**, 1-80.
61. Blom, H. (2008) A new anaspid fish from the Middle Silurian Cowie Harbour fish bed of Stonehaven, Scotland. *Journal of Vertebrate Paleontology* **28**, 594-600.
62. Blom H. & Goujet D. (2002) Thelodont scales from the Lower Devonian Red Bay Group, Spitsbergen. *Palaeontology* 45, 795-820.
63. Blom H., Märss T. & Miller G.C. (2001) Silurian and earliest Devonian Birkeniid anaspids

from the Northern Hemisphere. *Transactions of the Royal Society of Edinburgh: Earth Science* **92**, 263-323.

64. Bockelie T. (1976) An early Ordovician vertebrate. *Nature* **260**, 36-38.
65. Bone Q. (1972) Buoyancy and hydrodynamic functions of integument in the castor oil fish, *Ruvettus pretiosus* (Pisces: Gempylidae). *Copeia* **1972**, 78-87.
66. Bone Q. (1975) Muscular and energetic aspects of fish swimming. In: *Swimming and Flying in Nature* (eds C.J. Brokaw and C. Brennen). Plenum Press, New York, 493-528.
67. Borazjani I. & Sotiropoulos F. (2010) On the role of form and kinematics on the hydrodynamics of self-propelled body/caudal fin swimming. *Journal of Experimental Biology* **213**, 89-107.
68. Botella H., Blom H., Dorka M., Ahlberg P. E & Janvier P. (2007) Jaws and teeth of the earliest bony fishes. *Nature* **448**, 583-586.
69. Botella H. & Fariña R. A. (2008) Flow pattern around the rigid cephalic shield of the Devonian agnathan *Errivaspis waynensis* (Pteraspidiformes: Heterostraci). *Palaeontology* **51**, 1141-1150.
70. Botella H., Valenzuela-Ríos J. I. & Carls P. (2006) A new early Devonian thelodont from Celtiberia (Spain), with a revision of Spanish thelodonts. *Palaeontology* **49**, 141-154.
71. Boucot A. J. & Janis C. (1983) Environment of the early Paleozoic vertebrates. *Palaeogeography, Palaeoclimatology, Palaeoecology*, 41, 251–287.
72. Boyajian G. E. & Labarbera M. (1987) Biomechanical analysis of passive flow of Stromatoporoids - morphologic, paleoecologic, and systematic implications. *Lethaia* **20**, 223-229.
73. Braun J. & Reif W.-E. (1982) A new terminology of aquatic propulsion in vertebrates. *Neues Jahrbuch für Geologie und Paläontologie* **164**, 162-171.
74. Brazeau M. D. (2012) A revision of the anatomy of the Early Devonian jawed vertebrate *Ptomacanthus anglicus* Miles. *Palaeontology* **55,** 355-367.
75. Brazeau M. D. & Friedman M. (2014) The characters of Palaeozoic jawed vertebrates. *Zoological Journal of the Linnean Society* **170**, 779–821.
76. Briggs D. E. G. (1992) Conodonts: a major extinct group added to the vertebrates. *Science* **256**, 1285-1286.
77. Briggs D. E. G., Clarksone N. K. & Aldridge R. J. (1983) The conodont animal. *Lethaia* **16**, 1–14.
78. Brown K. J., Britz R., Bills R., Rüber L. & Day J. J. (2011) Pectoral fin loss in the Mastacembelidae: a new species from Lake Tanganyika. *Journal of Zoology* **284**, 286-293.
79. Browning A., Ortiz C. & Boyce M. C. (2013) Mechanics of composite elasmoid fish scale assemblies and their bioinspired analogues. *Journal of the Mechanical Behavior of*

Biomedical Materials **19**, 75-86.

80. Bruet B. J. F., Song J., Boyce M. C. & Ortiz C. (2008) Materials design principles of ancient fish armour. *Nature Materials* **7**, 748-756.
81. Bunker S. J. & Machin K. E. (1991) The hydrodynamics of cephalaspids. In J. M. V. Rayner and R. J. Wootton, eds. *Biomechanics in Evolution*. Cambridge University Press, Cambridge, UK.
82. Burdak V.D. (1972) Hydrodynamic function of the cycloid fish scale. *Zoologicheskii Zhurnal* **51**, 1086-1090.
83. Burrow C. (1994) Form and function in scales of *Ligulalepis toombsi* Schultze, a palaeoniscoid from the early Devonian of Australia. *Records of the South Australian Museum (Adelaide)* **27**, 175-185.
84. Burrow C. J. (1996) Placoderm scales from the Lower Devonian of New South Wales, Australia. *Modern Geology* **20**, 351-370.
85. Burrow C. J. (2002) Lower Devonian acanthodian faunas and biostratigraphy of south-eastern Australia. *Memoirs of the Association of Australasian Palaeontologists* **27**, 75-137.
86. Burrow C. J. (2003a) Earliest devonian gnathostome microremains from central New South Wales (Australia). *Geodiversitas*, *25*(2), 273-288.
87. Burrow C. J. (2003b) Poracanthodid acanthodian from the Upper Silurian (Pridoli) of Nevada. *Journal of Vertebrate Paleontology* **23**, 489-493.
88. Burrow C. J. (2004) A redescription of *Atopacanthus dentatus* Hussakof and Bryant, 1918 (Acanthodii, Ischnacanthidae). *Journal of Vertebrate Paleontology* **24**, 257-267.
89. Burrow C. J. (2011) A partial articulated acanthodian from the Silurian of New Brunswick, Canada. *Canadian Journal of Earth Sciences* **48**, 1329-1341.
90. Burrow C. J. (2013) Reassessment of *Ischnacanthus scheii* Spjeldnaes (Acanthodii, Ischnacanthiformes) from the latest Silurian or earliest Devonian of Ellesmere Island, arctic Canada. *Canadian Journal of Earth Sciences* **50**, 945-954.
91. Burrow C. J., Janvier P. & Villarroel C. (2003) Late Devonian acanthodians from Colombia. *Journal of South American Earth Sciences* **16**, 155-161.
92. Burrow C. J., Lelièvre H., & Janjou D. (2006) Gnathostome microremains from the Lower Devonian Jawf Formation, Saudi Arabia. *Journal Information* **80***,* 537-560.
93. Burrow C. J., Lon J. A. & Turner S. (1998) Lower Devonian microvertebrates from the Point Hibbs Formation, Tasmania. *Alcheringa* **22**, 9-20.
94. Burrow C. J., Long J. A. & Trinajstic K. (2009) Disarticulated acanthodian and chondrichthyan remains from the upper Middle Devonian Aztec Siltstone, Southern Victoria Land, Antarctica. *Antarctic Science* **21**, 71-88.
95. Burrow C. J., Newman M. J., Davidson R. G., & den Blaauwen J. L. (2013) Redescription of

Parexus recurvus, an Early Devonian acanthodian from the Midland Valley of Scotland. *Alcheringa: An Australasian Journal of Palaeontology* **37**, 392-414.

96. Burrow C. J. & Simpso A. J. (1995) A new ischnacanthid acanthodian from the Late Silurian (Ludlow, Ploeckensis Zone) Jack Formation, north Queensland. *Memoirs - Queensland Museum* **38**, 383-396.
97. Burrow C. J., Trinajstic K., & Long J. (2012) First acanthodian from the Upper Devonian (Frasnian) Gogo Formation, Western Australia. *Historical Biology* **24**, 349-357.
98. Burrow C. J. & Turner S. (1999) A review of placoderm scales, and their significance in placoderm phylogeny. *Journal of Vertebrate Paleontology* **19**, 204-219.
99. Burrow C. J. & Turner S. (2012) Fossil fish taphonomy and the contribution of microfossils in documenting Devonian vertebrate history. In *Earth and Life,* Springer, Netherlands.
100. Burrow C., Turner, S., & Wang, S. T. (2000). Devonian microvertebrates from Longmenshan, China: taxonomic assesssment. *Courier-Forshungsintitut Senckenberg*, *223*, 391-451.
101. Burrow C. J., Turner S. & Young G. C. (2010) Middle Palaeozoic microvertebrate assemblages and biogeography of East Gondwana (Australasia, Antarctica). *Palaeoworld* **19**, 37-54.
102. Burrow C. J., Vergoossen J. M., Turner S., Uyeno T. T., & Thorsteinsson R. (1999) Microvertebrate assemblages from the Upper Silurian of Cornwallis Island, Arctic Canada. *Canadian Journal of Earth Sciences* **36**, 349-361.
103. Burrow C. J. & Young G. C. (1999) An articulated teleostome fish from the Late Silurian (Ludlow) of Victoria, Australia. *Records of the Western Australian Museum* **57**, 1-14.
104. Burton T. E. (1973) Wall pressure fluctuations at smooth and rough surfaces under turbulent boundary layers with favorable and adverse pressure gradients (No. A/V-70208-9). Massachusetts Institute of Technology, Cambridge Acoustics and Vibration Lab.
105. Bushnell D. M. & Moore K. J. (1991) Drag reduction in nature. *Annual Review of Fluid Mechanics* **23**, 65-79.
106. Butler P. M. (1995) Ontogenetic aspects of dental evolution. *International Journal of Developmental Biology* 39, 25.
107. Bystrow A. P. (1957) The microstructure of dermal bones in arthrodires. *Acta Zoologica* **38**, 239-275.
108. Caldwell M. W. & Wilson M. V. (1995) Comparison of the body formand squamation of "fork-tailed" agnathans with that of conventional thelodonts. *Géobios* **28**, 23-29.
109. Caldwell M. W. & Sasso C. D. (2004) Soft-tissue preservation in a 95 million year old marine lizard: form, function, and aquatic adaptation. *Journal of Vertebrate Paleontology* **24**, 980-985.
110. Carey F. G., Kanwisher J. W., Brazie O., Gabrielson G., Casey J. G. & Pratt Jr H. L. (1982)

Temperature and activities of a white shark, *Carcharodon carcharias*. *Copeia* **1982**, 254-260.

111. Carey F. G., & Clark E. (1995) Depth telemetry from the sixgill shark, *Hexanchus griseus*, at Bermuda. *Environmental Biology of Fishes* **42**, 7-14.
112. Carlson R. L. & Laude G. V. (2011) Escaping the flow: boundary layer use by the darter *Etheostoma tetrazonum* (Percidae) during benthic station holding. *Journal of Experimental Biology* **214**, 1181-1193.
113. Carlson J. K., Palmer C. L., & Parsons G. R. (1999) Oxygen consumption rate and swimming efficiency of the blacknose shark, *Carcharhinus acronotus*. *Copeia* **1999**, 34-39.
114. Carman M. L., Estes T. G., Feinberg A. W., Schumacher J. F., Wilkerson W., Wilson L. H. & Brennan A. B. (2006) Engineered antifouling microtopographies–correlating wettability with cell attachment. *Biofouling* **22**, 11-21.
115. Carnevale G. & Santini F. (2006) † *Archaeotetraodon cerrinaferoni*, sp. nov. (Teleostei: Tetraodontidae), from the Miocene (Messinian) of Chelif Basin, Algeria. *Journal of Vertebrate Paleontology* **26**, 815-821.
116. Carpenter P. W., Davies C. & Lucey A. D. (2000) Hydrodynamics and compliant walls: Does the dolphin have a secret. *Current Science* **79**, 758-765.
117. Carr R. (1995) Placoderm diversity and evolution. *Bulletin du Muséum national d'histoire naturelle. Section C, Sciences de la terre, paléontologie, géologie, minéralogie* **17**, 85-125.
118. Carrier J. C., Musick J. A., & Heithaus M. R. eds (2012) Biology of sharks and their relatives. CRC press.
119. Carroll R. L. (1985) Evolutionary constraints in aquatic diapsid reptiles. *Special Papers in Palaeontology* **33**, 145-155.
120. Carter J. T. (1919) On the occurrence of denticles on the snout of *Xiphias gladius*. In Proceedings of the Zoological Society of London (Vol. 89, No. 3-4, pp. 321-326). Blackwell Publishing Ltd.
121. Castro J. I. (1993) The shark nursery of Bulls Bay, South Carolina, with a review of the shark nurseries of the southeastern coast of the United States. In The reproduction and development of sharks, skates, rays and ratfishes (pp. 37-48). Springer Netherlands.
122. Castro J. I. (2011) *The Sharks of North America*. Oxford University Press.
123. Chamberlain Jr J. A. & Westermann G. E. (1976) Hydrodynamic properties of cephalopod shell ornament. *Paleobiology* **1976**, 316-331.
124. Chan M. D. (2001) Fish ecomorphology: predicting habitat preferences of stream fishes from their body shape (Doctoral dissertation, Virginia Polytechnic Institute and State University).
125. Chen D. (2010) Squamation in *Andreolopis* from the late Silurian of Sweden. A degree

project in Biology, Master of Science, Biology Education Center, Uppsala University and Department of Organismal Biology, 31 pp.

126. Chen H., Zhang X., Zhang D., Pan J. & Hagiwara, I. (2013) Large-scale equal-proportional amplification bio-replication of shark skin Based on solvent-swelling PDMS. *Journal of Applied Polymer Science* **130**, 2383-2389.
127. Chernova O. F. & Vorob'eva E. I. (2012) Polymorphism of the surface sculpture of placoid scales of sharks (Selachomorpha, Elasmobranchii). *Doklady Biological Sciences* **446**, 316-319.
128. Cheung P. J. & Ruggieri G. D. (1983) *Dermophthirius nigrellii* n. sp. (Monogenea: Microbothriidae), an ectoparasite from the skin of the lemon shark, *Negaprion brevirostris*. *Transactions of the American Microscopical Society* **1983**, 129-134.
129. Choi H., Moin P. & Kim J. (1994) Active turbulence control for drag reduction in wall-bounded flows. *Journal of Fluid Mechanics* **262**, 75-110.
130. Choi H., Park H., Sagong W. & Lee S. (2012) Biomimetic flow control based on morphological features of living creatures. *Physics of Fluids* **24**, 121302.
131. Choi K.-S., Yang X., Clayton B. R., Glover E. J., Atlar M., Semenov B. N. & Kuli M. (1997) Turbulent drag reduction using compliant surfaces. *Proceedings of the Royal Society A: Mathematical, Physical & Engineering Sciences* **453**, 2229-2240.
132. Cigala-Fulgosi F. & Gandolfi G. (1983) Re-description of the external morphology of *Somniosus rostratus* (Risso, 1826), with special reference to its squamation and cutaneus sensory organs, and aspects of their functional morphology (Pisces Selachii Squalidae). *Monitore Zoologico Italiano (N.S.)* **17**, 27-70.
133. Clark R. B. (1964) Dynamics in Metazoan Evolution. Oxford University Press, Oxford.
134. Cloudsley-Thompson J. L. (2005) Plesiosaurs and Ichthyosaurs. *Ecology and Behaviour of Mesozoic Reptiles*, 45-60.
135. Coates M. I. (1999) Endocranial preservation of a Carboniferous actinopterygian from Lancashire, UK, and the interrelationships of primitive actinopterygians. *Philosophical Transactions of the Royal Society of London. Series B: Biological Sciences* **354**, 435-462.
136. Coates M. I., & Sequeira S. E. K. (2001) A new stethacanthid chondrichthyan from the Lower Carboniferous of Bearsden, Scotland. *Journal of Vertebrate Paleontology* **21**, 438-459.
137. Coates M. I. (2003) The evolution of paired fins. *Theory in Biosciences* **122**, 266-287.
138. Cochran-Biederman J. L., & Winemiller K. O. (2010) Relationships among habitat, ecomorphology and diets of cichlids in the Bladen River, Belize. *Environmental Biology of Fishes* **88**, 143-152.
139. Cote S., Carroll R., Cloutier R., & Bar-Sagi L. (2002) Vertebral development in the Devonian sarcopterygian fish *Eusthenopteron foordi* and the polarity of vertebral evolution in non-

amniote tetrapods. *Journal of Vertebrate Paleontology* **22**, 487-502.

140. Cressey R. & Boxshall G. (1989) *Kabatarina pattersoni*, a fossil parasitic copepod (Dichelesthiidae) from a Lower Cretaceous fish. *Micropaleontology* **35**, 150-167.
141. Criswell K. E., Coates, M. I. & LaBarbera M. (2013) Drag forces and wake production in the spine brush complex of stethacanthid sharks. Poster presentation at the annual Society of Vertebrate Paleontology meeting in Los Angeles, California.
142. Crooks N., Babey L., Haddon W. J., Love A. C. & Warin C. P. (2013) Sexual Dimorphisms in the dermal denticles of the lesser-spotted catshark, *Scyliorhinus canicula* (Linnaeus, 1758). *PLoS ONE* **8***,* e76887.
143. Cruickshank A. R. I. & Skews B. W. (1980) The functional significance of nectridean tabular horns (Amphibia: Lepospondyli). *Proceedings of the Royal Society of London. Series B. Biological Sciences* **209**, 513-537.
144. Daget J., Gayet M., Meunier F. J. & Sire J-Y. (2001) Major discoveries on the dermal skeleton of fossil and recent polypteriforms: a review. *Fish and Fisheries* **2**, 113–124.
145. Dahl T. W., Hammarlund E. U., Anbar A. D., Bond D. P., Gill B. C., Gordon G. W. & Canfield D. E. (2010) Devonian rise in atmospheric oxygen correlated to the radiations of terrestrial plants and large predatory fish. *Proceedings of the National Academy of Sciences* **107**, 17911-17915.
146. Daniel T. L. (1981) Fish mucus – in situ measurements of polymer drag reduction. *Biological Bulletin* **160**, 376-382.
147. Davidson R. G. & Trewin N. H. (2005) Unusual preservation of the internal organs of acanthodian and actinopterygian fish in the Middle Devonian of Scotland. *Scottish Journal of Geology* **41**, 129-134.
148. Davies B. E. (2009) An experimental morphological investigation into the hydrodynamics and locomotion of the Palaeozoic jawless vertebrates *Poraspis*, *Errivaspis* and *Ateleaspis* (Doctoral dissertation, University of Leicester).
149. Dean B. (1907) Notes on acanthodian sharks. *American Journal of Anatomy* **7**, 209-226.
150. Dean B. & Bhushan B. (2010) Shark-skin surfaces for fluid-drag reduction in turbulent flow: a review. *Philosophical Transactions of the Royal Society A: Mathematical, Physical & Engineering Sciences* **368**, 4775-4806.
151. Dean B. D. (2011) The effect of shark skin inspired riblet geometries on drag in rectangular duct flow (Doctoral dissertation, The Ohio State University).
152. DeBlois M. C. (2013) Quantitative reconstruction and two-dimensional, steady flow hydrodynamics of the plesiosaur flipper. *Theses, Dissertations and Capstones.* 501.
153. Deliagina T. (1997) Vestibular compensation in lampreys: impairment and recovery of equilibrium control during locomotion. *Journal of Experimental Biology* **200**, 1459-1471.

154. Denison R. (1978) Placodermi, Handbook of Palaeoichthyology. Ed. Schultze H. P. *Gustav Fischer Verlag*, Stuttgart, NY.
155. Denison R. (1979) Acanthodii, Handbook of Palaeoichthyology. Ed. Schultze H. P., Volume 5. *Gustav Fischer Verlag*, Stuttgart, 62 p.
156. Dennis K. & Miles R. S. (1979) Eubrachythoracid arthrodires with tubular rostral plates from Gogo, Western Australia. *Zoological Journal of the Linnean Society* **67**, 297-328.
157. DeWindt J. T. (1974) Acanthodian scales from the Bloomsburg Formation (?Middle and Upper Silurian) of central Pennsylvania. *Journal of Paleontology* **48**, 594-595.
158. Deynat P. P. (1998) Le revêtement cutané des raies (Chondrichthyes, Elasmobranchii, Batoidea). II. Morphologie et arrangement des tubercules cutanés. *Annales des Sciences Naturelles-Zoologie et Biologie Animale* **19**, 155-172.
159. Doligalski T. L., Smith C. R. & Walker J. D. A. (1994) Vortex interactions with walls. *Annual Review of Fluid Mechanics* **26**, 573-616.
160. Domenici P. (Ed.)(2010) Fish locomotion: an eco-ethological perspective. *CRC Press.*
161. Donley J. M., Sepulveda C. A., Konstantinidis P., Gemballa S. & Shadwick R. E. (2004) Convergent evolution in mechanical design of lamnid sharks and tunas. *Nature* **429**, 61–65.
162. Donoghue P. C. (1998) Growth and patterning in the conodont skeleton. *Philosophical Transactions of the Royal Society of London. Series B: Biological Science* **353**, 633-666.
163. Donoghue P. C. (2002) Evolution of development of the vertebrate dermal and oral skeletons: unravelling concepts, regulatory theories, and homologies. *Paleobiology* **2002**, 474-507.
164. Donoghue P. C., Forey P. L. & Aldridge R. J. (2000) Conodont affinity and chordate phylogeny. *Biological Reviews of the Cambridge Philosophical Society* **75**, 191-251.
165. Donoghue P. C. & Purnell M. A. (1999) Growth, function, and the conodont fossil record. *Geology* **27**, 251-254.
166. Donoghue P. C. & Purnel M. A. (2005) Genome duplication, extinction and vertebrate evolution. *Trends in Ecology & Evolution* **20**, 312-319.
167. Donoghue P. C. & Smith M. P. (2001) The anatomy of *Turinia pagei* (Powrie), and the phylogenetic status of the Thelodonti. *Earth and Environmental Science Transactions of the Royal Society of Edinburgh* **92**, 15-37.
168. Downs J. P. & Donoghue P. C. (2009) Skeletal histology of *Bothriolepis canadensis* (Placodermi, Antiarchi) and evolution of the skeleton at the origin of jawed vertebrates. *Journal of Morphology* **270**, 1364-1380.
169. Drucker E. G & Lauder G. V. (2000) A hydrodynamic analysis of fish swimming speed: wake structure and locomotor force in slow and fast labriform swimmers. *Journal of Experimental Biology* **203**, 2379-2393.

170. Drucker E. G & Lauder G. V. (2001) Locomotor function of the dorsal fin in teleost fishes: experimental analysis of wake forces in sunfish. *Journal of Experimental Biology* **204**, 2943-2958.
171. Drucker E. G. & Lauder G. V. (2002) Experimental hydrodynamics of fish locomotion: functional insights from wake visualization. *Integrative and Comparative Biology* **42**, 243-257.
172. Drucker E. G. & Lauder G. V. (2002) Wake dynamics and locomotor function in fishes: interpreting evolutionary patterns in pectoral fin design. *Integrative and Comparative Biology* **42**, 997-1008.
173. Donley J. M., Sepulveda C. A., Konstantinidis P., Gemballa S. & Shadwick R. E. (2004) Convergent evolution in mechanical design of lamnid sharks and tunas. *Nature* **429**, 61-65.
174. Donovan D. A., Bingham B. L., From M., Fleisch A. F. & Loomis E. S. (2003) Effects of barnacle encrustation on the swimming behaviour, energetics, morphometry and drag of the scallop *Chlamys hastata*. *Journal of the Marine Biological Association of the United Kingdom* **83**, 813–819.
175. Dupret V., Sanchez S., Goujet D., Tafforeau P., & Ahlberg P. E. (2014) A primitive placoderm sheds light on the origin of the jawed vertebrate face. *Nature* **507**, 500-503.
176. Ebert D. A., Fowler S. & Compagno L. (2013) Sharks of the world: a fully illustrated guide. *Wild Nature Press*, Plymouth, United Kingdom.
177. Ehrlich H. (2015) Fish Scales as mineral-based composites. In *Biological Materials of Marine Origin,* Springer Netherlands.
178. Elliott D. K. (2013) A new cyathaspid (Agnatha, Heterostraci) with an articulated oral cover from the Late Silurian of the Canadian Arctic. *Journal of Vertebrate Paleontology* **33**, 29-34.
179. Elliott D. K. & Loeffler E. J. (1989) A new agnathan from the Lower Devonian of Arctic Canada, and a review of the tessellated heterostracans. *Palaeontology* **32**, 883-891.
180. Elliott D. K. & Petriello M. A. (2011) New poraspids (Agnatha, Heterostraci) from the Early Devonian of the western United States. *Journal of Vertebrate Paleontology* **31**, 518–530.
181. Férron H., Pla C., Martinez-Perez C., Escudero-Mozo M. J. & Botella H. (2014) Morphometric discriminant analysis of isolated chondrichthyan scales for palaeoecological inferences: the Middle Triassic of the Iberian Chain (Spain) as a case of study. *Journal of Iberian Geology* **40**, 87-97.
182. Ferry L. A. & Lauder G. V. (1996) Heterocercal tail function in leopard sharks: a three-dimensional kinematic analysis of two models. *Journal of Experimental Biology* **199**, 2253–2268.
183. Fierstine H. L. & Voigt N. L. (1996) Use of rostral characters for identifying adult billfishes (Teleostei: Perciformes: Istiophoridae and Xiphiidae). *Copeia* **1996**, 148-161.

184. Fischer-Rousseau L., Chu K. P. & Cloutier R. (2010) Developmental plasticity in fish exposed to a water velocity gradient: a complex response. *Journal of Experimental Zoology Part B: Molecular and Developmental Evolution* **314**, 67-85.
185. Fish F. E. (1990) Wing design and scaling of flying fish with regard to flight performance. *Journal of the Zoological Society of London* **221**, 391-403.
186. Fish F. E. (1993) Influence of hydrodynamic design and propulsive mode on mammalian swimming energetics. *Australian Journal of Zoology* **42**, 79-101.
187. Fish F. E. (1994) Energy conservation by formation swimming: metabolic evidence from ducklings. In Maddock L., Bone Q. & Rayner J. M. V. (eds.) *Mechanics and physiology of animal swimming*, Cambridge University Press, Cambridge
188. Fish F. E. (1995) Kinematics of ducklings swimming in formation: Energetic consequences of position. Journal of Experimental Zoology **272**, 1-11.
189. Fish F. E. (1998) Imaginative solutions by marine organisms for drag reduction. *Proceedings of the International Symposium on Seawater Drag Reduction*, 443-450.
190. Fish F. E. & Battle J. M. (1995) Hydrodynamic design of the humpback whale flipper. *Journal of Morphology* **225**, 51-60.
191. Fish F. E., Goetz K. T., Rugh D. J. & Brattström, L. V. (2013) Hydrodynamic patterns associated with echelon formation swimming by feeding bowhead whales (*Balaena mysticetus*). *Marine Mammal Science* **29**, 498-507.
192. Fish F. E. & Hui C. A. (1991) Dolphin swimming–a review. *Mammal Review* **21**, 181–195.
193. Fish F. E. & Shannahan L. D. (2000) The role of the pectoral fins in body trim of sharks. *Journal of Fish Biology* **56**, 1062-1073.
194. Fish F. E. & Lauder G. V. (2006) Passive and active flow control by swimming fishes and mammals. *Annual Review of Fluid Mechanics* **38**, 193-224.
195. Flammang B. E., Lauder G. V., Troolin D. R. & Strand T. (2011) Volumetric imaging of shark tail hydrodynamics reveals a three-dimensional dual-ring vortex wake structure. *Proceedings of the Royal Society B: Biological Sciences*, 20110489.
196. Fletcher T. M., Janis C. M. & Rayfield E. J. (2010) Finite element analysis of ungulate jaws: can mode of digestive physiology be determined. *Palaeontologia Electronica* **13**, 1-15.
197. Fortey R. A. (1985) Pelagic trilobites as an example of deducing the life habits of extinct arthropods. *Transactions of the Royal Society of Edinburgh: Earth Sciences* **76**, 219-230.
198. Francis M. P. & Duffy C. (2005) Length at maturity in three pelagic sharks (*Lamna nasus, Isurus oxyrinchus*, and *Prionace glauca*) from New Zealand. *Fishery Bulletin* **103**, 489-500.
199. Friedman M. (2008) The evolutionary origin of flatfish asymmetry. *Nature* **454**, 209-212.
200. Friedman M. (2009) Ecomorphological selectivity among marine teleost fishes during the end-Cretaceous extinction. *Proceedings of the National Academy of Sciences* **106**, 5218-

5223.

201. Friedman M. (2010) Explosive morphological diversification of spiny-finned teleost fishes in the aftermath of the end-Cretaceous extinction. *Proceedings of the Royal Society B* **277**, 1675-1683.
202. Friedman M. & Blom H. (2006) A new actinopterygian from the Famennian of East Greenland and the interrelationships of Devonian ray-finned fishes. *Journal of Paleontology* **80**, 1186-1204.
203. Friedman M. & Brazeau M. D. (2010) A reappraisal of the origin and basal radiation of the Osteichthyes. *Journal of Vertebrate Paleontology* **30**, 36-56.
204. Friedman M. & Sallan L. C. (2012) Five hundred million years of extinction and recovery: a phanerozoic survey of large-scale diversity patterns in fishes. *Palaeontology* **55**, 707-742.
205. Froese R. & Pauly D. (2011-2015) *Fishbase*. World Wide Web Electronic Publication. www.Fishbase.Org, (accessed 11/2011 - 08/2015).
206. Gabbott S. E., Aldridge R. J. & Theron J. N. (1995) A giant conodont with preserved muscle-tissue from the Upper Ordovician of South Africa. *Nature* **374**, 800-803.
207. Gad-el-Hak M. (1996) Compliant coatings: a decade of progress. *Applied Mechanics Reviews* **49**, S147-S157.
208. Gagnier P. Y. (1993) *Sacabambaspis janvieri*. *Vertébré ordovicien de Bolivie* **2**, 119-166.
209. Gagnier P. Y. & Wilson M. V. (1996) Early Devonian acanthodians from northern Canada. *Palaeontology* **39**, 241-258.
210. Gai Z., Donoghue P. C., Zhu M., Janvier P. & Stampanoni M. (2011) Fossil jawless fish from China foreshadows early jawed vertebrate anatomy. *Nature* **476**, 324-327.
211. Gai Z-K., Zhu M., Jia L-T. & Zhao W-J. (2015) A streamlined jawless fish (Galeaspida) from the Lower Devonian of Yunnan, China and its taxonomic and paleoecological implications. *PalAsiatica* **53**, 93-109.
212. Ganguly D. N. & Mookerje S. (1947) On the structure and development of ctenoid scales in certain Indian fishes. *Proceedings of the National Institute of Science India* **13**, 331-337.
213. García-Mayoral R. & Jiménez J. (2011) Drag reduction by riblets. *Philosophical Transactions of the Royal Society A* **369**, 1412-1427.
214. Gazzola M., Argentina M. & Mahadevan L. (2014) Scaling macroscopic aquatic locomotion. *Nature Physics* **10**, 758-761.
215. Gemballa S. & Bartsch P. (2002) Architecture of the integument in lower teleostomes: functional morphology and evolutionary implications. *Journal of Morphology* **253**, 290–309.
216. Ghanadi F., Arjomandi M., Zander A. C. & Cazzolato B. S. (2012) A review of skin friction drag reduction within the turbulent boundary layer. In Proceedings: the 7th Australasian Congress on Applied Mechanics (ACAM 7), 9-12 December 2012, the University of Adelaide,

North Terrace Campus/National Committee on Applied Mechanics of Engineers Australia (p. 817). Engineers Australia.

217. Goldman K. J. & Anderson S. D. (1999 Space utilization and swimming depth of white sharks, *Carcharodon carcharias*, at the South Farallon Islands, central California. *Environmental Biology of Fishes* **56**, 351-364.
218. Graham J. B., DeWar H., Lai N. C., Lowell W. R. & Arce S. M. (1990) Aspects of shark swimming performance determined using a large water tunnel. *Journal of Experimental Biology* **151**, 175-192.
219. GRAHAM, J. B., LOWELL, W. R., RUBINOFF, I., & MOTTA, J. (1987). Surface and subsurface swimming of the sea snake Pelamis platurus. Journal of experimental biology, 127(1), 27-44.
220. Grande, L., Jin, F., Yabumoto, Y. & Bemis, W. E. 2002 *Protopsephurus liui*, a well-preserved primitive paddlefish (Acipenseriformes: Polyodontidae) from the Lower Cretaceous of China. *Journal of Vertebrate Paleontology* 22, 209-237. (doi:10.1671/0272-4634(2002)022[0209:plawpp]2.0.co;2)
221. Gray J. 1936. Studies in animal locomotion VI. The propulsive powers of the dolphin. J. Exp. Biol. 13:192–99
222. Greeniaus, J. W. & Wilson, M. V. H. 2003 Fossil juvenile cyathaspididae (Heterostraci) reveal rapid cyclomorial development of the dermal skeleton. *Journal of Vertebrate Paleontology* 23, 483-487. (doi:10.1671/0272-4634(2003)023[0483:FJCHRR]2.0.CO;2)
223. Grove A. J. & Newell G. E. (1936) A mechanical investigation in to the effectual action of the caudal fin of some aquatic chordates. *Annual Magazine of Natural History* **17**, 280-290.
224. Grover C.A. (1974) Juvenile denticles of the swell shark *Cephaloscylliym ventriosum*: function in hatching. *Canadian Journal of Zoology* **52**, 359-363.
225. Gunn J. S., Stevens J. D., Davis T. L. O., & Norman B. M. (1999) Observations on the short-term movements and behaviour of whale sharks (*Rhincodon typus*) at Ningaloo Reef, Western Australia. Marine Biology **135**, 553-559.
226. Hairapetian V., Blom H., & Miller C. G. (2008) Silurian thelodonts from the Niur Formation, central Iran. *Acta Palaeontologica Polonica* **53**, 85-95.
227. Hairapetian V., Valiukevicius J. & Burrow C. J. (2006) Early Frasnian acanthodians from central Iran. *Acta Palaeontologica Polonica* **51**, 499.
228. Halstead L. B. (1973) The heterostracan fishes. *Biological Reviews* **48**, 279–332.
229. Hammer Ø., Harper D.A.T. & Ryan P.D. (2001) PAST: Paleontological statistics software package for education and data analysis. *Palaeontologia Electronica* **4**, 9.
230. Hanke G. F. (2002) *Paucicanthus vanelsti* gen. et sp. nov., an Early Devonian (Lochkovian) acanthodian that lacks paired fin-spines. *Canadian Journal of Earth Sciences* **39**, 1071-1083.

231. Hanke G. F. (2008) *Promesacanthus eppleri* n. gen., n. sp., a mesacanthid (Acanthodii, Acanthodiformes) from the Lower Devonian of northern Canada. *Geodiversitas* **30**, 287-302.
232. Hanke G. F. & Davis S. P. (2012) A re-examination of *Lupopsyrus pygmaeus* Bernacsek & Dineley, 1977 (Pisces, Acanthodii). *Geodiversitas* **34**, 469-487.
233. Hanke G. F. & Wilson M. V. (2006) Anatomy of the Early Devonian acanthodian *Brochoadmones milesi* based on nearly complete body fossils, with comments on the evolution and development of paired fins. *Journal of Vertebrate Paleontology* **26**, 526-537.
234. Hanke G. F. & Davis S. P. (2008) Redescription of the acanthodian *Gladiobranchus probaton* Bernacsek & Dineley, 1977, and comments on diplacanthid relationships. *Geodiversitas* **30**, 303-330.
235. Hanke G. F. & Davis S. P. (2012) A re-examination of *Lupopsyrus pygmaeus* Bernacsek & Dineley, 1977 (Pisces, Acanthodii). *Geodiversitas* **34**, 469-487.
236. Harris J. E. (1936) The role of the fins in the equilibrium of the swimming fish. I. Wind tunnel tests in a model of *Mustelus canis*. *Journal of Experimental Biology* **13**, 474–493.
237. Hawthorn J. R., Wilson M. V. & Falkenberg A. B. (2008) Development of the dermoskeleton in *Superciliaspis gabrielsei* (Agnatha: Osteostraci). *Journal of Vertebrate Paleontology* **28**, 951-960.
238. Hebrank M. R. & Hebrank J. H. (1986) The mechanics of fish skin: lack of an “external tendon” role in two teleosts. *Biological Bulletin* **71**, 236-247.
239. Helfman G. S., Collette B. B., Facey D. E. & Bowen B. W. (2009) *The Diversity of Fishes: Biology, Evolution, and Ecology*. West Sussex: Blackwell Publishing.
240. Hopson J. A. (1974) The functional significance of the hypocercal tail and lateral fin fold of anaspid ostracoderms. *Fieldiana* **33**, 83-93.
241. Hove J. R., O'Bryan L. M., Gordon M. S., Webb P. W., & Weihs D. (2001) Boxfishes (Teleostei: Ostraciidae) as a model system for fishes swimming with many fins: kinematics. *Journal of Experimental Biology* **204**, 1459-1471.
242. Hoyt J. W. (1975) Hydrodynamic drag reduction due to fish slimes. *Swimming and Flying In Nature* **2**, 653–672.
243. Hui C. A. (1987) The porpoising of penguins: an energy conserving behavior for respiratory ventilation? *Canadian Journal of Zoology* **65**, 209-211.
244. Hui C. A. (1989) Surfacing behavior and ventilation in free-ranging dolphins. *Journal of Mammalogy* 70, 833-835.
245. Huish, M. T. & Benedict, C. (1977) Sonic tracking of dusky sharks in cape fear river, north-Carolina. *Journal of the Elisha Mitchell Scientific Society* **93**, 21-26.
246. Hurley I. A., Mueller R. L., Dunn K. A., Schmidt E. J., Friedman M., Ho R. K. & Coates M. I.

(2007). A new time-scale for ray-finned fish evolution. *Proceedings of the Royal Society B: Biological Sciences* **274**, 489-498.

247. Ibanez A. L., Cowx I. G. & O'HIGGINS P. (2009) Variation in elasmoid fish scale patterns is informative with regard to taxon and swimming mode. *Zoological Journal of the Linnean Society* **155**, 834-844.
248. Ikoma T., Kobayashi H., Tanaka J., Walsh D. & Mann S. (2003) Microstructure, mechanical, and biomimetic properties of fish scales from *Pagrus major*. *Journal of Structural Biology* **142**, 327-333.
249. Janvier P. (1987) The paired fins of Anaspids: one more hypothesis about their function. *Journal of Paleontology* **61**, 850-853.
250. Janvier P. (1996) Early Vertebrates. *Oxford Monographs on Geology and Geophysics*. New York: Oxford University Press.
251. Janvier P. (2003) Vertebrate characters and the Cambrian vertebrates. *Comptes Rendus Palevol* **2**, 523-531.
252. Janvier P. (2015) Facts and fancies about early fossil chordates and vertebrates. *Nature* **520**, 483-489.
253. Jetz W. & Freckleton R. P. (2015) Towards a general framework for predicting threat status of data-deficient species from phylogenetic, spatial and environmental information. *Philosophical Transactions of the Royal Society B: Biological Sciences* **370**, 20140015.
254. Johnson R., Bester M. N., Dudley S. F., Oosthuizen W. H., Meÿer M., Hancke L., & Gennari E. (2009) Coastal swimming patterns of white sharks (*Carcharodon carcharias*) at Mossel Bay, South Africa. *Environmental Biology of Fishes* **85**, 189-200.
255. Jones F. H. (1973) Tail beat frequency, amplitude, and swimming speed of a shark tracked by sector scanning sonar. *Journal du Conseil* **35**, 95-97.
256. Kajiura S. M., Forni J. B. & Summers A. P. (2003) Maneuvering in juvenile carcharhinid and sphyrnid sharks: the role of the hammerhead shark cephalofoil. *Zoology* **106**, 19-28.
257. Kane E. A. & Higham T. E. (2012) Life in the flow lane: differences in pectoral fin morphology suggest transitions in station-holding demand across species of marine sculpin. *Zoology* **115**, 223-232.
258. Karatajūtė-Talimaa V. N. (1995) The Mongolepidida: scale structure and systematic position. *Geobios* **19**, 35–37.
259. Karatajūtė-Talimaa V. N. (1997) Chondrichthyan scales from Lochkovian (Lower Devonian) of Podolia (Ukraine). *Geologija* **22**, 5-17. (In Märss et al., 2007)
260. Karatajute-Talimaa V. N. (1998) Determination Methods for the Exoskeletal Remains of Early Vertebrates. *Fossil Record* **1**: 21–51.
261. Karatajūtė-Talimaa V. N. (2002) Lower Devonian (Lochkovian) thelodonts from October

Revolution Island (Severnaya Zemlya Archipelago, Russia). *Geodiversitas* **24**, 791-804.

262. Karatajute-Talimaa V. N. & Smith M. M. (2002) Early acanthodians from the Lower Silurian of Asia. *Earth and Environmental Science Transactions of the Royal Society of Edinburgh* **93**, 277-299.
263. Kardong K. (2009) *Vertebrates: Comparative Anatomy, Function, Evolution*. New York: McGraw-Hill.
264. Keating J. N., Sansom R. S. & Purnell M. A. (2012) A new osteostracan fauna from the Devonian of the Welsh Borderlands and observations on the taxonomy and growth of Osteostraci. *Journal of Vertebrate Paleontology* **32**, 1002-1017.
265. Keating J. N., Marquart C. L. & Donoghue P. C. J. (2015) Histology of the heterostracan dermal skeleton: Insight into the origin of the vertebrate mineralised skeleton. *Journal of Morphology* **276**, 657–680.
266. Kermack K. A. (1943) The functional significance of the hypocercal tail in *Pteraspis rostrata*. *Journal of Experimental Biology* **20**, 23-27.
267. Kerr T. (1952) The scales of primitive living actinopterygians. *Proceedings of the Zoological Society of London* **122**, 55–78.
268. Kim S. H., Shimada K. & Rigsby C. K. (2013) Anatomy and evolution of heterocercal tail in lamniform sharks. *The Anatomical Record* **296**, 433-442.
269. Kimmel C. B. (1993) Patterning the brain of the zebrafish embryo. *Annual Review of Neuroscience* **16**, 707–732.
270. Kirschner C. M. & Brennan A. B. (2012) Bio-inspired antifouling strategies. *Annual Review of Materials Research* **42**, 211-229.
271. Klimley A. P., Beavers S. C., Curtis T. H. & Jorgensen S. J. (2002) Movements and swimming behavior of three species of sharks in La Jolla Canyon, California. *Environmental Biology of Fishes* **63**, 117-135.
272. Klug C., Kröger B., Kiessling W., Mullins G. L., Servais T., Frỳda J., Korn D. & Turner S. (2010) The Devonian nekton revolution. *Lethaia* **43**, 465–477.
273. Knappertsbusch M. W., Binggeli D., Herzig A., Schmutz L., Stapfer S., Schneider C., Eisenecker J. & Widmer L. (2009) AMOR – A new system for automated imaging of microfossils for morphometric analyses*, Palaeontologia Electronica* **12**, 2.
274. Kocher T. D., Conroy J. A., McKaye K. R. & Stauffer J. R. (1993) Similar morphologies of cichlid fish in Lakes Tanganyika and Malawi are due to convergence. *Molecular Phylogenetics and Evolution* **2**, 158-165.
275. Koeltzsch K., Dinkelacker A. & Grundmann R. (2002) Flow over convergent and divergent wall riblets. *Experiments in Fluids* **33**, 346-350.
276. Kogan I., Rudert A., Licht M. & Brandt S. (2011) Hydrodynamic properties of the Triassic fish

Saurichthys compared to the extant fish *Belone belone* (Linnaeus, 1761). *Beiträge zur Paläontologie* **32**, 62.

277. Kong F. Y. & Schetz J. A. (1982) Turbulent boundary layer over porous surfaces with different surface geometries. *AIAA paper*, 82-0030.
278. Kottelat M., Britz R., Hui T. H., & Witt K. E. (2006) *Paedocypris*, a new genus of Southeast Asian cyprinid fish with a remarkable sexual dimorphism, comprises the world's smallest vertebrate. Proceedings of the Royal Society B: Biological Sciences, 273(1589), 895-899.
279. Kramer M. O. (1960) Boundary layer stabilization by distributed damping. *Journal of the American Society for Naval Engineers* **72**, 25–34.
280. Kramer M. O. (1961) The Dolphins' Secret. *Journal of the American Society for Naval Engineers* **73**, 103–108.
281. Kriwet J. & Benton M. J. (2004) Neoselachian (Chondrichthyes, Elasmobranchii) diversity across the Cretaceous–Tertiary boundary. *Palaeogeography, Palaeoclimatology, Palaeoecology* **214**, 181-194.
282. Kudryashov A. F. & Barsukov V. V. (1980) Hydrodynamic role of fish squamosal integument as an analog of the surfaces directly formed by the turbulent flow. Report 2: Hydrodynamic function of squamosal integument. *NASA STI/Recon Technical Report* **81**, 18320.
283. Landreneau E. & Schaefer S. (2010) Scales and Scale-like Structures. *Computer Graphics Forum* **29**, 1653–1660.
284. Lang A., Motta P., Habegger M. L., Hueter R. & Afroz F. (2011) Shark skin separation control mechanisms. *Marine Technology Society Journal* **45**, 208-215.
285. Lang A. W., Motta P., Hidalgo P. & Westcott M. (2008) Bristles shark skin: a microgeometry for boundary layer control? *Bioinspiration & Biomimetics* **3**, 046005.
286. Lang A. W., Bradshaw M. T., Smith J. A., Wheelus J. N., Motta P. J., Habegger M. L. & Hueter R. E. (2014) Movable shark scales act as a passive dynamic micro-roughness to control flow separation. *Bioinspiration & Biomimetics* **9**, 036017.
287. Lang T. G. (1966) Hydrodynamic analysis of cetacean performance. In *Whales, Dolphins and Porpoises*. Ed. KS Norris, Berkley, CA, University of California Press.
288. Lang T. G. & Daybell D. A. (1963) Porpoise performance tests in a seawater tank. *Naval Ordnance Test Station China Lake CA* **1963**, No. NOTS-TP-3063.
289. Langerhans R. B. & Reznick D. N. (2010) Ecology and evolution of swimming performance in fishes: predicting evolution with biomechanics. In *Fish locomotion: an eco-ethological perspective.* Eds. Domenici P. & Kapoor B.G.
290. Lauder G. V. (1989) Caudal fin locomotion in ray-finned fishes: historical and functional analyses. *American Zoologist* **29**, 85-102.
291. Lauder G. V. (2000) Function of the caudal fin during locomotion in fishes: kinematics, flow

visualization, and evolutionary patterns. *American Zoologist* **40**, 101-122.

292. Lauder G. V. (2010) Swimming hydrodynamics: ten questions and the technical approaches needed to resolve them. In *Animal Locomotion*. Springer Berlin Heidelberg.
293. Lauder G. V. & Drucker E. G. (2002) Forces, fishes, and fluids: hydrodynamic mechanisms of aquatic locomotion. *Physiology* **17**, 235-240.
294. Lauder G. V. & Drucker E. G. (2004) Morphology and experimental hydrodynamics of fish fin control surfaces. *IEEE Journal of Oceanic Engineering* **29**, 556-571.
295. Lauder G.V. & Liem K.F. (1983) The evolution and interrelationships of the actinopterygian fishes. *Bulletin of the Museum of Comparative Anatomy* **150**, 95–197.
296. Lee C. & Kim J. (2002) Control of the viscous sublayer for drag reduction. *Physics of Fluids* **14**, 2523-2529.
297. Lee C. Y. (Ed.)(2012). *Snake venoms* (Vol. 52). Springer Science & Business Media.
298. Lehtola K. A. (1983). Articulated Ordovician fish from Cañon City, Colorado. *Journal of Paleontology* **57**, 605-607.
299. Leis J. M. & Carson-Ewart B. M. (Eds)(2000). The larvae of Indo-Pacific coastal fishes: an identification guide to marine fish larvae (Vol. 2). Brill.
300. Le Rouzic A., ØSTBYE K., Klepaker T. O., Hansen T. F., Bernatchez L., Schluter D. & VØLLESTAD L. A. (2011) Strong and consistent natural selection associated with armour reduction in sticklebacks. *Molecular Ecology* **20**, 2483-2493.
301. Liao J. C. & Lauder G. V. (2000) Function of the heterocercal tail in white sturgeon: flow visualization during steady swimming and vertical manoeuvring. *Journal of Experimental Biology* **203**, 3585-3594.
302. Liao J. C. (2007) A review of fish swimming mechanics and behaviour in altered flows. *Philosophical Transactions of the Royal Society B: Biological Sciences* **362**, 1973-1993.
303. Lighthill M. J. (1969) Hydrodynamics of aquatic propulsion. *Annual Review of Fluid Mechanics* **1**, 413-446.
304. Li-mei T., Lu-quan R., Zhi-wu H. & Shi-cun Z (2005) Experiment about drag reduction of bionic non-smooth surface in low speed wind tunnel. *Journal of Bionics Engineering* **2**, 15-24
305. Lin J. C., Howard F.G. & Selby G. V. (1989) Turbulent flow separation control through passive techniques. *AIAA paper 89-0976*
306. Lin J. C. (2002) Review of research on low-profile vortex generators to control boundary-layer separation. *Progress in Aerospace Sciences* **38**, 389-420.
307. Lin Y. S., Wei C. T., Olevsky E. A. & Meyers M. A. (2011) Mechanical properties and the laminate structures of *Arapaima gigas* scales. *Journal of Mechanical Behaviour of Biomedical Materials* **4**, 1145-1156.

308. Lindgren J., Alwmark C., Caldwell M. W. & Fiorillo A. R. (2009) Skin of the Cretaceous mosasaur *Plotosaurus*: implications for aquatic adaptations in giant marine reptiles. *Biology letters* **5**, 528-531.
309. Lindgren J., Everhart M. J. & Caldwell M. W. (2011) Three-dimensionally preserved integument reveals hydrodynamic adaptations in the extinct marine lizard *Ectenosaurus* (Reptilia, Mosasauridae). *PloS One* **6**, e27343.
310. Lindgren J., Polcyn M. J. & Young B. A. (2011) Landlubbers to leviathans: evolution of swimming in mosasaurine mosasaurs. *Paleobiology* **37**, 445-469.
311. Lingham-Soliar T. (2005a) Caudal fin in the white shark, *Carcharodon carcharias* (Lamnidae): a dynamic propeller for fast, efficient swimming. *Journal of morphology* **264**, 233-252.
312. Lingham-Soliar T. (2005b) Dorsal fin in the white shark, *Carcharodon carcharias*: A dynamic stabilizer for fast swimming. *Journal of Morphology* **263**, 1-11.
313. Lingham-Soliar T & Plodowski G. (2007). Taphonomic evidence for high-speed adapted fins in thunniform ichthyosaurs. *Naturwissenschaften* **94**, 65-70.
314. Liston J. J., Newbrey M. G., Challands T. J., Adams C. E. (2013) Growth, age and size of the Jurassic pachycormid *Leedsichthys problematicus* (Osteichthyes: Actinopterygii). In: Arratia G, Schultze H-P, Wilson MVH, editors. Mesozoic Fishes 5 – global diversity and evolution. Munchen: Verlag Dr. F. Pfeil.
315. Litvinenko M. V., Chernorai V. G., Kozlov V. V., Grek G. R. & Lofdal L. L. (2002) Role of the streaky structures in a transition mechanism of the boundary layers and jets. Chalmers University of Technology Goeteborg (Sweden).
316. Long J. A. (1983) A new diplacanthoid acanthodian from the Late Devonian of Victoria. *Memoirs of the Association of Australasian Palaeontologists*, *1*, 51-65.
317. Long J. A. (2011) The Rise of Fishes: 500 Million Years of Evolution. Baltimore: The Johns Hopkins University Press.
318. Long J. A. & Trinajstic K. (2010) The Late Devonian Gogo Formation lägerstatte of Western Australia: exceptional early vertebrate preservation and diversity. *Annual Review of Earth and Planetary Sciences* **38**, 255-279.
319. Long J. A., Young G. C., Holland T., Senden T. J. & Fitzgerald E. M. (2006) An exceptional Devonian fish from Australia sheds light on tetrapod origins. *Nature* **444**, 199-202.
320. Long J. H., Hale M. E., McHenry M. J. & Westneat M. W. (1996) Functions of fish skin: flexural stiffness and steady swimming of longnose gar *Lepisosteus osseus*. *Journal of Experimental Biology* **199**, 2139-2151.
321. Long J. H. & Nipper K. S. (1996) The importance of body stiffness in undulatory propulsion. *American Zoologist* **36**, 678-694.
322. Lowe C. G., Holland K. N. & Wolcott T. G. (1998) A new acoustic tailbeat transmitter for

fishes. *Fisheries Research* **36**, 275-283.

323. Luchini P., Manzo F. & Pozzi A. (1991) Resistance of a grooved surface to parallel flow and cross-flow. *Journal of Fluid Mechanics* **228**, 87-109.
324. Lucifora L. O., García V. B., Menni R. C., Escalante A. H. & Hozbor N. M. (2009) Effects of body size, age and maturity stage on diet in a large shark: ecological and applied implications. *Ecological Research* **24**, 109-118.
325. Lukševics E., Lebedev O., Mark-Kurik E. & Karatajūtė-Talima V. (2009) The earliest evidence of host-parasite interactions in vertebrates. *Acta Zoologica* **90**, 335-343.
326. Lund R. (1990) Chondrichthyan life history styles as revealed by the 320 million years old Mississippian of Montana. *Environmental Biology of Fishes* **27**, 1-19.
327. Maia A. M., Wilga C. A. & Lauder G. V. (2012) Biomechanics of locomotion in sharks, rays, and chimaeras. *Biology of sharks and their relatives*, 2nd ed. Boca Raton, Florida: CRC Press.
328. Maia A. & Wilga C. A. (2013) Function of dorsal fins in bamboo shark during steady swimming. *Zoology* **116**, 224-231.
329. Mark-Kurik E. (1992) Functional aspects of the armour in the early vertebrates. In *Fossil fishes as living animals*, Academia 1, 107-116.
330. Mark-Kurik E. & Carls P. (2002) A long-snouted Late Eifelian arthrodire from Aragón, Spain. *Revista Espańola de Paleontología* **17**, 117-135.
331. Mark-Kurik E. & Botella H. (2009) On the tail of *Errivaspis* and the condition of the caudal fin in heterostracans. *Acta Zoologica* **90**, 44-51.
332. Märrs T. (1986) Squamation of the Thelodont Agnathan *Phlebolepis*. *Journal of Vertebrate Paleontology* **6**, 1-11.
333. Märss T. (1999) A new late silurian or early Devonian thelodont from the Boothia Peninsula, Arctic Canada. *Palaeontology* **42**, 1079-1099.
334. Märrs T. (2003) *Paralogania* from the Rootsiküla (Wenlock) and Paadla (Ludlow) stages of Estonia. *Proceedings of the Estonian Academy Of Sciences* **52**, 98-112.
335. Märss T. (2006a) Exoskeletal ultrasculpture of early vertebrates. *Journal of Vertebrate Paleontology* **26**, 235-252.
336. Märss T. (2006b) Thelodonts (Agnatha) from the basal beds of the Kuressaare Stage, Ludlow, Upper Silurian of Estonia. In *Proceedings of the Estonian Academy of Sciences, Geology* **55**, 43-66.
337. Märss T. (2011) A unique Late Silurian *Thelodus* squamation from Saaremaa (Estonia) and its ontogenetic development. *Estonian Journal of Earth Sciences* **60**, 137.
338. Märs T. & Karatajute-Talimaa V. (2002) Ordovician and Lower Silurian thelodonts from Severnaya Zemlya Archipelago (Russia). *Geodiversitas* **24**, 381-404.
339. Märss T. & Miller C. G. (2004) Thelodonts and distribution of associated conodonts from

the Llandovery – lowermost Lochkovian of the Welsh Borderland. *Palaeontology* **47**, 1211-1265.

340. Märrs T. & Ritchie A. (1998) Articultaed thelodonts (Agnatha) of Scotland. *Transactions of the Royal Society of Edinburgh: Earth Sciences* **88**, 143-195.
341. Märss T., Wilson M. V. & Thorsteinsson R. (2002) New thelodont (Agnatha) and possible chondrichthyan (Gnathostomata) taxa established in the Silurian and Lower Devonian of the Canadian Arctic Archipelago. In *Proceedings of the Estonian Academy of Sciences, Geology* **51**, 88-120.
342. Märss T., Wilson M. V. H. & Thorsteinsson R. (2006) Silurian and Lower Devonian thelodonts and putative chondrichthyans from the Canadian Arctic Archipelago. *Special Papers in Palaeontology* **75**, 1–140.
343. Märss T., Turner S. & Karatajūtė-Talimaa V. (2007) *Handbook of Palaeoichthyology: Agnatha II, Thelodonti.* Verlag Dr. Friedrich Pfeil, München.
344. Martin A. J., Vazquez-Prokopec G. M. & Page M. (2010) First known feeding trace of the Eocene bottom-dwelling fish *Notogoneus osculus* and its paleontological significance. *PloS One* **5**, e10420.
345. Massare J. A. (1988) Swimming capabilities of Mesozoic marine reptiles: implications for method of predation. *Paleobiology* **1988**, 187-205.
346. Massare J. A. (1994) Swimming capabilities of Mesozoic marine reptiles: a review. *Mechanics and Physiology of animal swimming*, 133-149.
347. Matoltsy A. G. & Richards K. S. (1986) *Biology of the Integument 2: Vertebrates*. Berlin: Springer-Verlag.
348. Maxwell E. E. & Wilson L. A. (2013) Regionalization of the axial skeleton in the 'ambush predator' guild - are there developmental rules underlying body shape evolution in ray-finned fishes? *BMC Evolutionary Biology* **13**, 265.
349. McGowan C. (1999) A practical guide to vertebrate mechanics. Cambridge University Press.
350. McHenry M. J. & Lauder G. V. (2006) Ontogeny of form and function: locomotor morphology and drag in zebrafish (*Danio rerio*). *Journal of Morphology* **267**, 1099-1109.
351. Mckenzie R. W., Motta P. J. & Rohr J. R. (2014) Comparative squamation of the lateral line canal pores in sharks. *Journal of Fish Biology* **84**, 1300–1311.
352. McKibben J. N. & Nelson D. R. (1986) Patterns of movement and grouping of gray reef sharks, *Carcharhinus amblyrhynchos*, at Enewetak, Marshall Islands. *Bulletin of Marine Science* **38**, 89-110.
353. Medved R. J. & Marshall J. A. (1983) Short-term movements of young sandbar sharks, *Carcharhinus plumbeus* (Pisces, Carcharhinidae). *Bulletin of Marine Science* **33**, 87-93.
354. Melchin M. J. & Douce K. M. (1996) Modelling flow patterns in conical dendroid graptolites.

Lethaia **29**, 39-46.

355. Metz J. R., Leeuwis R. H. J., Zethof J. & Flik G. (2014) Zebrafish (*Danio rerio*) in calcium-poor water mobilise calcium and phosphorus from scales. *Journal of Applied Ichthyology* **30**, 671–677.
356. Meyer W. & Seegers U. (2012) Basics of skin structure and function in elasmobranchs: a review. *Journal of Fish Biology* **80**, 1940-1967.
357. Miller J. (1975) Structure and function of trilobite terrace lines. *Fossils and Strata* **4**, 155-1 78.
358. Miklosovic D. S., Murray M. M., Howle L. E. & Fish F. E. (2004) Leading-edge tubercles delay stall on humpback whale (*Megaptera novaeangliae*) flippers. *Physics of Fluids* **16**, 39 -42.
359. Morris S. C. (1981) Parasites and the fossil record. *Parasitology* **82**, 489-509.
360. Morrissey L. B., Braddy S. J., Bennett J. P., Marriott S. B. & Tarrant P. R. (2004) Fish trails from the Lower Old Red Sandstone of Tredomen Quarry, Powys, southeast Wales. *Geological Journal* **39**, 337–358.
361. Motani R. (2005) Evolution of fish-shaped reptiles (Reptilia: Ichthyopterygia) in their physical environments and constraints. *Annual Review of Earth and Planetary Science* **33**, 395-420.
362. Motta P. J. (1977) Anatomy and functional morphology of dermal collagen fibers in sharks. *Copeia* **1977**, 454-464.
363. Motta P. J., Habegger M. L., Lang A., Hueter R. & Davis J. (2012) Scale morphology and flexibility in the shortfin mako *Isurus oxyrinchus* and the blacktip shark *Carcharhinus limbatus*. *Journal of Morphology* **273**, 1096–1110.
364. Motta P. J., Norton S. F. & Luczkovich J. J. (1995) Perspectives on the ecomorphology of bony fishes. *Environmental Biology of Fishes* **44**, 11-20.
365. Moy-Thomas J. A. & Miles R. S. (1971) Palaeozoic fishes. Saunders Company, Philadelphia.
366. Müller U., Heuvel B., Stamhuis E. & Videler J. (1997) Fish foot prints: morphology and energetics of the wake behind a continuously swimming mullet (*Chelon labrosus* Risso). *Journal of Experimental Biology* **200**, 2893-2906.
367. Müller U. K., Stamhuis E. J. & Videler J. J. (2000) Hydrodynamics of unsteady fish swimming and the effects of body size: comparing the flow fields of fish larvae and adults. *Journal of Experimental Biology* **203**, 193-206.
368. Müller U. K. & Videler J. J. (1996) Inertia as a 'safe harbour': do fish larvae increase length growth to escape viscous drag? *Reviews in Fish Biology and Fisheries* **6**, 353-360.
369. Murdock D. J., Rayfield E. J. & Donoghue P. C. (2014) Functional adaptation underpinned the evolutionary assembly of the earliest vertebrate skeleton. *Evolution & Development*, **16**, 354-361.

370. Nachtigall W. (2001) Some aspects of Reynolds number effects in animals. *Mathematical Methods in the Applied Sciences* **24**, 1401–1408.
371. Nadesan T., Mitsudharmadi H., Lee T. S., & Winoto S. H. (2014) Quasi-streamwise counter-rotating vortices generated by convergent riblets in flat plate boundary layer. *Journal of Visualization* **17**, 319-325.
372. Nagamatsu H. T., Orozco R. D. & Ling D. C. (1984) Porosity effect on supercritical airfoil drag reduction by shock wave/boundary layer control. AIAA paper 84-1682.
373. Nagamine H., Yamahata K., Hagiwara Y. & Matsubara R. (2004) Turbulence modification by compliant skin and strata-corneas desquamation of a swimming dolphin. *Journal of Turbulence* **5**, 1–25
374. Nakamura I., Watanabe Y. Y., Papastamatiou Y. P., Sato K. & Meyer C. G. (2011) Yo-yo vertical movements suggest a foraging strategy for tiger sharks Galeocerdo cuvier. *Marine Ecology Progress Series* **424**, 237-246.
375. Nakaya K. (1995) Hydrodynamic function of the head in the hammerhead sharks (Elasmobranchii: Sphyrnidae). *Copeia* **1995**, 330-336.
376. Natanson L. J., Mello J. J. & Campana S. E. (2002) Validated age and growth of the porbeagle shark, *Lamna nasus*, in the western North Atlantic Ocean. *Fishery Bulletin* **100**, 266-278.
377. Neat F. C. & Campbell N. (2013) Proliferation of elongate fishes in the deep sea. *Journal of Fish Biology* **83**, 1576-1591.
378. Nelson D. R., McKibben J. N., Strong Jr W. R., Lowe C. G., Sisneros J. A., Schroeder D. M. & Lavenberg R. J. (1997) An acoustic tracking of a megamouth shark, Megachasma pelagios: a crepuscular vertical migrator. *Environmental Biology of Fishes* **49**, 389-399.
379. Nelson J. S. (2006) Fishes of the World. John Wiley & Sons.
380. Newman M. J., Davidson R. G., Den Blaauwen J. L. & Burrow C. J. (2011) The early Devonian acanthodian *Euthacanthus gracilis* from the Midland Valley of Scotland. *Scottish Journal of Geology* **47**, 101-111.
381. Newman M. J., Davidson R. G., Blaauwen J. L. D. & Burrow C. J. (2012 The Early Devonian Acanthodian *Uraniacanthus curtus* (Powrie, 1870) n. comb. from the Midland Valley of Scotland. *Geodiversitas* **34**, 739-759.
382. Newman M. J. & Trewin N. H. (2001) A new jawless vertebrate from the Middle Devonian of Scotland. *Palaeontology* **44**, 43-51.
383. Noren S. R., Biedenbach G., Redfern J. V. & Edwards E. F. (2008) Hitching a ride: the formation locomotion strategy of dolphin calves. *Functional Ecology* **22**, 278-283.
384. Nugroho B., Hutchins N. & Monty J. P. (2013) Large-scale spanwise periodicity in a turbulent boundary layer induced by highly ordered and directional surface roughness. *International Journal of Heat and Fluid Flow* **41**, 90–102.

385. Oeffner J. & Lauder G. V. (2012) The hydrodynamic function of shark skin and two biomimetic applications. *Journal of Experimental Biology* **215**, 785–795.
386. Onozato H. & Watabe N. (1979) Studies on fish scale formation and resorption. *Cell and tissue research* **201**, 409-422.
387. Orme D., Freckleton R., Thomas G., Petzoldt T., Fritz S., Isaac N. & Pearse W. (2013) Caper: comparative analyses of phylogenetics and evolution in R. R package version 0.5.2; http://CRAN.R-project.org/package=caper
388. Reynolds O. (1883) An experimental investigation of the circumstances which determine whether the motion of water shall be direct or sinuous, and of the law of resistance in parallel channels. *Philosophical Transactions of the Royal Society* **174**, 935–982.
389. Östlund-Nilsson S., Curtis L., Nilsson G. E. & Grutter A. S. (2005) Parasitic isopod *Anilocra apogonae*, a drag for the cardinal fish *Cheilodipterus quinquelineatus*. *Marine Ecology Progress Series* **287**, 209–216.
390. Otto M. & Laurin M. (2001) Microanatomy of the dermal skeleton of *Balticaspis latvica* (Osteostraci, Middle Devonian). *Journal of Vertebrate Paleontology* **21**, 186-189.
391. Pabst D. A. (2000) To bend a dolphin: convergence of force transmission designs in cetaceans and scombrid fishes. *American Zoologist* **40**, 146-155.
392. Page L. M. (1976) The modified midventral scales of Percina (Osteichthyes; Percidae). Journal of Morphology **148**, 255–264.
393. Palmer C. & Young M. T. (2015) Surface drag reduction and flow separation control in pelagic vertebrates, with implications for interpreting scale morphologies in fossil taxa. *Royal Society Open Science* **2**, 140163.
394. Partridge B. L., Johansson J. & Kalish J. (1983) The structure of schools of giant bluefin tuna in Cape Cod Bay. *Environmental Biology of Fishes* **9**, 253-262.
395. Pavlov V. V. (2006) Dolphin skin as a natural anisotropic compliant wall. *Bioinspiration & Biomimetics* 1, 31.
396. Peach M. B. & Marshall N. J. (2000) The pit organs of elasmobranchs: a review. *Philosophical Transactions of the Royal Society of London B* **355**, 1131-1134.
397. Pearson D. M. (1982) Primitive bony fishes, with especial reference to *Cheirolepis* and palaeonisciform actinopterygians. *Zoological Journal of the Linnean Society* **74**, 35–67.
398. Pernègre V. N. (2002) The genus *Doryaspis* White (Heterostraci) from the lower Devonian of Vestspitsbergen, Svalbard. *Journal of Vertebrate Paleontology* **22**, 735-746.
399. Pershin S. V., Chernyshov L. F., Kozlov L. F., Koval A. P. & Zayets V. A. (1976) Patterns in the integuments of fast-swimming fishes. *Bionika* **1976**, 3-21
400. Plotnick R. E. & Bauer J. (2014) Crinoids Aweigh: experimental biomechanics of ancyrocrinus holdfasts. in experimental approaches to understanding fossil organisms. Springer

Netherlands.

401. Plotnick R. E. Baumiller T. K. (1988) The pterygotid telson as a biological rudder. *Lethaia* **21**, 13–27.
402. Pough F. H. & Janis C. M. (eds)(2005) Vertebrate Life (7th Ed). New Jersey: Pearson Prentice Hall.
403. Poyato-Ariza F. J. (2005) Pycnodont fishes: morphologic variation, ecomorphological plasticity, and a new interpretation of their evolutionary history. *Bulletin of the Kitakyushu Museum of Natural History and Human History, Series A (Natural History)* **3**, 169–184.
404. Pradel A., Sansom I. J., Gagnier P. –Y., Cespedes R. & Janvier P. (2007) The tail of the Ordovician fish *Sacambaspis*. *Biology Letters* **22**, 72-75.
405. Priede I. G. (1984) A basking shark (*Cetorhinus maximus*) tracked by satellite together with simultaneous remote sensing. *Fisheries Research* **2**, 201-216.
406. Přikryl T. (2011) Lepidological review on the fish fauna of the Kučlín locality (Upper Eocene, Czech Republic). *Acta Musei Nationalis Pragae, Series B, Historia Naturalis* **67**, 149–156.
407. Pulcini D., Costa C., Aguzzi J. & Cataudell S. (2008) Light and shape: A contribution to demonstrate morphological differences in diurnal and nocturnal teleosts. *Journal of Morphology* **269**, 375-385.
408. Purnell M. A. (2001) Scenarios, selection and the ecology of early vertebrates.), In *Major Events in Early Vertebrate Evolution: Palaeontology, Phylogeny, Genetics and Development*. Ed. Ahlberg P.E., Taylor & Francis.
409. Purnell M. A. (2002) Feeding in extinct jawless heterostracan fishes and testing scenarios of early vertebrate evolution. *Proceedings of the Royal Society of London. Series B: Biological Sciences* **269**, 83-88.
410. Qu Q., Sanchez S., Blom H., Tafforeau P. & Ahlberg P. E. (2013) Scales and tooth whorls of ancient fishes challenge distinction between external and oral 'teeth'. *PloS One* **8**, E71890.
411. Raschi W. G. & Musick J. A. (1986) Hydrodynamic aspects of shark scales. *NASA STI/Recon Technical Report* **86**, 22889.
412. Raschi W. & Tabit C. (1992) Functional aspects of placoid scales: a review and update. *Australian Journal of Marine and Freshwater Research* **43**, 123-147.
413. Reif W-E. (1974) Morphogenese und Musterbildung des Hautzahnchen - Skelettes von Heterodontus. *Lethaia* **7**, 25-42.
414. Reif W-E. (1976) Morphogenesis, pattern formation and function of the dentition ofHeterodontus (Selachii). *Zoomorphologie* **83**, 1-47.
415. Reif W-E. (1978) Protective and hydrodynamic function of the dermal skeleton of elasmobranchs. *Neues Jahrbuch Geologie und Palaontologie Abhandlungen* **157**, 133-41.
416. Reif W-E. (1978) Types of morphogenesis of the dermal skeleton in fossil

sharks. *Paläontologische Zeitschrift* **52**, 110-128.

417. Reif W-E. (1978) Wound healing in sharks. *Zoomorphologie* **90**, 101-111.
418. Reif W-E. (1979) Morphogenesis and histology of large scales of batoids (Elasmobranchii). *Paläontologische Zeitschrift* **53**, 26-37.
419. Reif W-E. (1982a) Evolution of dermal skeleton and dentition in vertebrates. The odontode-regulation theory. *Evolutionary Biology* **15**, 287-368.
420. Reif W-E. (1982b) Morphogenesis and function of the squamation in sharks. 1. Comparative functional morphology of shark scales, and ecology of scales. *Neues Jahrbuch fur Geologie und Palaontologie Abhandlungen* **164**, 172-183.
421. Reif W-E. (1983) Functional morphology and evolutionary ecology. *Paläontologische Zeitschrift* **57**, 255-266.
422. Reif W-E. (1985a) Squamation and ecology of sharks. *Courier Forschungsinstitut Senckenberg* **78**, 1-255.
423. Reif W-E. (1985b) Functions of scales and photophores in mesopelagic luminescent sharks. *Acta Zoologica* **66**. 111-118.
424. Reif W-E. & Dinkelacker A. (1982) Hydrodynamics of the squamation in fast swimming sharks. *Neues Jahrbuch fur Geologie und Paleontologie Abhandlungen* **164**, 184-187.
425. Reif W-E. & Weishampel D. B. (1986) Anatomy and mechanics of the lunate tail in lamnid sharks. *Zoologische Jahrbücher Anatomie* **114**, 221-234.
426. Richardson W. J., Fraker M. A., Wursig B. & Wells R. S. (1985) Behaviour of bowhead whales *Balaena mysticetus* summering in the Beaufort Sea: Reactions to industrial activities. *Biological Conservation* **32**, 195–230.
427. Rickards B., Rigby S., Rickards J. & Swales C. (1998) Fluid dynamics of the graptolite rhabdosome recorded by laser Doppler anemometry. *Palaeontology* **41**, 737-752.
428. Ridgway S. H. & Carder D. A. (1993) Features of dolphin skin with potential hydrodynamic importance. *IEEE Engineering in Medicine and Biology Magazine* **12**, 83–88
429. Roberts C. D. (1993) Comparative morphology of spined scales and their phylogenetic significance in the teleostei. *Bulletin of Marine Science* **52**, 60-113.
430. Romano C., Kogan I., Jenks J., Jerjen I. & Brinkmann W. (2012) *Saurichthys* and other fossil fishes from the late Smithian (Early Triassic) of Bear Lake County (Idaho, USA), with a discussion of saurichthyid palaeogeography and evolution. *Bulletin of Geosciences* **87**, 543-570.
431. Romer A. S. (1933) Eurypterid influence on vertebrate history. *Science* **78**, 114-117.
432. Rosen M. W. & Cornford N. E. (1971) Fluid friction of fish slimes. *Nature* **234**, 49-51.
433. Rücklin M., Giles S., Janvier P. & Donoghue P. C. (2011) Teeth before jaws? Comparative analysis of the structure and development of the external and internal scales in the extinct

jawless vertebrate *Loganellia scotica*. *Evolution & development* 13, 523-532.

434. Russo R. A. (2013) Observations on the ectoparasites of elasmobranchs in San Francisco Bay, California. *California Fish and Game* **99**, 233-236.
435. Rygg A. D., Cox J. P. L., Abel R., Webb A. G., Smith N.B. & Craven B. A. (2013) A computational study of the hydrodynamics in the nasal region of a hammerhead shark (*Sphyrna tudes*): implications for olfaction. *Plos One* **8**, E59783.
436. Sagnes P. & Statzner B. (2009) Hydrodynamic abilities of riverine fish: a functional link between morphology and velocity use. *Aquatic Living Resources* **22**, 79-91.
437. Sagong W., Jeon W. P., & Choi H. (2013) Hydrodynamic Characteristics of the Sailfish (*Istiophorus platypterus*) and Swordfish (*Xiphias gladius*) in Gliding Postures at Their Cruise Speeds. *PloS one* **8**, e81323.
438. Sagong W., Kim C., Choi S., Jeon W-P. & Choi H. (2008) Does the sailfish skin reduce skin friction like the shark skin? *Physics of Fluids* **20**, 101510.
439. Sallan L. C. & Coates M. I. (2010) End-Devonian extinction and a bottleneck in the early evolution of modern jawed vertebrates. *Proceedings of the National Academy of Sciences* **107**, 10131-10135.
440. Sambilay Jr V. C. (1990) Interrelationships between swimming speed, caudal fin aspect ratio and body length of fishes. *Fishbyte* **8**, 16-20.
441. Sansom I. J., Smith M. M. & Smith P. M. (1996) Scales of thelodont and shark-like fishes from the Ordovician of Colorado. *Nature* **379**, 628-630.
442. Sansom I. J., Smith M. M. & Smith M. P. (2001) The Ordovician radiation of vertebrates. Major events in early vertebrate evolution: palaeontology, phylogeny, genetics and development, 156-171.
443. Sansom I. J., Davies N. S., Coates M. I., Nicoll R. S. & Ritchie A. (2012) Chondrichthyan-like scales from the Middle Ordovician of Australia. *Palaeontology* **55**, 243-247.
444. Sansom R. S. (2009) Phylogeny, classification and character polarity of the Osteostraci (Vertebrata). *Journal of Systematic Palaeontology* **7**, 95-115.
445. Sansom R. S., Freedman K. I. M., Gabbott S. E., Aldridge R. J. & Purnell M. A. (2010) Taphonomy and affinity of an enigmatic Silurian vertebrate, *Jamoytius kerwoodi* White. *Palaeontology* **53**, 1393-1409.
446. Sansom R. S., Gabbott S. E. & Purnell M. A. (2013) Unusual anal fin in a Devonian jawless vertebrate reveals complex origins of paired appendages. *Biology Letters* **9**, 20130002.
447. Sayles L. P. & Hershkowit S. G. (1937) Placoid scale types and their distribution in Squalus acanthias. *Biological Bulletin*, 51-66.
448. Scacco U., La Mesa G. & Vacchi M. (2010) Body morphometrics, swimming diversity and niche in demersal sharks: a comparative case study from the Mediterranean Sea. *Scientia*

Marina **74**, 37-53.

449. Schlichting H., Gersten K. & Gersten K. (2000). Boundary-layer theory. Springer Science & Business Media.
450. Schönbörner A. A., Boivin G. & Baud C. A. (1979) The mineralization processes in teleost fish scales. *Cell and tissue research* **202**, 203-212.
451. Schultze H.-P. (1984) Juvenile specimens of *Eusthenopteron foordi* Whiteaves, 1881 (Osteolepiform Rhipidistian, Pisces) from the Late Devonian of Miguasha, Que´bec, Canada. *Journal of Vertebrate Paleontology* **4**, 1–16.
452. Schumacher J. F., Aldred N., Callow M. E., Finlay J. A., Callow J. A., Clare A. S. & Brennan A. B. (2007) Species-specific engineered antifouling topographies: correlations between the settlement of algal zoospores and barnacle cyprids. *Biofouling* **23**, 307-317.
453. Schumacher J. F., Carman M. L., Estes T. G., Feinberg A. W., Wilson L. H., Callow M. E. & Brennan A. B. (2007) Engineered antifouling microtopographies–effect of feature size, geometry, and roughness on settlement of zoospores of the green alga Ulva. *Biofouling* **23**, 55-62.
454. Semmens J. M., Payne N. L., Huveneers C., Sims D. W. & Bruce B. D. (2013) Feeding requirements of white sharks may be higher than originally thought. *Scientific reports* **3**.
455. Sfakiotakis M., Lane D. M. & Davies J. B. C. (1999) Review of fish swimming modes for aquatic locomotion. *IEEE Journal of Oceanic Engineering* **24**, 237-252.
456. Shadwick R. E. & Lauder G. V. (Eds.)(2006) Fish Physiology: Fish Biomechanics (Vol. 23). Academic Press.
457. Shephard K. L. (1994) Functions for fish mucus. *Reviews in Fish Biology & Fisheries* **4**, 401-429.
458. Shoele K. & Zhu Q. (2009) Fluid–structure interactions of skeleton-reinforced fins: performance analysis of a paired fin in lift-based propulsion. *Journal of Experimental Biology* **212**, 2679-2690.
459. Shu D. G., Luo H. L., Morris S. C., Zhang X. L., Hu S. X., Chen L. & Chen L. Z. (1999) Lower Cambrian vertebrates from south China. *Nature* **402**, 42-46.
460. Shu D. G., Morris S. C., Han J., Zhang Z. F., Yasui K., Janvier P. & Liu H. Q. (2003) Head and backbone of the Early Cambrian vertebrate *Haikouichthys*. *Nature* **421**, 526-529.
461. Silas E. G. & Selvaraj G. S. D. (1972) Descriptions of the adult and embryo of the bramble shark *Echinorhinus brucus* (Bonnaterre) obtained from the continental slope of India. *Journal of the Marine Biological Association of India* **14**, 395–401.
462. Simons J. R. (1970) The direction of the thrust produced by the heterocercal tails of two dissimilar elasmobranchs: the Port Jackson shark, *Heterodontus portusjacksoni* (Meyer), and the piked dogfish, *Squalus megalops* (Macleay). *Journal of Experimental Biology* **52**, 95-

107.

463. Sims D. W. (2000) Filter-feeding and cruising swimming speeds of basking sharks compared with optimal models: they filter-feed slower than predicted for their size. *Journal of Experimental Marine Biology and Ecology* **249**, 65-76.
464. Sire J. Y. (1986) Ontogenic development of surface ornamentation in the scales of Hemichromis bimaculatus (Cichlidae). *Journal of Fish Biology* **28**, 713-724.
465. Sire J. Y. (1990) From ganoid to elasmoid scales in the actinopterygian fishes. *Netherlands Journal of Zoology* **40**, 75-92.
466. Sire Y., Géraudie J., Meunter F. J. & Zylberberg L. (1987) On the origin of ganoine: histological and ultrastructural data on the experimental regeneration of the scales of *Calamolchthys calabaricus* (Osteichthyes, Brachyopterygii, Polypteridae). *American Journal of Anatomy* **180**, 391–402.
467. Sire J-Y. & Akimenko M. A. (2004) Scale development in fish: a review, with description of sonic hedgehog (shh) expression in the zebrafish (*Danio rerio*). *International Journal of Developmental Biology* **48**, 233-247.
468. Sire J-Y., Donoghue P. C. J. & Vickaryous M. K. (2009) Origin and evolution of the integumentary skeleton in non-tetrapod vertebrates. *Journal of Anatomy* **214**, 409-440.
469. Smith M. M. & Hall B. K. (1990) Development and evolutionary origins of vertebrate skeletogenic and odontogenic tissues. *Biological Reviews* **65**, 277-373.
470. Smith J. A. (2011) Turbulent separation control effects of mako shark skin samples on a NACA 4412 hydrofoil (Doctoral dissertation, University of Alabama Tuscaloosa).
471. Smith J. B., Grandstaff B. S. & Abdel-Ghani M. S. (2006) Microstructure of polypterid scales (Osteichthyes: Actinopterygii: Polypteridae) from the upper Cretaceous Bahariya Formation, Bahariya Oasis, Egypt. *Journal of Paleontology* **80**, 1179-1185.
472. Smith M. M., Coates M. I. & Ahlberg P. E. (Ed)(2001) The evolution of vertebrate dentitions: phylogenetic pattern and developmental models. In *Major Events in Early Vertebrate Evolution* **61**, 223–240. Systematics Association Special Volume Series.
473. Smith M. P. & Sansom I. J. (1995) The affinity of *Anatolepis* Bockelie & Fortey. *Geobios* **28**, 61-63.
474. Smith W. L. & Wheeler W. C. (2006) Venom evolution widespread in fishes: a phylogenetic road map for the bioprospecting of piscine venoms. *Journal of Heredity* **97**, 206-217.
475. Soehn K. L., Märss T., Caldwell M. W. & Wilson M. V. (2001) New and biostratigraphically useful thelodonts from the Silurian of the Mackenzie Mountains, Northwest Territories, Canada. *Journal of Vertebrate Paleontology* **21**, 651-659.
476. Sokolov V., Bulina I. & Rodionov V. (1969) Interaction of dolphin epidermis with flow boundary layer. *Nature* **222**, 267–68.

477. Song J., Ortiz C. & Boyce M. C. (2011) Threat-protection mechanics of an armored fish. *Journal of the Mechanical Behavior of Biomedical Materials* **4**, 699-712.
478. Southall E. J. & Sims D. W. (2003) Shark skin: a function in feeding. *Proceedings of the Royal Society of London B: Biological Sciences* **270,** 47-49.
479. Stetson H. C. (1931) Studies on the morphology of the Heterostraci. *The Journal of Geology*, 141-154.
480. Stevens J. D. (2008) The biology and ecology of the shortfin mako shark, *Isurus oxyrinchus*. *Sharks of the open ocean: Biology, fisheries and conservation*, 87-94.
481. Stokes M. (1997) Larval locomotion of the lancelet. *Journal of Experimental Biology* **200**, 1661-1680.
482. Südkamp W. H. & Burrow C. J. (2007) The acanthodian *Machaeracanthus* from the Lower Devonian Hunsrück Slate of the Hunsrück region (Germany). *Palaeontologische Zeitschrift* **81**, 97-104.
483. Sullivan T. & Regan F. (2011) The characterization, replication and testing of dermal denticles of *Scyliorhinus canicula* for physical mechanisms of biofouling prevention. *Bioinspiration & Biomimetics* **6**, 046001.
484. Sundström L. F., Gruber S. H., Clermont S. M., Correia J. P., de Marignac J. R., Morrissey J. F. & Oliveira M. T. (2001) Review of elasmobranch behavioral studies using ultrasonic telemetry with special reference to the lemon shark, *Negaprion brevirostris*, around Bimini Islands, Bahamas. *Environmental Biology of Fishes* **60**, 225-250.
485. Talay T. A. (1975) Introduction to the Aerodynamics of Flight (Vol. 367). Scientific and Technical Information Office, National Aeronautics and Space Administration.
486. Tamura Y. & Takagi T. (2009) Morphological features and functions of bluefin tuna change with growth. *Fisheries Science* **75**, 567-575.
487. Tanaka S., Kitamura T. & Nakano H. (2001) Identification of shark species by SEM observation of denticle of shark fins. *ICCAT* **54**, 1386-1394.
488. Thomson K. S. (1971) The adaptation and evolution of early fishes. *Quarterly Review of Biology*, 139-166.
489. Thomson K. S. & Simanek D. E. (1977) Body form and locomotion in sharks. *American Zoologist* **17**, 343-354.
490. Tintori A. & Sassi, D. (1992). *Thoracopterus* Bronn (Osteichthyes: Actinopterygii): A gliding fish from the upper Triassic of Europe. *Journal of Vertebrate Paleontology*, **12**, 265-283.
491. Trewin N. H. (2000) The ichnogenus Undichna, with examples from the Permian of the Falkland Islands. *Palaeontology* **43**, 979-997.
492. Tricas T. C., Taylor L. R. & Naftel G. (1981) Diel behavior of the tiger shark, *Galeocerdo cuvier*, at French Frigate Shoals, Hawaiian Islands. *Copeia*, 904-908.

493. Trinajstic K. (2001) Acanthodian microremains from the Frasnian Gneudna Formation, Western Australia. *Records of the Western Australian Museum* **20**, 187-198.
494. Turner S. (1973) Siluro-Devonian thelodonts from the Welsh Borderland. *Journal of the Geological Society* **129**, 557-582.
495. Turner S. (1982) A new articulated thelodont (Agnatha) from the Early Devonian of Britain. *Palaeontology* **25**, 879-889.
496. Turner S. (1992) Thelodont lifestyles. In *Fossil Fishes as Living Animals* (Ed. Mark-Kurik E) Akademia, 1. Tallinn, Estonia: Publishing Dept Estonian Academy of Sciences.
497. Turner S. (1995) Devonian thelodont scales (Agnatha, Thelodonti) from Queensland. *Memoirs of the Queensland Museum* **38**, 677-686.
498. Turner S. (1997) Sequence of Devonian thelodont scale assemblages in East Gondwana. *Geological Society of America, Special Publications* **321**, 295–315.
499. Turner S. (1999) Early Silurian to Early Devonian thelodont assemblages and their possible ecological significance. In *Palaeocommunities — a case study from the Silurian and Lower Devonian.* EdsBoucot A.J. & Lawson J. International Geological Correlation Programme 53, Project Ecostratigraphy, Final Report, Cambridge University Press, Cambridge, UK.
500. Turner S., Burrow C. J., Gholamalian H. & Yazdi M. (2002) Late Devonian (early Frasnian) microvertebrates and conodonts from the Chahriseh area near Esfahan, Iran. *Memoirs of the Association of Australasian Palaeontologists* **27**, 149-159.
501. Turner S., Burrow C. J., Schultze H. P., Blieck A., Reif W-E., Rexroad C. B. & Nowlan, G. S. (2010) False teeth: conodont-vertebrate phylogenetic relationships revisited. *Geodiversitas* **32**, 545-594.
502. Turner S., Kuglitsch J. J. & Clark D. L. (1999) Llandoverian thelodont scales from the Burnt Bluff Group of Wisconsin And Michigan. *Journal of Paleontology* **73**, 667-676.
503. Turner S. & Murphy M. A. (1988) Early Devonian vertebrate microfossils from the Simpson Park Range, Eureka County, Nevada. *Journal of Paleontology*, 959-964.
504. Turner, S. & Nowlan, G. S. (1995) Early Silurian microvertebrates of eastern Canada. *Bulletin du Muséum national d'histoire naturelle. Section C, Sciences de la terre, paléontologie, géologie, minéralogie* **17**, 513-529.
505. Turner S. & Young G. C. (1992) Thelodont scales from the Middle-Late Devonian Aztec Siltstone, southern Victoria Land, Antarctica. *Antarctic Science **4***, 89-105.
506. Tway L. E. & Zidek J. (1982) Catalog of Late Pennsylvanian ichthyoliths, part I. *Journal of Vertebrate Paleontology* **2**, 328-361.
507. Tway L. E. & Zidek J. (1983) Catalog of late Pennsylvanian ichthyoliths, Part II. *Journal of Vertebrate Paleontology* **2**, 414-438.
508. Tytell E. D., Borazjani I., Sotiropoulos F., Baker T. V., Anderson E. J. & Lauder G. V. (2010)

Disentangling the functional roles of morphology and motion in the swimming of fish. *Integrative and Comparative Biology* **50**, 1140-1154.

509. Uskova Y. T., Shmyrev A. N., Rayevskiy V. S., Bogdanova L. N., Momot L. N. (1983) The nature and hydrodynamic activity of dolphin eye secretions. *Bionika* **17**, 72–75 (from Russian, in Fish & Lauder, 2006)
510. Valiukevicius J. (1992) First articulated *Poracanthodes* from the Lower Devonian of Severnaya Zemlya. *Fossil fishes as living animals. Academy of Sciences of Estonia, Tallinn*, 193-214.
511. Valiukevičius, J. (2003). Devonian acanthodians from Severnaya Zemlya Archipelago (Russia). *Geodiversitas* **25**, 131-204.
512. Valiukevičius J. (2004) New Wenlock–Pridoli (Silurian) acanthodian fishes from Lithuania. *Acta Palaeontologica Polonica* **49**, 147-160.
513. Valiukevičius J. (2005) Silurian acanthodian biostratigraphy of Lithuania. *Geodiversitas* **27**, 349-380
514. Valiukevičius J. & Burrow C. J. (2005) Diversity of tissues in acanthodians with “Nostolepis”-type histological structure. *Acta Palaeontologica Polonica 50*, 635-649.
515. Vélez-Zuazo X. & Agnarsson I. (2011) Shark tales: a molecular species-level phylogeny of sharks (Selachimorpha, Chondrichthyes). *Molecular phylogenetics and evolution* **58**, 207-217.
516. Vergoossen J. M. J. (2004) Fish microfossils from Ramsåsa, site E, Scania, southern Sweden (mid Palaeozoic). *Scripta Geologica*, 127, 1-70.
517. Vermeij G. J. (1987) Evolution and escalation: an ecological history of life. Princeton, NJ: Princeton University Press.
518. Vernerey F. J. & Barthelat F. (2010) On the mechanics of fish scale structures. *International Journal of Solids and Structures* **47**, 2268-2275.
519. Vernerey F. J. & Barthelat F. (2014) Skin and scales of teleost fish: Simple structure but high performance and multiple functions. *Journal of the Mechanics and Physics of Solids* **68**, 66-76.
520. Vickers-Rich P. & Komarower P. (Eds)(2007) The rise and fall of the Ediacaran biota. Geological Society of London. Chicago
521. Videler J. J. (1993) *Fish Swimming*. London: Chapman & Hall
522. Videler J. J. (1995) Body surface adaptations to boundary-layer dynamics. In *Biological fluid dynamics*. Eds Ellington C. P. & Pedley T. J. Society of Experimental Biology, Cambridge.
523. Viswanath P. R. (2007) Some thoughts on separation control strategies. *Sādhanā* **32**, 83-92.
524. Wagner G. N., Mckinley R. S., Bjorn P. A. & Finstad B. (2003) Physiological impact of sea lice on swimming performance of atlantic salmon. *Journal of Fish Biology* **62**, 1000–1009.

525. Wahl M. (1997) Increased drag reduces growth of snails: comparison of flume and in situ experiments. *Marine Ecology Progress Series* **151**, 291–293.
526. Walker J. A. (2000) Does a rigid body limit maveuverability? *Journal of Experimental Biology* **203**, 3391 – 3396.
527. Walsh M. J. & Lindemann A. M. (1984) Optimization and application of riblets for turbulent drag reduction. *AIAA 22nd Aerospace Sciences Meeting*, AIAA-84-0347.
528. Walters V. (1962) Body form and swimming performance in the scombroid fishes. *American Zoologist*, 143-149.
529. Wainwright P. C. (1996) Ecological explanation through functional morphology: the feeding biology of sunfishes. *Ecology*, 1336-1343.
530. Wainwright P. C., Bellwood D. R. & Westneat M. W. (2002) Ecomorphology of locomotion in labrid fishes. *Environmental Biology of Fishes* **65**, 47-62.
531. Wainwright S. A., Vosburgh F. & Hebrank J. H. (1978) Shark skin: function in locomotion. *Science* **202**, 747-749.
532. Walters V. (1962) Body form and swimming performance in scombrid fishes. *American Zoology* **2**, 143-149.
533. Walters V. (1963) The trachipterid integument and an hypothesis on its hydrodynamic function. *Copeia 1963*, 260-270.
534. Wang J., Gai Z. & Zhu M. (2004) A new species of {Macrothyraspis}(Galeaspida, Agnatha) from wenshan, Yunnan, China. *Vertebrata Pal Asiatica* **43**, 304-311.
535. Wang J. J., Lan S. L. & Chen, G. (2000) Experimental study on the turbulent boundary layer flow over riblets surface. *Fluid dynamics research* **27**, 217-229.
536. Ware D. M. (1978) Bioenergetics of pelagic fish: theoretical change in swimming speed and ration with body size. *Journal of the Fisheries Board of Canada* **35**, 220-228.
537. Watanabe Y. Y., Lydersen C., Fisk A. T. & Kovacs, K. M. (2012) The slowest fish: swim speed and tail-beat frequency of Greenland sharks. *Journal of Experimental Marine Biology and Ecology* **426**, 5-11.
538. Watson D. M. S. (1937) The acanthodian fishes. *Philosophical Transactions Of The Royal Society Of London B: Biological Sciences* **228**, 49-146.
539. Watts P. & Fish F. E. (2001) The influence of passive, leading edge tubercles on wing performance. In Proceedings of the Twelfth International Symposium on Unmanned Untethered Submersible Technology. Durham New Hampshire.
540. Webb P. W. (1975) Hydrodynamics and energetics of fish propulsion. *Bulletin of the Fisheries Research Board of Canada,* 190.
541. Webb P. W. (1977) Effects of median-fin amputation on fast-start performance of Rainbow Trout (*Salmo gairdneri*). *Journal of Experimental Biology* **68**, 123-135.

542. Webb P. W. & Smith G. R. (1980) Function of the caudal fin in early fishes. *Copeia* **1980**, 559-562.
543. Webb P. W. & Keyes R. S. (1982) Swimming kinematics of sharks. *Fishery Bulletin* **80**, 803-812.
544. Webb P. W. (1984) Body form, locomotion and foraging in aquatic vertebrates. *American Zoologist* **24**, 107-120.
545. Webb P. W. (1984) Form and function in fish swimming. *Scientific American*.
546. Webb P. W. (1988) 'Steady' swimming kinematics of Tiger Musky, an esociform accelerator, and Rainbow Trout, a generalist cruiser. *Journal of Experimental Biology* **138**, 51-69.
547. Webb P. W., Sims D. & Schultz W. W. (1991) The effects of an air/water surface on the fast-start performance of rainbow trout (*Oncorhynchus mykiss*). *Journal of Experimental Biology* **155**, 219-226.
548. Webb P. W., Hardy D. H. & Mehl V. L. (1992) The effect of armored skin on the swimming of longnose gar, *Lepisosteus osseus*. *Canadian Journal of Zoology* **70**, 1173-1179.
549. Webb P. W. (2002) Control of posture, depth, and swimming trajectories of fishes. *Integrative and Comparative Biology* **42**, 94-101.
550. Webb P. (2006) Stability and maneuverability. In *Fish Biomechanics: Fish Physiology.* Vol. 23 (ed. R. E. Shadwick and G. V. Lauder). San Diego: Academic Press
551. Webb P. W. & Cotel A. J. (2010) Turbulence: does vorticity affect the structure and shape of body and fin propulsors? *Integrative and Comparative Biology* **50**, 1155-1166.
552. Weihs D. (1973) Hydromechanics of fish schooling. *Nature* **241**, 290–291.
553. Weihs D. (1974) Energetic advantages of burst swimming of fish. *Journal of Theoretical Biology* **48**, 215-229.
554. Weihs D. (1980) Energetic significance of changes in swimming modes during growth of larval anchovy, *Engraulis mordax*. *Fishery Bulletin* **77**, 597-604.
555. Weihs D. (1981). Body section variations in sharks: an adaptation for efficient swimming. *Copeia* **1981**, 217-219.
556. Weihs D. (2004) The hydrodynamics of dolphin drafting. *Journal of Biology* **3**, 1–23.
557. Wendruff A. J. & Wilson M. V. H. (2011) A fork-tailed coelacanth, *Rebellatrix divaricerca*, gen. et sp. nov. (Actinistia, Rebellatricidae, fam. nov.), from the Lower Triassic of Western Canada. *Journal of Vertebrate Paleontology* **32**, 499-511.
558. Whitear M. (1986) The skin of fishes including cyclostomes. In *Biology of the Integument*. Eds Bereiter-Hahn J., Matoltsy A.G. & Richards K.S. Springer-Verlag. Berlin.
559. Wilga C. D. & Lauder G. V. (2002) Function of the heterocercal tail in sharks: quantitative wake dynamics during steady horizontal swimming and vertical manoeuvring. *Journal of Experimental Biology* **205**, 2365-2374.

560. Wilga C. D. & Lauder G. V. (2004) Biomechanics: Hydrodynamic function of the shark's tail. *Nature* **430**, 850-850.
561. Wilga C. D. & Lauder G. V. (2004) Biomechanics of Locomotion in Sharks, Rays, and Chimaeras. *Biology of Sharks and Their Relatives*. New York: CRC Press.
562. Wilga C. D. & Lauder G. V. (2004) Biomechanics: Hydrodynamic function of the shark's tail. *Nature* **430**, 850-850.
563. Williams T. M., Friedl W. A., Fong M. L., Yamada R. M., Sedivy P. & Haun J. E. (1992) Travel at low energetic cost by swimming and wave-riding bottlenose dolphins. *Nature* **355**, 821–23
564. Wilkinson S. P. (1983) Influence of wall permeability on turbulent boundary-layer properties. In *AIAA, Aerospace Sciences Meeting* (Vol. 1).
565. Wilson M. V. & Caldwell M. W. (1993) New Silurian and Devonian fork-tailed 'thelodonts' are jawless vertebrates with stomachs and deep bodies. *Nature* **361**, 442-444.
566. Wilson M. V. H. & Caldwell M. W. (1998) The furcacaudiformes: a new order of jawless vertebrates with thelodont scales, based on articulated Silurian and Devonian fossils from northern Canada. *Journal of Vertebrate Paleontology* **18**, 10-29.
567. Wilson M. V. & Märss T. (2009). Thelodont phylogeny revisited, with inclusion of key scale-based taxa. *Estonian Journal of Earth Sciences* **58**, 297-310.
568. Wilson M. V. & Märss T. (2012) Anatomy of the Silurian thelodont *Phlebolepis elegans* Pander. *Estonian Journal of Earth Sciences* **61**, 261.
569. Wisshak M., Volohonsky E. & Blomeier D. (2004) Acanthodian fish trace fossils from the Early Devonian of Spitsbergen. *Acta Palaeontologica Polonica* **49**, 629-634.
570. Witzmann F. (2011) Morphological and histological changes of dermal scales during the fish-to-tetrapod transition. *Acta Zoologica* **92**, 281-302.
571. Wolfgang M. J., Anderson J. M., Grosenbaugh M. A., Yue D. K. & Triantafyllou M. S. (1999) Near-body flow dynamics in swimming fish. *The Journal of Experimental Biology* **202**, 2303-2327.
572. Wu T. Y. T. (1975) Swimming and flying in nature (Vol. 2). Plenum Pub Corp.
573. Xian-Guang H., Aldridge R. J., Siveter D. J., Siveter D. J. & Xiang-Hong F. (2002) New evidence on the anatomy and phylogeny of the earliest vertebrates. *Proceedings of the Royal Society of London. Series B: Biological Sciences* **269**, 1865-1869.
574. Xu G-H., Zhao L-J., Gao K-Q. & Wu F-X. (2012) A new stem-neopterygian fish from the Middle Triassic of China shows the earliest over-water gliding strategy of the vertebrates. *Proceedings of the Royal Society B* **280**, 1471-2954.
575. Yamanoue Y., Setiamarga D. H. E. & Matsuura K. (2010) Pelvic fins in teleosts: structure, function and evolution. *Journal of Fish Biology* **77**, 1173-1208.

576. Yang S. Q. (2009) Drag reduction in turbulent flow with polymer additives. *Journal of Fluids Engineering* **131**, 051301.
577. Yang W., Gludovatz B., Zimmermann E. A., Bale H. A., Ritchie R. O. & Meyers M. A. (2013). Structure and fracture resistance of alligator gar (*Atractosteus spatula*) armored fish scales. *Acta Biomaterialia* **9**, 5876-5889.
578. Yeh T. T. & Hall J. M. (2008) Airspeed calibration service. *NIST Special Publication* **250**, 79.
579. Young G. C. (1991) The first armoured agnathan vertebrates from the Devonian of Australia. In *Early Vertebrates and Related Problems of Evolutionary Biology*. Chang M. M., LIu Y. H. & Zhang G. R. (eds) Science Press, Beijing, China.
580. Young G. C. (1997) Ordovician microvertebrate remains from the Amadeus Basin, central Australia. *Journal of Vertebrate Paleontology* **17**, 1-25.
581. Young G. C. (2010) Placoderms (armored fish): dominant vertebrates of the Devonian Period. *Annual Review of Earth and Planetary Sciences* **38**, 523-550.
582. Young G. C. & Burrow C. J. (2004) Diplacanthid acanthodians from the Aztec Siltstone (late Middle Devonian) of southern Victoria Land, Antartica. *Fossils and Strata* **50**, 23-43.
583. Young G. C., Karatajute-Talimaa V. N. & Smith M. M. (1996) A possible Late Cambrian vertebrate from Australia. *Nature* **383**, 810-812.
584. Zangerl R. & Case G. R. (1973) Iniopterygia, a new order of chondrichthyan fishes from the Pennsylvanian of North America. *Fieldiana Geological Memoirs* **6**, 1–67.
585. Zhang X-G. & Hou, X-G. (2004) Evidence for a single median fin-fold and tail in the Lower Cambrian vertebrate, *Haikouichthys ercaicunensis*. *Journal of Evolutionary Biology* **17**, 1162–1166.
586. Zhu M. & Gai Z. (2007) Phylogenetic relationships of galeaspids (Agnatha). *Frontiers of Biology in China* **2**, 151-169.
587. Zhu D., Ortega C. F., Motamedi R., Szewciw L., Vernerey F. & Barthelat F. (2012) Structure and mechanical performance of a "modern" fish scale. *Advanced Engineering Materials* **14**, 185194.
588. Zhu D., Szewciw L., Vernerey F. & Barthelat F. (2013) Puncture resistance of the scaled skin from striped bass: collective mechanisms and inspiration for new flexible armor designs. *Journal of the Mechanical Behavior of Biomedical Materials* **24**, 30–40.
589. Zhu Q., Wolfgang M. J., Yue D. K. P. & Triantafyllou M. S. (2002) Three-dimensional flow structures and vorticity control in fish-like swimming. *Journal of Fluid Mechanics* **468**, 1-28.
590. Zidek J. (1976) Kansas Hamilton Quarry (Upper Pennsylvanian) Acanthodes with remarks on the previously reported North American occurrences of the genus. *University Kansas Paleontological Contributions* **83**, 1–41.
591. Zidek J. (1985) Growth in acanthodes (acanthodii: pisces) data and

implications. *Paläontologische Zeitschrift* **59**, 147-166.

592. Zigaite Ž., & Ciurlionio M. K. (2004) A new thelodont from Lower Silurian of Tuva and north-west Mongolia. *Acta Universitatis Latviensis* **679**, 158-165.
593. Žigaitė, Ž., & Karatajūtė-Talimaa, V. (2008) New genus of chondrichthyans from the Silurian–Devonian boundary deposits of Tuva (Russia). *Acta Geologica Polonica* ***58***, 127-131.
594. Žigaitė Ž., Karatajūtė-Talimaa V., Goujet D. & Blom H. (2013) Thelodont scales from the Lower and Middle Devonian Andrée Land Group, Spitsbergen. *Geologiska Föreningen* **135**, 57-73.
595. Žigaitė Ž., Richter M., Karatajūtė-Talimaa V. & Smith M. M. (2013) Tissue diversity and evolutionary trends of the dermal skeleton of Silurian thelodonts. *Historical Biology* **25**, 143-154.
596. Zimmermann E. A., Gludovatz B., Schaible E., Dave N. K. N., Yang W., Meyers M. A. & Ritchie R. O. (2013) Mechanical adaptability of the bouligand-type structure in natural dermal armour. *Nature Communications* **4**, 2634.

Appendix I. Supplementary Data Relating to Comparative Analysis

A1.1. Modern Shark Variability Analysis – *Centrophorus granulosus*

a) Specimen

Figure Supplementary S1.1. Photographs of a stuffed gulper shark (*Centrophorus granulosus)* specimen before sampling; a single 480mm male caught in Zamboanga, Mindanao, Phillipines in 2013. Top, lateral view; centre, dorsal view; and bottom shows dorsal detail of the flank region. Scale bar fine intervals are 1 cm.

b) Sampling locations

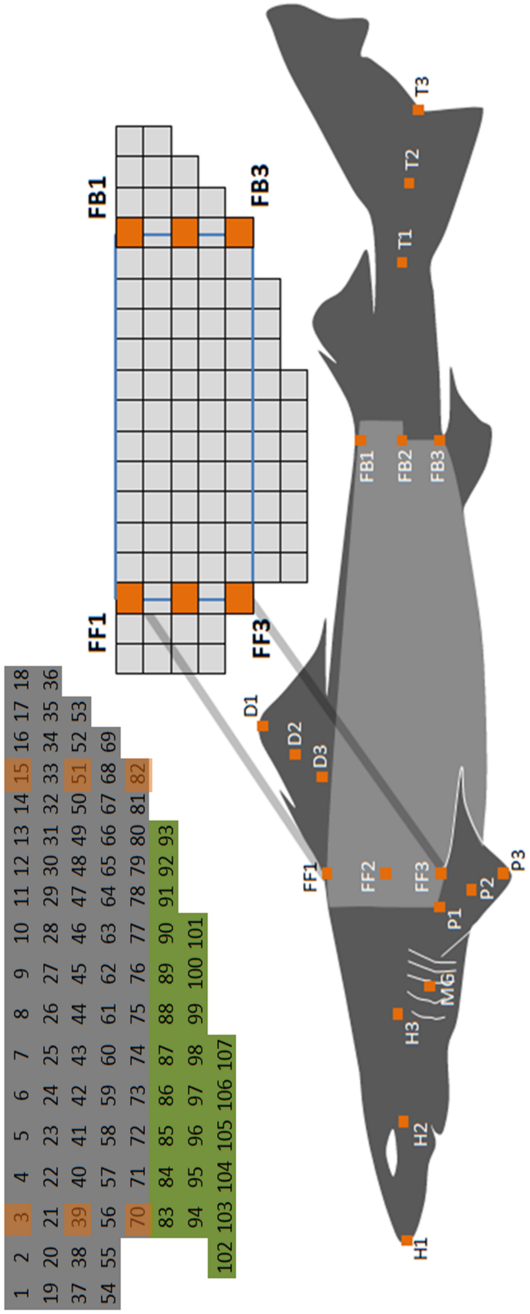

Figure S1.2. Sampling locations of *Centrophorus granulosus*, showing region of high resolution sampling on flank. Green squares indicate data collected but not classified as the flank proper during analyses. Orange squares indicate sampling locations used for both high resolution and low resolution mapping of scale width and length.

c) Scanning electron microscopy

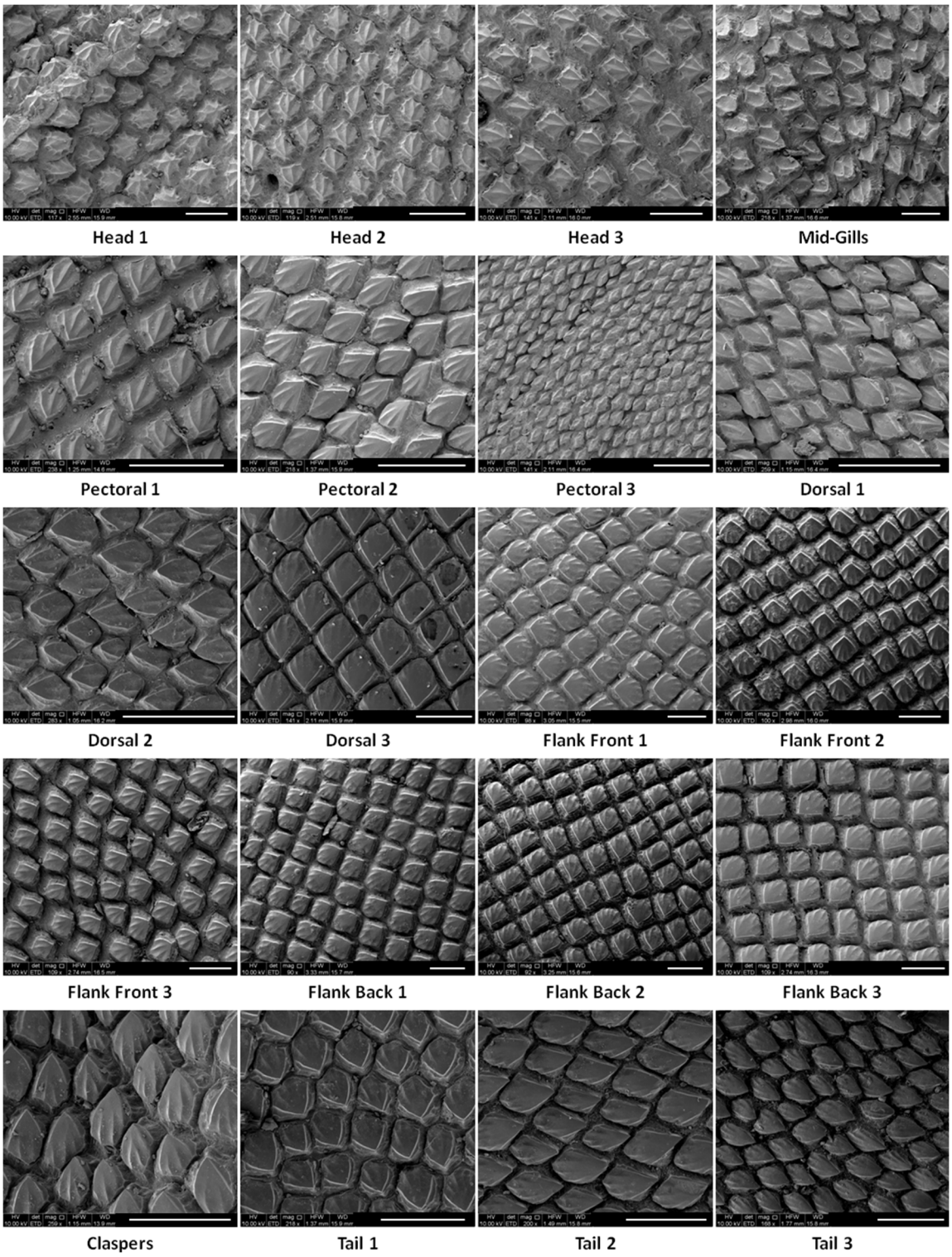

Figure S1.3. Examples of scanning electron micrographs of modern shark skin used for scale measurements and comparative analysis at different sampling locations. Specimen is *Centrophorus granulosus*, a 480mm male. See Chapter 3.1.3. for sampling locations. Scale bars are 500µm.

c) Raw scale crown measurement data

Table S1.1. Raw width measurements (µm) of 15 scale crowns from 20 body locations of a 480mm male *Centrophorus granulosus.* Values rounded to whole digits.

	H1	H2	H3	MG	Pec1	Pec2	Pec3	Dors1	Dors2	Dors3	FF1	FF2	FF3	FB1	FB2	FB3	Cl	Tail1	Tail2	Tail3
Scale 1	268	213	174	150	179	182	77	110	133	333	358	302	259	303	307	350	166	206	192	152
Scale 2	257	228	182	148	138	159	67	95	133	334	279	275	263	300	308	343	157	191	195	154
Scale 3	265	222	179	157	130	167	96	99	156	330	333	275	248	335	298	331	185	187	174	174
Scale 4	232	220	217	156	152	157	97	96	120	325	337	306	245	333	326	309	158	206	162	140
Scale 5	276	227	221	162	142	151	79	105	144	316	333	327	284	344	316	312	187	206	153	158
Scale 6	198	178	208	158	171	165	92	106	118	326	364	256	242	341	305	269	193	206	177	154
Scale 7	225	215	192	182	163	166	80	119	110	319	343	307	260	322	315	309	180	195	200	150
Scale 8	233	210	158	169	188	167	100	107	123	267	295	312	235	330	299	342	149	179	224	162
Scale 9	221	215	146	150	174	137	85	128	142	318	323	271	270	348	278	304	168	219	148	173
Scale 10	259	206	171	150	163	139	67	116	141	355	332	286	224	328	301	316	176	183	160	173
Scale 11	198	225	175	154	176	156	72	115	98	342	334	298	234	337	291	335	179	200	162	164
Scale 12	232	237	143	179	153	147	74	114	103	288	337	292	248	369	317	288	162	189	197	148
Scale 13	259	217	214	168	160	152	66	124	89	319	332	272	216	334	314	284	145	184	222	147
Scale 14	245	230	214	151	174	125	75	129	134	360	320	276	231	343	324	261	-	222	215	131
Scale 15	243	218	172	171	141	142	66	121	126	337	373	286	190	297	292	301	-	175	233	124

Table S1.2. Raw length measurements (µm) of 15 scale crowns from 20 body locations of a 480mm male *Centrophorus granulosus.* Values rounded to whole digits.

	H1	H2	H3	MG	Pec1	Pec2	Pec3	Dors1	Dors2	Dors3	FF1	FF2	FF3	FB1	FB2	FB3	Cl	Tail1	Tail2	Tail3
Scale 1	325	259	232	154	179	218	132	192	193	417	344	259	275	308	272	391	252	227	345	268
Scale 2	193	222	231	172	215	246	117	175	225	343	310	251	256	348	254	340	212	228	303	280
Scale 3	241	258	249	159	199	209	141	174	218	364	355	274	249	354	281	338	260	195	307	293
Scale 4	230	223	219	151	236	211	158	178	193	346	394	262	238	365	272	336	255	191	324	272
Scale 5	233	262	244	139	193	247	168	158	202	357	381	263	271	372	281	340	242	195	352	318
Scale 6	269	244	257	135	238	259	158	159	196	342	400	268	236	393	299	370	304	238	329	223
Scale 7	213	218	211	166	221	221	179	188	211	343	345	268	254	389	338	341	202	212	366	275
Scale 8	225	242	213	147	197	221	162	182	162	345	289	253	239	378	292	333	229	224	351	258
Scale 9	264	260	211	139	220	179	156	213	190	416	341	256	284	414	317	330	279	208	311	261
Scale 10	341	279	210	155	185	236	155	163	180	418	363	270	266	359	284	304	251	229	304	303
Scale 11	269	251	233	198	182	225	156	179	141	416	371	268	293	394	261	301	258	228	344	247
Scale 12	278	227	245	166	185	246	170	189	167	396	322	286	286	394	296	292	207	231	316	290
Scale 13	277	221	240	180	206	189	153	182	108	410	402	280	272	354	311	306	214	234	352	267
Scale 14	270	228	226	169	179	211	167	191	165	441	379	245	212	376	333	298	-	244	345	250
Scale 15	305	223	250	122	178	219	128	196	177	456	388	254	243	359	323	301	-	191	373	262

Table S1.3. Mean width and length measurements (µm) used for high resolution flank study. Mean of 15 scale crowns from 120 body locations of a 480mm male *Centrophorus granulosus*. Sampling locations detailed in Chapter 3.1.3. of main text and supplementary figure A1.2 which precedes this table. Asterisks denotes data from locations detailed in Table 1 and 2.

Sample Location	Mean Width (n=15)	Mean Length (n=15)
CG_001	343.2022	355.7148
CG_002	352.9967333	353.1551333
***CG_003 (FF1)**	332.8147333	359.0219333
CG_004	306.2500667	348.2068
CG_005	287.4680667	301.3404667
CG_006	238.5742	238.1581333
CG_007	213.4942667	227.1436667
CG_008	238.6156	253.8282667
CG_009	232.0419333	253.5458
CG_010	260.2537333	277.4511333
CG_011	289.9298	317.9884667
CG_012	302.1193333	349.6306667
CG_013	283.9075333	337.3041333
CG_014	286.3078	321.8882667
***CG_015 (FB1)**	330.9742667	370.4362667
CG_016	276.6521333	317.4204667
CG_017	294.906	340.4233333
CG_018	236.7892	292.2907333
CG_019	341.0988	360.5124667
CG_020	300.4616	304.7328
CG_021	274.4744667	320.2222
CG_022	283.3530667	309.4782
CG_023	270.2181333	295.4958
CG_024	285.1635333	308.6301333
CG_025	287.8741333	321.2779333
CG_026	320.6712	322.9095333
CG_027	324.3097333	354.9341333
CG_028	300.2768	331.5708667
CG_029	319.4705333	352.7454
CG_030	344.8656	348.0449333
CG_031	320.7544667	371.7474667
CG_032	323.6776667	309.2988
CG_033	312.8450667	345.2823333
CG_034	324.7070667	359.8592667
CG_035	315.1111333	334.4718667
CG_036	339.7396667	354.9452667
CG_037	302.9805333	301.9738
CG_038	236.5091333	255.4742
***CG_039 (FF2)**	289.3248667	263.9144
CG_040	288.437	269.974

CG_041	309.719	304.3975333
CG_042	300.5356	309.2054
CG_043	290.5626	336.3720667
CG_044	305.2065333	315.3381333
CG_045	316.3632	357.3482667
CG_046	312.7708667	329.5219333
CG_047	308.1211333	358.0902
CG_048	318.9006667	324.3064
CG_049	340.1048	349.6798667
CG_050	317.7593333	331.3307333
***CG_051 (FB2)**	306.0026667	294.3224
CG_052	323.7414667	353.2922667
CG_053	320.1056667	332.7737333
CG_054	211.5312	231.5557333
CG_055	210.1222667	225.3413333
CG_056	252.9958	259.0394667
CG_057	249.1372667	270.6431333
CG_058	265.8541333	290.9726
CG_059	268.9488667	290.3234
CG_060	294.8490667	321.6198667
CG_061	293.5878667	309.0010667
CG_062	292.2068	314.7822667
CG_063	298.3280667	301.1434667
CG_064	278.1637333	299.7860667
CG_065	287.1298	316.7651333
CG_066	267.5128	286.0952667
CG_067	264.4452	305.3991333
CG_068	236.8315333	284.4640667
CG_069	269.684	283.8637333
***CG_070 (FF3)**	243.3992	258.2494
CG_071	241.5594	267.3918667
CG_072	267.5684	299.3847333
CG_073	275.7359333	303.1803333
CG_074	281.4974	300.3226
CG_075	272.1116667	298.6636
CG_076	271.8015333	290.8284667
CG_077	290.0711333	311.8188667
CG_078	303.3436667	312.1494667
CG_079	296.9876667	296.5674
CG_080	294.1258	308.5588
CG_081	299.1325333	321.3729333
***CG_082 (FB3)**	310.3322667	328.1878
CG_083	234.1302667	255.5161333
CG_084	242.3046667	273.4233333
CG_085	248.1509333	284.6248667
CG_086	266.5854	292.5008

CG_087	296.8594	325.8781333
CG_088	299.7863333	353.4679333
CG_089	331.1356	360.5499333
CG_090	354.236	387.2304
CG_091	366.2528667	452.4502667
CG_092	395.0169333	429.1254667
CG_093	321.4921333	383.3107333
CG_094	269.5779333	309.4416667
CG_095	297.6537333	333.9079333
CG_096	304.0614667	363.4905333
CG_097	310.4851333	336.7329333
CG_098	316.2746	370.6933333
CG_099	367.7267333	399.8726
CG_100	347.768	370.0480667
CG_101	279.7222667	319.0768667
CG_102	241.0214667	274.3878667
CG_103	247.7571333	279.1179333
CG_104	265.5458667	296.5334667
CG_105	265.8666	291.3410667
CG_106	264.765	289.1823333
CG_107	237.9094667	266.3213333
***CG_Dorsal_01**	112.3004	181.2226667
***CG_Dorsal_02**	124.7366	181.8934
***CG_Dorsal_03**	324.5824	387.3578667
***CG_Head_01**	240.8515333	262.2556
***CG_Head_02**	217.5345333	241.1225333
***CG_Head_03**	184.4107333	231.2929333
***CG_MidGill_01**	160.4341333	156.7788667
***CG_Pec_01**	160.2597333	200.9680667
***CG_Pec_02**	154.1594667	222.5358667
***CG_Pec_03**	79.3728	153.3443333
***CG_Tail_01**	196.5402	218.3247333
***CG_Tail_02**	187.5908	334.8146
***CG_Tail_03**	153.5048	271.0940667

A1.2. Modern Shark Variability Analysis – *Lamna nasus*

a) Specimens

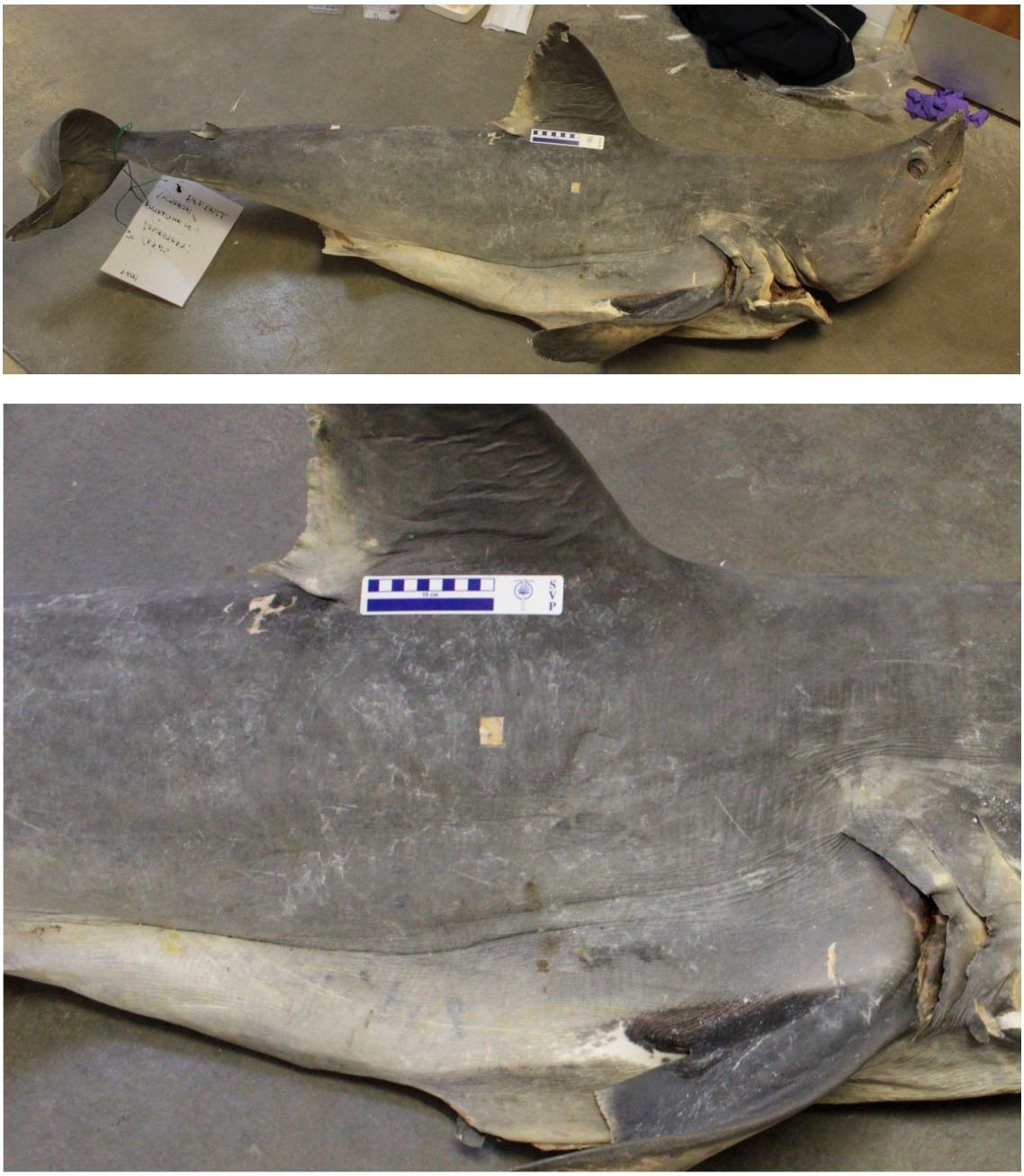

Figure S1.4. Photographs of a porbeagle shark (*Lamna nasus)* specimen during sampling; a 215cm female (see Chapter 3.1.3.) caught in United Kingdom between 2012-2013, and stored at Centre for Environment Fisheries and Aquaculture Science (CEFAS), Lowestoft, UK. Top, lateral view of entire specimen; and bottom shows lateral detail of the flank region. Scale bar fine intervals are 1 cm. Note: test sample removed at centre of flank, not retained for analysis.

Table S1.4. *Lamna nasus* specimens and specimen numbers used in the analysis. All specimens were wild caught and sourced by Victoria Bendall (CEFAS, Lowestoft, United Kingdom).

Species	Specimen Number	Sex	Maturity	Total Length (cm)
Lamna nasus	***LN 01***	**F**	Mature	**215**
Lamna nasus	***LN 03***	**F**	Immature	**186**
Lamna nasus	***LN 04***	**F**	Immature	**127**
Lamna nasus	***LN 05***	**M**	Immature	**146**
Lamna nasus	***LN 06***	**M**	Mature	**183**

Maturity = Males over 165cm and females over 195cm defined as mature, according to Ebert *et al.* 2013.

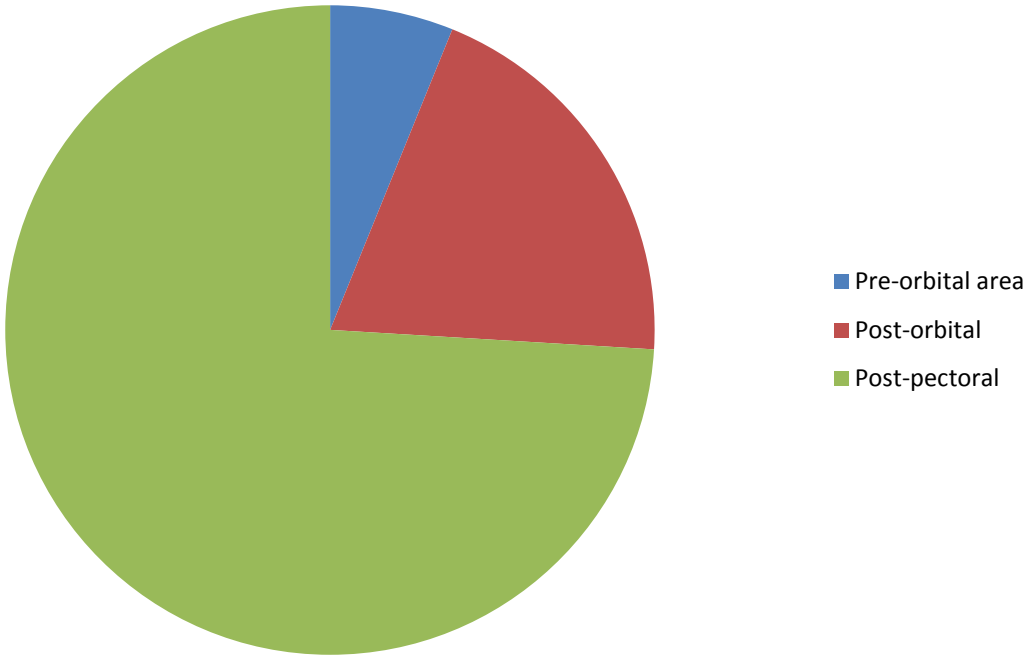

Figure S1.5. Mean percentage area of different regions (defined in body text) of fish bodies (n =123).

b) Scanning electron microscopy

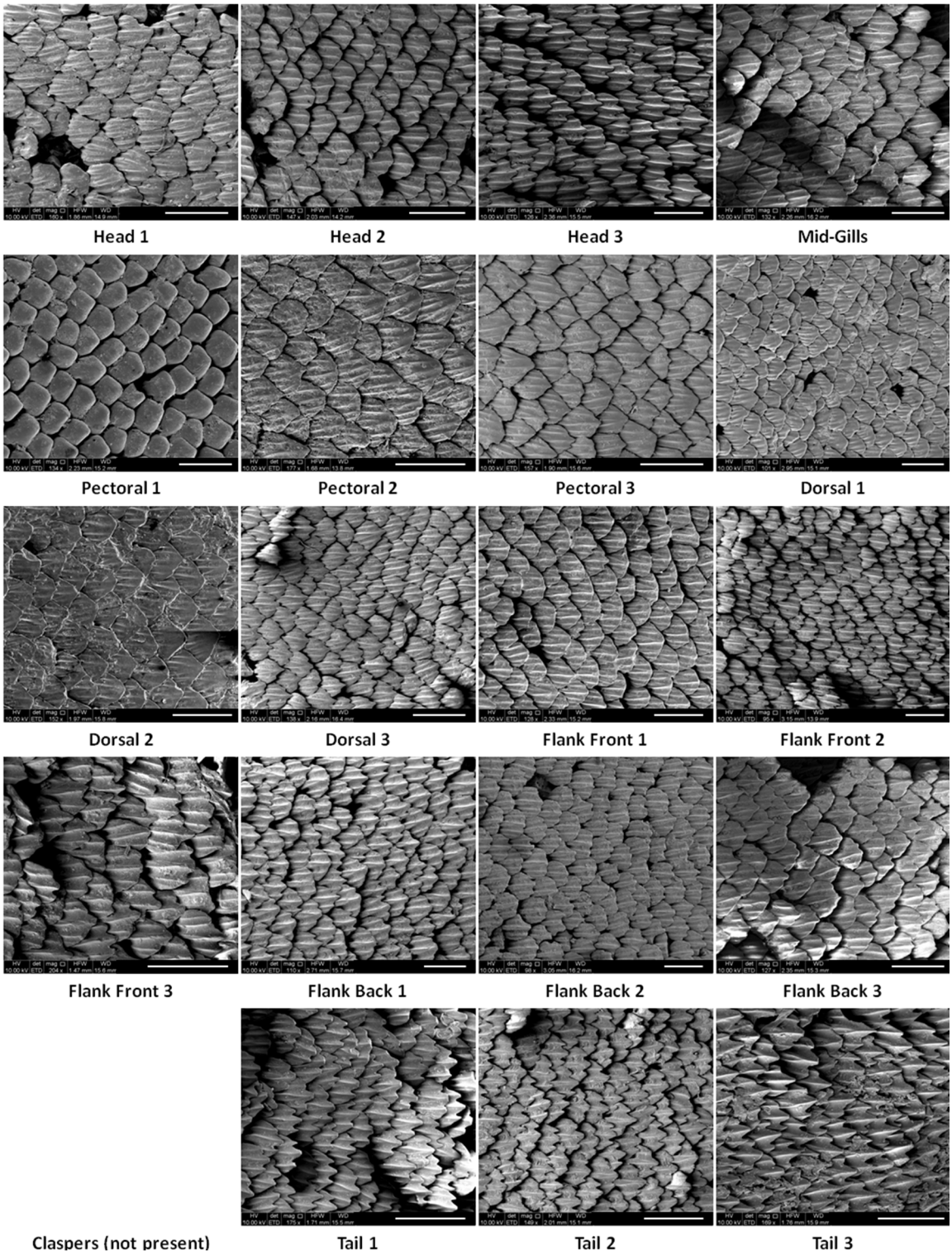

Figure 1.6. Examples of scanning electron micrographs of modern shark skin used for scale measurements and comparative analysis at different sampling locations. Specimen is *Lamna nasus* LN01, a 215cm mature female. See Chapter 3.1.3. for sampling locations. Scale bars are 500µm.

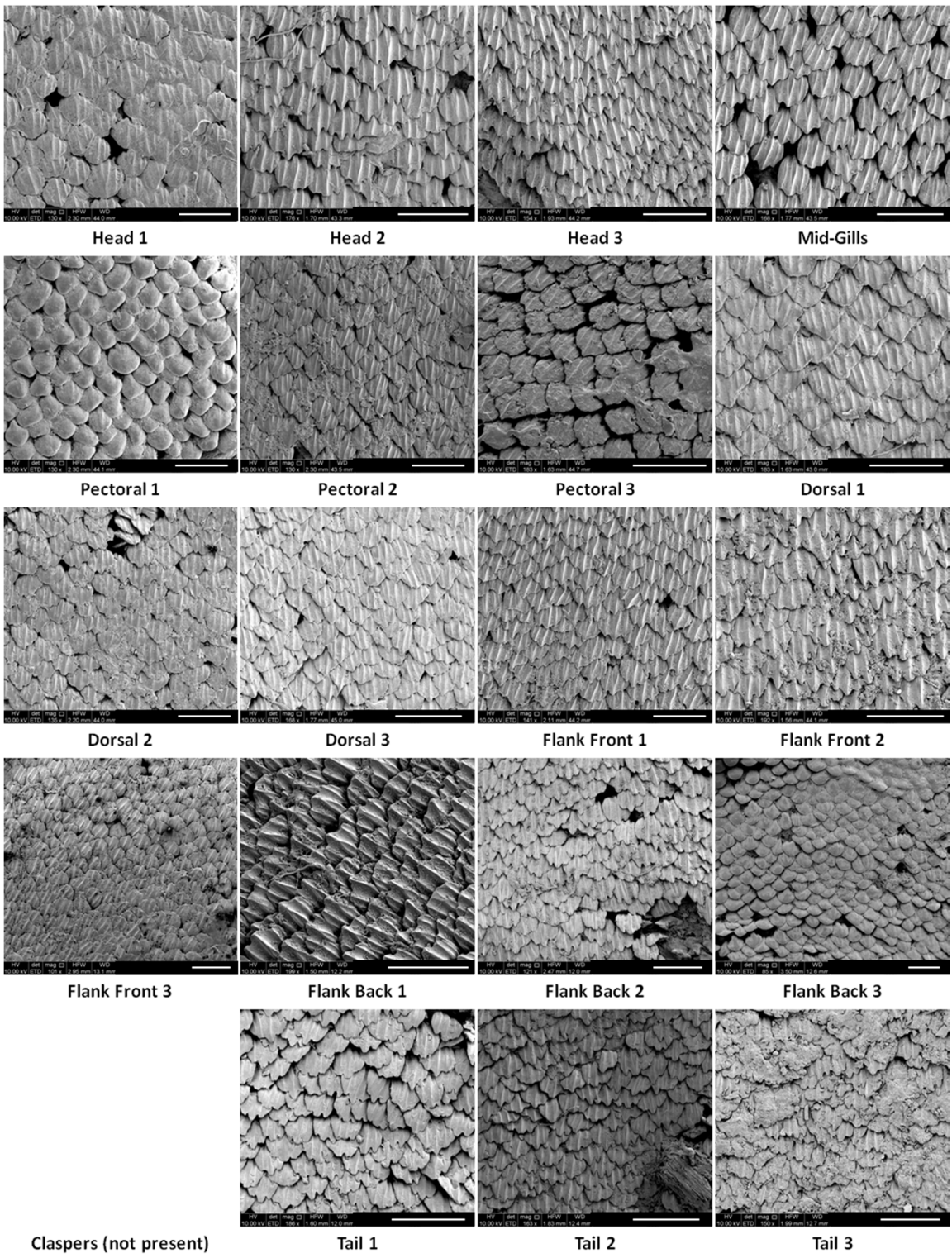

Figure S1.7. Examples of scanning electron micrographs of modern shark skin used for scale measurements and comparative analysis at different sampling locations. Specimen is *Lamna nasus* LN03, a 186cm immature female. See Chapter 3.1.3. for sampling locations. Scale bars are 500µm.

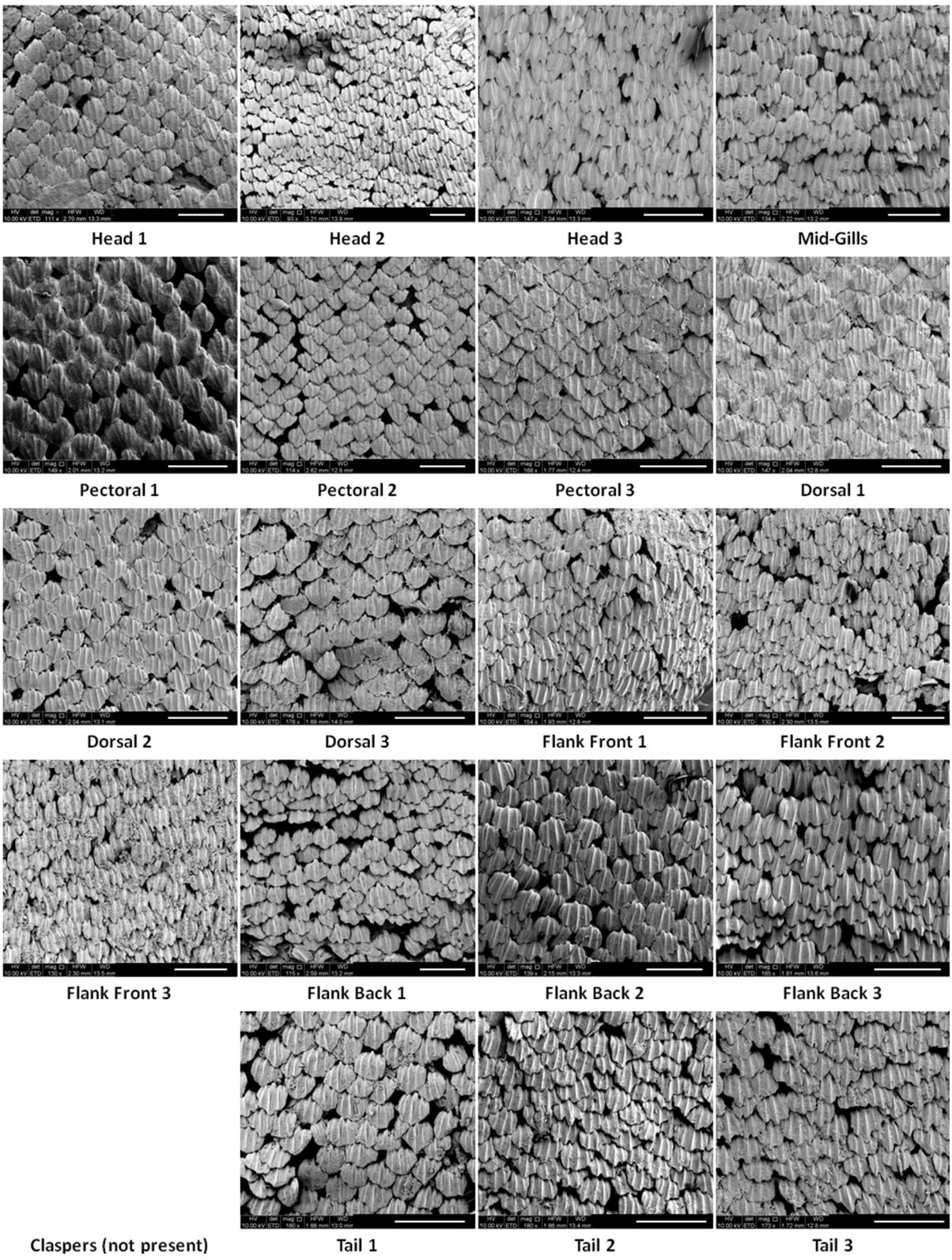

Figure S1.8. Examples of scanning electron micrographs of modern shark skin used for scale measurements and comparative analysis at different sampling locations. Specimen is *Lamna nasus* specimen LN04, a 127cm immature female. See Chapter 3.1.3. for sampling locations. Scale bars are 500µm.

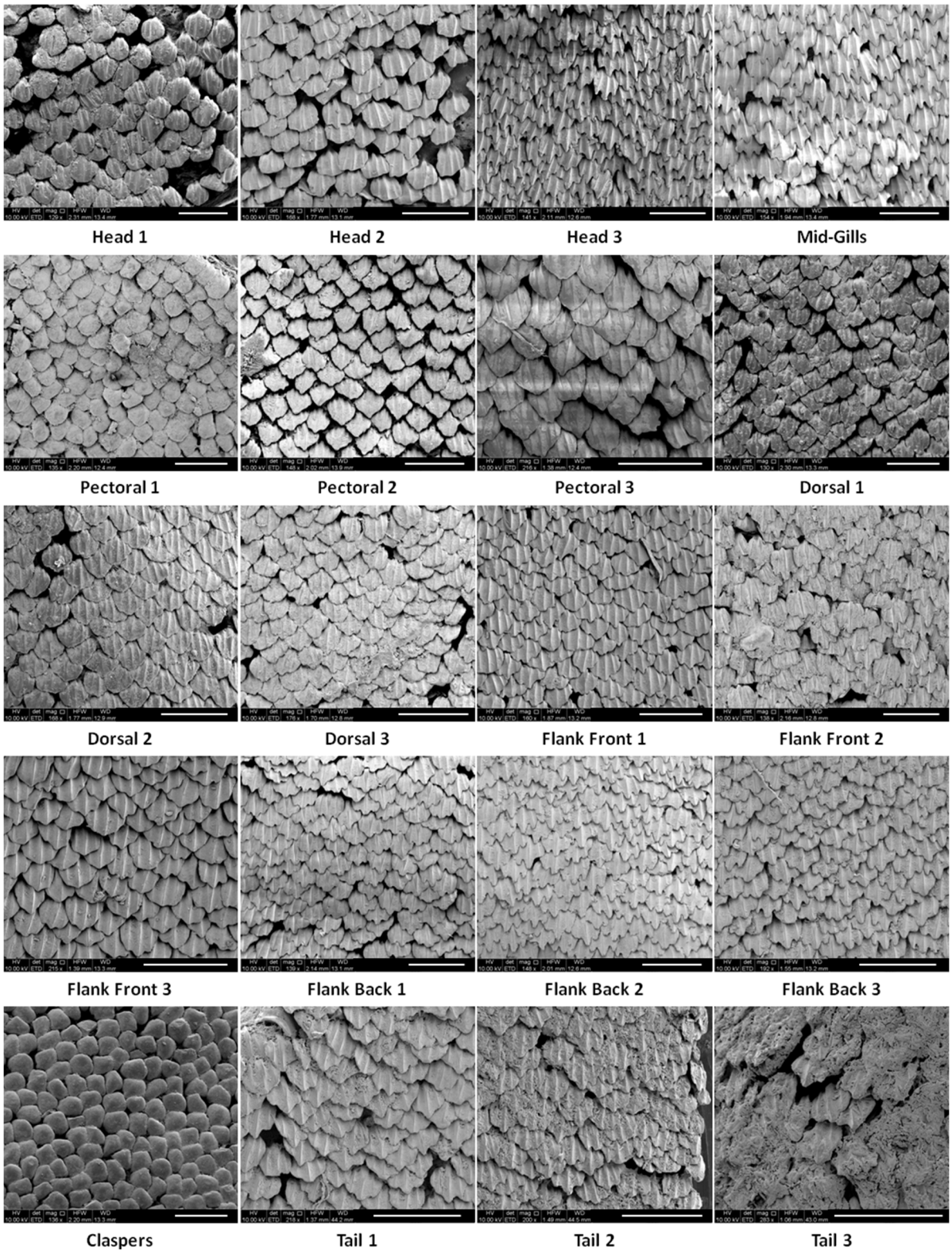

Figure S1.9. Examples of scanning electron micrographs of modern shark skin used for scale measurements and comparative analysis at different sampling locations. Specimen is *Lamna nasus* specimen LN05, a 146cm immature male. See Chapter 3.1.3. for sampling locations. Scale bars are 500µm.

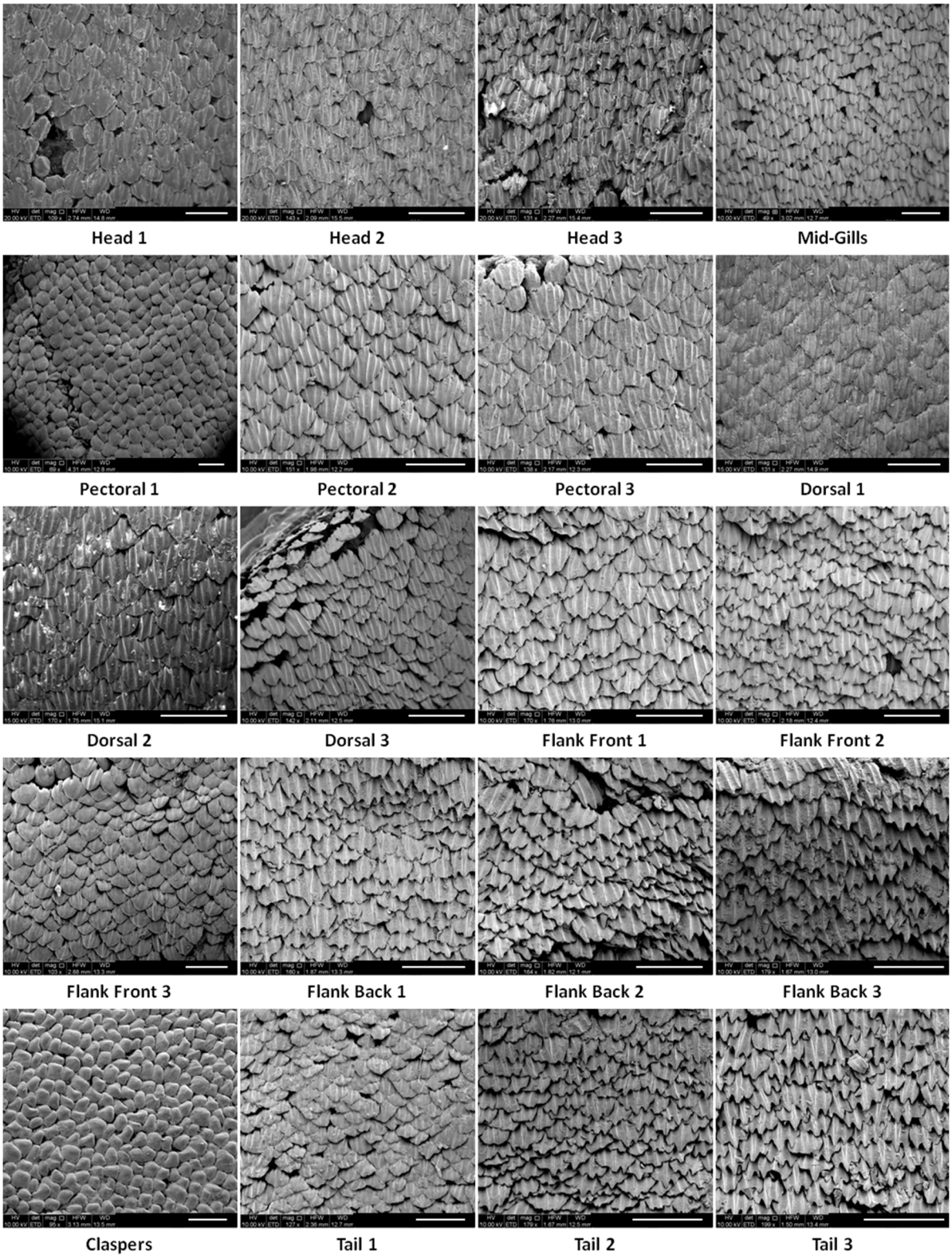

Figure S1.10. Examples of scanning electron micrographs of modern shark skin used for scale measurements and comparative analysis at different sampling locations. Specimen is *Lamna nasus* specimen LN06, a 183cm mature male. See Chapter 3.1.3. for sampling locations. Scale bars are 500µm.

c) Riblet spacing measurements

Table S1.5. Riblet spacing measurements (µm) for scales at different sampling locations of *Lamna nasus* specimen LN01, a 215cm mature female. See Chapter 3.1.3. for sampling locations. Note pelvic claspers were not present, other missing data denotes riblets were not present on the scale crowns. Values have been rounded to whole digits.

	H1	**H2**	**H3**	**MG**	**Pec1**	**Pec2**	**Pec3**	**Dors1**	**Dors2**	**Dors3**	**FF1**	**FF2**	**FF3**	**FB1**	**FB2**	**FB3**	**Cl**	**Tail1**	**Tail2**	**Tail3**
Scale 1	59	64	67	56	-	57	52	38	57	44	56	80	60	65	71	71	-	57	70	68
Scale 2	44	55	64	57	-	47	42	42	45	37	61	72	55	74	58	71	-	53	66	78
Scale 3	53	64	71	55	-	39	45	48	41	49	61	85	55	77	70	69	-	55	74	74
Scale 4	54	60	70	64	-	44	48	41	51	39	55	61	56	79	58	68	-	66	62	81
Scale 5	41	62	68	61	-	45	40	47	48	44	53	71	66	63	64	64	-	49	64	81
Scale 6	54	69	64	65	-	41	42	39	47	42	58	70	59	80	79	68	-	51	77	77
Scale 7	47	71	75	48	-	40	48	40	38	39	58	70	56	73	65	68	-	64	67	61
Scale 8	44	73	67	53	-	42	48	45	40	38	49	67	55	66	70	63	-	56	71	65
Scale 9	40	57	61	66	-	40	46	41	41	39	54	70	65	77	56	54	-	70	72	88
Scale 10	46	73	57	67	-	40	49	44	40	45	55	67	69	71	69	61	-	51	69	79
Scale 11	47	71	71	48	-	43	48	40	42	39	48	70	59	62	67	57	-	65	72	75
Scale 12	56	70	59	58	-	40	45	40	49	52	47	71	55	73	67	61	-	60	72	67
Scale 13	51	67	61	48	-	39	46	36	58	37	56	60	61	81	61	66	-	62	65	73
Scale 14	43	61	57	55	-	45	52	45	62	44	55	67	64	79	74	67	-	62	67	70
Scale 15	53	77	68	55	-	39	53	44	47	47	55	72	55	82	61	65	-	66	74	69

Table S1.6. Riblet spacing measurements (µm) for scales at different sampling locations of *Lamna nasus* specimen LN03, a 186cm immature female. Note pelvic claspers were not present; other missing data denotes riblets were not present on the scale crowns. See Chapter 3.1.3. for sampling locations. Values have been rounded to whole digits.

	H1	H2	H3	MG	Pec1	Pec2	Pec3	Dors1	Dors2	Dors3	FF1	FF2	FF3	FB1	FB2	FB3	Cl	Tail1	Tail2	Tail3
Scale 1	70	59	63	47	-	43	39	43	46	44	51	65	58	44	60	45	-	44	45	37
Scale 2	56	59	54	48	-	51	46	50	41	28	45	58	59	60	62	54	-	46	59	40
Scale 3	55	52	42	62	-	39	63	44	40	33	59	67	51	60	59	60	-	47	55	50
Scale 4	65	56	60	61	-	46	56	44	39	32	54	60	57	62	75	44	-	42	50	42
Scale 5	54	58	59	65	-	44	48	44	37	42	63	52	56	89	64	49	-	44	49	47
Scale 6	58	68	56	53	-	41	46	39	37	32	48	63	55	61	75	45	-	42	36	46
Scale 7	52	61	55	59	-	50	43	33	40	32	65	69	48	71	67	44	-	47	47	39
Scale 8	59	62	52	56	-	45	48	42	39	43	49	68	67	63	72	48	-	45	40	41
Scale 9	64	55	52	57	-	44	44	46	46	31	45	52	58	74	73	38	-	48	40	42
Scale 10	59	48	56	50	-	46	49	44	31	46	44	75	56	63	72	42	-	39	45	36
Scale 11	45	44	56	57	-	37	43	49	36	35	43	75	59	69	63	45	-	54	39	36
Scale 12	56	61	55	55	-	45	49	36	38	30	59	83	49	51	76	-	-	37	53	43
Scale 13	59	53	54	63	-	44	49	42	47	46	67	67	48	80	69	-	-	44	48	38
Scale 14	67	57	52	58	-	46	52	45	50	46	46	66	52	55	56	-	-	44	41	49
Scale 15	49	55	62	46	-	44	43	40	40	42	59	57	64	50	66	-	-	40	53	49

Table S1.7. Riblet spacing measurements (µm) for scales at different sampling locations of *Lamna nasus* specimen LN04, a 127cm immature female. Note pelvic claspers were not present; other missing data denotes riblets were not present on the scale crowns. See Chapter 3.1.3. for sampling locations. Values have been rounded to whole digits.

	H1	H2	H3	MG	Pec1	Pec2	Pec3	Dors1	Dors2	Dors3	FF1	FF2	FF3	FB1	FB2	FB3	Cl	Tail1	Tail2	Tail3
Scale 1	59	67	51	57	-	47	50	47	49	43	59	59	70	70	65	49	-	47	50	48
Scale 2	58	59	65	55	-	53	52	44	39	43	44	73	57	89	50	52	-	46	47	49
Scale 3	60	66	47	56	-	39	60	41	38	39	47	54	59	83	67	54	-	39	39	48
Scale 4	53	75	54	54	-	44	52	38	44	39	55	60	56	76	59	62	-	43	42	52
Scale 5	58	59	65	51	-	50	56	35	41	41	49	65	59	64	47	73	-	40	41	51
Scale 6	58	51	68	55	-	48	58	42	46	42	53	59	55	62	63	56	-	35	36	42
Scale 7	59	73	59	57	-	47	43	43	44	37	55	60	60	78	73	72	-	47	53	49
Scale 8	61	58	57	69	-	54	58	42	33	41	51	60	53	65	53	59	-	37	44	52
Scale 9	56	60	66	54	-	44	63	41	38	38	53	58	61	84	55	56	-	45	46	52
Scale 10	65	62	67	68	-	52	59	39	46	42	46	71	54	69	49	51	-	36	46	52
Scale 11	57	62	64	58	-	56	54	46	39	45	48	66	46	76	57	61	-	40	43	51
Scale 12	52	74	59	53	-	56	56	44	38	45	49	62	57	66	63	50	-	45	47	51
Scale 13	64	64	74	63	-	41	57	43	39	39	55	55	60	73	74	53	-	44	42	51
Scale 14	56	55	64	63	-	41	55	42	36	40	50	54	52	67	47	49	-	41	44	51
Scale 15	56	73	67	59	-	47	54	42	42	35	52	51	48	54	51	62	-	46	39	48

Table S1.8. Riblet spacing measurements (µm) for scales at different sampling locations of *Lamna nasus* specimen LN05, a 146cm immature male. Note pelvic claspers were present; however missing data denotes riblets were not present on the scale crowns. See Chapter 3.1.3. for sampling locations. Values have been rounded to whole digits.

	H1	H2	H3	MG	Pec1	Pec2	Pec3	Dors1	Dors2	Dors3	FF1	FF2	FF3	FB1	FB2	FB3	Cl	Tail1	Tail2	Tail3
Scale 1	57	55	62	61	-	52	50	42	48	50	53	58	49	61	87	55	-	51	58	59
Scale 2	49	60	59	65	-	49	52	45	46	48	51	64	55	68	69	55	-	50	56	55
Scale 3	50	62	64	56	-	47	54	44	47	43	48	64	55	56	69	64	-	50	52	51
Scale 4	66	53	60	64	-	46	44	50	47	46	57	54	65	65	79	58	-	58	53	47
Scale 5	61	55	67	54	-	43	47	47	50	37	52	59	49	53	70	59	-	54	46	43
Scale 6	59	52	63	54	-	35	48	45	48	50	45	75	56	63	69	46	-	49	46	46
Scale 7	47	49	67	77	-	52	44	49	48	43	46	50	56	58	79	58	-	50	45	42
Scale 8	56	51	54	56	-	49	39	55	41	39	61	55	63	64	58	61	-	48	57	40
Scale 9	62	45	65	62	-	47	47	50	61	45	55	67	52	65	65	61	-	56	43	38
Scale 10	58	55	58	55	-	48	42	42	51	49	55	67	54	62	67	72	-	45	50	42
Scale 11	61	56	61	62	-	46	45	51	42	41	49	64	51	64	72	68	-	50	51	40
Scale 12	56	51	68	58	-	46	46	48	49	55	46	60	53	61	76	57	-	46	37	36
Scale 13	58	58	69	56	-	58	55	49	53	47	55	63	56	59	71	65	-	56	57	43
Scale 14	63	60	66	55	-	45	47	39	40	42	44	66	62	53	56	60	-	57	52	40
Scale 15	47	48	61	53	-	47	47	43	40	44	42	66	62	58	66	55	-	45	47	38

Table S1.9. Riblet spacing measurements (µm) for scales at different sampling locations of *Lamna nasus* specimen LN06, a 183cm mature male. Note pelvic claspers were present; however missing data denotes riblets were not present on the scale crowns. See Chapter 3.1.3. for sampling locations. Values have been rounded to whole digits.

	H1	H2	H3	MG	Pec1	Pec2	Pec3	Dors1	Dors2	Dors3	FF1	FF2	FF3	FB1	FB2	FB3	Cl	Tail1	Tail2	Tail3
Scale 1	80	69	60	68	-	57	68	54	49	39	55	57	55	78	73	58	-	43	58	45
Scale 2	58	59	60	60	-	51	55	47	49	43	62	70	56	68	64	72	-	58	49	63
Scale 3	73	74	54	51	-	50	48	48	55	45	52	58	62	69	71	57	-	45	58	56
Scale 4	62	58	63	60	-	58	55	44	44	38	58	59	55	67	63	80	-	50	46	48
Scale 5	72	67	60	65	-	57	54	55	47	37	57	52	51	70	66	64	-	56	55	46
Scale 6	73	62	67	73	-	52	57	48	52	42	65	58	55	75	54	66	-	49	45	59
Scale 7	76	61	62	61	-	42	54	50	49	42	68	60	58	66	69	64	-	51	49	47
Scale 8	65	65	78	79	-	50	55	52	46	39	62	62	63	64	62	67	-	48	44	53
Scale 9	60	54	61	69	-	51	53	46	54	46	61	72	51	54	63	68	-	50	58	52
Scale 10	60	60	56	65	-	51	52	57	49	37	53	70	54	66	59	70	-	55	52	45
Scale 11	56	58	59	69	-	52	55	45	51	39	64	71	54	70	72	62	-	55	50	59
Scale 12	69	62	67	64	-	55	50	51	50	43	66	66	56	68	58	63	-	50	55	56
Scale 13	62	65	62	69	-	52	60	50	50	44	63	74	54	74	70	72	-	49	48	45
Scale 14	51	73	61	61	-	52	48	44	49	47	61	58	56	72	67	67	-	49	59	50
Scale 15	54	55	64	60	-	53	58	51	52	38	58	72	55	62	58	65	-	50	51	46

c) Crown width measurements

Table S1.10. Crown width measurements (µm) for scale crowns at different sampling locations of *Lamna nasus* specimen LN01, a 215cm mature female. See Chapter 3.1.3. for sampling locations. Values have been rounded to whole digits.

	H1	H2	H3	MG	Pec1	Pec2	Pec3	Dors1	Dors2	Dors3	FF1	FF2	FF3	FB1	FB2	FB3	Cl	Tail1	Tail2	Tail3
Scale 1	294	307	334	290	300	285	292	301	282	254	311	306	271	319	328	322	-	274	274	277
Scale 2	269	321	312	277	265	253	248	312	296	228	320	335	290	340	294	328	-	226	246	261
Scale 3	315	265	308	307	321	253	302	294	285	229	360	370	288	355	322	358	-	267	266	284
Scale 4	273	239	326	385	265	221	253	307	286	242	332	297	246	305	319	297	-	263	276	305
Scale 5	258	317	313	308	276	232	233	312	322	231	319	282	260	320	350	286	-	260	325	293
Scale 6	292	275	298	340	259	283	281	313	302	257	309	318	300	401	378	297	-	239	320	255
Scale 7	252	308	339	306	338	243	260	251	303	228	366	303	255	328	310	307	-	271	274	293
Scale 8	280	312	305	313	290	277	299	306	295	223	338	279	275	307	390	323	-	226	285	237
Scale 9	275	309	312	328	270	288	227	301	300	222	417	290	304	341	328	323	-	296	279	266
Scale 10	300	267	290	313	288	239	311	358	303	218	393	303	281	321	330	266	-	248	276	240
Scale 11	342	266	384	323	224	246	301	291	291	219	323	306	234	382	330	261	-	263	306	248
Scale 12	283	268	328	302	299	249	272	265	241	272	300	318	232	365	338	253	-	245	302	215
Scale 13	258	283	303	328	277	233	254	250	295	228	332	269	252	344	382	298	-	307	268	261
Scale 14	279	272	318	283	283	267	283	262	293	269	266	339	268	392	328	340	-	265	275	257
Scale 15	292	328	290	296	245	210	274	244	320	277	285	307	212	326	322	294	-	293	287	255

Table S1.11. Crown width measurements (µm) for scale crowns at different sampling locations of *Lamna nasus* specimen LN03, a 186cm immature female. See Chapter 3.1.3. for sampling locations. Values have been rounded to whole digits.

	H1	H2	H3	MG	Pec1	Pec2	Pec3	Dors1	Dors2	Dors3	FF1	FF2	FF3	FB1	FB2	FB3	Cl	Tail1	Tail2	Tail3
Scale 1	276	256	252	231	213	267	195	272	236	237	251	263	215	260	239	234	-	259	184	196
Scale 2	305	251	242	249	222	245	237	279	246	181	251	245	239	256	275	285	-	225	224	210
Scale 3	299	227	233	252	228	208	246	281	258	179	352	263	261	256	249	292	-	246	234	221
Scale 4	272	275	272	262	200	248	230	277	197	208	268	260	206	259	254	239	-	195	230	210
Scale 5	273	262	256	251	209	218	223	222	235	191	339	248	254	289	254	229	-	244	210	180
Scale 6	301	279	266	247	235	220	184	208	254	209	239	229	243	278	284	240	-	208	188	212
Scale 7	367	252	255	256	222	226	193	215	253	177	314	260	208	248	264	230	-	237	212	201
Scale 8	279	296	246	241	245	251	242	256	201	235	238	240	253	271	282	256	-	184	193	186
Scale 9	330	256	255	260	257	229	173	270	253	202	261	251	223	303	290	221	-	253	210	214
Scale 10	299	248	323	234	259	217	225	265	218	216	272	260	221	266	274	222	-	204	224	191
Scale 11	255	259	251	252	214	203	209	343	216	174	229	276	252	282	283	229	-	210	240	187
Scale 12	269	270	250	258	312	223	233	221	204	199	344	272	230	290	341	-	-	213	272	182
Scale 13	318	241	260	258	237	201	173	282	238	204	197	243	230	291	265	-	-	202	245	192
Scale 14	304	258	236	272	223	240	172	247	241	205	268	256	217	230	273	-	-	187	194	190
Scale 15	276	267	233	258	221	259	214	243	240	177	331	227	229	243	265	-	-	178	281	247

Table S1.12. Crown width measurements (µm) for scale crowns at different sampling locations of *Lamna nasus* specimen LN04, a 127cm immature female. See Chapter 3.1.3. for sampling locations. Values have been rounded to whole digits.

	H1	H2	H3	MG	Pec1	Pec2	Pec3	Dors1	Dors2	Dors3	FF1	FF2	FF3	FB1	FB2	FB3	Cl	Tail1	Tail2	Tail3
Scale 1	228	263	206	259	237	203	196	237	233	192	265	262	255	304	251	201	-	237	227	261
Scale 2	260	230	232	270	221	225	232	254	193	187	250	262	244	289	220	214	-	232	204	223
Scale 3	252	224	212	230	245	187	202	223	195	177	246	228	232	341	285	243	-	215	189	223
Scale 4	251	244	238	248	251	216	221	230	220	211	258	258	215	315	294	262	-	210	178	255
Scale 5	302	250	230	260	246	215	231	244	206	196	236	252	235	268	215	264	-	194	188	239
Scale 6	267	193	249	257	230	206	205	249	223	181	252	254	212	275	243	227	-	182	177	194
Scale 7	273	267	231	215	218	212	214	256	239	173	249	256	233	290	282	251	-	191	216	263
Scale 8	305	273	224	239	231	203	219	252	193	185	226	273	206	299	244	234	-	213	210	233
Scale 9	253	234	255	255	216	171	246	236	232	187	281	244	215	284	247	230	-	216	213	261
Scale 10	271	257	262	260	231	230	224	262	247	204	217	273	233	317	236	227	-	196	205	232
Scale 11	265	217	242	249	230	214	222	252	244	193	223	267	210	340	267	245	-	190	243	210
Scale 12	249	239	219	270	240	229	196	225	232	216	245	259	218	286	276	216	-	231	239	223
Scale 13	240	252	267	242	239	177	201	242	211	175	276	223	250	312	285	253	-	209	202	251
Scale 14	227	218	257	237	242	219	205	231	223	185	286	282	195	278	256	240	-	219	235	256
Scale 15	284	243	247	253	232	236	193	223	250	171	250	229	192	303	261	253	-	219	242	221

Table S1.13. Riblet Crown width measurements (µm) for scale crowns at different sampling locations of *Lamna nasus* specimen LN05, a 146cm immature male. See Chapter 3.1.3. for sampling locations. Values have been rounded to whole digits.

	H1	H2	H3	MG	Pec1	Pec2	Pec3	Dors1	Dors2	Dors3	FF1	FF2	FF3	FB1	FB2	FB3	Cl	Tail1	Tail2	Tail3
Scale 1	265	244	237	251	206	212	243	182	229	229	218	254	179	221	284	189	-	194	250	208
Scale 2	273	261	214	223	184	215	216	225	224	196	259	242	235	246	239	208	-	216	238	234
Scale 3	235	262	197	224	180	213	248	218	235	192	219	212	220	224	258	232	-	187	193	206
Scale 4	270	201	241	233	221	195	200	221	249	217	204	225	213	266	269	194	-	233	175	205
Scale 5	263	234	221	234	182	205	201	240	228	175	261	255	182	246	259	200	-	229	210	221
Scale 6	268	205	219	204	233	188	211	225	210	242	222	262	191	225	235	185	-	217	175	238
Scale 7	229	232	229	228	182	241	200	234	213	196	230	224	216	223	288	204	-	204	167	192
Scale 8	220	229	162	228	205	213	197	215	216	197	262	213	216	268	242	213	-	180	210	186
Scale 9	243	189	212	240	212	242	228	237	208	177	210	255	211	255	270	208	-	214	170	257
Scale 10	250	228	212	211	222	211	189	213	220	233	244	246	229	254	289	218	-	204	228	181
Scale 11	296	231	231	224	224	249	234	223	208	202	220	238	200	249	280	230	-	204	200	195
Scale 12	237	253	213	226	203	213	202	205	225	226	267	274	227	234	247	176	-	213	197	138
Scale 13	234	222	258	234	193	204	240	223	224	190	228	246	226	270	265	218	-	215	204	162
Scale 14	285	244	218	242	230	198	222	228	239	174	206	268	230	240	227	213	-	209	207	138
Scale 15	241	218	224	198	182	225	222	220	210	189	189	239	235	253	265	207	-	198	208	173

Table S1.14. Crown width measurements (µm) for scale crowns at different sampling locations of *Lamna nasus* specimen LN06, a 183cm mature male. See Chapter 3.1.3. for sampling locations. Values have been rounded to whole digits.

	H1	H2	H3	MG	Pec1	Pec2	Pec3	Dors1	Dors2	Dors3	FF1	FF2	FF3	FB1	FB2	FB3	Cl	Tail1	Tail2	Tail3
Scale 1	342	277	242	240	267	302	355	216	255	219	283	261	259	332	301	230	-	224	196	235
Scale 2	380	225	222	260	257	302	324	208	279	216	326	339	259	267	279	328	-	248	286	265
Scale 3	328	260	248	238	226	296	307	296	260	193	310	206	269	232	264	225	-	191	264	237
Scale 4	275	222	274	247	235	298	296	219	247	198	283	263	259	274	259	291	-	270	185	175
Scale 5	327	286	255	231	273	282	291	257	204	158	309	255	262	256	278	256	-	278	262	170
Scale 6	325	260	235	254	223	305	342	293	283	200	348	259	234	288	253	258	-	275	269	286
Scale 7	323	243	300	234	291	197	324	235	237	192	356	216	265	244	321	282	-	324	223	212
Scale 8	331	329	301	283	271	211	294	277	222	201	279	228	256	254	329	251	-	282	215	192
Scale 9	321	228	232	278	258	282	271	272	303	216	291	314	253	244	248	227	-	228	231	212
Scale 10	273	247	211	246	183	263	335	311	235	179	291	252	246	343	239	262	-	227	203	214
Scale 11	220	246	314	287	279	276	282	249	273	170	293	305	235	342	311	217	-	277	251	250
Scale 12	310	219	322	248	230	278	325	237	271	199	305	241	232	340	256	231	-	263	245	204
Scale 13	299	256	222	249	256	294	320	257	289	214	306	303	234	329	290	299	-	282	175	192
Scale 14	228	291	248	272	215	239	285	221	229	183	343	260	246	349	294	230	-	286	226	207
Scale 15	236	227	251	257	297	266	315	227	260	159	331	336	307	260	264	222	-	277	255	204

d) Exposed scale length measurements

Table S1.15. Exposed crown length measurements (µm) for scales at different sampling locations of *Lamna nasus* specimen LN01, a 215cm mature female. See Chapter 3.1.3. for sampling locations. Values have been rounded to whole digits.

	H1	H2	H3	MG	Pec1	Pec2	Pec3	Dors1	Dors2	Dors3	FF1	FF2	FF3	FB1	FB2	FB3	Cl	Tail1	Tail2	Tail3
Scale 1	304	229	338	311	241	262	384	254	306	300	297	304	241	320	296	309	-	219	269	326
Scale 2	225	236	308	235	278	279	283	297	274	263	265	330	276	334	274	360	-	267	239	229
Scale 3	216	216	330	306	272	258	312	302	252	261	307	356	220	304	299	365	-	286	247	236
Scale 4	255	234	323	412	407	262	268	248	207	267	240	338	284	340	293	341	-	185	238	341
Scale 5	269	191	301	295	262	239	307	227	248	239	289	270	307	327	332	325	-	216	247	262
Scale 6	279	222	311	342	285	287	270	218	260	252	281	337	219	333	360	351	-	186	288	320
Scale 7	288	246	309	370	315	223	343	217	278	205	248	310	292	274	246	256	-	226	277	175
Scale 8	231	263	322	283	264	272	266	252	257	259	285	307	239	327	344	318	-	242	222	223
Scale 9	270	238	348	332	287	232	301	257	303	259	221	327	324	296	317	274	-	253	245	281
Scale 10	293	238	314	309	304	288	381	310	302	242	314	283	218	300	343	262	-	194	235	255
Scale 11	263	237	342	382	268	327	260	303	258	251	281	369	240	337	341	294	-	187	224	225
Scale 12	266	248	298	363	270	221	305	211	232	266	280	314	197	324	301	258	-	219	233	198
Scale 13	330	254	356	353	267	319	254	235	325	307	325	337	241	305	330	275	-	210	254	236
Scale 14	271	242	290	261	306	251	316	263	299	272	256	370	223	317	311	280	-	283	197	229
Scale 15	375	261	327	259	261	270	311	320	279	323	259	332	296	347	288	336	-	209	233	221

Table S1.16. Exposed crown length measurements (µm) for scales at different sampling locations of *Lamna nasus* specimen LN03, a 186cm immature female. See Chapter 3.1.3. for sampling locations. Values have been rounded to whole digits.

	H1	H2	H3	MG	Pec1	Pec2	Pec3	Dors1	Dors2	Dors3	FF1	FF2	FF3	FB1	FB2	FB3	Cl	Tail1	Tail2	Tail3
Scale 1	288	238	222	262	233	311	197	256	244	203	214	216	203	213	226	214	-	175	201	215
Scale 2	276	235	281	271	252	271	178	276	233	176	205	236	236	214	241	220	-	172	150	177
Scale 3	293	213	225	250	223	266	207	282	192	217	271	246	209	234	247	194	-	205	195	198
Scale 4	268	251	294	270	197	284	232	189	218	216	215	262	195	230	242	199	-	175	201	206
Scale 5	265	230	230	216	199	197	239	211	238	198	239	243	235	222	219	221	-	181	154	161
Scale 6	274	283	310	323	249	275	210	234	240	239	218	249	225	219	177	190	-	131	179	205
Scale 7	340	254	180	295	211	275	238	220	258	173	251	225	260	190	272	233	-	186	197	226
Scale 8	337	187	242	313	214	291	218	239	228	217	235	246	193	201	198	226	-	146	193	195
Scale 9	339	281	328	310	237	211	218	313	230	193	192	258	166	215	228	187	-	233	179	165
Scale 10	297	200	297	267	212	243	225	257	196	216	221	250	223	175	257	198	-	188	178	192
Scale 11	276	221	187	265	226	245	214	342	215	230	239	224	203	224	246	227	-	157	188	151
Scale 12	290	238	232	277	291	286	231	272	202	229	278	167	152	215	240	-	-	196	201	137
Scale 13	282	242	185	292	209	248	192	244	237	185	211	203	218	212	238	-	-	156	183	133
Scale 14	288	276	240	275	196	307	182	324	233	160	186	256	198	238	245	-	-	222	208	162
Scale 15	277	260	199	316	207	264	178	290	230	239	264	173	115	217	213	-	-	222	231	187

Table S1.17. Exposed crown length measurements (µm) for scales at different sampling locations of *Lamna nasus* specimen LN04, a 127cm immature female. See Chapter 3.1.3. for sampling locations. Values have been rounded to whole digits.

	H1	H2	H3	MG	Pec1	Pec2	Pec3	Dors1	Dors2	Dors3	FF1	FF2	FF3	FB1	FB2	FB3	Cl	Tail1	Tail2	Tail3
Scale 1	249	209	208	242	255	235	194	188	191	165	258	248	243	289	241	234	-	198	132	215
Scale 2	212	235	284	267	264	259	216	178	192	189	205	246	258	176	185	250	-	213	177	178
Scale 3	252	257	262	251	241	221	204	169	191	160	200	229	253	265	307	234	-	190	169	187
Scale 4	275	210	295	232	263	199	249	215	183	214	262	292	259	260	300	275	-	209	159	163
Scale 5	269	270	243	265	257	192	242	228	195	200	214	283	237	215	230	208	-	217	158	187
Scale 6	254	222	275	276	276	202	194	239	203	159	251	208	204	265	250	228	-	198	151	179
Scale 7	268	201	210	232	272	190	222	222	143	178	222	277	283	268	268	214	-	213	165	182
Scale 8	285	254	247	264	276	240	227	267	200	196	236	299	261	276	242	195	-	230	166	217
Scale 9	262	257	255	287	242	232	251	238	227	165	271	265	193	239	272	215	-	187	184	237
Scale 10	240	271	294	262	213	255	222	253	176	166	228	284	247	225	267	204	-	167	201	245
Scale 11	226	217	227	243	259	233	192	235	189	191	189	215	211	297	230	262	-	163	127	195
Scale 12	222	258	294	236	284	220	218	164	183	176	254	237	237	241	277	202	-	194	174	212
Scale 13	282	191	234	259	251	245	170	232	178	189	226	243	263	219	244	211	-	171	160	175
Scale 14	279	181	257	238	271	164	176	269	196	180	249	279	238	256	251	251	-	221	201	229
Scale 15	286	202	221	273	313	218	159	228	182	216	225	222	202	263	254	258	-	152	183	203

Table S1.18. Exposed crown length measurements (µm) for scales at different sampling locations of *Lamna nasus* specimen LN05, a 146cm immature male. See Chapter 3.1.3. for sampling locations. Values have been rounded to whole digits.

	H1	H2	H3	MG	Pec1	Pec2	Pec3	Dors1	Dors2	Dors3	FF1	FF2	FF3	FB1	FB2	FB3	Cl	Tail1	Tail2	Tail3
Scale 1	300	159	238	227	217	239	208	201	218	221	201	248	153	264	156	151	-	121	218	140
Scale 2	270	220	188	183	175	151	260	256	186	184	201	247	196	227	171	155	-	166	194	227
Scale 3	220	216	187	224	185	194	214	253	230	198	223	192	167	200	176	160	-	159	113	140
Scale 4	288	186	219	245	160	164	196	217	205	195	180	216	193	194	229	210	-	145	116	212
Scale 5	311	225	175	216	173	221	219	246	203	178	190	243	158	210	198	135	-	136	144	178
Scale 6	211	181	214	221	192	194	195	269	188	196	177	233	131	151	150	129	-	154	181	210
Scale 7	177	224	190	177	204	230	158	246	206	182	171	268	165	214	193	172	-	159	165	221
Scale 8	229	209	123	280	185	210	259	230	212	223	217	264	159	202	247	155	-	161	176	204
Scale 9	270	181	182	195	220	188	268	233	175	151	185	222	143	150	175	176	-	173	125	301
Scale 10	207	231	221	200	202	207	171	146	216	200	206	214	202	195	159	150	-	168	142	163
Scale 11	264	222	238	205	234	180	199	188	205	207	153	209	188	187	170	173	-	155	196	132
Scale 12	244	204	167	213	203	194	194	221	234	133	180	294	171	230	133	152	-	182	176	130
Scale 13	221	213	200	160	158	219	201	153	199	187	212	241	212	195	197	160	-	174	141	179
Scale 14	257	202	198	165	203	224	199	196	181	178	104	221	154	241	182	166	-	152	163	151
Scale 15	205	177	238	174	191	183	193	231	227	195	181	157	163	162	194	147	-	130	177	125

Table S1.19. Exposed crown length measurements (µm) for scales at different sampling locations of *Lamna nasus* specimen LN06, a 183cm mature male. See Chapter 3.1.3. for sampling locations. Values have been rounded to whole digits.

	H1	H2	H3	MG	Pec1	Pec2	Pec3	Dors1	Dors2	Dors3	FF1	FF2	FF3	FB1	FB2	FB3	Cl	Tail1	Tail2	Tail3
Scale 1	284	248	196	210	276	341	316	170	226	237	177	233	215	268	225	203	-	175	127	231
Scale 2	337	245	220	262	262	292	345	173	219	219	176	174	247	240	194	252	-	140	172	218
Scale 3	340	177	226	248	202	298	282	278	223	258	236	178	257	223	166	228	-	164	146	228
Scale 4	253	235	262	192	238	271	293	174	214	157	154	117	240	230	164	158	-	178	139	160
Scale 5	342	189	217	245	329	290	333	238	260	144	228	224	238	171	198	203	-	168	224	153
Scale 6	262	222	205	197	247	335	305	274	226	171	259	226	229	174	174	223	-	182	195	208
Scale 7	304	252	253	254	262	212	261	203	205	175	209	253	201	203	266	230	-	202	136	180
Scale 8	321	246	251	280	195	225	303	251	171	159	135	268	204	176	187	211	-	204	137	209
Scale 9	235	200	213	275	236	323	294	277	258	223	175	214	197	211	196	169	-	144	169	174
Scale 10	275	248	223	283	193	233	297	294	173	194	252	240	232	286	188	175	-	140	172	169
Scale 11	249	215	282	241	263	326	229	255	166	150	277	159	245	259	191	162	-	180	189	233
Scale 12	335	211	240	284	230	264	248	232	226	148	247	244	213	253	227	220	-	178	189	181
Scale 13	294	239	164	213	262	291	296	182	229	237	177	278	176	182	178	214	-	143	150	192
Scale 14	192	220	207	229	258	245	198	220	196	168	230	215	270	177	207	169	-	168	137	181
Scale 15	244	195	297	285	275	230	330	260	237	174	179	242	251	184	221	172	-	163	150	168

e) Riblet number

Table S1.20. Riblet number for scale crowns at different sampling locations of *Lamna nasus* specimen LN01, a 215cm mature female. See Chapter 3.1.3. for sampling locations.

	H1	H2	H3	MG	Pec1	Pec2	Pec3	Dors1	Dors2	Dors3	FF1	FF2	FF3	FB1	FB2	FB3	Cl	Tail1	Tail2	Tail3
Scale 1	4	4	5	4	-	5	5	4	5	5	4	4	4	3	3	3	-	3	3	3
Scale 2	5	5	5	4	-	5	4	6	5	5	4	5	5	4	3	4	-	3	3	3
Scale 3	4	3	4	4	-	6	5	6	5	5	5	4	4	4	4	5	-	3	3	4
Scale 4	4	5	4	5	-	4	4	5	3	5	5	4	4	3	4	3	-	3	3	3
Scale 5	4	5	5	4	-	4	5	5	3	4	5	4	3	5	4	3	-	4	5	3
Scale 6	4	4	5	5	-	5	5	5	4	5	4	4	5	4	3	3	-	4	4	4
Scale 7	4	5	5	5	-	4	5	5	6	5	5	4	4	3	4	3	-	3	3	4
Scale 8	5	4	4	4	-	5	5	5	4	4	5	4	5	3	4	4	-	3	3	3
Scale 9	4	4	5	5	-	5	4	6	5	3	6	3	4	3	5	4	-	4	3	3
Scale 10	5	4	5	5	-	4	5	6	4	4	5	3	3	4	4	4	-	5	3	3
Scale 11	4	3	5	5	-	4	5	5	5	4	5	3	3	5	4	4	-	5	3	3
Scale 12	3	4	5	5	-	4	5	6	5	5	5	4	3	3	4	3	-	3	3	3
Scale 13	4	4	5	5	-	5	5	5	4	4	5	3	4	3	5	3	-	5	3	4
Scale 14	4	4	5	4	-	6	5	6	5	5	4	5	3	4	4	3	-	3	3	3
Scale 15	4	4	4	5	-	5	5	5	5	5	5	3	3	3	5	3	-	5	3	3

Table S1.21. Riblet number for scale crowns at different sampling locations of *Lamna nasus* specimen LN03, a 186cm immature female. See Chapter 3.1.3. for sampling locations.

	H1	H2	H3	MG	Pec1	Pec2	Pec3	Dors1	Dors2	Dors3	FF1	FF2	FF3	FB1	FB2	FB3	Cl	Tail1	Tail2	Tail3
Scale 1	4	4	4	5	-	5	4	5	4	5	5	3	3	5	4	5	-	4	3	3
Scale 2	5	5	5	5	-	4	5	4	5	4	5	4	3	4	3	5	-	4	3	3
Scale 3	4	4	5	3	-	4	3	5	4	3	6	3	5	4	3	4	-	4	3	3
Scale 4	4	4	4	3	-	4	3	5	4	3	4	3	3	4	3	3	-	4	3	3
Scale 5	4	4	4	3	-	5	5	5	5	4	5	4	4	3	3	3	-	5	3	3
Scale 6	4	4	5	5	-	4	4	4	5	5	4	3	3	5	3	3	-	4	6	3
Scale 7	6	3	4	3	-	3	4	5	4	4	5	3	4	3	3	3	-	4	3	3
Scale 8	5	5	4	3	-	5	4	4	4	4	5	3	4	3	3	4	-	3	3	3
Scale 9	5	4	4	4	-	4	3	5	4	5	5	4	3	4	3	3	-	5	4	4
Scale 10	4	4	5	4	-	3	5	4	4	4	5	3	3	4	3	3	-	4	3	3
Scale 11	4	5	5	4	-	3	5	5	4	3	5	3	4	5	3	3	-	4	5	3
Scale 12	4	4	4	4	-	4	3	4	3	4	5	3	4	5	4	-	-	4	4	3
Scale 13	4	5	5	3	-	5	4	5	3	4	3	3	3	4	3	-	-	4	4	3
Scale 14	4	4	3	4	-	3	3	5	3	3	5	3	3	3	4	-	-	3	3	3
Scale 15	4	4	3	4	-	4	4	4	4	3	5	3	3	4	3	-	-	3	5	4

Table S1.22. Riblet number for scale crowns at different sampling locations of *Lamna nasus* specimen LN04, a 127cm immature female. See Chapter 3.1.3. for sampling locations.

	H1	H2	H3	MG	Pec1	Pec2	Pec3	Dors1	Dors2	Dors3	FF1	FF2	FF3	FB1	FB2	FB3	Cl	Tail1	Tail2	Tail3
Scale 1	3	5	4	4	3	3	3	5	5	4	5	3	4	4	4	3	-	5	4	4
Scale 2	4	4	3	5	3	5	4	5	5	4	5	4	4	3	4	3	-	5	3	3
Scale 3	5	3	4	4	3	4	3	4	3	3	4	3	4	3	4	4	-	5	3	3
Scale 4	5	4	3	5	3	3	4	5	5	5	4	3	3	3	5	4	-	4	3	5
Scale 5	5	5	4	5	3	3	4	5	3	4	3	4	3	3	3	5	-	4	3	5
Scale 6	5	3	5	5	3	5	4	4	5	3	4	3	3	3	4	3	-	4	3	3
Scale 7	3	3	4	3	4	4	4	5	5	4	3	3	3	3	4	3	-	3	4	5
Scale 8	5	4	3	4	3	4	4	5	5	4	3	3	3	3	3	4	-	5	3	3
Scale 9	5	3	3	5	3	3	3	4	5	3	4	3	3	3	3	5	-	3	4	5
Scale 10	5	5	3	5	3	4	3	5	5	2	3	4	4	4	3	3	-	3	3	5
Scale 11	4	3	4	5	3	3	4	5	4	3	3	3	3	5	4	3	-	4	5	3
Scale 12	5	4	3	5	4	3	4	4	5	3	4	3	3	4	4	3	-	4	5	3
Scale 13	4	4	3	5	3	3	3	4	4	3	5	3	4	3	4	5	-	3	4	4
Scale 14	4	3	3	5	3	5	3	4	4	3	5	3	3	3	3	4	-	4	5	5
Scale 15	5	3	3	5	4	5	3	4	5	5	4	3	3	4	4	4	-	4	5	3

Table S1.23. Riblet number for scale crowns at different sampling locations of *Lamna nasus* specimen LN05, a 146cm immature male. See Chapter 3.1.3. for sampling locations.

	H1	H2	H3	MG	Pec1	Pec2	Pec3	Dors1	Dors2	Dors3	FF1	FF2	FF3	FB1	FB2	FB3	Cl	Tail1	Tail2	Tail3
Scale 1	5	3	4	4	-	3	4	3	5	4	4	4	4	3	4	3	-	3	5	3
Scale 2	4	5	3	3	-	3	4	4	4	3	5	3	5	3	3	3	-	3	3	3
Scale 3	4	4	3	4	-	3	4	3	4	4	5	3	5	4	3	3	-	3	3	4
Scale 4	4	3	4	4	-	3	4	4	5	4	3	3	3	4	3	3	-	3	3	3
Scale 5	4	4	3	5	-	3	4	4	4	3	5	3	3	4	3	3	-	3	4	3
Scale 6	5	3	3	4	-	3	3	4	3	5	5	3	3	4	3	3	-	3	3	4
Scale 7	5	4	4	3	-	5	3	3	3	3	5	3	4	4	4	3	-	3	4	3
Scale 8	4	3	3	5	-	3	3	3	4	5	3	5	3	4	3	3	-	3	3	3
Scale 9	3	3	3	5	-	5	4	3	3	3	3	3	3	3	3	3	-	3	3	3
Scale 10	3	3	3	3	-	3	3	3	4	5	4	3	5	3	4	3	-	3	5	4
Scale 11	5	4	4	5	-	5	5	3	4	3	4	3	3	5	4	4	-	3	3	3
Scale 12	3	5	4	4	-	3	3	3	4	3	5	5	5	3	3	3	-	3	3	3
Scale 13	3	4	3	5	-	3	4	4	3	3	4	3	5	5	3	3	-	3	3	3
Scale 14	4	4	3	5	-	3	4	3	4	3	4	4	3	3	3	3	-	3	3	3
Scale 15	4	4	3	3	-	4	4	3	4	3	5	3	3	4	4	3	-	3	3	3

Table S1.24. Riblet number for scale crowns at different sampling locations of *Lamna nasus* specimen LN06, a 183cm mature male. See Chapter 3.1.3. for sampling locations.

	H1	H2	H3	MG	Pec1	Pec2	Pec3	Dors1	Dors2	Dors3	FF1	FF2	FF3	FB1	FB2	FB3	Cl	Tail1	Tail2	Tail3
Scale 1	4	4	4	3	-	5	5	3	4	5	5	3	3	4	4	3	-	3	3	5
Scale 2	5	4	3	4	-	5	5	3	5	4	5	4	4	3	4	5	-	3	5	5
Scale 3	5	4	3	5	-	5	5	5	5	5	5	3	3	3	3	4	-	3	5	5
Scale 4	4	4	4	4	-	5	4	4	5	5	4	3	4	4	3	3	-	4	3	3
Scale 5	5	3	4	3	-	5	4	5	5	4	5	4	4	3	4	3	-	4	5	3
Scale 6	4	5	3	3	-	5	5	5	5	5	5	4	3	4	4	3	-	5	5	4
Scale 7	3	3	4	4	-	4	5	4	4	5	3	3	4	3	4	4	-	4	3	3
Scale 8	4	5	4	3	-	3	4	5	4	5	5	3	3	3	5	3	-	5	4	3
Scale 9	5	4	3	5	-	5	5	4	5	5	5	3	3	3	3	3	-	3	4	4
Scale 10	5	3	3	4	-	5	5	3	3	4	4	3	3	5	3	3	-	3	3	3
Scale 11	4	3	4	4	-	5	4	4	4	4	4	3	4	5	3	3	-	3	4	5
Scale 12	5	3	4	3	-	4	5	4	5	4	4	3	3	5	4	4	-	3	5	3
Scale 13	4	4	3	3	-	5	5	4	5	5	5	3	3	4	4	3	-	5	3	3
Scale 14	3	4	3	5	-	5	4	4	4	5	5	4	3	5	4	3	-	4	3	3
Scale 15	4	3	4	3	-	5	5	3	4	4	5	4	5	3	3	3	-	5	4	3

Table S1.25. Riblet convergence and divergence angles (degrees) for scale crowns at different sampling locations of *Lamna nasus* specimen LN01, a 215cm mature female. See Chapter 3.1.3. for sampling locations. Note negative values are diverging in the streamwise direction (anterior to posterior of crown), and positive values indicate riblets converge to a point at the posterior.

	H1	H2	H3	MG	Pec1	Pec2	Pec3	Dors1	Dors2	Dors3	FF1	FF2	FF3	FB1	FB2	FB3	Cl	Tail1	Tail2	Tail3
Scale 1	12	-7	-6	-3	-	7	6	3	3	0	-6	-9	-6	-6	-4	0	-	-7	-12	-4
Scale 2	9	-13	-9	-3	-	17	10	-8	2	0	4	-11	-7	1	-8	1	-	2	-2	2
Scale 3	13	-9	-4	3	-	7	5	5	3	0	-10	-7	-11	-3	-4	-4	-	-5	-9	-5
Scale 4	5	-2	-9	1	-	17	23	4	2	-1	3	-9	-8	-5	-9	0	-	-4	-5	-1
Scale 5	6	-11	-6	4	-	8	9	5	0	8	-5	-9	-12	-4	-9	0	-	-7	-1	4
Scale 6	2	-3	-7	-1	-	15	3	0	-5	4	-2	-11	-9	-1	-6	-4	-	-9	-1	4
Scale 7	3	-2	-6	1	-	4	10	-1	-1	-9	-6	-12	-10	-2	-8	-1	-	-5	0	0
Scale 8	11	-3	-6	1	-	5	9	3	-2	0	-9	-7	-13	-3	-4	0	-	-9	1	3
Scale 9	2	-5	-6	-1	-	5	1	7	1	-4	-6	-9	-4	1	-6	0	-	-5	-4	-5
Scale 10	8	-9	-9	-5	-	6	5	0	4	0	-6	-10	-10	-3	-3	-2	-	-11	-3	1
Scale 11	2	-11	-11	-4	-	4	25	10	16	-4	-11	-9	-9	-4	-5	0	-	-7	-2	-1
Scale 12	13	1	-3	1	-	12	8	5	19	-2	-5	-6	-7	3	-10	1	-	-5	-5	2
Scale 13	6	-6	-6	-3	-	10	-1	2	-2	-4	-4	-10	0	-1	-6	0	-	-1	1	2
Scale 14	11	-2	-18	-1	-	18	14	-1	2	3	-5	-7	4	-2	-10	0	-	2	2	2
Scale 15	5	1	-7	-5	-	2	6	-1	10	2	-1	-5	-6	-4	-9	0	-	-5	-2	1
Scale 16	-3	-3	-12	-5	-	4	8	-3	-2	2	-2	-4	-7	-2	-16	0	-	-6	2	0
Scale 17	-4	0	-9	-9	-	18	8	6	4	-2	-5	-9	-5	-4	-2	5	-	0	-9	-4
Scale 18	10	-5	-5	-3	-	10	11	9	18	5	-7	-11	-5	-1	-11	2	-	-3	-5	-5
Scale 19	1	-6	-3	-10	-	9	-3	6	-2	0	-2	-6	-6	3	-8	1	-	-4	-3	-2
Scale 20	11	-1	-8	4	-	13	4	5	15	-3	-2	-3	-7	0	-10	2	-	-6	5	0

Table S1.26. Riblet convergence and divergence angle (degrees) for scale crowns at different sampling locations of *Lamna nasus* specimen LN03, a 186cm immature female. See Chapter 3.1.3. for sampling locations. Note negative values are diverging in the streamwise direction (anterior to posterior of crown), and positive values indicate riblets converge to a point at the posterior.

	H1	H2	H3	MG	Pec1	Pec2	Pec3	Dors1	Dors2	Dors3	FF1	FF2	FF3	FB1	FB2	FB3	Cl	Tail1	Tail2	Tail3
Scale 1	4	-9	-12	-8	-	6	2	-1	-5	-2	-7	-3	1	4	-11	-	-	-7	-3	-13
Scale 2	17	-12	-9	-8	-	4	0	-1	-3	-3	0	-6	-6	3	-5	-	-	-5	-7	-11
Scale 3	4	-10	-5	-10	-	7	4	0	0	0	1	-10	14	-1	-7	-	-	-1	-1	-3
Scale 4	1	-2	-8	-9	-	2	-4	-2	1	1	-6	-6	10	-7	-10	-	-	-3	-4	-11
Scale 5	8	-3	-15	-8	-	5	-3	-8	-4	-3	-2	-11	-2	-17	-8	-	-	-2	-6	-10
Scale 6	0	-7	-15	-13	-	3	3	1	0	4	2	-8	9	-18	-8	-	-	3	-6	-8
Scale 7	5	-3	-8	-9	-	3	3	-8	-2	0	-7	-7	10	-10	-4	-	-	-10	-5	-7
Scale 8	4	-14	-6	-12	-	2	-5	-7	-3	1	-1	-7	3	-3	-7	-	-	-7	-5	-6
Scale 9	-2	-3	-11	-14	-	10	-7	-4	-9	-1	-4	-8	2	-10	-8	-	-	-8	-1	-9
Scale 10	6	-4	-5	-14	-	8	-5	-1	-12	8	-4	-16	-1	-7	-9	-	-	-1	-5	-1
Scale 11	1	-9	-3	-6	-	11	-3	-7	-4	-1	2	-10	2	-8	-3	-	-	-11	0	-4
Scale 12	25	-13	-7	-8	-	8	2	-1	-3	1	-5	-10	2	-12	-9	-	-	-7	-4	-8
Scale 13	3	0	-8	-1	-	2	-2	-2	-3	-1	4	-5	4	-17	-4	-	-	-3	1	-8
Scale 14	13	-6	-16	-6	-	3	-3	-2	2	-1	10	-7	-2	-5	-11	-	-	-3	4	-8
Scale 15	12	-11	-5	-2	-	6	5	-3	0	-4	-6	-3	20	-10	-5	-	-	-3	1	-10
Scale 16	12	-4	-5	-4	-	6	-5	-4	-5	-1	2	-11	9	1	-13	-	-	-5	-6	-9
Scale 17	2	-9	-11	-7	-	12	2	0	4	0	3	-8	13	-11	-2	-	-	-4	0	-8
Scale 18	12	-11	-15	-4	-	5	-2	-1	0	3	-1	-15	4	-11	-5	-	-	-5	1	-4
Scale 19	5	-13	-9	-10	-	3	2	-2	5	1	2	-8	-4	-11	-4	-	-	-3	10	-3
Scale 20	1	-4	-5	2	-	7	-3	0	-1	2	-5	-14	14	0	-14	-	-	-13	1	-6

Table S1.27. Riblet convergence and divergence angle (degrees) for scale crowns at different sampling locations of *Lamna nasus* specimen LN04, a 127cm immature female. See Chapter 3.1.3. for sampling locations. Note negative values are diverging in the streamwise direction (anterior to posterior of crown), and positive values indicate riblets converge to a point at the posterior.

	H1	H2	H3	MG	Pec1	Pec2	Pec3	Dors1	Dors2	Dors3	FF1	FF2	FF3	FB1	FB2	FB3	Cl	Tail1	Tail2	Tail3
Scale 1	4	-5	-15	-16	14	-3	-1	-10	-4	-4	-11	-14	-8	-17	-15	-18	-	-16	-12	-11
Scale 2	5	-10	-11	-20	12	8	2	-5	-6	-3	-14	-18	-6	-14	-16	-13	-	-14	4	-11
Scale 3	12	-4	-21	-19	28	6	-2	-4	-7	-4	-10	-12	-13	-14	-9	-10	-	-7	-13	-13
Scale 4	7	-5	-12	-14	24	3	-4	-4	-1	-3	-10	-17	-11	-23	-14	-16	-	-14	-7	-9
Scale 5	7	-11	-18	-12	26	-5	-1	1	3	-4	-10	-18	-12	-9	-18	-15	-	-11	-13	-5
Scale 6	5	-17	-18	-17	26	-9	-4	-7	-6	-7	-9	-10	-14	-7	-16	-18	-	-10	-15	-9
Scale 7	7	-4	-15	-8	18	3	-4	-5	-7	0	-4	-19	-14	-10	-18	-8	-	-11	-13	-10
Scale 8	15	-8	-16	-14	25	-6	-8	-3	-8	-5	-17	-14	-7	-13	-15	-15	-	-15	-16	-9
Scale 9	8	-14	-24	-9	20	-2	0	-2	-5	-2	-9	-16	-13	-12	-14	-17	-	-12	-2	-9
Scale 10	9	-12	-20	-17	26	10	-2	-4	-2	-4	-8	-15	-15	-12	-13	-14	-	-7	-14	-20
Scale 11	14	-2	2	-12	23	2	-1	-2	-10	3	-9	-15	-13	-5	-6	-28	-	-13	-13	-12
Scale 12	15	-10	-10	-10	13	-19	-3	-6	-6	-2	-12	-19	-6	-13	-11	-18	-	-11	-8	-11
Scale 13	-6	-12	-14	-16	20	-8	-1	-2	-5	0	0	-9	-14	-9	-10	-13	-	-11	-16	-3
Scale 14	8	-8	-13	-18	31	-20	-1	-5	-7	-4	-5	-11	-13	-14	-15	-17	-	-10	-11	-11
Scale 15	11	-12	-6	-11	27	0	-5	4	-2	-4	-11	-16	-9	-6	-19	-18	-	-8	-13	-8
Scale 16	6	-5	-20	-14	26	5	-3	-5	-11	2	-6	-20	-6	-12	-11	-17	-	-13	-6	-15
Scale 17	10	-21	1	-11	34	-2	-1	-6	-9	2	-4	-18	-5	-20	-19	-19	-	-10	-19	-11
Scale 18	3	-12	-18	-13	31	-2	-5	0	-8	0	-18	-9	-12	-4	-17	-17	-	-15	-13	-12
Scale 19	1	-16	-20	-14	21	6	-1	0	-7	0	-14	-13	-20	-15	-7	-13	-	-7	-6	-10
Scale 20	2	-5	-13	-12	27	3	1	-5	-5	0	-1	-17	-9	-10	-17	-17	-	-8	-18	-14

Table S1.28. Riblet convergence and divergence angle (degrees) for scale crowns at different sampling locations of *Lamna nasus* specimen LN05, a 146cm immature male. See Chapter 3.1.3. for sampling locations. Note negative values are diverging in the streamwise direction (anterior to posterior of crown), and positive values indicate riblets converge to a point at the posterior.

	H1	H2	H3	MG	Pec1	Pec2	Pec3	Dors1	Dors2	Dors3	FF1	FF2	FF3	FB1	FB2	FB3	Cl	Tail1	Tail2	Tail3
Scale 1	-2	-16	-25	-5	-	0	2	-1	-5	-6	-17	-17	2	-4	-13	-16	-	-14	-8	-14
Scale 2	-4	-16	-15	-8	-	2	2	-8	-6	-4	-7	-13	-4	-14	-19	-10	-	-8	-3	-16
Scale 3	3	-21	-27	-12	-	-4	-8	-4	-1	-7	-12	-22	-10	-10	-15	-4	-	-6	-12	-15
Scale 4	7	-15	-24	-15	-	-4	-3	-15	-6	-12	-21	-13	-1	-16	-23	-12	-	-16	-15	-22
Scale 5	-5	-12	-24	-24	-	-7	1	-1	-9	0	-12	-13	3	-13	-7	-17	-	-11	-16	-12
Scale 6	-1	-11	-22	-19	-	5	5	-6	-7	-5	-21	-15	-4	-15	-16	-14	-	-10	-14	-9
Scale 7	4	-17	-21	-18	-	-1	3	-21	-9	-10	-15	-15	1	-10	-14	-17	-	-11	-13	-12
Scale 8	3	-5	-17	-21	-	-5	-5	-4	-6	-6	-3	-26	0	-18	-20	-13	-	-12	-17	-20
Scale 9	-2	-18	-17	-24	-	-2	-1	-4	0	-1	-9	-19	-9	-5	-22	-3	-	-20	-11	-13
Scale 10	0	-17	-19	-18	-	2	0	-2	0	-3	-4	-19	-9	-9	-14	-17	-	-23	-18	-11
Scale 11	5	-20	-19	-25	-	-10	4	-5	-11	-3	-8	-21	-8	-13	-25	-14	-	-11	-7	-19
Scale 12	-3	-11	-24	-22	-	-2	0	-10	-9	-11	-15	-18	-3	-5	-19	-13	-	-6	-11	-18
Scale 13	-1	-22	-16	-14	-	-2	1	-9	0	-2	-15	-17	-1	-5	-20	-3	-	-16	-3	-13
Scale 14	8	-12	-25	-20	-	-5	-2	-19	-11	-3	-4	-13	1	-16	-11	-16	-	-7	-16	-17
Scale 15	9	-23	-18	-19	-	2	2	4	-7	1	-10	-21	2	-8	-17	-14	-	-12	-20	-18
Scale 16	-2	-21	-28	-9	-	-6	3	-1	-4	-7	0	-9	0	-11	-17	-20	-	-5	-19	-15
Scale 17	2	-19	-6	-4	-	-4	3	-3	-8	-2	-13	-13	-1	-12	-9	-14	-	-15	-3	-10
Scale 18	5	-10	-22	-17	-	2	0	-3	-4	-8	-6	-19	4	-18	-16	-11	-	-6	-4	-13
Scale 19	4	-13	-16	-17	-	-5	-2	1	-17	-5	-13	-24	-2	-10	-14	-13	-	-11	-19	-9
Scale 20	7	-16	-10	-16	-	2	-5	-3	-4	-3	-19	-15	2	-15	-6	-10	-	-10	-10	-6

Table S1.29. Riblet convergence and divergence angle (degrees) for scale crowns at different sampling locations of *Lamna nasus* specimen LN06, a 183cm mature male. See Chapter 3.1.3. for sampling locations. Note negative values are diverging in the streamwise direction (anterior to posterior of crown), and positive values indicate riblets converge to a point at the posterior.

	H1	H2	H3	MG	Pec1	Pec2	Pec3	Dors1	Dors2	Dors3	FF1	FF2	FF3	FB1	FB2	FB3	Cl	Tail1	Tail2	Tail3
Scale 1	15	9	-17	0	-	17	11	2	7	-2	5	-1	11	-5	-4	1	-	-1	4	-10
Scale 2	14	-3	-4	-3	-	7	15	-1	2	3	1	-1	16	5	-5	3	-	-3	-3	3
Scale 3	35	2	-4	1	-	14	16	3	1	-3	-10	-7	17	-2	0	0	-	-7	6	0
Scale 4	-2	2	-4	-4	-	9	9	1	-5	6	2	-2	12	-2	-6	6	-	2	2	-1
Scale 5	16	-3	-5	-5	-	10	0	4	8	4	8	-2	14	-6	-7	7	-	3	-2	-11
Scale 6	13	-1	-5	1	-	19	8	3	1	7	-14	-3	7	2	-3	-10	-	1	-2	0
Scale 7	23	1	-5	-4	-	9	6	0	8	0	-3	-7	14	1	1	1	-	3	5	-2
Scale 8	38	2	1	2	-	-10	18	-1	8	9	1	4	15	-5	1	2	-	-2	4	-5
Scale 9	22	1	-7	-2	-	0	4	3	-4	-1	2	-1	8	3	-2	1	-	-7	-2	-9
Scale 10	17	0	-7	-5	-	14	6	1	-1	9	1	0	12	3	-2	5	-	-1	5	-11
Scale 11	27	1	-1	-10	-	5	16	4	-7	3	3	0	17	3	-8	-2	-	4	6	3
Scale 12	20	6	7	-8	-	6	12	3	-1	6	-5	-10	6	-4	-9	-7	-	12	2	-2
Scale 13	29	1	-1	-5	-	11	19	1	9	9	17	5	11	1	-4	2	-	10	3	-5
Scale 14	9	1	-6	-1	-	10	26	-1	0	-4	-1	-1	15	-2	-8	3	-	3	4	-9
Scale 15	16	-2	-19	-15	-	9	11	7	1	-6	0	-3	32	-1	-9	0	-	7	-7	2
Scale 16	16	10	-3	-11	-	12	16	8	0	0	4	0	17	2	-3	0	-	-1	7	-3
Scale 17	7	1	-10	-15	-	15	20	-7	-1	-3	-5	-2	26	4	-3	-11	-	8	5	1
Scale 18	2	1	-8	-4	-	7	7	0	5	-4	3	-5	24	-7	-5	-2	-	-7	0	-10
Scale 19	28	-2	2	3	-	1	5	1	6	-3	-3	-10	9	-5	-7	0	-	3	4	-10
Scale 20	4	-1	-4	9	-	10	18	5	1	6	2	-3	11	-1	-4	6	-	6	-4	-13

d) Heat maps of preceding data

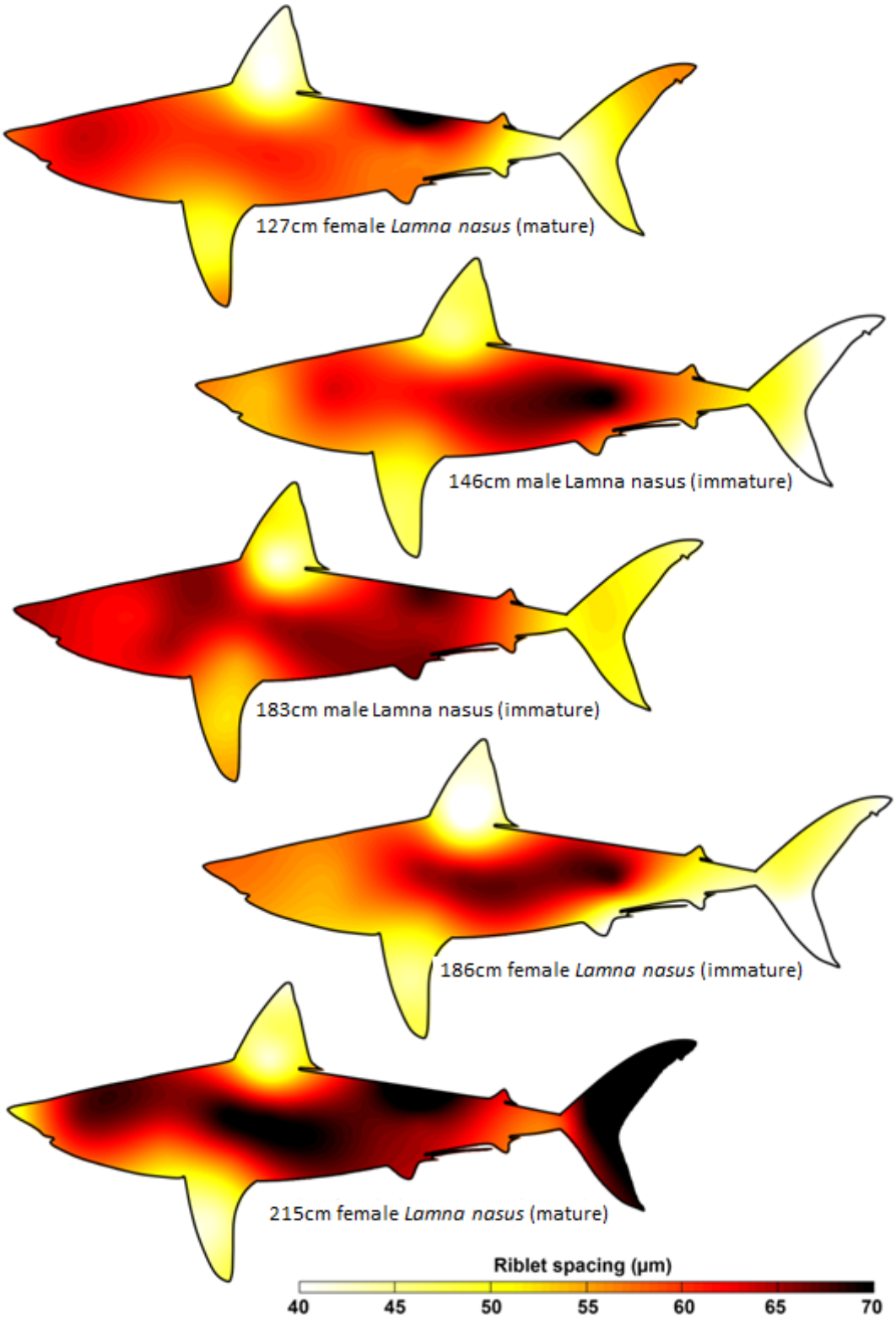

Figure S1.11 Heat maps of mean riblet spacing (µm) distribution in individual *Lamna nasus* specimens, generated from sampling points detailed in Chapter 3.1.3.

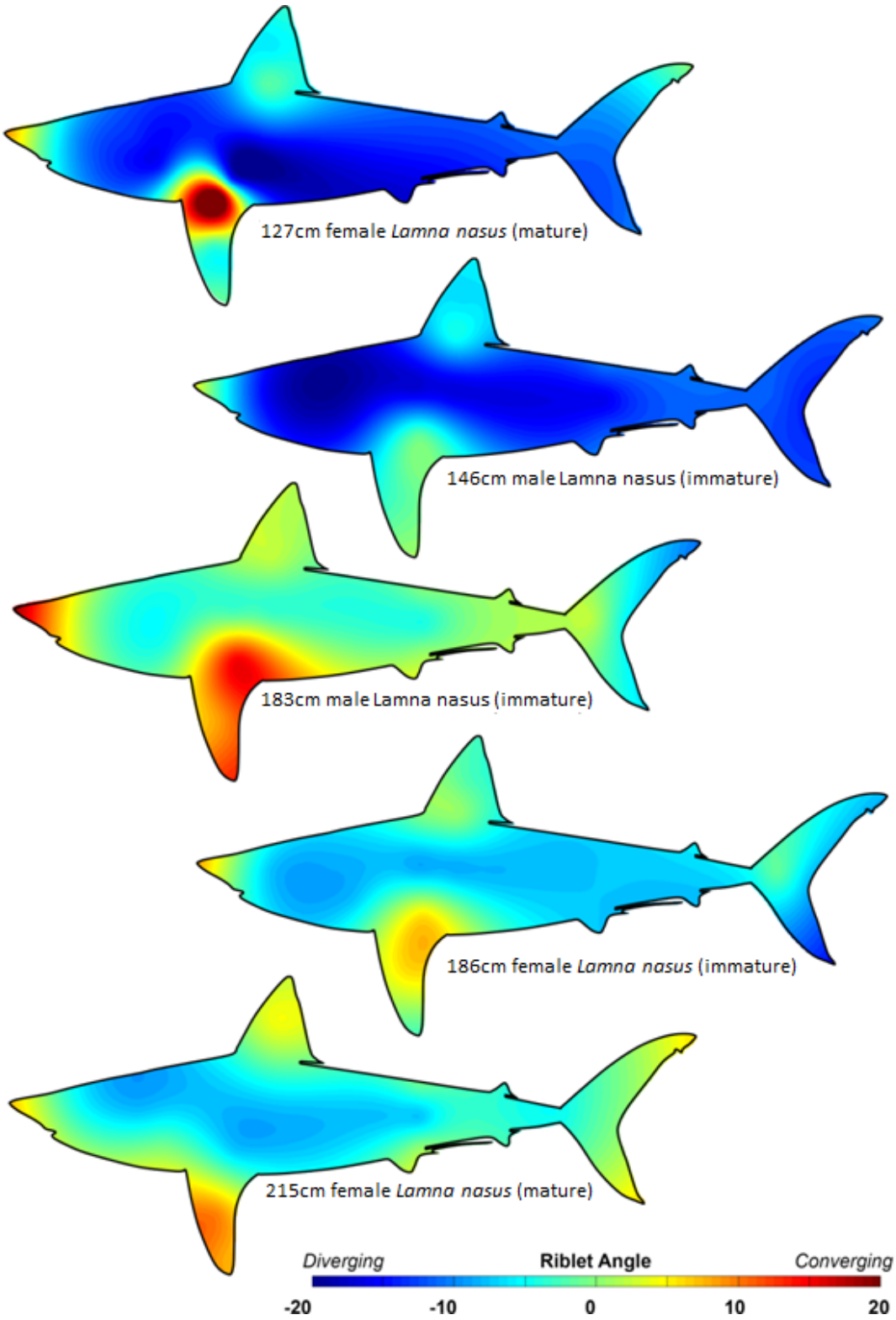

Figure S1.12. Heat maps of mean riblet convergence/divergence angles (degrees) in individual *Lamna nasus* specimens, generated from sampling points detailed in Chapter 3.1.3.

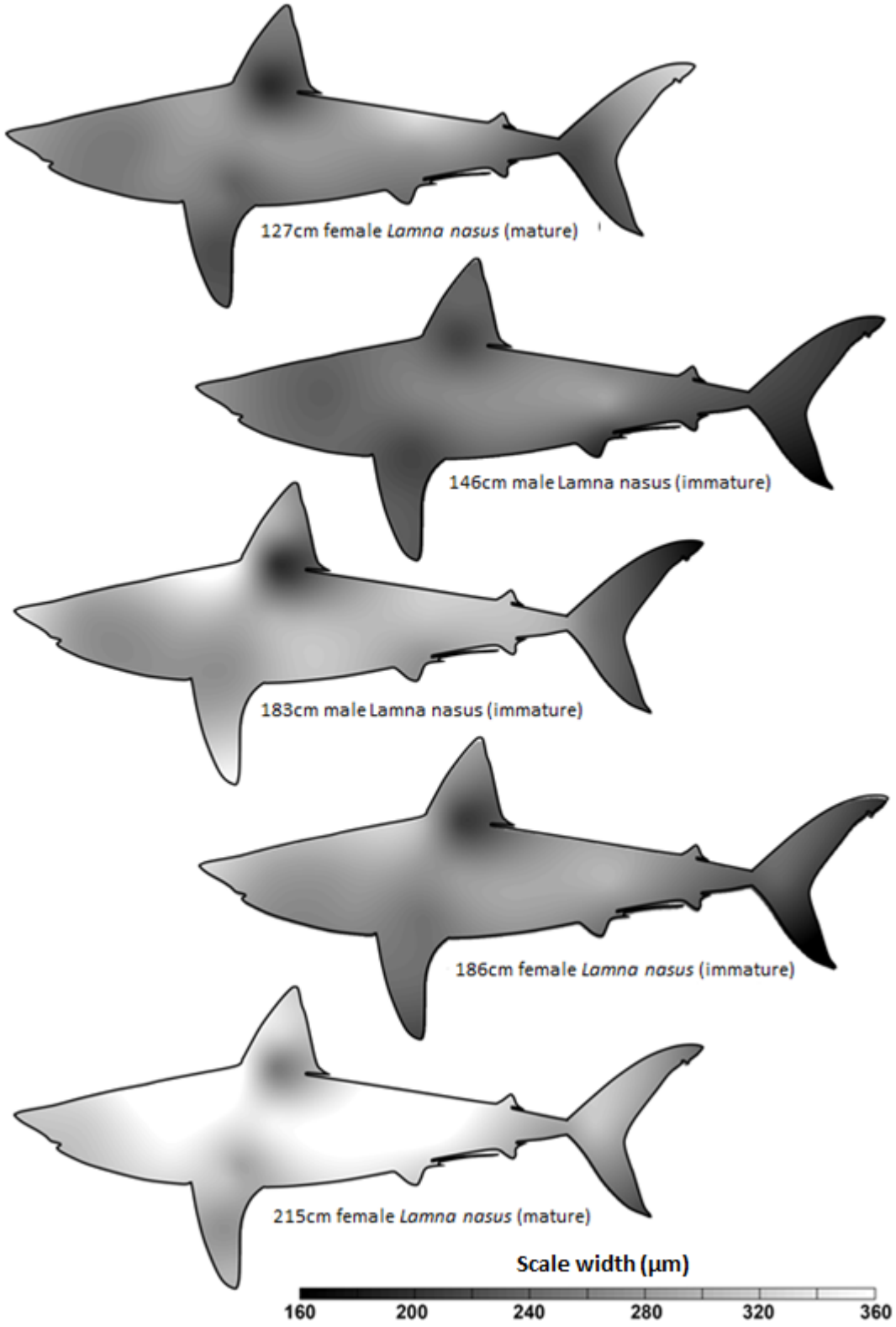

Figure S1.13. Heat maps of mean scale width (µm) distribution in individual *Lamna nasus* specimens, generated from sampling points detailed in Chapter 3.1.3.

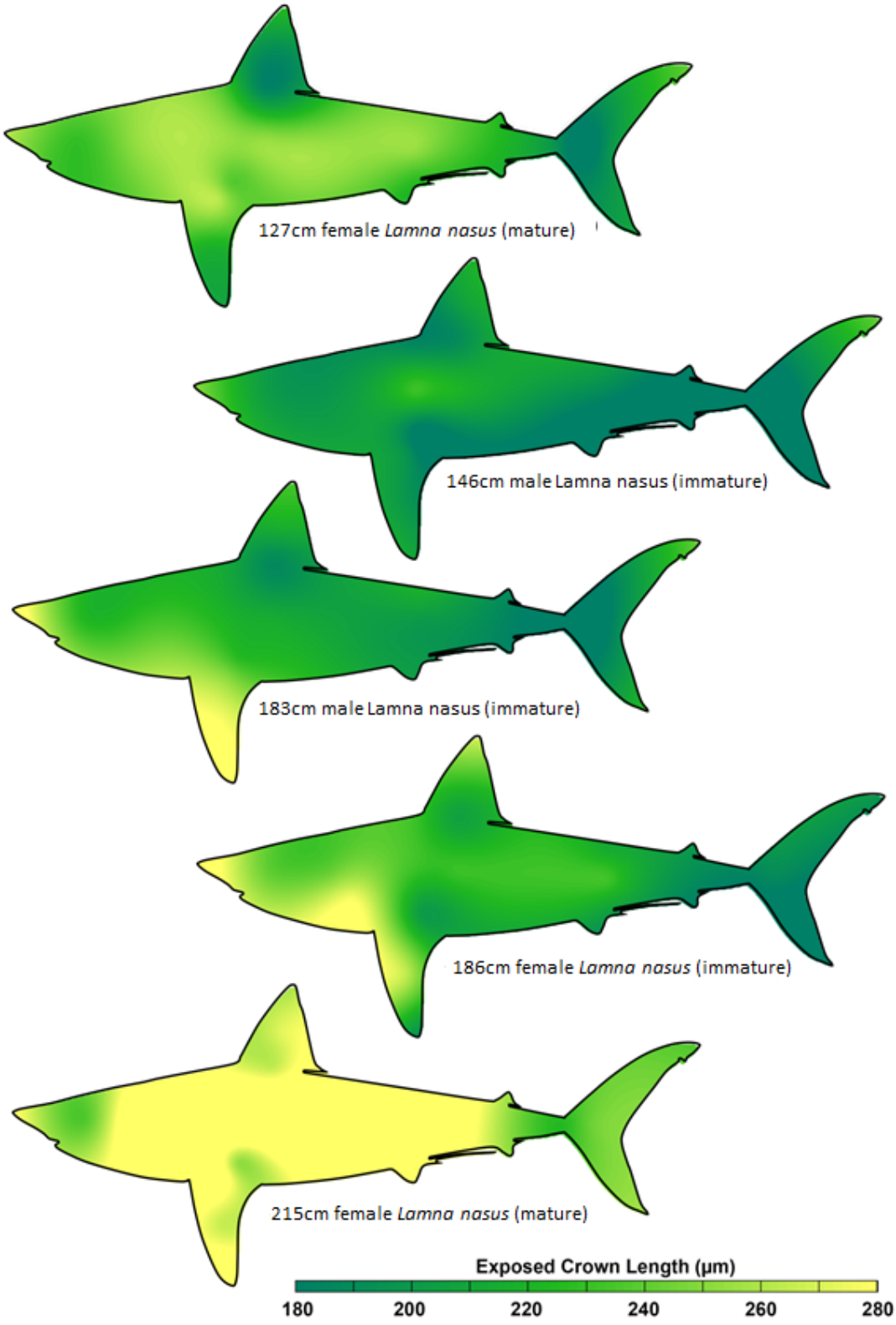

Figure S1.14. Heat maps of mean exposed scale length (µm) distribution in individual *Lamna nasus* specimens, generated from sampling points detailed in Chapter 3.1.3.

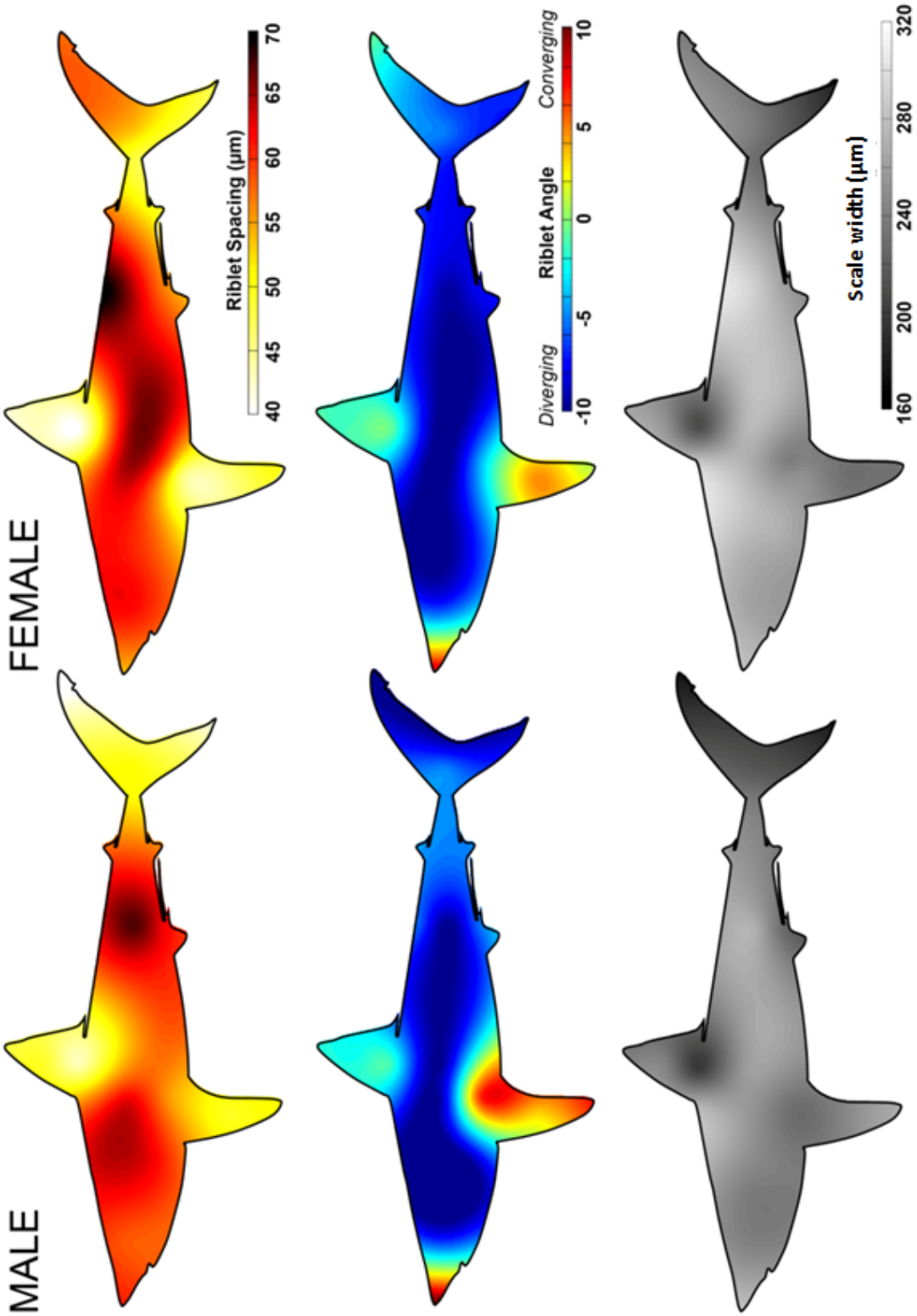

Figure S1.15. Heat maps of mean riblet spacing (top), mean riblet angle (middle), and mean scale width (bottom) distribution for all male (left) and female (right) *Lamna nasus* specimens. Images generated using sampling points detailed in Chapter 3.1.3.

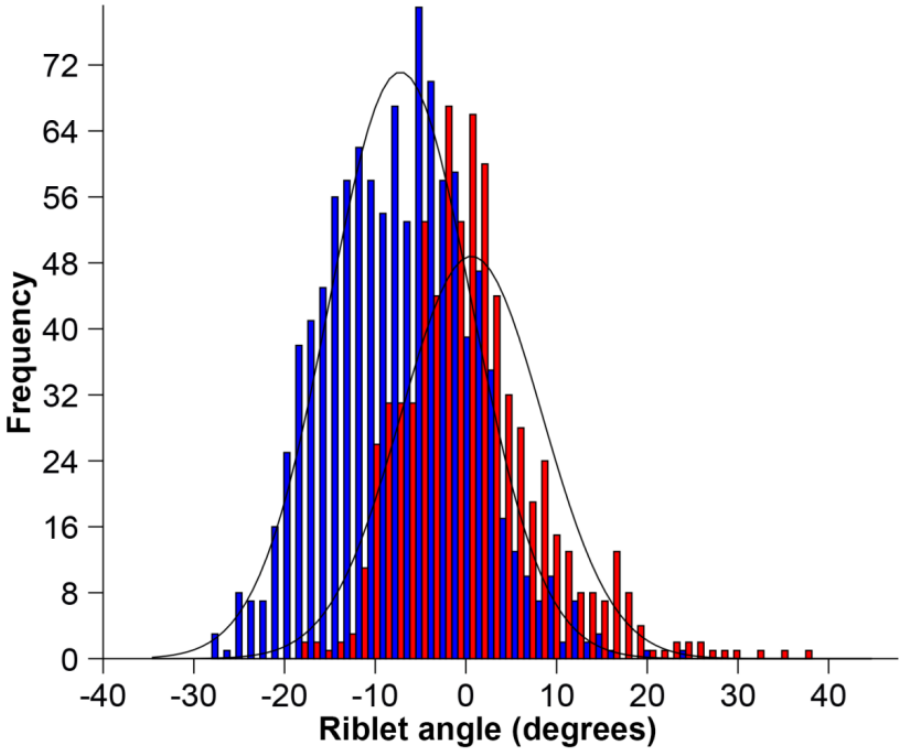

Figure S1.16. Histogram showing mean riblet angle of immature (blue) and mature (red) *Lamna nasus*. Mature males over 165 cm and females over 195 cm, defined according to Ebert *et al.* (2013).

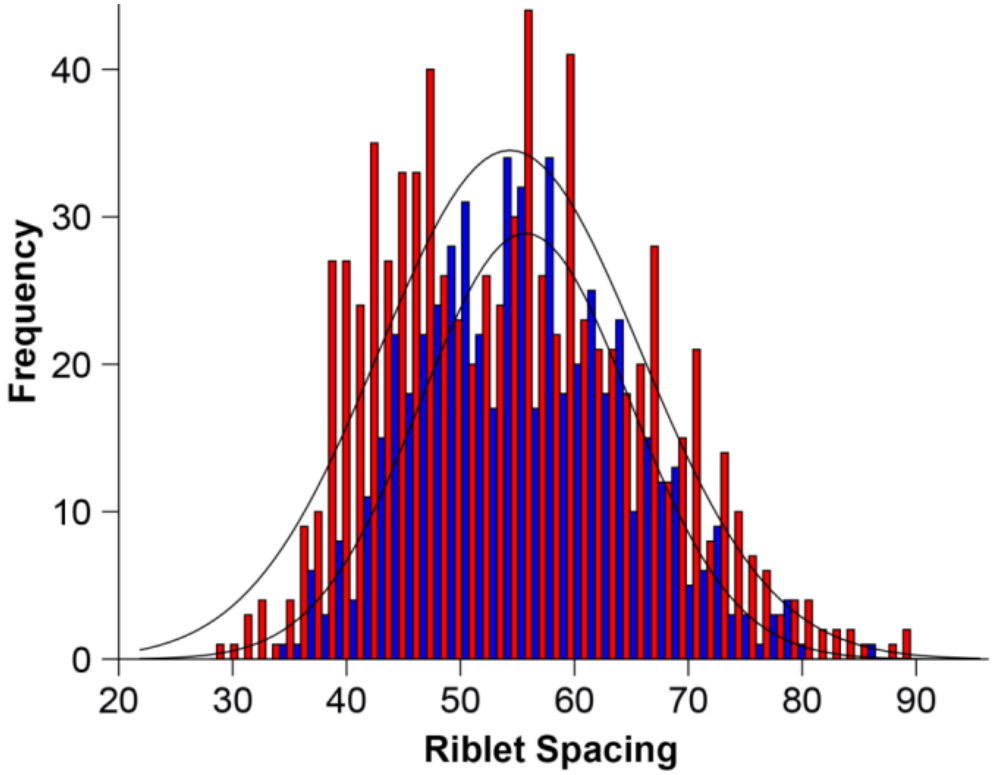

Figure S1.17. Histogram showing mean riblet spacing for all body regions of male (blue) and female (red) *Lamna nasus* specimens.

A1.3. Modern Shark Comparative Anatomy – Other Sampled Species

a) Specimens

Figure S1.18. Photographs of stuffed *Chiloscyllium plagiosum* specimen pre-sampling, a single 680mm male caught in the Phillipines in 2013. Top, lateral view; centre, dorsal view; and bottom shows dorsal detail of the flank region. Scale bar fine intervals are 1 cm.

Figure S1.19. Photographs of stuffed *Chiloscyllium punctatum* specimen pre-sampling, a single 730mm female caught in Surigao, the Phillipines in 2013. Top, lateral view; centre, dorsal view; and bottom shows dorsal detail of the flank region. Scale bar fine intervals are 1 cm.

Figure S1.20. Photographs of a *Squatina squatina* specimen before sampling, a 124cm female (see Chapter 3.1.3.) caught in United Kingdom between 2012-2013, and stored at Centre for Environment Fisheries and Aquaculture Science (CEFAS), Lowestoft, UK. Top, dorsal view of entire specimen; and bottom, ventral view of entire specimen. Scale bar fine intervals are 1 cm.

Figure S1.21. Photographs of a *Squalus acanthias* specimen before sampling, a 102cm female (see Chapter 3.1.3.) caught in United Kingdom in 2013, and sampled at the Centre for Environment Fisheries and Aquaculture Science (CEFAS), Lowestoft, UK. Top, lateral view; centre, dorsal view; and bottom shows lateral detail of the flank region. Scale bar fine vertical intervals are 1 cm.

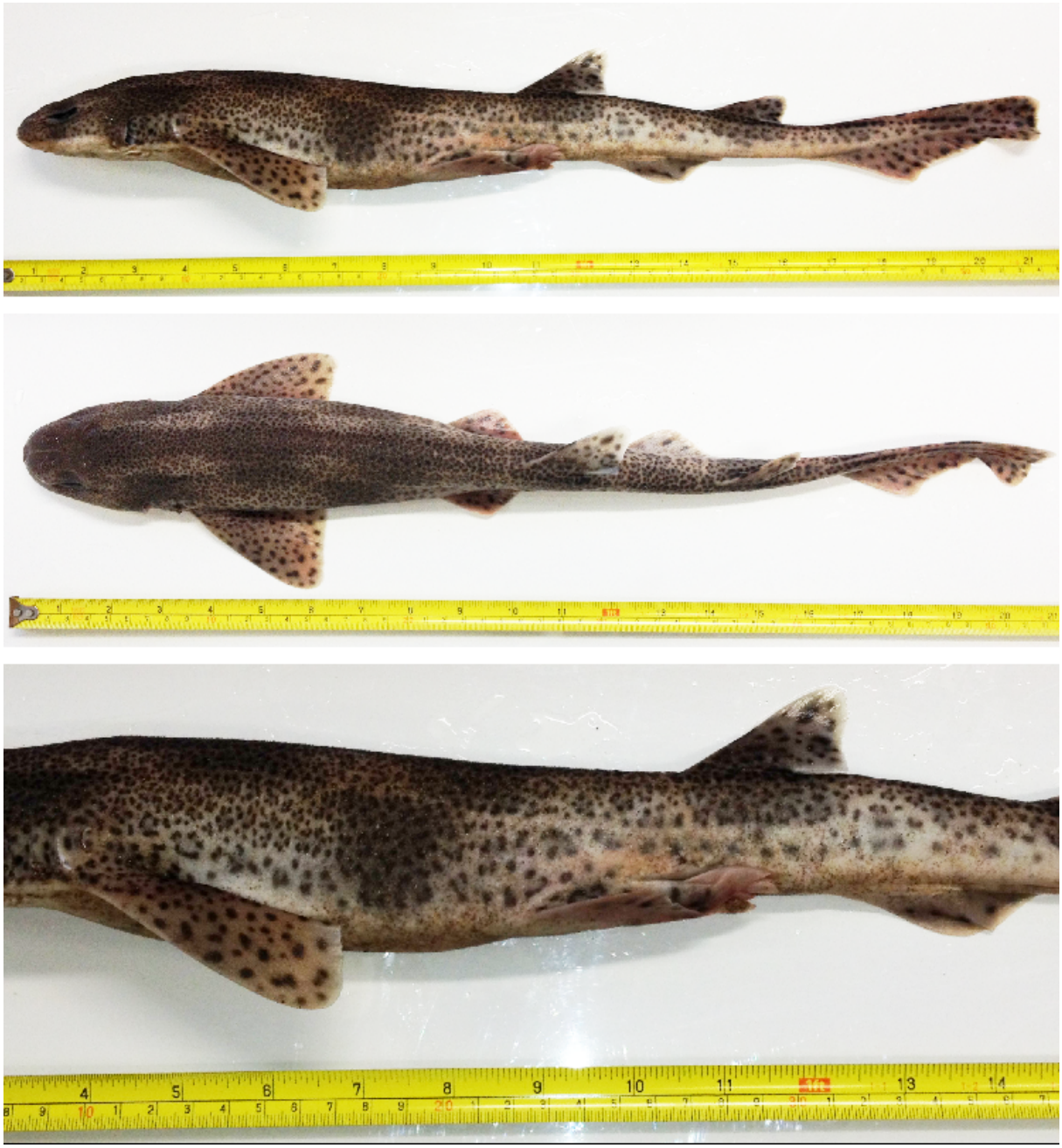

Figure S1.22. Photographs of a *Scyliorhinus canicula* specimen before sampling, a 535mm male (see Chapter 3.1.3.) beached in Pembrokeshire, United Kingdom in 2014. Top, lateral view; centre, dorsal view; and bottom shows lateral detail of the flank region. Scale bar fine numbers are centimetre intervals.

b) Scanning electron microscopy

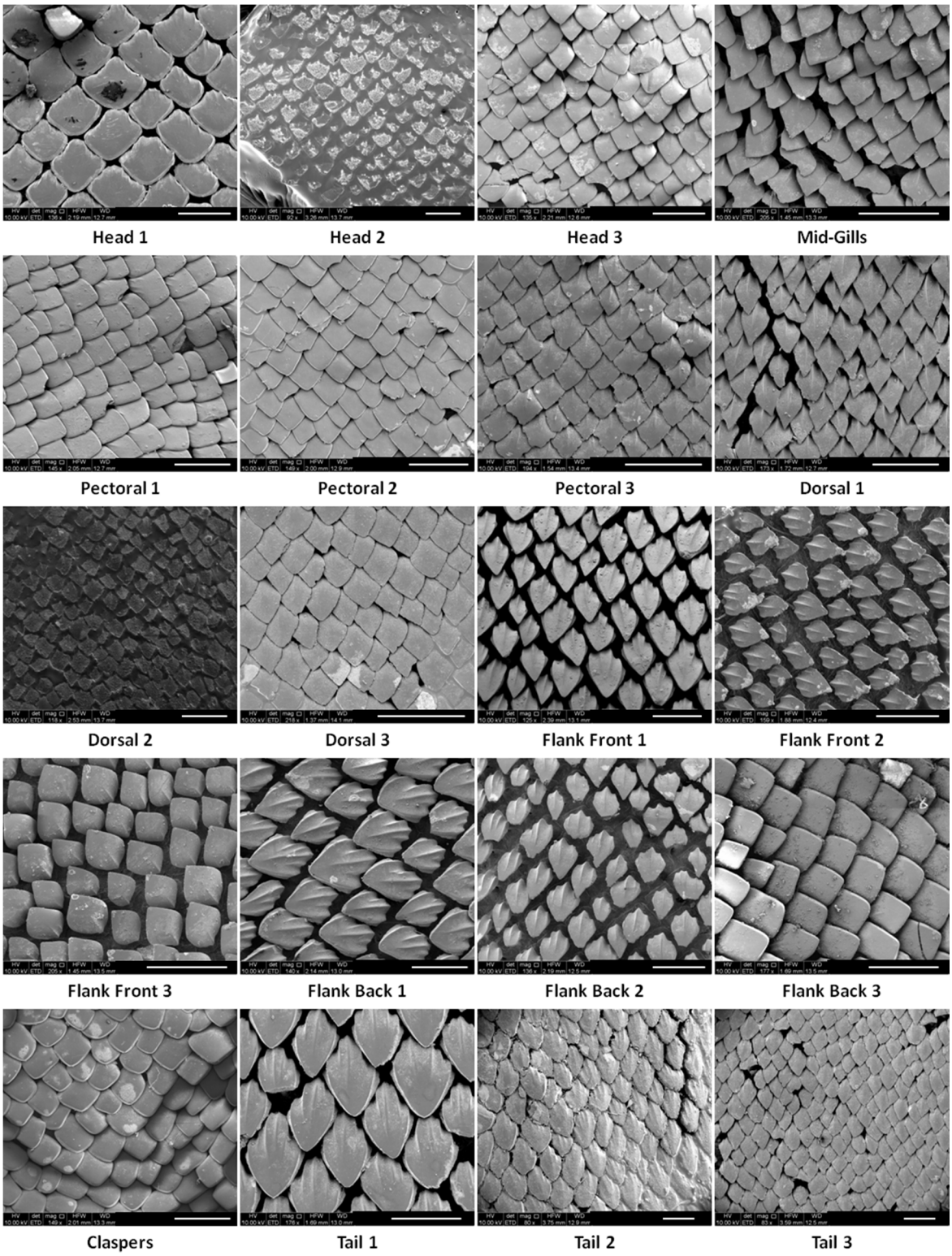

Figure S1.23. Examples of scanning electron micrographs of modern shark skin used for scale measurements and comparative analysis at different sampling locations. Specimen is a 680mm male *Chiloscyllium plagiosum*. See Chapter 3.1.3. for sampling locations. Scale bars are 500µm.

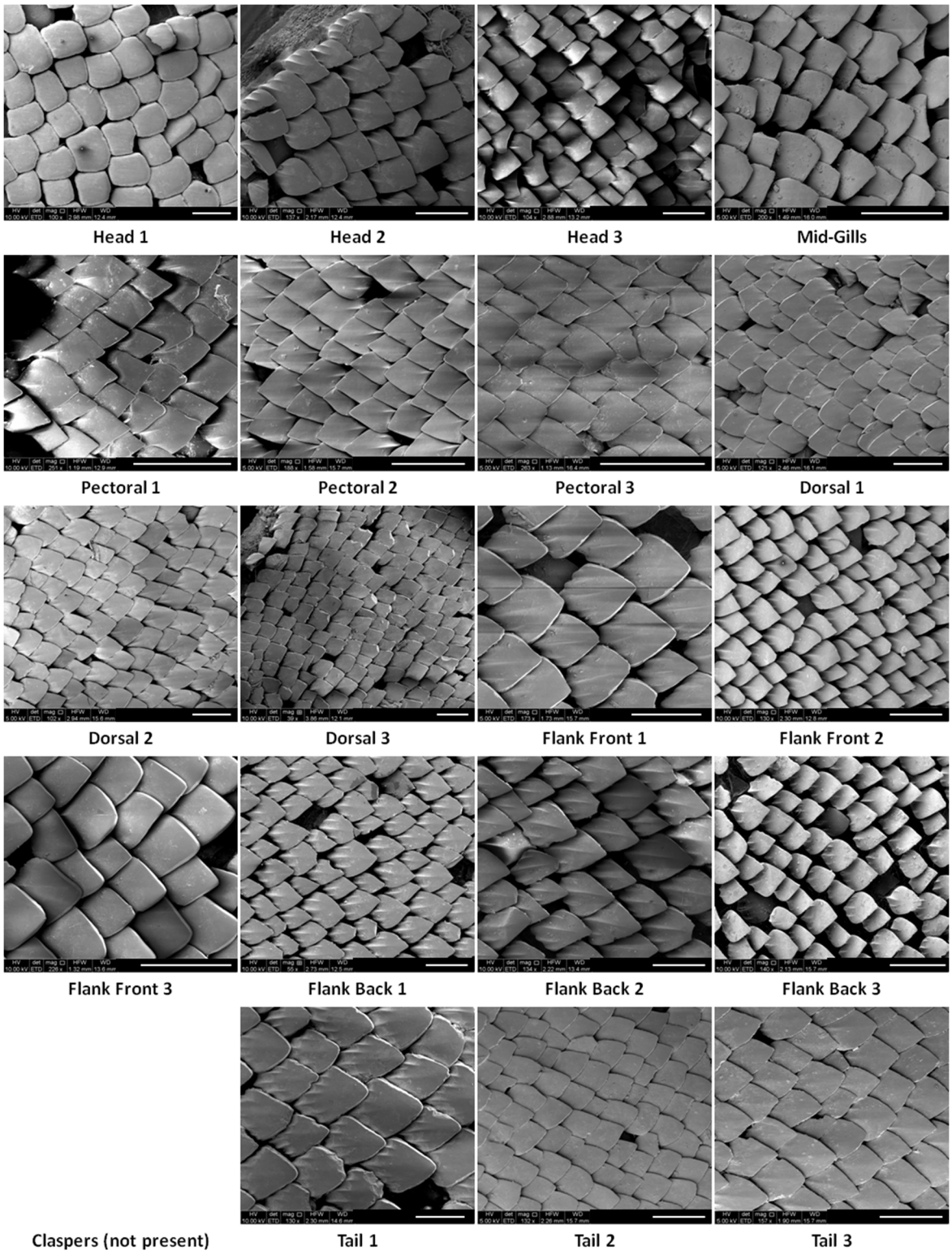

Figure S1.24. Examples of scanning electron micrographs of modern shark skin used for scale measurements and comparative analysis at different sampling locations. Specimen is a 730mm female *Chiloscyllium punctatum*. See Chapter 3.1.3. for sampling locations. Scale bars are 500µm.

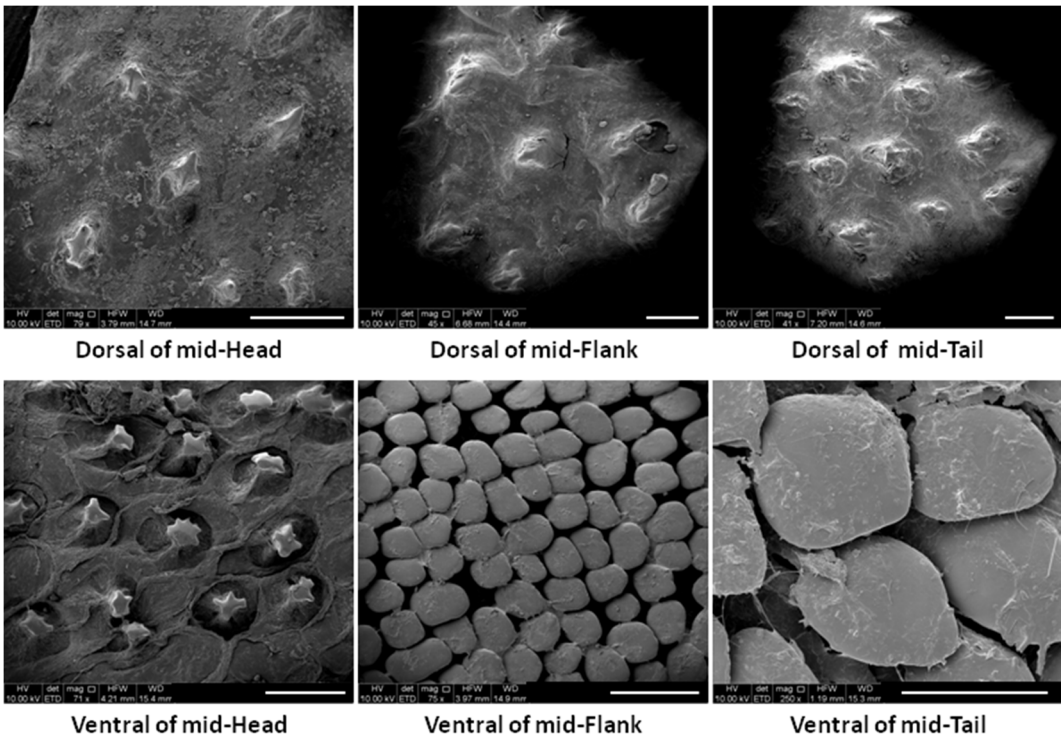

Figure S1.25. Examples of scanning electron micrographs of modern shark skin used for scale comparative analysis at different sampling locations. Specimen is a 1240mm female *Squatina squatina*. Note that the dorsoventrally compressed body form of this species limits the use of the analogous landmarks detailed in Chapter 3.1.3, and so brief descriptions of sampling location are provided for clarity. Scale bars are 1mm, except 'Ventral of mid-Tail' which is 500µm.

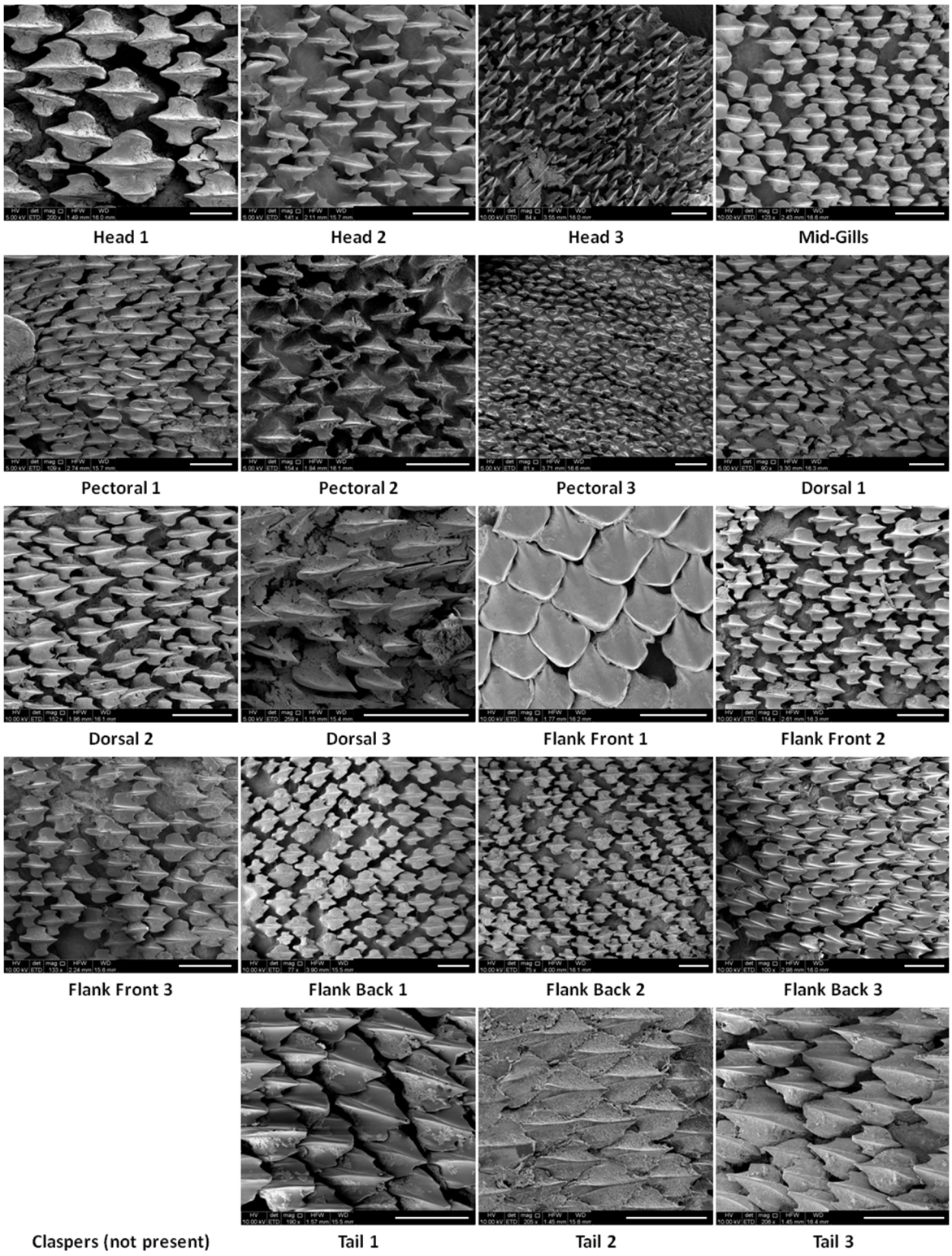

Figure S1.26. Examples of scanning electron micrographs of modern shark skin used for scale measurements and comparative analysis at different sampling locations. Specimen is a 1020mm female *Squalus acanthias*. See Chapter 3.1.3. for sampling locations. Scale bars are 500µm.

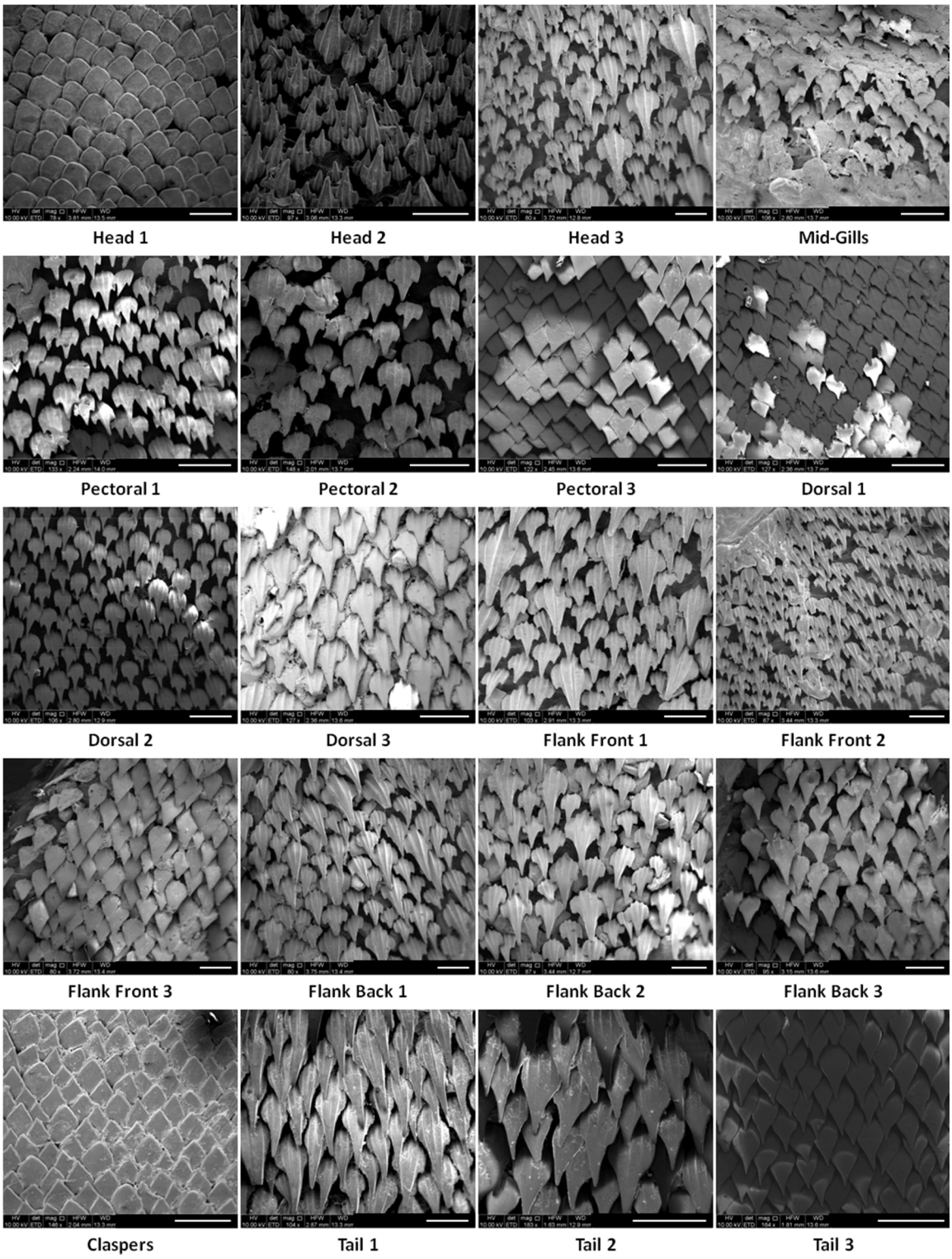

Figure S1.27. Examples of scanning electron micrographs of modern shark skin used for scale measurements and comparative analysis at different sampling locations. Specimen is a 535mm male *Scyliorhinus canicula*. See Chapter 3.1.3. for sampling locations. Scale bars are 500µm.

A1.4. Inter-species riblet spacing analysis

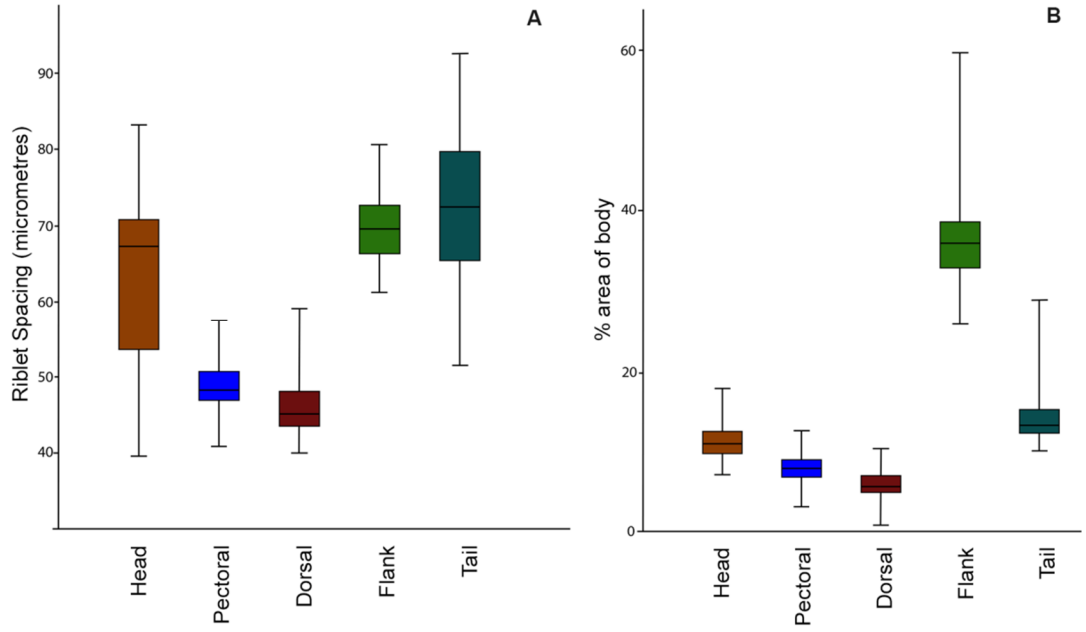

Figure S1.28 A. Box and whisker plot of mean scale riblet spacing in different regions of *Lamna nasus* (215 cm, female) as detailed in Figure 1a. B. Plot of body regions by percentage area, calculated from lateral view figured images of modern sharks species in this study (n=50).

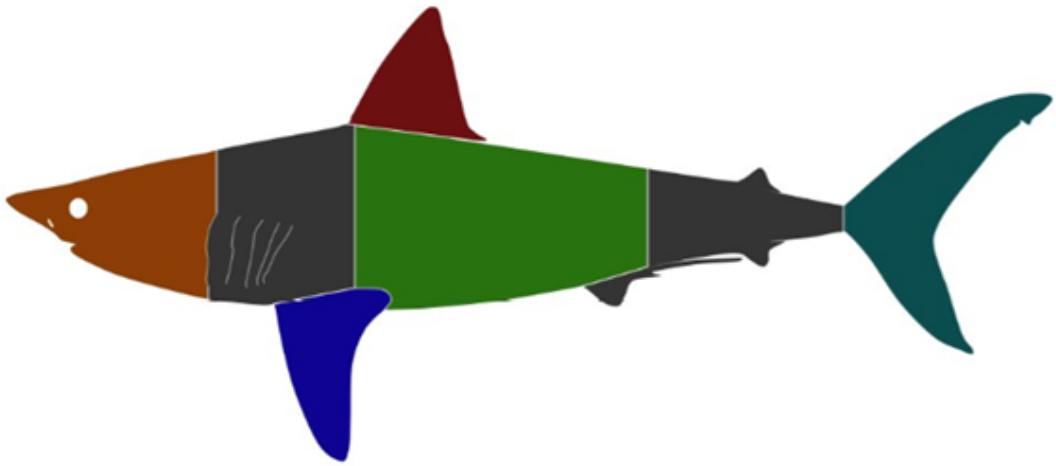

Figure S1.29 Standardised body regions for area calculations, head (orange), pectoral fin (blue), dorsal fin (red), flank (green), and tail/caudal fin (turquoise).

Table S1.30. Percentage area of shark regions (defined in previous figure)

Species	Head	Pectoral	Dorsal	Flank	Tail	Other
Alopias_pelagicus	7.6	12.1	3.9	33.7	25.3	17.3
Alopias_vulpinus	8.1	9.2	4.7	30.9	28.9	18.2
Apisturus_canutus	11.7	7.7	0.8	28.7	16.3	34.7
Apristurus kampae	11.8	13.4	1.1	47.4	21.6	4.7
Apristurus laurussoni	11.6	13.3	1.1	49.7	19.9	4.2
Carcharhinus_acronotus	11.8	7.9	5.8	33.7	13.3	27.5
Carcharhinus_albimarginatus	11.3	6.5	5.6	42.8	12.8	20.9
Carcharhinus_altimus	12.5	8.9	6.2	36.6	12.6	23.1
Carcharhinus_amblyrhynchos	13.5	7.0	6.6	36.5	16.4	20.0
Carcharhinus_brachyurus	9.2	8.9	5.1	36.3	14.0	26.5
Carcharhinus_brevipinna	12.3	6.8	5.5	38.0	12.3	25.0
Carcharhinus_cerdale	10.6	10.1	7.2	31.2	14.1	26.8
Carcharhinus_falciformis	10.1	7.8	5.0	36.5	15.2	25.4
Carcharhinus_galapagensis	11.8	8.7	7.1	33.9	16.2	22.3
Carcharhinus_isodon	10.1	8.1	6.0	36.0	14.6	25.2
Carcharhinus_leucus	14.1	7.9	7.5	39.0	12.3	19.3
Carcharhinus_limbatus	11.6	8.4	6.3	34.5	13.2	26.0
Carcharhinus_longimanus	9.6	12.6	8.7	35.0	14.9	19.2
Carcharhinus_melanopterus	12.1	8.4	5.8	33.1	12.9	27.6
Carcharhinus_obscurus	10.7	9.0	5.0	40.0	12.6	22.7
Carcharhinus_perezii	11.0	7.4	6.0	39.4	14.6	21.7
Carcharhinus_plumbeus	12.4	11.4	10.0	27.1	14.8	24.4
Carcharhinus_porosus	9.6	6.9	5.1	38.6	13.7	26.1
Carcharhinus_signatus	12.5	9.3	4.5	41.0	12.1	20.6
Carcharodon_carcharias	14.8	10.5	5.4	32.7	11.3	25.3
Galeocardo_cuvier	12.6	7.1	5.2	40.8	13.2	21.1
Galeorhinus galeus	10.4	6.0	4.7	41.7	11.3	25.9
Hexanchus_griseus	12.9	5.1	1.5	40.8	13.0	26.8
Hexanchus_nakamurai	10.0	4.7	1.9	43.3	15.2	25.0
Isurus_oxyrhinchus	13.1	8.3	5.4	37.6	11.5	24.1
Isurus_paucus	10.6	11.5	5.3	37.4	12.0	23.1
Lamna_ditropis	14.1	7.2	6.9	32.9	10.3	28.6
Lamna_nasus	13.3	8.9	6.9	34.2	14.3	22.4
Megachasma_pelagios	17.8	8.3	3.1	26.0	21.0	23.7
Nasolamia_velox	13.2	8.5	7.0	37.9	10.8	22.6
Negaprion_brevirostris	10.9	10.2	4.7	35.6	10.8	27.6
Odontaspis_ferox	10.3	5.9	5.6	36.9	12.6	28.7
Prionace_glauca	11.1	9.8	4.7	39.4	12.6	22.5
Rhincodon_typus	9.8	9.1	5.4	30.8	14.3	30.6
Rhizoprionodon_longurio	11.3	6.3	5.8	36.6	12.5	27.4
Rhizoprionodon_terraenovae	12.1	7.7	6.1	36.9	12.2	25.0
Sphyrna_corona	9.7	7.4	10.3	25.8	17.6	29.1
Sphyrna_lewini	10.5	5.5	7.2	34.9	14.3	27.6
Sphyrna_media	8.3	5.3	6.8	34.4	15.1	30.2
Sphyrna_mokarran	7.8	6.7	8.5	31.2	15.9	30.0

Sphyrna_tiburo	7.6	8.5	8.1	30.2	16.9	28.7
Sphyrna_tudes	8.3	7.0	9.1	29.3	17.9	28.3
Sphyrna_zygaena	7.1	5.9	7.6	34.9	16.3	28.2
Triaenodon_obesus	9.0	8.1	5.3	36.3	12.9	28.3
Zameus_squamulosus	10.6	3.2	1.8	59.7	10.1	14.7

Table S1.31. Source figures and mean riblet distances of taxa included in this study.

Taxa	Figure Source (s)	N Scales Measured	N Total Measurements	Mean Spacing / Standard Error (µm)
Modern Sharks				
Alopias pelagicus	1	15	225	47.52 ±0.3
Alopias vulpinus	1	15	225	44.26 ±0.3
Apristurus canutus	1	4	60	87.22 ±1.1
Apristurus kampae	1	3	48	121.87 ±1.1
Apristurus laurussoni	1	8	120	82.77 ±0.5
Carcharhinus acronotus	1	15	225	75.12 ±0.8
Carcharhinus albimarginatus	1	15	225	51.69 ±0.4
Carcharhinus altimus	1	15	225	85.48 ±0.5
Carcharhinus amblyrhynchos	1, 2	30	449	88.61 ±0.7
Carcharhinus brachyurus	1, 3	15	225	79.27 ±0.5
Carcharhinus brevipinna	1	15	225	74.69 ±0.7
Carcharhinus cerdale	1	15	225	111.88 ±0.5
Carcharhinus falciformis	1, 2	45	675	48.56 ±0.4
Carcharhinus galapagensis	1	15	225	72.73 ±0.4
Carcharhinus isodon	1	10	150	82.66 ±1.2
Carcharhinus leucus	1	11	165	145.12 ±2.0
Carcharhinus limbatus	1	15	225	49.22 ±0.5
Carcharhinus longimanus	1	15	225	78.88 ±0.8
Carcharhinus melanopterus	2	15	225	103.70 ±2.1
Carcharhinus obscurus	1, 3	30	450	67.86 ±0.6
Carcharhinus perezii	1	15	225	64.86 ±0.7
Carcharhinus plumbeus	1,2	9	585	107.11 ±1.1
Carcharhinus porosus	1	15	225	64.30 ±0.4
Carcharhinus signatus	1	15	225	70.65 ±0.5
Carcharodon carcharias	1, 2	25	369	82.14 ±0.5
Galeocardo cuvier	1, 2	14	210	274.63 ±2.5
Galeorhinus galeus	1	15	225	96.21 ±0.6
Hexanchus griseus	1, 2	25	375	161.75 ±1.0
Hexanchus nakamurai	1	15	225	99.47 ±0.5
Isurus oxyrhinchus	1, 2	26	390	46.14 ±0.3
Isurus paucus	1	15	225	61.92 ±0.4
Lamna ditropus	1	15	225	72.29 ±0.6
Lamna nasus	1, 4	20	265	57.7 ±0.9
Megachasma pelagios	1	11	165	96.88 ±0.6

Nasolamia velox	1	15	225	80.04 ±0.5
Negaprion brevirostris	2	18	256	52.44 ±0.9
Odontaspis ferox	1	15	225	107.46 ±0.8
Prionace glauca	1, 2	51	699	119.04 ±1.1
Rhincodon typus	1,5	23	345	81.62 ±0.6
Rhizoprionodon longurio	1	30	225	64.50 ±0.4
Rhizoprionodon terraenovae	1	15	225	73.29 ±0.5
Sphyrna corona	1	15	225	49.31 ±0.4
Sphyrna lewini	1, 2	16	236	46.83 ±0.2
Sphyrna media	1	15	225	56.52 ±0.4
Sphyrna mokarran	1	15	225	69.04 ±0.5
Sphyrna tiburo	1	14	210	48.82 ±0.4
Sphyrna tudes	1	15	225	65.90 ±0.4
Sphyrna zygaena	1, 2	45	675	45.37 ±0.2
Triaenodon obesus	1, 2	15	225	98.21 ±1.4
Zameus squamulosus	1	8	120	171.93 ±2.2
'Acanthodians'				
Gladiobranchus probaton	6	7	137	44.35 ±1.4
Milesacanthus ancestralis	7, 8	2	94	41.90 ±1.0
Milesacanthus antarcticus	9	5	119	38.72 ±1.0
Nostolepis gaujensis	7,8	5	103	99.16 ±2.9
Nostolepis gracilis	10	2	56	51.08 ±1.1
Vernicomacanthus waynensis	11	15	225	96.74 ±0.7
Thelodonts				
Canonia costulata	12	3	45	38.10 ±0.6
Canonia grossi	12-15	13	384	35.71 ±0.6
Kataporodus gemellus	12,16	5	151	51.23 ±0.6
Nikolivia milesi	17	3	90	66.83 ±1.8
Thelodus bicostatus	18	1	30	59.98 ±2.3
Extinct Chondricthayns (unknown body location)				
Areyonga oervigi	19	5	60	77.26±3.7
Tantalepis gatehousei	4	2	56	69.05±1.8

Source Data for Supplementary Table 1.31.

1. Castro JI. The sharks of North America. New York: Oxford University Press; 2011.

2. Reif WE. Squamation and ecology of sharks. Courier Forschungsinstitut. Senckenberg Frankfurt am Main. 1985; 78: 1-255.

3. Sue Lindsay, Microscopy and Microanalysis Unit, Australian Museum, Sydney

4. Tom Fletcher, School of Earth and Environment, University of Leeds

5. Kuthalingam MDK, Luther G, Livingston P, Murty VS. Further occurrences of the whale shark, Rhincodon typus Smith in the Indian coastal waters. Indian Journal of Fisheries 1973; 20: 646-651.

6. Hanke GF, Davis SP. Redescription of the acanthodian Gladiobranchus probaton Bernacsek & Dineley, 1977, and comments on diplacanthid relationships. Geodiversitas. 2008; 30: 303–330.

7. Hairapetian V, Valiukevicius J, Burrow CJ. Early Frasnian acanthodians from central Iran. Acta Palaeontologica Polonica. 2006; 51: 499-520.

8. Burrow CJ, Long JA, Trinajstic K. Disarticulated acanthodian and chondrichthyan remains from the upper Middle Devonian Aztec Siltstone, southern Victoria Land, Antarctica. Antarctic Science. 2009; 21: 71-88.

9. Burrow CJ, Lelièvre H, Janjou D. Gnathostome microremains from the Lower Devonian Jawf Formation, Saudi Arabia. Journal of Paleontology. 2006; 80: 537-560.

10. Valiukevičius J. Silurian acanthodian biostratigraphy of Lithuania. Geodiversitas. 2005; 27: 349-380.

11. Märss T, Wilson MVH, Thorsteinsson R. Silurian and Lower Devonian thelodonts and putative chondrichthyans from the Canadian Arctic Archipelago. Special Papers in Palaeontology. 2006; 75: 1–144.

12. Märss, T. A new Late Silurian or Early Devonian thelodont from the Boothia Peninsula, Arctic Canada. Palaeontology. 1999; 42: 1079-1099.

13. Karatajūtė-Talimaa VN. Lower Devonian (Lochkovian) thelodonts from October Revolution Island (Severnaya Zemlya Archipelago, Russia). Geodiversitas. 2002; 24: 791–804.

14. Blom H. Vertebrate remains from Upper Silurian–Lower Devonian beds of Hall and North Greenland. Geology of Greenland Survey Bulletin. 1999; 182: 1–80.

15. Märss T, Wilson MVH, Thorsteinsson R. New thelodont (Agnatha) and possible chondrichthyan (Gnathostomata) taxa established in the Silurian and Lower Devonian of the Canadian Arctic Archipelago. Proceedings of the Estonian Academy of Sciences, Geology. 2002; 51: 88-120.

16. Turner S. A new articulated thelodont (Agnatha) from the Early Devonian of Britain. Palaeontology. 1982; 25: 879–889.

17. Turner S. Siluro-Devonian thelodonts from the Welsh Borderland. Journal of the Geological Society. 1973; 129: 557–584.

18. Young GC. Ordovician microvertebrate remains from the Amadeus Basin, central Australia. Journal of Vertebrate Paleontology. 1997; 17: 1-25.

19. Sansom IJ, Davies NS, Coates MI, Nicoll RS, Ritchie A. Chondrichthyan-like scales from the Middle Ordovician of Australia. Palaeontology. 2012; 55: 243-247. doi: 10.1111/j.1475-4983.2012.01127.x

Table S1.32. Ecological data informing category decisions for modern sharks.

Species	Size Range (cm)	Reifs 1985 Category	Diet	Habitat	Oceanodromous?	Prey on Fast Fish?	Category Decision
Alopias pelagicus	262-316			Coastal/oceanic	Yes	Yes	**Fast**
A. vulpinus	260-762	Fast		Coasta/oceanic	Yes	Yes	**Fast**
Apisturus canutus	42.8-45.5			Demersal	No		**Slow/Scavenger/Ambush**
A. kampae							**Slow/Scavenger/Ambush**
A. laurissonis							**Slow/Scavenger/Ambush**
Carcharhinus acronotus	103-141.3			Coastal, Reef	No	No	**Moderate**
C. albimarginatus	174-275			Coastal, Reef	No	Yes	**Fast**
C. altimus	200-282			Deep, Reef	No	Yes	**Moderate**
C. amblyrhynchos		Nearshore		Reef	Yes	No	**Moderate**
C. brachyurus	193-305		*car, clup*	Coastal, Reef	Yes	Yes	**Moderate**
C. brevipinna	171-242		*clup, scoph*	Coastal, Reef	Yes	Yes	**Fast**
C. cerdale	85-116			Demersal			**Moderate**
C. falciformis	203-305	Fast	*car, scom*	Oceanic, Reef	Yes	Yes	**Fast**
C. galapagensis	205-330	Fast	*balist, pleur, ser*	Coastal, Reef	No	No	**Moderate**
C. isodon	129.8-189		*clup, scia, scom*	Coastal, Demersal	No	Yes	**Fast**
C. leucus	160-324		*car, cent, meg, mug, scom*	Coastal, Reef	No	Yes	**Moderate**
C. limbatus	142.5-202		*car, clup, elop, haem, inverts, mug* squid	Coastal, Reef	No	Yes	**Fast**
C. longimanus	180-350		*cor, scom,*	Oceanic	Yes	Yes	**Fast**
C. melanopterus				Reef	No	No	**Moderate**

C. obscurus	270.1-384	Fast	*car, mug,* octopus, *pleur, ser, sph*	Coastal/oceanic, Reef	Yes	Yes	**Fast**
C. perezii	170-249		*exo, sco*	Coastal, Reef	No	No	**Moderate**
C. plumbeus	180-234	Nearshore	*car,* catfish, *clup, lut, mug, sciaen, scom,* small sharks, *spar, sph, syn*	Coastal, Reef	Yes	Yes	**Moderate**
C. porosus	73-110		small bony fish	Coastal, Demersal	No	Yes	**Moderate**
C. signatus	287			Bathyal, Demersal	No	Yes	**Fast**
Carcharodon carcharias	339.5-600	Fast	mammals, sharks	Pelagic, Coastal, Oceanic	Yes	Yes	**Fast**
Galeocardo cuvier	290-472	Nearshore		Coastal/oceanic, Demersal	Yes	Scavenger	**Moderate**
Galeorhinus galeus	155-198		*scom*	Coastal, Demersal	Yes	Rarely	**Moderate**
Hexanchus griseus	325-482	Slow		Bathyal, Bathydemersal, Demersal	Yes	Ambush	**Slow/Scavenger/Ambush**
H. nakamurai	144-169			Bathyal, Bathydemersal, Demersal	No	Scavenger	**Slow/Scavenger/Ambush**
Isurus oxyrhinchus	195-380	Fast	*inverts, istio, Prionace glauca, xiph*	Coastal/oceanic	Yes	Yes	**Fast**
I. paucus	228.6-427	Fast	*dio,* squid	Oceanic	Yes		**Fast**
Lamna ditropis	158-282	Fast	*gad, salm*	Coastal/Oceanic	Yes	Yes	**Fast**
L. nasus	186-263	Fast	*alep, clup, gad, scom, sebas, str*	Coastal/Oceanic	Yes	Yes	**Fast**
Megachasma pelagios	450-544		Planktonic	Bathydemersal, Oceanic	Yes	No	**Slow/Scavenger/Ambush**
Nasolamnia velox	125-161			Coastal/oceanic, Demersal	No	No	**Moderate**

Negaprion brevirostris	227-291	Nearshore	*bat, eng, ger, haem, hem, lutjan, spar*	Coastal, Reef	Yes	Yes	**Moderate**
Odontaspis ferox	364			Coastal/oceanic, Demersal		Yes	**Moderate**
Prionace glauca	182-383	Nearshore	*bram, clup, gad, sal, scom, str*	Pelagic/oceanic	Yes	Yes	**Fast**
Rhincodon typus	900-1218		*clup,* Planktonic, occassional *scom,*	Pelagic/oceanic	Yes	Yes	**Slow/Scavenger/Ambush**
Rhizoprionodon longurio	83-116		fishes, *inverts*	Coast, Demersal	No		**Moderate**
R. terraenovae	80-106.5		small fishes, *pleur*	Coast, Demersal	No	Yes	**Moderate**
Sphyrna corona	67.2			Coastal, Demersal	No		**Fast**
S. lewini	135-326	Fast		Coastal/oceanic	Yes	Yes	**Fast**
S. media	82.7-111		fishes, shrimp, squid	Demersal	No		**Moderate**
S. mokarran	210-548		*car, meg,* Sharks	Coastal/oceanic	Yes	Yes	**Fast**
S. tiburo	68-130.8		*inverts, spa*	Coastal, Reef	No	No	**Moderate**
S. tudes	80-148	Fast	*ari, inverts*	Coastal/oceanic, Demersal	No	No	**Moderate**
S. zygaena	240-266	Fast		Pelagic/oceanic	Yes	Yes	**Fast**
Triaenodon obesus	105-168	Nearshore	reef fishes, Crustaceans	Benthic, Reef	No	No	**Moderate**
Zameus squamulosus				Demersal	No		**Slow/Scavenger/Ambush**

Abbreviations: alep = Alepisauriformes; ari = Ariidae; balist = Balistidae; bat = Batrachoididae; bram = Bramidae; car = Carangiformes; cent = Centropomidae; clup = Clupidae; cor = Coryphaenoides; dio = Diodontidae; elop = Elopidae; eng = Engraulidae; exo = Exocoetidae; gad = Gadiformes; ger = Gerreidae; haem = Haemulidae; hem = Hemiramphidae; Inverts = Invertebrates; ist = Istiophoridae; lut = Lutjanidae; meg = Megalopidae; mug = Mugilidae; pleur = Pleuronectiformes; sal = Salmonidae; scia = Sciaenidae; scop = Scophthalmidae; scom = Scombridae; ser = Serranidae; Spa = Sparidae; sph = Sphyraenidae; str = Stromateidae; syn = Syngnathidae; xiph = Xiphiidae

Principle Source Data for Supplementary Table 2

Castro JI. The sharks of North America. New York: *Oxford University Press*; 2011.

Froese R, Pauly D. FishBase 2011. World Wide Web electronic publication. www.fishbase.org, (06/2014)

Reif WE. Squamation and ecology of sharks. *Courier Forschungsinstitut*. Senckenberg Frankfurt am Main. 1985; 78: 1-255.

Appendix II Supplementary Data Relating to Experimental Analysis

A2.1. Examined material

Table S2.1 List of institutions and notable fossil specimens used to inform the design of scaled plate blocks.

Institution	Taxa (uncorrected / as catalogued)	Specimen number (on label)	Figure	Squamation		
				Scale overlap (not including spines)	Well-ordered rows	Packing / interscale spacing
Natural History Museum, London, UK	*Acanthodes sulcatus*	P57555/6	S2.1.	No	Yes	Tight
	Cheiracanthus latus	P50105	S2.2.	No	Yes	Tight
	Climatius reticulates	P1343a	S2.3.	No	Yes	Tight
	Diplacanthus longispinus	P1369	S2.4.	No	Yes Variable	Tight
	Lanarkia horrida	P11030		No	Variable	Tight
		P42009		No	Yes	Tight
	Loganellia scotica	P11282	S2.6.	No	Yes	Tight
		P13026		No	Yes	Tight
	Parexus falcatus	P130		No	Yes	Tight
	Ptomacanthus anglicus	P16615.1		No	Yes	Tight
		P19998		No	Yes	Tight
	Thelodus mackintoshi	P52444		No	Yes	Tight
	Uraniacanthus spinosus	P20000.1		No	Yes	Tight
	Vernicomacanthus waynensis	P24938a		No		Tight
National Museum of Scotland, Edinburgh, UK.	*Acanthodes sp.*	1950 38 9		No	Yes	Tight
	Climatius reticulates	1887 35 5C		No	Yes	Tight
						Tight
	Diplacanthus longispinus	1891 92 199		No	Yes	Tight
	Ischnacanthus gracilis	1953 4 3		No	Yes	Tight
	Lanarkia horrida	1956 14 16		No	Yes	Tight
		1991 48 3		No	Partially	Tight
		1991 48 8		No	?	Tight
	Lanarkia lanceolota	1991 48 6	S2.5.	No	Partially	Tight
	Loganellia scotica	1902 39 1		No	Yes	Tight
		1995 93 2		No	Yes	Tight
		1995 93 5		No	Yes	Tight
		1905 3 2		No	Yes	Tight
		FR 1623		No	Yes	Tight

	Logania scotica	1965 59 7		No	Yes	Tight
		1905 3 4		No	Yes	Tight
		1905 3 5		No	Yes	?Tight
		1905 4		No	Yes	Tight
		1967 65 18		No	Yes	Tight
		1967 65 20		No	Yes	Tight
		1967 65 21		No	Yes	Tight
		1986 34 1		No	Partially	?Tight
	Parexus falcatus	1887 35 4		No	Yes	Tight
	Shielia taiti	1929 5 41		No	Yes	Tight
		1901 68 2		No	Yes	?
	Thelodus sp.	FR 1422		?	?	Tight
	Vernicomacanthus uncinatus	189192208		No	Yes	Tight
				No	Yes	
Sedgwick Museum of Earth Sciences, Cambridge, UK (including off-site store)	*Canobius politus*	E4855		No	Yes	Tight
	Cheirolepis cummingiae	H9927		No	Yes	Tight
	Cheirolepis trailli	H4477		No	Yes	Tight
		H4488		No	Yes	Tight
	Ctenothrissa radians	B94763		Yes	Yes	Tight
	Diplacanthus longispinnus	H4406		No	?	Tight
	Diplacanthus striatus	H4410		No	Yes	Tight
	Diplopterus agassizii	H4587		Partially	Yes	Tight
	Eugnathus orthostomus	J61279		Yes	Yes	Tight
	Holoptychius andersoni	P594		Yes	Yes	Tight
		H4667		Yes	?	Tight
	Hoplopteryx lewisiensis	B8961		Yes	Yes	Tight
	Hoplopteryx superbus	B8969		Yes	Yes	Tight
	Pholidophorus latiusculus	N/A		Yes	Yes	Tight
University Museum of Zoology, Cambridge, UK	Indet. Acanthodian	GN13		No	Yes	Tight
		GN19		No	Yes	Tight
		GN21		No	?	Tight
	Homalacanthus affinis	GN25		No	Yes	Tight
	Meidiichthys browni	GN311.2		Partially	Yes	Tight
	Mesacanthus mitchelli	GN1		No	Yes	Tight
	Indet. Palaeoniscid	GN411		Partially	Yes	Tight

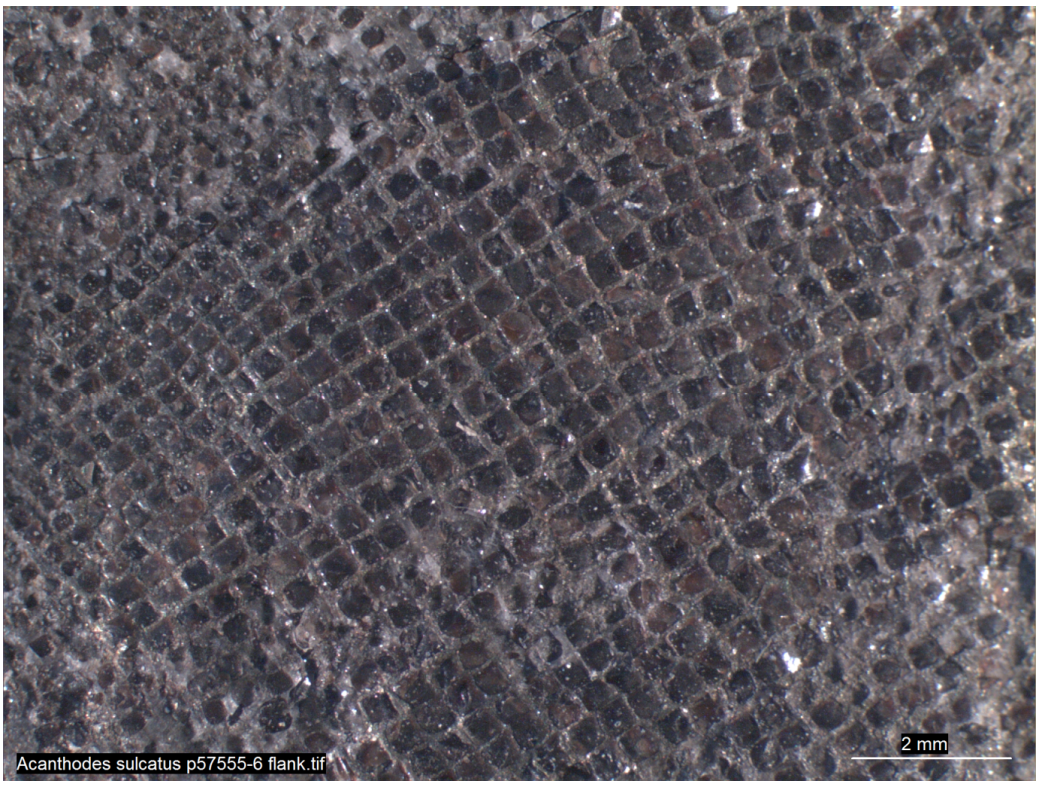

Figure S2.1. Flank scales of the acanthodian *Acanthodes sulcatus*, NHMUK P57555. Scale bar = 2mm.

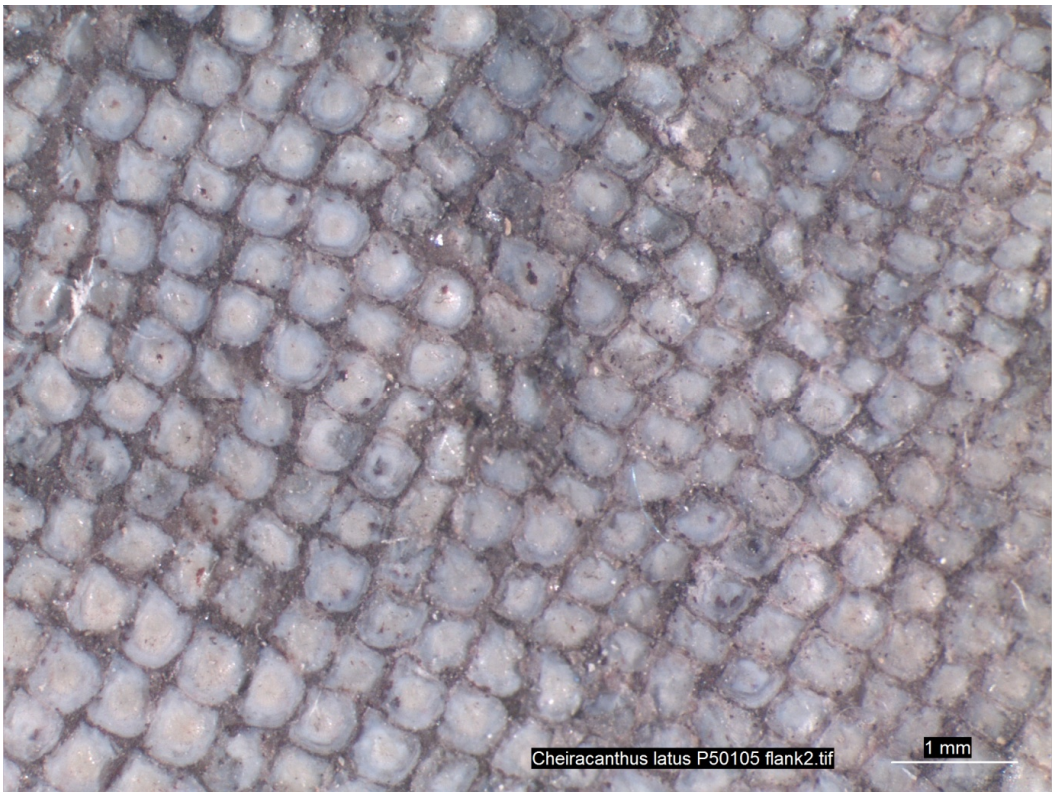

Figure S2.2. Flank scales of the acanthodian *Cheiracanthus latus*, NHMUK P50105. Scale bar = 1mm.

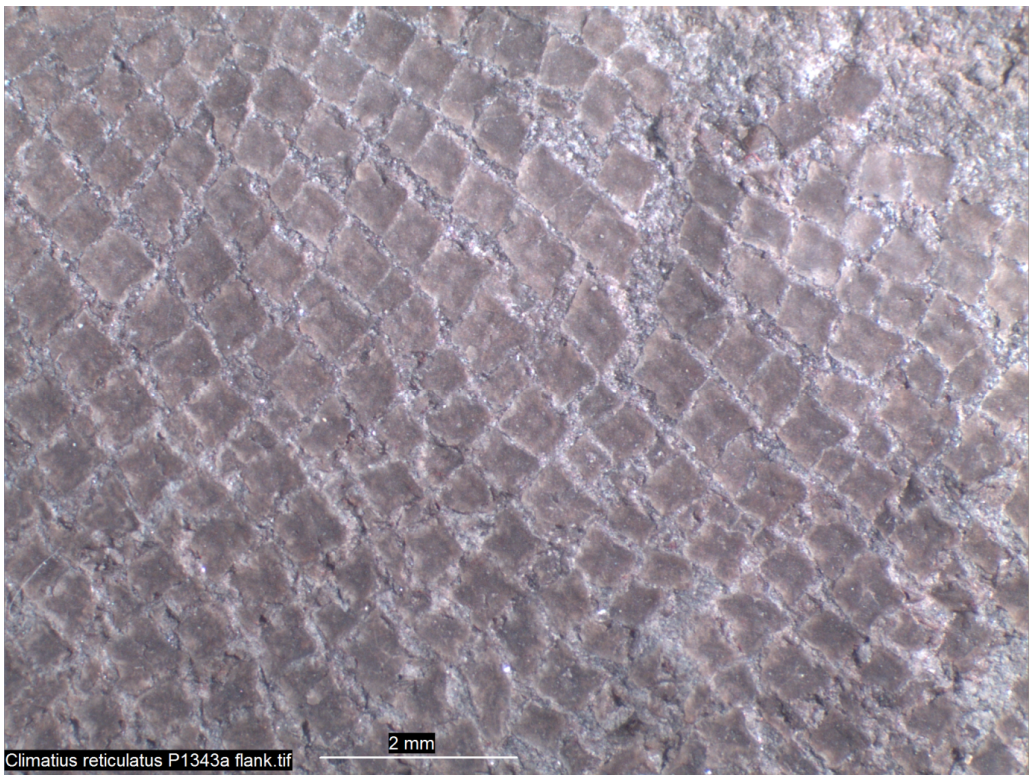

Figure S2.3. Flank scales of the acanthodian *Climatius reticulatus*, NHMUK P1343a. Scale bar = 2mm.

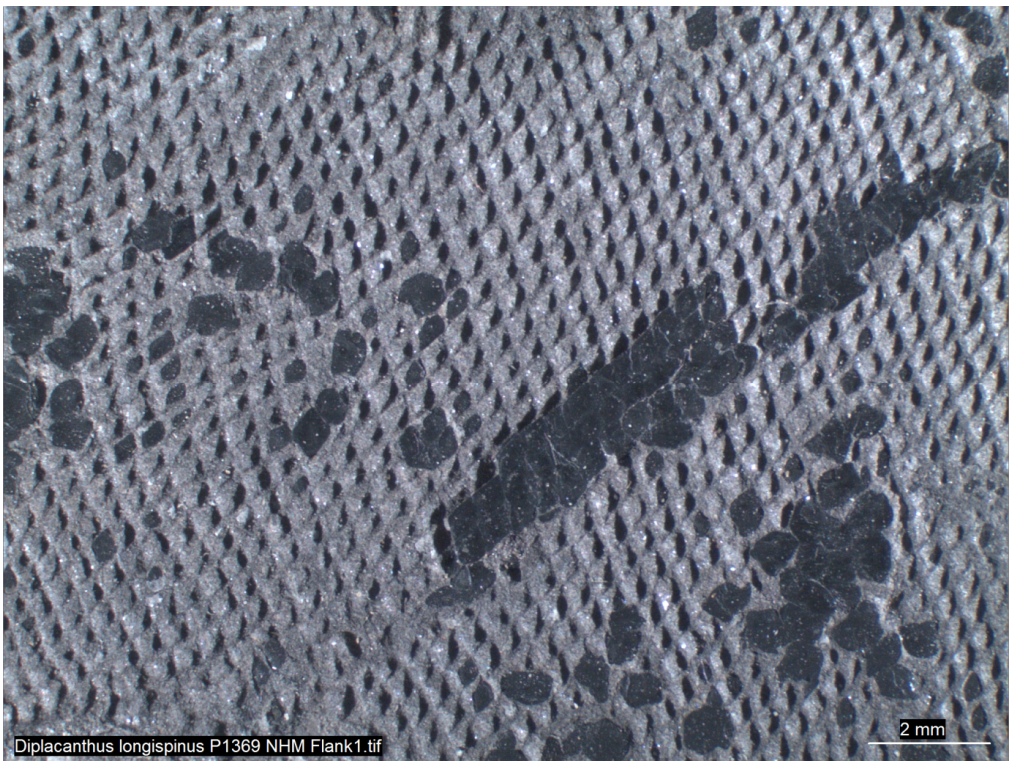

Figure S2.4. Flank scales of the acanthodian *Diplacanthus longispinus*, NHMUK P1369. Scale bar = 2mm.

Figure S2.5. Flank scales of the thelodont *Lanarkia lanceolata*, NMS 1991486. Scale bar increments = 10 mm.

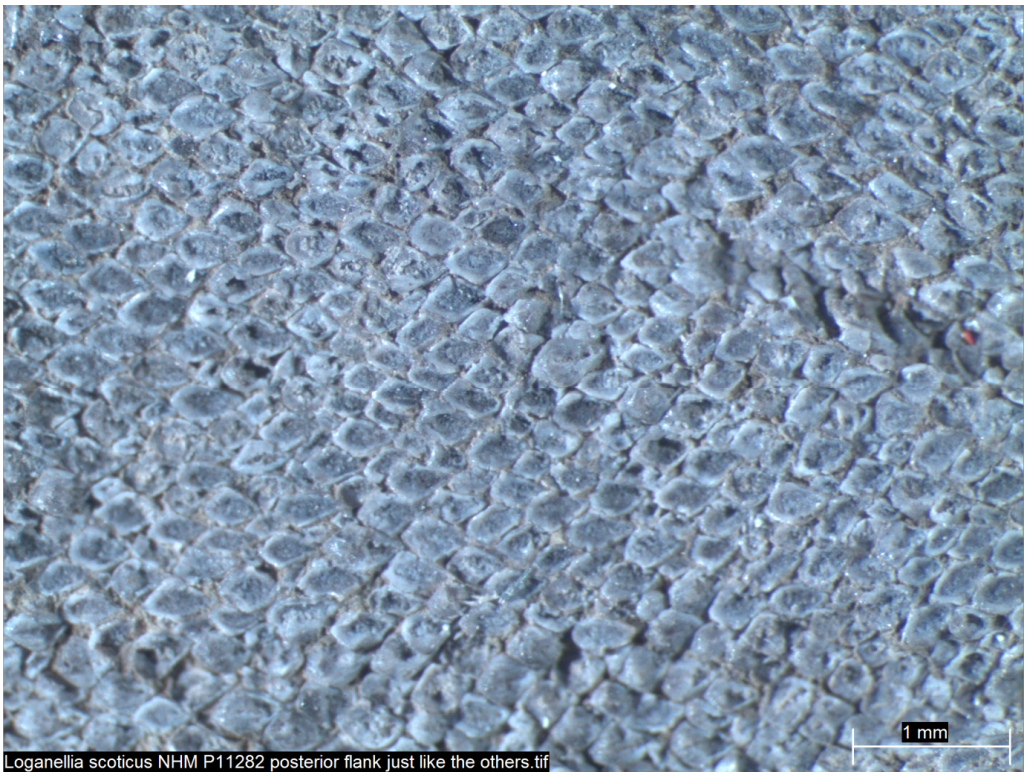

Figure S2.6. Flank scales of the thelodont *Loganellia scotica*, NHMUK P11282. Scale bar = 1mm.

b) Modern examined material

Polypterus senegalus

Figure S2.7. *Polypterus senegalus* bichir specimen used to examine scale tessellation of a 'ganoid fish', and, informing the design of the *Lophosteus* scale blocks using the primitive condition of actinopterygian squamation. Specimen was 363mm.

A2.2. Laser Doppler Anemometry Data Acquisition

Table S2.2. Raw LDA data acquisition during smooth plate experimental run, showing number of measurements used to calculate mean velocity, and validation (%).

Vertical (mm)	Smooth Plate Horizontal Profile Position									
	200 mm		250 mm		300 mm		350 mm		400 mm	
	n	V. (%)	n	V. (%)	n	V. (%)	n	V. (%)	n	V. (%)
0	6	50	1	100	0	NaN	1	100	24	87.5
0.01	11	53.54	1	100	0	NaN	8	86.67	48	91.92
0.02	9	30.1	0	NaN	0	NaN	7	64.38	28	96.43
0.03	16	36.4	0	NaN	0	NaN	1	0	81	87.86
0.04	6	33.86	8	50	0	NaN	4	50	89	85.73
0.05	3	100	10	80.95	1	100	2	100	117	85.06
0.06	2	20	11	51.67	0	NaN	1	100	214	87.04
0.07	0	NaN	19	57.22	4	50	3	100	250	87.59
0.08	2	16.67	995	87.89	24	98.44	2	100	358	91.52
0.09	0	NaN	5913	81.09	7	90	4	83.33	378	89.69
0.1	6	26.73	4800	80.93	19	68.89	7	58.33	490	87.93

0.2	81	84.46	2028	72.38	1531	82.15	1392	82.93	1615	86.68
0.3	778	87.11	3596	60.94	675	87.02	5237	79.38	2475	89.64
0.4	1673	74.08	5565	76.43	1483	86.18	4045	84.22	2439	89.8
0.5	1743	87.99	2823	86.37	1257	87.14	1566	89.92	1926	88.93
0.6	1491	90.79	1972	84.86	1401	86.43	1150	90	1703	87.3
0.7	1676	90.79	1826	78.06	1419	90.71	1237	92.35	1794	89.4
0.8	1778	92.22	1945	89.62	1366	92.82	1051	90.19	2190	91.65
0.9	1492	89.57	1849	92.31	1318	92.13	1066	90.75	2605	90.42
1	1542	90.05	1823	91.77	1168	92.82	1110	91.25	2935	90.21
1.1	1604	90.5	1866	90.62	1194	92.67	1428	92.18	3009	89.88
1.1	1534	91.16	1782	92.63	1250	91.91	1474	92.26	3345	88.98
1.2	1930	90.55	2037	91.19	1369	93.1	1637	93.06	3406	88.94
1.3	2363	92.57	2036	93.36	1431	94.06	1871	93.42	3774	89.63
1.4	2557	91.16	2105	92.38	1468	93.5	1966	92.67	3596	89.27
1.5	2816	92.66	2292	92.03	1543	94.74	2034	91.86	3831	90.73
1.6	2882	91.66	2297	92.57	1588	93.77	1940	92.11	3773	91.07
1.7	2959	92.22	2123	91.62	1738	94.93	2002	93.08	3967	89.45
1.8	2875	90.83	2216	93.11	1690	93.61	1997	89.42	3767	89.26
1.9	2874	92.12	2304	93.02	1860	94.64	2092	94.31	4015	91.66
2	3105	92.83	2313	93.26	1802	93.6	2149	91.9	3944	91.01
2.1	2906	92.74	2180	94.01	1712	94.25	2156	92.82	3859	90.78
2.2	3000	93.32	2307	93.34	1737	94.28	2143	93.92	3989	91.16
2.3	3017	91.02	2264	93.58	1787	94.09	2062	93.66	4043	90.72
2.4	2966	94.02	2215	94.38	1742	94.06	2144	92.93	3982	91.17
2.5	2965	92.55	2133	94.02	1836	94.69	2129	94.42	3953	90.53
2.6	2866	93.05	2252	93.48	1831	95.18	2167	94.89	3854	91.83
2.7	3052	92.31	2265	94.65	1801	93.38	2121	94.23	4160	91.35
2.8	3031	93.32	2282	94.08	1842	93.67	2172	92.53	4077	90.38
2.9	3085	93.16	2311	93.4	1947	94.88	2232	93.54	4218	91.63
3	3147	93.67	2259	92.89	1986	92.91	2121	92.4	4244	91.15
3.15	3271	94.27	2269	94.36	1849	95.2	2274	94.77	4146	91.86
3.3	3159	92.83	2219	93.19	1837	94.37	2334	93	4174	91.04
3.5	3023	93.16	2346	93.22	1924	96.2	2361	93.74	4061	91.67
3.7	3467	93.47	2294	92.21	1970	95.15	2397	93.5	4134	92.4
3.9	3345	93.54	2409	94.59	1884	96.2	2395	93.49	4406	93.75
4.1	3113	93.82	2370	95.08	1812	95.14	2370	93.2	4277	93.51
4.3	2918	93.78	2284	94.33	1868	94.8	2442	93.96	4459	92.85
4.5	3043	93.56	2450	93.66	1914	94.99	2276	93.74	4529	92.12
4.75	3069	93.97	2332	94.12	1908	94.54	2411	95.13	4411	92.53
5	3173	93.67	2385	94.27	1917	95.9	2352	94.43	4577	92.87
5.25	3096	93.48	2401	95.39	2012	91.71	2267	92.58	4781	92.73
5.5	3088	93.43	2389	94.37	1971	95.7	2344	94.05	4871	91.91
5.75	3055	94.28	2417	93.61	1823	95.42	2251	94.33	4652	91.86
6.05	3073	91.97	2415	95.29	2008	96.15	2350	95.01	4619	92.43
6.68	3084	93.66	2401	94.52	1934	96.74	2277	94.79	4934	92.35
7.39	3145	93.29	2486	95.72	2022	95.48	2325	95.33	5057	93.02
8.16	3205	93.63	2345	94.25	2063	95.74	2342	94.42	4849	92.53
9.02	3018	94.15	2401	94.71	2213	95.78	2470	94.62	4484	93.53
9.97	2992	93.77	2433	94.52	2014	94.64	2441	93.52	4569	93.3
11.02	3171	93.29	2578	95.08	2110	94.96	2484	94.46	4734	93.75
12.18	3084	92.42	2895	94.07	2263	96.2	2478	94.76	5236	94.13
13.46	3361	94.46	2548	96.02	2304	95.82	2551	96.05	5112	93.29
14.88	3197	93.31	2541	94.94	2363	94.9	2666	95.69	4972	93.73
16.44	3257	94.23	2546	94.82	2293	94.85	2763	94.41	4763	93.53
18.17	3347	94.57	2532	96.28	2275	95.13	2538	94.16	5195	94.04
20.08	3444	94.81	2446	95.02	2702	95.93	2564	93.53	5420	93.5
22.19	3467	94.41	2406	96.41	2408	95	2572	95.55	5065	94.08
24.53	3254	94.76	2510	94.5	2365	95.1	2558	94.71	5185	93.39
27.11	3541	94.87	2399	95.52	2354	96.2	2621	95.4	5046	94.57

29.96	3374	93.98	2317	95.34	2459	94.19	2807	94.88	4864	93.56
33.11	3435	95.11	2394	95.52	2387	95.28	2658	94.9	5049	94.26
36.59	3522	95.59	2487	96.4	2561	96.13	1069	97.58	5408	94.03
40.44	3332	94.01	2112	95.93	2527	96.06	2566	95.28	5065	93.86
44.69	3137	95.47	2454	96.16	2315	95.55	1500	93.89	4861	94.41
49.39	3430	94.95	2536	94.85	2444	96.5	2129	93.91	5140	94.2
54.59	3189	95.21	1932	95.15	2306	95.96	2394	92.24	4519	95.29
60.33	3147	94.99	2150	95.68	2442	96.97	1988	96.01	4194	94.69
66.67	2876	95.37	2001	96.33	2080	95.49	1639	95.06	4323	94.56
73.69	2834	94.89	2086	96.2	2495	96.2	4445	92.28	3542	94.14
81.44	2594	95.55	1936	95.53	1884	95.33	3832	93.89	3703	94.08
90	3178	94.69	1923	97.15	1873	95.61	4285	94.72	3387	94.13

Table S2.3. (Below) Raw LDA data acquisition during *Loganellia scotica* plate experimental run, showing number of measurements used to calculate mean velocity, and validation (%).

Vertical (mm)	*Loganellia scotica* Plate Horizontal Profile Position									
	200 mm		**250 mm**		**300 mm**		**350 mm**		**400 mm**	
	n	V. (%)	n	V. (%)	n	V. (%)	n	V. (%)	n	V. (%)
0	14449	94.31	4156	61.21	19699	94.5	23643	97.5	10032	98.41
0.01	21512	96.79	3546	70.08	23904	94.69	21244	97.33	16799	97.79
0.02	19412	95.39	5066	79.36	21307	93.48	19857	95.33	17720	97.25
0.03	373	67.68	12057	93.4	19847	90.9	0	80.86	22485	94.77
0.04	338	65.53	9552	77.62	20916	90.23	7278	86.58	17262	91.36
0.05	374	68.3	5481	94.31	26678	92.75	18058	97.55	12990	85.93
0.06	288	69.03	410	76.49	29361	92.83	0	65.66	16116	83.93
0.07	378	64.4	3447	98.25	18591	90.81	1853	95.46	11792	82.44
0.08	142	70.13	1110	98.62	2365	65.16	334	81.23	3659	63.97
0.09	275	64.15	4748	87.63	2559	66.37	2097	96.99	3209	62.73
0.1	225	70.19	16090	95.61	2855	70.27	10214	98.61	3587	63.14
0.2	1155	84.08	32494	83.65	1370	50.49	19764	95.77	1601	53.16
0.3	620	77.09	7631	82.11	1239	52.61	1477	54.1	1816	52.78
0.4	595	64.1	32933	79.55	1503	55.79	1155	50.77	2362	71.77
0.5	1079	52.79	11640	63.87	1602	81.84	1468	61.69	2750	83.63
0.6	934	81.46	2855	63.89	1838	79.11	1776	67.34	2544	91.08
0.7	1266	82.91	2295	60.2	1720	84.52	1598	63.84	2818	89.77
0.8	1341	86.64	1940	66.08	1707	89.86	1639	84.89	3334	90.59
0.9	1221	88.6	2680	90.28	1883	91.37	2115	90.31	5198	90.81
1	1302	89.43	2737	89.59	2619	89.45	2548	91.39	5997	89.52
1.1	1490	83.17	3211	89.24	3168	90.01	3226	91.62	6389	89.2
1.1	1385	79.27	3229	89.73	3189	90.27	3082	91.68	6458	90.01
1.2	2017	90.55	3745	90.23	3476	92.07	3477	91.68	6479	89.49
1.3	2477	89.27	4069	90.81	3686	90.44	3624	91.1	6494	88.99
1.4	2814	89.27	3889	91.42	3892	90.57	4050	91.4	7067	89.34
1.5	2940	88.2	3747	91.37	3953	91.97	6740	90.53	7334	90.92
1.6	3124	89.96	4169	91.05	4105	91.07	5972	90.27	7374	90.97
1.7	3262	90.17	4227	89.86	4146	90.48	6284	91.23	7434	89.96
1.8	3434	89.62	4330	92.03	4189	91.92	6812	89.61	7400	90.64
1.9	3445	90.31	4250	91.49	4410	92.27	6962	90.51	7587	90.87
2	3676	88.63	4270	91.75	4294	92.13	6874	90.13	7854	90.57
2.1	3549	89.8	4205	91.49	4472	92.47	6880	90.72	7867	90.24
2.2	3583	89.9	4454	92.65	4268	91.98	7251	90.78	8009	90.54
2.3	3763	90	4677	91.35	4436	92.22	7277	90.43	8027	90.31
2.4	3703	91.53	4793	92.69	4612	90.56	7019	90.76	8336	90.07
2.5	3867	91.5	4980	91.83	4769	92.44	7554	89.98	8297	90.67

2.6	3777	90.52	5252	91.17	4758	91.41	7161	90.07	8339	90.4
2.7	3937	91.81	5108	92.76	4855	92.15	7352	91.51	8558	90.28
2.8	4060	92.15	5195	91.97	4784	91.36	7192	91.86	8462	90.39
2.9	3700	91.73	5048	91.96	4868	92.98	7329	92.06	8722	90.6
3	3692	92.1	5129	92.11	4684	93.41	7454	92.4	8783	91.67
3.15	3869	91.84	5127	92.12	4674	93.2	7508	91.95	8544	90.75
3.3	3744	92.06	5213	92.18	4723	92.65	7295	91.32	8770	91.05
3.5	3737	91.49	5031	92.66	4727	93.16	7660	91.82	8800	91.2
3.7	3750	92.34	5183	92.84	4469	93.49	8140	91.34	8721	91.2
3.9	3703	92.43	5196	92.2	4447	93.32	7748	91.77	8950	91.06
4.1	3711	92.61	5121	93.26	4686	92.61	8197	91.84	9189	91.47
4.3	3811	93.16	5132	91.82	4477	93.39	8123	91.58	8602	91.41
4.5	3727	93.35	5230	92.67	4626	93.83	7721	92.48	8880	90.77
4.75	5658	91.83	5328	92.92	4724	94.71	7835	92.66	8834	92.07
5	5243	92.53	5348	93.3	4731	94.06	7677	92.06	8995	91.95
5.25	5186	92.51	5100	93.54	4488	94.17	7774	92.66	8952	91.86
5.5	5199	91.89	5122	93.38	4556	92.37	7513	91.93	8805	90.72
5.75	5330	92.18	5009	93.38	4602	93.32	7867	92.63	8821	92.83
6.05	5345	92.45	5389	93.79	4621	94.84	8160	92.69	8776	92.35
6.68	5359	93.01	5208	94.02	4675	94.26	8207	93.32	8758	92.19
7.39	5312	92.14	5329	93.51	4657	93.85	7906	93.07	9388	92.23
8.16	5327	93.46	5338	93.59	4548	94.65	8276	92.97	9632	92.52
9.02	5546	93.24	5385	94.35	4718	94.96	8009	92.67	9608	92.5
9.97	5532	92.63	5339	94.56	4670	94.7	8258	93.28	9332	93.27
11.02	6106	93.91	5403	93.85	4776	93.92	8148	93.39	9383	92.12
12.18	5809	92.76	5887	93.11	4707	95.38	8167	94.04	9178	93.97
13.46	5798	93.12	6320	94.68	4851	94.25	8354	93.17	9206	92.59
14.88	5889	94.1	5451	94.67	4846	94.07	7691	93.96	9157	93.88
16.44	5802	92.89	5550	95.04	4856	94.12	8279	93.92	9520	92.84
18.17	5574	94.06	5375	94.52	4786	95.08	8149	94.63	9461	93.57
20.08	5760	93.78	5425	94.47	4689	94.43	8041	93.86	9673	93.65
22.19	5751	94.49	5496	95.13	4506	95.12	8391	93.91	9509	93.85
24.53	5666	92.97	5365	95.2	4797	95.04	8091	94.04	9263	93.3
27.11	5612	94.32	5442	94.81	4838	95.37	8314	94.16	9721	93.67
29.96	5593	94.33	5329	94.23	4758	94.88	8875	93.24	9494	93.8
33.11	5611	93.97	5387	93.92	4564	95.43	7944	94.06	9406	93.26
36.59	5430	94.79	5123	93.83	4832	94.78	7254	93.64	9154	93.52
40.44	5429	94.36	5104	95.1	4578	95.5	7509	93.58	9189	93.47
44.69	5307	94.3	4685	93.51	4623	94.66	5122	88.39	8564	94.09
49.39	5355	94.71	5095	94.13	4581	93.63	7530	94.16	8403	94.03
54.59	5190	94.13	5304	94.64	4494	95.67	6942	94	8161	93.18
60.33	5321	94.72	4990	94.99	4160	95.28	6703	94.25	8005	93.78
66.67	5114	92.5	5486	94.15	4450	95.11	5632	94.1	7929	94.01
73.69	4839	94.23	4905	95.03	3894	94.32	6401	94.1	7720	94.6
81.44	4782	93.45	5790	94.53	4332	95.05	9181	94.01	6838	92.4
90	6434	94.44	4313	94.69	3694	96.15	6362	94.41	7124	93.33

Table S2.4. (below) Raw LDA data acquisition during *Lophosteus sp.* plate experimental run, showing number of measurements used to calculate mean velocity, and validation (%).

Vertical (mm)	***Lophosteus sp.* Plate Horizontal Profile Position**									
	200 mm		**250 mm**		**300 mm**		**350 mm**		**400 mm**	
	n	V. (%)	n	V. (%)	n	V. (%)	n	V. (%)	n	V. (%)
0	18145	93.81	0	98.42	5324	97.09	34496	89.77	15961	95.33
0.01	21421	92.61	0	99.46	494	59.24	31086	90.3	35125	91.8

0.02	23601	91.14	0	95	620	53.89	31284	89.81	32360	88.19
0.03	25926	91.94	0	95.45	254	45.28	19692	80.86	10688	73.93
0.04	23970	93.33	0	98.08	199	47.46	11899	76.31	6188	67.14
0.05	24526	93.94	0	95.14	11224	91.85	4985	67.3	1682	53.93
0.06	25091	94.61	0	92.33	30598	91.04	4475	65.66	2283	57.32
0.07	23525	94.56	0	95.01	33880	90.82	4348	65.43	2368	58.16
0.08	23195	94.06	0	93.3	38522	87.19	3886	65.14	1666	56.95
0.09	25284	94.53	0	94.43	14440	91.12	3273	66.88	1518	56.87
0.1	22065	94.8	0	95.53	18776	92.55	3183	64.83	1525	55.65
0.2	14577	95.06	1	0	1475	58.17	2907	65.12	2164	72.38
0.3	2958	68.06	7	50	1426	47.75	2476	83.33	2372	67.66
0.4	1833	51.82	758	67.43	2086	80.9	3632	88.5	2911	80.26
0.5	2055	49.97	3494	69.05	2313	80.24	3786	88.91	3129	87.13
0.6	2439	74.94	4176	77.3	2713	82.93	3725	88.98	2947	89.57
0.7	2968	81.69	4196	81.82	2315	86.23	3789	88.89	3250	89.79
0.8	2917	67.71	3885	82.22	2348	90.11	4000	89.43	3889	88.38
0.9	3333	82.94	3788	83.15	2676	87.01	4498	88.37	4184	87.14
1	3677	87.22	4164	85.48	3197	88.96	5164	88.98	4297	90.03
1.1	4143	88.12	4271	86.48	3537	89.79	5660	89.07	4867	89.76
1.1	4172	87.46	4417	86.46	3577	89.93	5283	89.44	4823	89.64
1.2	4181	86.5	4729	87.16	3899	88.28	5645	87.31	4926	90.27
1.3	4619	87.81	5327	87.22	4143	88.98	5619	88.41	5132	89.51
1.4	5058	86.59	5274	87.26	4323	89.47	5949	89.55	5005	90.47
1.5	5287	87.64	5128	87.34	4318	89.28	5846	88.98	5298	88.13
1.6	5643	88.21	5171	87.87	4374	89.65	6128	88.81	7568	88.35
1.7	5875	87.73	5325	88.23	4573	89.61	6127	89.33	6842	88.72
1.8	5688	86.76	5365	88.66	4586	88.89	6199	89.55	7126	89.42
1.9	6031	87.59	5376	89.54	4471	90.16	6131	90.07	7585	88.3
2	5861	87.18	5387	90.19	4652	90.6	6183	89.48	7539	89.06
2.1	6139	88.98	5491	89.91	4758	88.04	6122	89.77	7554	89.07
2.2	6119	88.22	5389	90.14	4572	91.13	6349	90.28	7543	87.98
2.3	5932	87.79	5567	89.52	4753	89	6187	91.12	7925	89.61
2.4	6301	88.04	5501	90.19	4651	90.06	6053	89.86	7952	89.96
2.5	6147	88.24	5331	89.73	7241	89.31	6245	90.31	8080	89.28
2.6	6483	88.5	5375	90.59	6874	88.89	6232	91.35	7820	89.68
2.7	6294	89.16	5690	90.61	7281	88.94	6304	90.95	8106	89.83
2.8	6345	88.17	5582	90.71	7860	89.2	6123	90.45	8151	88.89
2.9	6220	88.01	5740	90.9	7950	89.65	6301	90.83	7888	90.06
3	6228	88.33	5509	90.05	8246	89.32	6007	90.65	8510	89.87
3.15	6526	88.53	5505	90.77	8215	89.74	6240	90.84	8516	89.09
3.3	6724	89.52	5522	90.53	7827	90.67	6304	91.34	8491	89.21
3.5	6394	89.36	5534	91.19	7414	89.66	6319	91.53	8350	90.31
3.7	6595	89.8	5446	91.57	7624	90.54	6445	90.73	8377	89.89
3.9	6636	89.69	5572	92.12	7765	90	6452	90.68	8613	90.12
4.1	6423	87.88	5570	90.43	7372	91.36	7100	91.5	8424	90.91
4.3	6584	89.88	5704	90.14	7513	91.03	7124	92.24	8256	90.44
4.5	6661	89.98	5558	91.21	7530	90.87	7183	91.63	8265	90.68
4.75	6613	89.93	5559	91.43	7270	90.63	6531	92.49	8298	90.98
5	6307	89.48	5564	91.36	7519	90.45	6456	91.82	8101	91.43
5.25	6446	90.47	5646	91.68	7441	91.2	6578	91.8	8160	92.14
5.5	6721	90.63	5605	92.23	7609	91.7	6536	91.03	8115	91.05
5.75	6664	90.36	5783	91.19	7477	92	6537	92.93	8046	90.88
6.05	6464	90.17	5756	92.09	7624	91.87	6531	91.24	7952	91.51
6.68	6630	91.42	5460	92.4	7401	92.24	6741	92.78	7909	91.44
7.39	6850	90.31	5217	93.41	7403	92.68	6556	92.47	8085	92.07
8.16	6818	90.73	5668	91.5	7287	92.45	6629	93.29	8555	92.33
9.02	6897	90.17	5726	92.1	7491	92.24	6760	93.59	8137	92.99
9.97	6904	91.37	6002	91.25	7484	92.49	6830	92.95	8603	92.32
11.02	7366	91.31	5972	91.57	7412	92.91	6850	91.98	8285	92.51

12.18	7106	91.65	6843	92.49	7711	92.46	6864	93.7	8207	92.17
13.46	7483	91.22	6861	93.11	7668	93.38	6857	93.27	8074	92.87
14.88	7441	91.74	6125	92.93	7597	93.63	6509	94.19	8187	92.42
16.44	7506	92.58	5977	92.96	7559	92.8	6728	93.61	8165	92.4
18.17	7098	91.3	5926	93.21	7543	93.41	6987	93.27	8428	92.34
20.08	7554	92.54	5825	93.37	9643	92.43	6748	93.21	8087	93.22
22.19	7335	92.38	6434	93.36	7226	92.99	6757	93.2	8483	92.66
24.53	7373	92.88	5763	92.77	7486	92.24	6706	93.42	8279	93.08
27.11	7106	92.34	5856	93.75	7612	93.43	6570	92.98	8508	92.21
29.96	6904	93.3	5878	93.84	7678	93.57	7478	94.09	8240	93.69
33.11	6752	93.03	5850	93.77	7297	93.84	6530	93.86	8425	92.68
36.59	6720	93.08	6023	94.31	7380	93.18	3700	95.71	9267	92.95
40.44	6972	93.42	5514	93.31	7148	93.3	6427	93.3	7764	93.41
44.69	6691	93.38	5600	93.6	7689	94.13	4591	93.26	8122	93
49.39	6807	93.11	6574	93.62	6623	92.83	5887	94.31	7710	93.18
54.59	6312	93.24	4975	93.5	7366	93.92	5578	90.99	6674	93.14
60.33	7068	93.21	5035	93.78	7450	93.54	5100	95.07	6074	92.47
66.67	6694	92.08	5421	93.49	6759	93.64	4997	94.37	7551	93.07
73.69	5856	91.97	4810	93.88	7819	93.34	5405	94.34	7073	92.48
81.44	5975	93.48	5233	94.03	5955	93.69	5905	93.1	6741	93.65
90	8113	92.99	4197	93.98	5325	93.41	6741	93.15	5632	92.93

Table S2.5. (Below) Raw LDA data acquisition during *Phlebolepis elegans* plate experimental run, showing number of measurements used to calculate mean velocity, and validation (%).

Vertical (mm)	***Phlebolepis elegans* Plate Horizontal Profile Position**									
	200 mm		**250 mm**		**300 mm**		**350 mm**		**400 mm**	
	n	V. (%)	n	V. (%)	n	V. (%)	n	V. (%)	n	V. (%)
0	63	35.75	13511	92.74	632	57.96	1073	59.82	28150	93.45
0.01	41	27.73	16636	95.93	2682	80.15	1880	64.69	30570	93.34
0.02	51	27.62	16098	95.51	4786	84.94	2603	66.94	28047	92.66
0.03	72	36.94	22073	96.46	11187	91.11	4220	73.44	11177	84.12
0.04	63	29.31	16772	96.79	12273	91.41	7663	80.95	4115	71.12
0.05	76	34.29	21358	97.5	8460	89.19	19212	87.82	2005	60.69
0.06	91	34.69	17142	98.22	13484	91.96	16773	84.12	1597	55.36
0.07	91	34.25	9488	99.21	17687	92.79	18652	87.93	1446	54.37
0.08	105	36.47	669	78.16	21940	94.72	11557	81.77	1407	56.02
0.09	118	37.34	483	69.77	23559	95.23	10855	81.15	1416	52.02
0.1	302	48	4069	91.99	24086	94.68	6899	73.37	2266	50.34
0.2	6465	85.57	3152	69.97	27734	93.7	2137	54.83	2487	73.96
0.3	15201	93.44	3080	62.08	2156	53.19	2046	48.73	3235	71.36
0.4	14152	81.44	2301	51.9	2309	70.84	3166	65.09	3537	78.4
0.5	2170	53.47	2492	56.78	2564	76	4277	88.39	3167	78.37
0.6	3067	59.21	3463	63.34	3312	86.88	4540	87.66	3587	87.41
0.7	3401	68.87	3718	87.71	3389	86.71	4483	90.93	3893	87.15
0.8	3625	89.27	3739	87.69	3124	84.2	4216	90.25	4936	89.22
0.9	3493	88.5	3790	83.14	3839	90.24	4781	89.32	6308	88.17
1	3750	85.81	4422	91.37	4788	91.3	5784	91.39	6808	90.26
1.1	4590	90.48	5426	91.33	5539	90.45	5948	91.54	7336	89.33
1.1	4677	89.79	5235	91.08	5370	90.22	6178	90.7	7251	90.38
1.2	5492	89.2	6341	90.18	6276	91.21	6283	91.84	7560	89.7
1.3	6428	91.52	7045	90.69	6475	91.27	6540	91.64	7877	89.63
1.4	8734	89.81	7818	90.67	6514	91.94	6821	91.2	8131	90.53
1.5	8669	89.88	8084	90.63	6893	91.35	6800	91.42	8188	90.76
1.6	9244	88.55	8085	89.95	7106	92.15	6879	91.84	8268	90.02

1.7	9896	89.49	8530	90.92	7440	91.66	6892	91.79	8279	89.15
1.8	9678	90.46	8583	90.66	7270	91.95	6964	91.17	8498	90.57
1.9	9941	89.94	8418	90.89	7333	91.57	7044	91.76	8702	90.44
2	10106	89.32	8662	90.97	7683	91.13	7105	92.34	8485	90.63
2.1	10469	89.11	8871	91.29	8191	90.73	7466	91.17	8829	91.38
2.2	10406	89.74	8902	90.72	8485	91.43	7537	91.86	8951	91.54
2.3	10330	88.83	8709	91.33	8254	90.75	7499	91.17	8863	91.01
2.4	10301	89.27	9017	91.81	8363	91.58	7057	92.72	9281	90.62
2.5	10405	89.97	8613	91.58	8205	92.1	7522	92.56	9098	91.54
2.6	10300	89.54	8427	90.65	8290	90.67	7490	91.85	9437	90.5
2.7	10485	89.57	8702	90.25	8399	91.23	7415	92.27	9051	91.27
2.8	10388	90.24	8759	90.18	8425	91.13	7394	92.46	9539	90.6
2.9	10493	89.61	8707	91.35	8626	91.44	7405	92.44	9366	90.99
3	10601	90.06	8840	91.77	8498	92.34	7272	93.46	9471	91.45
3.15	10901	90.92	8947	92.48	8864	92.03	7309	92.4	9489	91.57
3.3	10700	90.34	8967	92.04	8740	92.65	7375	91.18	9789	90.55
3.5	10756	90.47	9018	91.9	8399	92.7	7683	93.36	9678	91.7
3.7	10863	89.89	8998	92.06	8583	91.97	7752	93.59	9519	91.9
3.9	10830	90.66	9231	91.75	8867	92.25	7550	92.76	9720	91.07
4.1	10666	90.96	9208	91.37	8694	92.16	7828	92.68	9901	91.27
4.3	11415	90.71	9243	92.02	8746	92.38	8077	93.08	9987	91.75
4.5	10577	89.95	9262	91.42	8682	91.62	7647	93.37	9996	93.02
4.75	10786	90.5	9253	92.79	8972	92.8	8019	93.6	9863	92.16
5	10825	90.76	9226	91.41	9002	91.92	7696	92.91	9597	92.98
5.25	10586	90.12	9259	92.52	9028	91.93	7734	93.68	9607	92.49
5.5	10942	91.12	9382	92.68	8864	92.94	7674	92.95	9882	92.44
5.75	10882	91.1	9166	92.48	8685	92.77	7470	93.28	9811	92.47
6.05	10710	90.08	9213	92.4	9036	92.92	7661	93.75	9906	93.32
6.68	11114	91.35	9207	92.82	8742	93.15	8176	93.4	9582	93.15
7.39	11018	91.18	9076	92.44	8369	93.3	7635	92.49	9980	92.6
8.16	11237	90.21	9369	93.14	8636	93.4	7527	93.65	10223	93.15
9.02	11227	90.57	9717	93.02	8722	93.48	8026	93.68	10329	93.85
9.97	11231	91.25	10086	91.89	8778	93.08	7923	94.23	10414	93.55
11.02	11680	91.12	9890	92.67	8794	93.1	8133	94.17	10352	93.3
12.18	10875	91.04	9862	92.81	9034	93.96	8122	93.77	10118	93.3
13.46	11882	91.25	10686	92.84	9438	92.95	8036	95.28	10251	94.14
14.88	12205	91.66	10045	92.88	9119	93.02	8053	94.82	10124	93.17
16.44	12150	92.09	9828	92.68	8902	92	7969	94.73	10348	93.9
18.17	12107	92.42	10038	92.86	9198	94.28	8554	94.18	10217	93.45
20.08	11990	92.42	9929	93.99	9972	93.48	8221	94.39	10221	93.91
22.19	12018	92.63	10136	93.38	9273	94.01	8100	94.98	10498	93.23
24.53	12245	93.46	10020	93.32	9107	93.08	8022	94.2	10468	93.52
27.11	11950	92.95	9969	93.5	9222	93.78	8188	94.93	10673	93.42
29.96	12037	93.11	9881	94.08	9393	94.06	7889	94.42	10002	93.62
33.11	11796	93.29	9799	93.44	9212	93.36	8025	95.08	10431	93.99
36.59	11748	92.22	9903	92.71	9280	93.92	6690	94.57	10652	93.89
40.44	11992	93.31	8902	93.77	8984	94.72	7304	94.45	9764	94.14
44.69	11744	93.35	9527	94.07	9291	93.84	6160	94.8	10008	94.01
49.39	11445	93.03	10036	93.83	8282	94.4	7883	95.07	9247	93.19
54.59	11474	94	9308	93.6	8793	93.73	7000	93.95	9233	94.89
60.33	11789	93.7	9153	94.17	8521	93.51	7099	94.94	8773	94.51
66.67	11881	93.49	9437	93.88	8983	95.29	6092	95.64	9418	93.43
73.69	11149	92.83	9228	94.25	9366	93.98	6327	94.99	9779	93.59
81.44	11237	92.35	9260	93.86	8171	94.51	7430	94.88	7500	94.23
90	11872	92.86	8456	95.12	7337	95.09	7123	95.23	9146	94.73

Table S2.6. (Below) Raw LDA data acquisition during *Poracanthodes sp.* plate experimental run, showing number of measurements used to calculate mean velocity, and validation (%).

Vertical (mm)	*Poracanthodes sp.* Plate Horizontal Profile Position									
	200 mm		250 mm		300 mm		350 mm		400 mm	
	n	V. (%)	n	V. (%)	n	V. (%)	n	V. (%)	n	V. (%)
0	0	50	0	100	0	NaN	0	100	1130	70.24
0.01	0	53.54	0	100	0	NaN	0	86.67	2395	81.67
0.02	0	30.1	0	NaN	0	NaN	0	64.38	2032	85.76
0.03	0	36.4	0	NaN	0	NaN	0	0	12159	91.02
0.04	0	0	0	50	0	NaN	0	50	11558	92.74
0.05	0	0	0	80.95	0	100	0	100	22092	95.85
0.06	0	14.29	0	51.67	0	NaN	0	100	28423	96.64
0.07	0	0	0	57.22	0	50	2	100	22789	96.38
0.08	0	0	0	87.89	0	98.44	1	0	22860	95.75
0.09	0	NaN	0	81.09	0	90	0	83.33	23575	95.25
0.1	0	26.73	0	80.93	0	68.89	0	58.33	10712	88.17
0.2	0	84.46	0	72.38	0	82.15	6	6.22	1517	55.19
0.3	0	87.11	1	0	2	33.33	5	6.28	2519	59.21
0.4	1	0	0	76.43	0	86.18	31	17.33	2016	69.45
0.5	4	7.75	1	0	29	22.51	129	35.8	2404	61.85
0.6	0	90.79	2	16.67	1226	64.85	596	48.83	2824	89.41
0.7	0	90.79	12	11.62	7816	87.02	1032	54.83	2784	91.4
0.8	4	11.01	121	36.82	4642	71.28	1984	70.96	3062	89.47
0.9	12260	92.77	362	48.69	2919	54.89	2037	74.35	3465	90
1	9972	84.42	1016	56.88	3353	71.79	2184	84.21	4004	89.1
1.1	2225	71.59	2203	68.29	3691	86.03	2387	85.9	4616	89.23
1.1	2141	73.89	2253	68.55	3657	85.57	2383	86.15	4464	88.5
1.2	3175	81.19	3636	67.99	3542	75.25	2954	89.99	4976	90.08
1.3	4443	81.84	3508	68.24	3849	88.31	3900	89.65	5262	89.93
1.4	4805	81.81	3833	74.85	3823	88.97	4887	89.83	5468	89.9
1.5	5101	77.16	4383	88.25	3968	89.24	5217	89.23	5546	91.16
1.6	5617	76.27	4634	88.95	4731	88.26	5734	88.35	5571	90.34
1.7	5140	87.8	4774	88.11	4954	89.8	6121	88.55	5711	90.75
1.8	6080	88.42	4517	88.41	5751	89.71	6440	89.55	5611	89.42
1.9	6415	88.22	4890	90.39	6067	88.51	6751	90.04	5580	89.66
2	7179	87.94	5708	89.88	6653	89.07	6642	89.2	5716	90.46
2.1	7974	87.62	6484	89.17	6907	88.71	6754	88.95	5738	90.19
2.2	8444	87.42	7188	90.24	6819	89.24	6801	90.52	5828	90.6
2.3	8579	87.54	7293	89.58	7032	89.63	6770	90.19	5871	90.93
2.4	8781	87.48	7389	89.16	7248	89.69	6887	89.95	5715	90.65
2.5	9112	87.15	7518	88.51	7768	88.93	7176	89.55	5659	91
2.6	9430	87.98	7605	88.92	7701	89.28	7099	89.27	5812	90.2
2.7	9272	88.28	7853	89.48	7243	90.08	7269	90.68	5530	91.6
2.8	9378	87.99	7816	89.58	7199	88.53	7142	89.54	5733	91.11
2.9	9539	88.1	7919	88.88	7285	89.11	7173	90.36	5603	92.08
3	9775	87.9	8081	89.52	7362	90.77	7243	90.76	5493	91.29
3.15	9895	88.72	8285	90.98	7643	89.86	7219	90.85	5536	91.85
3.3	9796	87.25	7952	90.42	7606	89.29	7258	91.31	5420	91.77
3.5	9789	88.9	8130	88.82	7772	91.5	7346	90.2	5680	91.98
3.7	9677	89.45	8110	88.87	7120	90.4	7816	90.88	5708	91.94
3.9	9489	88.8	8208	89.57	7719	90.62	7703	91.35	5575	92.26
4.1	9860	89.95	8213	90.25	7739	90.47	7358	91.28	5686	93.22
4.3	9734	89.51	8215	89.46	7854	91.16	7411	90.75	5861	92.63
4.5	9768	88.54	8279	90.35	7695	91.7	7222	91.17	5996	92.63
4.75	9957	89.01	8420	90.61	7835	91.98	7026	91.32	5841	92.14
5	9827	89.8	8643	90.82	7923	91.58	7102	90.06	6107	92.27

5.25	9985	89.11	8405	91.28	7943	91.87	7142	91.68	6139	92.34
5.5	9995	89.82	8725	91.18	8080	90.81	7173	91.59	5942	92.53
5.75	9964	89.78	8623	91.68	8142	91.97	6997	91.92	6324	92.78
6.05	9796	89.79	8753	91.63	7929	90.71	7100	92.47	6383	93.31
6.68	10126	89.17	8887	90.72	7591	91.5	7355	92.85	6315	92.22
7.39	10087	90.74	8941	91.36	8140	91.54	7236	92.68	6315	92.85
8.16	10154	89.96	8773	90.06	8197	90.86	7541	92.34	6257	92.99
9.02	10218	90.48	8742	90.28	8137	91.4	7632	92.23	6049	94.06
9.97	10053	90.68	9259	91.78	8325	91.55	7561	92.01	6298	93.4
11.02	10684	90.36	9533	91.06	8475	91.66	7151	92.05	6742	92.36
12.18	10309	90.87	10329	91.27	8257	92.51	7443	92.59	6919	93.34
13.46	10677	89.99	9805	91.12	8422	91.81	7541	92.91	6815	93.02
14.88	10710	90.19	9106	91.91	8977	91.73	7647	92.29	6833	93.55
16.44	10687	89.93	9352	92.34	9037	92.16	7602	92.67	6667	93.61
18.17	10976	91.32	9370	92.07	8942	92.01	7397	92.9	6591	93.48
20.08	10812	91.96	9257	91.84	8933	92.22	7860	92.52	6745	93.2
22.19	11101	91.33	9145	91.47	8875	92.96	7511	92.53	6333	93.15
24.53	10834	91.99	9547	93.01	8702	92.56	7676	93.3	6300	94
27.11	11136	91.72	9569	92.11	8668	92.12	7919	93.15	6396	93.13
29.96	11032	92.34	9514	93.13	8475	92.3	8160	93.01	6229	93.46
33.11	11123	91.39	9529	92.76	8899	92.86	7736	92.82	6185	93.38
36.59	10627	91.91	9134	93.21	9091	92.28	6352	93.57	6343	93.67
40.44	10739	92.35	9115	93.41	8619	92.39	6772	93.42	6260	93.21
44.69	11008	92.16	9375	91.92	8344	93	5082	93	5596	93.12
49.39	11073	91.49	8790	92.22	8719	92.87	7177	93.12	6326	93.34
54.59	10395	91.7	8598	92.85	8143	92.88	6835	93.35	5831	93.88
60.33	10039	91.95	8686	92.7	8076	92.72	6357	92.77	5542	93.74
66.67	9600	92.16	8746	93.35	7715	92.28	5528	93.38	4960	93.57
73.69	9571	92.86	8474	92.69	8351	93.05	5897	92.96	5501	93.61
81.44	9325	92.3	8452	93.11	8713	92.42	7135	93.07	5554	92.98
90	11757	91.61	7773	93.72	6859	93.08	5706	93.43	3833	93.63

Table S2.7. (below) Raw LDA data acquisition during *Nostolepis striata* plate experimental run, showing number of measurements used to calculate mean velocity, and validation (%).

Vertical (mm)	*Nostolepis striata* Plate Horizontal Profile Position									
	200 mm		**250 mm**		**300 mm**		**350 mm**		**400 mm**	
	n	V. (%)	n	V. (%)	n	V. (%)	n	V. (%)	n	V. (%)
0	42	27.84	19466	98.42	31581	92.52	30313	94.06	18738	97.43
0.01	115	44.55	5877	99.46	35543	92.95	31128	93.8	16187	90.71
0.02	145	52.8	1172	95	33359	94.64	31300	94.1	7520	91.38
0.03	138	50.98	1309	95.45	18959	95.92	30224	93.3	8890	93.38
0.04	115	45.42	9727	98.08	16796	95.63	28576	93.07	9848	85.6
0.05	121	48.9	17838	95.14	32017	95.09	17820	90.54	5395	83.91
0.06	321	62.84	21742	92.33	17159	93.68	19139	89.6	7157	81.99
0.07	307	58.39	23541	95.01	15390	93.35	25230	92.99	15854	89.94
0.08	875	71.78	22245	93.3	19881	92.79	26742	94.5	24485	92.11
0.09	339	60.61	13755	94.43	8722	92.65	26967	91.34	24849	91.08
0.1	1929	79.02	16382	95.53	17370	97.37	25298	91.12	11984	81.22
0.2	7213	87.84	23147	88.18	23593	85.57	1990	63.29	1545	63.36
0.3	4067	75.96	2519	60.64	27648	68.08	1918	56.27	1816	64.62
0.4	3204	60.74	2597	58.58	3989	61.68	2017	67.04	1887	53.97
0.5	3250	55.94	2911	66.04	2055	57.09	2181	61.95	4092	72.37
0.6	3766	52.68	3708	55.81	2393	52.65	2052	55.36	3842	84.63
0.7	4016	53.65	3424	59.46	2628	52.76	2324	80.17	3708	86.35

0.8	4315	69.63	4059	65.69	2502	53.47	2781	87.83	4453	86.95
0.9	4290	72.94	4606	79.37	2949	77.01	3418	88	5562	88.39
1	4003	66.89	5250	87.01	3407	88.85	4168	89.27	6194	85.46
1.1	4645	77.37	5467	85.29	3872	88.04	4271	88.29	6331	85.88
1.1	4461	72.39	5501	84.98	3950	88.47	4471	88.89	6187	85.61
1.2	5701	86.59	5694	86.79	4707	87.61	4820	88.19	6801	87.48
1.3	6704	82.57	6347	87	5436	89.09	4986	87.46	7016	87.65
1.4	7151	80.74	6542	88.28	5582	87.72	5344	88.13	7181	87.54
1.5	7612	81.83	6954	86.7	5824	89.01	5480	89.23	7353	86.93
1.6	8243	85.91	7464	87.32	5681	88.81	5402	87.6	7530	87.9
1.7	8587	86.3	7332	88.07	6245	87.44	5538	89.21	7699	87.42
1.8	8893	86.42	7683	87.31	6591	87.15	5691	88.79	8201	87.97
1.9	8818	86.21	7425	88.88	6569	89.18	5520	90.2	7851	88.01
2	9163	84.51	7689	88.22	6700	88.84	5552	89.95	8258	87.31
2.1	9109	87.01	8050	87.58	6874	88.96	5674	89.95	8032	87.74
2.2	9451	85.97	7840	87.1	7182	89.05	5877	89.49	8336	88.35
2.3	9588	85.31	8106	88.31	6830	88.8	6039	89.55	8166	87.35
2.4	9932	87.4	8379	87.62	7417	88.54	6010	89.88	8420	88.53
2.5	9931	86.99	8568	87.98	7456	89.27	5883	88.65	8678	86.61
2.6	10232	86.41	8710	87.98	7189	88.75	6035	89.8	8573	88.13
2.7	10327	87.6	8520	86.97	7572	88.35	6071	89.07	8721	85.88
2.8	10177	86.03	8962	87.5	7002	88.9	6291	90.73	8723	88
2.9	10105	86.78	9175	88.3	7190	89.45	6167	90.69	8736	87.66
3	10366	87.27	8946	88.48	7494	89.46	6244	90.43	8899	88.32
3.15	10596	87.16	9145	88.82	7727	88.71	6200	90.31	9042	87.73
3.3	10560	87.54	8997	89.11	7705	89.46	6336	88.09	9285	88.31
3.5	10305	87.85	9223	87.72	7300	90.63	6728	89.3	9190	87.42
3.7	10414	87.38	9066	89.07	7657	90.01	6931	90.01	9512	88.28
3.9	10367	87.41	9257	88.14	7717	90.02	6636	90.66	9411	89.17
4.1	10496	87.47	9446	88.74	7859	89.34	6712	90.66	9514	88.09
4.3	10823	87.49	9145	89.28	7899	90.41	6523	90.97	9353	89.34
4.5	10594	87.8	9444	87.78	8110	89.28	6708	90.09	9498	90.19
4.75	10787	87.94	9660	89.45	8095	89.86	6768	90.62	9694	89.38
5	10592	86.66	9625	89.62	7707	90.24	6748	90.27	9584	89.45
5.25	10906	87.73	9596	88.21	7737	90.54	6597	90.68	9597	89.35
5.5	10712	88.62	9883	89.66	8148	90.26	6483	91.22	9466	88.43
5.75	10588	87.16	9657	89.83	8272	90.24	6888	91.92	9851	89.77
6.05	10993	87.53	9622	89.66	8312	89.78	6898	92.01	9540	90.5
6.68	11138	88.43	9075	89.91	8089	91.3	6765	92.05	9763	90.04
7.39	10807	89.47	9802	90.2	8609	91.17	6742	91.82	10256	89.2
8.16	10328	89.27	10074	89.89	8811	91.33	6830	92.82	10203	89.94
9.02	11121	89.53	9993	90.34	8881	91.11	7013	91.85	10321	90.22
9.97	11567	89.58	10314	91.23	9005	91.39	7180	91.52	10403	91.21
11.02	9348	90.97	10669	90.56	8972	91.54	7397	92.53	10492	91.4
12.18	11857	90.51	11405	90	9049	90.33	7357	92.66	10412	91.64
13.46	12079	88.96	10531	90.41	9015	91.54	7524	92.89	10521	91.09
14.88	11958	90.11	10579	90.17	9043	92.07	7521	93.48	10729	91.81
16.44	11930	90.12	10326	91.38	9128	92.29	7647	93.46	10408	92.11
18.17	12190	91.17	10650	91.44	9214	91.43	7387	92.3	10858	92.02
20.08	11752	90.8	10291	91.54	8895	92.53	7203	92.95	10888	92.63
22.19	11969	89.95	10456	90.52	9023	91.82	7350	93.26	10810	91.31
24.53	11929	91.17	10399	91.86	9074	91.2	7167	92.9	10629	91.52
27.11	12079	90.61	10301	91.81	9214	92.49	7560	92.88	11152	92.21
29.96	11908	91.48	10375	91.09	8976	92.73	7959	93.05	10772	91.57
33.11	11952	90.71	10109	92.38	8958	93.67	7458	93.05	10978	92.36
36.59	11350	91.58	9907	92.53	8762	92.04	6583	93.47	10342	91.71
40.44	11736	91.01	9176	92.12	8803	92.84	7458	93.83	10334	91.64
44.69	11265	91.57	8493	92.96	8380	92.87	5437	94	9720	92.67
49.39	11298	91.74	10113	92.69	9219	92.99	7126	93.46	9386	92.04

54.59	10618	91.63	9670	91.85	8718	92.8	6338	94.03	9657	92.55
60.33	10492	91.97	9010	92.65	8067	92.66	6028	93.97	8563	92.51
66.67	10536	92	9600	92.52	7977	93.64	5478	93.74	8554	91.54
73.69	10359	91.69	8888	92.25	8045	92.3	5447	93.82	9421	92.81
81.44	9655	92.33	8310	93.16	8738	92.93	7643	93.68	7346	91.99
90	11742	91.54	9456	92.36	6564	92.99	5946	93.54	7425	92.77

A2.3. Raw velocity data and profile corrections

Table S2.8. (below) Smooth control plate. Raw LDA data showing mean velocity at different vertical positions (z), for five horizontal locations (200-400mm), and the corrected base of each profile (red line) and data subsequently excluded from analysis (red).

Raw vertical position Z (mm)	Smooth Plate Mean velocity (m/s)				
	200 mm	250 mm	300 mm	350 mm	400 mm
0	0.003	0.022	0.000	-0.038	0.182
0.01	-0.002	0.005	0.000	0.012	0.179
0.02	-0.002	0.000	0.000	-0.004	0.166
0.03	0.003	0.000	0.000	0.007	0.171
0.04	-0.004	0.028	0.000	0.024	0.176
0.05	0.045	0.036	-0.003	0.041	0.181
0.06	0.010	0.030	0.000	0.034	0.192
0.07	0.000	0.028	-0.003	0.009	0.184
0.08	0.002	0.004	0.002	0.020	0.189
0.09	0.000	0.003	0.012	0.011	0.193
0.1	0.001	0.003	0.016	0.049	0.200
0.2	0.177	0.012	0.033	0.037	0.214
0.3	0.194	0.059	0.162	0.047	0.226
0.4	0.204	0.080	0.189	0.095	0.237
0.5	0.245	0.180	0.211	0.230	0.248
0.6	0.266	0.249	0.247	0.240	0.256
0.7	0.285	0.263	0.266	0.263	0.268
0.8	0.297	0.284	0.269	0.264	0.278
0.9	0.304	0.306	0.279	0.284	0.286
1	0.309	0.307	0.288	0.285	0.292
1.1	0.322	0.323	0.294	0.294	0.298
1.1	0.317	0.310	0.298	0.290	0.295
1.2	0.326	0.323	0.306	0.300	0.302
1.3	0.334	0.325	0.313	0.300	0.309
1.4	0.327	0.333	0.311	0.307	0.310
1.5	0.335	0.340	0.320	0.315	0.313
1.6	0.356	0.342	0.328	0.312	0.320
1.7	0.348	0.351	0.328	0.327	0.337
1.8	0.356	0.350	0.339	0.329	0.338
1.9	0.353	0.363	0.333	0.320	0.343
2	0.360	0.367	0.341	0.333	0.340
2.1	0.360	0.359	0.341	0.337	0.334
2.2	0.368	0.372	0.346	0.349	0.349
2.3	0.369	0.376	0.353	0.343	0.350
2.4	0.370	0.368	0.347	0.346	0.353
2.5	0.373	0.374	0.363	0.350	0.352
2.6	0.377	0.374	0.363	0.346	0.345
2.7	0.371	0.376	0.360	0.358	0.367
2.8	0.375	0.379	0.373	0.366	0.363

2.9	0.382	0.382	0.363	0.370	0.363
3	0.377	0.383	0.373	0.369	0.366
3.15	0.389	0.388	0.375	0.372	0.365
3.3	0.390	0.385	0.377	0.375	0.378
3.5	0.387	0.398	0.379	0.387	0.379
3.7	0.398	0.398	0.394	0.388	0.375
3.9	0.396	0.404	0.390	0.378	0.382
4.1	0.399	0.407	0.403	0.393	0.384
4.3	0.390	0.405	0.402	0.387	0.395
4.5	0.408	0.410	0.401	0.389	0.396
4.75	0.397	0.416	0.403	0.402	0.405
5	0.419	0.418	0.418	0.412	0.409
5.25	0.415	0.415	0.418	0.410	0.417
5.5	0.420	0.417	0.415	0.417	0.415
5.75	0.414	0.428	0.411	0.402	0.416
6.05	0.425	0.428	0.421	0.424	0.417
6.68	0.428	0.438	0.431	0.425	0.428
7.39	0.438	0.451	0.431	0.431	0.441
8.16	0.442	0.447	0.439	0.446	0.450
9.02	0.444	0.456	0.451	0.460	0.450
9.97	0.446	0.462	0.459	0.463	0.451
11.02	0.453	0.476	0.470	0.468	0.471
12.18	0.463	0.487	0.470	0.473	0.475
13.46	0.479	0.479	0.478	0.479	0.477
14.88	0.474	0.493	0.481	0.482	0.481
16.44	0.486	0.499	0.490	0.493	0.487
18.17	0.500	0.502	0.495	0.493	0.497
20.08	0.511	0.507	0.494	0.497	0.504
22.19	0.512	0.512	0.498	0.502	0.512
24.53	0.507	0.528	0.504	0.511	0.509
27.11	0.513	0.527	0.514	0.506	0.513
29.96	0.522	0.515	0.521	0.519	0.514
33.11	0.518	0.509	0.520	0.517	0.530
36.59	0.519	0.508	0.509	0.528	0.521
40.44	0.516	0.512	0.519	0.526	0.526
44.69	0.517	0.516	0.526	0.514	0.525
49.39	0.520	0.518	0.519	0.521	0.529
54.59	0.524	0.519	0.527	0.533	0.512
60.33	0.526	0.509	0.513	0.522	0.519
66.67	0.523	0.513	0.513	0.522	0.528
73.69	0.518	0.512	0.516	0.524	0.524
81.44	0.522	0.525	0.516	0.522	0.522
90	0.520	0.512	0.516	0.521	0.524

Table S2.9. (below) *Loganellia scotica* plate. Raw LDA data showing mean velocity at different vertical positions (z), for five horizontal locations (200-400mm), and the corrected base of each profile (red line) and data subsequently excluded from analysis (red).

Raw vertical position Z (mm)	*Loganellia scotica* Mean velocity (m/s)				
	200 mm	250 mm	300 mm	350 mm	400 mm
0	0.000	0.000	0.000	0.000	0.000
0.01	0.000	0.000	0.000	0.000	0.000
0.02	0.000	0.000	0.000	0.000	0.000
0.03	0.000	0.000	0.001	0.000	0.000

0.04	-0.001	0.000	0.001	0.000	0.000
0.05	0.000	0.000	0.001	0.000	0.002
0.06	0.000	0.006	0.001	0.000	0.002
0.07	0.000	0.000	0.001	0.000	0.004
0.08	0.000	0.000	0.007	0.001	0.019
0.09	0.000	0.000	0.005	0.000	0.018
0.1	0.000	0.000	0.005	0.000	0.016
0.2	0.000	0.004	0.035	0.000	0.109
0.3	0.000	0.002	0.141	0.053	0.158
0.4	0.037	0.001	0.213	0.134	0.242
0.5	0.067	0.093	0.270	0.219	0.281
0.6	0.242	0.235	0.287	0.264	0.293
0.7	0.262	0.222	0.302	0.281	0.316
0.8	0.273	0.278	0.311	0.305	0.323
0.9	0.290	0.324	0.323	0.326	0.332
1	0.309	0.327	0.327	0.327	0.330
1.1	0.312	0.333	0.339	0.332	0.342
1.1	0.313	0.331	0.342	0.336	0.337
1.2	0.326	0.344	0.340	0.335	0.348
1.3	0.333	0.346	0.345	0.344	0.344
1.4	0.340	0.353	0.353	0.359	0.357
1.5	0.342	0.355	0.358	0.360	0.358
1.6	0.351	0.362	0.356	0.358	0.365
1.7	0.344	0.359	0.360	0.360	0.362
1.8	0.351	0.360	0.372	0.369	0.363
1.9	0.355	0.366	0.379	0.372	0.360
2	0.364	0.374	0.377	0.374	0.372
2.1	0.364	0.377	0.377	0.383	0.370
2.2	0.359	0.382	0.383	0.387	0.378
2.3	0.377	0.387	0.381	0.383	0.385
2.4	0.371	0.383	0.385	0.380	0.386
2.5	0.368	0.384	0.390	0.393	0.386
2.6	0.378	0.391	0.391	0.385	0.385
2.7	0.381	0.392	0.395	0.391	0.395
2.8	0.382	0.396	0.403	0.392	0.390
2.9	0.380	0.391	0.407	0.391	0.395
3	0.380	0.394	0.397	0.403	0.396
3.15	0.395	0.396	0.400	0.404	0.393
3.3	0.394	0.412	0.405	0.400	0.405
3.5	0.389	0.399	0.418	0.408	0.398
3.7	0.392	0.403	0.404	0.413	0.409
3.9	0.399	0.408	0.412	0.408	0.412
4.1	0.398	0.406	0.419	0.417	0.420
4.3	0.409	0.420	0.418	0.428	0.418
4.5	0.398	0.418	0.417	0.429	0.414
4.75	0.406	0.421	0.422	0.433	0.420
5	0.409	0.432	0.427	0.425	0.427
5.25	0.415	0.422	0.429	0.431	0.428
5.5	0.409	0.419	0.439	0.432	0.446
5.75	0.420	0.421	0.432	0.438	0.444
6.05	0.419	0.437	0.433	0.451	0.442
6.68	0.428	0.435	0.438	0.454	0.442
7.39	0.424	0.446	0.453	0.453	0.453
8.16	0.443	0.456	0.456	0.464	0.466
9.02	0.443	0.455	0.462	0.466	0.466
9.97	0.446	0.454	0.461	0.475	0.469
11.02	0.455	0.469	0.470	0.474	0.484
12.18	0.473	0.473	0.466	0.476	0.478
13.46	0.469	0.482	0.483	0.488	0.487

14.88	0.480	0.484	0.495	0.492	0.488
16.44	0.485	0.487	0.502	0.491	0.496
18.17	0.483	0.495	0.496	0.489	0.496
20.08	0.481	0.493	0.507	0.502	0.500
22.19	0.485	0.495	0.505	0.502	0.498
24.53	0.491	0.500	0.503	0.507	0.504
27.11	0.486	0.496	0.503	0.511	0.505
29.96	0.489	0.505	0.501	0.504	0.506
33.11	0.489	0.506	0.504	0.506	0.504
36.59	0.492	0.497	0.509	0.506	0.508
40.44	0.487	0.501	0.504	0.508	0.508
44.69	0.485	0.498	0.507	0.511	0.501
49.39	0.491	0.498	0.507	0.513	0.500
54.59	0.495	0.504	0.504	0.512	0.502
60.33	0.489	0.499	0.507	0.506	0.507
66.67	0.489	0.498	0.508	0.509	0.514
73.69	0.493	0.501	0.503	0.511	0.504
81.44	0.488	0.503	0.500	0.509	0.505
90	0.494	0.496	0.502	0.511	0.500

Table S2.10. (below) *Lophosteus sp.* plate. Raw LDA data showing mean velocity at different vertical positions (z), for five horizontal locations (200-400mm), and the corrected base of each profile (red line) and data subsequently excluded from analysis (red).

Raw vertical position Z (mm)	*Lophosteus sp.* Mean velocity (m/s)				
	200 mm	250 mm	300 mm	350 mm	400 mm
0	0.000	0.000	0.000	0.001	0.001
0.01	-0.001	0.000	0.002	0.001	0.001
0.02	-0.001	0.000	0.002	0.001	0.002
0.03	-0.001	0.000	0.003	0.005	0.012
0.04	0.000	0.000	0.000	0.008	0.021
0.05	0.000	0.000	0.002	0.027	0.098
0.06	-0.001	0.000	0.003	0.036	0.087
0.07	-0.001	0.000	0.003	0.038	0.091
0.08	-0.001	0.000	0.003	0.049	0.135
0.09	-0.001	0.000	0.002	0.061	0.134
0.1	-0.001	0.000	0.002	0.072	0.143
0.2	0.000	0.257	0.078	0.138	0.235
0.3	0.012	0.045	0.108	0.247	0.260
0.4	0.058	0.045	0.228	0.270	0.292
0.5	0.106	0.070	0.262	0.300	0.309
0.6	0.213	0.140	0.299	0.315	0.318
0.7	0.260	0.197	0.315	0.328	0.335
0.8	0.256	0.234	0.322	0.344	0.345
0.9	0.289	0.275	0.336	0.343	0.353
1	0.306	0.296	0.342	0.357	0.353
1.1	0.317	0.317	0.353	0.369	0.370
1.1	0.332	0.326	0.356	0.357	0.369
1.2	0.328	0.332	0.357	0.366	0.366
1.3	0.335	0.337	0.359	0.369	0.382
1.4	0.348	0.357	0.369	0.376	0.375
1.5	0.345	0.364	0.366	0.366	0.378
1.6	0.352	0.373	0.374	0.383	0.385
1.7	0.364	0.381	0.369	0.387	0.393

1.8	0.360	0.388	0.391	0.388	0.396
1.9	0.369	0.386	0.380	0.400	0.406
2	0.375	0.386	0.387	0.404	0.392
2.1	0.366	0.390	0.396	0.400	0.395
2.2	0.373	0.392	0.402	0.403	0.393
2.3	0.372	0.403	0.395	0.403	0.409
2.4	0.380	0.403	0.395	0.409	0.414
2.5	0.383	0.399	0.403	0.403	0.410
2.6	0.390	0.406	0.413	0.418	0.414
2.7	0.389	0.417	0.401	0.416	0.410
2.8	0.389	0.414	0.413	0.417	0.416
2.9	0.381	0.423	0.408	0.417	0.407
3	0.390	0.408	0.413	0.424	0.428
3.15	0.395	0.420	0.416	0.420	0.428
3.3	0.394	0.418	0.418	0.422	0.428
3.5	0.392	0.425	0.425	0.427	0.424
3.7	0.404	0.422	0.427	0.430	0.435
3.9	0.405	0.425	0.438	0.435	0.435
4.1	0.407	0.421	0.432	0.438	0.435
4.3	0.418	0.430	0.434	0.443	0.448
4.5	0.419	0.428	0.443	0.446	0.433
4.75	0.420	0.439	0.446	0.449	0.453
5	0.409	0.438	0.448	0.454	0.445
5.25	0.425	0.439	0.449	0.458	0.449
5.5	0.435	0.441	0.446	0.459	0.456
5.75	0.433	0.444	0.460	0.452	0.460
6.05	0.434	0.453	0.457	0.463	0.459
6.68	0.440	0.454	0.462	0.463	0.462
7.39	0.450	0.448	0.472	0.469	0.477
8.16	0.449	0.461	0.466	0.478	0.482
9.02	0.453	0.463	0.481	0.484	0.480
9.97	0.459	0.480	0.484	0.490	0.491
11.02	0.468	0.483	0.489	0.493	0.491
12.18	0.474	0.479	0.496	0.496	0.500
13.46	0.482	0.487	0.492	0.500	0.499
14.88	0.495	0.492	0.496	0.502	0.501
16.44	0.491	0.497	0.507	0.505	0.512
18.17	0.498	0.499	0.507	0.507	0.515
20.08	0.503	0.507	0.521	0.522	0.514
22.19	0.504	0.518	0.506	0.524	0.516
24.53	0.513	0.520	0.517	0.529	0.520
27.11	0.520	0.518	0.526	0.527	0.521
29.96	0.511	0.524	0.527	0.530	0.524
33.11	0.517	0.526	0.528	0.527	0.527
36.59	0.510	0.524	0.517	0.524	0.529
40.44	0.512	0.532	0.538	0.526	0.536
44.69	0.511	0.518	0.525	0.534	0.529
49.39	0.512	0.529	0.525	0.538	0.535
54.59	0.517	0.517	0.537	0.532	0.520
60.33	0.518	0.524	0.524	0.533	0.529
66.67	0.522	0.519	0.528	0.531	0.526
73.69	0.513	0.516	0.525	0.529	0.528
81.44	0.520	0.527	0.525	0.530	0.529
90	0.530	0.515	0.525	0.532	0.525

Table S2.11. (below) *Phlebolepis elegans* plate. Raw LDA data showing mean velocity at different vertical positions (z), for five horizontal locations (200-400mm), and the corrected base of each profile (red line) and data subsequently excluded from analysis (red).

Raw vertical position Z (mm)	*Phlebolepis elegans* Mean velocity (m/s)				
	200 mm	250 mm	300 mm	350 mm	400 mm
0	-0.001	0.000	0.002	0.006	0.001
0.01	0.000	0.000	0.001	0.006	0.001
0.02	0.000	0.000	0.000	0.006	0.001
0.03	-0.001	0.000	0.000	0.005	0.002
0.04	0.000	0.000	0.000	0.003	0.005
0.05	-0.001	0.000	0.001	0.002	0.010
0.06	0.000	0.000	0.000	0.004	0.019
0.07	0.001	0.000	0.000	0.002	0.021
0.08	0.000	0.000	0.000	0.005	0.029
0.09	-0.001	0.003	0.000	0.004	0.029
0.1	0.000	0.001	0.000	0.007	0.051
0.2	0.001	0.003	0.000	0.100	0.185
0.3	0.000	0.034	0.051	0.137	0.222
0.4	0.015	0.091	0.197	0.231	0.254
0.5	0.075	0.167	0.234	0.284	0.274
0.6	0.190	0.221	0.276	0.300	0.305
0.7	0.240	0.272	0.291	0.314	0.302
0.8	0.271	0.300	0.306	0.321	0.323
0.9	0.296	0.311	0.327	0.331	0.333
1	0.305	0.322	0.334	0.344	0.330
1.1	0.314	0.339	0.352	0.334	0.343
1.1	0.319	0.329	0.349	0.346	0.346
1.2	0.330	0.345	0.352	0.350	0.356
1.3	0.332	0.348	0.346	0.357	0.357
1.4	0.341	0.356	0.359	0.365	0.364
1.5	0.339	0.360	0.364	0.357	0.357
1.6	0.346	0.358	0.370	0.369	0.364
1.7	0.354	0.370	0.379	0.366	0.368
1.8	0.356	0.366	0.366	0.378	0.380
1.9	0.355	0.375	0.380	0.383	0.377
2	0.363	0.376	0.381	0.380	0.373
2.1	0.369	0.385	0.385	0.385	0.388
2.2	0.370	0.378	0.387	0.408	0.388
2.3	0.384	0.381	0.388	0.398	0.391
2.4	0.373	0.389	0.389	0.389	0.396
2.5	0.378	0.392	0.391	0.398	0.393
2.6	0.380	0.381	0.400	0.399	0.404
2.7	0.387	0.394	0.398	0.403	0.399
2.8	0.381	0.388	0.396	0.404	0.411
2.9	0.380	0.391	0.409	0.413	0.404
3	0.374	0.395	0.404	0.410	0.411
3.15	0.384	0.387	0.414	0.403	0.405
3.3	0.386	0.403	0.405	0.412	0.415
3.5	0.391	0.394	0.406	0.410	0.420
3.7	0.398	0.404	0.407	0.416	0.420
3.9	0.407	0.405	0.414	0.420	0.416
4.1	0.397	0.409	0.416	0.432	0.426
4.3	0.405	0.412	0.426	0.429	0.428
4.5	0.405	0.414	0.422	0.430	0.427
4.75	0.415	0.419	0.430	0.436	0.442

5	0.416	0.424	0.439	0.435	0.435
5.25	0.408	0.429	0.434	0.439	0.425
5.5	0.422	0.426	0.437	0.432	0.439
5.75	0.417	0.437	0.439	0.444	0.438
6.05	0.409	0.424	0.446	0.448	0.445
6.68	0.428	0.427	0.445	0.460	0.448
7.39	0.426	0.447	0.450	0.458	0.458
8.16	0.436	0.444	0.457	0.460	0.463
9.02	0.442	0.446	0.460	0.464	0.459
9.97	0.440	0.462	0.468	0.471	0.466
11.02	0.460	0.461	0.477	0.474	0.480
12.18	0.453	0.467	0.468	0.479	0.486
13.46	0.466	0.467	0.483	0.491	0.479
14.88	0.483	0.471	0.489	0.487	0.493
16.44	0.481	0.480	0.487	0.488	0.491
18.17	0.479	0.484	0.488	0.497	0.492
20.08	0.485	0.492	0.498	0.498	0.497
22.19	0.483	0.493	0.495	0.494	0.502
24.53	0.495	0.497	0.501	0.499	0.508
27.11	0.488	0.506	0.502	0.510	0.509
29.96	0.495	0.499	0.509	0.509	0.513
33.11	0.498	0.508	0.513	0.511	0.514
36.59	0.502	0.503	0.512	0.515	0.514
40.44	0.496	0.502	0.505	0.507	0.503
44.69	0.496	0.506	0.510	0.515	0.512
49.39	0.489	0.505	0.508	0.515	0.505
54.59	0.488	0.506	0.509	0.515	0.510
60.33	0.494	0.499	0.506	0.518	0.512
66.67	0.496	0.500	0.511	0.512	0.519
73.69	0.502	0.510	0.514	0.503	0.514
81.44	0.509	0.496	0.506	0.505	0.510
90	0.487	0.492	0.509	0.506	0.511

Table S2.12. (below) *Poracanthodes sp.* plate. Raw LDA data showing mean velocity at different vertical positions (z), for five horizontal locations (200-400mm), and the corrected base of each profile (red line) and data subsequently excluded from analysis (red).

Raw vertical position Z (mm)	*Poracanthodes sp.* Mean velocity (m/s)				
	200 mm	250 mm	300 mm	350 mm	400 mm
0	0.000	0.000	0.000	0.000	0.000
0.01	0.000	0.000	0.000	0.000	0.000
0.02	0.000	0.000	0.000	0.000	0.000
0.03	0.000	0.000	0.000	0.000	0.000
0.04	0.000	0.000	0.000	0.000	0.000
0.05	0.000	0.000	0.000	0.000	0.000
0.06	0.000	0.000	0.000	0.000	0.000
0.07	0.000	0.000	0.000	0.000	0.000
0.08	0.000	0.000	0.000	0.006	0.000
0.09	0.000	0.000	0.000	0.000	0.000
0.1	0.000	0.000	0.000	0.000	0.000
0.2	0.000	0.000	0.000	-0.001	0.048
0.3	0.000	-0.023	-0.011	0.000	0.097
0.4	0.000	0.000	0.000	-0.001	0.194
0.5	-0.008	-0.126	0.001	0.017	0.210

0.6	0.000	0.004	0.001	0.046	0.268
0.7	0.000	-0.001	0.000	0.097	0.291
0.8	0.045	0.002	0.007	0.178	0.302
0.9	0.000	0.007	0.052	0.226	0.311
1	0.017	0.080	0.196	0.261	0.326
1.1	0.160	0.165	0.243	0.284	0.332
1.1	0.170	0.157	0.230	0.282	0.328
1.2	0.178	0.179	0.264	0.298	0.342
1.3	0.202	0.222	0.282	0.309	0.344
1.4	0.230	0.253	0.309	0.319	0.352
1.5	0.251	0.290	0.311	0.324	0.353
1.6	0.274	0.306	0.328	0.332	0.362
1.7	0.296	0.321	0.330	0.353	0.363
1.8	0.314	0.333	0.337	0.355	0.368
1.9	0.322	0.337	0.346	0.357	0.378
2	0.330	0.357	0.350	0.361	0.377
2.1	0.341	0.350	0.354	0.367	0.372
2.2	0.336	0.361	0.355	0.369	0.374
2.3	0.343	0.357	0.365	0.366	0.386
2.4	0.342	0.363	0.366	0.375	0.380
2.5	0.343	0.369	0.373	0.389	0.391
2.6	0.362	0.361	0.373	0.388	0.395
2.7	0.356	0.377	0.386	0.392	0.397
2.8	0.355	0.378	0.378	0.391	0.399
2.9	0.364	0.383	0.386	0.390	0.394
3	0.369	0.391	0.387	0.399	0.393
3.15	0.367	0.395	0.402	0.402	0.398
3.3	0.383	0.389	0.399	0.400	0.407
3.5	0.384	0.397	0.406	0.405	0.406
3.7	0.377	0.401	0.401	0.413	0.409
3.9	0.385	0.402	0.410	0.412	0.418
4.1	0.383	0.402	0.407	0.420	0.418
4.3	0.388	0.409	0.416	0.425	0.431
4.5	0.398	0.412	0.420	0.421	0.426
4.75	0.401	0.420	0.416	0.432	0.427
5	0.398	0.422	0.426	0.435	0.434
5.25	0.403	0.425	0.431	0.434	0.438
5.5	0.415	0.438	0.437	0.441	0.440
5.75	0.415	0.425	0.429	0.440	0.442
6.05	0.413	0.443	0.443	0.440	0.446
6.68	0.421	0.446	0.431	0.447	0.456
7.39	0.423	0.445	0.459	0.454	0.458
8.16	0.429	0.445	0.456	0.459	0.466
9.02	0.441	0.456	0.458	0.470	0.478
9.97	0.441	0.466	0.463	0.480	0.469
11.02	0.457	0.461	0.480	0.477	0.478
12.18	0.460	0.467	0.477	0.480	0.491
13.46	0.469	0.488	0.485	0.490	0.496
14.88	0.483	0.479	0.492	0.496	0.496
16.44	0.482	0.484	0.495	0.502	0.507
18.17	0.484	0.494	0.498	0.500	0.500
20.08	0.490	0.500	0.501	0.501	0.506
22.19	0.512	0.505	0.508	0.513	0.504
24.53	0.509	0.504	0.514	0.516	0.507
27.11	0.500	0.512	0.512	0.517	0.520
29.96	0.511	0.510	0.511	0.511	0.512
33.11	0.508	0.518	0.524	0.517	0.516
36.59	0.510	0.507	0.519	0.521	0.519
40.44	0.508	0.513	0.521	0.525	0.526

44.69	0.509	0.523	0.522	0.525	0.531
49.39	0.514	0.516	0.518	0.522	0.528
54.59	0.509	0.524	0.531	0.524	0.527
60.33	0.510	0.517	0.522	0.523	0.522
66.67	0.510	0.514	0.518	0.531	0.534
73.69	0.513	0.518	0.524	0.527	0.524
81.44	0.508	0.514	0.512	0.527	0.529
90	0.506	0.513	0.514	0.513	0.515

Table S2.13. (below) *Nostolepis striata* plate. Raw LDA data showing mean velocity at different vertical positions (z), for five horizontal locations (200-400mm), and the corrected base of each profile (red line), data subsequently excluded from analysis (red).

Raw vertical position Z (mm)	*Nostolepis striata* Mean velocity (m/s)				
	200 mm	250 mm	300 mm	350 mm	400 mm
0	-0.001	0.000	0.000	0.000	0.000
0.01	0.000	0.000	0.000	0.000	0.000
0.02	0.000	0.000	0.000	0.000	0.000
0.03	-0.001	0.000	0.000	0.000	0.000
0.04	0.000	0.000	0.000	0.000	0.000
0.05	0.001	0.000	0.000	0.001	0.000
0.06	0.000	0.000	0.000	0.001	0.001
0.07	0.000	0.000	0.000	0.001	0.001
0.08	0.000	0.000	0.000	0.000	0.001
0.09	0.000	0.000	0.000	0.000	0.002
0.1	0.000	0.000	0.000	0.001	0.005
0.2	0.000	0.004	0.000	0.087	0.131
0.3	0.008	0.050	0.003	0.094	0.185
0.4	0.035	0.033	0.048	0.182	0.173
0.5	0.058	0.140	0.128	0.198	0.232
0.6	0.092	0.115	0.127	0.195	0.246
0.7	0.129	0.168	0.120	0.246	0.256
0.8	0.215	0.215	0.179	0.260	0.272
0.9	0.236	0.256	0.265	0.271	0.272
1	0.236	0.268	0.275	0.285	0.281
1.1	0.263	0.279	0.284	0.286	0.291
1.1	0.265	0.282	0.289	0.290	0.289
1.2	0.275	0.290	0.295	0.299	0.287
1.3	0.291	0.290	0.306	0.301	0.302
1.4	0.290	0.305	0.311	0.310	0.317
1.5	0.294	0.302	0.314	0.317	0.311
1.6	0.300	0.315	0.320	0.321	0.315
1.7	0.311	0.318	0.326	0.319	0.319
1.8	0.312	0.320	0.331	0.332	0.336
1.9	0.318	0.322	0.328	0.331	0.327
2	0.323	0.336	0.332	0.331	0.333
2.1	0.324	0.337	0.343	0.333	0.328
2.2	0.323	0.333	0.336	0.340	0.343
2.3	0.335	0.339	0.341	0.355	0.340
2.4	0.341	0.348	0.350	0.345	0.345
2.5	0.338	0.348	0.357	0.347	0.354
2.6	0.347	0.351	0.356	0.356	0.348
2.7	0.346	0.351	0.365	0.358	0.358
2.8	0.351	0.355	0.359	0.358	0.365

2.9	0.350	0.366	0.367	0.364	0.363
3	0.356	0.362	0.371	0.369	0.361
3.15	0.362	0.366	0.370	0.362	0.375
3.3	0.361	0.369	0.376	0.373	0.373
3.5	0.369	0.377	0.381	0.384	0.378
3.7	0.376	0.375	0.382	0.385	0.381
3.9	0.366	0.384	0.387	0.379	0.389
4.1	0.377	0.385	0.390	0.392	0.396
4.3	0.393	0.387	0.393	0.397	0.393
4.5	0.387	0.394	0.401	0.403	0.394
4.75	0.391	0.397	0.401	0.409	0.402
5	0.402	0.395	0.399	0.413	0.406
5.25	0.403	0.402	0.408	0.406	0.420
5.5	0.404	0.414	0.409	0.415	0.417
5.75	0.409	0.416	0.416	0.420	0.433
6.05	0.428	0.409	0.420	0.429	0.426
6.68	0.430	0.424	0.428	0.434	0.434
7.39	0.423	0.436	0.446	0.446	0.439
8.16	0.438	0.448	0.455	0.446	0.449
9.02	0.441	0.448	0.461	0.460	0.462
9.97	0.452	0.459	0.469	0.469	0.476
11.02	0.462	0.465	0.470	0.475	0.479
12.18	0.470	0.472	0.493	0.486	0.482
13.46	0.489	0.484	0.494	0.493	0.499
14.88	0.479	0.493	0.499	0.494	0.495
16.44	0.490	0.498	0.510	0.493	0.498
18.17	0.502	0.505	0.514	0.508	0.500
20.08	0.509	0.509	0.519	0.505	0.513
22.19	0.508	0.514	0.517	0.519	0.533
24.53	0.510	0.511	0.523	0.524	0.526
27.11	0.521	0.525	0.525	0.522	0.525
29.96	0.519	0.526	0.530	0.524	0.533
33.11	0.518	0.521	0.515	0.525	0.524
36.59	0.510	0.517	0.526	0.524	0.530
40.44	0.518	0.523	0.516	0.537	0.525
44.69	0.509	0.520	0.531	0.530	0.532
49.39	0.512	0.519	0.525	0.538	0.528
54.59	0.517	0.526	0.534	0.529	0.535
60.33	0.504	0.524	0.533	0.538	0.531
66.67	0.510	0.516	0.527	0.528	0.520
73.69	0.513	0.526	0.529	0.523	0.531
81.44	0.509	0.524	0.525	0.534	0.534
90	0.510	0.524	0.526	0.525	0.539

A2.4. Corrected velocity profiles

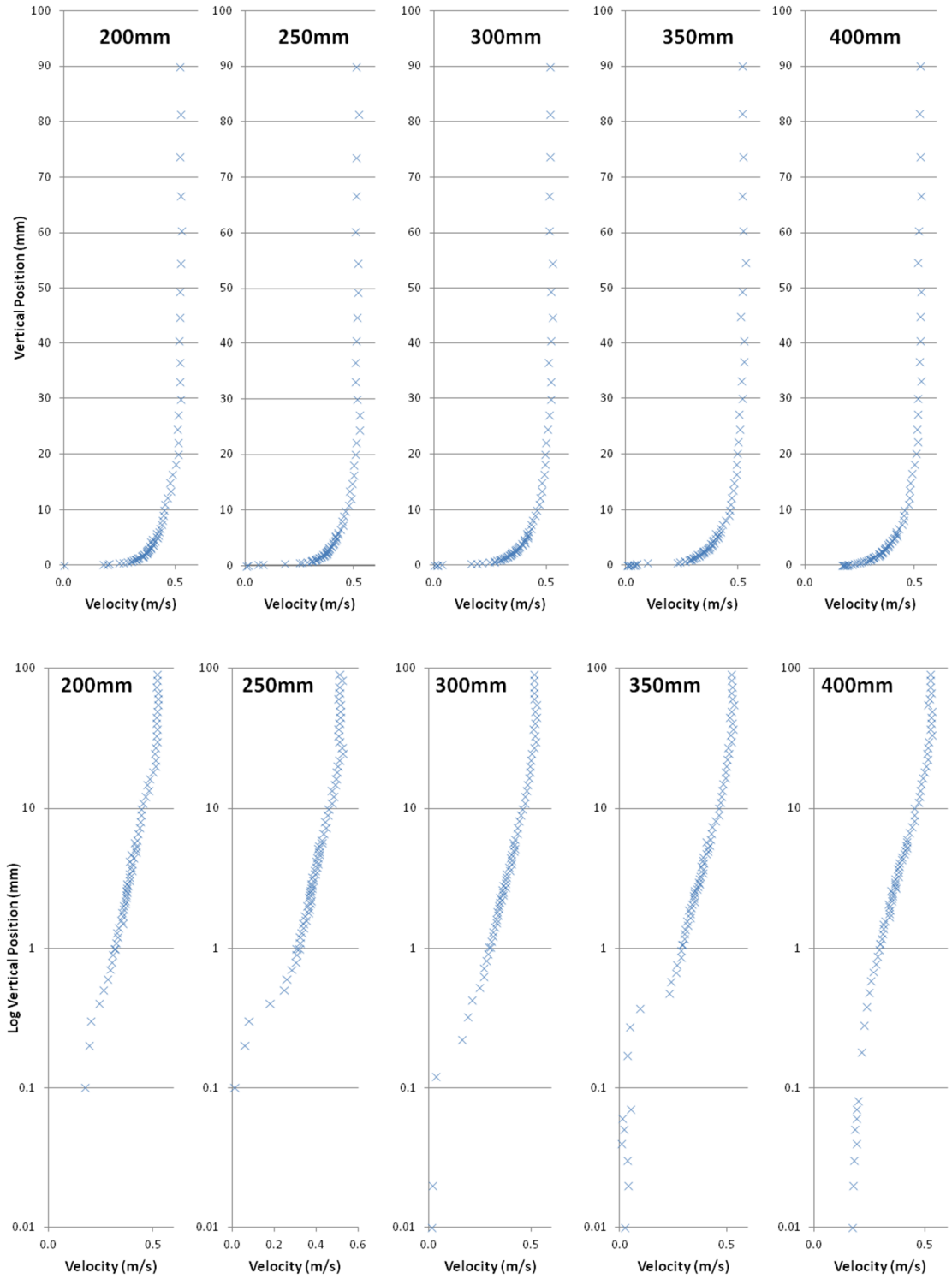

Figure S2.8. Top, corrected velocity profiles of smooth control plate at different horizontal locations (200-400mm). Bottom, semilog plots of same data.

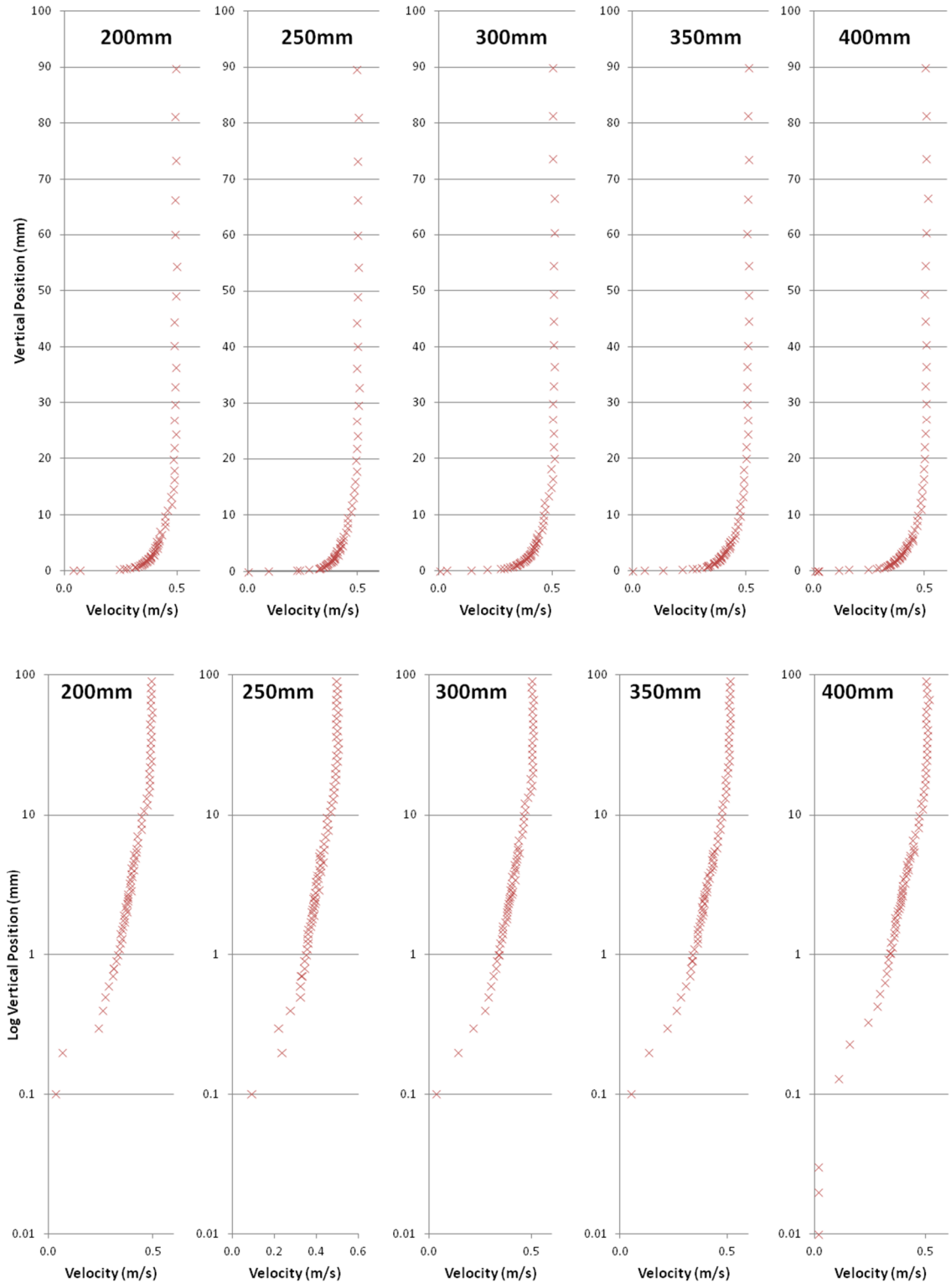

Figure S2.9. Top, corrected velocity profiles of *Loganellia scotica* plate at different horizontal locations (200-400mm). Bottom, semilog plots of same data.

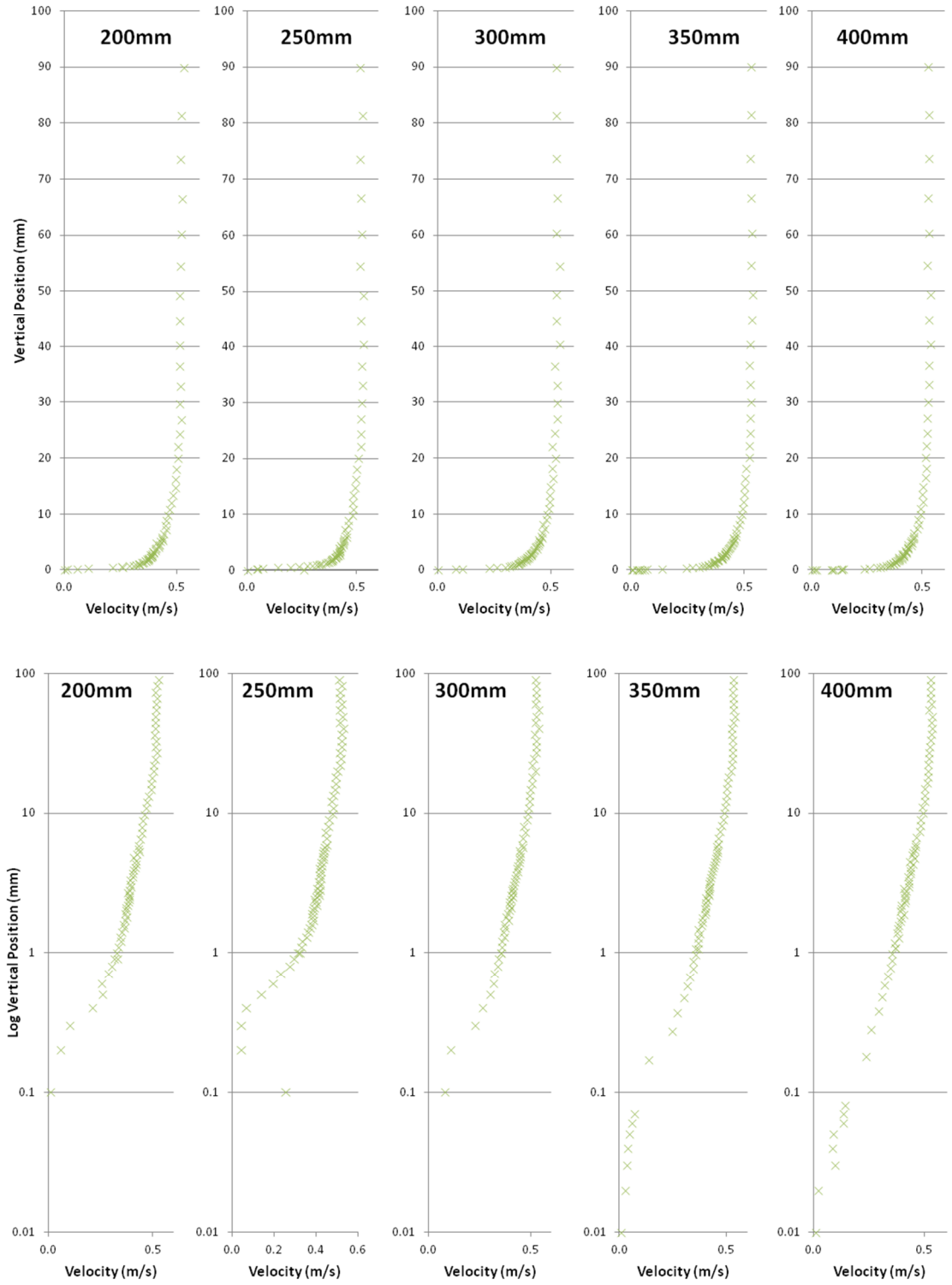

Figure S2.10. Top, corrected velocity profiles of *Lophosteus sp*. plate at different horizontal locations (200-400mm). Bottom, semilog plots of same data.

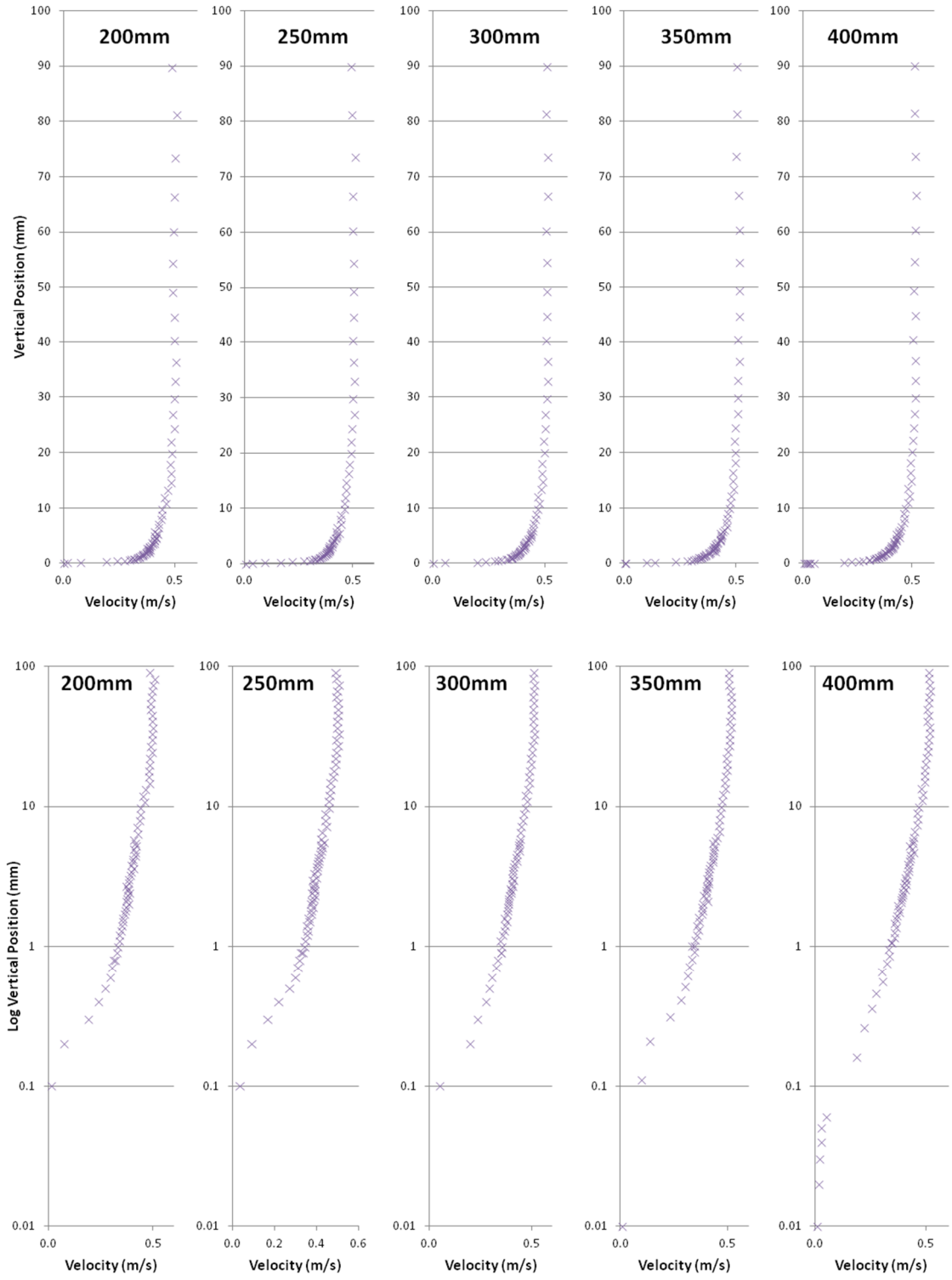

Figure S2.11. Top, corrected velocity profiles of *Phlebolepis elegans* plate at different horizontal locations (200-400mm). Bottom, semilog plots of same data.

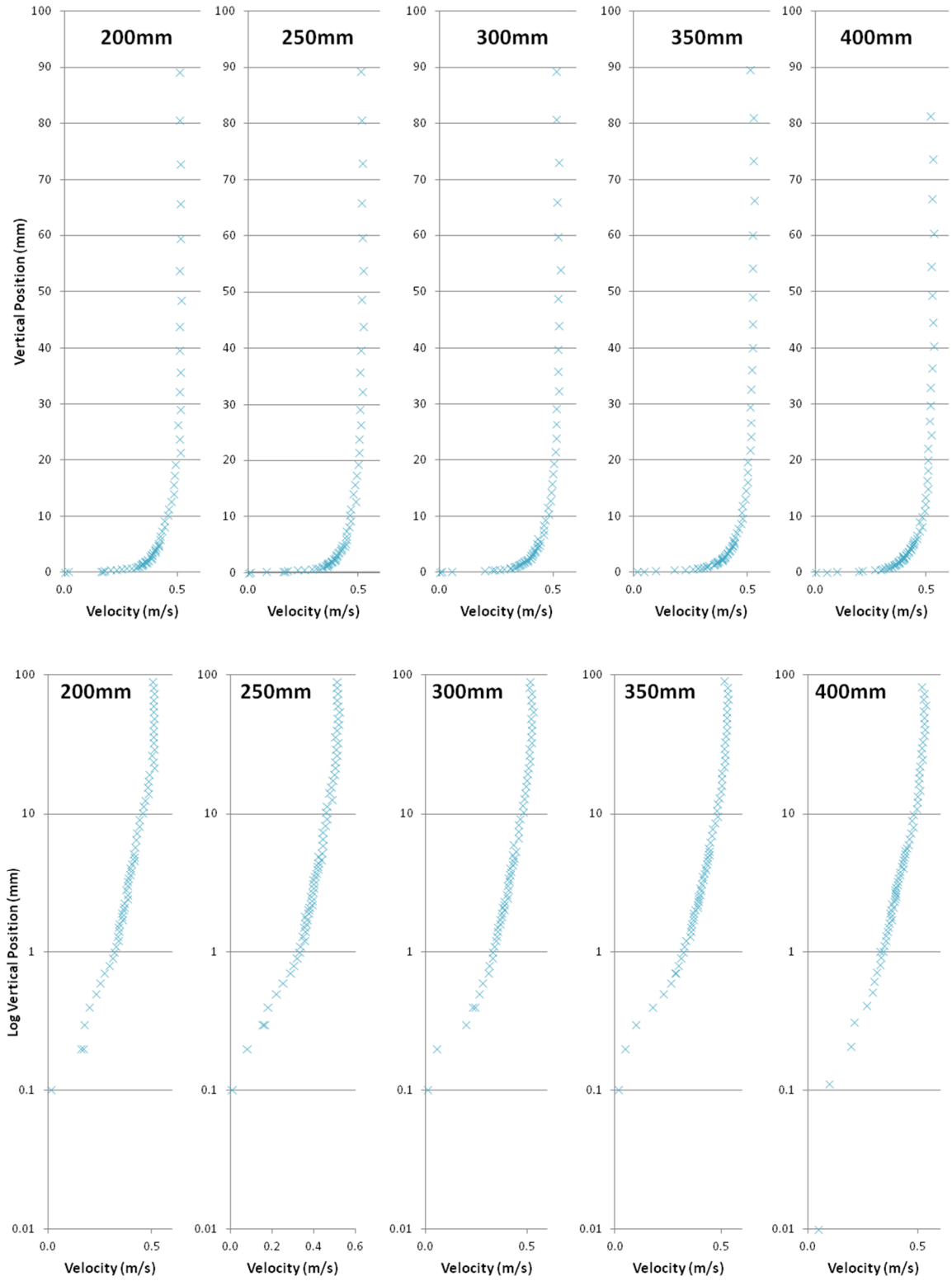

Figure S2.12. Top, corrected velocity profiles of *Poracanthodes sp.* plate at different horizontal locations (200-400mm). Bottom, semilog plots of same data.

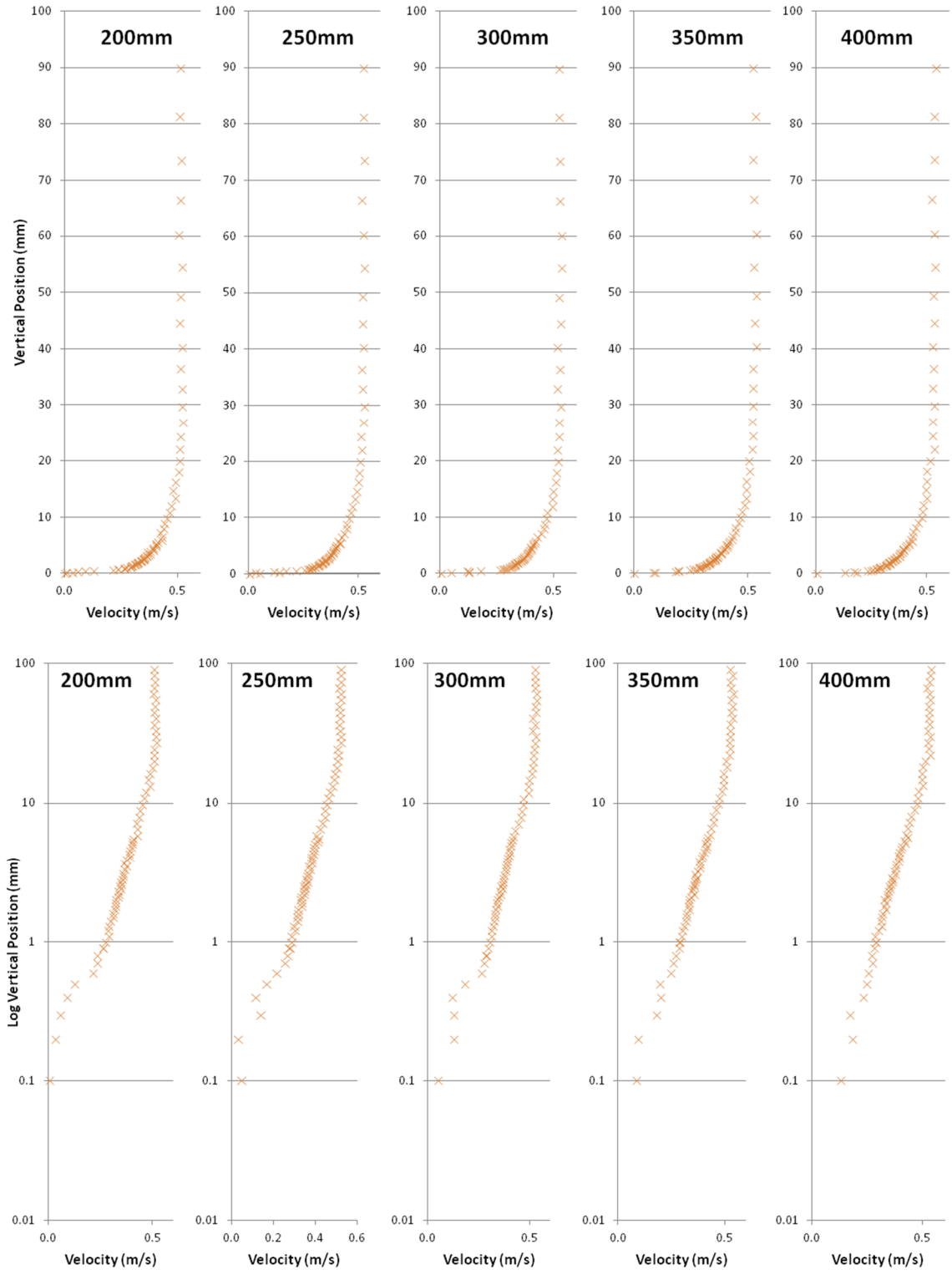

Figure S2.13. Top, corrected velocity profiles of *Nostolepis striata* plate at different horizontal locations (200-400mm). Bottom, semilog plots of same data.

A2.5. Shear stresses

Table S2.14. Shear stresses for 200 mm horizontal position of all plates.

200mm Horizontal Position											
Smooth Control		***Loganellia***		***Lophosteus***		***Phlebolepis***		***Poracanthodes***		***Nostolepis***	
Z [mm]	t (Pa)	Z [mm]	t (Pa)	Z [mm]	t (Pa)	Z [mm]	t (Pa)	Z [mm]	t (Pa)	Z [mm]	t (Pa)
0	0.005	0	0.004	0	0.003	0	0.008	0	0.005	0	0.003524
0.1	0.092	0.1	0.080	0.1	0.035	0.1	0.047	0.1	0.055	0.1	0.030762
0.2	0.078	0.2	0.103	0.2	0.079	0.2	0.105	0.2	0.086	0.2	0.067025
0.3	0.087	0.3	0.075	0.3	0.110	0.3	0.114	0.2	0.087	0.3	0.089177
0.4	0.079	0.4	0.074	0.4	0.077	0.4	0.088	0.3	0.091	0.4	0.11222
0.5	0.076	0.5	0.070	0.5	0.077	0.5	0.067	0.4	0.097	0.5	0.120134
0.6	0.076	0.6	0.067	0.6	0.093	0.6	0.068	0.5	0.093	0.6	0.09501
0.7	0.074	0.7	0.066	0.7	0.075	0.7	0.069	0.6	0.090	0.7	0.086578
0.8	0.075	0.8	0.070	0.8	0.069	0.8	0.065	0.7	0.090	0.8	0.094046
0.9	0.070	0.8	0.070	0.9	0.070	0.8	0.065	0.8	0.070	0.9	0.073318
1	0.068	0.9	0.063	0.9	0.069	0.9	0.068	0.9	0.068	0.9	0.07755
1	0.066	1	0.063	1	0.068	1	0.060	1	0.069	1	0.068392
1.1	0.067	1.1	0.063	1.1	0.062	1.1	0.064	1.1	0.066	1.1	0.067631
1.2	0.069	1.2	0.062	1.2	0.069	1.2	0.059	1.2	0.064	1.2	0.067661
1.3	0.067	1.3	0.059	1.3	0.066	1.3	0.059	1.3	0.065	1.3	0.06685
1.4	0.063	1.4	0.059	1.4	0.061	1.4	0.059	1.4	0.063	1.4	0.065647
1.5	0.066	1.5	0.055	1.5	0.060	1.5	0.055	1.5	0.062	1.5	0.06593
1.6	0.062	1.6	0.055	1.6	0.059	1.6	0.059	1.6	0.061	1.6	0.063497
1.7	0.064	1.7	0.058	1.7	0.060	1.7	0.054	1.7	0.064	1.7	0.063931
1.8	0.062	1.8	0.057	1.8	0.061	1.8	0.058	1.8	0.058	1.8	0.064454
1.9	0.064	1.9	0.056	1.9	0.057	1.9	0.058	1.9	0.059	1.9	0.062132
2	0.064	2	0.054	2	0.061	2	0.059	2	0.059	2	0.058921
2.1	0.062	2.1	0.054	2.1	0.055	2.1	0.059	2.1	0.063	2.1	0.063328
2.2	0.064	2.2	0.052	2.2	0.056	2.2	0.055	2.25	0.061	2.2	0.060072
2.3	0.064	2.3	0.056	2.3	0.056	2.3	0.054	2.4	0.060	2.3	0.062418
2.4	0.063	2.4	0.056	2.4	0.056	2.4	0.059	2.6	0.061	2.4	0.061975
2.5	0.059	2.5	0.060	2.5	0.059	2.5	0.055	2.8	0.055	2.5	0.061835
2.6	0.062	2.6	0.056	2.6	0.057	2.6	0.053	3	0.056	2.6	0.060386
2.7	0.059	2.7	0.054	2.7	0.055	2.7	0.053	3.2	0.056	2.7	0.062719
2.8	0.060	2.85	0.056	2.8	0.057	2.85	0.051	3.4	0.057	2.8	0.061909
2.9	0.063	3	0.054	2.95	0.058	3	0.054	3.6	0.057	2.95	0.063399
3.05	0.062	3.2	0.053	3.1	0.055	3.2	0.053	3.85	0.056	3.1	0.06073
3.2	0.065	3.4	0.055	3.3	0.057	3.4	0.064	4.1	0.061	3.3	0.061335
3.4	0.059	3.6	0.056	3.5	0.055	3.6	0.062	4.35	0.057	3.5	0.063125
3.6	0.066	3.8	0.055	3.7	0.057	3.8	0.057	4.6	0.055	3.7	0.061262
3.8	0.063	4	0.056	3.9	0.051	4	0.055	4.85	0.059	3.9	0.057117
4	0.062	4.2	0.052	4.1	0.056	4.2	0.056	5.15	0.054	4.1	0.066087
4.2	0.059	4.45	0.052	4.3	0.057	4.45	0.056	5.78	0.054	4.3	0.060649
4.4	0.058	4.7	0.051	4.55	0.053	4.7	0.059	6.49	0.056	4.55	0.062075

4.65	0.058	4.95	0.056	4.8	0.053	4.95	0.053	7.26	0.055	4.8	0.059432
4.9	0.063	5.2	0.050	5.05	0.057	5.2	0.053	8.12	0.063	5.05	0.063313
5.15	0.066	5.45	0.053	5.3	0.056	5.45	0.058	9.07	0.056	5.3	0.058612
5.4	0.064	5.75	0.050	5.55	0.060	5.75	0.052	10.12	0.054	5.55	0.06188
5.65	0.062	6.38	0.050	5.85	0.060	6.38	0.052	11.28	0.053	5.85	0.06194
5.95	0.062	7.09	0.050	6.48	0.056	7.09	0.046	12.56	0.061	6.48	0.06135
6.58	0.060	7.86	0.054	7.19	0.062	7.86	0.053	13.98	0.055	7.19	0.060794
7.29	0.067	8.72	0.053	7.96	0.055	8.72	0.055	15.54	0.049	7.96	0.0623
8.06	0.059	9.67	0.051	8.82	0.060	9.67	0.053	17.27	0.049	8.82	0.056687
8.92	0.065	10.72	0.053	9.77	0.054	10.72	0.052	19.18	0.052	9.77	0.057425
9.87	0.065	11.88	0.050	10.82	0.052	11.88	0.056	21.29	0.046	10.82	0.056157
10.92	0.059	13.16	0.049	11.98	0.058	13.16	0.050	23.63	0.042	11.98	0.056505
12.08	0.061	14.58	0.045	13.26	0.055	14.58	0.054	26.21	0.042	13.26	0.063864
13.36	0.063	16.14	0.040	14.68	0.050	16.14	0.047	29.06	0.040	14.68	0.054279
14.78	0.057	17.87	0.044	16.24	0.052	17.87	0.048	32.21	0.038	16.24	0.051088
16.34	0.055	19.78	0.039	17.97	0.050	19.78	0.044	35.69	0.044	17.97	0.051638
18.07	0.060	21.89	0.044	19.88	0.047	21.89	0.045	39.54	0.037	19.88	0.041653
19.98	0.044	24.23	0.039	21.99	0.050	24.23	0.039	43.79	0.039	21.99	0.042782
22.09	0.053	26.81	0.039	24.33	0.046	26.81	0.038	48.49	0.040	24.33	0.04572
24.43	0.042	29.66	0.038	26.91	0.048	29.66	0.039	53.69	0.042	26.91	0.039375
27.01	0.044	32.81	0.042	29.76	0.044	32.81	0.040	59.43	0.044	29.76	0.039022
29.86	0.047	36.29	0.039	32.91	0.041	36.29	0.039	65.77	0.046	32.91	0.04242
33.01	0.040	40.14	0.032	36.39	0.044	40.14	0.037	72.79	0.043	36.39	0.038627
36.49	0.040	44.39	0.034	40.24	0.039	44.39	0.042	80.54	0.044	40.24	0.045264
40.34	0.038	49.09	0.035	44.49	0.041	49.09	0.039	89.1	0.051	44.49	0.038294
44.59	0.044	54.29	0.039	49.19	0.035	54.29	0.040			49.19	0.0401
49.29	0.041	60.03	0.035	54.39	0.034	60.03	0.041			54.39	0.038289
54.49	0.040	66.37	0.040	60.13	0.039	66.37	0.044			60.13	0.037198
60.23	0.047	73.39	0.040	66.47	0.049	73.39	0.044			66.47	0.042335
66.57	0.040	81.14	0.040	73.49	0.042	81.14	0.042			73.49	0.041912
73.59	0.039	89.7	0.048	81.24	0.043	89.7	0.041			81.24	0.038832
81.34	0.043			89.8	0.049					89.8	0.04042
89.9	0.044										

Table S2.15. (below) Shear stresses for 250 mm horizontal position of all plates.

250 mmm Horizontal Position											
Smooth Control		***Loganellia***		***Lophosteus***		***Phlebolepis***		***Poracanthodes***		***Nostolepis***	
Z [mm]	t (Pa)	Z [mm]	t (Pa)	Z [mm]	t (Pa)	Z [mm]	t (Pa)	Z [mm]	t (Pa)	Z [mm]	t (Pa)
0	0.013	0	0.015	0	0.000	0	0.018	0	0.028	0	0.024
0.1	0.049	0.1	0.116	0.1	0.000	0.1	0.066	0.1	0.034	0.1	0.071
0.2	0.087	0.2	0.110	0.2	0.043	0.2	0.103	0.2	0.080	0.2	0.073
0.3	0.098	0.3	0.125	0.3	0.047	0.3	0.113	0.3	0.086	0.3	0.101
0.4	0.115	0.4	0.096	0.4	0.066	0.4	0.111	0.3	0.090	0.4	0.117
0.5	0.085	0.5	0.073	0.5	0.069	0.5	0.073	0.4	0.101	0.5	0.117
0.6	0.088	0.6	0.067	0.6	0.079	0.6	0.071	0.5	0.099	0.6	0.102

0.7	0.073	0.7	0.065	0.7	0.080	0.7	0.076	0.6	0.085	0.7	0.077
0.8	0.071	0.7	0.063	0.8	0.079	0.8	0.071	0.7	0.073	0.8	0.071
0.9	0.071	0.8	0.063	0.9	0.078	0.9	0.067	0.8	0.070	0.9	0.069
1	0.072	0.9	0.062	1	0.077	0.9	0.067	0.9	0.074	0.9	0.068
1	0.069	1	0.062	1	0.078	1	0.064	1	0.070	1	0.067
1.1	0.071	1.1	0.063	1.1	0.073	1.1	0.062	1.1	0.066	1.1	0.063
1.2	0.068	1.2	0.061	1.2	0.070	1.2	0.061	1.2	0.068	1.2	0.068
1.3	0.067	1.3	0.059	1.3	0.068	1.3	0.060	1.3	0.063	1.3	0.065
1.4	0.069	1.4	0.059	1.4	0.066	1.4	0.059	1.4	0.063	1.4	0.066
1.5	0.065	1.5	0.061	1.5	0.063	1.5	0.063	1.5	0.060	1.5	0.063
1.6	0.066	1.6	0.052	1.6	0.064	1.6	0.055	1.6	0.060	1.6	0.064
1.7	0.064	1.7	0.057	1.7	0.059	1.7	0.058	1.7	0.062	1.7	0.062
1.8	0.065	1.8	0.056	1.8	0.064	1.8	0.057	1.8	0.060	1.8	0.064
1.9	0.064	1.9	0.060	1.9	0.059	1.9	0.058	1.9	0.059	1.9	0.063
2	0.064	2	0.055	2	0.057	2	0.056	2	0.060	2	0.062
2.1	0.065	2.1	0.053	2.1	0.060	2.1	0.056	2.1	0.058	2.1	0.063
2.2	0.064	2.2	0.056	2.2	0.059	2.2	0.052	2.2	0.058	2.2	0.064
2.3	0.063	2.3	0.058	2.3	0.057	2.3	0.054	2.35	0.059	2.3	0.061
2.4	0.064	2.4	0.057	2.4	0.054	2.4	0.055	2.5	0.059	2.4	0.062
2.5	0.060	2.5	0.054	2.5	0.058	2.5	0.055	2.7	0.057	2.5	0.063
2.6	0.066	2.6	0.050	2.6	0.062	2.6	0.055	2.9	0.054	2.6	0.059
2.7	0.066	2.75	0.051	2.7	0.059	2.7	0.056	3.1	0.055	2.7	0.062
2.8	0.061	2.9	0.057	2.8	0.061	2.8	0.055	3.3	0.050	2.8	0.062
2.9	0.063	3.1	0.057	2.9	0.057	2.95	0.051	3.5	0.057	2.95	0.061
3.05	0.059	3.3	0.053	3.05	0.057	3.1	0.051	3.7	0.053	3.1	0.063
3.2	0.061	3.5	0.051	3.2	0.055	3.3	0.049	3.95	0.055	3.3	0.063
3.4	0.067	3.7	0.049	3.4	0.058	3.5	0.056	4.2	0.056	3.5	0.059
3.6	0.061	3.9	0.052	3.6	0.056	3.7	0.049	4.45	0.053	3.7	0.061
3.8	0.063	4.1	0.047	3.8	0.055	3.9	0.052	4.7	0.055	3.9	0.058
4	0.063	4.35	0.049	4	0.050	4.1	0.051	4.95	0.057	4.1	0.057
4.2	0.062	4.6	0.050	4.2	0.055	4.3	0.049	5.25	0.055	4.3	0.064
4.4	0.062	4.85	0.053	4.4	0.053	4.55	0.053	5.88	0.053	4.55	0.061
4.65	0.061	5.1	0.053	4.65	0.060	4.8	0.055	6.59	0.052	4.8	0.063
4.9	0.062	5.35	0.050	4.9	0.058	5.05	0.051	7.36	0.056	5.05	0.059
5.15	0.060	5.65	0.055	5.15	0.053	5.3	0.050	8.22	0.051	5.3	0.060
5.4	0.062	6.28	0.045	5.4	0.051	5.55	0.050	9.17	0.053	5.55	0.060
5.65	0.062	6.99	0.052	5.65	0.053	5.85	0.048	10.22	0.050	5.85	0.057
5.95	0.060	7.76	0.053	5.95	0.053	6.48	0.051	11.38	0.053	6.48	0.060
6.58	0.061	8.62	0.050	6.58	0.050	7.19	0.055	12.66	0.054	7.19	0.057
7.29	0.056	9.57	0.047	7.29	0.052	7.96	0.052	14.08	0.054	7.96	0.057
8.06	0.062	10.62	0.054	8.06	0.051	8.82	0.054	15.64	0.058	8.82	0.055
8.92	0.059	11.78	0.045	8.92	0.049	9.77	0.049	17.37	0.053	9.77	0.055
9.87	0.056	13.06	0.046	9.87	0.056	10.82	0.056	19.28	0.049	10.82	0.053
10.92	0.062	14.48	0.042	10.92	0.058	11.98	0.052	21.39	0.040	11.98	0.058
12.08	0.058	16.04	0.043	12.08	0.053	13.26	0.046	23.73	0.053	13.26	0.053
13.36	0.064	17.77	0.045	13.36	0.050	14.68	0.052	26.31	0.049	14.68	0.048
14.78	0.060	19.68	0.038	14.78	0.050	16.24	0.051	29.16	0.036	16.24	0.049
16.34	0.056	21.79	0.041	16.34	0.052	17.97	0.052	32.31	0.047	17.97	0.048

18.07	0.053	24.13	0.036	18.07	0.047	19.88	0.045	35.79	0.041	19.88	0.053
19.98	0.051	26.71	0.040	19.98	0.044	21.99	0.041	39.64	0.043	21.99	0.044
22.09	0.053	29.56	0.041	22.09	0.044	24.33	0.037	43.89	0.045	24.33	0.048
24.43	0.046	32.71	0.032	24.43	0.050	26.91	0.036	48.59	0.043	26.91	0.047
27.01	0.052	36.19	0.038	27.01	0.044	29.76	0.045	53.79	0.045	29.76	0.050
29.86	0.045	40.04	0.036	29.86	0.040	32.91	0.037	59.53	0.045	32.91	0.045
33.01	0.034	44.29	0.036	33.01	0.044	36.39	0.038	65.87	0.039	36.39	0.036
36.49	0.035	48.99	0.045	36.49	0.040	40.24	0.045	72.89	0.045	40.24	0.041
40.34	0.038	54.19	0.041	40.34	0.045	44.49	0.041	80.64	0.042	44.49	0.041
44.59	0.039	59.93	0.045	44.59	0.039	49.19	0.038	89.2	0.040	49.19	0.038
49.29	0.044	66.27	0.042	49.29	0.037	54.39	0.040			54.39	0.041
54.49	0.043	73.29	0.037	54.49	0.039	60.13	0.038			60.13	0.043
60.23	0.035	81.04	0.041	60.23	0.044	66.47	0.047			66.47	0.039
66.57	0.039	89.6	0.040	66.57	0.045	73.49	0.041			73.49	0.040
73.59	0.039			73.59	0.041	81.24	0.040			81.24	0.048
81.34	0.045			81.34	0.050	89.8	0.040			89.8	0.044
89.9	0.037			89.9	0.040						

Table S2.16. (below) Shear stresses for 300 mm horizontal position of all plates.

300mm Horizontal Position											
Smooth Control		***Loganellia***		***Lophosteus***		***Phlebolepis***		***Poracanthodes***		***Nostolepis***	
Z [mm]	t (Pa)	Z [mm]	t (Pa)	Z [mm]	t (Pa)	Z [mm]	t (Pa)	Z [mm]	t (Pa)	Z [mm]	t (Pa)
0	0.011	0	0.028	0	0.013	0	0.009	0	0.006	0	0.029
0.01	0.018	0.1	0.080	0.1	0.084	0.1	0.091	0.1	0.032	0.1	0.085
0.02	0.037	0.2	0.120	0.2	0.111	0.2	0.090	0.2	0.089	0.2	0.115
0.12	0.039	0.3	0.118	0.3	0.081	0.3	0.083	0.3	0.098	0.3	0.125
0.22	0.088	0.4	0.077	0.4	0.078	0.4	0.078	0.4	0.079	0.4	0.132
0.32	0.092	0.5	0.082	0.5	0.072	0.5	0.074	0.4	0.079	0.5	0.136
0.42	0.081	0.6	0.074	0.6	0.075	0.6	0.074	0.5	0.085	0.6	0.079
0.52	0.076	0.7	0.070	0.7	0.071	0.7	0.069	0.6	0.074	0.7	0.069
0.62	0.076	0.8	0.066	0.8	0.068	0.8	0.068	0.7	0.072	0.8	0.070
0.72	0.070	0.9	0.065	0.9	0.070	0.9	0.071	0.8	0.074	0.8	0.070
0.82	0.070	1	0.067	1	0.066	0.9	0.065	0.9	0.071	0.9	0.069
0.92	0.071	1	0.065	1	0.065	1	0.067	1	0.070	1	0.068
1.02	0.066	1.1	0.060	1.1	0.063	1.1	0.060	1.1	0.065	1.1	0.069
1.02	0.071	1.2	0.060	1.2	0.066	1.2	0.061	1.2	0.064	1.2	0.067
1.12	0.071	1.3	0.063	1.3	0.064	1.3	0.062	1.3	0.066	1.3	0.066
1.22	0.070	1.4	0.062	1.4	0.063	1.4	0.058	1.4	0.066	1.4	0.066
1.32	0.068	1.5	0.061	1.5	0.066	1.5	0.061	1.5	0.062	1.5	0.067
1.42	0.066	1.6	0.059	1.6	0.059	1.6	0.060	1.6	0.063	1.6	0.063
1.52	0.064	1.7	0.057	1.7	0.059	1.7	0.061	1.7	0.062	1.7	0.065
1.62	0.066	1.8	0.059	1.8	0.060	1.8	0.056	1.8	0.062	1.8	0.068
1.72	0.066	1.9	0.059	1.9	0.058	1.9	0.057	1.9	0.061	1.9	0.065
1.82	0.064	2	0.056	2	0.058	2	0.055	2	0.060	2	0.062
1.92	0.067	2.1	0.057	2.1	0.059	2.1	0.054	2.1	0.061	2.1	0.063

2.02	0.063	2.2	0.057	2.2	0.057	2.2	0.054	2.2	0.058	2.2	0.066
2.12	0.062	2.3	0.059	2.3	0.058	2.3	0.053	2.3	0.054	2.3	0.064
2.22	0.067	2.4	0.054	2.4	0.058	2.4	0.057	2.45	0.059	2.4	0.069
2.32	0.061	2.5	0.058	2.5	0.059	2.5	0.054	2.6	0.058	2.5	0.063
2.42	0.066	2.6	0.059	2.6	0.056	2.6	0.053	2.8	0.058	2.6	0.066
2.52	0.062	2.7	0.059	2.7	0.056	2.7	0.054	3	0.057	2.7	0.065
2.62	0.061	2.8	0.060	2.8	0.056	2.8	0.058	3.2	0.057	2.85	0.061
2.72	0.061	2.9	0.055	2.9	0.057	2.95	0.056	3.4	0.056	3	0.062
2.82	0.063	3.05	0.055	3.05	0.057	3.1	0.049	3.6	0.054	3.2	0.062
2.92	0.062	3.2	0.052	3.2	0.055	3.3	0.049	3.8	0.054	3.4	0.062
3.07	0.064	3.4	0.057	3.4	0.056	3.5	0.051	4.05	0.053	3.6	0.061
3.22	0.065	3.6	0.050	3.6	0.051	3.7	0.058	4.3	0.051	3.8	0.062
3.42	0.060	3.8	0.053	3.8	0.055	3.9	0.053	4.55	0.052	4	0.060
3.62	0.062	4	0.056	4	0.056	4.1	0.052	4.8	0.052	4.2	0.064
3.82	0.061	4.2	0.051	4.2	0.055	4.3	0.049	5.05	0.050	4.45	0.061
4.02	0.063	4.4	0.051	4.4	0.058	4.55	0.052	5.35	0.053	4.7	0.056
4.22	0.062	4.65	0.053	4.65	0.056	4.8	0.055	5.98	0.048	4.95	0.058
4.42	0.063	4.9	0.050	4.9	0.055	5.05	0.053	6.69	0.054	5.2	0.059
4.67	0.061	5.15	0.051	5.15	0.053	5.3	0.052	7.46	0.053	5.45	0.057
4.92	0.059	5.4	0.054	5.4	0.052	5.55	0.051	8.32	0.051	5.75	0.057
5.17	0.058	5.65	0.050	5.65	0.057	5.85	0.049	9.27	0.050	6.38	0.065
5.42	0.061	5.95	0.049	5.95	0.052	6.48	0.051	10.32	0.050	7.09	0.061
5.67	0.056	6.58	0.049	6.58	0.050	7.19	0.055	11.48	0.052	7.86	0.061
5.97	0.058	7.29	0.047	7.29	0.057	7.96	0.045	12.76	0.055	8.72	0.057
6.6	0.055	8.06	0.050	8.06	0.051	8.82	0.051	14.18	0.048	9.67	0.059
7.31	0.055	8.92	0.045	8.92	0.050	9.77	0.051	15.74	0.057	10.72	0.053
8.08	0.051	9.87	0.055	9.87	0.047	10.82	0.048	17.47	0.045	11.88	0.058
8.94	0.050	10.92	0.052	10.92	0.054	11.98	0.050	19.38	0.047	13.16	0.055
9.89	0.057	12.08	0.047	12.08	0.054	13.26	0.043	21.49	0.050	14.58	0.051
10.94	0.055	13.36	0.042	13.36	0.052	14.68	0.047	23.83	0.046	16.14	0.053
12.1	0.056	14.78	0.050	14.78	0.048	16.24	0.047	26.41	0.036	17.87	0.047
13.38	0.054	16.34	0.048	16.34	0.050	17.97	0.048	29.26	0.046	19.78	0.048
14.8	0.052	18.07	0.039	18.07	0.048	19.88	0.044	32.41	0.043	21.89	0.047
16.36	0.051	19.98	0.044	19.98	0.048	21.99	0.041	35.89	0.038	24.23	0.046
18.09	0.049	22.09	0.042	22.09	0.049	24.33	0.041	39.74	0.046	26.81	0.040
20	0.049	24.43	0.041	24.43	0.042	26.91	0.044	43.99	0.039	29.66	0.048
22.11	0.048	27.01	0.045	27.01	0.043	29.76	0.044	48.69	0.043	32.81	0.045
24.45	0.040	29.86	0.034	29.86	0.046	32.91	0.040	53.89	0.040	36.29	0.038
27.03	0.043	33.01	0.038	33.01	0.045	36.39	0.040	59.63	0.039	40.14	0.041
29.88	0.041	36.49	0.043	36.49	0.045	40.24	0.042	65.97	0.039	44.39	0.040
33.03	0.043	40.34	0.036	40.34	0.040	44.49	0.036	72.99	0.042	49.09	0.040
36.51	0.038	44.59	0.040	44.59	0.040	49.19	0.038	80.74	0.044	54.29	0.043
40.36	0.038	49.29	0.037	49.29	0.043	54.39	0.038	89.3	0.042	60.03	0.036
44.61	0.047	54.49	0.035	54.49	0.042	60.13	0.039			66.37	0.045
49.31	0.038	60.23	0.043	60.23	0.042	66.47	0.039			73.39	0.044
54.51	0.035	66.57	0.036	66.57	0.041	73.49	0.041			81.14	0.045
60.25	0.042	73.59	0.043	73.59	0.040	81.24	0.041			89.7	0.039
66.59	0.040	81.34	0.046	81.34	0.041	89.8	0.044				

73.61	0.038	89.9	0.039	89.9	0.040						
81.36	0.041										
89.92	0.039										

Table S2.17. (overleaf) Shear stresses for 350 mm horizontal position of all plates.

350 mm Horizontal Position											
Smooth Control		***Loganellia***		***Lophosteus***		***Phlebolepis***		***Poracanthodes***		***Nostolepis***	
Z [mm]	t (Pa)	Z [mm]	t (Pa)	Z [mm]	t (Pa)	Z [mm]	t (Pa)	Z [mm]	t (Pa)	Z [mm]	t (Pa)
0	0.000	0	0.004	0	0.024	0	0.023	0	0.004	0	0.012
0.01	0.026	0.1	0.091	0.01	0.030	0.01	0.035	0.1	0.116	0.1	0.091
0.02	0.002	0.2	0.126	0.02	0.054	0.11	0.103	0.2	0.066	0.2	0.101
0.03	0.000	0.3	0.110	0.03	0.065	0.21	0.125	0.3	0.087	0.3	0.092
0.04	0.001	0.4	0.093	0.04	0.065	0.31	0.108	0.4	0.086	0.4	0.102
0.05	0.007	0.5	0.097	0.05	0.076	0.41	0.074	0.5	0.085	0.5	0.115
0.06	0.011	0.6	0.073	0.06	0.080	0.51	0.071	0.6	0.078	0.6	0.072
0.07	0.051	0.7	0.071	0.07	0.084	0.61	0.071	0.7	0.076	0.7	0.071
0.17	0.061	0.8	0.066	0.17	0.112	0.71	0.068	0.7	0.075	0.8	0.068
0.27	0.063	0.9	0.064	0.27	0.079	0.81	0.063	0.8	0.074	0.9	0.069
0.37	0.099	0.9	0.069	0.37	0.080	0.91	0.067	0.9	0.069	1	0.071
0.47	0.075	1	0.063	0.47	0.074	1.01	0.063	1	0.071	1	0.068
0.57	0.074	1.1	0.066	0.57	0.072	1.01	0.065	1.1	0.066	1.1	0.069
0.67	0.068	1.2	0.063	0.67	0.072	1.11	0.059	1.2	0.066	1.2	0.068
0.77	0.068	1.3	0.061	0.77	0.070	1.21	0.062	1.3	0.064	1.3	0.070
0.87	0.071	1.4	0.059	0.87	0.067	1.31	0.064	1.4	0.066	1.4	0.068
0.97	0.075	1.5	0.059	0.97	0.067	1.41	0.062	1.5	0.064	1.5	0.068
1.07	0.071	1.6	0.059	1.07	0.066	1.51	0.058	1.6	0.061	1.6	0.065
1.07	0.072	1.7	0.059	1.07	0.067	1.61	0.057	1.7	0.059	1.7	0.070
1.17	0.071	1.8	0.058	1.17	0.062	1.71	0.059	1.8	0.056	1.8	0.067
1.27	0.066	1.9	0.059	1.27	0.067	1.81	0.059	1.9	0.058	1.9	0.064
1.37	0.070	2	0.063	1.37	0.064	1.91	0.058	2	0.057	2	0.066
1.47	0.067	2.1	0.056	1.47	0.061	2.01	0.055	2.1	0.061	2.1	0.064
1.57	0.066	2.2	0.055	1.57	0.063	2.11	0.061	2.2	0.059	2.2	0.071
1.67	0.066	2.3	0.057	1.67	0.058	2.21	0.057	2.3	0.059	2.3	0.064
1.77	0.065	2.4	0.056	1.77	0.059	2.31	0.055	2.4	0.058	2.4	0.065
1.87	0.063	2.5	0.059	1.87	0.059	2.41	0.058	2.5	0.058	2.5	0.067
1.97	0.067	2.6	0.058	1.97	0.060	2.51	0.055	2.6	0.053	2.6	0.065
2.07	0.067	2.7	0.054	2.07	0.057	2.61	0.055	2.75	0.055	2.7	0.064
2.17	0.066	2.8	0.056	2.17	0.057	2.71	0.055	2.9	0.058	2.8	0.065
2.27	0.063	2.95	0.051	2.27	0.062	2.81	0.055	3.1	0.056	2.9	0.065
2.37	0.066	3.1	0.060	2.37	0.056	2.91	0.053	3.3	0.055	3.05	0.064
2.47	0.064	3.3	0.060	2.47	0.059	3.06	0.051	3.5	0.054	3.2	0.064
2.57	0.064	3.5	0.054	2.57	0.058	3.21	0.052	3.7	0.055	3.4	0.066
2.67	0.064	3.7	0.054	2.67	0.064	3.41	0.053	3.9	0.059	3.6	0.063
2.77	0.065	3.9	0.053	2.77	0.060	3.61	0.055	4.1	0.057	3.8	0.063
2.87	0.064	4.1	0.057	2.87	0.058	3.81	0.053	4.35	0.052	4	0.062

2.97	0.068	4.3	0.055	2.97	0.056	4.01	0.054	4.6	0.053	4.2	0.062
3.12	0.061	4.55	0.057	3.12	0.060	4.21	0.053	4.85	0.052	4.4	0.063
3.27	0.059	4.8	0.049	3.27	0.054	4.41	0.054	5.1	0.051	4.65	0.062
3.47	0.062	5.05	0.055	3.47	0.059	4.66	0.051	5.35	0.054	4.9	0.062
3.67	0.067	5.3	0.051	3.67	0.053	4.91	0.054	5.65	0.054	5.15	0.059
3.87	0.058	5.55	0.050	3.87	0.054	5.16	0.056	6.28	0.049	5.4	0.062
4.07	0.064	5.85	0.050	4.07	0.053	5.41	0.051	6.99	0.050	5.65	0.060
4.27	0.057	6.48	0.049	4.27	0.058	5.66	0.053	7.76	0.052	5.95	0.059
4.47	0.060	7.19	0.053	4.47	0.055	5.96	0.053	8.62	0.053	6.58	0.065
4.72	0.066	7.96	0.051	4.72	0.051	6.59	0.056	9.57	0.052	7.29	0.058
4.97	0.062	8.82	0.052	4.97	0.055	7.3	0.049	10.62	0.048	8.06	0.058
5.22	0.060	9.77	0.050	5.22	0.055	8.07	0.049	11.78	0.048	8.92	0.059
5.47	0.063	10.82	0.044	5.47	0.058	8.93	0.047	13.06	0.049	9.87	0.054
5.72	0.059	11.98	0.044	5.72	0.049	9.88	0.047	14.48	0.049	10.92	0.060
6.02	0.063	13.26	0.044	6.02	0.048	10.93	0.049	16.04	0.049	12.08	0.056
6.65	0.057	14.68	0.042	6.65	0.048	12.09	0.050	17.77	0.049	13.36	0.056
7.36	0.061	16.24	0.044	7.36	0.053	13.37	0.050	19.68	0.042	14.78	0.050
8.13	0.054	17.97	0.046	8.13	0.052	14.79	0.041	21.79	0.052	16.34	0.051
8.99	0.054	19.88	0.046	8.99	0.057	16.35	0.041	24.13	0.048	18.07	0.047
9.94	0.057	21.99	0.039	9.94	0.057	18.08	0.044	26.71	0.045	19.98	0.046
10.99	0.050	24.33	0.035	10.99	0.054	19.99	0.040	29.56	0.041	22.09	0.045
12.15	0.052	26.91	0.036	12.15	0.050	22.1	0.042	32.71	0.046	24.43	0.045
13.43	0.050	29.76	0.041	13.43	0.052	24.44	0.040	36.19	0.043	27.01	0.040
14.85	0.049	32.91	0.038	14.85	0.049	27.02	0.044	40.04	0.036	29.86	0.044
16.41	0.050	36.39	0.036	16.41	0.046	29.87	0.044	44.29	0.041	33.01	0.038
18.14	0.047	40.24	0.040	18.14	0.046	33.02	0.039	48.99	0.037	36.49	0.039
20.05	0.050	44.49	0.043	20.05	0.041	36.5	0.040	54.19	0.047	40.34	0.037
22.16	0.044	49.19	0.036	22.16	0.041	40.35	0.036	59.93	0.046	44.59	0.042
24.5	0.041	54.39	0.037	24.5	0.041	44.6	0.043	66.27	0.040	49.29	0.047
27.08	0.042	60.13	0.044	27.08	0.043	49.3	0.038	73.29	0.043	54.49	0.039
29.93	0.038	66.47	0.041	29.93	0.040	54.5	0.040	81.04	0.043	60.23	0.041
33.08	0.042	73.49	0.039	33.08	0.042	60.24	0.037	89.6	0.039	66.57	0.039
36.56	0.042	81.24	0.042	36.56	0.038	66.58	0.037			73.59	0.040
40.41	0.047	89.8	0.038	40.41	0.042	73.6	0.036			81.34	0.039
44.66	0.038			44.66	0.043	81.35	0.039			89.9	0.044
49.36	0.039			49.36	0.040	89.91	0.036				
54.56	0.042			54.56	0.036						
60.3	0.033			60.3	0.040						
66.64	0.041			66.64	0.044						
73.66	0.046			73.66	0.040						
81.41	0.043			81.41	0.040						
89.97	0.039			89.97	0.044						

Table S2.18. (below) Shear stresses for 400 mm horizontal position of all plates.

400 mm Horizontal Position

Smooth Control		***Loganellia***		***Lophosteus***		***Phlebolepis***		***Poracanthodes***		***Nostolepis***	
Z [mm]	t (Pa)	Z [mm]	t (Pa)	Z	t (Pa)	Z	t (Pa)	Z	t (Pa)	Z	t (Pa)
0	0.070	0	0.023	0	0.019	0	0.026	0	0.004	0	0.030
0.01	0.072	0.01	0.051	0.01	0.044	0.01	0.038	0.01	0.071	0.1	0.101
0.02	0.062	0.02	0.048	0.02	0.061	0.02	0.053	0.11	0.100	0.2	0.094
0.03	0.067	0.03	0.050	0.03	0.103	0.03	0.055	0.21	0.094	0.3	0.115
0.04	0.083	0.13	0.111	0.04	0.101	0.04	0.066	0.31	0.114	0.4	0.082
0.05	0.076	0.23	0.131	0.05	0.107	0.05	0.063	0.41	0.074	0.5	0.071
0.06	0.073	0.33	0.089	0.06	0.112	0.06	0.079	0.51	0.070	0.6	0.072
0.07	0.075	0.43	0.072	0.07	0.105	0.16	0.085	0.61	0.068	0.7	0.069
0.08	0.076	0.53	0.070	0.08	0.104	0.26	0.093	0.71	0.069	0.8	0.068
0.18	0.074	0.63	0.071	0.18	0.086	0.36	0.077	0.81	0.066	0.9	0.068
0.28	0.075	0.73	0.065	0.28	0.099	0.46	0.077	0.91	0.066	1	0.067
0.38	0.070	0.83	0.069	0.38	0.075	0.56	0.070	1.01	0.069	1	0.068
0.48	0.073	0.93	0.065	0.48	0.074	0.66	0.069	1.01	0.067	1.1	0.066
0.58	0.073	1.03	0.061	0.58	0.073	0.76	0.068	1.11	0.065	1.2	0.067
0.68	0.073	1.03	0.061	0.68	0.067	0.86	0.068	1.21	0.062	1.3	0.068
0.78	0.068	1.13	0.062	0.78	0.070	0.96	0.063	1.31	0.059	1.4	0.067
0.88	0.071	1.23	0.063	0.88	0.067	1.06	0.064	1.41	0.063	1.5	0.069
0.98	0.069	1.33	0.060	0.98	0.064	1.06	0.064	1.51	0.063	1.6	0.065
1.08	0.065	1.43	0.059	1.08	0.069	1.16	0.065	1.61	0.060	1.7	0.068
1.08	0.067	1.53	0.062	1.08	0.066	1.26	0.064	1.71	0.059	1.8	0.066
1.18	0.067	1.63	0.059	1.18	0.062	1.36	0.063	1.81	0.060	1.9	0.068
1.28	0.064	1.73	0.058	1.28	0.068	1.46	0.058	1.91	0.061	2	0.066
1.38	0.067	1.83	0.058	1.38	0.062	1.56	0.060	2.01	0.058	2.1	0.066
1.48	0.064	1.93	0.058	1.48	0.061	1.66	0.059	2.11	0.059	2.2	0.065
1.58	0.065	2.03	0.057	1.58	0.058	1.76	0.058	2.21	0.062	2.3	0.067
1.68	0.069	2.13	0.058	1.68	0.059	1.86	0.059	2.31	0.060	2.4	0.068
1.78	0.067	2.23	0.057	1.78	0.059	1.96	0.060	2.41	0.057	2.5	0.064
1.88	0.066	2.33	0.054	1.88	0.057	2.06	0.059	2.51	0.055	2.6	0.068
1.98	0.063	2.43	0.060	1.98	0.057	2.16	0.054	2.61	0.060	2.7	0.065
2.08	0.067	2.53	0.059	2.08	0.058	2.26	0.059	2.71	0.056	2.8	0.068
2.18	0.065	2.63	0.055	2.18	0.056	2.36	0.058	2.81	0.056	2.9	0.066
2.28	0.064	2.73	0.057	2.28	0.059	2.46	0.058	2.91	0.056	3.05	0.066
2.38	0.066	2.83	0.057	2.38	0.056	2.56	0.056	3.06	0.058	3.2	0.067
2.48	0.065	2.93	0.059	2.48	0.056	2.66	0.055	3.21	0.054	3.4	0.066
2.58	0.060	3.08	0.056	2.58	0.059	2.76	0.057	3.41	0.055	3.6	0.068
2.68	0.070	3.23	0.055	2.68	0.059	2.86	0.052	3.61	0.054	3.8	0.062
2.78	0.068	3.43	0.051	2.78	0.060	2.96	0.056	3.81	0.051	4	0.063
2.88	0.063	3.63	0.056	2.88	0.055	3.11	0.051	4.01	0.054	4.2	0.065
2.98	0.067	3.83	0.056	2.98	0.056	3.26	0.051	4.21	0.052	4.4	0.063
3.13	0.062	4.03	0.055	3.13	0.057	3.46	0.055	4.41	0.055	4.65	0.064
3.28	0.066	4.23	0.054	3.28	0.060	3.66	0.053	4.66	0.050	4.9	0.063
3.48	0.063	4.43	0.054	3.48	0.052	3.86	0.051	4.91	0.053	5.15	0.063
3.68	0.063	4.68	0.051	3.68	0.059	4.06	0.054	5.16	0.053	5.4	0.064
3.88	0.060	4.93	0.052	3.88	0.053	4.26	0.055	5.41	0.056	5.65	0.059
4.08	0.060	5.18	0.052	4.08	0.057	4.46	0.051	5.66	0.053	5.95	0.061

4.28	0.062	5.43	0.057	4.28	0.052	4.71	0.052	5.96	0.051	6.58	0.062
4.48	0.059	5.68	0.054	4.48	0.051	4.96	0.053	6.59	0.052	7.29	0.062
4.73	0.067	5.98	0.049	4.73	0.056	5.21	0.048	7.3	0.051	8.06	0.056
4.98	0.064	6.61	0.052	4.98	0.054	5.46	0.050	8.07	0.059	8.92	0.058
5.23	0.063	7.32	0.050	5.23	0.055	5.71	0.050	8.93	0.047	9.87	0.058
5.48	0.066	8.09	0.052	5.48	0.055	6.01	0.048	9.88	0.055	10.92	0.050
5.73	0.059	8.95	0.055	5.73	0.055	6.64	0.049	10.93	0.047	12.08	0.055
6.03	0.057	9.9	0.052	6.03	0.055	7.35	0.047	12.09	0.058	13.36	0.054
6.66	0.059	10.95	0.048	6.66	0.053	8.12	0.053	13.37	0.050	14.78	0.053
7.37	0.065	12.11	0.043	7.37	0.052	8.98	0.045	14.79	0.047	16.34	0.049
8.14	0.061	13.39	0.041	8.14	0.050	9.93	0.047	16.35	0.047	18.07	0.045
9	0.054	14.81	0.039	9	0.048	10.98	0.050	18.08	0.045	19.98	0.043
9.95	0.053	16.37	0.046	9.95	0.050	12.14	0.051	19.99	0.046	22.09	0.048
11	0.057	18.1	0.043	11	0.047	13.42	0.046	22.1	0.039	24.43	0.050
12.16	0.048	20.01	0.041	12.16	0.048	14.84	0.045	24.44	0.043	27.01	0.044
13.44	0.045	22.12	0.035	13.44	0.045	16.4	0.041	27.02	0.045	29.86	0.043
14.86	0.046	24.46	0.042	14.86	0.042	18.13	0.039	29.87	0.037	33.01	0.045
16.42	0.044	27.04	0.039	16.42	0.043	20.04	0.041	33.02	0.040	36.49	0.033
18.15	0.046	29.89	0.036	18.15	0.046	22.15	0.040	36.5	0.042	40.34	0.043
20.06	0.047	33.04	0.042	20.06	0.048	24.49	0.040	40.35	0.038	44.59	0.041
22.17	0.043	36.52	0.040	22.17	0.045	27.07	0.039	44.6	0.041	49.29	0.033
24.51	0.045	40.37	0.040	24.51	0.040	29.92	0.042	49.3	0.042	54.49	0.044
27.09	0.042	44.62	0.038	27.09	0.044	33.07	0.034	54.5	0.037	60.23	0.042
29.94	0.041	49.32	0.035	29.94	0.043	36.55	0.039	60.24	0.046	66.57	0.041
33.09	0.049	54.52	0.036	33.09	0.041	40.4	0.038	66.58	0.036	73.59	0.039
36.57	0.045	60.26	0.038	36.57	0.047	44.65	0.044	73.6	0.040	81.34	0.047
40.42	0.043	66.6	0.040	40.42	0.035	49.35	0.037	81.35	0.041	89.9	0.040
44.67	0.043	73.62	0.037	44.67	0.041	54.55	0.040				
49.37	0.041	81.37	0.040	49.37	0.041	60.29	0.040				
54.57	0.042	89.93	0.039	54.57	0.043	66.63	0.035				
60.31	0.039			60.31	0.036	73.65	0.040				
66.65	0.039			66.65	0.047	81.4	0.036				
73.67	0.040			73.67	0.042	89.96	0.045				
81.42	0.039			81.42	0.033						
89.98	0.048			89.98	0.045						

A2.6. Frictional velocity calculations

Code used for the generation of U* approximations (see body text of section 3.2):

```
nu=1.004*1e-6; %viscocity
I=100;%iteration count max out
load fm.mat %load the file with all the data

for j=1:length(fm(1,1:end))/3; %take the file loaded , number of columns with
data in, not the first, it's the second to the end ignoring every other one

    a(:,1)=fm(:,1+(j-1)*3); %a= picks out the distance/depth column (in
millimetres)
```

```
    a(:,2)=fm(:,2+(j-1)*3);  %picks out u
    y=zeros(I+1,length(a(2:end,1))); %preallocates variables for speed
    yp=zeros(I+1,length(a(2:end,1)));
    u=zeros(I+1,length(a(2:end,1)));

    for i=1:I+1 %iteration loop to find friction velocity
        u(i,:)=a(2:end,2); %defines velocity ignoring the first term because
we don't want a zero depth (can't take a log of zero)
        if i==1 %saying it's fitting a slope of best fit between all of the
experimental data
            y(i,:)=log(a(2:end,1)/1e3); %log distance (adjusted to metres)
            p=polyfit(y(i,:),u(i,:),1); %this is calculating the slope

        else
            [spv,pos]=max(a(:,2));
            vec1=find(a(1:pos,2)<=0.99*a(pos,2));
            yul=0.3*max(a(vec1,1));
            yp(i,:)=a(2:end,1)/1e3*us(i-1,j)/nu; %here we're defining
dimnesionless distance away from the wall (distance in mm divided by 1000,
times by shear stress we calculated, divided by kinematic viscocity
            y(i,:)=log(yp(i,:)); %log dimensionless distance/depth
            vec2=find(yp(i,:)>=30 & a(2:end,1)'<yul); %finds the dimensionless
distance greater than 30 less than 100 wall units
            p=polyfit(y(i,vec2),u(i,vec2),1); %finds the slope again based on
previous subset of data
        end
        us(i,j)=p(1)*0.41; %defines the shear velocity as the slope of best
fit times Von Karmens constant K
        if i>1 && abs(us(i,j)-us(i-1,j))/abs(us(i,j))<=1e-4 %terminates the
loop if results are converging to 4 decimal places
            break
        end
    end
    us(find(us==0))=NaN; %turns all zeros to NaN (not a number)
    plot(us(:,j)) %plotting the shear velocity against the number of
iterations made until constant for every plate
    hold on
end
```

A2.7. Skin friction coefficients

Table S2.19. Skin friction coefficients for all plates at horizontal positions 200-400mm. See Chapter 7 for plots.

Plate	Horizontal Position (mm)				
	200	**250**	**300**	**350**	**400**
Smooth	0.015705	0.018109	0.023481	0.02612	0.020061
Loganellia	0.01128	0.009823	0.015886	0.015794	0.015728
Lophosteus	0.011518	0.008594	0.017565	0.01577	0.013479
Phlebolepis	0.012344	0.011044	0.012964	0.016818	0.019087
Poracanthodes	0.015185	0.017103	0.020675	0.027195	0.017331
Nostolepis	0.028856	0.027693	0.022026	0.023082	0.02398